Surface functionalization of bioactive glasses with natural molecules of biological significance

POLITECNICO DI TORINO

Doctoral Thesis in Biomedical Engneering

XXVI cycle

Surface functionalization of bioactive glasses with natural molecules of biological significance

Xin Zhang

Tutors: Enrica Vern é

Enrico Prenesti

December 2013

Contents

Introduction

Natural or artificial materials used for replacement or supplement the functions of living tissues, termed as biomaterials, may be bioinert (i.e. alumina and zirconia,) resorbable (i.e. tricalcium phosphate), bioactive (i.e. hydroxyapatite, bioactive glasses, and glass-ceramics) or porous for tissue ingrowth (i.e. hydroxyapatite-coated metals). Among all the biomaterials, bioactive glasses and glass-ceramics are widely used in orthopedic and dental applications and are being developed for tissue engineering. However, to a large extent, the behavior and overall performance of biomaterials are governed by surface properties. Surface modifications therefore provide unique possibilities to control the subsequent surface interaction and response which are required for particular application. By tailoring the material surface, a wide portfolio of additional functionalities is enabled to overcome material deficiencies while maintaining its bulk material properties. As a consequence, the surface functionalization of materials has become pivotal for academic research as well as industrial product development.

Plant-derived polyphenols are compounds possessing one or more aromatic rings with one or more hydroxyl groups. They are broadly distributed in the plant kingdom and are the most abundant secondary metabolites of plants, with more than 8,000 phenolic structures currently known, ranging from simple molecules such as phenolic acids to highly polymerized substances such as tannins. Numerous researches and investigation reported the notable biological activities of polyphenols, such as cardiovascular protection, cancer prevention and treatment, antiaging activity as well as applications in Alzheimer’s disease, oral health, immune function diabetes and other neurodegenerative disorders.

Till now, numerous investigations provide a number of surface functionalization techniques and make it possible to graft various kinds of biomolecules such as proteins, growth factors and enzymes to the surface of bioactive glass and glass-ceramics. However, very few researches have

been focused on the coupling of natural bioactive polyphenols on surface of bioactive glasses and glass-ceramics.

As a conclusion, the aim of this thesis is to combine bioactive glasses and glass-ceramics with natural polyphenols, in this case they are grape polyphenol and tea polyphenol extracted from grape skin and green tea respectively, in order to make it possible to immobilize biomolecules as well as prepare smart biomaterials with both typical inorganic activity and specific biological benefits from natural molecule. Surface functionalization of the same substrates with gallic acid as model molecule for polyphenols has been carried out in order to investigate more in depth the mechanisms of surface modification with a simple molecule.

This thesis can be divided into five chapters. The first chapter introduces the composition, chemical structure, biological properties and potential applications of plant polyphenols. In chapter II, the extraction methods and analysis techniques involved in polyphenol investigation are reviewed. Chapter III mainly illustrated the structure, property and biomedical application of biomaterials as well as methodologies and evaluation of surface functionalization. Materials and techniques related to this thesis are demonstrated in chapter IV. The last chapter, also the core chapter of this thesis, describes the results and discussions in five separate sections: i) surface functionalization of SCNA and CEL2 with gallic acid; ii) surface functionalization of SCNA and CEL2 with polyphenol extracted from grape skin; iii) surface functionalization of SCNA and CEL2 with polyphenol extracted from green tea; iv) surface functionalization of SC-45 with gallic acid and buffered gallic acid and v) surface functionalization of SC-45 with folic acid.

Chapter I

Functional polyphenols from plants: composition, chemical structure, biological properties and potential applications

1 Introduction

Phenolics are the most abundant secondary metabolites present in the plant kingdom. In plant, phenolic compounds participate in growth, fertility and reproduction and play a role in various defense reactions to protect against abiotic stress like UV-light, or biotic stresses such as predator and pathogen attacks [1, 2]. They also constitute the basic component of pigment, essences and flavors. At the tissue, cellular and sub-cellular level, soluble phenolics are found within plant cell vacuoles, while insoluble phenolics such as lignins and hydroxycinnamic acids are the components of cell wall [3, 4] and these compounds contribute to the mechanical strength of cell walls and plant growth and morphogenesis by linking with carious cell components [5-8]. It was reported that the ferulic and *p*-coumaric acids may be esterified to pectin and arabinoxylans or cross-linked to cell wall polysaccharides and this cross-links may play a role in adhesion among cells, serve as a lignins formation site and do contributions to the thermal stability of plant texture [9-13].

For decades, plant polyphenols have interested researchers for their essential contribution to plant physiology, providing plants with resistance to pathogens and predators and their abilities of antioxidant, free radical scavenging capacities and their potential effects on human health. Nowadays, polyphenol gets an increasing recognition not only by the scientific community but also by the general public due to the presence and abundance of polyphenol in fruits, vegetables, seeds and derived foodstuffs and beverages, whose daily consumption has been claimed to be beneficial for human health. Their ability to scavenge oxidative generated free radicals, such as lipids and nucleic acid free radicals, has often been underlined as the fundamental chemical event that emphasizes their utility in reducing the risk of certain age-related degeneration and diseases.

Due to the great benefits of polyphenols for human health, nowadays, it is highly recommended and heavily advertised to eat five servings of fruits and vegetables per day and drink green tea on a regular basis as well as a couple of glasses of red wine per day. As a result, this chapter includes contents such as a short history of polyphenol, chemical structure and composition as well as biological activities of phenolics.

2 The history of polyphenols

Before being termed polyphenols, these plant-derived natural products were globally referred to as vegetable tannis for the original application of various polyphenol extracts in leather-making process during which the animal skins or furs were converted into leather. Literature verified that the Ancient Greeks of archaic period (ca. 800-500 BC) firstly developed this technology by using oak galls in Europe [14].

It was until second half of the 20^{th} century that research about polyphenols starts to address objectives beyond the leather manufacture, accompanied with the first glimpse of the definition of plant polyphenols. In 1957, White mentioned that the term "tannin" should strictly refer to the plant polyphenols with molecular masses between 500 and 3000 Da and to be capable of forming cross-linked hydrogen group with collagen molecules. In brief, he indicated that all tannins belong to polyphenols while the reciprocal is not necessarily true [15-17]. The definition of plant polyphenols was given by Bate-Smith and Swain in their own proposal in 1962, as"water-soluble phenolic compounds having molecular weights between 500 and 3000 (Da) and, besides giving the usual phenolic reactions, they have special properties such as the ability to precipitate alkaloids, gelatin and other proteins from solution [18] ", which was a slight variation of White's earlier proposal. Then the scientist Edwin Haslam refined the definition at the molecular level. He expanded the definitions of Bata-Smith, Swain and White as descriptor for water soluble plant phenolic compounds possessing molecular masses ranging from 500 to 3000-4000 Da and having 12-16 phenolic hydroxyl groups on five to seven aromatic rings per 1000 Da of relative molecular mass. Furthermore, the compounds should have the common phenolic reaction and the ability to precipitate some alkaloids, gelatin or proteins in solution [19].

3 Phenolic compounds and their structures

Polyphenols or phenolic compounds constitute one of the most abundant and ubiquitous groups of plant metabolites and an integral part of both human and animal diets. Chemically, phenolics can be defined as substances possessing an aromatic ring linked with one or more hydroxyl groups, including their functional derivatives [20]. Until now, more than 8000 phenolic structures have been known and there were two main biogenetical synthetic pathways: the shikimate pathway and the acetate pathway [21, 22]. Natural polyphenols always include simple phenols, phenolic acid (both benzoic and cinnamic acid derivatives), coumarins, flavonids, stibenes, hydrolysable and condensed tannins, lignans and ligins [23]. According to literature [22], polyphenols can be divided into at least 10 classes (Table 1) based on their molecular structure and flavonoids considered as the most important single group, can be subdivided into 13 classes (Table 2). In food science research, polyphenol found are usually divided into four main classes: phenolic acid, flavonoids, lignans and stilbenes [24].

Table 1 Main classes of phenolic compounds

Class	**Basic skeleton**	**Basic structure**
Simple phenols	C_6	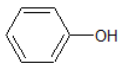
Benzoquinones	C_6	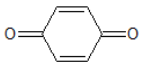
Phenoilc acids	C_6-C_1	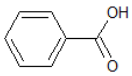
Acetophenones	C_6-C_2	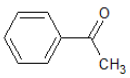
Phenylacetic acids	C_6-C_2	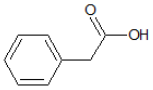
Hydroxycinnamic acids	C_6-C_3	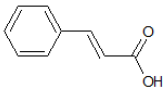
Phenylpropenes	C_6-C_3	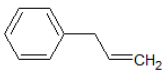

Coumarins, isocoumarin	C_6-C_3	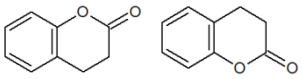
Chromones	C_6-C_3	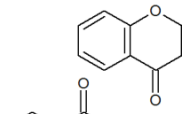
Naftoquinones	C_6-C_4	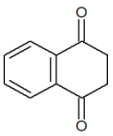
Xanthones	C_6-C_1-C_6	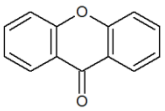
Stilbenes	C_6-C_3	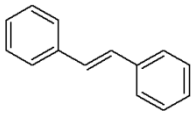
Anthraquinones	C_6-C_3	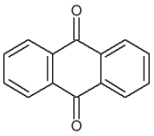
Flavonoids	C_6-C_3-C_6	
Lignans, neolignans	$(C_6$-$C_3)_2$	
Lignins	$(C_6$-$C_3)_n$	

Table 2 Classification of food flavonoids

Flavonoid	**Basic structure**
Chalcones	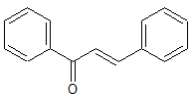
Dihydrochalcones	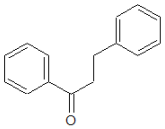
Aurones	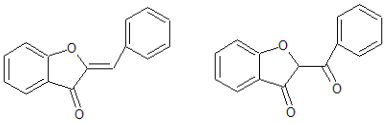
Flavones	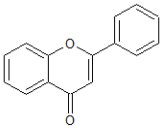
Flavonols	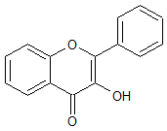

Dihydroflavonol	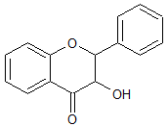
Flavanones	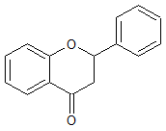
Flavanol	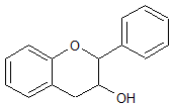
Flavandiol or leucoanthocyanidin	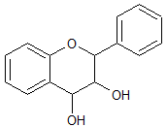
Anthocyanidin	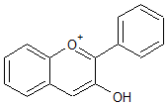
Isoflavonoids	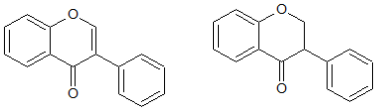
Biflavonoids	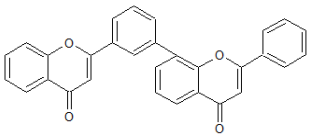
Proanthocyanidins or condensed tannins	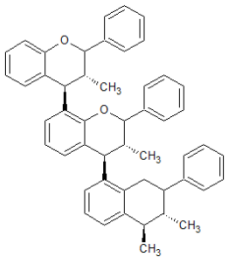

Simple phenols (C_6) derivatives and flavonoids are the most common and important phenols among the low-molecular mass phenols. Simple phenols, such as phenol itself, cresol, thymol, orcinol, resorcinol and so on, widely exist in various species, while phenolics with a C_6-C_1 structure, such as phenolic acid and aldehydes, are fairly common in higher plants and ferns.

Phenolic acids are phenols which have one carboxylic acid functional group and are divided into hydroxycinnamic acids and hydroxybenzoic acid. The latter ones are less common than the former ones, which mainly include gallic acid, *p*-coumaric, caffeic, chlorogenic acid, ferulic acid and sinapic acids. These acids are usually present as the bound forms that are glycosylated derivative or esters of quinic acid, shikimic acid and tartaric acid [25].

Phenylpropanoid derivatives (C_6-C_3) as another important group of low-molecular weight phenolics are usually covalently linked to cell wall polysaccharides (predominantly ester-linked to arabinose units of hemicellulose) or to the so-called core lignin. Chromones, coumarin, and cinnamyl alcohols etc are the common members in this group [26, 27].

Flavonoids, as one of the most abundant phenolic compounds, possess a common C_6-C_3-C_6-skeleton composed of three rings (Figure 1) including two aromatic rings linked through three carbons. This molecules family is constituted by different sub-classes, flavones, flavonols, flavanones, flavanols and anthocyanins differing by the insaturation degree and substituent of ring C. Biogenetically, the A ring is usually from a molecule of resorcinol or phloroglucinol synthesized in the acetate pathway, whereas B ring is synthesized from the shikimate pathway [28].

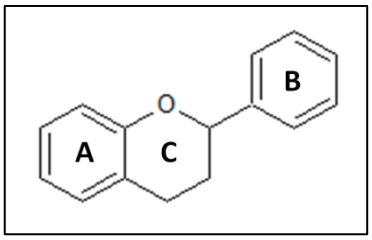

Figure 1: Basic structure of flavonoids

Tannins are compounds of intermediate to high molecular weight. According to literature, the molecular weight of tannins found in carob pods was up to 30,000 Da [29]. Tannis are highly hydroxylated molecules and can precipitate carbohydrates and protein. Plant tannins can be subdivided into two main catagories: i) hydrolysable and ii) condensed tannins. Hydrolyzable tannins are composed gallic acid and its dimeric condensation products hexahydroxydiphnic acid [30]. The best known hydrolyzable tannin is tannic acid (Figure 2).

Major stilbenoids found in foods of plant origin are resveratrol (Figure 3) and its glucosiders. Resveratrol (3, 4', 5-trihydroxystibene) as one kind of phytochemicals is a low molecular mass natural product and an early product from the biosynthesis of phenyalanine. It is also taken as an intermediate leading to some polyphenols and flavonoids with more complicated structures [31].

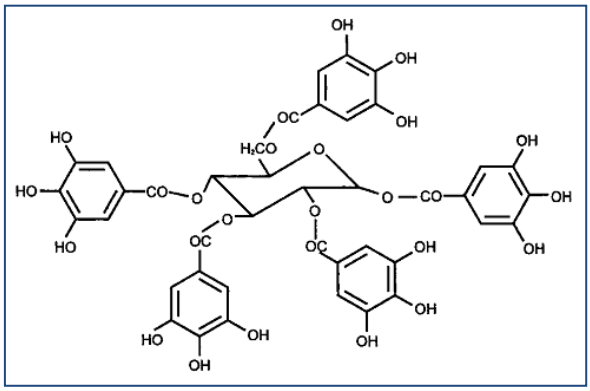

Figure 2: Chemical structure of tannic acid [29]

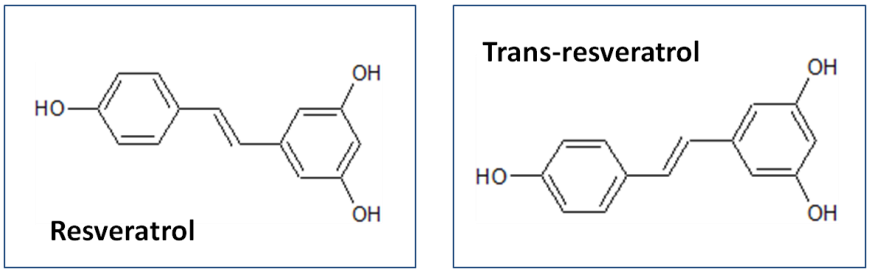

Figure 3: The chemical structure of resveratrol and trans-resveratrol

3.1 The composition and structure of grape polyphenol (GP)

Grapes as table food and winemaking sources had a long and abundant history, dated to the Ancient Greek and Roman civilizations. Due to the various nutrient elements in grape, such as vitamins, minerals, carbohydrates, edible fibers and phytochemicals, nowadays substantial scientific attention has been focused on the potential biomedical effect of grapes and grape products [32]. Furthermore, as one of the main sources of bioactive components, grapes are rich in phenolic compounds in its skins, short stems, seeds, leaves, even in grape pomace after wine-making industry [33, 34]. The total phenolic content in grape seed, skin, flesh and leaf has been estimated as 2178.8, 374.6, 23.8, 351.6 mg/g respectively, with gallic acid as the equivalent [35]. Anthocyanins, catechins, proanthocyanidins, flavonol glucosides, stilbenes and phenolic acids are the principal phenolic constituents found in GP [34, 36]. Chemical structures of a number of phenolic compounds from grape have been reported in the literature, the most important ones are shown in figure 4.

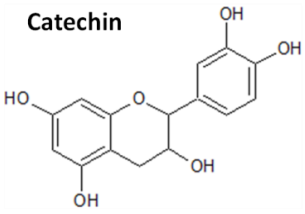

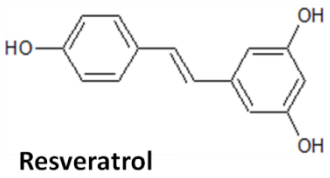

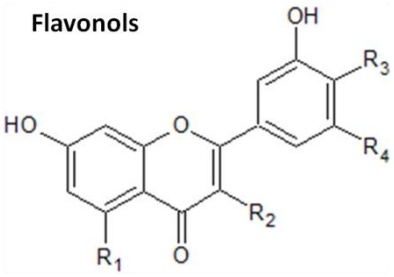

	R_1	R_2	R_3	R_4
Quercetin	OH	OH	OH	H
Rutin	OH	*O*-Rutinose	OH	H
Morin	OH	OH	H	OH
Myricetin	OH	OH	OH	OH
Fisetin	OH	OH	OH	H

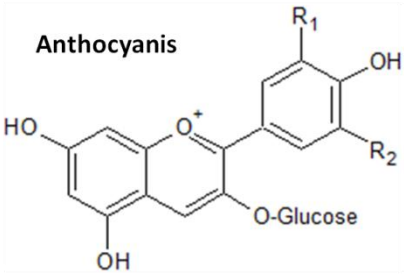

	R_1	R_2
Cyaniding-3-*O*-gluc	OH	H
Delphindin-3-*O*-gluc	OH	OH
Peaonidin-3-*O*-gluc	OCH_3	H
Petunidin-3-*O*-gluc	OCH_3	OH
Malvidin--3-*O*-gluc	OCH_3	OCH_3

Figure 4: Chemical structures of some phenols from grapes

The polyphenol composition and quantity of GP usually vary with grape cultivars, soil composition, geographic origin, climate and cultivation practices or exposure to diseases, such as fungal infections [37]. For instance anthocyaninins are abundant in red grapes but neglected in white varieties. Xia [38] has reviewed the phenolic compound distribution in different parts of grapes (Table 3) and it was proved that the grape skin was rich in anthocyanins, hydroxycinnamic acids, flavanols and flavonol glysides. Overall, grape seeds contained lower amount of phenolic acid than grape skin, but higher amount of catechins and procyandins [39, 40].

Table 3 The phenolic compounds in different parts of grape and its products [38]

Resource	**Phenolic compounds**
Seed	Gallic acid, catechin, epicatechin, dimeric procyanidin, proanthocyanidins
Skin	Proanthocyanidins, ellagic acid, myricetin, quercetin, kaempferol, *trans*-resveratrol
Leaf	Myricetin, ellagic acid, kaempferol, quercetin, gallic acid
Stem	Rutin, quercetin 3-*O*-glucuronide, *trans*-resveratrol, astilbin
Raisin	Hydroxycinnamic acid, hydroxymethylfurfural
Red wine	Malvidin-3-glucoside, catechin, resveratrol, hydroxycinnamic acid, peonidin-3-glucoside, petunidin-3-glucoside, cyaniding-3-glucoside, quercetin,

Scientists all over the world have intensively investigated the phenolic profile of grape skins and seeds of European variety (*vitis vinifera*). Among the scientists, Montealegre et al. [34] has studied the composition and quantity of polyphenols of ten grape species (including six white grape varieties and four red grape varieties) grown in warm climate of Spain. They found that the red grape skin contained higher amount of hydroxycinnamates than white grape, but lower amount of catechins, procyandiin dimmers and total flavonols. Furthermore, the composition of polyphenol of same grape variety was influenced by the growing location, climate, maturity and the time of fermentation [41, 42]. El ás et al. [43] evaluated the phenolic compositions of grape seeds extracts from four different grape varieties (Carm énère (CA), Merlot (M), Cabernet Franc

(CF) and Cabernet Sauvignon (CS)) by HPLC -DAD and spectrophotometric analysis during four ripening stages. Significant differences between CA and CF were observed in seed weights, total tannins and polymeric flavanol fraction. Besides, M seeds showed higher concentration of (+)-catechin and (-)-epicatechin and CA seeds presented higher concentrations of a series of other proanthocyanidins. In their other research [44], the phenolic composition of skin extracts of these four grape varieties was investigated. Cabernet Sauvignon skins showed the highest contents of monomeric, oligomeric and polymeric flavan-3-ols with respect to other varieties at harvest maturity. Likewise the sum of glucoside and cumarilglucoside anthocyanins in Carménère was higher than in Cabernet. Franc and Cabernet Sauvignon in some sampling date. According to the study of Yu et al. [45], the Muscadine (one native grape variety grown in the United States) grape had more skin (5%) and less seeds (8%) than Cabernet (one European grape variety). Moreover, the polyphenol compostion of Muscadine and Cabernet was different. The total extractable polyphenol, total anthocyanin content and total flavonoid content were 36.4, 0.88 and 21.02 mg/g DM in Muscadine seeds, 19.39, 8.15, 4.78 mg/g DM in Muscadine skin, respectively.

3.2 The composition and structure of tea polyphenol (TP)

Tea, the second popular beverage in the world next to water has been consumed for thousands of years and has attracted attention in recent years due to its numerous health benefits such as antioxidant, antimicrobial, anti-carcinogenic and anti-arteriosclerotic properties [46, 47]. Tea is produced by brewing the dried tea leaves and buds of the plant *Camellia sinensis*, which was first cultivated in China and later in Japan. During the 15^{th} to 17^{th} centuries, the commercial cultivation gradually expanded to Indonesia and then to the Indian subcontinent with the opening of ocean routes to the East [48]. Annual production of about 1.8 million tons of dried leaf provides world per capita consumption of 40 L of beverages [49]. Based on the different degree of fermentation during manufacturing process, tea can generally be classified into three types, specifically, green tea (no fermented tea), oolong tea (partially fermented tea), and black tea (fully fermented tea) [50].

The chemical composition of tea is complicated, including polyphenols, alkaloids (caffeine,

threobromine, theophylline), polysaccharides, amino acids, volatile oils, lipids, vitamin C minerals and other uncharacterized constituents [51]. The main polyphenols in tea are flavonoids, particularly flavanols (i.e., catechins), and phenolic acids. Catechins (figure 4) are colorless water-soluble compounds which impart bitterness and astringency to green tea infusions [52]. These catechins are synthesized in tea leaves through malonic acid and shikimic acid metabolic pathways with gallic acid as an intermediate derivative [53]. The total content of catechin in green tea infusion is 420 mg/L [54] and catechin constitute 15-30% of dry weight of green tea leaves, compared with 8-20% of oolong and 3-10% of black tea [55]. Green tea extracts are mainly constituted of four primary catechins (figure 5): (-)-epicatechin (EC), (-)-epicatechingallate (ECG), (-)-epigallocatechin (EGC) and (-)-epigallocatechingallate (EGCG) [56]. Among them, EGCG is the most important and wildly studied tea catechin due to its high content (up to 50%) [57]. Additionally, EGCG, in particular, is known to inhibit tolemerase, urokinase, nitric-oxide snthase, tumor necrosis factor alpha, the proteasome and so on [58-62]. Later， 3-galloylquinic acid, 4-galloylquinic acid, 1,3,5-trigalloylquinic acid, 4-(di-galloyl) quinic acid, 5-(digalloyl) quinic acid, and either 3-galloyl-5-(d igalloyl) quinic acid or 3-(digalloyl) -5-galloylquinic acid were also identified in green tea [63]. Tea is also an important source of gallic acid (hydroxybenzoic acid). It is reported that the content of gallic acid in Chinese Pu-er teas is highest (about 15 g/kg of dry weight) as opposed to other types of tea [58].

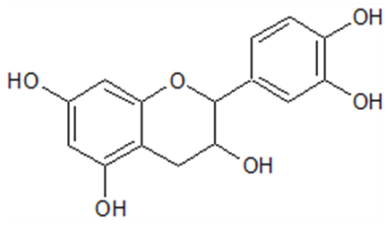

(-)-Epicatechin (EC)

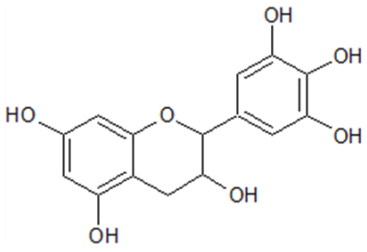

(-)-Epigallocatechin (EGC)

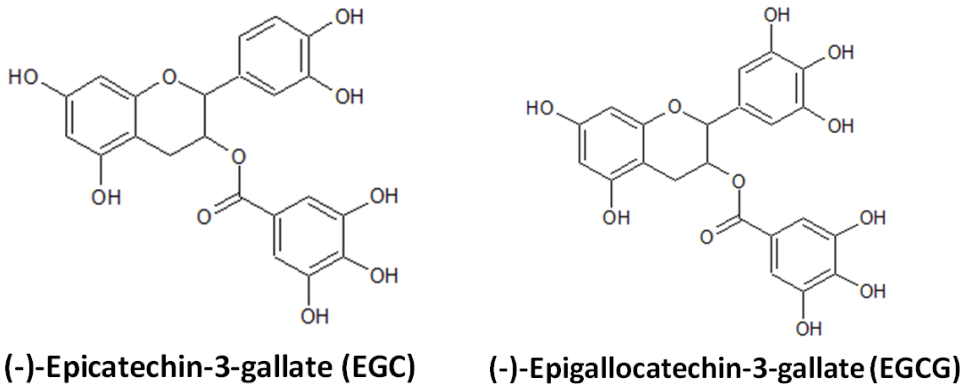

Figure 5: Structure of major tea catechins present in green tea extracts

As for black tea, during the fermentation process, some important chemical changes happen; polyphenol oxidase and peroxidase are the responsibles for the oxidation of flavanols oxidize pyrogallol and cathchol into their form of *o*-quinones. Two characteristic black tea polyphenols, theaflavins and thearubigins are generated during fermentation. Till now, four major theaflavins (shown in figure 6) have been identified from black tea, including theaflavin, theaflavin-3-gallate, theaflavin-3'-gallate and theaflavin-3, 3'-digallate [64]. Takino et al. [65] revealed that theaflavin was the coupling oxidation product of EC and EGC.

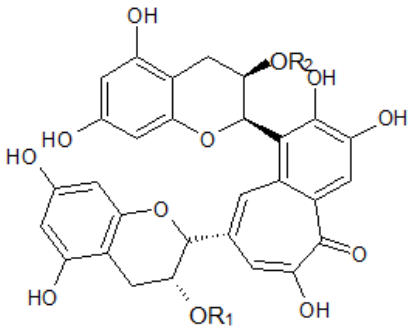

		R_1	R_2
Theaflavin	TF	H	H
Theaflavin-3-gallate	TF3G	Gallate	H
Theaflavin-3'-gallate	TF3'G	H	Gallate
Theaflavin-3, 3'-digallate	TFDG	Gallate	Gallate

Figure 6: Chemical structures of theaflavins

4 Biological properties of polyphenols

Numerous studies have demonstrated that plant polyphenols have many health benefits such as antioxidant and anti-inflammatory properties, antimutagenic and anticarcinogenic activities, prevention and delay of cardiovascular diseases, increase in lifespan and retarded the onset of age-related markers. Among all the sources for phenolics extraction, grape and tea are the most important two plant materials and have been widely investigated due to their great contribution to human health care. Grape and its products have been consumed for centuries and since the ancient Greece and Roma age, grapes have served for the winemaking. And from the clue of "French paradox", lots of investigations have been carried out and found the evidences of grape beneficial health effects, including inhibiting some degenerative diseases and reducing plasma oxidation stress and slowing ageing [66, 67]. Some recent studies showed that taking grape seed extract can reduce food intake in rats and the energy intake of human [68]. As for tea, the famous beverage all over the world, in the past few years, numerous evidences associated with tea consumption and health benefits come from epidemiological studies, in vitro studies, animal studies as well as an increasing number of human intervention studies [38].

4.1 Basic physicochemical properties of the phenol functional group

There are numerous reasons to investigate plant polyphenols. Plant phenolics, one kind of the secondary metabolisms of plants, deserve a special mention considering the wide-raging benefits, such as plant resistance against microbial pathogens and animal herbivores, protection against solar radiation as well as reproduction, nutrition, and growth, they offer to plants and to other living organisms. These characteristics are essentially a result of their inherent physicochemical properties deriving from the phenol functional group [69] (figure 7).

A phenyl ring bearing a hydroxyl group (Ph-OH), as the most elementary structural form of polyphenol, determines a phenol function of amphiphilic moiety which combines the hydrophobic character of the planar aromatic nucleus with the hydrophilic character of the polar hydroxyl substituent, which can act as a hydrogen-bond donor or an acceptor. Moreover, hydrophobic π-stacking (van der Waals) interactions and the formation of hydrogen bonds are

often complementary effects that plant phenolics can use to interact physically with other biomolecules [70].

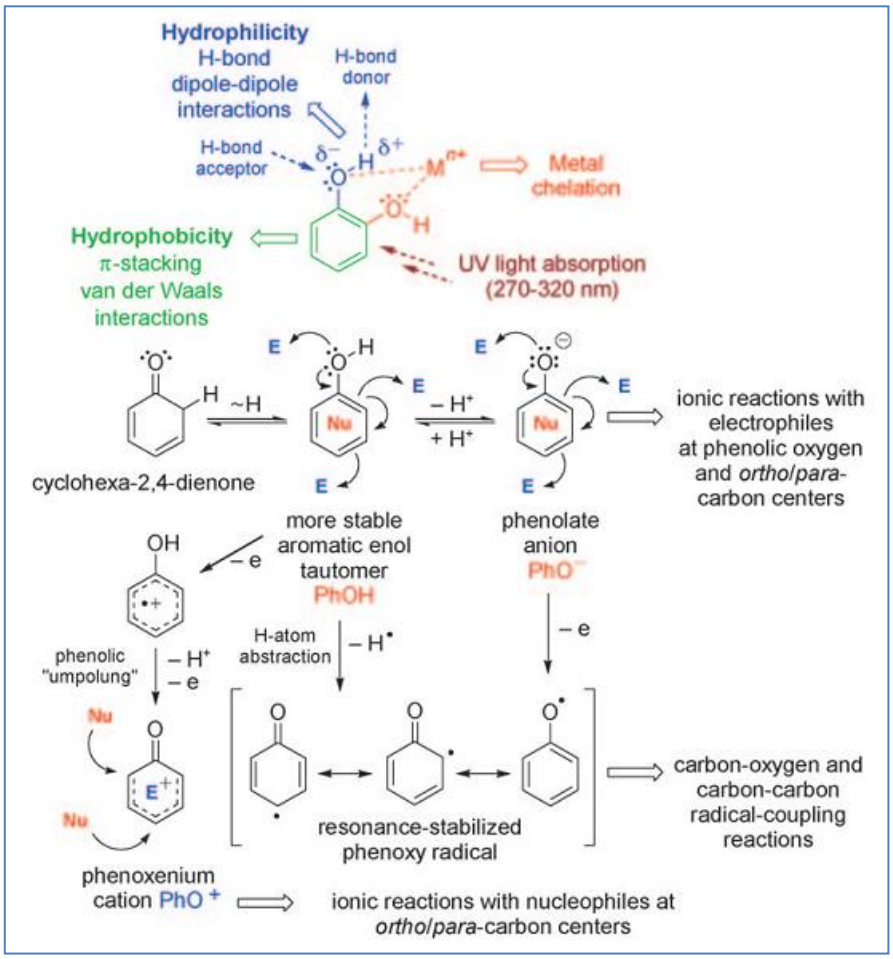

Figure 7: Basic physicochemical properties and reactivities of the phenol functional group [69] E = Electrophile, Nu = Nucleophile

When there are at least two adjacent hydroxyl groups on a phenyl ring, the main reaction of phenolics is metal chelation, which plays an important role in the plant pigmentation [71, 72] and cationic nutrient such as Ca, Mg, Fe, Cu, Mn [73, 74, 75] through the plant-litter-soil interaction. In addition, the secondary maximum absorption of polyphenol aqueous solution is red-shifted to 270 nm, compared to benzene at 254 nm. The presence of an additional hydroxyl group and/or an electron-withdrawing group (carbonyl or propenoyl ester group et al.) on the *para*-position can also shift the maximum absorption into the UV-Blight range (280-320 nm).

Otherwise, the adjunction of a single hydroxyl group on a benzene (phenyl) ring can also change

the chemical properties of its quasi-inert aromatic system. Phenols can be taken as the stabilized enol tautomers with a soft nucleophilic character, while it can be transformed into harder nuclephilic character by deprotonation into phenolate anions (PhO^-), if the moderate and exploitable acidic phenolic O-H bond is in biological system. Phenols and phenolate anions are also sensitive to oxidation processes. The relatively weak bond dissociation energy (BDE) of the phenolic O-H bond enables the production of phenoxy radicals ($PhO^•$) by hydrogen abstraction [76-78].

4.2 Antioxidant properties

When it refers to polyphenols and plant phenolics, their most notable biological activity should undoubtedly be antioxidant characteristics.Antioxidant ability refers to the capability to scavenge reactive oxygen species (ROS), which include radical and non-radical oxygen species, such as O_2^-, $HO^•$, $NO^•$, H_2O_2， HOCl, as well as oxidatively generated free radicals $RO^•$ and $ROO^•$, like those derived from biomolecules such as low-density lipoproteins (LDLs) [79-83], proteins and oligonucleic acids (DNA and RNA) [84, 85]. This so-called antioxidant capability is cited to be the key property emphasizing the prevention and/or reduction of oxidative stress-related chronic diseases and age-related disorders such as cardiovascular diseases (for example, atherosclerosis), neurodegeneration (for example, Alzheimer's disease, Parkinson's), carcinogenesis, as well as skin deterioration, by intake plant phenolics and other plant polyphenol-containing products. Furthermore, several methods have been developed to evaluate the antioxidant capacities of phenolic compounds, such as the 1, 1-dipheyl-2-picryhidrazyl (DPPH) assay, crocin bleaching assay (CBA), oxygen radical absorbance capacity (ORAC) assay, Trolox equivalent antioxidant capacity (TEAC) assay, the thiobarbituric acid reactant substances (TBARS), lipid peroxidation (MDA) colorimetric/fluorometric assay and the ferric reducing antioxidant power (FRAP) assay.

4.2.1 Mechanism of antioxidant properties

4.2.1.1 Mechanism of free radical scavenging

In food products, lipid oxidation is considered as one of the main factor limiting commodity quality and acceptability due to the generation of reactive oxygen species and off-flavors from unsaturated fatty acids [86, 87]. Scheme 1 showed the mechanism involved in lipid oxidation in foods. Step one illustrates that in the initiation reaction, the unsaturated fatty acid (RH) loses hydrogen radicals (H) then reacts with oxygen in the presence of light, heat or trace metals and finally forms the peroxyl radicals (ROO•). In the propagation process, peroxyl radicals react with more unsaturated fatty acids to obtain lipid hydroperoxides (ROOH). In the end, the oxidation chain reaction terminates when two proxyl radical reacts to generate a non-radical species (ROOR or RR). In this situation, the function of antioxidants is to delay or inhibit the oxidation of lipids or other molecules by inhibiting the initiation or propagation step of the oxidative chain reactions [88].

Step 1: Initiation	$RH \rightarrow R^{\bullet} + H^{\bullet}$
	$R^{\bullet} + O_2 \rightarrow ROO^{\bullet}$
Step 2: Propagation	$ROO^{\bullet} + RH \rightarrow ROOH + R^{\bullet}$
Step 3: Termination	$ROO^{\bullet} + ROO^{\bullet} \rightarrow ROOR + O2$
	$ROO^{\bullet} + R^{\bullet} \rightarrow ROOR$
	$R^{\bullet} + R^{\bullet} \rightarrow RR$

Scheme 1: the mechanism of lipid oxidation production

As for human being, lots of factors (figure 8) can increase the production of free radicals and reactive oxygen species which are the sources of oxidative stress in cells, damaging proteins, lipids and DNA [89]. The antioxidants can put an end to the oxidative stress and stop the cycle of free radical cell damage by donating one of their electrons to the unstable free radical and replace them by relatively stable radicals.

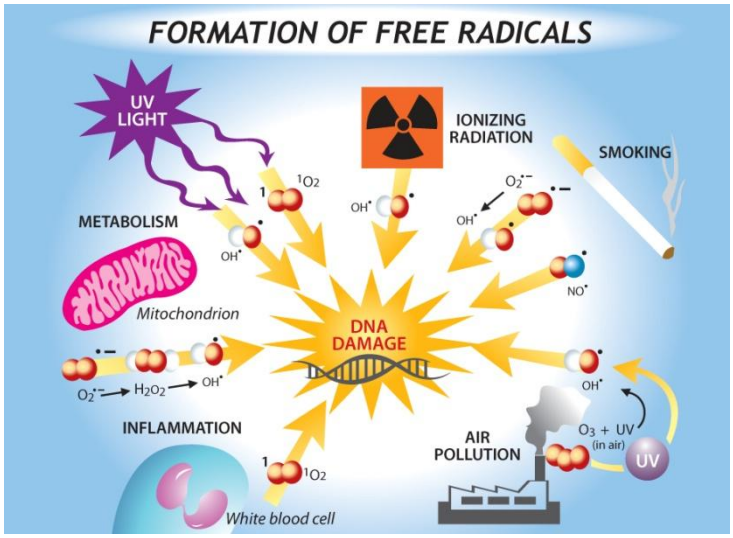

Figure 8: Formation of free radicals [90]

According to literature, two main antioxidant mechanisms (scheme 2) have been proposed [91]. The first one is named as hydrogen-atom transfer (HAT) which is based on the capability of the phenol functional group to donate a hydrogen atom to a free radical R•, such as the aforementioned peroxyl radicals ROO•. In this case, phenol plays a role as the chain breaking antioxidant and after reacting with free radicals, phenol itself becomes a free radical (PhO•). The efficiency of the antioxidant action depends on the transfer speed of the hydrogen atom to ROO• and the stability of the new formed phenoxyl radical PhO•, since the PhO• may react with ROOH or RH and as a result terminates the propagating radical chain reaction. The factor that influences the formation and stability of PhO• is the structural features of the phenol parent compound. The most important factors playing a determining role include the number, presence and relative position of additional phenolic hydroxyl groups, their implication in the formation of intramolecular hydrogen bonds, and the conformationally dependent possibility of allowing electronic delocalization throughout the largest part of the molecule [69]. All the factors affect the bond dissociation energy (BDE) of phenol O-H bond: the weaker the O-H bond, the easier the H-atom transfer and more stable the PhO• will be. The second one is the single-electron transfer (SET) mechanism based on the transfer of electron from PhOH to free radical R• with the formation of a stable radical cation $PhOH^{\bullet+}$ (scheme 2).

HAT mechanism	$R^{\bullet} + PhOH \rightarrow PhO^{\bullet} + RH$
SET mechanism	$R^{\bullet} + PhOH \rightarrow R^{-} + PhOH^{\bullet+}$

Scheme 2: Two main mechanisms (HAT and SET) of phenol radical-scavenging-based antioxidant action

4.2.1.2 Mechanism of iron bonding

Plant phenolic compounds can also show their antioxidant activity by chelating metal ions such as iron (II)/copper (I), and iron (III)/copper (II) ions that participate in the conversion of O_2^- and H_2O_2 in to highly aggressive $HO^{\bullet}$ through Haber-Weiss/Fenton-type reactions [92-96]. Hydroxyl radicals ($HO^{\bullet}$) which is known as the most reactive ROS can abstract a hydrogen atom from biological substrates[97] and can be generated by multiple pathways, such as decomposition of peroxynitrous acid [98] and the metal-mediated reduction of peroxide. For the first pathway, for example, $O_2^{\bullet -}$ and $NO^{\bullet}$ can react to form $OONO^-$ [99, 100], which can decompose into $HO^{\bullet}$ [98] later. H_2O_2 as a biological peroxide can be produced in the process of cellular respiration [101] and cell signaling mechanism. However, the amount of H_2O_2 is commonly reduced in vivo by Fe^{2+} or Cu^+ through Fenton-type reaction.

$$Fe^{2+} (Cu^+) + H_2O_2 + H^+ \rightarrow Fe^{3+} (Cu^{2+}) + HO^{\bullet} + H_2O$$

Research showed that DNA can be directly damaged by $HO^{\bullet}$[102-104], and indirectly by the oxidation of [4Fe-4S] iron-sulfur cluster by $O2^{\bullet -}$ to form H_2O_2 [105].

$$[2Fe^{2+}2Fe^{3+}\text{-}4S] + O_2^{\bullet -} + 2H^+ \rightarrow [Fe^{2+}3Fe^{3+}\text{-}4S] + H_2O_2$$

In addition, the Haber-Weiss reaction was thought to be another source for cellular $HO^{\bullet}$ [106, 107].

$$O_2^{\bullet -} + H_2O_2 + H^+ \rightarrow O_2 + HO^{\bullet} + H_2O$$

The radical-induced damage to DNA usually happens to both the phosphate backbone (strand breakage) and the nucleotide bases, because DNA backbone is composed of negatively charged phosphate groups as well as electron-rich nucleotide bases with the localization of metal ions such as Na^+, Mg^{2+}, Fe^{2+}, Fe^{3+}, Cu^+, Cu^{2+}, by electrostatic interaction near the phosphate backbone and transition metal ions. With the presence of H_2O_2 as a result of oxidative stress, redox active metal ions like Fe^{2+} or Cu^+ bonded to DNA can react with H_2O_2 to form highly reactive $HO^{\bullet}$ in immediate proximity to DNA. Then $HO^{\bullet}$ abstracts hydrogen atom from the deoxyribose sugar backbone leaving a DNA radical adduct that rearranges, cleaves the phosphodiester backbone and ultimately leads to a strand scission [102, 103, 108, 109]. Alternatively, $HO^{\bullet}$ may damage the nucleotide bases and produce oxidized base products such as 8-oxo-guanine and fragmented or ring-opened derivatives [110-112]. As a result, both damages to DNA can cause genetic mutations, cancers or cell death [110]. Even if the iron-mediated oxidative damage of DNA by $HO^{\bullet}$ is the primary reason for cell death, the intracellular non-protein-bond iron [113] generated during this damage process exists as Fenton-active iron Fe^{2+} [114] investigated by electron paramagnetic resonance (EPR) is associated with both Alzherimer's and Parkinson's [115, 116], and cardiovascular disease [117].

To summarize, iron plays an important role in the generation of ROS in vivo, for example, $HO^{\bullet}$ and H_2O_2, and due to its pivotal contributions to oxidative stress, DNA damage and cell death, iron becomes the target of many antioxidant therapies. Polyphenol, because of its ability to coordinate iron, is extensively examined and as antioxidant for prevention of conditions associated with iron-generated ROS and oxidative stress.

Catechol and gallol (figure 9) as well as many functionalized derivatives thereof are well known as effective metal chelators. After deprotonation required for metal bind, catechol and gallol are named as catecholate and gallate groups, respectively.

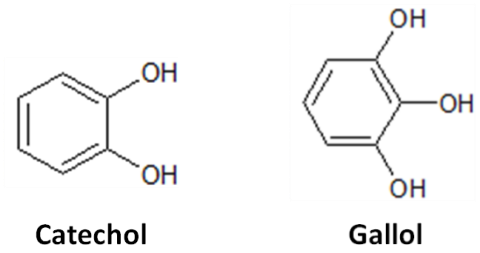

Figure 9: chemical structure of catechol and gallol

Metal ions prefer octahedral geometry and can coordinate up to three catecholate or gallate groups. For instance, Fe^{2+} and Fe^{3+} might bind with catechol or gallol in a 3:1 fashion [118] (figure 10).

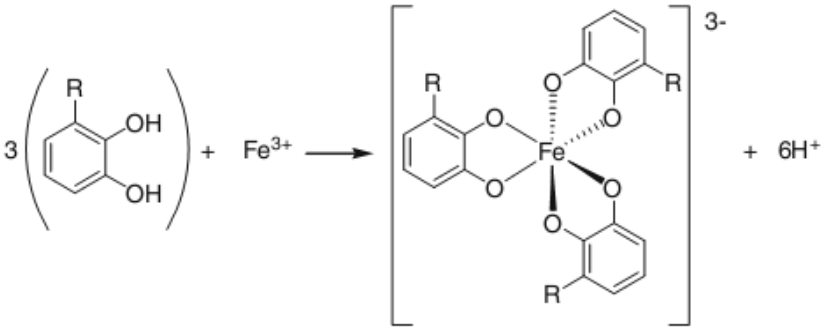

Figure 10: Expected octahedral coordination between iron and polyphenol. (gallol, R=OH; catechol, R=H) [118]

Because Fe^{3+} is great prior to Fe^{2+} in the stabilization with polyphenol ligands, one process called autooxidation carries out, during which the catecholate or gallate complexes of Fe^{2+} can be oxidized rapidly to Fe^{3+}-complexes with the presence of O_2 (figure 11a). Otherwise, binding of a catecholate or gallate ligand to Fe^{3+}, polyphenols can reduce the iron to Fe^{2+} and at the same time polyphenol is oxidized into semiquinone (figure 11b). [118]

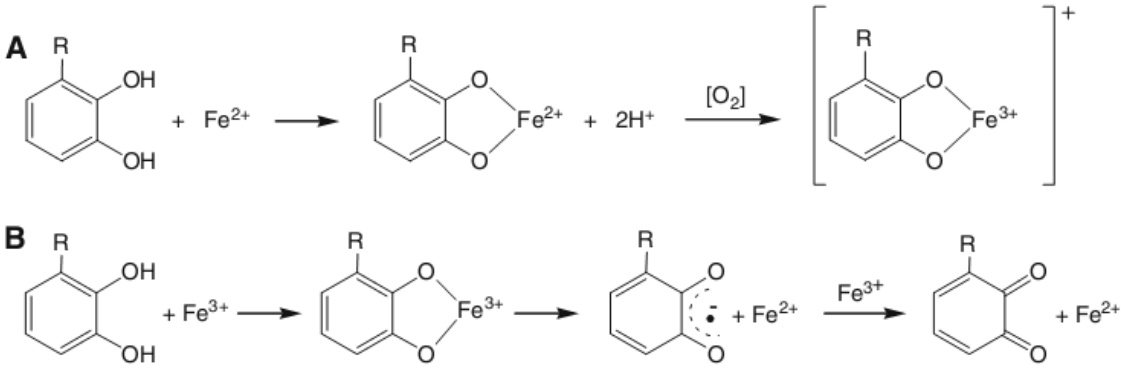

Figure 11: a) Coordination between Fe^{2+} and polyphenols and subsequent by electron transfer reaction with the presence of oxygen and generation of the Fe^{3+}-polyphenol complex; b) Coordination between Fe^{3+} and polyphenols, subsequent iron with reduction of Fe^{3+} and semiquinone formation (gallol, R=OH; catechol, R=H) [118]

Till now, researches have been done on the cytoprotective effects of polyohenols related to iron-binding. Kawabata et al. and Yoshino and Murakami have indicated that iron chelation by several different polyphenols protects rat microsomes from lipid proxidation by blocking the Fenton reaction [119, 120]. Morel et al. [121, 122] showed that the ability of polyphenols to chelate and remove iron from iron-loaded hepatocytes correlates with cytoprotective effects of those compounds. Ferrali et al. [123] have found quercetin can protect mouse erythrocytes from iron-mediated lipid peroxidation by binding irons. Similarly, Anghileri and Thouvenot [124] have investigated that polyphenols from mate tea, green tea and red wine extracts can prevent against the iron-induced lipid peroxidation of mouse liver tissue suspensions (MDA assay) as well as the iron-dependent calcium uptake in this suspensions due to the inhibition of iron bioavailability.

Attentions are also paid to protective effects of polyphenols in blood and plasma. Polyphenols from green and black tea are reported to have protective effects by iron-chelation against red blood cell lipid peroxidation, with a concentration-dependent inhibition on the generation of HO•, and cytoprotection of red blood cells in vitro from primaquine-induced oxidative stress due to the production of $O_2^{\bullet -}$ and H_2O_2 [125]. Similar results have been achieved by Srichairatanakool et al [126]. They found that green tea polyphenols enabled prevent β-thalassemia patients from iron-overload symptoms by chelating iron, with non-protein-bond,

in thalassemic plasma and radical scavenging measured by TEAC assay.

Some animal experiments showed that green tea catechins are able to cross the highly selective blood-brain barrier (BBB) and inhibit the iron-induced neuro-degeneration in mice by measuring the down-regulation of the amyloid precursor protein (APP) in the hippocampus region of the brain [127, 128]. Polyphenols from green tea and wine have shown a great inhibition to aggregation and accumulation of amyloid beta (Aβ) fibrils [129] and Aβ neurotoxicity [130], which may be a direct result of the iron-chelation ability.

Since whole-cell assays involve many variables and make it difficult to evaluate the attribution of polyphenol antioxidant activity to metal binding, many in vitro methods have been employed to examine the iron-binding antioxidant mechanism of polyphenols, for instance the quantification of the inhibition of iron-mediated DNA damage by polyphenols. Two common methods for this kind of quantification are DNA gel electrophoresis and the deoxyribose assay, which employs UV-visible spectroscopy to quantify malonaldehyde (a production from OH•induced degration of 2-deoxyribose) by its condensation reaction with thiobarbituric acid [131-133]. For gel electrophoresis, Zhao et al. observed that verbascoside can inhibited DNA damage by blocking the Fenton reaction with a dose-dependent manner, by iron-bind with polyphenols [134]. To extend this research, Perron et al. [135] investigated 12 different phenolic compounds and achieved the results that all of the compounds with catechol or gallol groups can inhibit 50% of the DNA damage from Fe^{2+} and H_2O_2 (IC_{50}) at concentrations between 1-59 μM.

4.2.1.3 Mechanism of pro-oxidant activity

Under certain conditions, some phenolic antioxidants can initiate an autoxidation process and act as prooxidants [136]. The phenoxyl radical (PhO•) may also interact with oxygen and form quinones (Ph=O) and superoxide anion ($O_2^{\bullet -}$) instead of blocking a free radical chain reaction by react with a second radical [137].

$$PhO^{\bullet} + O_2 \rightarrow Ph{=}O + O_2^{\bullet -}$$

Additionally, in some cases, prooxidant activity of phenolic antioxidants can be induced by transition metal ions as demonstrated by the following reactions [88]:

$$Cu^{2+}\ (Fe^{3+}) + PhOH \rightarrow Cu^{+}\ (Fe^{2+}) + PhO\bullet + H^{+}$$

$$PhO\bullet + RH \rightarrow PhOH + R\bullet$$

$$R\bullet + O_2 \rightarrow ROO\bullet$$

$$ROO\bullet + RH \rightarrow ROOH + R\bullet$$

$$ROOH + Cu^{+}\ (Fe^{2+}) \rightarrow Cu^{2+}\ (Fe^{3+}) + RO\bullet + OH^{-}$$

When phenolic antioxidants are under the condition that favors their autoxidation, they tend to behave like prooxidants, for instance, at high pH with high concentration of transition metal ions and with the presence of oxygen. It is reported that small and simple phenolics are easily oxidized and show pro-oxidant activity such as quercetin and gallic acid, while high molecular weight phenolics, such as condensed and hydrolysable tannins, barely show pro-oxidant activity [138].

4.2.2 Antioxidant properties of grape polyphenol (GP)

With the methods mentioned previously, notable antioxidant activities were evaluated in grape polyphenol extracted from grape seeds, skins, leaves as well as grape juice, wine and pomace after winemaking industry. The values of antioxidant capacities have great differences among different assays and polyphenol sources. Xia [38] et al reviewed the antioxidant capacities of the extracts from different parts of grape and its products (Table 4).

Numerous publications are associated with the antioxidant activities of grape phenols, such as grape seeds with the capacity of decreasing of oxidated LDL in plasma [139], grape juice reducing oxidative stress in serum [140], the protection from grape red wine against membrane oxidation os *Sacchiaromyces cerevisiae* induced by H_2O_2 [141], as well as the antioxidation of white grape dietary fiber concentrate for polyunsaturated fatty acid in oil [142].

Table 4 Antioxidant capacities of the extracts from different parts of grape and its products

Resource	TEAC	FRAP	DPPH	ORAC
Grape pomace	0.91 g/L (EC_{50})		0.20 g/L (EC_{50})	-
Defatted grape seed	36.36 mol TE/100g	21.6mol TE/100g	-	-
Whole seed	76.3 mol TE/100g	58.04mol TE/100g	-	-
Grape seed 1	-	-	> 663 μmol TE/g	-
Grape seed 2	-	-	16.8-92mmol TE/g	42.18 mmol TE/g
Grape seed 3	281.3μmol TE/g	-	-	-
Grape skin 1	-	-	15.7-113.3mmol TE/g	36.40 mmol TE/g
Grape skin 2	12.8μmol TE/g	-	-	-
Grape leaf	236.1 μmol TE/g	-	-	-
Grape fresh	2.4μmol TE/g	-	-	-
Grape juice	25 mmol TE/L	32 mmol Fe2+/L	15 mmol TE/L	-
Grape wine 1	-	8.8μmol TE/g	22.9-26.7μmol TE/g	-
Grape wine 2	-	3.098 mg TE/L	70.7 % inhibition	10.724μmol /L

Some studies showed the antioxidant activity of phenol is not highly concentrate-dependent but with a concentration saturation limit above which the antioxidant capacity may not increase further [143]. Pinelo et al. [144] revealed the impact of solvent on the antioxidant activity of catechin, resveratrol and grape extracts dissolved in ethanol, methanol and water, respectively. The maximum radical scavenging capacity was the phenol in ethanol while the minimum was in water. Besides, Arora et al. [145] found that flavonoids showed higher antioxidant capacity against metal-ion-induced peroxidation than peroxyl-radical peroxidation due to the direct reaction to generate phenoxyl radicals, which was stable and could cut off the reaction chain [146].

4.2.3 Antioxidant properties of tea polyphenol (TP)

Tea is particularly rich in polyphenols, including catechins, theaflavins and thearubigins, which do contributions to the health benefits of tea, especially antioxidant property. Tea polyphenols take a role as antioxidants in vitro mainly by scavenging reactive oxygen and

nitrogen species as well as chelating redox-active transition metal ions. The possible indirect function pathways of tea polyphenol are: 1) inhibition of the redox-sensitive transcription factors, nuclear factor-κB and activator protein-1; 2) inhibition of "pro-oxidant" enzymes, such as inducible nitric oxide synthase, lipoxygenases, cyclooxygenases and xanthine oxidase; and 3) induction of phase II and antioxidant enzymes, such as glutathione S-transferases and superoxide dismutases [147].

In brief, five potential mechanisms for the antioxidant capacity of tea have been summarized as follows:

i. Radical and oxidant scavenging
ii. Metal chelation
iii. Inhibition of redox-sensitive transcription factors
iv. Inhibition of "pro-oxidant" enzymes
v. Induction of phase II enzymes

The standard one-electron reduction potential ($E°'$) of a compound acting as a free radical scavenger can be employed to measure the reactivity of an antioxidant as hydrogen or electron donor under standard conditions. Under nonstandard conditions, such as in vivo, the Nernst equation can be used to correct$\Delta E°'$ of a redox reaction for the actual concentrations encountered in vivo [148].

$$\text{Nernst equation: } \Delta E = \Delta E°' - 60\ \text{mV}\ \log_{10}\frac{[\text{products}]}{[\text{reactants}]}$$

A lower $E°'$ value means that less energy is required for hydrogen or electron donation. Tea catechins and theaflavins have higher $E°'$values (Table 5), compared to α-tocopherol (vitamin E) and ascorbate (vitamin C) which is a superior hydrogen donor to tea polyphenol [149, 150].

Table 5 *E°'* value of tea catechin, TP and other physiological antioxidants

Antioxidant	**Reduction potential* (*mV*)**
Ascorbate	280
α-tocopherol	480
Uric acid 590	590
Glutathione (Cysteine)	920
(-)-Epigallocatechin gallate	430
(-)-Epigallocatechin	430
(-)-Epicatechin	570
(-)-Epicatechin gallate	550
Theaflavin	510
Theaflavin digallate	540

*standard reduction potential at pH 7.0, 20℃

When referred to the inhibition of pro-oxidant enzymes, green tea catechin can limit the activity of xanthine oxidase in vitro [151] and similar results demonstrated the inhibition effects of EGCG from green tea and theaflavin from black tea in cultured human leukemia cells [152]. In addition, numerous animal models were developed to analyze the antioxidant activities of tea and tea polyphenols. Green tea extract, provided to male rats in their drinking water, prevented decreases in liver glutathione (GSH) concentrations induced by ethanol administration [153]. Oral administration of green tea extract to mice infected with *M. tuberculosis* attenuated inhibits erythrocyte superoxide dismutase (SOD) activity [154], on the other hand, oral administration of black or green tea extract increased serum SOD activity in mice exposed to the carcinogen, 3-methylcolanthrene [155]. Feeding green tea polyphenols dose-dependently decrease the concentration of TBARS (thiobarbituric acid-reacting substances) in LDL from cholesterol-fed rats after 4h of copper-mediated oxidation [156]. Feeding red wine, quercetin or catechin in their drinking water to ApoE-deficient mice can decrease the Basal levels of lipid hydroper-oxides (LOOH) by measuring iodometrically in LDL [157]. Tea polyphenol can also act as a biomarker of oxidative damage to proteins and this damage may result in chemical modifications of amino acids, aggregation or cross linking of proteins or protein fragmentation. Providing old rats (up to 22 age of mouse) with

green tea extract in their drinking water can decrease aortic collagen-linked Maillard-type fluorescence, a marker for advanced glycation endproducts [158]. The most commonly analyzed oxidated DNA base in animal models of tea administration is 8-OHdG (8-hydroxy 2'-deoxyguanosine). Topical EGCG prevented the epidermal formation of the oxidized DNA bases, 5-hydroxymethyl-2-deoxyuridine and 8-OHdG and thymidine glycol in mice induced by phorbol ester-type tumor promoters [159]. Providing green tea or EGCG to mice in their drinking can not only decrease lung adenomas, but also significantly inhibit increases in lung DNA level of 8-OHdG induced by tobacco carcinogen, 4-(methylnitrosamino)-1-(3-pyridyl)-1-butanone [160].

4.3 Anticancer activities

Cancer, known medically as a malignant neoplasm, is a broad group of diseases involving unregulated cell growth. The cancer cells divide and grow uncontrollably result in forming malignant tumors and invading nearby parts of the body. There are over 200 different known cancers that affect humans. Various factors like environmental, chemical, physical, metabolic, and genetic factors can directly or indirectly induce cancers. Strong and consistent epidemiology evidence indicates a diet with high consumption fruits and vegetables, rich in antioxidants agents, can reduce the risk of many cancers and decrease cancer incidence and mortality [161]. As a result, in recent years, experimental cancer researchers focus on the identification and development of these compounds, among which polyphenols, as one of the most numerous and ubiquitous group of plant metabolites, are an integral part of the human diet due to their safety and low toxicity [162]. In addition to their primary antioxidant capacity, phenolic compounds display a wide variety of biological activities related to the anticarcinogenic and anticancer potential.

4.3.1 Anticancer effects of phenolics in vitro

Phenolic extracted or isolated from different plants have been investigated with in vitro models in a number of cancer cell lines representing different evolutionary stages of cancer. For example, berry extracts isolated from blackberry, raspberry, blueberry, cranberry,

strawberry and the phenolic compounds isolated from strawberry including anthocyanins, quercetin, kaempferol, esters of coumaric acid and ellagic acid, showed a significant inhibition of the growth of human oral (KB, CAL-27), breast (MCF-7), colon (HT-29, HCT-116), and prostate (LNCaP, DU-145) tumor cell lines in a dose-dependent manner with different sensitivity between cell lines [163, 164]. The antiprolierative activity of ethanol extracts from 10 edible berries on HL-60 human leukemia cells and HCT-116 cells is compared by Katsube et al [165], and the bilberry showed the highest activity. Extracts and phenolic compounds isolated from wine, such as resveratrol, quercetin, catechin, and epicatechin [166, 167], as well as green tea polyphenols (epicatechin, epigallocatechin, epicatechin-3-gallate) [168-170], also display notable antiprolierative activity in different cancer cell line systems. In addition, although a number of polyphenols such as flavones (apigenin, baicalein, luteolin and rutin), flavanones (hesperidin and naringin) and sesame lignans (sesaminol, sesamin, and episesamin), are not widely studied previously, they had growth inhibitory effects in different cancer cell lines like colon [117], prostate [172, 173], breast [174], stomach, liver [175], cervix, leukemia [176] and pancreas.

4.3.2 Anticancer effects of phenolics in vivo

Additionally, a number of in vivo animal experiments have been performed to study the antitumor effectiveness of plant-derived phenolic extracts or phenolic compounds on tumor incidence and multiplicity [177-180]. The animals were induced to have tumor by chemical, genetically or ultraviolet light methods as well as xenograft methods in colon, breast, lung, liver, stomach, prostate, esophagus, pancreas mammary gland, small intestine and skin. For instance, Ding et al. [181] investigated the major anthocyanin (cyanidin-3-glucoside (C3G)), from blackberry for its potential ability to inhibit 7, 12-dimethylbenz[a]anthracene (DMBA)-12-O-tetradecanolyphorbol-13-acetate (TPA)-induced skin papillomas in animal skin model. After 20 weeks of TPA promotion, the inhibition of papillomagenesis by C3G was observed. 22 weeks later, four tumors greater than 4-5 mm in diameter in the TPA-treated group were observed, whereas no large tumors were found in the C3G plus TPA-treated group. Martin et al. [182] summarized the contribution of cocoa and phenolic components from cocoa to prevention of cancer through different models of carcinogenesis (Table 6).

Table 6 summary of cancer prevention effect of cocoa and cocoa flavonoids in animal models [182]

Cancer type	Model (carcinogen)	Intervention dose	Duration[a]	Main outcomes[b]
Mammary Pancreatic	Female Sprague–Dawley rats (PhIP)	Procianidims of cocoa liquor (0.025% or 0.25%)	48w (d) or (p)	↓ Incidence and multiplicity of pancreatic lesions
Lung Thyroid	Male F344 (DMBDD)	Procianidims of cocoa liquor (0.025% or 0.25%)	36w (p)	↓ Incidence and multiplicity of carcinomas in lung and thyroid
Prostate	Male Wistar-Unilever rats (MNU + TP)	Cocoa rich-polyphenolic extract (24 or 48 mg/kg body weight)	36w (b–d–p)	↓ Incidence of prostate tumours at 24 mg/kg body weight.
Leukaemia	Brown Norway rat (leukaemia cells)	(−)-Epicatechin (40 mg/kg body weight)	3w (p)	↑ Necrosis of leukaemia bone marrow cells
Hepatic	Male Wistar rats (DEN)	Cocoa rich-diet (16%)	6w (b–d–p) or (p)	↓ Post-necrotic proliferation and reduced initiated cells.
Colon	Female C57BL/6J-Min/1 mouse	(+)-Catechin (0.1% or 1%)	10w	↓ Intestinal tumour number
Colon	Male Wistar (AOM)	Cocoa-rich diet (12%)	8 w (b–d–p)	↓ pre-neoplastic lesions (aberrant crypt foci)

[a] w, weeks; dietary intervention before (b), during (d), post (p) carcinogen treatment.
[b] The arrow indicate an increase (↑) or decrease (↓).

4.3.3 Anticancer activity of grape polyphenols

Numerous evidences have proved that the extracts from grapes and its products had great anticancer activity. Hudson et al. [183] reported that the extract from grape skins could lead to apoptosis of prostate tumor cell lines with a high rate. The extracts from grape pomace after winemaking industry inhibited activities of matrix metalloproteinases-2 and -9, and showed a significant antiproliferative effect on human colon adenocarcinoma cells (Caco-2) [184, 185]. In the study of Bagchi et al. [186], the grape seed procyanidin extract (GSPE) showed greater protection against lipid oxidation and DNA damage than vitamin C and E. GSPE also displayed protection against skin cancer by inhibiting UV-radiation-induced oxidative stress and activation of mitogen-activated protein kinase and NF-κB signaling in human epidermal keratinocytes [1187, 188]. An in vitro study [189] demonstrated that GSPE inhibited pancreatic carcinoma cells MIA PaCa-2 and BxPC-3 proliferation in a dose-dependent manner and induced G1-phase arrest of the cell cycle in BxPC-3 or mitochondria- mediated apoptosis in MIA PaCa-2. GSPE also induced apoptosis of non-small cell lung cancer (NSCLC) cells, A549 and H1299 in vitro [190]. Recent findings suggest that grape seed extracts (GSE) may be an effective alternative and complementary medicine against colorectal cancer due to its strong growth inhibitory and apoptosis-inducing effects. For example, Kaur et al [191] found that GSE could strongly inhibit the growth of LoVo, HT29 and SW480 cells as well as the apoptosis in all three cell lines. Moreover, phenolics

from grape juice significantly inhibited carcinogen-induced DNA adduct formation in rat model [192], and limited DNA synthesis in breast cancer cells [193].

4.3.4 Anticancer activity of tea polyphenol

The cancer-preventive effect of tea and its main constituents has been demonstrated in epidemiological, cell culture, animal and clinical studies in the recent decade. Numerous mechanisms have been proposed to account for the cancer preventive effects of green tea and EGCG in laboratory animal models, including the inhibition of growth factor signaling, inhibition of key cellular enzymes, inhibition of gene transcription, as well as induction of tumor suppressor genes [194].

In vitro cell culture studies show that tea polyphenols potently induce apoptotic cell death and cell cycle arrest in tumor cells but not in their normal cell counterparts [19532]. In one experiment, SKH-1 mice were exposed to UVB light twice a week for 22 weeks and fed with green tea (6 mg solid/mL) for another 23 weeks by oral administration. It was found that green tea could decrease the incidence of skin tumor formation compared to the control group (water-fed) [196]. It was reported [197] that the incidence of hepatocellular tumors was 73.3% if mice were chemically induced by pentachlorophenol (PCP, 600 ppm) after treatment with the initiator diethylnitrosamine (DEN). The incidence of hepatocellular tumors could be decreased to 33.3% if the mice were given green tea infusion before the chemical treatment and during the treatment period. A study of the inhibitory effect of green tea on lung cancer demonstrated that mice given 1 % green tea infusion exhibited a significantly lower lung tumor multiplicity from 0.72/mouse to 0.41/mouse [198].

Among all the compounds of tea polyphenol, EGCG (epigallocatechin-3-gallate) is the most abundant one in tea and one of the most well studied polyphenolics in relation to HCC (hepatocellular carcinoma), which is one of the most frequent tumors representing the fifth commonest malignancy worldwide and the third cause of mortality from cancer [199]. Evidences from in vitro studies showed that EGCG could inhibit the growth of different human hepatoma cell lines, such as HepG2, HuH-7, Hep3B and HLE [200, 201]. Also, in

vivo study reported that EGCG could enhance the activity of the anticancer drug doxorubicin in a murine model for chemo-resistant HCC by inhibiting the P-glyco-protein (P-gp) efflux pump activity and reducing the expression of multidrug resistance (MDR)1 protein [202].

4.4 Antimicrobial effects

In addition to antioxidant activities, lots of plant-derived phenolic extracts have been demonstrated potential antibacterial, antifungal and antiviral activities. Some studies showed that phenolic extracts have inhibitory effects against specific strains of bacteria such as *Streptococcus Mutans*, *Staphylococcus aureus*, *Escherichia coli* and *Candida albicans* [203]. Various bacterial species exhibit different sensitivities to polyphenols. For example, *Staphylococcus aureus* have the highest sensitivities towards grape wine extracts, followed by *Escherichia coli* and the lowest sensitivities was detected in *Candida albicans* [204]. The time of reaction also affect the antibacterial activities of phenolic compounds. Karapinar et al. [205] demonstrated that a kind of grape juice immediately acted against *Salmonella typhimurium* at the concentration of 1-3.5 log cfu/g while in study of Baydar et al. [206], it took the grape seed extracts 48 hours to show the inhibition against *Staphylococcus aureus*. The phenolic compounds from different parts of grape showed different antimicrobial activities. The increasing order of the antimicrobial activity was flesh, whole fruit grape extracts, fermented pomace, skin, leave and seed [38]. Study indicated that the minimum inhibition concentration (MICs) of grape seed was 0.26 mg/L (gallic acid as the equivalent), while that of grape stem extract was 0.34 mg/L [207]. Brown et al. [208] verified that the grape skin exhibited the strongest inhibition against *Helicobacter pylori*, compared to grape synergy (skin and seed) and seed. Some researchers revealed the structure-activity relationship between polyphenol and its antimicrobial effects. Results indicated that the number of hydroxyl group and the degree of polymerization may influence the antimicrobial activities of phenolics [209. In addition, Rhodes et al. [210] found that the red pigmented polymeric phenolics from grape juice or skin showed pH-dependent antilisterial activity, while the antilisterial activity of unpigmented phenolics such as that from grape seed was independent of pH.

Polyphenols isolated from green tea also exhibited great antimicrobial effects such as

Gram-positive and Gram-negative bacteria [211]. Among the catechins from green tea extracts, EGCG and ECG are the most potent in exhibiting antimicrobial activity due to the galloyl moiety present in their structures [212]. It is reported that EGCG possessed antibacterial effects on various strains of *Staphylococcus* (Gram positive cocci) and Gram negative rods such as *E. coli*, *Klebsiella pneumonia* and *Salmonella* and the concentration required for inhibiting the growth of *Staphylococcus* was 50-100 μg/mL, while for Gram-negative rods the concentration should be higher than 800μg/mL [213]. In vivo and in vitro experiments showed that a green tea extract inhibited caries formation in hamsters and increased the resistance of human enamel to acid [214]. Friedman et al. [215] evaluated the antibacterial effects on *Ba. Cereus* (a widely distributed foodborne pathogen that causes vomiting and diarrhea in mammals) of seven green tea catechins and four black tea theaflavins as well as infusions of 36 commercial green, black, oolong, white, and herbal teas. Results demonstrated that GCG, EGCG, CG, ECG, TF339 G, TF39G, as well as TF3G displayed antimicrobial activities at nanomolar levels and some of them had higher activities than medicinal antibiotics such as tetracycline or vancomycin. They also indicated that the bactericidal activities of tea could be roughly attributed to the levels of catechin and theaflavins.

4.5 Anti-inflammation activities

Inflammation is defined as part of the complex biological response of vascular tissues to harmful stimuli, such as pathogens, damaged cells, or irritants [216]. Due to the antibacterial, antioxidant properties of polyphenol, the phenolic compounds showed great potential in anti-inlfammation filed. Significant anti-inflammation effects of phenolics from grapes especially grape seeds have been exhibited on rats, mice and human, mainly attributed to molecules like flavonols, flavanols and procyanidins [38]. In the study of Bralley et al. [217], extracts from grape skins and seeds inhibited mouse ear inflammation, edema and polymorphonuclear leukocyte infiltration induced by 12-O-tetradecanoylphorbol 13-acetate. For grape phenolics, immunomodulation and antioxidative action are the two main pathways for the anti-inflammation effect. Panico et al. [218] proved the mechanism of anti-inflammation of procyanidins might be that they inhibited the release of proinflammation factors through human chondrocytes assays. Mejia et al. [219] summarized the anti-inflammation activities of tea and its bioactive components such as EGCG,

EGC, ECG, theaflavin, as well as tea extracts from green and green tea, in vitro and in animal models. Cytokines, such as tumor necrosis factor-α (TNF-α), IL-6, IL-1, GM-CSF, interferon-γ (IFN-γ), and IL-12, are a group of multifunctional proteins involved in several steps related to inflammatory responses. Almost all cell types, when exposed to TNF, can activate NF-κB (nuclear factor kappa B) leading to the expression of inflammatory genes such as cyclooxy-genase-2 (COX-2), lipoxygenase-2 (LOX-2), cell-adhesion molecules, inflammatory cytokines, chemokines, and inducible nitric oxide synthase (iNOS) [220]. Some investigation indicated that tea polyphenols could modulate at different targets (in this case, the targets are NOS and NF-κB) of the anti-inflammation effects related to arachidonic acid-dependent pathways such as COX inhibition [221].

4.6 Cardioprotection action

Epidemiological studies suggest that consumption of grape products, wine, green tea and other foods rich in polyphenols is associated with decreased risk of cardiovascular disease, which is induced by modifications in fatty acid metabolism and excessive lipid peroxidation of LDL. Moreover, these oxidation products also cause the formation of thromboxane with the process of platelet aggregation, then the artery blockage and finally thrombosis [222]. Grape seed procyanidins had significant effectiveness in laser-induced thrombus formation in the carotid artery of mice through intravenous and oral administration [223]. Grape seeds extracts were found to exhibit higher inhibition in platelet adhesion, aggregation and generation of superoxide anion than pure resvertrol [224]. Dohadwala et al. [225] indicated that the mechanisms of grape polyphenol in reducing atherosclerosis included inhibition of oxidation of LDL, platelet aggregation and other favorable effects on cellular redox state, improvement in endothelial function, lowering blood pressure, anti-inflammation and activating novel proteins that prevent cell senescence. As for tea, Wolfram [226] found that the regular daily consumption of 5-6 or more cups of green tea, containing 200-300 mg of EGCG, had beneficial effects on cardiovascular and metabolic health. Recent research indicated that tea consumption improves endothelium-dependent vasodilation and that flava-3-ols increase nitric oxide (NO) generation and therefore could prevent cardiovascular disease (CVD).

4.7 Other biological properties

In addition to the biological properties above, numerous evidences referred to the health benefits of phenolic compounds, such as anti-aging activity, improvement of immunity, weight management. For example, it is reported a synergistic interaction between caffeine and catechin polyphenols from green tea extract appears to prolong sympathetic stimulation of thermogenesis and therefore processes the weight management [227, 228]. Some researchers investigated the potential positive effect of L-theanine on immunity and found that the supplementation of capsules containing L-theaine and flavan-3-ols from tea can decrease the incidence of cold and flu [229].

5 Bioavailability of polyphenols

It is important and necessary to know the bioavailability of polyphenol, since their nutritional significance and potential systemic effects will greatly rely on their behavior in the digestive tract. The absorption and metabolism of food polyphenols primarily depend on their chemical structure, which may be influenced by the factors such as the degree of glycosylation/acylation or polymerization, the basic structure (for example, benzene or flavones derivatives), conjunction with other phenolic compounds, molecule size and solubility [230]. Several researches showed that phenolics such as procyanidins, quercetin and flavanols were rapidly absorbed from grapes to plasma, with plasma concentration peaking at two or three hours later after ingestion [231, 232]. In order to detect digestion of polyphenol, some researchers employed the method to test the increase of lipid-bound polyphenols in serum as well as the decrease of lipid peroxidation in serum due to the antioxidant activity of polyphenol. It is found that after daily red wine consumption for two weeks, plasma levels of total phenolic concentration increased significantly and trace levels of metabolites were detected [233]. Ten healthy human subjects consumed 500 mL of Choladi green tea (containing 648 mumol of flavan-3-ols) after which plasma and urine were collected over a 24 h period and analysed by HPLC-MS. Plasma contained a total of ten metabolites, in the form of O-methylated, sulphated and glucuronide conjugates of (epi)catechin and (epi)gallocatechin, with 29-126 nM peak plasma concentrations (C(max)) occurring 1.6-2.3 h after ingestion, indicative of absorption in the small intestine [234]. In some cases,

supplementations or additions can enhance the availability of polyphenol by improving the solubility. For example, addition of vitamin C and sucrose may improve bioaccessibility of catechin in stimulated human digestive condition and accumulation of catechin by human intestinal cells [235].

6 The stability of polyphenol

Since polyphenols possess significant biological activities, great benefits for human health as well as potential applications such as food or medicine industry, the stability of phenolics plays an important role and should be taken into consideration. For example, in certain processing operations involving crystalline drugs, such as milling, lyophilization, spray drying, and wet granulation, the thermodynamical and chemical stability nature of the polyphenol should be understood well before the process. Experimental evidences demonstrated that several factors may influence the stability of polyphenol such as heat, pH and irradiation. Generally speaking, anthocyanins are highly susceptible to degradation during processing and storage of food products. The rate and extent of degradation depend on extrinsic factors such as processing and storage temperature, availability of oxygen, light etc. and the intrinsic properties of the product such as pH, the structure of the anthocyanins, the presence of metallic ions and oxidative enzymes [236]. It is reported that in food processing such as juice making, nut roasting and raw material drying, both polyphenol content and antioxidant activity decrease during the thermal processing and long-term storage [237, 236]. Li et al [239] found that the degradation of EGCG was concentration-dependent. After heating for 35 min, EGCG was more stable in solution with higher concentration (in this case, it is 5 mg/mL) than solutions with lower concentration. Biesaga et al. [240] investigated the influence of irradiation on stability of phenolic compound from honey, such as quercetin, kaempferol, luteolin, rhamnetin and myricet, and found that all compounds degraded during the extraction procedure with irradiation (ultrasonic and microwave). Research about the effect of pH on Galla chinensis extract's (GCE) stability indicated that GCE solution was not stable at neutral and alkaline conditions and its anti-caries activity could be strong at about pH 5.5 [241]. In addition, pH may affect the biological properties of polyphenol. For instance, according to literature, the radical scavenger activity of polyphenols is strongly pH-dependent with higher pH values which significantly increase the capacity, and this increase

has been attributed to the deprotonation of the hydroxyl moieties present on the aromatic rings of the phenolic compounds [242].

7 Safety and toxicity of polyphenol

Table 7 Summary of doses which were required for systemic toxicity in single in vivo studies [247]

Flavonoid or other dietary phenolic	Systemic toxicity dose
Isoflavone	
Genistein	140 mg/kg (mice) (no effect)
Daidzein	250 mg/kg (rats) (no effect)
Phenoxodiol	
Other flavonoid	
Flavonoids of *Vitex negundo*	15 mg/day (rats) (male reproductive toxicity)
Naringenin	10 mg/l (amphibian) (teratogenic)
EGCG	100 mg/kg i.p. (mice) (hepatotoxicity)
Other phenolic	
Pyrogallol	100 mg/kg i.p. (rats) (hepatotoxicity)
Propyl gallate	5 g/kg oral (rats) (hepatotoxicity)
Tannic acid	10 mg/kg i.p. (fish, carp); 120 mg/kg i.p. (mice) (hepatotoxicity)

Even though plants rich in polyphenols are generally regarded as safe based on their long history of dietary usage, the potential toxicity and safety of polyphenol were investigated if for example, highly purified and standardized phenolic compounds are involved in drug development due to their great benefits in anti-cancer or antioxidant. Numerous human intervention studies proved that daily consumption of tea polyphenols with relatively high dose (600-1800 mg/day) showed no adverse reactions [243-245]. However, an increasing number of cases exhibited that hepatoxicity in humans was related to intake of green tea dietary supplements. Some reports demonstrated that green tea supplements with the dose range from 700 to 2100 mg/day may clinically present elevated serum transaminase and bilirubin levels, abdominal pain and occasionally jaundice [246]. Galati et al. [247] reviewed the potential toxicity of flavonoids and isoflavones and indicated that potential safety issues exist if megadoses (Table 7) of these phenolics were consumed daily. Phenol ring-containing flavonoids, if oxidized by peroxidases, generate phenoxyl radicals which are cytotoxic as well as co-oxidize unsaturated lipids, GSH,

NADH, ascorbate, and nucleic acids, and cause ROS formation and mitochondrial toxicity.

8 Potential applications of polyphenols

A number of natural products found in plant extracts possess a wide range of applications in food, textile, pharmaceutical and cosmetic and so on, due to their excellent biological capacity like antioxidant, antiaging, anticancer and antimicrobial activities etc.

Green tea extracts have been employed in various food applications such as bread, extra virgin olive oil, meat, sausages, fish and biscuits [248]. Tea catechins showed higher antioxidant activities against lipid oxidation of cooked patties, compared to ginseng, mustard, rosemary, sage, butylated hydroxyanisole (BHA), butylated hydroxyl toluene (BHT), and vitamins C and E [249]. The inhibition of lipid oxidation in meats such as red meat, poultry and fish, was dose dependent. Addition of tea catechin (200-400 mg/kg) has significant inhibitory effects on lipid oxidation displayed in red meat and poultry patties [250]. Tea extracts also have the ability to inhibit the human salivary amylase and thus consuming tea could reduce cariogenic potential of starch rich foods such as crackers and cakes [251]. It is found that the antimicrobial activity of tea remains functional even at high temperatures (100 ℃/60 min) or at pasteurization temperatures (121 ℃/15 min) [252]. Moreover, green tea extract have shown inhibitory effects on bacteria causing dental caries *Streptococcus mutans* with a minimum inhibitory concentration of 250 μg/mL [253].

Significant effort has been made over past decade to explore the potential of using GP to produce function al food ingredients, such as natural antioxidants for nutrition fortification and food preservation, health promoting grape seed oil and dietary fiber [222]. Grape phenols have been reported to use in the baked food products such as bread to increase the antioxidant activity of the bread and inhibit lipid oxidation of raw and cooked chicken [254]. Grape seed extract (GSE) at 0.1% (w/w) is an effective radical scavenger in muscle tissues and shown to reduce the secondary oxidation products (TBARS and head space hexanal) in beef, chicken, and turkey during refrigerated storage [255, 256]. GSE can also be used in preventing periodontal diseases by exhibiting bacteriostatic effect on the oral anaerobes (Fusobacterium nucleatum and

Porphyromonas gingivalis) at a concentration of 2000 μg/mL [257].

References

[1] Weisshaar B, Jenkins GI. Phenylpropanoid biosynthesis and its regulation. Curr. Opin. Plant Biol 1998; 1: 251-257

[2] Winkel-Shirley B. Biosynthesis of flavonoids and effects of stress. Curr Opin Plant Biol 2002; 5: 218-223

[3] Bengoechea ML, Sancho AI, B. Bartolome B, et al. Phenolic composition of industrially manufactured purees and concentrates from peach and apple fruits J. Agric. Food Chem 1997; 45: 4071-4075

[4] Wink M. Compartmentation of secondary metabolites and xenbiotics in plant vacuoles. Adv Bot Res 1997; 25: 141-169

[5] Wallace G, Fry S. Phenolic components of the plant cell wall. Int Rev Cytol 1994; 151: 229-267

[6] Musel G, Schindler T, Bergfeld R, et al. Structure and distribution of lignin in primary and secondary cell walls of maize coleoptiles analyzed by chemical and immunological probes. Planta 1997; 201: 146-159

[7] Baucher M, Monties B, Van Montagu M, et al. Biosynthesis and genetic engineering of lignin. Crit Rev Plant Sci 1998; 17: 125-197

[8] Scalbert JA. Polyphenolic Phenomena, INRA edition: Paris, France, 1993; pp: 222-235

[9] Brett CT, Wende G, Smith AC, et al. Biosynthesis of cell-wall ferulate and diferulates. J Sci Food Agric 1999; 79 (3): 421-424

[10] Ishii T. Structure and functions of feruloylated polysaccharides. Plant Sci 1997; 127 (2): 111-127

[11] Renger A, Steinhart H. Ferulic acid dehydrodimers as structural elements in cereal dietary fibre. Eur Food Res Technol 2000; 211: 422-428

[12] Waldron KW, Ng A, Parker ML, et al. Ferulic Acid Dehydrodimers in the Cell Walls of Beta vulgaris and their Possible Role in Texture. J Sci Food Agric 1997; 74 (2): 221-228

[13] Wende G, Waldron KW, Smith AC, et al. Developmental changes in cell-wall ferulate and dehydroferulate in sugar beet. Phytochemistry 1999; 52: 819-827

[14] Van Driel-Murray C. In Ancient Egyptian Materials and Technology (Eds.: Nicholson PT, Shaw I), Cambridge University Press: Cambridge, 2000; pp: 299-319

[15] White T. In The Chemistry of Vegetable Tannins-A Symposium, Society of Leather Trades Chemists press: Croydon, 1956; pp: 7-29

[16] White T. Tannins-their occurrence and significance. J Sci Food Agric 1957; 8 (7): 377-385

[17] Williams AH. The simpler phenolic substances of plants. J Sci Food Agric 1957; 8: 385-389

[18] Swain T, Bate-Smith EC. In Comparative Biochemistry (Eds.: Mason HS, Florkin AM), Academic Press: New York, 1962; pp: 755-809

[19] Haslam E, Cai Y. Plant polyphenols (vegetable tannins): gallic acid metabolism. Nat Prod Rep 1994; 11: 41-66

[20] Shahidi F, Naczk, M. Phenolics. In: Food and Nutraceuticals. CRC Press LLC: Boca Raton, FL, 2004; pp: 443-482

[21] Harborne JB. The flavonoids: advances in research since 1986. Chapman and Hall press: London, 1993; pp: 27

[22] Harborne JB. Methods in plant biochemistry, I: plant phenolics. Academic Press: London, 1989; pp: 1-28

[23] Naczk M, Shahidi F. Extraction and analysis of phenolics in food. J chromatogr A 2004; 1054: 95-111

[24] Spencer JPE, Mohsen AE, Minihane MM, et al. Biomarkers of the intake of dietary polyphenols: strengths, limitations and application in nutrition research. Br J Nutr 2008; 99: 12-22

[25] Vermerris W, Nicholson R. Phenolic Compound Biochemistry. West Lafayette IN: Springer, 2006; pp: 1-34

[26] Jung HG. Forage lignins and their effects on fiber digestibility. Agron J 1989; 81: 33-8

[27] Wallace G, Chesson A, Lomax JA, et al. Lignin-carbohydrate complexes in graminaceous cell walls in relation. Anim Feed Sci Tech 1991; 32:193-199

[28] Harborne JB, Mabry TJ. The flavonoids: advances in research. Chapman and Hall press: London, 1982

[29] Wursch P, del Vedovo S, Rosset J, et al. The tannin granules from ripe carob pod. Lebens Wiss Techno1 1984; 17: 351-354

[30] Porter LW. Tannins. In: Methods in plant biochemistry, I: plant phenolics (Ed.: Harborne JB), Academic Press: London, 1989; pp: 389-419

[31] Fernandes MI, Pedro JR, Seoane E. Two polyhydroxystilbenes from stems of phoenix dactylifera. Phytochemistry 1983; 22: 2819-2821

[32] Zhang X, Ferraris S, Prenesti E, et al. Surface functionalization of bioactive glasses with natural molecules of biological significance, part II: Grafting of polyphenols extracted from grape skin. Appl Surf Sci 2013; 287: 341-348

[33] Poudel PR, Tamura H, Kataoka I, et al. Phenolic compounds and antioxidant activities of skins and seeds of five wild grapes and two hybrids native to Japan. J Food Compos Anal 2008; 21: 622-625

[34] Rodriguez MR, Romero Peces R, Chacon Vozmediano JL, et al. Phenolic compounds in skins and seeds of ten grape *Vitis vinifera* varieties grown in a warm climate. J Food Compos Anal 2006; 19: 687-693

[35] Pastrana-Bonilla E, Akoh CC, Sellappan S, et al. Phenolic content and antioxidant capacity of muscadine grapes. J Agric Food Chem 2003; 51: 5497-5503

[36] Hernandez-Jimenez A, Gomez-Plaza E, Martinez-Cutillas A, et al. Grape skin and seed proanthocyanidins from Monastrell × Syrah grapes. J Agric Food Chem 2009; 57: 10798-10803

[37] Bruno G, Sparapano L. Effects of three esca-associated fungi on Vitis vinifera L.: V. Changes in the chemical and biological profile of xylem sap from diseased cv. Sangiovese vines. Physiol Mol Plant Pathol 2007; 71: 210-229

[38] Xia E, Deng G, Guo Y, et al. Biological activities of polyphenols from grapes. Inter J Mol Sci 2010; 11: 622-646

[39] Gómez-Plaza E, Miñano A, López-Roca JM. Comparison of chromatic properties, stability and antioxidant capacity of anthocyanin-based aqueous extracts from grape pomace obtained from different vinification methods. Food Chem 2006; 97: 87-94

[40] Castillo-Muñoz N, Gómez-Alonso S, García-Romero E, et al. Flavonol profiles of Vitis vinifera white grape cultivars. J Food Compos Anal 2010; 23:699-705

[41] Kennedy JA, Matthews MA, Waterhouse AL. Changes in grape seed polyphenols during fruit ripening. Phytochemistry 2000; 55: 77-85

[42] Shi J, Yu J, Pohorly JE, et al. Polyphenolics in grape seeds-biochemistry and functionality. J Med Food 2003a; 6: 291-299

[43] Obreque-Slier E, López-Solís R, Castro-Ulloa L, et al. Phenolic composition and physicochemical parameters of Carménère, Cabernet Sauvignon, Merlot and Cabernet Franc grape seeds (Vitis vinifera L.) during ripening. LWT-Food Sci Tech 2012; 48: 134-141

[44] Obreque-Slier E, Peña-Neira Á, López-Solís R, et al. Phenolic composition of skins from four Carmenet grape varieties (Vitis vinifera L.) during ripening. LWT-Food Sci Tech 2013; 54: 404-413

[45] Yu J, Smith I, Melton B, et al. Stability of different classes of polyphenols in grape pomace as affected by drying method. 2011 IFT Annual Meeting, June 11-14, 2011, New Orleans, LA, USA.

[46] Cooper R, Morre DJ, Morre DM. Medicinal benefits of green tea: Part I. Review of noncancer health benefits. J Altern Complement Med 2005; 11(3): 521-528

[47] Matthews CM. Steep your genes in health: Drink tea. Proceedings (Baylor University Medical Centre) 2010; 23(2): 142-144

[48] Forrest D. The World Trade: A Survey of the Production, Distribution and Consumption of Tea. Woodhead -Faulkner: Cambridge, U.K., 1985

[49] Balentine DA. Phenolic Compounds in Food and Their Effects on Health I. Analysis, Occurrence, and Chemistry (Eds.: Ho CT, Lee CY, Huang MT), American Chemical Society: Washington, DC, 1998; pp: 35-72

[50] Lin YS, Tsai YJ, Tsay JS, et al. Factors affecting the levels of tea polyphenols and caffeine in tea leaves. J Agric Food Chem 2003; 51: 1864-1873

[51] Karori SM, Wachira FN, Wanyoko JK, et al. Antioxidant capacity of different types of tea products. Afr J Biotechnol 2007; 6(19): 2287-2296

[52] Wang R, Zhou W. Stability of tea catechins in the breadmaking process. J Agric Food Chem 2004; 52: 8224-8229

[53] Naidu AS. In Catechins in Natural food antimicrobial systems (Eds.: Juneja LR, Okubo T, Hung P), CRC press LLC: Florida, 2000; pp: 382

[54] Auger C, Al-Awwadi N, Bornet A, et al. Catechins and procyanidins in Mediterranean diets. Food Res Inter 2004; 37: 233-245

[55] Amidor T. Wholesome green tea. Food product design Available from. http://www.foodproductdesign.com/articles/2009/07/wholesome-green-tea.aspx (Acessed on September 21, 2010)

[56] Kajiya K, Hojo H, Suzuki M, et al. Relationship between Antibacterial Activity of (+)-Catechin Derivatives and Their Interaction with a Model Membrane. J Agric Food Chem 2004; 52(6): 1514-1519

[57] Stewart JA, Mullen W, Crozier A. On-line high performance liquid chromatography of the antioxidant of phenolic in green and black tea. Mol Nutr Food Res 2004; 49: 52 -60

[58] Lin JK, Lin CL, Liang YC, et al. Survey of catechins, gallic acid, and methylxanthines in green, oolong, pu'erh, and black teas. J Agric Food Chem 1998; 46: 3635-3642

[59] Lin YL, Lin JK. (-)-Epigallocatechin-3-gallate blocks the induction of nitric oxide synthase by down-regulating lipopolysaccharide-induced activity of transcription factor nuclear factor-kappa B. Mol Pharmacol 1997; 52: 465-472

[60] Naasani I, Seimiya H, Tsuruo T. Telomerase inhibition, telomere shortening, and senescence of cancer cells by tea catechins. Biochem Biophys Res Commun 1998; 249: 391-396

[61] Okabe S, Ochiai Y, Aida M, et al. Mechanistic aspects of green tea as a cancer preventive: effect of components on human stomach cancer cell lines. Jpn J Cancer Res 1999; 90:733-739

[62] Nam S, Smith DM, Dou QP. Ester bond-containing tea polyphenols potently inhibit proteasome activity in vitro and in vivo. J Biol Chem 2001; 276: 13322-13330

[63] Clifford MN, Stoupi S, Kuhnert N. Profiling and characterization by LC-MS of the galloyl quinic acids of green tea, tara tannin, and tannic acid. J Agric Food Chem 2007; 55: 2797-2807

[64] Sanderson GW, Ranadive AS, Eisenberg LS, et al. In Contribution of polyphenolic compounds to the taste of tea In Phenolic, Sulfur, and Nitrogen Compounds in Food Flavors, ACS Symposium Series 26 (Eds.: Charalambous G, Katz I), American Chemical Society: Washington, DC, 1976; pp: 14-46

[65] Takino Y, Ferretti A, Flanagan V, et al. The structure of theaflavin, a polyphen ol of black tea. Tetr ahedron Lett 1965; 4019-4025

[66] Meyer AS, Yi OS, Pearson DA, et al. Inhibition of human low-density lipoprotein oxidation in relation to composition of phenolic antioxidants in g rapes (Vitis vinifera). J Agric Food Chem 1997; 45: 1638-1643

[67] Sato M, Ramarathnam N, Suzuki Y, et al. Varietal differences in the phenolic content and superoxide radical scavenging potential of wines from different sources. J Agric Food Chem 1996; 44: 37-41

[68] Vogels N, Plantenga MSW. The effect of grape-seed extract on 24h energy intake in humans. Eur J Clin Nutr 2004; 58, 667-673

[69] Quideau S, Deffieux D, Douat-Casassus C, et al. Plant Polyphenols: Chemical Properties, Biological Activities, and Synthesis. Angew Chem Int Ed 2011; 5: 586-621

[70] Dangles O, Dufour C. In Recent Advances on Polyphenol Research, Vol. 1 (Eds.: Daayf F, Lattanzio V), Wiley-Black-well: Oxford, 2008, pp: 67-87

[71] Yoshida K, Mori M, Kondo T. Blue flower color development by anthocyanins: from chemical structure to cell physiology. Nat Prod Rep 2009; 26: 884-915

[72] De Freitas V, Mateus N. Chemical transformations of anthocyanins yielding a variety of colours. Environ Chem Lett 2006; 4: 175-183

[73] Scalbert A, Mila I, Expert D, et al. In Plant Polyphenols-2 Chemistry, Biology, Pharmacology, Ecology (Eds.: Gross GG, Hemingway RW, Yoshida T), Kluwer Academic/Plenum Publishers: New York, 1999; pp: 545-554

[74] Lattanzio V, Kroon P, Quideau S, et al. In Recent Advances in Polyphenol Research, Vol. 1 (Eds.: Daayf F, Lattanzio V), Wiley-Blackwell, Oxford, 2008; pp: 1-35

[75] Hättenschwiler S, Vitousek PM. The role of polyphenols in terrestrial ecosystem nutrient cycling. Trends Ecol Evol 2000; 15: 238-243

[76] Mulder P, Korth HG, Pratt DA, et al. Critical re-evaluation of the O-H bond dissociation enthalpy in phenol. J Phys Chem A 2005; 109: 2647-2655

[77] Blanksby SJ, Ellison GB. Bond dissociation energies of organic molecules. Acc Chem Res 2003; 36: 255-263

[78] Wayner DDM, Lusztyk E, Pagé D, et al. Effects of Solcation on the enthaplies of reaction of tert-butoxyl radicals with phenol and on the calculated O-H bond strength in phenol. J Am Chem Soc 1995; 117: 8737-8744

[79] Neudörffer A, Desvergne JP, Bonnefont-Rousselot D, et al. Protective effects of 4-hydroxycinnamic ethyl ester derivatives and related dehydrodimers against oxidation of LDL: Radical scavengers or metal chelators? J Agric Food Chem 2006; 54: 1898-1905

[80] Vaya J, Mahmood S, Goldblum A, et al. Inhibition of LDL oxidation by flavonoids in relation to their structure and calculated enthalpy. Phytochemistry 2003; 62: 89-99

[81] Terao J, Piskula M, Yao Q. Protective effect of epicatechin, epicatechin gallate, and quercetin on lipid peroxidation in phospholipid bilayers. Arch Biochem Biophys 1994; 308: 278-284

[82] Masaki H, Atsumi T, Sakurai H. Hamamelitannin as a new potent active oxygen scavenger. Phytochemistry 1994; 37: 337-343

[83] Okuda T, Yoshida T, Hatano T. In Phenolic Compounds in Food and their Effects on Health, ACS Symposium Series 507, Vol. II (Eds.: Huang MT, Ho CT, Lee CY), American Chemical Society: Washington, DC, 1992; pp: 87-97

[84] Li ASH, Bandy B, Tsang SS, et al. DNA-breaking versus DNA-protecting activity of four phenolic compounds in vitro. Free Radical Res 2000; 33: 551-566

[85] Shi X, Ye J, Leonard SS, et al. Antioxidant properties of (-)-epicatechin-3-gallate and its inhibition of Cr(VI)-induced DNA damage and Cr(IV)- or TPA-stimulated NF-kappa B activation. Mol Cell Biochem 2000; 206: 125-132

[86] Asghar A, Gray JI, Buckley DJ, et al. Perspectives on warmed over flavor. Food Tech 1988;

42(6): 102-108

[87] Frankel EN. In search for better methods to evaluate natural antioxidants and oxidative stability in food lipids. Trends Food Sci Tech 1993; 4: 220-225

[88] Huang D, Ou B, Prior RL. The chemistry behind antioxidant capacity assays. J Agric Food Chem 2005; 53: 1841-1856

[89] Orrenius S, Gogvadze V, Zhivotovsky B. Mito-chondrial oxidative stress: Implications for cell death. Annu Rev Pharmacol Toxicol 2007; 47: 143-183

[90] http://freedomwithessentialoils.wordpress.com/2012/06/19/free-radicals-antioxidants-orac-your-health/

[91] Wright JS, Johnson ER, DiLabio GA. Predicting the activity of phenolic antioxidants: theoretical method, analysis of substituent effects, and application to major families of antioxidants. J Am Chem Soc 2001; 123: 1173-1183

[92] Andjelkovic M, Van Camp J, De Meulenaer B, et al. Iron-chelation properties of phenolic acids bearing catechol and galloyl groups. Food Chem 2006; 98: 23-31

[93] Mira L, Fernandez MT, Santos M, et al. Interactions of flavonoids with iron and copper ions: a mechanism for their antioxidant activity. Free Radical Res 2002; 36: 1199-1208

[94] Sugihara N, Ohnishi M, Imamura M, et al. Differences in antioxidative efficiency of catechins in various metal-induced lipid peroxidations in cultured hepatocytes. J Health Sci 2001; 47: 99-106

[95] Pietta PG. Flavonoids as antioxidants. J Nat Prod 2000; 63: 1035-1042

[96] Lopes GKB, Schulman HM, Hermes-Lima M. Polyphenol tannic acid inhibits hydroxyl radical formation from Fenton reaction by complexing ferrous ions. Biochim Biophys Acta 1999; 1472: 142-152

[97] Keyer K, Gort AS, Imlay JA. Superoxide and the production of oxidative DNA damage. J Bacteriol 1995; 177: 6782-6790

[98] Beckman JS, Beckman TW, Chen J, et al. Apparent hydroxyl radical production by peroxynitrite: Implications for endothelial injury from nitric oxide and superoxide. Proc Natl Acad Sci U.S.A. 1990; 87: 1620-1624

[99] Koppenol WH, Moreno JJ, Pryor WA, et al. (1992). Peroxynitrite, a cloaked oxidant formed by nitric oxide and superoxide. Chem Res Toxicol 1992; 5: 834-842

[100] Squadrito GL, Pryor WA. The formation of peroxynitrite in vivo from nitric oxide and superoxide. Chem Biol Interact 1995; 96: 203-206

[101] Gilbert DL, Colton CA. Reactive oxygen species in biological systems. Plenum Publishers: New York, 1999

[102] Imlay JA, Linn S. DNA damage and oxygen radical toxicity. Science 1988; 240: 1302-1309

[103] Henle ES, Han Z, Tang N, et al. Sequence-specific DNA cleavage by Fe^{2+}-mediated Fenton reaction has possible biological implications. J Biol Chem 1999; 274: 962-971

[104] Battin EE, Perron NR, Brumaghim JL. The central role of metal coordination in selenium antioxidant activity. Inorg Chem 2006; 45: 499-501

[105] Flint DH, Tuminello JF, Emptage MH. The inactivation of Fe-S cluster containing hydro-lyases by superoxide. J Biol.Chem 1993; 268: 22369-22376

[106] Haber F, Weiss J. (1932). On the catalysis of hydroperoxide. Naturwiss 1932; 51: 948-950

[107] Koppenol WH. The Haber-Weiss cycle-70 years later. Redox Report 2001; 6: 229-234

[108] Rai P, Cole TD, Wemmer DE, et al. Localization of Fe^{2+} at an RTGR sequence within a DNA duplex explains preferential cleavage by Fe^{2+} and hydrogen peroxide. J Mol Biol 2001; 312: 1089-1101

[109] Rai P, Wemmer DE, Linn S. Preferential binding and structural distortion by Fe^{2+} at RGGG-containing DNA sequences correlates with enhanced oxidative cleavage at such sequences. Nuc Acids Res 2005; 33: 497-510

[110] Lu AL, Li X, Gu Y, et al.ERepair of oxidative DNA damage. Cell Biochem Biophys 2001; 35: 141-170

[111] Kennedy LJ, Moore K, Caulfield JL, et al. Quantitaion of 8-oxoguanine and strand breaks produced by four oxidizing agents. Chem Res Toxicol 1997; 10: 386-392

[112] Aruoma OI, Halliwell B, Gajewski E, et al. Copper-ion-dependent damage to the bases in DNA in the presence of hydrogen peroxide. Biochem J 1991; 273: 601-604

[113] Yamamoto Y, Fukui K, Koujin N, et al. Regulation of the intracellular free iron pool by Dpr provides oxygen tolerance to Streptococcus mutans. J Bacteriol 2004; 186: 5997-6002

[114] Woodmansee AN, Imlay JA. Quantitation of intracellular free iron by electron paramagnetic resonance spectroscopy. Methods Enzymol 2002; 349: 3-9

[115] Ke Y, Qian ZM. Iron misregulation in the brain: a primary cause of neurodegenerative disorders. Lancet Neurol 2003; 2: 246-253.

[116] Selima MH. Ratan RR. The role of iron neuro-toxicity in ischemic stroke. Ageing Res Rev 2004; 3: 345-353

[117] Wood RJ. The iron-heart disease connection: Is it dead or just hiding? Ageing Res Rev 2004; 3: 355-367

[118] Perron NR, Brumaghim JL. A review of the antioxidant mechanisms of pPolyphenol compounds related to iron binding. Cell Biochem Biophys 2009; 53: 75-100

[119] Yoshino M, Murakami K. Interaction of iron with polyphenolic compounds: Application to antioxidant characterization. Anal Biochem 1998; 257: 40-44

[120] Kawabata T, Schepkin V, Haramaki N, et al. Iron coordination by catechol derivative antioxidants. Biochem Pharmacol 1996; 51: 1569-1577

[121] Morel I, Lescoat G, Cogrel P, et al. Antioxidant and iron-chelating activities of the flavonoids catechin, quercetin and diosmetin on iron-loaded rat hepatocyte cultures. Biochem Pharmacol 1993; 45: 13-19

[122] Morel I, Lescoat G, Cillard P, et al. Role of flavonoids and iron chelation in antioxidant action. Methods Enzymol 1994; 234: 437-443

[123] Ferrali M, Signorini C, Caciotti B, et al. Protection against oxidative damage of erythrocyte membrane by the flavonoid quercetin and its relation to iron chelating activity. FEBS Letters 1997; 416: 123-129

[124] Anghileri LJ, Thouvenot P. Natural polyphenols-iron interaction. Biol Trace Elem Res 2000; 73: 251-258

[125] Grinberg LN, Newmark H, Kitrossky N, et al. (1997). Protective effects of tea polyphenols against oxidative damage to red blood cells. Biochem Pharmacol 1997; 54: 973-978

[126] Srichairatanakool S, Ounjaijean S, Thephinlap C, et al. Iron-chelating and free-radical scavenging activities of microwave processed green tea in iron overload. Hemoglobin 2006; 30: 311-327

[127] Mandel SA, Amit T, Zheng H, et al. The essentiality of iron chelation in neuroprotection: A potential role of green tea catechins. Oxidative Stress and Disease 2006; 22: 277-299

[128] Mandel SA, Avramovich-Tiorsh Y, Reznichenko L, et al. Multifunctional activities of green tea catechins in neuroprotection. Neurosignals 2005; 14: 46-60

[129] Ono K, Yoshiike Y, Takashima A, et al. Potent anti-amyloidogenic and fibril-destabilizing effects of polyphenols in vitro: implications for theprevention and therapeutics of Alzheimer's disease. J Neurochem 2003; 87: 172-181

[130] Levites Y, Amit T, Mandel S, et al. Neuroprotection and neurorescue against Ab toxicity and PKC-dependent release of nonamyloidogenic soluble precursor protein by green tea polyphenol (-)-epigallocatechin-3-gallate. FASEB J 2003; 17: 952-954

[131] Lopes GKB, Schulman HM, Hermes-Lima M. (1999). Polyphenol tannic acid inhibits hydroxyl radical formation from Fenton reaction by complexing ferrous ions. Biochim Biophys Acta 1999; 1472: 142-152

[132] Hermes-Lima M, Wang EM, Schulman HM, et al. (1994). Deoxyribose degradation catalyzed by Fe (III) EDTA: Kinetic aspects and potential usefulness for sub-micromolar iron measurements. Mol Cell Biochem 1994; 137: 65-73

[133] Winterbourn CC. The ability of scavengers to distinguish •OH production in the iron-catalyzed Haber-Weiss reaction: Comparison of four assays for •OH. Free Radic Biol Med 1987; 3: 33-39

[134] Zhao C, Dodin G, Yuan C, et al. "In vitro" protection of DNA from Fenton reaction by plant polyphenol verbascoside. Biochim Biophys Acta 2005; 1723: 114-123

[135] Perron NR, Hodges JN, Jenkins M, et al. Predicting how polyphenol antioxidants prevent DNA damage by binding to iron. Inorg Chem 2008; 47: 6153-6161

[136] Shahidi F, Wanasundara PK. Phenolic antioxidants. Crit Rev Food Sci Nutr 1992; 32: 67-103

[137] Cotelle N. Role of flavonoids in oxidative stress. Curr Top Med Chem 2001; 1: 569-590

[138] Hagerman AE, Riedl KM, Jones GA, et al. High molecular weight plant polyphenolics (tannins) as biological antioxidants. J Agric Food Chem 1998; 46: 1887-1892

[139] Sano A, Uchida R, Saito M. et al. Beneficial effects of grape seed extract on malondialdehyde-Modified LDL. J Nutr Sci Vitaminol 2007; 53: 174-182

[140] Garcia-Alonso J, Ros G, Vidal-Guevara ML, et al. Acute intake of phenolic-rich juice improves antioxidant status in healthy subjects. Nutr Res 2006; 26: 330-339

[141] Dani C, Bonatto D, Salvador M, et al. Antioxidant protection of resveratrol and catechin in Saccharomyces cerevisiae. J Agric Food Chem 2008; 56: 4268-4272

[142] Sanchez-Alonso I, Borderias J, Larsson K, et al. Inhibition of hemoglobin-mediated oxidation of regular and lipid-fortified washed cod mince by a white grape dietary fiber. J Agric Food Chem 2007; 55: 5299-5305

[143] Dani C, Oliboni LS, Vanderlinde R, et al. Antioxidant activity and phenolic and mineral content of rose grape juice. J Med Food 2009; 12: 188-192

[144] Pinelo M, Rubilar M, Sineiro J, et al. A thermal treatment to increase the antioxidant capacity of natural phenols: catechin, resveratrol and grape extract cases. Eur Food Res Technol 2005; 221: 284-290

[145] Arora A, Nair MG, Strasburg GM. Structure-activity relationships for antioxidant activities of a series of flavonoids in a liposomal system. Free Radic Biol Med 1998; 24: 1355-1363

[146] Yoshimura Y, Nakazawa H, Yamaguchi F. Valuation of the NO scavenging activity of procyanidin in grape seed by use of the TMA-PTIO/NOC 7 ESR system. J Agric Food Chem 2003; 51: 6409-6412

[147] Frei B, Higdon JV. Antioxidant activity of tea polyphenols in vivo: evidence from animal studies. J Nutr 2003; 133: 3275-3284

[148] Buettner GR. The pecking order of free radicals and antioxidants: lipid peroxidation, alpha-tocopherol, and ascorbate. Arch Biochem Biophys1993; 300: 535-543

[149] Jovanavic SV, Steenken S, Simic MG. Reduction potentials of flavonoid and model phenoxyl radicals. J Chem Soc Perkins Trans 1996; 2: 2497-2503

[150] Jovanavic SV, Hara Y, Steenken S, et al. Antioxidant potential of theaflavins: A pulse radiolysis study. J Am Chem Soc 1997; 119: 5337-5343

[151] Aucamp J, Gaspar A, Hara Y, et al. Inhibition of xanthine oxidase by catechins from tea (Camellia sinensis). Anticancer Res 1997; 17: 4381-4385

[152] Lin JK, Chen PC, Ho CT, et al. Inhibition of xanthine oxidase and suppression of intracellular reactive oxygen species in HL-60 cells by theaflavin-3, 3-digallate, (-)-epigallocatechin-3-gallate, and propyl gallate. J Agric Food Chem 2000; 48: 2736-2743

[153] Skrzydlewska E, Ostrowska J, Farbiszewski R, et al. Protective effect of green tea against lipid peroxidation in the rat liver, blood serum and the brain. Phytomedicine 2002; 9: 232-238

[154] Guleria RS, Jain A, Tiwari V, et al. Protective effect of green tea extract against the erythrocytic oxidative stress injury during myco-bacterium tuberculosis infection in mice. Mol Cell Biochem 2002; 236: 173-181

[155] Das M, Sur P, Gomes A, et al. Inhibition of tumour growth and inflammation by consumption

of tea. Phytother Res 2002; 16: 40-44

[156] Yokozawa T, Nakagawa T, Kitani K. Antioxidative activity of green tea polyphenol in cholesterol-fed rats. J Agric Food Chem 2002; 50: 3549-3552

[157] Hayek T, Fuhrman B, Vaya J, et al. Reduced progression of atherosclerosis in apolipoprotein E-deficient mice following consumption of red wine, or its polyphenols quercetin or catechin, is associated with reduced susceptibility of LDL to oxidation and aggregation. Arterioscler Thromb Vasc Biol 1997; 17: 2744-2752

[158] Song DU, Jung YD, Chay KO, et al. Effect of drinking green tea on age-associated accumulation of Maillard-type fluorescence and carbonyl groups in rat aortic and skin collagen. Arch Biochem Biophys 2002; 397: 424-429

[159] Wei H, Frenkel K. Relationship of oxidative events and DNA oxidation in SENCAR mice to in vivo promoting activity of phorbol ester-type tumor promoters. Carcinogenesis 1993; 14: 1195-1201

[160] Xu Y, Ho CT, Amin SG, et al. Inhibition of tobacco-specific nitrosamine-induced lung tumorigenesis in A/J mice by green tea and its major polyphenol as antioxidants. Cancer Res 1992; 52: 3875-3879

[161] Dai J, Mumper RJ. Plant Phenolics: Extraction, analysis and their antioxidant and anticancer properties. Molecules 2010; 15: 7313-7352

[162] Fresco P, Borges F, Diniz C, et al. New insights on the anticancer properties of dietary polyphenols. Med Res Rev 2006; 26: 747-766

[163] Zhang Y, Seeram NP, Lee R, et al. Isolation and identification of strawberry phenolics with antioxidant and human cancer cell antiproliferative properties. J Agric Food Chem 2008; 56: 670-675

[164] Seeram NP, Adams LS, Zhang Y, et al. Blackberry, black raspberry, blueberry, cranberry, red raspberry, and strawberry extracts inhibit growth and stimulate apoptosis of human cancer cells in vitro. J Agric Food Chem 2006; 54: 9329-9339

[165] Katsube N, Iwashita K, Tsushida T, et al. Induction of apoptosis in cancer cells by Bilberry (Vaccinium myrtillus) and the anthocyanins. J Agric Food Chem 2003; 51: 68-75

[166] Damianaki A, Bakogeorgou E, Kampa M, et al. Potent inhibitory action of red wine polyphenols on human breast cancer cells. J Cell Biochem 2000; 78: 429-441

[167] Kampa M, Hatzoglou A, Notas G, et al. Wine antioxidant polyphenols inhibit the proliferation of human prostate cancer cell lines. Nutr Cancer 2000; 37: 223-233

[168] Zhang G, Miura Y, Yagasaki K. Effects of green, oolong and black teas and related components on the proliferation and invasion of hepatoma cells in culture. Cytotechnology 1999; 31: 37-44

[169] Weisburg JH, Weissman DB, Sedaghat T, et al. In vitro cytotoxicity of epigallocatechin gallate and tea extracts to cancerous and normal cells from the human oral cavity. Basic Clin Pharmacol Toxicol 2004; 95: 191-200

[170] Nichenametla SN, Taruscio TG, Barney DL, et al. A review of the effects and mechanisms of polyphenolics in cancer. Crit Rev Food Sci Nutr 2006; 46: 161-183

[171] Kuntz S, Wenzel U, Daniel H. Comparative analysis of the effects of flavonoids on proliferation, cytotoxicity, and apoptosis in human colon cancer cell lines. Eur J Nutr 1999; 38: 133-142

[172] Knowles LM, Zigrossi DA, Tauber RA, et al. Flavonoids suppress androgen-independent human prostate tumor proliferation. Nutr Cancer 2000; 38: 116-122

[173] Gupta S, Afaq F, Mukhtar, H. Selective growth-inhibitory, cell-cycle deregulatory and apoptotic response of apigenin in normal versus human prostate carcinoma cells. Biochem Biophys Res Commun 2001; 287: 914-920

[174] Kanno S, Tomizawa A, Hiura T, et al. Inhibitory effect s of naringenin on tumor growth in human cancer cell lines and sarcoma S-180-implanted mice. Biol Pharm Bull 2005; 28: 527-530

[175] Zhang M, Zhang JP, Ji HT, et al. Effect of six flavonoids on proliferation of hepatic stellate cells in vitro . Acta Pharmacol Sin 2000; 21: 253-256

[176] Miyahara Y, Komiya T, Katsuzaki H, et al. Sesamin and episesamin induce apoptosis in human lymphoid leukemia Molt 4B cells. Int J Mol Med 2000; 6: 43-46

[177] Yang CS, Maliakal P, Meng, X. Inhibition of carcinogenesis by tea. Annu Rev Pharmacol Toxicol 2002; 42: 25-54

[178] Lambert JD, Yang CS. Cancer chemopreventive activity and bioavailability of tea and tea polyphenols. Mutat Res 2003; 523-524: 201-208

[179] Gerhauser C. Cancer chemopreventive potential of apples, apple juice, and apple components. Planta Med 2008; 74: 1608-1624

[180] Thomasset S, Teller N, Cai H, et al. Do anthocyanins and anthocyani dins, cancer chemopreventive pigments in the diet, merit development as potential drugs? Cancer Chemother Pharmacol 2009; 64: 201-211

[181] Ding M, Feng R, Wang SY, et al. Cyanidin-3-glucoside, a natural product derived from blackberry, exhibits chemopreventive and chemotherapeutic activity. J Biol Chem 2006; 281: 17359-17368

[182] Martin MA, Goya L, Ramos S. Potential for preventive effects of cocoa and cocoa polyphenols in cancer. Food Chem Toxicol 2013; 56: 336-351

[183] Hudson TS, Hartle DK, Hursting SD, et al. Inhibition of prostate cancer growth by muscadine grape skin extract and resveratrol through distinct mechanisms. Cancer Res 2007; 67: 8396-8405

[184] Lazze MC, Pizzala R, Pecharroman FJG, et al. Grape waste extract obtained by supercritical fluid extraction contains bioactive antioxidant molecules and induces antiproliferative effects in human colon adenocarcinoma cells. J Med Food 2009; 12: 561-568

[185] God JM, Tate P, Larcom LL. Anticancer effects of four varieties of muscadine grape. J Med Food 2007; 10: 54-59

[186] Bagchi D, Bagchi M, Stohs SJ, et al. Free radicals and grape seed proanthocyanidin extract, importance in human health and disease prevention. Toxicol 2000; 148: 187-197

[187] Mantena SK, Katiyar SK. Grape seed proanthocyanidins inhibit UV-radiation-induced

oxidative stress and activation of MAPK and NF-kB signaling in human epidermal keratinocytes. Free Radic Biol Med 2006; 40: 1603-1614

[188] White TI, Spencer JM, Flowers FP. Chemoprevention of nonmelanoma skin cancer. J Ame Dermatol 2006; 54, 933-946

[189] Chung YC, Huang CC, Chen CH, et al. Grape-seed procyanidins inhibit the in vitro growth and invasion of pancreatic carcinoma cells. Pancreas 2012; 41: 447-454

[190] Singh T, Sharma SD, Katiyar SK. Grape proanthocyanidins induce apoptosis by loss of mitochondrial membrane potential of human non-small cell lung cancer cells in vitro and in vivo. PLoS ONE 2011; 6: 27444

[191] Kaur M, Mandair R, Agarwal R, et al. Grape seed extract induces cell cycle arrest and apoptosis in human colon carcinoma cells. Nutr Cancer 2008; 60: 2-11

[192] Jung K, Wallig M, Singletary K. Purple grape juice inhibits 7,12-dimethylbenz-[a]anthracene(DMBA)- induced rat mammary tumorigenesis and in vivo DMBA-DNA adduct formation. Cancer Lett 2006; 233: 279-288

[193] Singletary KW, Stansbury MJ, Giusti M, et al. Inhibition of rat mammary tumorigenesis by concord grape juice constituents. J Agric Food Chem 2003; 51: 7280-7286

[194] Yang CS, Sang S, Lambert JD, et al. Possible mechanisms of the cancer-preventive activities of green tea. Mol Nutr Food Res 2006; 50: 170-175

[195] Chen D, Daniel KG, Kuhn DJ, et al. Green tea and tea polyphenols in cancer prevention. Front Biosci 2004; 9: 2618-2631

[196] Lu YP, Lou YR, Lin Y, et al. Conney: Inhibitory effects of orally administered green tea, black tea, and caffeine on skin carcinogenesis in mice previously treated with ultraviolet B light (high-risk mice): relationship to decreased tissue fat. Cancer Res 2001; 61: 5002-5009

[197] Umemura T, Kai S, Hasegawa R, et al. Prevention of dual promoting effects of pentachlorophenol, an environmental pollutant, on diethylnitrosamine-induced hepato- and cholangiocarcinogenesis in mice by green tea infusion. Carcinogenesis 2003; 24: 1105-1109

[198] Landau JM, Wang ZY, Yang GY, et al. Inhibition of spontaneous formation of lung tumors and rhabdomyosarcomas in A/ J mice by black and green tea. Carcinogenesis 1998; 19: 501-507

[199] Parkin DM, Bray F, Ferlay J, et al. Estimating the world cancer burden: Globocan 2000. Int J Cancer 2001; 94: 153-156

[200] Huang SP, Chen JC, Wu CC, et al. Capsaicin-induced apoptosis in human hepatoma HepG2 cells. Anticancer Res 2009; 29, 165-174.

[201] Nishikawa T, Nakajima T, Moriguchi M, et al. A green tea polyphenol, epigalocatechin-3-gallate, induces apoptosis of humanhepatocellular carcinoma, possibly through inhibition of Bcl-2 family proteins. J Hepatol 2006; 44: 1074-1082

[202] Liang G, Tang A, Lin X, et al. Green tea catechins augment the antitumor activity of doxorubicin in an in vivo mouse model for chemoresistant liver cancer. Int J Oncol 2010; 37: 111-123

[203] Daglia M, Papetti A, Grisoli P, et al. Antibacterial activity of red and white wine against oral streptococci. J Agric Food Chem 2007; 55: 5038-5042

[204] Papadopoulou C, Soulti K ,Roussis IG. Potential antimicrobial activity of red and white wine phenolic extracts against strains of Taphylococcus aureus, Escherichia coli and Candida albicans. Food Technol Biotechnol 2005; 43: 41-46

[205] Karapinar M, Sengun IY. Antimicrobial effect of koruk (unripe grape-*Vitis vinifera*) juice against Salmonella typhimurium on salad vegetables. Food Control 2007; 18: 702-706

[206] Jayaprakasha GK, Tamil S, Sakartah KK. Antibacterial and antioxidant activities of grape (*Vitis vinifera*) seed extracts. Food Res Int 2003; 36: 117-122

[207] Anastasiadi M, Chorianopoulos NG, George-John EN, et al. Antilisterial activities of polyphenol-rich extracts of grapes and vinification byproducts. J Agric Food Chem 2009; 57: 457-463

[208] Brown JC, Huang G, Haley-Zitlin V, et al. Antibacterial effects of grape extracts on *Helicobacter pylori*. Appl Environ Microbiol 2009; 75: 848-852

[209] Tagurt T. Tanaka T, Kouno I. Antimicrobial activity of 10 different plant polyphenols against bacteria causing food-borne disease. Biol Pharm Bull 2004; 27: 1965-1969

[210] Rhodes PL, Mitchell JW, Wilson MW, et al. Antilisterial activity of grape juice and grape extracts derived from *Vitis vinifera* variety Ribier. Int J Food Microbiol 2006; 107: 281-286

[211] Gadang VP, Hettiarachchy NS, Johnson MG, et al. Evaluation of antibacterial activity of whey protein isolate coating incorporated with nisin, grape seed extract, malic acid, and EDTA on a turkey frankfurter system. J Food Sci 2008; 73(8): 389-394

[212] Shimamura T, Zhao WH, Hu Z. Mechanism of action and potential for use of tea catechin as an anti- infective agent. Anti-Infective Agents Medic 2007; 6: 57-62

[213] Yoda Y, Hu ZQ, Zhao WH, et al. Different susceptibilities of Staphylococcus and Gram-negative rods to epigallocatechin gallate. J Infect Chemother 2004; 10: 55-58

[214] Yu H, Oho T, Tagomori S, et al. Anticariogenic effects of green tea. Fukuoka Igaku Zasshi 1992; 83: 174-180

[215] Friedman M, Henika PR, Levin CE, et al. Antimicrobial activities of tea catechins and theaflavins and tea extracts against Bacillus cereus. J. Food Prot 2006; 69: 354-361

[216] Ferrero Miliani L, Nielsen OH, Andersen PS, et al. Chronic inflammation: importance of NOD2 and NALP3 in interleukin-1beta generation. Clin Exp Immunol 2007; 147(2): 227-35

[217] Bralley EE, Hargrove JL, Greenspan P, et al. Topical anti-inflammatory activities of vitis rotundifolia (Muscadine Grape) extracts in the tetradecanoylphorbol acetate model of ear inflammation. J Med Food 2007; 10: 636-642

[218] Panico AM, Cardile V, Avondo S, et al. The in vitro effect of a lyophilized extract of wine obtained from Jacquez grapes on human chondrocytes. Phytomedicine 2006; 13: 522-526

[219] De Mejia EG , Ramirez-Mares MV, Puangpraphant S. Bioactive components of tea: Cancer, inflammation and behavior. Brain Behav Immun 2009; 23: 721-731

[220] Kundu JK, Surh J. Inflammation: gearing the journey to cancer. Mutation Res 2008; 659: 15-30

[221] Miles EA, Zoubouli P, Calder PC. Effects of polyphenols on human Th1 and Th2 cytokine production. Clin Nutr 2005; 24: 780-784

[222] Yu J, Ahmedna M. Functional components of grape pomace: their composition, biological properties and potential applications. Int Jf Food Sci Tech 2013; 48: 221-237

[223] Sano T, Oda E, Yamashita T. et al. Anti-thrombotic effect of proanthocyanidin, a purified ingredient of grape seed. Thromb Res 2005; 115: 115-121

[224] Olas B, Wachowicz B, Tomczak A, et al. Comparative antiplatelet and antioxidant properties of polyphenol-rich extracts from: berries of Aronia melanocarpa, seeds of grape and bark of Yucca schidigera in vitro. Platelets 2008; 19: 70-77

[225] Dohadwala MM, Vita JA. Grapes and cardiovascular disease. J Nutr 2009; 139: 1788-1793

[226] Wolfram S. Effects of green tea and EGCG on cardiovascular and metabolic health. J Am Coll Nutr 2007; 26: 373-388

[227] Dulloo AG, Duret C, Rohrer D, et al. Efficacy of a green tea extract rich in catechin polyphenols and caffeine in increasing 24h energy expenditure and fat oxidation in humans. Am J Clin Nutr 1999; 70: 1040-1045

[228] Dulloo AG, Seydoux J, Girardier L, et al. Green tea and thermogenesis: Interactions between catechin- polyphenols, caffeine, and sympathetic activity. Int J Obes Relat Metab Disord 2000; 24: 252-258

[229] Bukowski JF, Percival SS. L-Theanine intervention enhances human γδ Tlymphocyte function. Nutr Rev 2008; 66: 96-102

[230] Bravo L. Polyphenols: chemistry, dietary sources, metabolism, and nutritional significance. Nutr rev 1998; 56 (11): 317-333

[231] Baba S, Osakabe N, Natsume M, et al. Absorption and urinary excretion of (-)-epicatechin after administration of different levels of cocoa powder or (-)-epicatechin in rats. J Agric Food Chem 2001; 49: 6050-6056

[232] Baba S, Osakabe N, Natsume M, et al. In vivo comparison of the bioavailability of (+)-catechin, (-)-epicatechin and their mixture in orally administered rats. J Nutr 2001; 131: 2885-2891

[233] Tsanga C, Higginsa S, Duthiea GG, et al. The influence of moderate red wine consumption on antioxidant status and indices of oxidative stress associated with CHD in healthy volunteers. Br J Nutr 2005; 93: 233-240

[234] Stalmach A, Troufflard S, Serafini M, et al. Absorption, metabolism and excretion of Choladi green tea flavan-3-ols by humans. Mol Nutr Food Res 2009b; 53: S44-S53

[235] Peters CM, Green RJ, Janle EM, et al. Formulation with ascorbic acid and sucrose modulates catechin bioavailability from green tea. Food Res Inte 2010; 43: 95-102

[236] Patras A, Brunton NP, O'Donnell C, et al. Effect of thermal processing on anthocyanin stability

in foods; mechanisms and kinetic s of degradation. Trends Food Sci Tech 2010; 21(1): 3-11

[237] Klimczak I, Malecka M, Szlachta M. et al. Effect of storage on the content of polyphenols, vitamin C and the antioxidant activity of orange juices. J Food Compos Anal 2007; 20: 313-322

[238] Hager TJ, Howard LR, Prior RL. Processing and storage effects on monomeric anthocyanins, percent polymeric colour, and antioxidant capacity of processed blackberry products. J Agric Food Chem, 2008; 56: 689-695

[239] Li N, Taylor LS, Ferruzzi MG, et al. Color and chemical stability of tea polyphenol (-)-epigallocatechin-3- gallate in solution and solid states. Food Res Inte 2013; 53: 909-921

[240] Biesaga M, Pyrzynńska K. Stability of bioactive polyphenols from honey during different extraction methods. Food Chem 2013; 136: 46-54

[241] Huang X, Cheng L, Exterkate RAM, et al. Effect of pH on Galla chinensis extract's stability and anti-caries properties in vitro. Arch oral biol 2012; 57: 1093-1099

[242] Tagliazucchi D, Verzelloni E, Bertolini D, et al. In vitro bio-accessibility and antioxidant activity of grape polyphenols. Food Chem 2010; 120: 599-606

[243] Chow HH, Cai Y, Hakim IA, et al. Pharmacokinetics and safety of green tea polyphenols after multiple-dose administration of epigallocatechin gallate and polyphenon E in healthy individuals. Clin Cancer Res 2003; 9: 3312-3319

[244] Bettuzzi S, Brausi M, Rizzi F, et al. Chemoprevention of human prostate cancer by oral administration of green tea catechins in volunteers with high-grade prostate intraepithelial neoplasia: A preliminary report from a one-year proof-of-principle study. A Corti Cancer Res 2006; 66: 1234-1240

[245] Chow HH, Cai Y, Alberts DS, et al. Phase I pharmacokinetic study of tea polyphenols following single-dose administration of epigallocatechin gallate and polyphenon E. Cancer Epidemiol Biomarkers Prev 2001; 10: 53-58

[246] Mazzanti G, Menniti-Ippolito F, Moro PA, et al. Hepatotoxicity from green tea: a review of the literature and two unpublished cases. Eur J Clin Pharmacol 2009; 65: 331-341

[247] Galati G, O'Brien PJ. Potential toxicity of flavonoids and other dietary phenolics: significance for their chemopreventive and anticancer properties. Free Radic Biol Med 2004; 37(3): 287-303

[248] Perumalla AVS, Hettiarachchy NS. Green tea and grape seed extracts-Potential applications in food safety and quality. Food Res Inte 2011; 44: 827-839

[249] Sullivan CM, Lynch AM, Lynch PB, et al. Assessment of the antioxidant potential of food ingredients in fresh, previously frozen and cooked chicken patties. Inte J Poultry Sci 2004; 3(5): 337-344

[250] Mitsumoto M, O'Grady MN, Kerry JP, et al. Addition of tea catechins and vitamin C on sensory evaluation, colour and lipid stability during chilled storage in cooked or raw beef and chicken patties. Meat Sci 2005; 69: 773-779

[251] Zhang J, Kashket S. Inhibition of salivary amylase by black and green teas and their effects on the intraoral hydrolysis of starch. Caries Res 1998; 32: 233

[252] Oh D, Lee MK, Park BK. Antimicrobial activities of commercially available tea on the harmful foodborne organisms. J Korean Soc Food Nutr 1999; 28: 100-106

[253] Sakanka S, Kim M, Taniguchi M, et al. Antibacterial substances in Japanese green tea extract against Streptococcus mutans , a cariogenic bacterium. Agric Biol Chem 1989; 53: 2307-2311

[254] Peng X, Ma J, Cheng KW, et al. The effects of grape seed extract fortification on the antioxidant activity and quality attributes of bread. Food Chem 2009; 119: 49-53

[255] Mielnik MB, Olsen E, Vogt G, et al. Grape seed extract as antioxidant in cooked, cold stored turkey meat. Food Sci Tech 2006; 39: 191-198

[256] Rababah T, Hettiarachchy NS, Horax R, et al. Thiobarbituric acid reactive substances and volatile compounds in chicken breast meat infused with plant extracts and subjected to electron beam irradiation. Poultry Sci 2006; 85(6): 1107-1113

[257] Furiga A, Lonvaud-Funel A, Badet C. In vitro study of antioxidant capacity and antibacterial activity on oral anaerobes of a grape seed extract. Food Chem 2009; 113: 1037-1040

Chapter II

Polyphenol: evolution of extraction and analysis

1 Introduction

Phenolic compounds are widely distributed in roots, leaves, flesh, and peels of plants like cocoa, tea, peanut, grape as well as other vegetables and fruits. The polyphenols are always constituted by simple phenols, phenolic acids (both benzoic and cinnamic acid derivatives), coumarins, flavonoids, stilbenes, hydrolysable and condensed tannins, lignans, and lignins. The chemical structure and properties of the molecule influence the extraction method employed as well as the extraction conditions such as time, temperature, pH, solvent, solid and liquid ratio etc. Since the chemical nature of plant phenolics varies from simple to highly polymerized substance and may exist as complex with carbohydrates, proteins and other plant components, phenolic extracts of plant materials are always a mixture of different classes of phenolics with different extraction system. The phenolic extracts from plant materials are always a diversified mixture of plant phenolics soluble in the solvent system used. Additional steps may be required to remove the unwanted phenolics and non-phenolic substances such aswaxes, terpenes, fats and chlorophylls. This chapter mainly focuses on the methodology that was employed by both total phenolic extract and the extraction of some specific molecules, and technologies involved in the analysis of polyphenols.

2 Methodology of phenolic extraction

Considering the variations among bioactive compounds and large number of plant species, it is necessary to build up a standard and integrated approach to screen out these compounds with great human health benefits. Farnsworth et al. [1] reported an integrated approach showing the sequence of medicinal plant study, which started from name collection of plants frequently used and terminated at industrialization. Works of particular order for medicinal plant study and the

position of extraction techniques are shown by a flow chart in Figure 1.

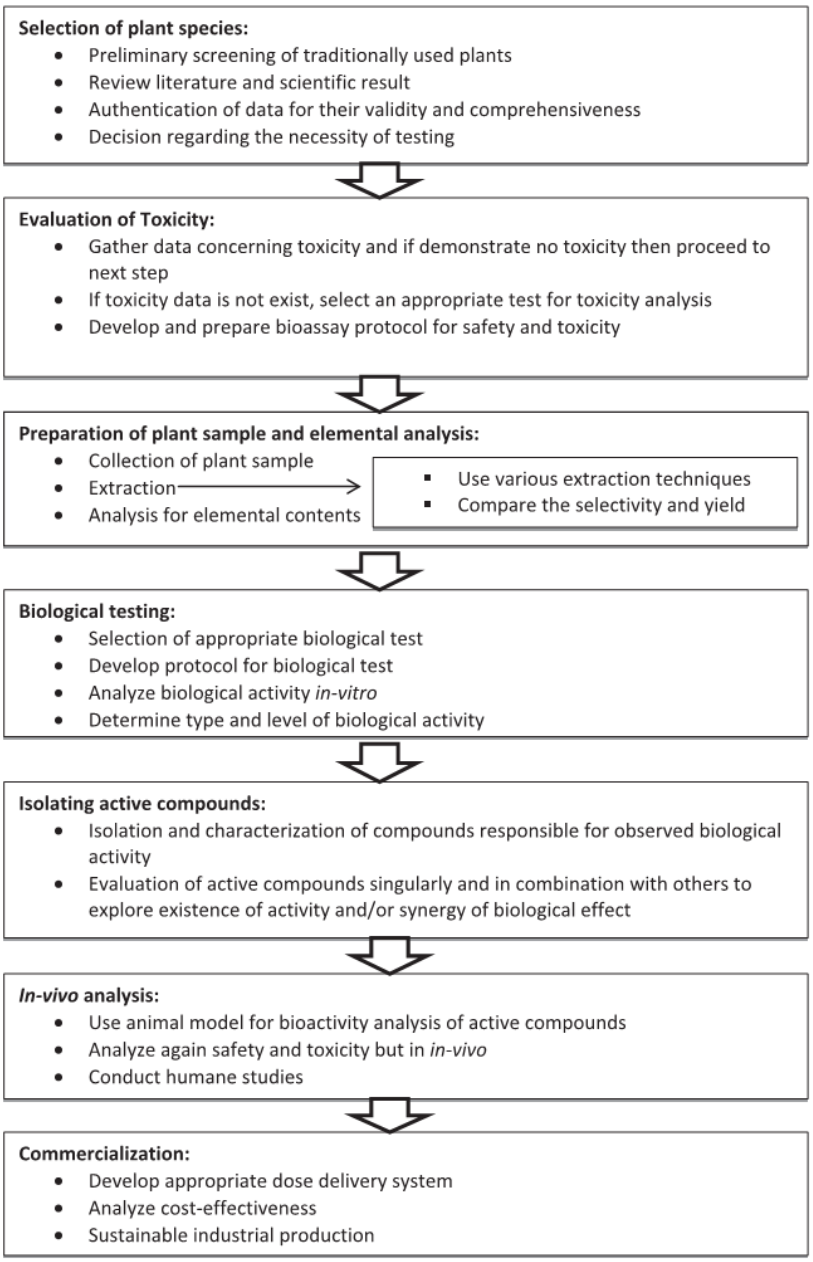

Figure 1: The flow chart of medicinal plant study and position of extraction techniques [1]

Only if an appropriate extraction process is carried out in advance, it is possible to process further steps such as separation, identification and characterization of bioactive compounds. Different extraction techniques should be used in diverse conditions for understanding the extraction selectivity from various natural sources. All these techniques have some objectives in common [2]:

i. Extract targeted bioactive compounds from complex plant sample

ii. Increase selectivity of analytical methods

iii. Increase sensitivity of bioassay by increasing the concentration of targeted compounds

iv. Convert the bioactive compounds into a more suitable form for detection and separation,

v. Provide a strong and reproducible method that is independent of variations in the sample matrix

2.1 Conventional extraction techniques

Bioactive compounds from plant materials can be extracted by various classical extraction techniques. Most of these techniques are based on the extracting power of different solvents in use and the application of heat and/or mixing. In order to obtain bioactive compounds from plants, the existing classical techniques are: i) soxhlet extraction, ii) maceration and iii) hydrodistillation.

2.1.1 Soxhlet extraction

Soxhlet extractor was first proposed by German chemist FranzRitter Von Soxhlet [3]. It was originally designed for the extraction of lipid from a solid test material, but now it can be used whenever it is difficult to extract any compound from a solid. The soxhlet extraction has widely been used for extracting valuable bioactive compounds from various natural sources. It is used as a model for the comparison of new extraction alternatives. Generally, a small amount of dry sample is placed in a thimble. The thimble is then placed in distillation flask which contains the solvent of particular interest. After reaching to an overflow level, the solution of the thimble-holder is aspirated by a siphon. Siphon unloads the solution back into the distillation flask. This solution carries extracted solutes into the bulk liquid. Solute is remained in the distillation flask and solvent passes back to the solid bed of plant. The process runs repeatedly until the extraction is completed.

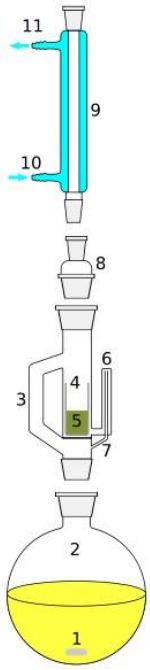

1. Stirrer bar/anti-bumping granules
2. Still pot (extraction pot)- still pot should not be overfilled and the volume of solvent in the still pot should be 3 to 4 times the volume of the soxhlet chamber
3. Distillation path
4. Soxhlet Thimble
5. Extraction solid (residue solid)
6. Syphon arm inlet
7. Syphon arm outlet
8. Reduction adapter
9. Condenser
10. Cooling water in
11. Cooling water out

Figure 2: Soxhlet extractor

2.1.2 Maceration

Initially, maceration was used in homemade preparation of tonic. Later, it became a popular and inexpensive way to obtain essential oils and bioactive compounds. In general, maceration is employed for small scale extraction and consists of several steps. Firstly, grinding of plant materials into small pieces or particles is carried out to increase the contact area between solid material and proper solvent when they are mixed together. Secondly, during maceration process, appropriate solvent named as menstruum is added in a closed vessel. Thirdly, the liquid is strained off but the marc which is the solid residue of this extraction process is pressed to recover large amount of occluded solutions. The obtained strained and the press out liquid are mixed and separated from impurities by filtration. Occasional shaking in maceration facilitates extraction by two ways: i) increase diffusion; ii) remove concentrated solution from the sample surface for bringing new solvent to the menstruum for more extraction yield.

2.1.3 Hydrodistillation

Hydrodistillation is a traditional method for extracting bioactive compounds and essential oils

from plants. Organic solvents are not involved in this method and it can be performed for dehydration of plant materials. In hydrodistillation, first, the plant materials are packed in a still compartment; second, water is added in sufficient amount and then brought to boil. Alternatively, direct steam is injected into the plant sample. Hot water and steam act as the main influential factors to free bioactive compounds of plant tissue. Indirect cooling by water condenses the vapor mixture of water and oil. Condensed mixture flows from condenser to a separator, where oil and bioactive compounds separate automatically from the water [6]. Hydrodistillation involves the following main physicochemical processes: hydrodiffusion, hydrolysis and decomposition by heat. Diffusion of essential oils and hot water through plant membranes is known as hydrodiffusion. Hydrolysis in the present context is defined as a chemical reaction between water and certain constituents of essential oils. The reactions are not complete in either direction and the relationship between the molal concentrations of various constituents at equilibrium is written as:

$$K = \frac{(\text{alcohol}) \times (\text{acid})}{(\text{ester}) \times (\text{water})}$$

where K is the equilibrium constant.

Almost all constituents of essential oils are unstable at high temperature. In order to obtain the best quality oil, distillation must be done at low temperatures. The temperature in steam distillation is determined entirely by the operating pressure, whereas in water distillation and in water and steam distillation the operating pressure is usually atmospheric. The same is true for the rate and extent of hydrolysis. However, it is possible to obtain better yield and quality of oils by: i) maintaining the temperature as low as possible, ii) using as little water as possible, in the case of steam distillation, and iii) thoroughly comminuting the plant material and packing it uniformly before distillation. According literature [5], there are roughly three types of hydrodistillation: i) water distillation, ii) water and steam distillation and iii) direct steam distillation. At a high extraction temperature some volatile components may be lost. This drawback limits its use for thermo labile compound extraction.

2.1.4 Factors involved in conventional extraction

Considering the variety in food matrixes involved, there is surprisingly a great deal of coherency in the choice of solvents for extracting bioactive compounds. Solvents, such as methanol, ethanol, propanol, acetone, ethyl acetate, dimethylformamide and their combinations have also been used for the extraction of phenolics, often with different proportions of water. Extraction efficiency of any conventional method mainly depends on the choice of solvents [6]. The polarity of the targeted compound is the most important factor for solvent choice. Molecular affinity between solvent and solute, mass transfer, use of co-solvent, environmental safety, human toxicity and financial feasibility should also consider in selection of solvent for bioactive compound extraction. Some examples of bioactive compound extracted using different solvents are given in Table 1.

Table 1Example of some extracted bioactive compounds by different solvents [6]

Water	**Ethanol**	**Methanol**	**Chloroform**	**Dichloromethanol**	**Ether**	**Acetone**
Anthocyanins	Tannins	Anthocyanin	Terpenoids	Terpenoids	Alkaloids	Flavonoids
Tannins	Polyphenols	Terpenoids	Flavonoids	Terpenoids	Tannins	
Saponins	Flavonol	Saponins				
Terpenoids	Terpenoids	Tannins				
	Alkaloids	Flavones				
		Polyphenols				

Other factors such as extraction time, temperature as well as solid and liquid ratio also influence the yield of bioactive compounds extracted. In some cases, orthogonal test or response surface methodology are employed to optimize the extraction process and obtain the optimal combination of all involved factors.

2.2 Ultrasonic-assisted extraction (UAE)

Ultrasound is a special type of sound wave with a frequency greater than the upper limit of human hearing. Generally, in chemistry the frequency of ultrasonic is from 20 kHz to 100 MHz. Ultrasonic wave works like other waves and passes through a medium by creating compression and expansion. UAE has been developed based on the principle of cavitation, a phenomenon

generated during ultrasonic work process and only between liquid and liquid containing solid materials, which means production, growth and collapse of bubbles. At the same time, large amount of energy can be produced from the conversion of kinetic energy into heating the contents of the bubble which possesses temperature about 5000 K, pressure 1000 atm and, heating and cooling rate above 10^{10} K/s [7].

The main benefit of UAE can be observed in solid plant samples because ultrasound energy facilitates organic and inorganic compounds leaching from plant matrix [8] and finally increases the yield of target products. The mechanism may be that ultrasound intensified mass transfer and accelerated access of solvent to cell materials of plant parts. The mechanism of ultrasonic-assisted extraction involves two types of physical phenomena: i) the diffusion across the cell wall and ii) rinsing the contents of cell after breaking the walls [9]. The advantages of UAE include reduction in extraction time, energy and use of solvent. Ultrasound energy for extraction also facilitates more effective mixing, faster energy transfer, reduced thermal gradients and extraction temperature, selective extraction, reduced equipment size, faster response to process extraction control, quick start-up, increased production and eliminates process steps [10].

Factors such as moisture content of sample, milling degree, particle size and solvent, greatly influence the efficient and effective extraction. Furthermore, temperature, pressure, frequency and time of sonication are factors governing the action of ultrasound. In some cases, UAE incorporated with various classical techniques as they are reported to enhance the efficiency of a conventional system.

A large number of researches employed UAE to isolate phenolic compounds from plants. Tabaraki et al. [11] used ultrasonic-assisted extraction of natural antioxidants from rice bran and optimized the extraction condition by response surface methodology (RSM). Results showed that UAE temperature of 51-54℃, extraction time in the range of 40-45 min and concentrations 65–67% of ethanol as modifier, can result in optimal total phenols (6.05 mg GA/g dw), antioxidant activity (54.14 μmol Fe^{2+}/g dw) and antiradical activity (52.83% inhibition) from rice bran. Gu et al. [12] employed UAE at 25 ℃ to extract the polyphenols present in tobaccos

into anhydrous methanol cooperated with novel filtration device. Cho et al. [13] compared the efficiency of UAE and conventional solvent extraction and found that the extraction yield of resveratrol from grape stems was increased by 24-30% when UAE was employed with ethanol/water (80:20%, v/v) maintained at 60 ℃ for 30 min. Anthocyanins and phenolic compounds were extracted from grape peel using UAE and the extraction process was optimized with reference to solvent, extraction temperature and time [14]. UAE technique was proved to have higher efficiency and shorter extraction time than conventional extraction methods in the extraction of phenolcarboxylic acids, carnosic acid and rosmarinic acid from Rosmarinus officinalis using Ionic liquid based UAE [15].

2.3 Microwave-assisted Extraction (MAE)

Another novel method for extracting soluble products into a fluid is microwave-assisted extraction (MAE). Microwaves are electromagnetic fields in the frequency range from 300 MHz to 300 GHz and made up of two oscillating fields that are perpendicular such as electric field and magnetic field. The extraction mechanism of microwave-assisted extraction is supposed to involve three sequential steps described by Alupului [16]: i) separation of solutes from active sites of sample matrix under increased temperature and pressure; ii) diffusion of solvent across sample matrix; iii) release of solutes from sample matrix to solvent. According to Cravottoa et al. [17], MAE has several advantages such as quicker heating for the extraction of bioactive substances from plant materials; reducing thermal gradients; reducing equipment size and increasing extract yield. Compared to conventional extraction processes, MAE can shorten extraction time and extract organic and organometallic compounds that are more intact with its selectivity. In addition, MAE is considered as a green technology due to the reduction of organic solvent usage [16].

In the study of Pan et al. [18], MAE achieved higher extraction yield at 4 min than any extraction methods at room temperature for 20 h on extraction of polyphenols and caffeine from green tea leaves. MAE shortened extraction time from 10 h to 15 min in Ginsenosides extraction from ginseng root compared with conventional solvent extraction [19]. Dhobi et al. [20] showed increased extraction efficiency of MAE by extracting a flavolignin, silybinin from Silybum

marianum compared with Soxhlet and maceration extraction. MAE was applied to release bound phenolic acids from bran and flour fractions of sorghum and maize of different hardness by Chiremba et al. [21]. Spigno et al. [22] investigated influence of microwave power (450–600–900 W) and irradiation duration (30–210 s) on total phenols concentration and antioxidant activity and found that MAE allowed higher recoveries compared to conventional brewing technique, without altering the antioxidant potential of the extracts. Ballard et al. [23] used MAE to extract phenolic antioxidants from peanut skins and investigated the effects of microwave power (10%, 50%, 90% nominal), irradiation time (30, 90, 150 s) and sample mass (1.5, 2.5, 3.5 g) on total phenolic content (TPC), ORAC (oxygen radical absorbance capacity) level and resveratrol content cooperated with response surface method which optimized extraction conditions on the basis of TPC, ORAC level and resveratrol content. The maximum predicted TPC, under the optimized conditions (90% microwave power, 30 s irradiation time and 1.5 g skins), was 143.6 mg gallic acid equivalent (GAE)/g skins.

2.4 Enzyme-assisted extraction (EAE)

Enzymatic pre-treatment has been considered as a novel and an effective way to release bounded compounds and increase overall yield [24]. The addition of specific enzymes like cellulase, α-amylase, and pectinase during extraction enhances recovery by breaking the cell wall and hydrolyzing the structural polysaccharides and lipid bodies [25]. Generally, two approaches are applied for EAE [26]: i) enzyme-assisted aqueous extraction (EAAE) and ii) enzyme-assisted cold pressing (EACP). Various factors including enzyme composition and concentration, particle size of plant materials, solid to water ratio, and hydrolysis time are key factors for extraction [27]. Dominguez et al. [28] reported that the moisture content of plant materials is also an important factor for enzymatic hydrolysis.

Meyer et al. [29] employed EAE in phenolic antioxidants extraction from grape pomace during wine production and found a correlation between yield of total phenols and degree of plant cell wall breakdown by enzyme. In their further study [30], various enzymes showed the improvement on the release of phenolic compounds from Ribes nigrum pomace. Extraction of phenolic antioxidant from raspberry solid wastes was increased by application of enzyme in

hydro-alcoholic extraction compared with non-enzymatic control [31]. Another important finding of that study was that the extraction of phenolic antioxidants improved significantly with higher enzyme concentration. Maier et al. [32] used a mixture of pectinolytic and cellulolytic enzymes, in the ratio of 2:1, to extract bioactive compounds (phenolic acids, non-anthocyanin flavonoids and anthocyanins) from grape pomace; they obtained yields higher compared with the ones of sulfite-assisted extraction.

2.5 Pressurized liquid extraction (PLE)

The concept of pressurized liquid extraction was first proposed by Richter et al. [33] in 1996 and now it is known by several names such as pressurized fluid extraction (PFE), accelerated fluid extraction (ASE), enhanced solvent extraction (ESE), and high pressure solvent extraction (HSPE) [34]. PLE applied high pressure to maintain solvent liquids beyond their normal boiling point in order to facilitate the extraction process. The advantages of PLE include the decrease of extraction time and solvents requirement, compared with the traditional soxhlet extraction [33]. Recently, PLE has also been considered as a potential alternative technique to supercritical fluid extraction for extraction of polar compounds and useful for the extraction of organic pollutants from environmental matrices, those are stable at high temperatures. PLE extraction of flavonoids from spinach, using a mixture of ethanol and water (70:30) solvent at 50-150 ℃, was more effective than water solvent at 50-130 ℃ [35]. Individual phenolic compounds such as gallocatechin (GCT), epicatechin gallate, catechin, caffeic acid, chlorogenic acid, and myricetin and total phenolic contents were obtained from Anatolia propolis by PLE at optimum condition (40 ℃, 1500 psi for 15 min) [36]. Additionally, PLE is reorganized as a green extraction technique due to small amount organic solvent used [37].

2.6 Pulsed-electric field extraction (PEF)

The pulsed electric field (PEF) treatment has been applied in improving the pressing, drying, extraction, and diffusion processes. The mechanism of PEF may be to destroy cell membrane structure for increasing extraction. On the basis of the dipole nature of membrane molecules, electric potential separates molecules according to their charge in the cell membrane. An electric

potential passes through the membrane of that cell and, at the same time, a living cell is suspended in electric field [38]. The effectiveness of PEF treatment strictly depends on the process parameters, such as field strength, specific energy input, pulse number, treatment temperature and properties of the materials to be treated [39]. The advantages of PEF include enhancing extraction yield and decreasing extraction time by increasing mass transfer and destroying the cell membrane structure.

It has been found that PEF treatment, at a moderate electric field (500 and 1000 V/cm; for 10^{-4}-10^{-2} s), damage cell membrane of plant tissue with little temperature increase [40] and therefore, PEF can minimize the degradation of heat sensitive compounds [41]. PEF has been also applied on plant materials as a pretreatment process prior to conventional extraction to lower extraction effort [42]. Corralesa et al. [43] demonstrated that PEF was a better method to extract anthocyanins from grape by-product than other techniques. The application of a PEF treatment on grape skin before maceration step can reduce the duration of maceration and improve the stability of bioactive substances (anthocyanin and polyphenols) during vinification [44].

2.7 Supercritical fluid extraction (SFE)

Supercritical fluid extraction is a process of extracting one component in to liquid by using supercritical fluid as the extracting solvent. The properties of a supercritical fluid can be altered by varying the temperature and pressure and therefore it allows selective extraction. Supercritical fluid possesses gas-like properties of diffusion, viscosity, and surface tension, as well as liquid-like density and solvation power. These properties make it suitable for extracting compounds in a short time with higher yields [45]. For SFE, carbon dioxide (CO_2) is considered as an ideal solvent; since its critical temperature is close to room temperature and its low critical pressure (74 bars) offers the possibility to operate at moderate pressures (100-450 bar). Factors involved in SFE include temperature, pressure, particle size and moisture content of feed material, time of extraction, flow rate of CO_2 and solvent-to-feed-ratio [46].

3 Purification and fraction technologies

Most of the extractions lead to a crude extract of polyphenols which can be stilled improved by purifying and specifying. Thus, further purification and fraction can be processed by liquid-solid phase procedures and liquid-liquid procedures.

3.1 Liquid-solid phase procedures

The application of ion exchange resins can partially purify phenolic extracts. Mullen et al. [47] employed both ion-exchange column (Diaion HP-20) and column containing 40μm C_{18} silica gel support to remove sugars and other contaminants from acidified extracts of raspberry. As for phenolics present in aqueous plant extracts, amberlite particles (XAD-2) can be a good choice for isolation and purification. Amberlite particles were stirred with aqueous extracts for up to 4h and then packed into a glass column. The column was first washed with water, or a combination of acidified water and water, to remove sugar and other polar constituents. Subsequently, the phenolics were washed out from the column with methanol [48, 49]. Moreover, Phenolics extracts can also be purified and fractionated using solid phase extraction or solid phase microextraction (SPME) on C_{18} cartridges. Salagoity-Auguste and Bertrand [50] as well as Jaworski and Lee [51] demonstrated that a C18 Sep-Pak cartridge may be used to separate grape phenolics into acidic and neutral fractions. Column chromatography has been also employed for fractionation of phenolics extracts. Souquet et al. [52] utilized a Fractogel (Toyopearl TSK HW-50(f) gel) column (35 cm× 8 cm) to separate the non-tannin phenolics and proanthocyanidins. The isolation of proanthocyanins (condensed tannins) is commonly carried out by employing Sephadex LH-20 column chromatography [53].

3.2 Liquid-liquid procedures

Countercurrent chromatography (CCC) has recently been explored as an alternative to liquid chromatographic techniques for fractionation of various classes of phenolic compounds [54]. High speed centrifugal counter-current chromatography (HSCCC) was used for preparative isolation of anthocyanins from red wines and grape skins [55]. Degenhart et al. [56] found that

HSCCC can be employed for isolation of theaflavins, epitheaflavic acids, and thearubigins from black tea with hexane-ethylacetate-methanol-water (2:5:2:5 and 1.5:5:1.5:5, v/v/v/v) solvent system. In the study of Vitrac et al. [57], HSCCC was used for fractionation of red wine phenolic extracts first in ethyl acetate which were chromatographed using a 1.5 cm × 60 cm cation-exchange Dowex (Sigma) column and washing by water and 75% aqueous methanol successively. Afterwards, the phenolic extract was fractionated by HSCCC in both ascendant and descendant modes with water-ethanol-hexane-ethyl acetate in the ratios of 3:3:4:5 (v/v/v/v) and 7:2:1:8 (v/v/v/v) solvent systems.

4 Quantification of polyphenols

A number of spectrophotometric methods for quantification of phenolic compounds in plant materials have been developed. These assays are based on different principles and are used to determine various structural groups present in phenolic compounds. Gas chromatographic (GC) and high performance liquid chromatographic (HPLC) techniques have been used widely for both separation and quantitation of phenolic compounds. Structure elucidation is often achieved using combination of GC and HPLC with mass spectrometric analysis, as well as other relevant techniques.

4.1 Spectrophotometric techniques for determination of global phenolics (Table 2)

The Folin-Denis assay [58] is the most widely used for quantification of total phenolics in plant materials. Reduction of phosphomolybdic-phosphotungstic acid (Folin-Denis) reagent to a blue colored complex in an alkaline solution occurs in the presence of phenolic compounds [59]. Another technique is the Folin-Ciocalteau assay used for determination of the total content of plant food phenolics [60]. Oxidations of phenolic compounds with the Folin-Ciocalteau reagent include reaction with the mixture of $H_3PW_{12}O_{40}$ and $H_3PMo_{12}O_{40}$ acids in the alkaline medium. At this reaction a mix of blue oxides is formed. The vanillin [61] assays has been utilized for the estimation of total proanthocyanidins. The vanillin test is specific for flavan-3-ols, dihydrochalcones and proanthocyanidins which have a single bond at the 2, 3-position and possess free meta-hydroxy groups on the B ring [62]. The 4-(dimethylamino)-cinnamaldehyde

(DMCA) assay has also been proposed for estimation of proanthocyanidins [63]. The formation of a green chromophore between catechin and DMCA was first reported by Thies and Fischer [64]. The proanthocyanidin assay has also been utilized for the estimation of total proanthocyanidins, which carried out in a solution of butanol and concentrated hydrochloric acid (95:5, v/v). In the presence of this acidic solution proanthocyanidins (condensed tannins) are converted to anthocyanidins [65]. The complexation of phenolic with Al (III) has been employed for determination of total caffeic acid, total flavonoids and total tannins [66-68]. The total caffeic acid was measured by adding a solution of $AlCl_3$ to the methanol based extract of phenolics and adjusting the pH to 4.8 with a solution of NH_4Cl. The absorbance of this solution was then measured at 355 nm with UV-visible spectrophotometry. On the other hand, the total content of flavonoids has been obtained by the complexation of flavonoids with $AlCl_3$ at pH 3.1. The total content of flavonoids and tannins was determined by measuring the absorbance of the solution at 407 and 323 nm, respectively [68].

Table 2 Spectrophotometric techniques for determination of global phenolics

Technique	Reagent	Molecule determined	Measurement	Ref.
Folin-Denis assay	Folin-Denis reagent (phosphomolybdic-phosphotungstic acid)	Total phenolic content	UV absorbance at 725 nm	[58,59]
Folin-Ciocalteau assay	Folin-Ciocalteau reagent	Total phenolic content	UV absorbance at 760 nm	[60]
Vanillin assay	Vanillin reagent	Flavan-3-ols dihydrochalcones proanthocyanidins	UV absorbance at 500 nm	[61, 62]
DMCA assay	DMCA reagent (4-(dimethylamino)-cinnamaldehyde)	Proanthocyanidin	UV absorbance at 613 nm	[63, 64]
Proanthocyanidin assay	Butanol and concentrated hydrochloric acid	Proanthocyanidin	UV absorbance at 550 nm	[65]

4.2 Chromatographic techniques

Various chromatographic techniques have been employed for separation, preparative isolation, purification and identification of phenolic compounds. Moreover, Chromatographic procedures have also been used to study the interaction of phenolics with other food components [69].

4.2.1 Liquid chromatography

Many liquid chromatographic methodologies have been described in the literature for fractionation of polyphenols using Sephadex G-25 [63, 71, 72], Sephadex LH-20 [72-74]; Sepharose CL-4B [75], Fractogel (Toyopearl TSK-HW 40(s) gel) [76-78], Fractogel (Toyopearl) TSK 50(f) [79], inert glass microparticles [79] as well as C18 Sep-Pak cartridge [50, 51, 80]. Hoff and Singleton [75] developed a chromatographic procedure for separation of tannins from non-tannin materials using bovine serum albumin immobilized on Sepharose CL-4B as a column packing material. The preparative isolation of proanthocyanins is most commonly achieved by using Sephadex LH-20 column chromatography [72, 74]. Derdelinckx and Jerumanis [76] employed Fractogel (Toyopearl TSK HW-40(s) gel) for separation of malt and hop proanthocyanidin dimers and trimers after chromatography of polyphenols on Sephadex LH-20 with methanol. Recently, Labarbe et al. [79] employed an inert glass powder (Pyrex microparticles, 200-400μm) for fractionation of grape-seed or skin proanthocyanidins. Fulcrand et al. [81] fractionated wine phenolics into simple (phenolic acids, anthocyanins, flavonols and flavanols) and polymeric components using a Fractogel (Toyopearl) HW-50(f) col-umn (bed 12 mm × 120 mm).

4.2.2 High-performance liquid chromatography

Nowadays, High Performance Liquid Chromatography (HPLC) is widely used not only for the separation but also for the quantitation of phenolic compounds. Table 3 shows some HPLC procedures for determination of flavones and flavonols in some plant sources, while Table 4 exhibits some HPLC procedures for determination of catechins and proanthocyanidins (PA) in some plant sources. Plant phenolics are commonly detected using

UV-vis and photodiode array (DAD) detectors.

Other methods used for the detection of phenolics include electro-chemical coulometric array (EC) detector, chemical reaction detection technique and fluorimetric detector [82]. Mass spectrometric (MS) detectors coupled to high-performance liquid chromatography (HPLCMS tandem) have been commonly employed for structural characterization of phenolics. In addition, electrospray ionization mass spectrometry (ESI-MS) has been applied for structural confirmation of phenolics in plums, peaches, nectarines [83], grape seeds [84], soyfoods [85] and cocoa [86]. Satterfield and Brodbelt [87] indicated that complexation of flavonoids with Cu^{2+} enhanced the detection of flavonoids by ESI-MS.

Table 3 Some HPLC procedures for determination of flavones and flavonols in some plant sources [82]

Food	Sample preparation	Stationary phase	Mobile phase
Red onions	Extraction with MeOH stabilized with BHT; dilution with MeOH	Supelcosil LC-18 (250 mm × 4.6 mm, 5 μm) column coupled with a Spherisorb Supelguard LC-18	A: 0.01 M sodium phosphate adjusted to pH 2.5 with H_3PO_4; B: MeOH; linear gradient: 87–60%A in B, 0–13.5 min; 60–10%A in B, 13.5–39 min; 10–0%A in B, 39–42 min; 0–87%A in B, 42–46 min
Orange peel oils	Filtration, chilling to precipitate waxes, molecular distillation, residue taken to analysis	OmniSpher C18 column (125 mm × 2 mm; 3 μm).	A: 35% aqueous acetonitrile containing 0.01% formic acid; B: acetonitrile containing 0.01% formic acid. Gradient: A–B, 0–55 min
Spinach	Extraction of freeze dried sample with 40% MeOH for 20 h at 4 °C; centrifugation	Phenomenex Luna phenyl-hexyl column (250 mm × 4.6 mm, 5 μm) coupled with security guard column Phenomenex C_{18} ODS (4 mm × 3 mm)	A: H_2O/MeOH/formic acid (69:30:1); B: MeOH; gradient: 15–45%B, 0–18 min; 45–100%B, 18–23 min; 100%B, 23–27 min
Buckwheat	Extraction with 80% MeOH, filtration, evaporation, dissolving in MeOH–H_2O–oxalic acid (13:36:1, v/v/v) filtration	Capcell Pak C_{18}-SG 120, column, (100 mm × 4.6 mm, 3 μm)	A: MeOH–H_2O–acetic acid (13:36:1, v/v/v); B: MeOH–H_2O–acetic acid (73:25:2, v/v/v); gradient: 10–50%B in A, 0–20 min; 50%B in A, 20–25 min; 50–10%B in A, 25–30 min
Tomatoes onions lettuce celery	Extraction with 1.2 M HCl in 50% MeOH for 2 h at 90 °C; extract adjusted to pH 2.5 with TFA, filtration	C_{18} symmetry (150 mm × 3.9 mm, 5 μm) reversed-phase column, coupled with C_{18} symmetry guard	A: acetonitrile; B: H_2O adjusted to pH 2.5 with TFA; gradient: 15–35% A in B, 0–20 min
Edible tropical plants	Extraction with 1.2 M HCl in 50% MeOH for 2 h at 90 °C, filtration	Nova Pak C_{18} column (150 mm × 3.9 mm; 4 μm)	Isocratic: MeOH–H_2O (1:1, v/v) adjusted to pH 2.5 with TFA

Table 4 Some HPLC procedures for determination of catechins and proanthocyanidins (PA) in some plant sources [82]

Food	Sample preparation	Stationary phase	Mobile phase
Grape seed	Extraction with EtOH; fractionation of PA using Sephadex LH-20	Exsil 100 ODS C_{18}, reversed-phase (250 mm × 4.6 mm, 5 μm) coupled to C_{18} column guard	A: 0.2% H_3PO_4 (v/v); B: 82% acetonitrile with 0.4% H_3PO_4; gradient: 100%A, 0%B–85%A, 15%B, 0–15 min; 85%A, 15%B–84%A, 16%B, 15–40 min; 84%A, 16%B–83%A, 17%B, 40–45 min; 83%A, 17%B–57%A, 43%B, 45–48 min; 57%A, 43%B–48%A, 52%B, 48–49 min; isocratic 48%A, 52%B, 49–56 min; 48%A, 52%B-57%A, 43%B, 56–57 min; 57%A, 43%B–83%A, 17%B, 57–58 min; 83%A, 17%B–100%A, 0%B, 58–60 min
Wine	Filtration; direct injection	Nucleosil 100 C_{18}, (250 × 4 mm, 5 μm) coupled to C_{18} column guard	A: 2 mM $NH_4H_2PO_4$, adjusted to pH 2.6 with H_3PO_4; B: 20%A with acetonitrile; C: 0.2 M H_3PO_4 adjusted to pH 1.5 with ammonia; gradient: 100%A, 0–5 min; 0–4% B, 5–15 min; 4–8%B, 15–25 min; 8%B, 92%C, 25.1 min; 8–20%B, 25.1–45 min; 20–30%B, 45–50 min; 30–40%, 50–55 min; 40–80%B, 55–60 min
Apples, grapes beans	Extraction with 90% MeOH (apples, grapes) or 70% MeOH (beans); filtration	Inertsil ODS –2 (150 × 4.6 mm, 5 μm) coupled with Opti-Guard PR C18 Violet A guard.	A: 5% acetonitrile in 0.025 M phosphate buffer pH 2.4; B: 25% acetonitrile in 0.025 M phosphate buffer pH 2.4; isocratic, 0–5 min, 10%B; 5–20 min, linear gradient: 5–20 min, 10–80%B; 20–22 min, 80–90%B; isocratic 22–25 min, 90%B; linear gradient, 25–28 min, 10%B; isocratic, 28–37 min, 10%B
Foods, beverages	Extraction with H_2O or 70% acetone; purification using Supercosil Envil-18 20mL SPE column conditioned with MeOH and then with H_2O; phenols eluted with acetone/H_2O/CH_3COOH (70:29.5:0.5)	Phenomenex Luna silica column (250 × 4.6 mm, 5 μm)	A: dichloromethane; B: MeOH; C: 50% CH_3COOH; gradient: 14%B and 4%C–28.4%B and 4%C, 0–30 min; 28.4%B and 4%C–50%B and 4%C, 30–60 min; 50%B and 4%C–86%B and 4%C, 60–65 min; 86%B and 4%C, 65–70 min
Wine	Dealcoholized under vacuum; fractionation of procyanidins and catechins using two C_{18} Sep Pak cartridges in series	Superspher 100 RP18 (250 × 4 mm; 4 μm)	A: H_2O; B: H_2O–acetic acid (90:10, v/v); *catechins*: 10–80%B, 0–5 min; 80–100% B, 5–29 min; 100%B, 29–45 min; procyaidins: 10–70%B, 0–40 min; 70–85%B, 40–55 min; 85–100%B, 55–74 min

4.2.3 High-speed countercurrent chromatography

High-speed countercurrent chromatography (HSCCC), a kind of centrifugal partitioning chromatography, is an all-liquid chromatography which is suitable for preparative isolation of pure compounds [88, 89]. Separation of compounds is based on their partitioning between two immiscible liquids [55]. According to Baumann et al. [90], HSCCC is a simple and efficient method for separation of catechin gallates from spray-dried tea extract. Tea phenolic extract was first subjected to liquid-liquid partitioning between ethyl acetate and water. The organic layer containing catechins was then submitted to high-speed centrifugal countercurrent chromatography operating in an ascending mode. Favorable partitioning was achieved using n-hexanes/ethyl acetate/water (1:5:5, v/v/v) or ethyl acetate/methanol/water (5:1:5 and 5:2:5, v/v/v). Sephadex LH-20 column with methanol as a mobile phase was used

for a final purification of catechin gallates.

4.2.4 Other chromatographic techniques

Additionally, other chromatographic techniques also play an important role in purification and separation of food polyphenols. For instance, paper chromatographic (PC) and thin-layer chromatographic (TLC) techniques are still widely employed for purification and isolation of anthocyanins, flavonols, condensed tannins and phenolic acids with different solvent systems [91, 92]. It is reported that PC on Whatman No. 3 was employed for separation of anthocyanins using butanol/acetic acid/water, chloroform/acetic acid/water, or butanol/formic acid/water as possible mobile phases [91]. Azar et al. [93] have identified phenolics of bilberry juice Vaccinium myrtillus by a two dimensional TLC. Various gas chromatographic (GC) methodologies have been used for separation and quantitation of phenolic acids, isoflavones, capsaicinoids, phenolic aldehydes and monomers of condensed tannins [94]. Novel high-temperature gas chromatographic columns, electronic pressure controllers and detectors have significantly improved the resolution and have also led to an increase in the upper range of molecular weights of substances that can be analyzed by GC [95].

Reference

[1] Farnsworth NR, Akerele O, Bingel AS, et al. Medicinal plants in therapy. Bull World Health Organ 1985; 63: 965-981

[2] Smith RM. Before the injection-modern methods of sample preparation for separation techniques. J Chromatogr A 2003; 1000 (1-2): 3-27

[3] Soxhlet F. Die gewichtsanalytische Bestimmung des Milchfettes. Dingler's Polyt J 1879; 232: 461-465

[4] Harwood LM, Moody CJ. Experimental organic chemistry: Principles and Practice. Blackwell Scientific Publications, 1989; pp: 122-125

[5] Vankar PS. Essential oils and fragrances from natural sources. Resonance 2004; 9 (4): 30-41

[6] Cowan MM. Plant products as antimicrobial agents. Clin Microbiol Rev 1999; 12 (4): 564-582

[7] Suslick KS, Doktycz SJ. The effects of ultrasound on solids. In: Advances in Sonochemistry (Ed.: Mason TJ), JAI Press: New York, 1990; pp: 197-230

[8] Herrera MC, Luque de Castro MD. Ultrasound-assisted extraction of phenolic compounds from strawberries prior to liquid chromatographic separation and photodiode array ultraviolet detection. J Chromatogr 2005; 1100 (1):1-7

[9] Mason TJ, Paniwnyk L, Lorimer JP. The uses of ultrasound in food technology. Ultrason Sonochem 1996; 3 (3): 253-260

[10] Chemat F, Tomao V, Virot M. Ultrasound-assisted extraction in food analysis. In: Handbook of Food Analysis Instruments (Ed.: Otles S), CRC Press, 2008; pp: 85-94

[11] Tabaraki R, Nateghi A. Optimization of ultrasonic-assisted extraction of natural antioxidants from rice bran using response surface methodology. Ultrason Sonochem 2011; 18: 1279-1286

[12] Gu XG, Cai JB, Yang J, et al. Ultrasonic extraction followed by a novel filtration and clean-up device for screening of some polyphenols in tobaccos. J Sep Sci 2005; 28: 184-188

[13] Cho YJ, Hong JY, Chun HS, et al. Ultrasonication-assisted extraction of resveratrol from grapes. J Food Eng 2006; 77: 725-730

[14] Ghafoor K, Hui T, Choi YH. Optimization of ultrasound-assisted extraction of total anthocyanins from grape peel. J Food Biochem 2011; 35: 735-746

[15] Zu G, Zhang R, Yang L, et al. Ultrasound-assisted extraction of carnosic acid and rosmarinic acid using ionic liquid solution from Rosmarinus officinalis. Inter J Mol Sci 2012; 13 (9): 11027–11043

[16] Alupului A, Călinescu I, Lavric V. Microwave extraction of active principles from medicinal plants. U.P.B. Sci Bull Series B 2012; 74 (2): 129-142

[17] Cravottoa G, Boffaa L, Mantegnaa S, et al. Improved extraction of vegetable oils under high-intensity ultrasound and/or microwaves. Ultrason Sonochem 2008; 15 (5): 898-902

[18] Pan X, Niu G, Liu H. Microwave-assisted extraction of tea polyphenols and tea caffeine from green tea leaves. Chem Eng Process 2003; 42 (2): 129-133

[19] Shu YY, Ko MY, Chang YS. Microwave-assisted extraction of ginsenosides from ginseng root. Microchem J 2003; 74 (2): 131-139

[20] Dhobi M, Mandal V, Hemalatha S. Optimization of microwave assisted extraction of bioactive flavolignan-silybinin. J Chem Metrol 2009; 3 (1): 13-23

[21] Chiremba C, Rooney LW, Trust BJ. Microwave-assisted extraction of bound phenolic acids in bran and flour fractions from sorghum and maize cultivars varying in hardness. J Chromatogr A 2012; 1012 (2): 119-128

[22] Spigno G, De Faveri DM. Microwave-assisted extraction of tea phenols: A phenomenological study. J Food Engi 2009; 93: 210-217

[23] Ballard TS, Mallikarjunan P, Zhou KQ, et al. Microwave-assisted extraction of phenolic antioxidant compounds from peanut skins. Food Chem 2010; 120: 1185-1192

[24] Rosenthal A, Pyle DL, Niranjan K. Aqueous and enzymatic processes for edible oil extraction. Enzyme Microb Tech 1996; 19 (6): 402-420

[25] Singh RK, Sarker BC, Kumbhar BK, et al. Response surface analysis of enzyme-assisted oil extraction factors for sesame, groundnut, and sunflower seeds. J Food Sci Tech 1999; 36 (6): 511-514

[26] Latif S, Anwar F. Physicochemical studies of hemp (*Cannabis sativa*) seed oil using enzyme-assisted cold-pressing. Eur J Lipid Sci Tech 2009; 111 (10): 1042-1048

[27] Niranjan K, Hanmoungjai P. Enzyme-aided aqueous extraction. In: Nutritionally Enhanced Edible Oil Processing (Eds.: Dunford NT, Dunford HB), AOCS Publishing: Champaign, USA, 2004; pp: 89-90

[28] Dominguez H, Ntiiiez MJ, Lema JM. Enzyme-assisted hexane extraction of soybean oil. Food Chem 1995; 54 (2): 223-231

[29] Meyer AS, Jepsen SM, Sørensen NS. Enzymatic release of antioxidants for human low-density lipoprotein from grape pomace. J Agric Food Chem 1998; 46 (7): 2439-2446

[30] Landbo AK, Meyer AS. Enzyme-assisted extraction of antioxidative phenols from black currant juice press residues (*Ribes nigrum*). J Agric Food Chem 2001; 49 (7): 3169-3177

[31] Laroze L, Soto C, Zúñiga ME. Phenolic antioxidants extraction from raspberry wastes assisted by-enzymes. Electron J Biotechnol 2010; 13 (6): http://dx.doi.org/10.2225/vol13-issue6-fulltext-12

[32] Maier T, Göppert A, Kammerer DR, et al. Optimization of a process for enzyme-assisted pigment extraction from grape (*Vitis vinifera L.*) pomace. Eur Food Res Tech 2008; 227 (1): 267-275

[33] Richter BE, Jones BA, Ezzell JL, et al. Accelerated solvent extraction: a technology for sample preparation. Anal Chem 1996; 68 (6): 1033-1039

[34] Nieto A, Borrull F, Pocurull E, et al. Pressurized liquid extraction: a useful technique to extract pharmaceuticals and personal-care products from sewage sludge. TRAC-Trend Anal Chem 2010; 29 (7): 752-764

[35] Howard L, Pandjaitan N. Pressurized liquid extraction of flavonoids from spinach. J Food Sci 2008; 73 (3): 151-157

[36] Erdogan S, Ates B, Durmaz G, et al. Pressurized liquid extraction of phenolic compounds from Anatolia propolis and their radical scavenging capacities. Food Chem Toxicol 2011; 49 (7): 1592-1597

[37] Ibañez E, Herrero M, Mendiola JA, et al. Extraction and characterization of bioactive compounds with health benefits from marine resources: macro and micro algae, cyanobacteria, and invertebrates. In: Marine Bioactive Compounds: Sources, Characterization and Applications (Ed.: Hayes M), Springer, 2012; pp: 55-98

[38] Vorobiev E, Jemai AB, Bouzrara H, et al. Pulsed electric field assisted extraction of juice from food plants. In: Novel Food Processing Technologies (Eds.: Barbosa-Canovas G, Tapia MS, Cano MP), CRC Press: New York, 2005; pp: 105-130

[39] Heinz V, Toepfl S, Knorr D. Impact of temperature on lethality and energy efficiency of apple juice pasteurization by pulsed electric fields treatment. Innov Food Sci Emerg 2003; 4 (2): 167-175

[40] Fincan M, Dejme, P. In situ visualization of the effect of a pulsed electric field on plant tissue. J Food Eng 2002; 55 (3): 223-230

[41] Ade-Omowaye BIO, Angersbach A, Taiwo KA, et al. Use of pulsed electric field pretreatment to improve dehydration characteristics of plant based foods. Trends Food Sci Tech 2001; 12 (8): 285-295

[42] López N, Puértolas E, Condón S, et al. Enhancement of the extraction of betanine from red beetroot by pulsed electric fields. J Food Eng 2009; 90 (1): 60-66

[43] Corralesa M, Toepflb S, Butza P, et al. Extraction of anthocyanins from grape by-products assisted by ultrasonics, high hydrostatic pressure or pulsed electric fields: a comparison. Innov Food Sci Emerg 2008; 9 (1): 85-91

[44] López N, Puértolas E, Condón S, et al. Effects of pulsed electric fields on the extraction of phenolic compounds during the fermentation of must of Tempranillo grapes. Innov Food Sci Emerg 2008; 9 (4): 477-482

[45] Sihvonen M, Järvenpää E, Hietaniemi V, et al. Advances in supercritical carbon dioxide technologies. Trends Food Sci Tech 1999; 10 (6-7): 217–222

[46] Temelli F, Güçü-Üstündağ Ö. Supercritical Technologies for Further Processing of Edible Oils. In: Bailey's Industrial Oil and Fat Products (Ed.: Shahidi F), John Wiley & Sons, 2005; pp: 397-401

[47] Mullen W, McGinn J, Lean MEJ, et al. Ellagitannins, flavonoids, and other phenolics in red raspberries and their contribution to antioxidant capacity and vasorelaxation properties. J Agric Food Chem 2002; 50: 5191-5196

[48] Llorach R, Gil-Izquierdo A, Ferreres F, et al. HPLC-DAD-MS/MS ESI characterization of unusual highly Gglycosylated acylated flavonoids from cauliflower (*Brassica oleracea L.var.botrytis*) agroindustrial byproducts. J Agric Food Chem 2003; 51: 3895-3899

[49] Yao L, Jiang Y, D'Arcy B, et al. Quantitative high-performance liquid chromatography analyses of flavonoids in Australian Eucalyptus honeys. J Agric Food Chem 2004; 52: 210-214.

[50] Salagoity-Auguste MH, Bertrand AJ. Wine phenolics-analysis of low molecular weight components by high performance liquid chromatography. J Sci Food Agric. 1984; 35: 1241-1247

[51] Jaworski AW, Lee CY. Fractionation and HPLC determination of grape phenolics. J Agric Food Chem 1987; 35: 257-259

[52] Souquet JM, Cheynier V, Brossaud F. Polymeric proanthocyanidins from grape skins. Phytochemistry 1996; 43: 509-512

[53] Thompson RS, Jacques D, Haslam E, et al. Plant proanthocyanidins. Part I. Introduction; the isolation, structure, and distribution in nature of plant procyanidins. J Chem Soc Perkin Trans 1 1972; 1387-1399

[54] Degenhart A, Knapp H, Winterhalter P. Separation and purification of anthocyanins by high-speed countercurrent chromatography and screening for antioxidant activity. J Agric Food Chem 2000; 48: 338-343

[55] Degenhart A, Hofmann S, Knapp H, et al. Preparative isolation of anthocyanins by high-speed countercurrent chromatography and application of the color activity concept to red wine. J Agric Food Chem 2000; 48: 5812-5818

[56] Degenhart A, Engelhardt UE, Wendt AS, et al. Isolation of black tea pigments using high-speed countercurrent chromatography and studies on properties of black tea polymers. J Agric Food Chem 2000; 48: 5200-5205

[57] Vitrac X, Castagnino C, Waffo-Teguo P, et al. Polyphenols newly extracted in red wine from southwestern France by centrifugal partition chromatography. J Agric Food Chem 2001; 49: 5934-5938

[58] Williams S. Official Methods of Analysis Association of Official Analytical Chemists(12th Ed.), AOAC: Washington DC, 1980

[59] Folin O, Denis W. On phospotungstic-phosphomolybdic compounds as color reagents. J Biol Chem 1912; 12: 239-243

[60] Singleton VL, Rossi Jr JA. Colorimetry of total phenolics with phosphomolybdic-phosphotungstic acid reagents. Am J Enol Vitic 1965; 16: 144-158

[61] Price ML, Van Scoyoc S, Butler LG. A critical evaluation of the vanillin reaction as an assay for tannin in sorghum grain. J Agric Food Chem 1978; 26: 1214-1218

[62] Gupta RK, Haslam E. Vegetable tannins: structure and biosynthesis. In Polyphenols in Cereals and Legumes (Ed.: Hulse JH), International Development Research Center: Ottawa, Canada, 1980; pp: 15-24

[63] McMurrough I, McDowell J. Chromatographic separation and automated analysis of flavanols. Anal Biochem 1978; 91: 92-100

[64] Thies M, Fischer R. Über eine neue Farbreaktion zum mikrochemischen Nachweis und zur quantitativen Bestimmung von Catechinen. Mikrochim Acta 1971; 59: 9-13

[65] Porter LJ, Hrtstich LN, Chan BG. The conversion of procyanidins and prodelphinidins to cyaniding and delphinidin. Phytochemistry 1986; 25: 223-230

[66] Lamaison JLC, Carnet A. Teneurs en principaux flavonoids des fleurs de Crataegeus monogyna Jacq et de Crataegeus laevigata (Poiret D.C) en fonction de la vegetation. Pharm. Helv. 1990; 65: 315-320

[67] Zhishen J, Mengcheng T, Jianming W. The determination of flavonoid contents in mulberry and their scavenging effects on superoxide radicals. Food Chem 1999; 64: 555-559

[68] Zaporozhets OA, Krushynska OA, Lipkovska NA, et al. A new test method for the evaluation of total antioxidant activity of herbal products. J Agric Food Chem 2004; 52: 21-25

[69] Oh HI, Hoff JE, Haff LA. Immobilized condensed tannins and their interaction with proteins. J Food Sci 1985; 50: 1652-1654

[70] Michaud MJ, Margail MA. Étude analytique des tanins catéchiques. I. Les oligomères flavanoliques de l'Actinidia chinensis Planchon. Bull Soc Pharm Bordeaux 1977; 116: 52-64

[71] Somers TC. Wine tannins: isolation of condensed flavonoid pigments by gel-filtration. Nature 1966; 209: 368-370

[72] Asquith TN, Izuno CC, Butler LG. Characterization of the condensed tannin (proanthocyanidin) from a group II sorghum. J Agric Food Chem 1983; 31: 1299-1303

[73] Boukharta M, Girardin M, Metche M. Procyanidines galloylées du sarment de vigne (*Vitis vinifera*). Séparation et identification par chromatographie liquide haute performance and chromatographie en phase gazeuse. J Chromatogr 1988; 455: 406-409

[74] Davis AB, Hoseney RC. Grain sorghum condensed tannins. II. Preharvest changes. Cereal Chem 1979; 56: 310-314

[75] Hoff JF, Singleton KI. A method for determination of tannin in foods by means of immobilized enzymes. J Food Sci 1977; 42: 1566-1569

[76] Derdelinckx G, Jerumanis J. Separation of malt and hop proanthocyandins on Fractogel TSK HW-40 (S). J Chromatogr 1984; 285: 231-234

[77] Wen D, Li C, Di H, et al. A universal HPLC method for the determination of phenolic acids in compound herbal medicines. J Agric Food Chem 2005; 53: 6624-6629

[78] Ricardo da Silva JM, Rigaud J, Cheynier V, et al. Procyanidin dimers and trimers from grape seeds. Phytochemistry 1991; 4: 1259-1264

[79] Labarbe B, Cheynier V, Brossaud F, et al. Quantitative fractionation of grape proanthocyanidins according to their degree of polymerization. J Agric Food Chem 1999; 47: 2719-2723

[80] Sun BS, Leandro MC, Ricardo-da-Silva JM, et al. Separation of grape and wine proanthocyanidins according to their degree of polymerization. J Agric Food Chem 1998; 46: 1390-1396

[81] Fulcrand H, Remy S, Souquet JM, et al. Study of wine tannin oligomers by on-line liquid chromatography electrospray ionization mass spectrometry. J. Agric. Food Chem. 1999; 47: 1023-1028

[82] Naczk M, Shahidi F. Phenolics in cereals, fruits and vegetables: Occurrence, extraction and analysis. J Pharmaceut Biomed 2006; 41: 1523-1542

[83] Tomás-Barberán FA, Gil MI, Cremin P, et al. HPLC-DAD-ESIMS analysis of phenolic compounds in nectarines, peaches, and plums. J. Agric. Food Chem. 2001; 49: 4748-4760

[84] Peng Z, Hayasaka Y, Iland PG, et al. Quantitative analysis of polymeric procyanidins (tannins) from grape (*Vitis vinifera*) seeds by reverse phase high-performance liquid chromatography. J. Agric.Food Chem. 2001; 49: 26-31

[85] Zafrilla P, Ferreres F, Tomás-Barberán FA. Effect of processing and storage on the antioxidant ellagic acid derivatives and flavonoids of red raspberry (Rubus idaeus) jams. J. Agric. Food Chem. 2001; 49: 3651-3655

[86] Hammerstone JF, Lazarus SA, Mitchell AE, et al. Identification of procyanidins in cocoa (Theobroma cacao) and chocolate using high-performance liquid chromatography/mass spectrometry. J. Agric. Food Chem. 1999; 47: 490-496

[87] M Satterfield, Brodbelt JS. Enhanced detection of flavonoids by metal complexation and electrospray ionization mass spectrometry. Anal Chem 2000; 72: 5898-5906

[88] Degenhart A, Engelhardt UE, Lakenbrink C, et al. Preparative separation of polyphenols from tea by high-speed countercurrent chromatography. J. Agric. Food Chem. 2000; 48: 3425-3430

[89] Conway WD, Petrovski RJ. ACS Symposium Series, vol. 593. American Chemical Society: Washington, DC, 1995; pp: 156-183

[90] Baumann D, Adler S, Hamburger M. A simple isolation method for the major catechins in green tea using high-speed countercurrent chromatography. J Nat Prod 2001; 64: 353-355

[91] Jackman RL, Yada RY, Tung MA. Anthocyanins as food colorants-a review. J Food Biochem 1987; 11: 279-308

[92] Leung J, Fenton TW, Mueller MM, et al. Condensed tannins of rapeseed meal. J Food Sci 1979; 44: 1313-1316

[93] Azar M, Verette E, Brun S. Identification of some phenolic compounds in bilberry juice Vaccinium myrtillus. J. Food Sci 1987; 52: 1255-1257

[94] Naczk M, Shahidi F. Extraction and analysis of phenolics in food. J Chromatogr A 2004; 1054: 95-111

[95] Hemes PJ, Hedges JJ. Determination of condensed tannin monomers in environmental samples by capillary gas chromatography of acid depolymerization extracts. Anal Chem 2000; 72: 5115-5124

Chapter III

Biomaterials and surface functionalization

1 Biomaterials

1.1 Introduction

Biomaterials are known as the natural or man-made materials, which are used to replace or supplement the functions of living tissues [1]. First of all, the biomaterials should be biocompatible; this means that in vivo they must not induce adverse reaction (e.g. toxicity). In addition to this, biomaterials must possess features like bioinert behavior, bioactivity, biostability as well as biodegradibilty, depending on the intended activity of the material in the organism. In general, biomaterials are categorized as follows [2]:

i. Natural or synthetic polymers

ii. Metals

iii. Composites

iv. Bioactive glasses and ceramics

Biomaterials have been successfully and widely applied [3] in the form of implants such as sutures, bone plates, joint replacements, ligaments, vascular grafts, heart valves, intraocular lenses, dental implants, etc. and medical devices like pacemakers, biosensors, artificial hearts, blood tubes, etc. in order to replace and/or restore the function of traumatized or degenerated tissues or organs, to assist in healing, to improve function, to correct abnormalities, and therefore improve the quality of life of the patients.

1.2 Glasses and glass-ceramics

Glass is an amorphous (non-crystalline) solid material which exhibits a reversible glass transition from a hard and relatively brittle state into a molten or rubber-like state. The glasses are commonly obtained by the progressive cooling of a liquid; the result is similar to supercooled liquids with high viscosity without long-range order in the positions of the atoms. Figure 1 reports a schematic comparison between crystalline solids (ordered atomic arrangement) and amorphous ones (disordered atomic arrangement). The amorphous state is infrequent in nature due to the unstable structure in thermodynamics; under appropriate thermodynamic conditions, the amorphous state will transfer into crystals arranged with a long-range order [4, 5].

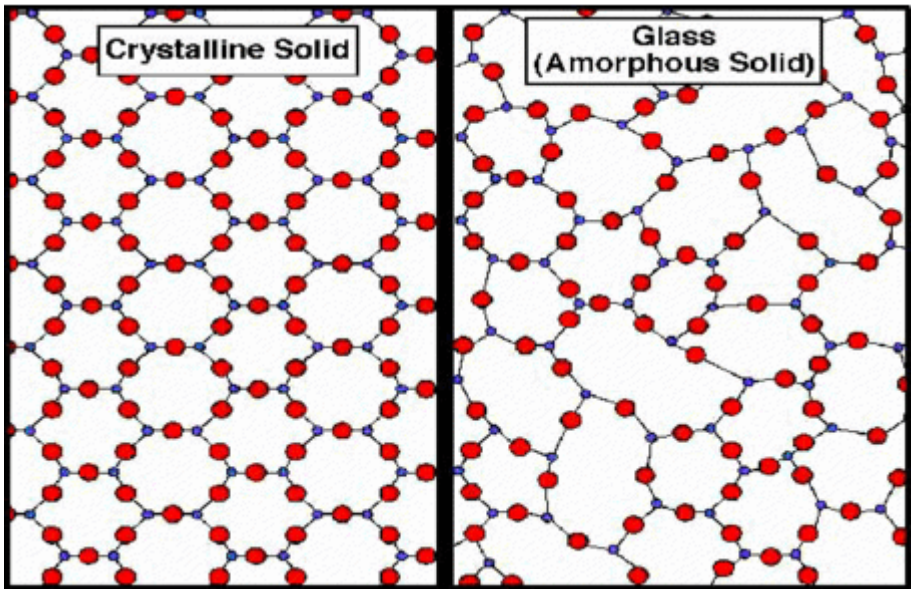

Figure 1: A comparison of crystalline and amorphous solid [6]

The general definition of "glass" refers to any substance that is in the amorphous state. The amorphous materials include several types:

a) Ceramics-inorganic oxides (traditional glasses), inorganic fluorides (fluoride glasses), inorganic chalcongenides (chalcongenide glasses)

b) Metals

c) Organic compounds (glycerin, glucose…)

d) Polymers

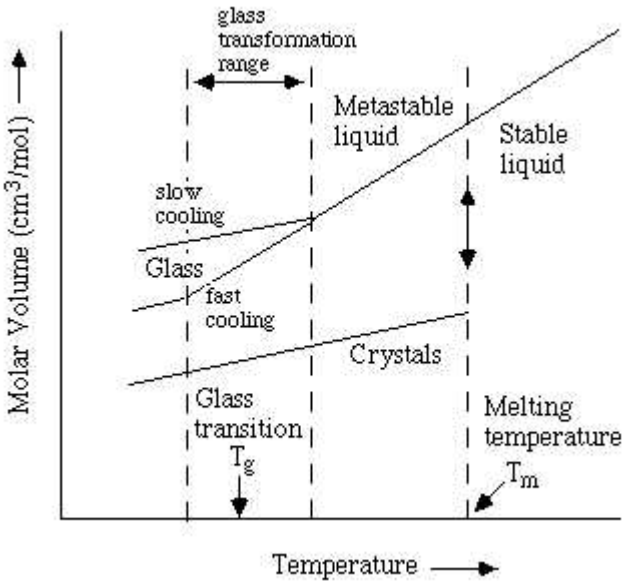

Figure 2: The volume-temperature diagram for a glass-forming liquid [7]

Most commercial glasses are obtained by rapid cooling of a viscous liquid below a typical "freezing" temperature, known as the glass transition temperature (T_g).

The cooling process of a viscous liquid (figure 2) includes characteristic regions:

a) $T>T_g$ – viscous liquid. The glass structural units will slide due to the viscous behavior with creep [8]

b) $T_g<T<T_m$ (melting temperature) - supercooled liquid

c) $T<T_g$ – amorphous solid-Fragile material

In addition, the glass transformation occurs over a range of temperature and cannot be characterized by any single temperature.

According to Zachariasen [9, 10], the criterions of glass formation are described as:

1) No oxygen atom may be linked to more than two cations.

2) The number of oxygen atoms surrounding the cations must be small (e.g., less than six).

3) The oxygen polyhedra shares corners with each other, but do not share edges or faces.

4) The polyhedra are linked in a three-dimensional network.

5) Cooling rate ≈ 10^6 K/s is required.

The object which starts as a glass and ends up as polycrystalline ceramic is termed as glass-ceramic. The processing of glass-ceramics is accomplished by first quenching a melt to form the glass object. Then, the glass is transformed into a glass-ceramics in two steps: i) glass is heat treated at a specific temperature range (i.e. 500-700 ^oC) to generate a large concentration of nuclei from which crystals can grow; ii) When sufficient nuclei are present to ensure that a fine-grained structure will be obtained, the temperature is raised to a range (i.e. 600-900 ^oC) that promotes crystal growth until crystals impinge and up to about 100% crystallization is achieved. The resulting microstructure is nonporous and contains fine-grained, randomly oriented crystals. There may also be a residual glassy matrix depending on the duration of the creaming heat treatment. [11]

1.3 Bioactive glasses

Bioactive glasses are a class of reactive materials, which can chemically bond with bone. They were firstly discovered by Hench and his colleagues in 1969. The group of glasses with specific composition was termed as bioactive glass. A definition of a bioactive material has been proposed by Hench as "a bioactive material is one that elicits a specific biological response at the interface of material that results in the formation of a bond between tissues and the material" [12]. Bioactive glasses have numerous applications in repair and reconstruction of diseased and damaged tissue, especially hard tissue like bone. The possibility of controlling a range of chemical properties and rate of bonding to tissues makes bioactive glass different from other bioactive ceramics and glass-ceramics. The most reactive glass even could develop a stable and bonded interface with soft tissues.

1.3.1 Parameters for bioactive glass design

The first bioactive glass was synthesized 40 years ago by Hench et al. [13] and belonged to the SiO_2-Na_2O-CaO-P_2O_5 system with excellent biocompatibility as well as the ability to

bond bone. This invention led to a revolution in the development of biomaterials and doped system of bioactive glasses as well as the development of inert materials for implantation and natural tissue regeneration.

In general, a bioactive material represents a material that is designed for inducing target specific biological activity. More specifically, a bioactive material represents a material, which follows a two-step process upon its implantation inside the body. In the first step it undergoes specific surface reactions with simulated body fluid (SBF) and during the second step it forms a HA-like layer, which is responsible for the interactions within hard and soft tissues [14].

Bioactive glasses designed should posses the ability to provide appropriate structural compatibility without toxicity. Hence, some basic parameters should be desired to make bioactive glass function as a suitable material [15, 16]. These requirements are listed as follows:

a) Biocompatibility of bioactive glasses, which is an indispensable property. They should be non-toxic and hence promote cell proliferation in addition to cell adhesion.

b) The nucleation and growth of crystalline phases in a matrix of glass during the thermal treatment of making scaffolds from bioglass should not induce cytotoxic effect in cell tissues.

c) A hydroxyapatite layer should be formed when bioglasses are immersed in SBF solution.

d) It should not exhibit any inflammatory response, demonstrate cytotoxicity or immunogenicity.

e) Bioglasses must meet the requirement for mechanical properties to withstand different kind of pressure depending on the implant site.

f) Bioglasses should possess controllable porosity to support vascularization if cells growth into the required physical structure in bone engineering is needed.

g) If porous, the architecture aspect of bioglasses should be three-dimensional (3D scaffolds) to propomte cell proliferation, vascularization and diffusion of nutrients.

h) For commercialization, the cost of bioglasses should be taken into consideration.

In addition to those requirement mentioned above, composition is an important factor for bioactive glass design. In most bioactive glass, the base components include SiO_2, Na_2O, CaO, P_2O_5. Hench and co-workers studied a series of glasses in this four component system and summarized the ternary SiO_2-Na_2O-CaO diagram shown in figure 3, which demonstrates the bioactive bonding boundary of compositions. In region A, glasses are bioactive and able to bond to bone. In a smaller region in the middle of area A, soft tissue bonding appears. Glasses in region B are nearly inert. Compositions in region C are resorbed within 10 to 30 days in tissue. In region D, the compositions are not technically practical [17].

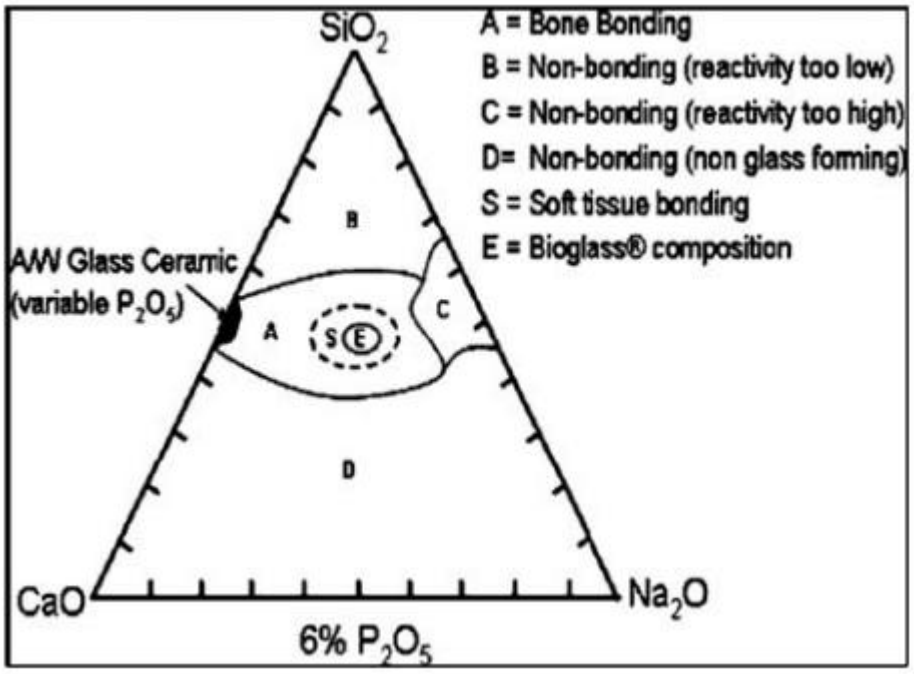

Figure 3: Compositional dependence of bone bonding and soft-tissue bonding of bioactive glasses and glass-ceramics. All compositions in region A have a constant 6 wt% of P_2O_5 [17].

1.3.2 Bioactivity

The basis of bonding property between bone and bioactive glasses is the chemical bioactivity of the glass in body fluids. The surface chemical reactions lead to the formation of a hydroxycarbonate apatite (HCA) layer where the bone can bond. When immersed in an aqueous solution, three general reactions happed to bioactive glass and solution: leaching, dissolution and precipitation. Leaching indicated the ion release, usually the ion exchange between H^+ or H_3O^+ and alkaline earth elements. This process is easy because these cations are not part of glass network; instead they just modify the network by forming non-bridging oxygen bonds (figure 4). The ion exchange process leads to an increase in interfacial pH (> 7.4).

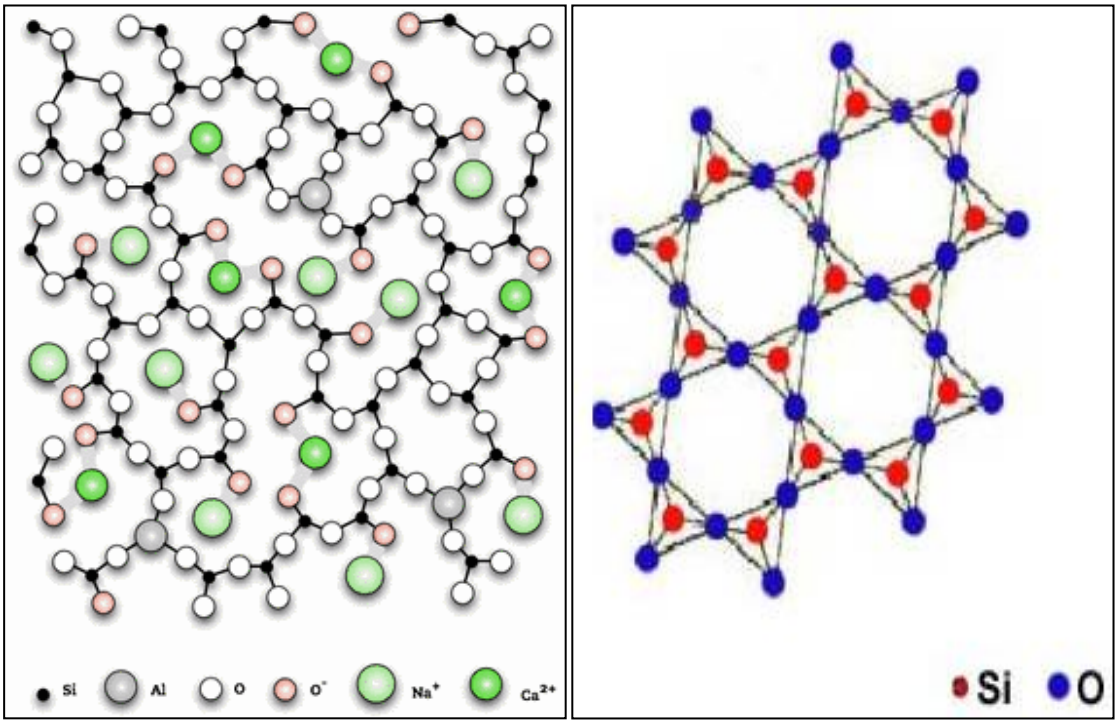

Figure 4: a) Structure of random glass network composed of network modifiers and b) structure of crystalline silicate [18, 19]

The second reaction process is network dissolution by breaking -Si-O-Si-O-Si- bonds and results in the release of silica into solution to form the silicic acid ($Si(OH)_4$). The rate of dissolution closely depends on the glass composition. For example, glass with compositions of > 60% SiO_2 possesses an extremely low dissolution rate due to the formation of the large number of bridging oxygen bonds. In the end, this process leads to the formation of a silica gel layer.

The calcium and phosphate ions released from the glass or present in the solution (e.g. SBF) can precipitate on the glass surface to form a calcium-phosphate layer, which later crystallizes to a hydroxycarbonate aptatite structure.

To summarize, bioactivity mechanism of bioactive glasses can be described in 12 stages [17]:

1) Rapid ion exchange of network modifying Ca^{2+} and Na^{+} ions from the glass with H_3O^{+} ions from solution. This step increases the pH at the implant-bone interface.

$$Si\text{-}O\text{-}Na^{+} + H^{+} + OH^{-} \rightarrow Si\text{-}OH^{+} + Na^{+}\,(solution) + OH^{-}$$

2) Loss of soluble silica and formation of silanols

$$Si\text{-}O\text{-}Si + H_2O \rightarrow Si\text{-}OH + OH\text{-}Si$$

3) Condensation and repolymerisation of the SiO_2-rich layer on the surface depleted in alkalis and alkaline-earth cations

4) Migration of Ca^{2+} and PO_4^{3-} groups to the surface through the silica-rich layer forming a $CaO\text{-}P_2O_5$-rich film on top of the silica-rich layer, followed by the growth of the amorphous calcium phosphate layer

5) Crystallization of the amorphous calcium phosphate layer into biologically equivalent hydroxycarbonate aptatite (HCA)

6) Adsorption of biological molecules in the hydroxyapatite layer

7) Action of macrophages

8) Attachment of stem cells

9) Differentiation of stem cells

10) Generation of matrix

11) Crystallization of matrix

12) Formation of new bone

The first five reaction stages (figure 5) that occur on the material side of the interface do not

depend on the presence of tissues. They can take place in distilled water, tris-buffer solution or stimulated body fluids. In a living organism the organic component of body fluids and tissues play a key role for the development of bioactive behaviour allowing the subsequent steps (6-12).

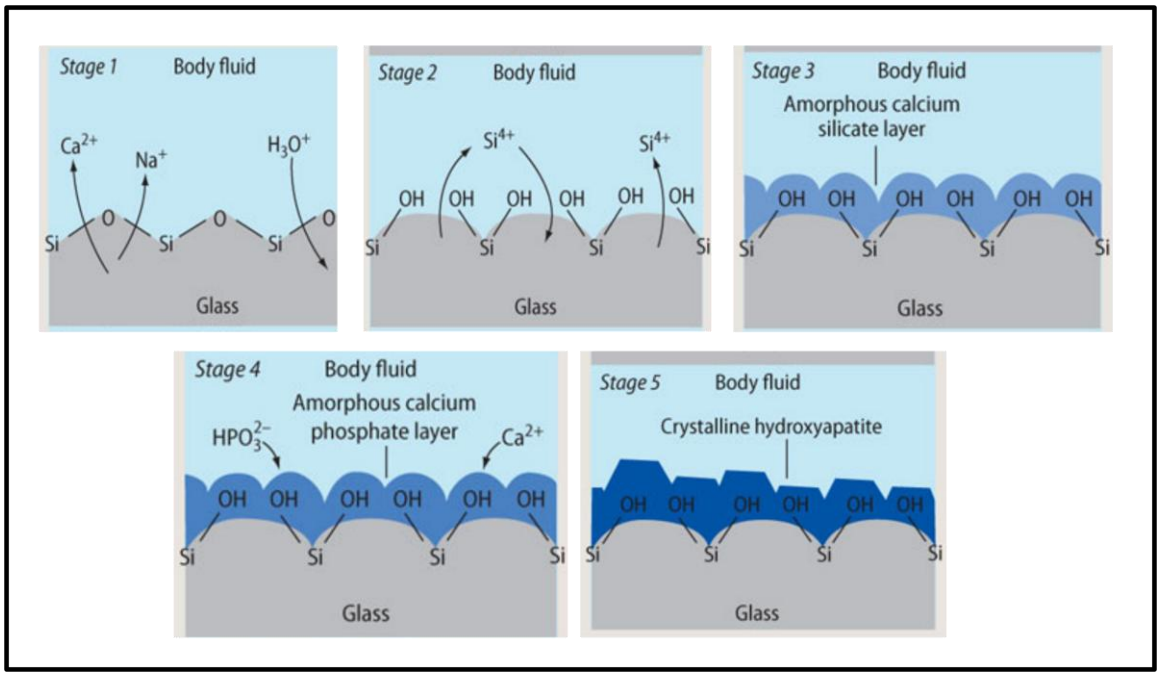

Figure 5: Bioactivity mechanisms in inorganic environment

The rate of development of the interfacial bond between implant and bone can be referred to as the level of bioactivity. Hench introduced an index (I_B) in order to measure the bioactivity level. The index is given by:

$$I_B = 100/t_{0.5bb}$$

where $t_{0.5bb}$ is the time for more than 50% of the implant interface to be bonded to bone.

1.3.3 Types of bioglasses

The generic name of glass is generally derived from its net work former. From the compositional aspect of glass, the glass structure is composed by the main oxide present in glass with various other oxides as dopants. In this section, some reported bioactive glasses and their structural components are introduced.

1.3.3.1 Silicate glasses

Commonly, the structure of silica-based bioactive glasses has been well characterized in terms of the arrangement of the SiO_4 coordination tetrahedron, a geometric unit in which a silicon atom, sitting in the center, is bonded to four oxygen atoms to form the four vertices of tetrahedron (figure 6).

The 45-S5 Bioglass (Na_2O-CaO-SiO_2-P_2O_5) is a silica-based composition, widely investigated and used in medical field as a bone regenerative material because of the deposition of a layer of hydroxy carbonate apatite (HCA) on the surface of the glass when immersed in body fluid. Cerruti et al [20] investigated the effect of pH and ionic strength on the reactivity of 45-S5 Bioglass. Results demonstrated that only at pH 8 a total reconstruction of the glass can be observed, with the formation of both a silica and a calcium phosphate rich layers. At higher pH, selective dissolution of the glass was hindered by the immediate precipitation of a layer of calcium phosphate, whereas at lower pH a total breakdown of the glass occurred and no calcium phosphate precipitation was noted.

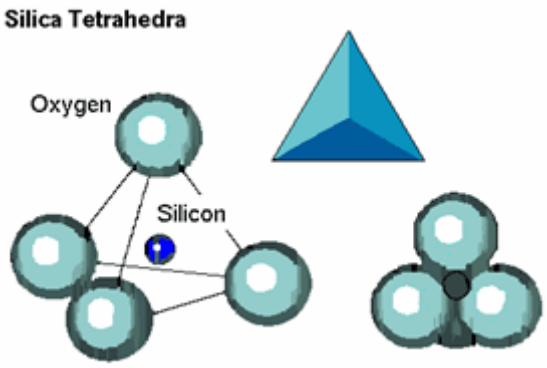

Figure 6: The form of single SiO_4 tetrahedron [21]

Recent findings showed that controlled release of the ionic dissolution products of bioactive glasses results in regeneration of tissues. In the research of Hench and co-workers [12], in the presence of critical concentrations of Si and Ca ions, within 48 h, osteoblasts, that are capable of differentiating into a mature osteocyte phenotype, begin to proliferate and regenerate new bone. Moreover, controlled release of soluble Ca and Si from bioactive glass-resorbable

polymer composites leads to vascularised soft tissue regeneration. Gene activation by controlled ion release provides the conceptual basis for molecular design of a third generation of biomaterials optimized for in situ tissue regeneration [22]. Other research showed that 45 S5 Bioglass exhibited an effect on promotion secretion of vascular endothelial growth factor in vitro [23].

Chen et al [24], synthesized 45-S5 Bioglass scaffolds by using the replication technique to obtain mechanically stable 3D scaffolds through a tailored sintering schedule and to assess the bioactivity and biodegradability of the scaffolds.

SCK (SiO_2-CaO-K_2O), another silicate glass, is Na_2O-free silica-based bioactive glasses and applied in making scaffolds in which the bioactivity phenomena involves H^+/K^+ exchange process [25]. The 13-93 glass (SiO_2-Na_2O-K_2O-MgO-CaO-P_2O_5) proposed by Fu et al. [26] remained amorphous even after heat-treatment confirmed from X-ray analysis.

Since silicon plays a significant role in bone mineralization along with gene activation, substitution of silicon for calcium into synthetic hydroxyapatites became an attractive area for many research groups [27].

1.3.3.2 Borate glasses

Bioactive borate glasses are a subset of the bioactive glass family that includes silicate, borate and phosphate glasses. In this case of bioactive borate glasses, the major glass former is B_2O_3 instead of SiO_2 or P_2O_5, and the compositions can include an array of alkali metal such as Li, Na, K etc and alkaline earth metal (Mg, Ca, Sr, Ba, etc) as well as transition-metal (Fe, Cu, Zn, Ag, Au) elements. The first borate glasses for biomedical application were proposed by Brink [28]. In order to get the desirable bioactive properties, the relative proportion of B_2O_3 was tailored.

Borate glasses are very reactive and have lower chemical durability, hence they convert more completely and rapidly to HA than their silica counterparts. The borate glasses, unlike silicate

glasses, form HCA (figure 7) directly on the surface of the underlying unreacted glass [29] without forming a borate-rich layer. The reason is that borate is readily soluble in body fluids. The degradation products of glass can be passed through the body naturally, predominantly through urine [30]. The complete degradation rate of the glasses can be controlled within a wide range of time periods by replacing silica with boron. In addition to this, the sintering behavior of borate/borosilicate glass is more controlled than silicate glasses. In vitro, borate glasses support cell proliferation along with differentiation while in vivo they are reported to enhance tissue infiltration [31].

However, $(BO_3)^{3-}$ ions are associated with a certain toxicity; in some reports, it indicate that certain compositions of borate glasses exhibited cytotoxicity under static conditions during in vitro culture testing, whereas non considerable toxicity was detected under more dynamic culture conditions [32-24].

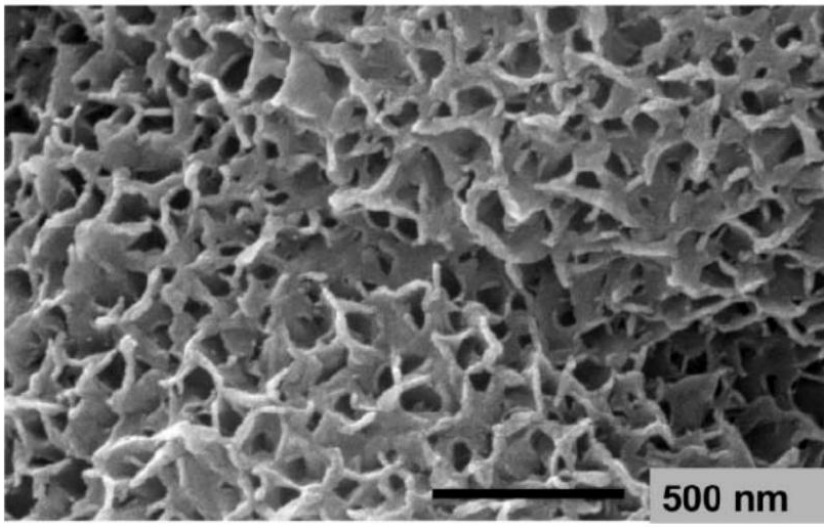

Figure 7: SEM image of HCA formed on borate glasses in vivo [29]

1.3.3.3 Phosphate glasses

Phosphate glasses, as the name suggests, consist of P_2O_5 as the network former oxide and were proposed in 1980. For instance, the composition of calcium phosphate glasses is similar to the mineral phase of bone and makes it an interesting material as a synthetic bone graft [35].

Same as silicate glasses, the structure of phosphate glass shows short-range order instead of any long-range order or significant symmetry of atomic arrangement. The basic unit in phosphate glass structure is the orthophosphate $(PO_4)^{3-}$ tetrahedron (figure 8a) with one phosphorus atom surrounded by four oxygen atoms. As one of the oxygen atoms is connected to the phosphorus atom by a double bond, the other three oxygen atoms can only act as bridges to other orthophosphate tetrahedral. In order to form the bridge, tetrahedral linked to each other by P-O-P bond (figure 8b). However, this tetrahedral is highly asymmetric in nature and this asymmetry results in low durability, along with the ease of P-O-P bonds hydration of phosphate glasses [36, 37].

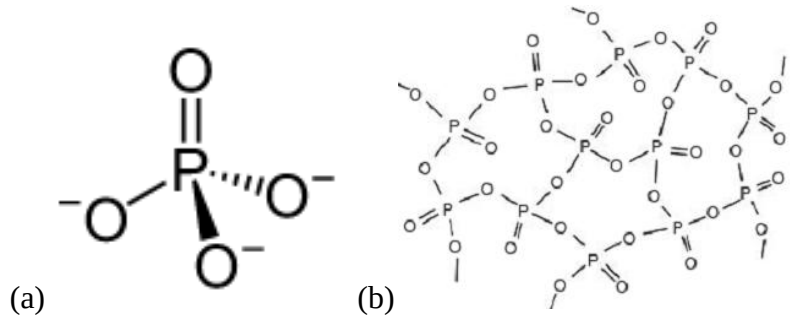

(a) (b)

Figure 8: (a) Basic phosphate tetrahedron in glass structure and (b) phosphate glass network [38]

The main reason why phosphate glasses are taken as great potential biomaterials is their ability to dissolve completely in aqueous solutions, releasing safe and non-toxic dissolution products. The dissolution rate of phosphate glasses strongly depends on the glass composition. For example, adding appropriate metal oxide, such as TiO_2, CuO, NiO, MnO, and Fe_2O_3 to the glass composition it is possible to tailor the dissolution rate effectively [39-43]. Moreover, the solubility is influenced by P_2O_5 content; lower P_2O_5 content presents lower solubility. Other factor like pH of the surrounding solution also affects glass dissolution. In an acidic environment, the dissolution of phosphate glass increased dramatically [36], while a basic pH also promotes glass dissolution although with a slower rate. On the other hand, during phosphate dissolution, pH of surrounding solution changes differently from silicate glasses. For instance, metaphosphate glasses tend to give an acidic pH, whereas pH increases towards neutral by decreasing phosphate content.

1.4 Magnetic biomaterials

Magnetism is known to all as the phenomenon by which some materials attract or repel other materials from a distance; examples of such materials include iron, lodestone and some steels. Magnetism, which is an intrinsic property of every atom, has a profound influence on living organisms. For instance, the hemoglobin in our blood is an iron complex and is magnetic in nature. There is now substantial evidence that all living organisms, including animals and humans, contain magnetic particles and act as magnetic receptors [44]. It is established that the magnetism and magnetic materials have a strong role to play in health care and biological applications [45-48]. In some early applications, magnetic materials were used for removal of metallic objects from the body of animals and humans [49]. In the last decades, research interests were focused on the use of materials in biological environment for implantation or for replacement of a part or a function of the body in a reliable and physiologically acceptable manner [50]. Recently, the use of magnetic micro and nano particles in the field of biology and biomaterials has been found useful in sophisticated biomedical applications such as cell separation, drug delivery as well as magnetic intracellular hyperthermia treatment of cancer. [51, 52] Moreover, the magnetically responsive microspheres were developed in vitro to direct the particle so that the remove bound cells and molecules and in vivo to target and hold the magnetic carriers at specific sites for protein and cell separation. In addition, the purification of bone marrow cells from tumor cells using immuno-magnetic beads is also applied in clinical therapy. The development of nano technology along with involvement of magnetism, opened new windows of sophisticated biomedical applications such as diagnostic, therapy and so on. [53]

1.4.1 Cancer and hyperthermia

Cancer is a term used for diseases in which abnormal cells divide without control and are able to invade other tissues (figure 9). Cancer cells can spread to various parts of the body through the blood and lymph systems. Cancer is not just one disease but it includes many diseases. There are more than 100 different types of cancer. Most cancers are named for the organ or type of cell in which they start.

Nowadays, cancer is the second leading cause of death following heart disease, accounting for 23% of all deaths per year. The threat from cancer raised great challenges to investigation and development of new methods for cancer treatment, diagnosis and prevention. Four standard methods are commonly employed for cancer treatment including surgery, chemotherapy, radiation therapy as well as immunotherapy and biologic therapy. However, as all of treatments present limitations and drawbacks, new strategies need to be developed.

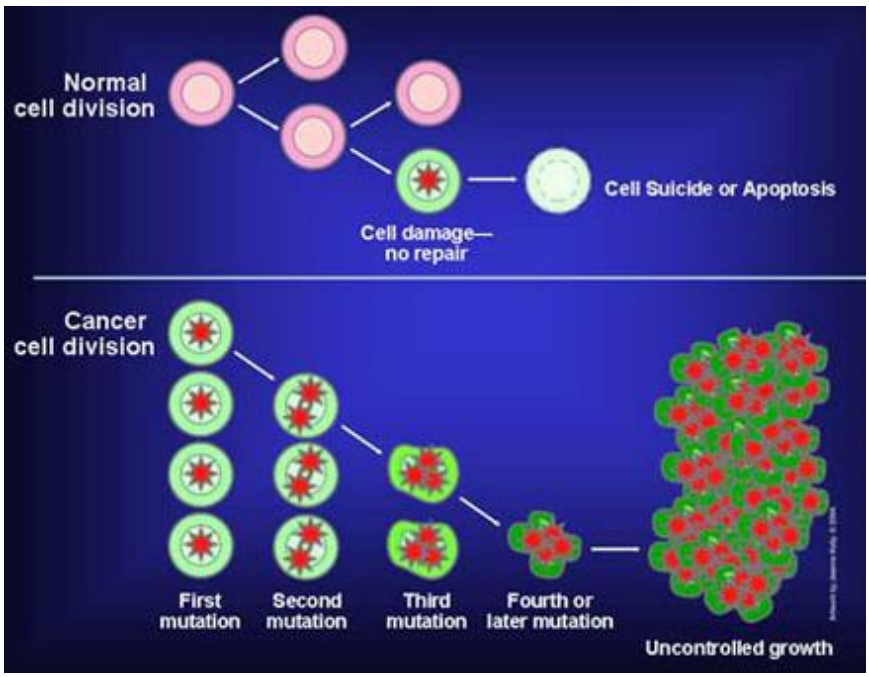

Figure 9: Normal cell division and cancer cell division [54]

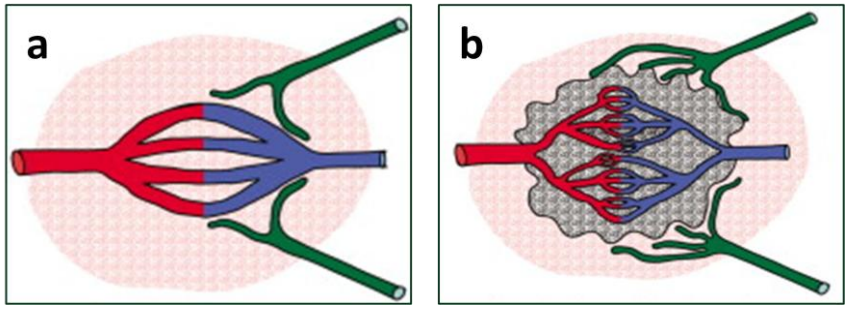

Figure 10: Vessels in (a) normal tissue and (b) tumor [56]

Hyperthermia (also called thermal therapy or thermotherapy) is a type of cancer treatment in which body tissue is exposed to controlled high temperatures (41-46 ^{o}C) in order to kill cancer cells or to make cancer cells more sensitive to the effects of radiation and certain anti-cancer drugs with minimal injury of normal tissues [55]. By killing cancer cells and

damaging proteins and structures within cells [56], hyperthermia may shrink tumors.

In normal tissues (figure 10a), during heating up to temperatures commonly used in clinical hyperthermia, the blood flow vastly increases and leading to an effective dissipation of heat. In contrast, at 41-42 ^{o}C, in most of the tumors (figure 10b) can lead to hemorrhage and cell damage because of a less efficient heat dissipation due to vascular occlusion and poorly organized blood vessels. The heat dissipation in the tumors is poor, particularly in the large tumors, due to the decrease in blood flow and vascular damage. Consequently, hyperthermia preferentially heats and causes greater damage in tumors than in normal tissues.

Hyperthermia is seldom applied alone but always used with other forms of cancer therapy such as radiation therapy and chemotherapy. Numerous clinical trials have investigated hyperthermia in combination with radiation therapy and/or chemotherapy on many types of cancer, such as head and neck, brain, lung, breast, bladder, rectum, liver etc. a certain of studies have shown a significant reduction in tumor size [57]. In current study, hyperthermia is performed in local, regional area and the whole body.

1.4.2 Categories of magnetic materials and factors affecting magnetic properties

On the basis of magnetic response, magnetic materials are classified as diamagnetic, paramagnetic and ferromagnetic materials (figure 11). Antiferromagnetism and ferrimagnetism fall within the broad category of ferromagnetism. Diamagnetism is very weak and not permanent; it persists only as long as the external field is present. It occurs due to a change in the orbital motion of electrons due to the external field; the direction of the induced magnetic moment is opposite to the field. In paramagnetism, each atom has a permanent dipole moment because of incomplete cancellation of its electron magnetic moments. Ferromagnetism is the most familiar type of magnetism. Ferromagnetic materials, unlike dia- and para-magnetic materials, show permanent magnetic moments even in the absence of an external field. Some materials, including the magnetic biomaterial magnetite (Fe_3O_4), exhibit ferrimagnetic behavior. Hexagonal ferrites and garnets are other ceramic materials that fall in this category. [58, 59]

Temperature will play an important role in determining magnetic properties, since entropy effects will be more dominant at high temperatures. The magnetic properties of both ferri- and ferro-magnets depend on the coupling forces between neighboring atoms; when temperatures are higher, entropy effects favor a random arrangement of spins, leading to a reduction in saturation magnetization. The saturation magnetization decreases with increasing temperature; at the Curie temperature T_c, it becomes zero and the material becomes paramagnetic above this temperature.

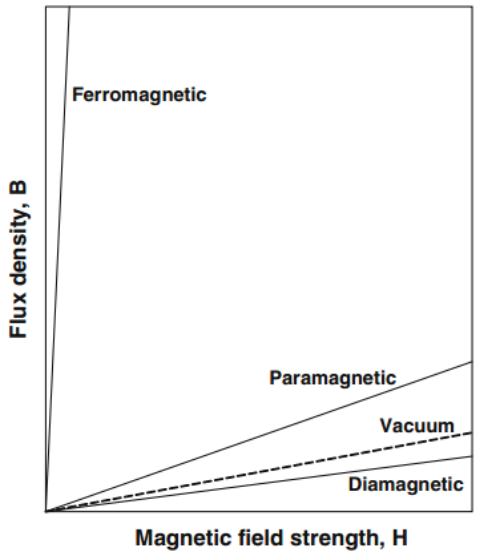

Figure 11: Schematic of the flux density B as a function of H for various materials [60]

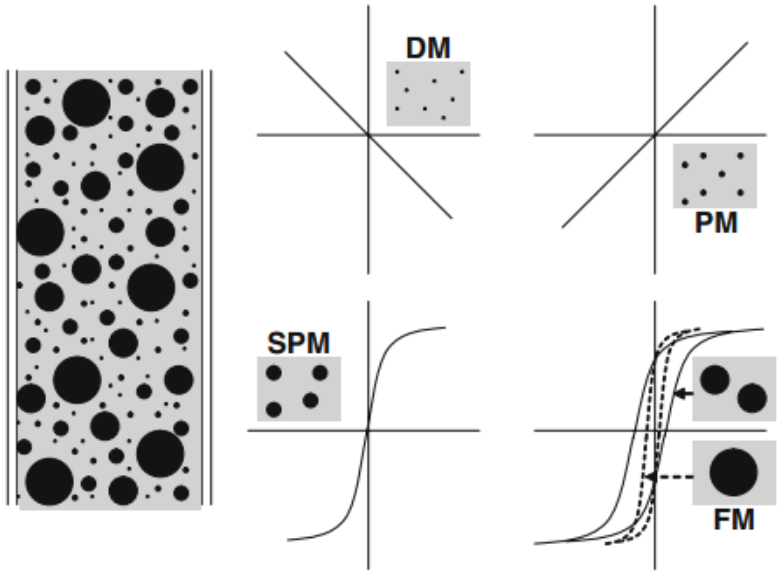

Figure 12: Magnetic properties are affected by the particle size (DM = diamagnetic, PM =

paramagnetic, SPM = superparamagnetic, FM =ferromagnetic) [60]

Manipulation of the magnetic properties can be performed by altering the composition, crystal structure, stress state and size of the material. Among these factors, size plays an important role in magnetic properties (figure 12). Large particles (greater than about 1 μm) with more magnetic domains which lead to a narrow hysteresis loop, are used in immunomagnetic separation of pathogenic microorganisms in microbiology. In drug delivery, gene delivery and hyperthermia, small magnetic particles are employed, since smaller particle sizes (less than about 1 μm) are energetically more favorable for only one domain to exist [60]. The response of such particles to a magnetic field is qualitatively different, resulting in a broader hysteresis loop. If the particle size is reduced further to about 20 nm, the material becomes superparamagnetic, which means that the magnetic moment of the particle fluctuates because of the thermal energy (~kT); at the atomic level the individual atomic moments continue to be ordered relative to each other.

1.4.3 Biomedical applications

1.4.3.1 Magnetic bioseparation

Bioseparation is an important phenomenon for the success of several biological processes. Magnetic separation of cells and biomolecules is based on the contrast of magnetic susceptibility between separand (magnetic) and medium (containing other nonmagnetic) materials. Magnetic bioseparation may be classified into two modes. For the first one, the separand may have sufficient intrinsic magnetic moment (e.g. red blood cells and magnetotactic bacteria) and can be directly separated by applying magnetic fields. For the other, the cells or biomolecules which are nonmagnetic in nature can be modified by attachment of magnetic responsive entity and thus can be manipulated using an external field. Entities that can be labeled include cells, bacteria and some types of vesicles. The first step is to label the entities with the particles followed by the separation of the labeled entities by magnetic separation (figure 13) [54]. This method has been applied to the selection of tumor cells from blood as well as to isolate enzymes, DNA and RNA from various sources including body fluids. Finely dispersed magnetic absorbent (ferro-carbon particle) has been used for

new methods of biological fluid detoxification. Magnetic bioseparation has been successfully used in the bioscience, biotechnology and biomedical fields, in both the laboratory and on a large scale.

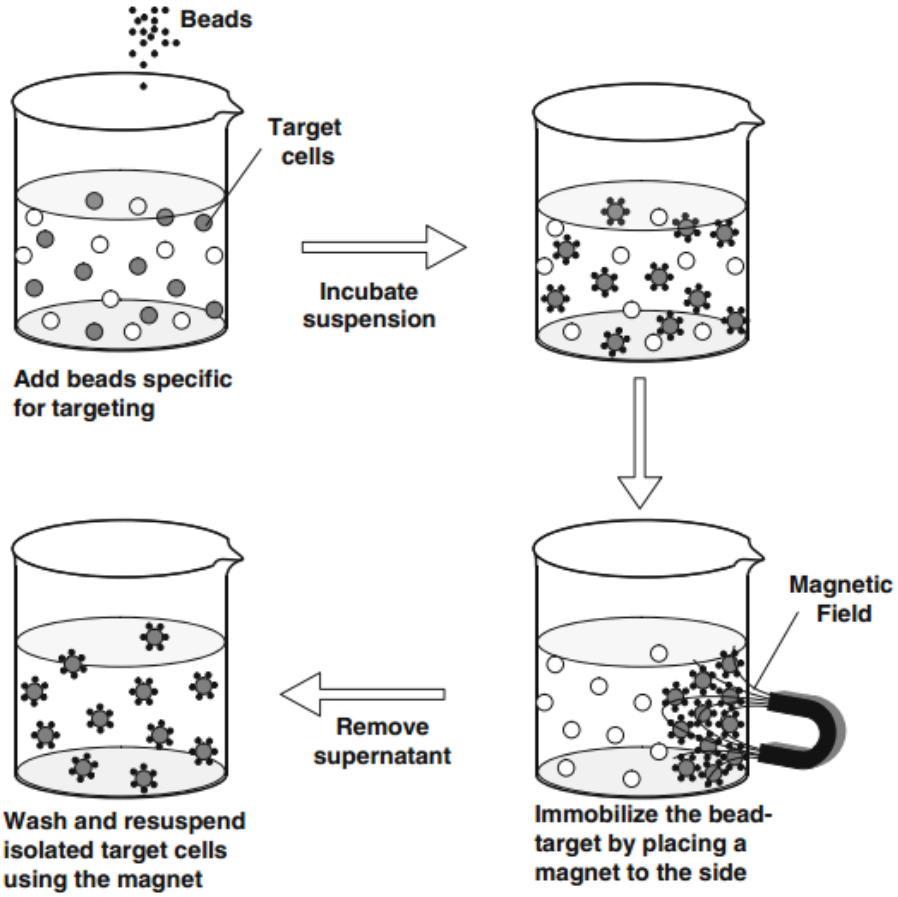

Figure 13: Magnetic separation [61]

1.4.3.2 Drug delivery

Since most methods of chemotherapy are relatively non-specific, they result in the waste of drug distributed to areas where they are not required with serious and undesirable side effects. The above problems may be solved by selectively and quantitatively accumulating the drug to the target site. Independent of the site and methods its administration, drug targeting at non-target sites should remain under certain minimum levels to avoid site reactions, whereas it should remain high at the disease sites. There are many different approaches to targeted drug delivery, e.g. direct application of drug into the affected zone, use of reactor molecules having high affinity to the affected site and physical targeting. Targeted drug delivery by

external physical force (magnetic field) is an innovative new approach, capable of effective drug targeting. [62]

1.4.3.3 Hyperthermia for treatment of cancer

Magnetic materials have been extensively used for hyperthermia of biological applications, based on the principle that the magnetization process determines the magnetic losses. These losses, depending upon the thermal conductivity and heat capacity of the surrounding medium, can be dissipated in the form of heat raising the temperature of the surrounding. The losses are of different kinds, which are determined both by the intrinsic and extrinsic properties and the particle sizes.

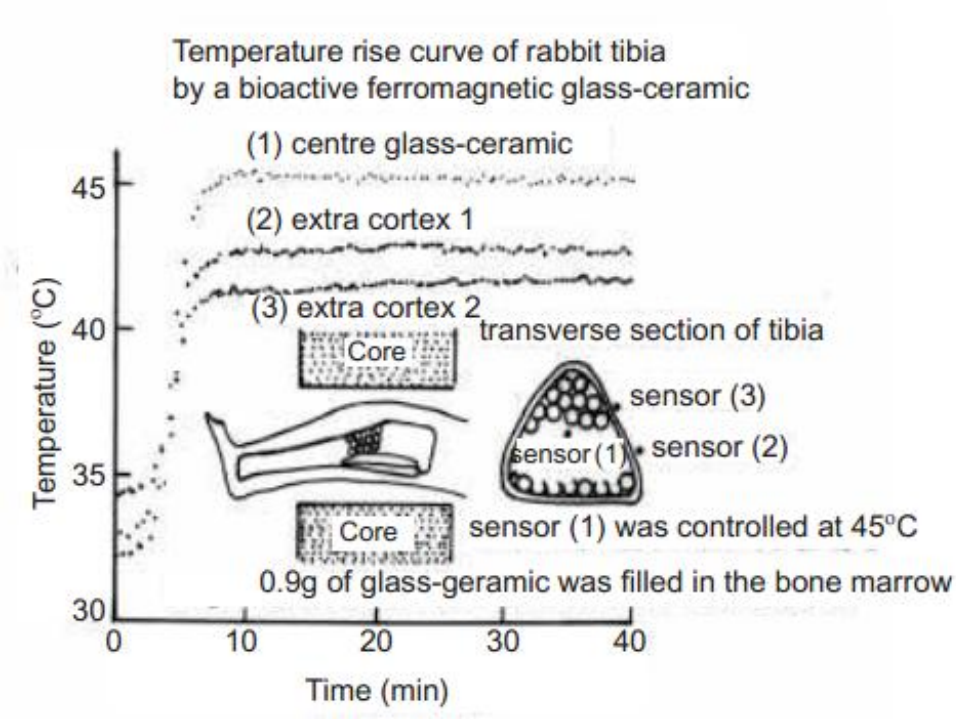

Figure 14: Schematic diagram showing bone heating and corresponding temperature rise [63]

Magnetic hyperthermia can be induced by two different methods. The first one is performed by surgically placing finite size magnetic implants within the tumor site, which absorbs energy from externally applied magnetic field and dissipates it in the form of heat to the surrounding tissue. The other one is to form bond on materials surface through the formation

of an apatite layer. In such a method, it is expected that temperature rise will be observed close to the implanted material and there will be non-uniformity in the temperature distribution in the tumor region. Figure 14 demonstrates a schematic diagram for application of alternating magnetic field to a bone packed with magnetic glass ceramics. The temperature of the glass ceramic and the outside of the bone is measured and reported in figure.

2 Surface functionalization

The properties of surface govern the behavior and overall performance of materials and therefore surface functionalization provide unique possibilities to control the subsequent surface interaction and biological response required for a particular application. Through tailoring material surfaces, a wide group of additional functionalities is enabled to overcome material deficiencies while maintaining its bulk properties. Hence, surface modification has become pivotal for academic research as well as industrial product development. Recently, numerous materials and commercial products with specific surface functionalities are readily available, and their usage in technical fields is potentially infinite. As a result, surface functionalization is considered of paramount importance for the development and design of new materials, as well as for prospective engineered systems [64, 65].

2.1 Functionalization routes

Multiple methods are used to modify material surfaces, which can be mechanical, physical, chemical, and biological (figure 15).

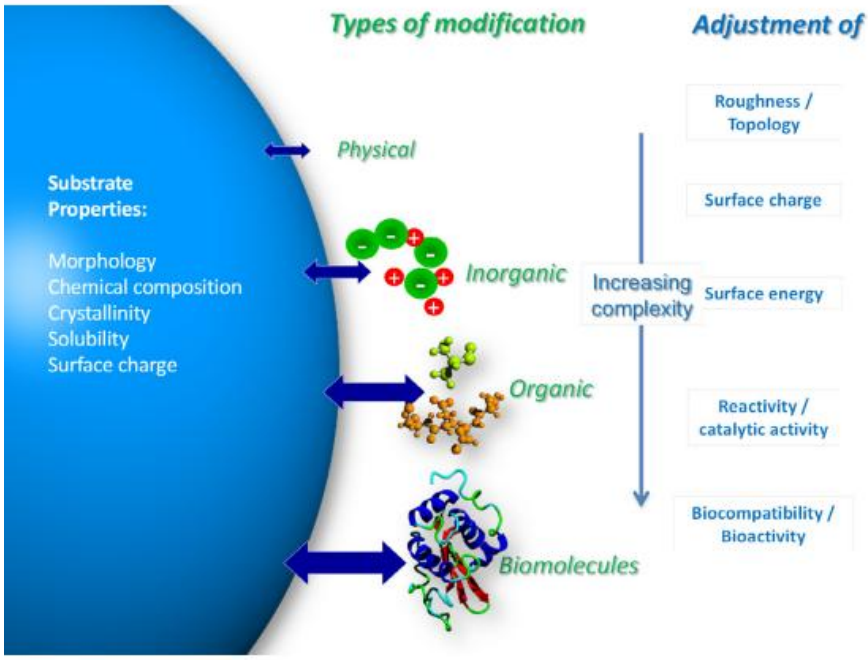

Figure 15: Substrate properties, modification routes and impact on material surface features [66].

2.1.1 Mechanical functionalization

Mechanical functionalization is any machining, polishing, etc., which provides the surface with a different but specific roughness, the structure or amplitude of which can optimize cell proliferation and cell adhesion [67, 68].

Polishing is used to remove small quantities of materials in order to obtain a desired smooth surface or a flat surface for following treatment. Usually mechanical polishing can be obtained by the use of SiC abrasive papers with decreasing grain size. The mechanical polishing can obtain mirror-like smooth surface with Ra of 0.1 μm [69]. In addition to this, electropolishing is also widely used for providing fine finishes with R < 10 nm [70].

It is reported that surface roughness alters osteoblast proliferation, differentiation, and matrix production in vitro. The implant surface roughness may play a role in determining phenotypic expression of cells in vivo [71]. Kieswetter et al. [72] found that substrate surface roughness influences growth factors and cytokine production of MG-63 osteoblast-like cells, suggesting that surface roughness can modulate the activity of cells interacting with an implant, and

therefore affect tissue healing and implant success.

2.1.2 Physical functionalization

Physical functionalization includes processes such as oxidation (i.e. passivation of metals and alloy), as well as any surface coating leading to a protection or activation. Multiple methods have been described [73-75]:

a) High temperature plasma sprays of Hydroxyapatite (HA), Tricalcium phosphate (TCP) or other metal oxides

b) chemical vapour deposition and cold vapour deposition (CVD)

c) Pulsed LASER Deposition (PL D)

d) Sol-gel deposits

e) Micro-arc oxidations

f) Hydrothermal treatments

g) Polyelectrolyte films and other electrochemical deposits

2.1.3 Chemical functionalization

Chemical functionalization consists mainly in the alteration of composition, energy and charge at the surface of a material. Popular methods for chemical modification are ion bombardment [76], treatment with acid or alkaline solutions [77, 78] and slurry-based techniques [79], as well as the attachment of organic functional groups to the material surface either by physisorption or covalent bonding [80].

The modification of inorganic substrates by anchoring organic molecules to the surfacec is a very powerful way to tailor surface properties, such as to control protein–material and cell-material interactions, to increase material biocompatibility and nanoparticle stabilization [81-83]. As for ceramic materials, surface functionalization through silanazation or poly (ethylene glycol) (PEG) is extensively investigated [84, 85]. Recently, organophosphorous

compounds are becoming of great interest as coupling agents for the surface modification of metal oxides by forming mono-, bi-, tri- or multidentate attachments with material surfaces which are very stable to hydrolysis over a large pH range and under physiological conditions. [86-88]. Figure 16 demonstrates the schematic diagram of silanization process on ceramic substrate.

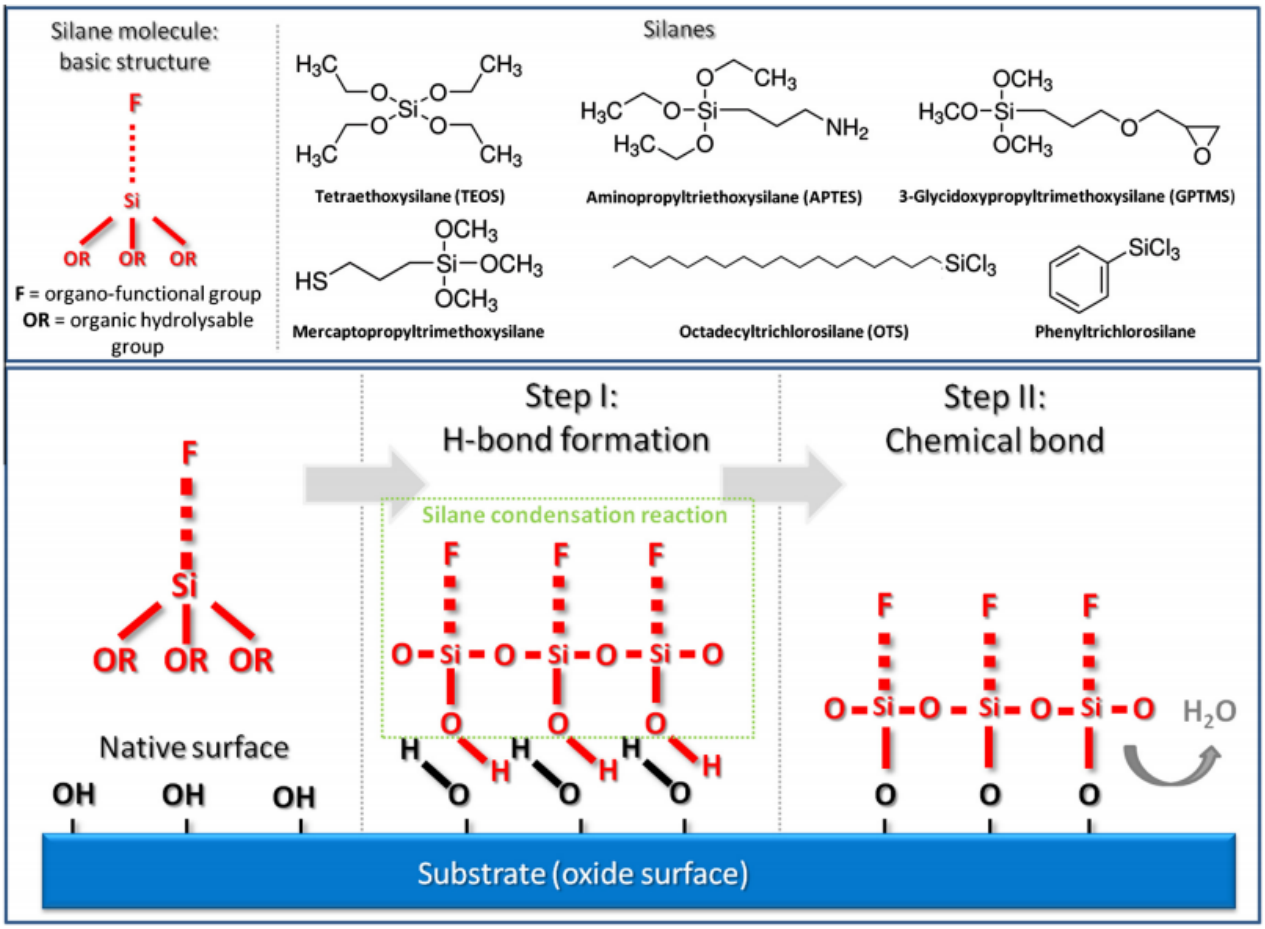

Figure 16: Silanization of ceramic surfaces [66].

Silanization is the most widely used technique to introduce surface functional groups on inorganic surfaces due to its straightforwardness, as it can be carried out at moderate temperatures, and no particular conditions or expensive equipments are required. Furthermore, it is applicable to any type of material and support, such as colloidal particles, porous materials, nanoporous membranes as well as 2-D planar surfaces [66]. In general, for surface silanization, silane molecules must first be activated (hydrolysed) and then condensation reactions occur between the Si–OH groups of the silanol and the OH groups of the surface, leading to the formation of a stable bond with the surface and the release of free alcohols as

side products.

Despite the wide variety of silane precursors available for surface modification, the majority of studies have employed aminosilanes, in particular 3-aminopropyltriethoxysilane (APTES). The popularity of APTES is related to its intrinsic chemical properties, since functional $–NH_2$ groups are employed to promote adhesion in glass–resin composites, for the attachment of negatively charged species (i.e. DNA and nanoparticles), or to promote and control biomolecular adhesion and enzyme stability, as well as cell adhesion and growth. [89-92]

2.1.4 Biological functionalization

Biological functionalization can be defined as the coupling of biological entities such as biomolecules, viruses, bacteria and cells and the material surfaces. Through this approach, unique properties and functionality of both the inorganic and biological entities are brought together to create an organic–inorganic hybrid material, often referred as ‘‘biohybrids’’ or ‘‘biodoped’’ materials [93]. The definition of biomolecular modification can be described as the attachment (immobilization) of molecules to a surface, resulting in reduction or loss of mobility. Numerous immobilization techniques have been developed based on three basic mechanisms: (i) physical, (ii) covalent and (iii) bioaffinity immobilization [94]. In this field, two principal concepts are considered: the molecule delivery (mainly drug delivery systems, DDS) and the molecule tight binding to the surface.

2.1.4.1 Functionalization with biomolecules by physisorption

Physical immobilization can be considered as the simplest functionalization method, it can be carried out by just immersing the material into a solution containing the target biomolecules. For highly porous substrates [95], this approach is the particularly suitable functionalization method. Physical immobilization is performed on the basis of electrostatic interactions, van der Waals forces, as well as hydrogen bonds and/or hydrophobic interactions. In general, physisorption can be used in combination with most types of surfaces. Furthermore, this approach is generally considered non-destructive and thus more suitable for preserving the

biological activity to be widely applied in, for instance, drug release purposes. Biomolecule immobilization methods based on physisorption, or more generally on non-covalent techniques, suffer from the problem of biomolecule leaching, and thus are often considered unsuitable for long-term or continuous usage [96].

2.1.4.2 Functionalization with biomolecules by covalent immobilization

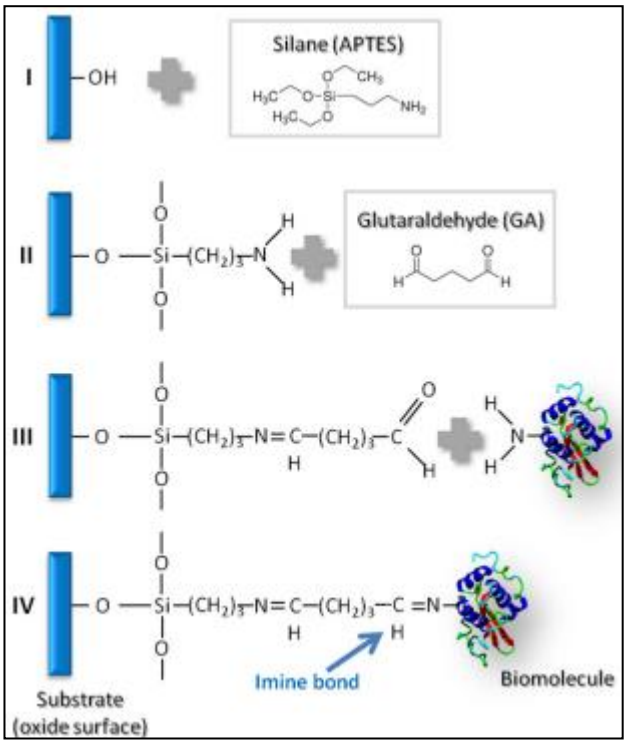

Figure 17: Covalent immobilization of biomolecules by glutaraldehyde (GA) [66]

Covalent immobilization of biomolecules on surfaces can improve the attachment to the material surface; they are particularly intended for enzyme immobilization due to the enhancement of enzyme stability or prevention of the enzyme from undergoing self-autolysis [97]. Covalent immobilization is potentially applicable to different materials and biomolecules. Recently researches have reported a range of applications of this approach: assay technologies, biosensors, medical imaging and therapy as well as biomaterials. The most common strategies for covalent immobilization of biomolecules are based on glutaraldehyde (GA) [98] or carbodiimide (EDC) [99] for immobilization of peptides, proteins and oligonucleotides [94]. Biomolecule attachment to inorganic carriers via glutaraldehyde (figure 17) is considered as the simplest coupling methods, through which

proteins, enzymes or amino-modified DNA molecules can be irreversibly immobilized on the activated surfaces via the covalent bond between the amino group on the biomolecule and the aldehyde [100]. The drawbacks are the potential toxicity, NPs cross-linking and aggregation [101].

2.2 Evaluation of modified surface

2.2.1 Characterization of modified surface

Since surface properties have a decisive effect on the applicability and efficiency of a material, an accurate and thorough analysis supported by an adequate set of different and complementary techniques is essential [102]. A comprehensive surface characterization must consider the evolution and changes of surface properties over time or in different environments. This is crucial for many systems, including NPs, biosensors, drug delivery systems and bioimplants, of which functionality and stability must be guaranteed for several days, months or years.

Analysis of surface topography and morphology is commonly carried out using microscopic methods [103]. Scanning electron microscopy (SEM) [104] and transmission electron microscopy (TEM) [105] can be taken as the standard methods for direct imaging and dimensional measurements in the range of hundreds of microns to the nanometer. For the measurement of large ensembles of particles yielding statistical results like size distributions, SEM and TEM investigations must be combined with other non-imaging techniques, such as dynamic light scattering, X-ray diffraction as well as and specific surface area analysis (Brunauer–Emmett–Teller, BET) [106-108]. Fluorescence and confocal microscopy are widely used for the simultaneous 2- and 3-D visualization of both material surfaces and biological components, such as biomolecules, cells and bacteria or tissues.

In order to obtain the information regarding the constituent elements, organic modifiers and chemical structure on the surface after modification, several standard spectroscopic methods such as energy-dispersive spectroscopy [109], secondary ion mass spectrometry [110],

induced coupled plasma spectroscopy (ICP) [111], infrared spectroscopy (IR) or attenuated total reflection Fourier transform infrared spectroscopy [112] and X-ray photoelectron spectroscopy (XPS) [113] are generally used. Thermal gravimetric analysis (TGV) [114] is widely applied in the study of interaction strength between the attached organic groups and the surface with increasing temperature.

In addition to the determination of surface functionalization, the characterization of the interaction of functionalized surfaces with the environment is necessary for drawing valuable conclusions on the surface characteristics and stability. It is popular to determine changes in surface charge after functionalization at a solid–liquid interface by means of electrokinetic analysis which is also used to determine the zeta potential and surface charge [115, 116], or to characterize the liquid phase adsorption processes as well as the interaction between surfaces and biomolecules [117].

Table 1 Characterization methods and techniques for detection of and quantification of organic surface modifiers [66].

Organic functional group	Method
Amino groups ($-NH_2$)	BET
	Chemical assay: (6-(2,4 dinitrophenyl)amino hexanoic acid succinimidyl ester)
	Chemical assay: picrate method
	Chemical assay: TNBS method (2,4,6-trinitrobenzenesulphonic acid)
	Fluorescence dye: fluorescamine
	Radiolabelling ([^{14}C] formaldehyde)
	TGA
	XPS
Carboxy groups (–COOH)	XPS
	TGA
	UV–Vis and gas chromatography
	NMR
	TGA
Hydroxyl groups (–OH)	Titration
	Water adsorption
	XPS
Phosphate groups ($-PO_3H_2$)	Chromatography
	Chemical assay: Ellmanns' reagent
Thiol groups (–SH)	NMR
	TGA
Functional groups (generic)	CHN-analysis

Organic surface compounds are analyzed and quantified with simply and cost-efficient methods which are usually colorimetric and fluorescence-based assays. Through the combination with ultraviolet–visible (UV–Vis) and fluorescent spectrometry, these assays are

able to perform a fast qualitative detection and a quantification of a wide range of reactive functional groups with high selectivity and good sensitivity. Some specific detection of amino, carboxy, hydroxyl, phosphate or thiol surface groups is listed in Table 1.

2.2.2 Biomolecule detection and activity of biofunctionalized surfaces

Determination of the quantity and conformation of biomolecules immobilized or adsorbed on a surface is still a great concern and fundamental to several applications, such as biomedical materials, drug delivery technologies, biosensors and imaging [118-120].

With the aim to measure the amount of adsorbed biomolecules, the depletion method, based on the decrease in biomolecule concentration in the solution after the solid surface has come into contact with the solution, is widely applied [121]. This approach is also widely employed for release studies and biomolecule concentration can be quantified by UV–Vis spectrometry [122] or by employing well-established colorimetric biochemical assays, such as the Lowry [123] and Bradford method [124]. The quantification of adsorbed biomolecules can be also performed by radioisotope-labelled proteins [120], which is a highly sensitive method used to study the competitive adsorption of various components of a mixture.

Direct measurement of the amount of a biomolecule on the surface can be performed by using several techniques, such as enzyme-linked immunosorbent assays (ELISAs) [120] and radio-labelling [120]. In situ measurements on planar surfaces can be conducted with a quartz crystal microbalance [120] or by optical methods, such as optical waveguide lightmode spectroscopy (OWLS) [119], ellipsometry [125] or total internal reflectance fluorescence [119].

2.2.3 In vitro and in vivo testing

In vitro and in vivo tests are considered powerful tools for screening the feasibility and functionality of devices. For functionalized, antibacterial materials, in vitro bacteria investigations are mainly aimed at determining bacteria viability by employing turbidity

measurements or agar-plate based tests (i.e. inhibition zone, diffusion test, colony-forming unit counting) [126-129]. Bacterial adhesion can be determined by microscopical methods, like SEM and/or fluorescence microscopy [130]. Moreover, specific fluorescence markers allow the simultaneous visualization and distinction between live and dead bacterial cells, and examine their interaction with material surfaces.

In vitro assays are in dispensable as initial screens for acute toxicity, acute toxicity, cytocompatibility, genotoxicity amd inflammatory responses, and are required prior to in vivo and clinical testing. During last decades, increasing interest is raised in the development of in vitro cell assays for the characterization of materials before their clinical use. Through cultivating cells on a material surface and monitoring their interaction with surface, sequences of events in vivo can be simulated and the material cytocompatibility and acute toxicity are able to be screened rapidly. According to material specific purposes, several parameters such as cell proliferation, activity, adhesion, inflammatory response and cellular uptake can be monitored. Microscopic techniques, like light microscopy fluorescence microscopy and electron microscopy are widely employed to simultaneously survey cell response, cell adhesion, particle uptake and localization, as well as material surface properties. Cell viability is typically evaluated with cell-type-specific markers. For instance, for bone cells, the activity and differentiation are measured with alkaline phosphatase (ALP)-based assays [131] or assessed with specific bone proteins like collagen, or osteogenic markers [132]. Bone cell mineralization capability can be determined by specific histological staining (i.e. von Kossa or alizarin red). For bone tissue engineering applications, bioactivity of a surface is often evaluated by examining the ability of apatite forming on its surface in a simulated body fluid (SBF) with ion concentrations nearly equal to those of human blood plasma. Kokubo et al. [133] concluded that examination of apatite formation in SBF is useful for predicting the in vivo bone bioactivity of a material, and the number of animals used in and the duration of animal experiments can be reduced remarkably by using this method. The ion concentration of SBFs and human blood plasma are reported in Table 2.

Table 2 Ion concentration of SBFs and human blood plasma [133]

	Ion concentration (mM)							
	Na^+	K^+	Mg^{2+}	Ca^{2+}	Cl^-	HCO_3^-	HPO_4^{2-}	SO_4^{2-}
Human blood plasma [15]	142.0	5.0	1.5	2.5	103.0	27.0	1.0	0.5
Original SBF	142.0	5.0	1.5	2.5	148.8	4.2	1.0	0
Corrected SBF (c-SBF)	142.0	5.0	1.5	2.5	147.8	4.2	1.0	0.5
Revised SBF (r-SBF)	142.0	5.0	1.5	2.5	103.0	27.0	1.0	0.5
Newly improved SBF (n-SBF)	142.0	5.0	1.5	2.5	103.0	4.2	1.0	0.5

After the initial in vitro screening, functionalized materials for biomedical applications must undergo in vivo testing prior to clinical use in humans. By means of in vivo testing, the performance of materials can be evaluated under real physiological conditions and physiological loading. Moreover, in vivo tests allow longer time evaluation of a material's behavior compared with in vitro testing. The in vivo material response and biocompatibility are typically assessed by histological examinations by means of different stains, such as haematoxylin–eosin, Masson's trichrome stain [134], Stevenel's Blue, Van Gieson's picrofuchsin [75] as well as toluidine blue [135] and so on.

References

[1] Ramakrishna S, Meyer J, Wintermantel E, et al. Biomedical applications of polymer-composite materials: A review. Comp Sci Tech 2001; 61:1189-1224

[2] Kaur G, Pandey OP, Singh K, et al. A review of bioactive glasses: Their structure, properties, fabrication, and apatite formation. Published online 2013 in Wiley Online Library (wileyonlinelibrary.com). DOI: 10.1002/jbm.a.34690

[3] Rawson H. Inorganic Glass-Forming Systems, Academic Press: London and New York, 1967

[4] Paul A. Chemistry of Glasses, Chapman and Hall: London and New York, 1990

[5] Mac Millan PW. Glass Ceramics, Academic Press: London and New York 1979; pp: 7-13

[6] http://apchemcyhs.wikispaces.com/A+Molecular+Comparison+of+Liquids+and+Solids

[7] http://courses.chem.psu.edu/chem112/materials/polymers.html

[8] Varshenya A. Fundamentals of inorganic glasses, Academic press: London and San Diego, 1994; pp: 15-17

[9] Kingery WD, Bowen HK, Uhlmann DR. Introduction to Ceramics, 2nd ed. John Wiley and Sons: New York, 1976

[10] Shelby JE. Introduction to Glass Science and Technology, 2 nd ed. The Royal Society of Chemistry: Cambridge, 2005

[11] Hench LL. Ceramics, glasses and glass-ceramics. In: Biomaterials Science: An Introduction to materials in medicine (Eds.: Ratner BD, Hoffman AS), Academic press: USA, 1996; pp: 73-77

[12] Hench LL, Splinter RJ, Greenlee TK, et al. Bonding mechanisms at the interface of ceramic prosthetic materials. J Biomed Mater Res 1971; 5 (6): 117-141

[13] Hench LL. Biomaterials: A forecast for the future. Biomaterials 1998;19: 1419-1423

[14] Kokubo T, Takadama H. How useful is SBF in predicting in vivo bone bioactivity? Biomaterials 2006; 27: 2907-2915

[15] Mikos AG, Temenoff JS. Formation of highly porous biodegrad-able scaffolds for tissue engineering. Electron J Biotechnol 2000;3:114-119

[16] Levenberg S, Langer R. Advances in tissue engineering. Curr Top Dev Biol 2004;61:113-134

[17] Hench LL, Andersson Ö. Bioactive glasses. In: An Introduction to Bioceramics (Eds.: Hench LL, Wilsom J), World Scientific publishing: London, River Edge, 1999; pp: 41-63

[18] http://en.wikipedia.org/wiki/Forest_glass

[19]http://www.ndt-ed.org/EducationResources/CommunityCollege/Materials/Structure/solidstate.htm

[20] Cerruti M, Greenspan D, Powers K. Effect of pH and ionic strength on the reactivity of Bioglass® 45S5. Biomaterials 2005; 26: 1665-1674

[22] Hench LL, Xynos ID, Polak JM. Bioactive glasses for in situ tissue regeneration. J Biomater Sci 2004; 15 (4): 543-562

[23] Day RM, Boccaccini AR, Shurey S, et al. Assessment of polyglycolic acid mesh and bioactive glass for soft tissue engineering scaffolds. Biomaterials 2004; 25: 5857-5866

[24] Qizhi Z. Chen QZ, Thompson ID, et al. 45S5 Bioglass®-derived glass-ceramic scaffolds for bone tissue engineering. Biomaterials 2006; 27: 2414-2425

[25] Vitale-Brovarone C, Verne E, Appendino P. Macroporous bioactive glass-ceramic scaffolds for tissue engineering. J Mater Sci Mater Med 2006; 17: 1069-1078

[26] Fu Q, Rahaman MN, Bal BS, et al. Mechanical and in vitro performance of 13-93 bioactive glass scaffolds prepared by a polymer foam replication technique. Acta Biomater 2008; 4: 1854-1864

[27] Xynos ID, Edgar AJ, Buttery LDK, et al. Ionic products of bioactive glass dissolution increase proliferation of human osteoblasts and induce insulin-like growth factor II mRNA expression and protein synthesis. Biochem Biophys Res Commun 2000; 276: 461-465

[28] Brink M. The influence of alkali and alkali earths on the working range for bioactive glasses. J Biomed Mater Res 1997; 36: 109-117

[29] Marion NW, Liang W, Reilly G, et al. Borate glass supports the in vitro osteogenic differentiation of human mesenchymal stem cells. Mech adv mater struc 2005; 12: 1-8

[30] Gorustovich AA, Steimetz T, Nielsen FH, et al. A histomophometric study of alverolar bone modeling and remodeling in mice fed a poron-deficient diet. Arch oral biol 2008; 53: 677-682

[31] Vitale-Brovarone C, Miola M, Balagna C, et al. 3D-glass-ceramic scaffolds with antibacterial properties for bone grafting. Chem Eng J 2008; 137: 129-136

[32] Yao A, Wang D, Huang W, et al. In vitro bioactive characteristics of borate-based glasses with controllable degradation behavior. J Am Ceram Soc 2007; 90: 303-306

[33] Huang WH, Day DE, Kittiratanapiboon K, et al. Kinetics and mechanisms of the conversion of silicate (45-S5), borate, and borosilicate glasses to hydroxyapatite in dilute phosphate solutions. J Mater Sci Mater Med 2006; 17: 583-596

[34] Zhang X, Jia W, Gua Y, et al. Teicoplanin-loaded borate bioactive glass implants for treating chronic bone infection in a rabbit tibia osteomyelitis model. Biomaterials 2010; 31: 5865-5874

[35] Knowles JC. Phosphate based glasses for biomedical applications. J mater chem, 2003; 13: 2395-2401

[36] Bunker BC, Arnold GW, Wilder JA. Phosphate glass dissolution in aqueous solutions. J Non-Cryst Solids 1984; 64: 291-316

[37] Gao H, Tan T, Wang D. Dissolution mechanism and release kinetics of phosphate controlled release glasses in aqueous medium. J Controlled Release 2004; 96: 29-36

[38] Brauer DS. Phosphate glasses. In: Bio-Glasses : An Introduction (Eds.: Julian J, Clare AG), John Wiely and sons press, 2012; pp: 45-47

[39] Abou Neel EA, Mizoguchi T, Ito M, et al. In vitro bioactivity and gene expression by cells cultured on titanium dioxide doped phosphate-based glasses. Biomaterials 2007; 28: 2967-2977

[40] Abou Neel EA, Knowles JC. Physical and biocompatibility studies of novel titanium dioxide doped phosphate-based glasses for bone tissue engineering applications. J Mater Sci Mater Med 2008; 19: 377-386

[41] Abou Neel EA, Ahmed I, Pratten J, et al. Characterisation of antibacterial copper releasing degradable phosphate glass fibres. Biomaterials 2005; 26: 2247-2254

[42] Ahmed I, Collins CA, Lewis MP, et al. Processing, characterisation and biocompatibility of iron-phosphate glass fibres for tissue engineering. Biomaterials 2004; 25: 3223-3232

[43] Abou Neel EA, Ahmed I, Blaker JJ, et al. Effect of iron on the surface, degradation and ion release properties of phosphate-based glass fibers. Acta Biomater 2005; 1: 553-563

[44] Hafeli U. The mystery and history of magnetism. In: Scientific and clinical applications of magnetic carriers (Eds.: Häfeli U, Schütt W, Teller J, Zborowski M), Plenum: New York and London, 1997; pp: 1-8

[45] Gruttner C, Rudershausen S, Teller J. Improved properties of magnetic particles by combination of different polymer materials as particle matrix. J Magn Magn Mater 2001; 225: 1-7

[46] Mykhaylyk O, Cherchenko A, Ilkin A, et al. Glial brain tumor targeting of magnetite nanoparticles in rats. J Magn Magn Mater 2001; 225: 241-247

[47] Kim DK, Zhang Y, Kehr J, et al. Characterization and MRI study of surfactant-coated superparamagnetic nanoparticles administered into the rat brain. J Magn Magn Mater 2001; 225: 256-261

[48] Poeckley-Schoeniger C, Koepke J, Gueckel F, et al. MRI with superparamagnetic iron oxide: efficacy in the detection and characterization of focal hepatic lesions. Magn Reson Imag 1999; 17: 383-392

[49] Häfeli UO. The history of magnetism of medicine. In: Magnetism in medicine (Eds: Andrä W, Novak H), John Wiley and Sons: Berlin, 2007; pp: 3-22

[50] Chatterjee J, Haik Y, Chen CJ. Modification and characterization of polystyrene based magnetic microspheres and its comparison with albumin based magnetic microspheres. J Magn Mag. Mater 2001; 225: 21-29

[51] Andrä W, Novak H. Magnetism in medicine (Hand book), John Wiley and Sons: Berlin, 1998

[52] Jordan A, Wust P, Scholz R, et al. cellular uptake of magnetic fluid particles and their effects on human adenocacinoma cells exposed to AC magnetic fields in vitro. Int J Hyperthermia 1996; 12: 705-722

[53] Olsvik-O, Popovic T, Skjerve E, et al. Magnetic separation techniques in diagnostic microbiology. Clin Microbiol Rev 1994; 7: 43-54

[54] http://www.cancer.gov/cancertopics/cancerlibrary/what-is-cancer

[55] Van der Zee J. Heating the patient: a promising approach? Ann Oncol 2002; 13(8):1173-1184

[56] Alitalo K, Carmeliet P. Molecular mechanisms of lymphangiogenesis in health and disease. Cancer cell 2002; 1: 219-227

[57] Wust P, Hildebrandt B, Sreenivasa G, et al. Hyperthermia in combined treatment of cancer.

Lancet Oncol 2002; 3(8):487-497

[58] Callister WD. Materials Science and Engineering, Wiley: New York, 2003

[59] Ramanujan RV. Magnetic Particles for Biomedical Applications. In: Biomedical Materials (Ed: Narayan R). Springer Science Business Media: USA, 2009; pp: 477-491

[60] Pankhurst QA, Connolly J, Jones SK, et al. Applications of magnetic nanoparticles in biomedicine. J Phys D Appl Phys 2003; 36: 167-181

[61] Tartaj P, del Puerto Morales M, Veintemillas-Verdaguer S, et al. The preparation of magnetic nanoparticles for applications in biomedicine. J Phys D: Appl Phys 2003; 36: 182-197

[62] Kuznetsov AA, Filippov VI, Kuznetsov OA et al. New ferro-carbon adsorbents for magnetically guided transport of anti-cancer drugs. J Magn Magn Mater 1999; 194: 22-30

[63] Giri J, Ray A, Sriharsha T, et al. Proc. 14th MRSI Annual Meeting, Hyderabad, 2002

[64] Castner DG, Ratner BD. Biomedical surface science: foundations to frontiers. Surf Sci 2002; 500: 28-60

[65] Kingshott P, Andersson G, McArthur SL, et al. Surface modification and chemical surface analysis of biomaterials. Curr Opin Chem Biol 2011; 15: 667-76

[66] Treccani L, Klein TY, Meder F, et al. Functionalized ceramics for biomedical, biotechnological and environmental applications. Acta Biomater 2013; 9: 7115-7150

[67] Ratner BD, Hoffman AS, Schoen FJ, et al. Biomaterials science: introduction to materials in medicine. Academic Press: San Diego, CA, 1996

[68] Linez-Bataillon P, Monchau F, Bigerelle M, et al. In citro MC3T3 osteoblast adhesion with respect to surface ruoughness of Ti6A14V substrates. Biomol Eng 2002; 19: 133-141

[69] Larsson C, Thomsen P, Lausmaa J, et al. Bone response to surface-modified titanium implants-studies on electropolished implants with different oxide thicknesses and morphology. Biomaterials 1994; 15(13): 1062-1074

[70] Lausmaa J. Mechanical, Thermal, Chemical and Electrochemical Surface Treatment of Titanium. In: Titanium Medicine, Springer-Verlag: Berlin, 2001; pp: 232-258

[71] Martin JY, Schwartz Z, Hummert TW, et al. Effect of titanium surface-roughness on proliferation, differentiation, and protein-synthesis of human osteoblast-like cells (MG63). J Biomed Mater Res 1995; 29(3): 389-401

[72] Kieswetter K, Schwartz Z, Hummert TW et al., Surface roughness modulates the local production of growth factors and cytokines by osteoblast-like MG-63 cells. J Biomed Mater Res 1996; 32(1): 55-63

[73] Breme J, Eisenbarth E, Hildebrand HF. Calcium phosphate materials fundamentals. Sauramps-médical, Montpellier, ISBN: 2-84023-173-5, 1998; 139

[74] Zhang YM, Bataillon-Linez P, Huang P, et al. Surface analyses of micro-arc oxidized and hydrothermally treated titanium and effect on osteoblast behavior. J Biomed Mater Res 2004; 68A: 383-391

[75] Hamadouche M, Meunier A, Greenspan DC, et al. Bioactivity of sol-gel bioactive glass coated alumina implants. J Biomed Mater Res 2000; 52: 422-429

[76] Yokoyama Y, Tsukamoto T, Kobayashi T, et al. The changes of cell adhesion to collagen-coated Al_2O_3 by ion bombardment. Surf Coat Technol 2005; 196: 298-302

[77] Zhao X, Liu X, Ding C. Acid-induced bioactive titania surface. J Biomed Mater Res, A 2005;75:888-894 .

[78] Faga MG, Valle'e A, Bellosi A, et al. Chemical treatment on alumina-zirconia composites inducing apatite formation with maintained mechanical properties. J Eur Ceram Soc 2012; 32: 2113-2120

[79] Wang Z, Xue D, Chen X, et al. Mechanical and biomedical properties of hydroxyapatite-based gradient coating on [alpha]-Al_2O_3 ceramic substrate. J Non-Cryst Solids 2005; 351:1675-1681

[80] Neouze MA, Schubert U. Surface modification and functionalization of metal and metal oxide nanoparticles by organic ligands. Monatsh Chem 2008; 139: 183-195

[81] Comas H, Laporte V, Borcard F, et al. Surface functionalization of alumina ceramic foams with organic ligands. ACS Appl Mater Interfaces 2012; 4: 573-576

[82] Pei J, Hall H, Spencer ND. The role of plasma proteins in cell adhesion to PEG surface-density-gradient- modified titanium oxide. Biomaterials 2011; 32: 8968–8978

[83] Sperling RA, Parak WJ. Surface modification, functionalization and bioconjugation of colloidal inorganic nanoparticles. Philos Transact A Math Phys Eng Sci 2010; 368: 1333-1383

[84] Kohler N, Fryxell GE, Zhang MQ. A bifunctional poly (ethylene glycol) silane immobilized on metallic oxide-based nanoparticles for conjugation with cell targeting agents. J Am Chem Soc 2004; 126: 7206-7211

[85] Zhang MZ, Ishii A, Nishiyama N, et al. PEGylated calcium phosphate nanocomposites as smart environment-sensitive carriers for siRNA delivery. Adv Mater 2009; 21: 3520-3525

[86] Pawsey S, Yach K, Reven L. Self-assembly of carboxyalkylphosphonic acids on metal oxide powders. Langmuir 2002; 18: 5205-5212

[87] Adden N, Gamble LJ, Castner DG, et al. Phosphonic acid monolayers for binding of bioactive molecules to titanium surfaces. Langmuir 2006; 22: 8197-8204

[88] Iafisco M, Palazzo B, Falini G, et al. Adsorption and conformational change of myoglobin on biomimetic hydroxyapatite nanocrystals functionalized with alendronate. Langmuir 2008; 24: 4924-4930

[89] Schickle K, Kaufmann R, Duarte Campos DF, et al. Towards osseointegration of bioinert ceramics: introducing functional groups to alumina surface by tailored self assembled monolayer technique. J Eur Ceram Soc 2012; 32: 3063-3071

[90] Yang CL, Cheng K, Weng WJ, et al. Immobilization of RGD peptide on HA coating through a chemical bonding approach. J Mater Sci-Mater M 2009; 20: 2349-2352

[91] Laurent S, Forge D, Port M, Roch A, Robic C, Vander Elst L, et al. Magnetic iron oxide nanoparticles: synthesis, stabilization, vectorization, physicochemical characterizations, and

biological applications. Chem Rev 2008; 108: 2064-2110.

[92] Zhu MJ, Lerum MZ, Chen W. How to prepare reproducible, homogeneous, and hydrolytically stable aminosilane-derived layers on silica. Langmuir 2012; 28: 416-423

[93] Ruiz-Hitzky E, Ariga K, Lvov YM. Bio-inorganic hybrid nanomaterials: strategies, syntheses, characterization and applications. Wiley-VCH Verlag: Weinheim, 2008

[94] Hermanson GT. Bioconjugate techniques (2nd ed.). Academic Press: New York, 2008

[95] Mura S, Greppi G, Roggio AM, et al. Polypeptide binding to mesostructured titania films. Micropor Mesopor Mater 2011; 142: 1-6

[96] Sassolas A, Blum LJ, Leca-Bouvier BD. Immobilization strategies to develop enzymatic biosensors. Biotechnol Adv 2012; 30: 489-510

[97] Ota S, Miyazaki S, Matsuoka H, et al. High-throughput protein digestion by trypsin-immobilized monolithic silica with pipette-tip formula. J Biochem Biophys Methods 2007; 70: 57-62

[98] Galliker P, Hommes G, Schlosser D, et al. Laccase-modified silica nanoparticles efficiently catalyze the transformation of phenolic compounds. J Colloid Interface Sci 2010; 349: 98-105

[99] Schuessele A, Mayr H, Tessmar J, et al. Enhanced bone morphogenetic protein-2 performance on hydroxyapatite ceramic surfaces. J Biomed Mater Res Part A 2009; 90: 959-971

[100] Stamov DR, Nguyen TAK, Evans HM, et al. The impact of heparin intercalation at specific binding sites in telopeptide-free collagen type I fibrils. Biomaterials 2011; 32: 7444-7453

[101] Kim WJ, Kim S, Lee BS, et al. Enhanced protein immobilization efficiency on a TiO_2 surface modified with a hydroxyl functional group. Langmuir 2009; 25: 11692-11697

[102] Castner DG, Guldberg RE. Imaging techniques for biomaterials characterization. Biomaterials 2007; 28: 2379

[103] LearySwan EE, Popat KC, Desai TA. Peptide-immobilized nanoporous alumina membranes for enhanced osteoblast adhesion. Biomaterials 2005; 26: 1969-1976

[104] Kroll S, Treccani L, Rezwan K, et al. Development and characterisation of functionalised ceramic microtubes for bacteria filtration. J Membr Sci 2010; 365: 447-455

[105] Hong RY, Feng B, Chen LL, et al. Synthesis, characterization and MRI application of dextran-coated Fe_3O_4 magnetic nanoparticles. Biochem Eng J 2008; 42: 290-300

[106] Kozlova D, Chernousova S, Knuschke T, et al. Cell targeting by antibody-functionalized calcium phosphate nanoparticles. J Mater Chem 2012; 22: 396-404

[107] Bose S, Tarafder S. Calcium phosphate ceramic systems in growth factor and drug delivery for bone tissue engineering: a review. Acta Biomater 2012; 8: 1401-1421

[108] Daberkow T, Meder F, Treccani L, et al. Fluorescence labeling of colloidal core-shell particles with defined isoelectric points for in vitro studies. Acta Biomater 2012; 8: 720-727

[109] Wu W, He QG, Chen H, et al. Sonochemical synthesis, structure and magnetic properties of air-stable Fe_3O_4/Au nanoparticles. Nanotechnology 2007; 18: 145609

[110] Gu HW, Xu KM, Yang ZM, et al. Synthesis and cellular uptake of porphyrin decorated iron oxide nanoparticles - a potential candidate for bimodal anticancer therapy. Chem Commun 2005; 41: 4270-4272

[111] Lam KF, Kassab H, Pera-Titus M, et al. MCM-41 "LUS": alumina tubular membranes for metal separation in aqueous solution. J Phys Chem C 2010; 115: 176-187

[112] Rovira-Bru M, Giralt F, Cohen Y. Protein adsorption onto zirconia modified with terminally grafted polyvinylpyrrolidone. J Colloid Interface Sci 2001; 235: 70-79

[113] Dehestani M, Ilver L, Adolfsson E. Enhancing the bioactivity of zirconia and zirconia composites by surface modification. J Biomed Mater Res Part B 2012; 100: 832-840

[114] Yu MK, Park J, Jon S. Targeting strategies for multifunctional nanoparticles in cancer imaging and therapy. Theranostics 2012; 2: 3-44

[115] Ashley CE, Carnes EC, Epler KE, et al. Delivery of small interfering RNA by peptide-targeted mesoporous silica nanoparticle-supported lipid bilayers. ACS Nano 2012; 6: 2174-2188

[116] Namgung R, Zhang Y, Fang QL, et al. Multifunctional silica nanotubes for dual-modality gene delivery and MR imaging. Biomaterials 2011; 32: 3042-3052

[117] Talbert JN, Goddard JM. Enzymes on material surfaces. Colloids Surf B 2012; 93: 8-19

[118] Tanvir S, Pantigny J, Morandat S, et al. Development of immobilization technique for liver microsomes. Colloids Surf B 2009; 68: 178-188

[119] Gray JJ. The interaction of proteins with solid surfaces. Curr Opin Struct Biol 2004; 14: 110-115

[120] Nakanishi K, Sakiyama T, Imamura K. On the adsorption of proteins on solid surfaces, a common but very complicated phenomenon. J Biosci Bioeng 2001; 91: 233-244

[121] Meder F, Brandes C, Treccani L, et al. Controlling protein-particle adsorption by surface tailoring colloidal alumina particles with sulfonate groups. Acta Biomater 2013; 9: 5780-5787

[122] Meder F, Daberkow T, Treccani L, Wilhelm M, et al. Protein adsorption on colloidal alumina particles functionalized with amino, carboxyl, sulfonate and phosphate groups. Acta Biomater 2012; 8: 1221-1229

[123] Tanvir S, Morandat S, Frederic N, et al. Activity of immobilized rat hepatic microsomal CYP2E1 using alumina membrane as a support. New Biotechnol 2009; 26: 222-228

[124] Mueller B, Zacharias M, Rezwan K. Bovine serum albumin and lysozyme adsorption on calcium phosphate particles. Adv Eng Mater 2010; 12 B: 53-61

[125] Hartono SB, Gu W, Kleitz F, et al. Poly l-lysine functionalized large pore cubic mesostructured silica nanoparticles as biocompatible carriers for gene delivery. ACS Nano 2012; 6: 2104-2117

[126] LingFeng Q, NamKim T, Wu J, et al. Antibacterial effects of Ag-HAp thin films on alumina substrates. Thin Solid Films 1998; 335: 214-219

[127] Hetrick EM, Shin JH, Stasko NA, et al. Bactericidal efficacy of nitric oxide-releasing silica nanoparticles. ACS Nano 2008; 2: 235-246

[128] Okada M, Yasuda S, Kimura T, et al. Optimization of amino group density on surfaces of titanium dioxide nanoparticles covalently bonded to a silicone substrate for antibacterial and cell adhesion activities. J Biomed Mater Res, Part A 2006; 76: 95-101

[129] Sabbani S, Gallego-Perez D, Nagy A, et al. Synthesis of silver-zeolite films on micropatterned porous alumina and its application as an antimicrobial substrate. Micropor Mesopor Mater 2010; 135: 131-136

[130] Statz AR, Park JP, Chongsiriwatana NP, et al. Surface-immobilised antimicrobial peptoids. Biofouling 2008; 24: 439-448

[131] Lozano D, Manzano M, Doadrio JC, et al. Osteostatin-loaded bioceramics stimulate osteoblastic growth and differentiation. Acta Biomater 2010; 6: 797-803

[132] Panzavolta S, Torricelli P, Bracci B, et al. Functionalization of biomimetic calcium phosphate bone cements with alendronate. J Inorg Biochem 2010; 104: 1099-1106

[133] Kokubo T, Takadama H. How useful is SBF in predicting in vivo bone bioactivity? Biomaterials, 2006; 27: 2907-2915

[134] Trejo CG, Lozano D, Manzano M, et al. The osteoinductive properties of mesoporous silicate coated with osteostatin in a rabbit femur cavity defect model. Biomaterials 2010; 31: 8564-8573

[135] Wieneke H, Dirsch O, Sawitowski T, et al. Synergistic effects of a novel nanoporous stent coating and tacrolimus on intima proliferation in rabbits. Catheter Cardiovasc Intervent 2003; 60: 399-407

Chapter IV

Materials and methods

1 Introduction

This chapter presents the preparation of materials involved in this thesis, such as the synthesis of bioactive glasses and glass-ceramics as well as polyphenols extraction from grape skin and green tea and their grafting onto bioactive glasses and glass-ceramics, the analysis technologies employed to characterize the material surface and to evaluate the changes of solution for functionalization, including XPS, FTIR, UV, and pH measurement etc. In addition, the instruments related to this research are introduced in this chapter as well.

2 Preparation of bioactive glass and molecule for functionalization

2.1 Synthesis of bioactive glasses

Bioactive glasses are traditionally obtained by fusion of inorganic precursors of the final oxides and pouring of the molten glass in order to have rapid cooling. In this way it is possible to obtain a glassy structure avoiding crystallization. In fact, the formation of a glass requires the solid phase to be formed by rapid melt quenching. Glass is therefore cooled sufficiently rapidly below a typical "freezing" temperature, which is known as glass transition temperature, T_g, so that the supercooled disordered atomic configuration at T_g is frozen into the solid state. In general, the structure of glass is relative metastable compared to its crystalline countepart. The disordered structure of glass is defined as the amorphous network.

2.1.1 Synthesis of SCNA and CEL2

SCNA is a silica-based glass belonging to the quaternary SiO_2-CaO-Na_2O-Al_2O_3 system [1];

its molar composition is reported in Table 1. The synthesis of SCNA follows the conventional melting and quenching route. Pure inorganic precursors, in this case, SiO_2, $CaCO_3$, Na_2CO_3, Al_2O_3 (Sigma-Aldrich), have been weighted according to the amount necessary for obtaining the molar percentages of the resulting oxides reported in Table 1. Reagents were mixed for a couple of hours and then introduced in a platinum crucible and molten at 1550 ℃ for 1 h in air. The molten glass was quenched on a brass plate to obtain a bar, which have been subsequently annealed in furnace at 600 ℃ for 10 hours in order to relax residual stresses. The selection of annealing condition is according to thermal analysis.

In order to obtain powders the melted glass was poured in water. The so obtained frit was then milled and sieved up to a grain size lower than 20 μm.

Table 1 Glass molar composition of SCNA and CEL2 and melting/annealing conditions

Oxide	**SCNA**	**CEL2**
	Composition (Mol %)	
SiO_2	57	45
CaO	34	26
P2O5	-	3
K2O	-	4
Na2O	6	15
Al2O3	3	-
MgO	-	7
Melting	1 h, 1550 ℃	1 h, 1400 ℃
Annealing	10 h, 600 ℃	12h, 500 ℃

The composition of SCNA was chosen to impart high mechanical properties to the glass, especially compressive strength and hardness. The composition results also in a reduced bioactive behavior. In this case, the silica content is 57 % mol close to 60 % mol, according to Hench [2], which was the upper limit for allowing melt derived silicate glasses to show a bioactive behavior. Glasses with a silica content ranged from 53 %-58 % showed a decrease in the kinetics of an apatite layer formation on their surface, however, not all the material

bioactive behavior is suppressed. In the composition of SCNA, the presence of Al_2O_3 further inhibits the bioactivity of glass by stabilizing the glass network and as a result, inhibiting the potential ion exchange phenomena on the material/biological fluids interface. One the other hand, SCNA possesses remarkable mechanical features due to its major chemical stability. Moreover, the presence of CaO and Na_2O, as the network modifier oxides, contributes to the decrease of melting temperature.

CEL2 [3] is a silicate glass belonging to the complex SiO_2-P_2O_5-CaO-MgO-Na_2O-K_2O system; its molar composition is reported in Table 1. The selection of molar composition aims to maximize the bioactivity and biocompatibility and meanwhile to avoid undesired effects due to the pH changes caused by the ion leaching phenomenon.

In brief, CEL2 was prepared by melting reagent-grade reactants (SiO2, $Ca_3(PO)_4$, $CaCO_3$, $4MgCO_3Mg(OH)_2$ $5H_2O$, Na_2CO_3, K_2CO_3, Sigma-Aldrich) in a platinum crucible at 1400 ℃ for 1 h in air; the melt was poured onto a brass plate to obtain bars, which were annealed at 500 ℃ for 12 h to release internal stresses.

In order to obtain powders the melted glass was poured in water. The so obtained frit was then milled and sieved up to a grain size lower than 20 μm.

2.1.2 Preparation of bulk and powder samples

In this thesis, each type of bioactive glass was investigated in both the bulk and powder forms. As described in the previous paragraph, the bulk materials were obtained by pouring the melted glass on a brass plate to obtain glass bars which were annealed in a furnace then cut in to slices with an automatic cutter (ATA brilliant 220) showed in Figure 1. The bars were cut into 2 mm-thickness bulk with the size of about 1cm × 1 cm for subsequent treatment and analysis. The bulks of SCNA and CEL2 are polished with a polisher (Figure 2) on both sides using SiC abrasive papers, 120 > 320> 600 > 800> 1000 > 1200 > 2400 >4000 grit. The surface of well polished bulk samples is smooth, plane and homogeneous.

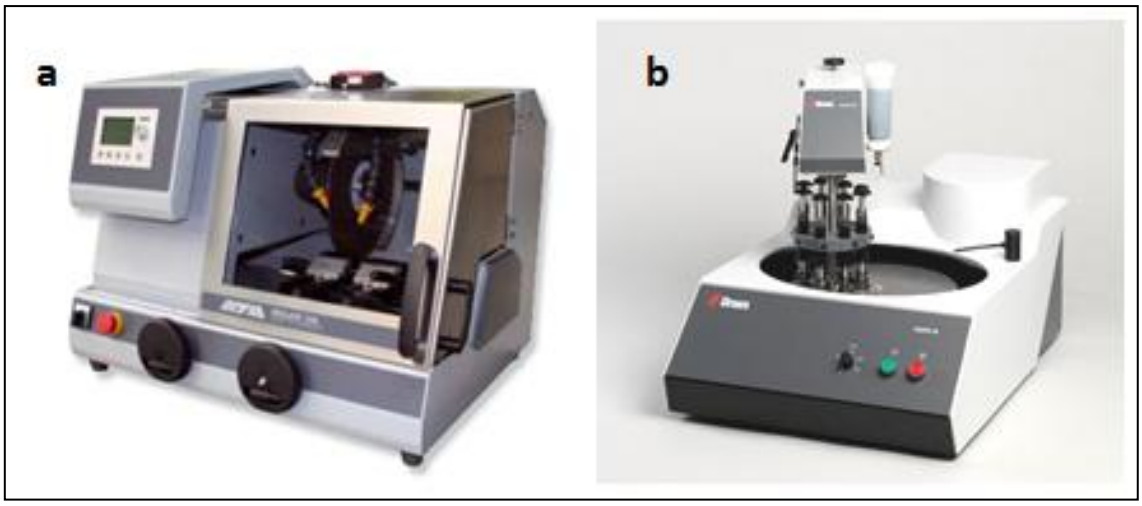

Figure 1: (a) ATA® BR220 Precision Cutter and (b) Struers® polisher

The powder samples were prepared by pouring the melted glass into water to obtain a frit. The frit was then ball milled and sieved up to a grain size lower than 20 μm. The glass bar, bulk as well as powder samples are showed in Figure 2.

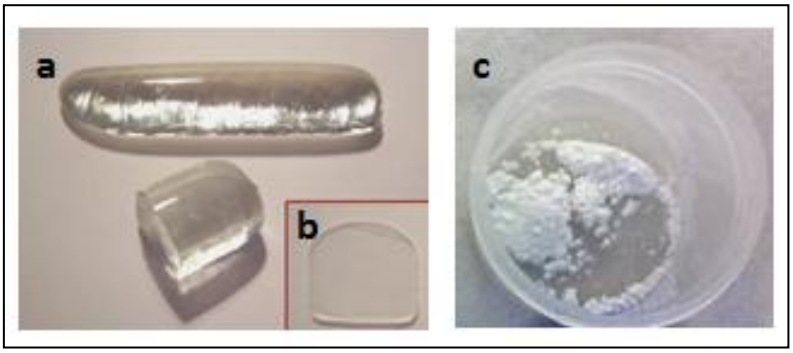

Figure 2: (a) Glass bar, (b) bulk and (c) powder

2.2 Synthesis of bioactive and ferrimagnetic glass-ceramic (SC-45)

A glass-ceramic material, named SC-45 belonging to complex SiO_2-Na_2O-CaO-P_2O_5-FeO-Fe_2O system was considered as ferromagnetic glass ceramic with potential application in the cancer therapy field thanks to its heating ability (hyperthermia effect, described in chapter III). Its molar composition is exhibited in Table 2. SC-45 was prepared by traditional melting of pure commercial reagents (SiO_2, Na_2CO_3, $CaCO_3$, $Ca_3(PO)_4$, $FeSO_4 \cdot 7\ H_2O$, Fe_2O_3, Sigma-Aldrich) in

a furnace at 1550 ℃ for 30 minutes in air, as described in literature [4, 5].

A part of the melt was poured into a brass mould to obtain glass bars, which were subsequently annealed at 600 ℃ for 12 hours. In order to prepare the bulk samples, the glass bars were cut into slices with the size of 10 x 10 x 1.5 mm^3 with an automatic cutter (Struers Accutom 5). Each slice was polished with SiC abrasive papers, up to 1200 grit and then with 6 microns diamond paste. Another part was cast into water to obtain frit, which was milled and sieved (below 20μm grain size) to powders. The glass bar, bulk as well as powder samples are showed in Figure 3.

Table 2 SC-45 molar composition

Oxide	SiO_2	Na_2O	CaO	P_2O_5	FeO	Fe_2O_3
% molar	24.7	13.5	13.5	3.3	14	31

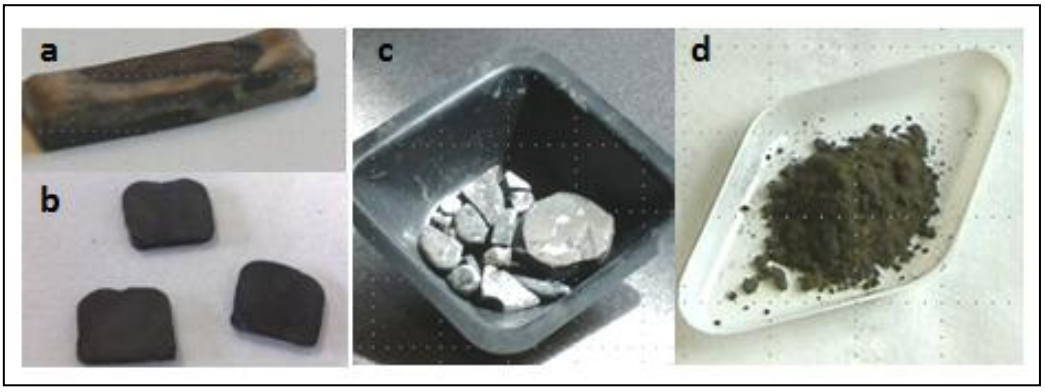

Figure 3: (a) Bar, (b) bulk, (c) frit and (d) powder of SC-45

2.3 Molecules for functionalization

2.3.1 Gallic acid

Gallic acid (3, 4, 5-trihydroxybenzoic acid, henceforth GA) and its derivatives are endogenous plant polyphenol found abundantly in tea, grapes, berries and other fruits as well as in wine [6]. It is a yellowish-white crystal (molecular mass 170.12 g/mol) with

melting point 250 ℃ and water solubility 1.1% at 20 ℃ [7]. On the basis of its chemical structure (Figure 4), gallic acid belongs to phenolic acids which are which have one carboxylic acid functional group. Like other polyphenols, gallic acid possesses a number of remarkable bioactivities such as antiallergic, anticarcinogenic, antimutagenic and antibacterial capacity, especially antioxidant and anticancer activities which had drawn wide attention to both investigations on human benefits and potential applications in industry such as food additives, cosmetics and pharmacy.

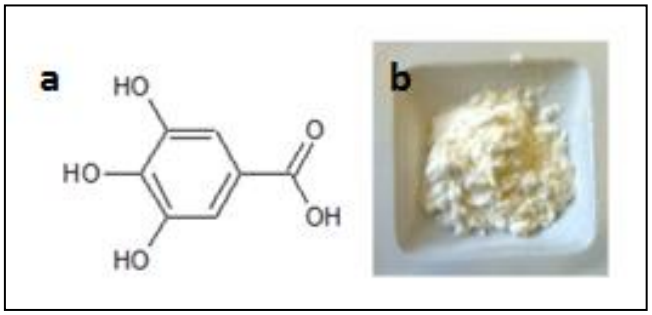

Figure 4: (a) Chemical structure of gallic acid and (b) commercial gallic acid powder

Gallic acid is also investigated to possess the pro-oxidant property in concentration dependent manner in presence of metal ions. Moreover, pro-oxidant property of gallic acid has been recognized as the apoptosis inducer in cancer cell lines [8].

In this thesis Gallic Acid (GA 97.5-102.5% titration, G7384, Sigma Aldrich) was employed for the functionalization of bioactive glasses (SCNA and CEL2) and glass-ceramic (SC-45) as model molecule for polyphenols and also for its potential properties, described above.

2.3.2 Folic acid

Folic acid, a member in vitamin B9 family is a critical molecule which is used in supplements and as a fortificant in foods. As shown in figure 5, folic acid consists of a pterin moiety linked via a methylene group to a para-aminobenzoylglutamate moiety. Its metabolic activity requires reduction to the tetrahydrofolic acid (THF) derivative, addition of a chain of glutamate residues in γ-peptide linkage, and acquisition of one-carbon unit [9].

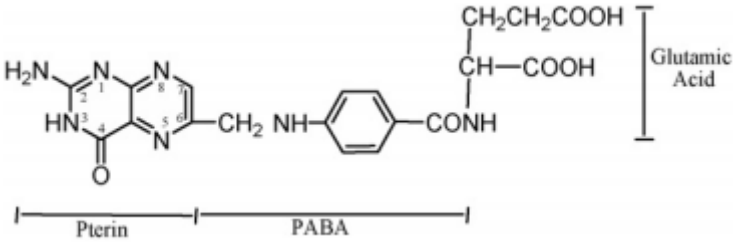

Figure 5: chemical structure of folic acid [9]

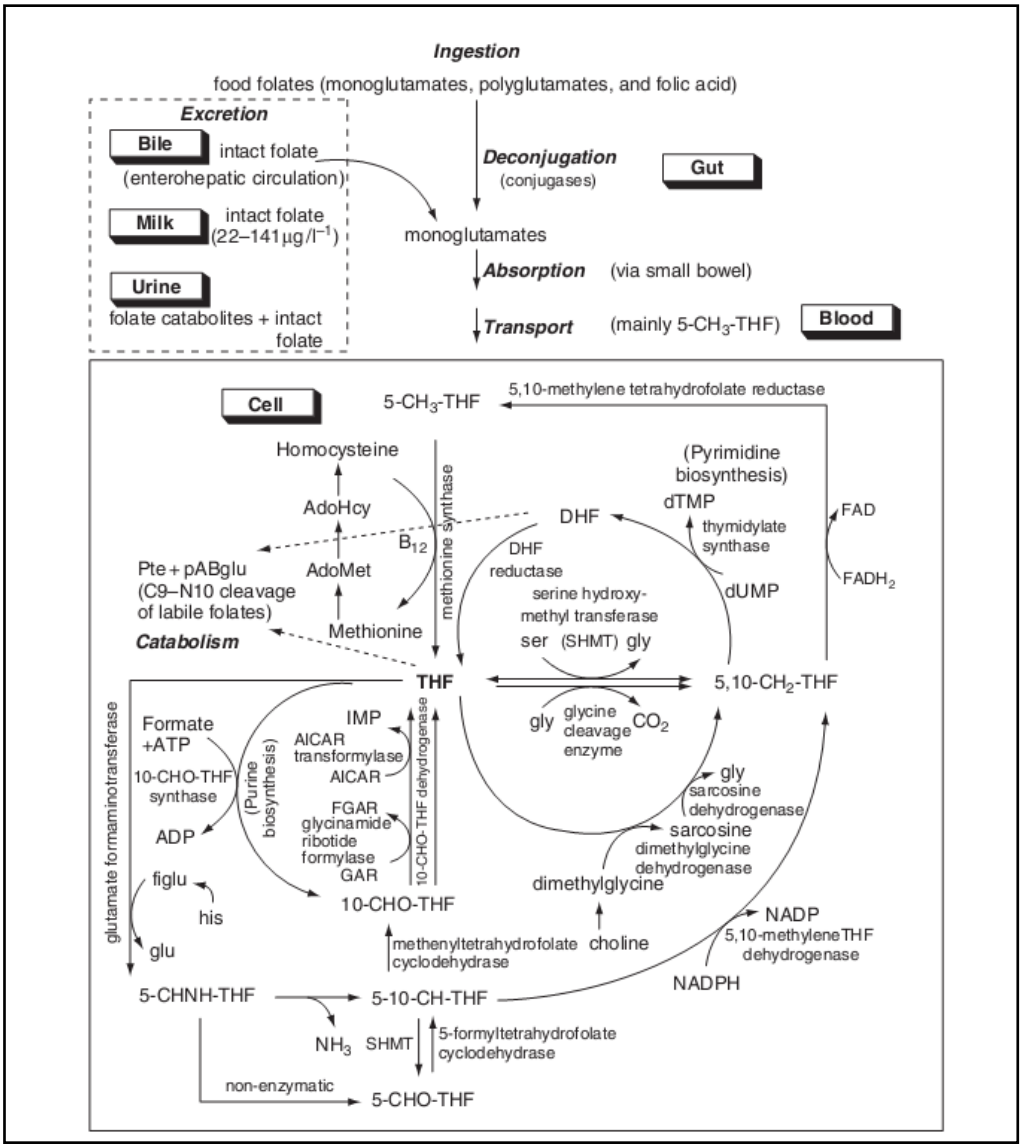

Figure 6: Physiology and metabolism of folic acid [9]. (GAR, glycinamide ribonucleotide; FGAR, formylglycinamide ribonucleotide; AICAR,aminoimidazolecarboxamide ribonucleotide; FIGLU, formiminoglutamic acid; IMP, inosine monophosphate)

The biochemical function of folic acid substrates (figure 6) is to transfer and use one-carbon

units in a variety of essential reactions including *de novo* purine biosynthesis, pyrimidine nucleotide biosynthesis, amino acid interconversions, and the generation and use of formate [9]. Since it is required by DNA synthesis, folic acid is involved in cell division. Moreover, the over expression of receptor of folic acid can be detected in several types of cancers in lung, colon, kidney and ovarian while in healthy human tissues the receptors just have limited distributions. Hence, folic acid can be used as an ideal molecule for tumour detection and treatment.

In this thesis Folic Acid (Folic acid ≥ 97 %, Sigma Aldrich) was used in preliminary experiments for the functionalization of SC-45 glass ceramic. The coupling of SC-45 and folic acid is of potential interest for the recognition and treatment of cancer.

2.3.3 Extraction of polyphenol from grape skin

Fresh red grapes (Barbera) were provided by a small-scale producer in the north of Italy (vineyard situated in Vagli Serra, Asti, Piedmonte, Italy) (Figure 7a). The fresh grapes were divided into four parts: flesh, skin, seed and stem (in this case only grape skin was employed).

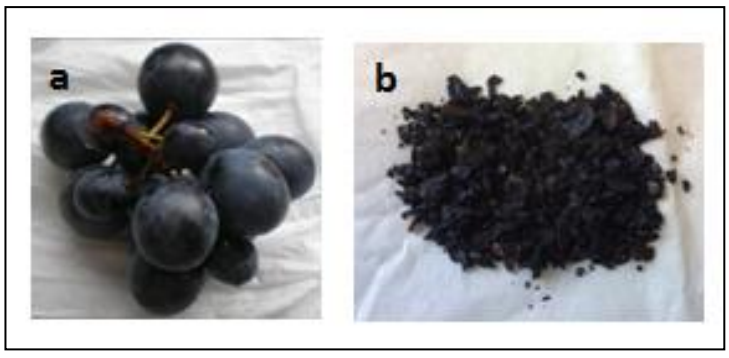

Figure 7: (a) fresh grape and (b) dried grape skin pieces

Fresh red grape skin was dried in oven at 60 ℃ and then grinded into small pieces (2-3 mm^2, Figure 7b). One type of conventional solvent extractions named as maceration was performed in this thesis according to literature [10]. The brief procedures are described as follows:

a) Weight dried grape skin (i.e. 10 g)

b) Solvent preparation: water-ethanol (20/80, v/v) with a solid-liquid ratio 1:20

c) Add solvent to immerse grape skin at 60 ℃ in a thermostatic bath (figure 8) for 60 min

d) Filter with filter paper to separate grape skin and extract solution (figure 9a)

e) Collect extraction solution and dry it in oven at 60 ℃ to remove the residual ethanol

f) Dissolve the extract in double distilled water and freeze at -18 ℃

g) Freeze dry and obtain the polyphenol extract (figure 9b)

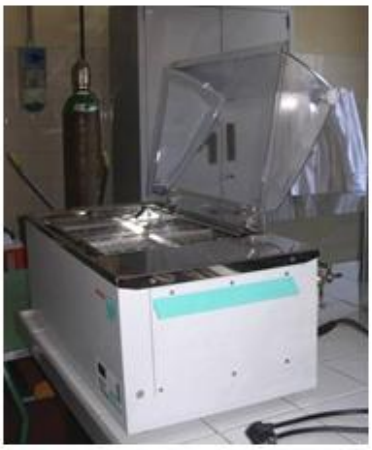

Figure 8: Thermostatic bath

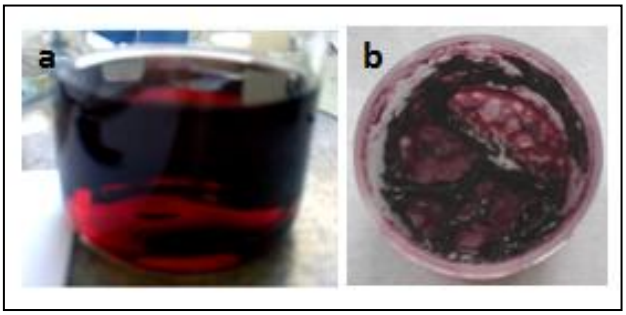

Figure 9: (a) Polyphenol extract in 80% ethanol and (b) polyphenol extract after freeze drying

2.3.4 Extraction of polyphenol from green tea

Green tea (Longjing) was bought from China; its origin is in Hangzhou, P. R. China (figure 10a). Since the green tea leaves were completely dry as brought, the extraction work started from the grinding of dried green tea leaves. As showed in figure 10b and 10c, green tea was put into a ceramic mortar and grinded into small pieces in order to increase the contact surface with solvent during extraction.

Figure 10: (a) green tea leaves, (b) green tea in a ceramic mortar and (c) grinded green tea

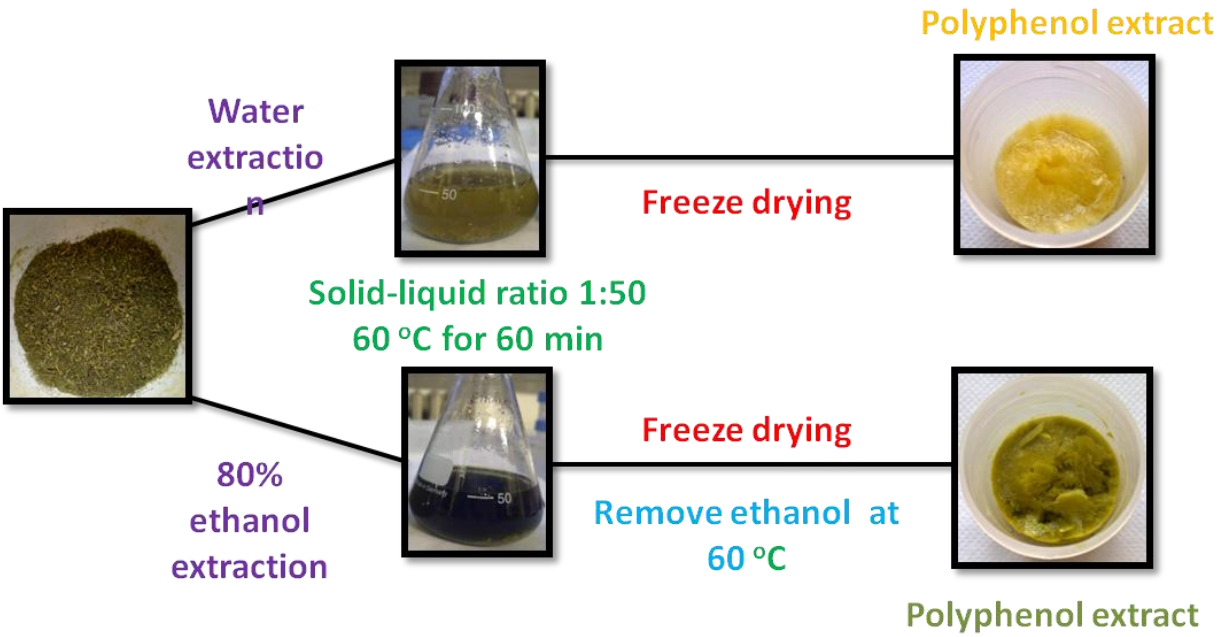

Scheme 1: Extraction of green tea polyphenol with water and 80% ethanol

Conventional solvent extraction [11] was selected to isolate tea polyphenols from green tea with two kinds of solvents (pure water, water-ethanol mixture). The procedures can be

summarized in the scheme 1. Tea phenol extracts with 80% ethanol were employed in the subsequent analysis due to its higher yield compared with the water extracted tea polyphenol.

3 Determination of total phenol content

3.1 Folin-Ciocalteau colorimetry

The Folin-Ciocalteau (FC) procedure is one of the standard procedures in grape polyphenol analysis such as in wine analysis, as well as in tea analysis [12]. Folin-Ciocalteau (FC) colorimetry is based on a chemical reduction of the reagent, a mixture of tungsten and molybdenum oxide. Singleton [13] first adapted this method to wine analysis. The products of the metal oxide reduction have a blue color that exhibits a broad light absorption with a maximum at 760 nm. The intensity of light absorption at that wavelength is proportional to the concentration of phenolics. Hence, gallic acid usually is employed as the calibration standard in FC method and the detection of light intensity is processed by UV-visible spectroscopy. In this thesis, Folin-Ciocalteau technique was employed both for standard curve and phenol content determination. The determination of standard curve is described as follows (figure 11):

a) Place 2 ml of gallic acid of each concentration into a container.

b) Add 6 ml double distilled water.

c) 0.5 ml Folin-ciocalteau reagent was added

d) Swirl to mix and incubate 1 to 8 minutes at room temperature.

e) Add 1.5 ml 20 % sodium carbonate solution.

f) Incubate for 2 hours at room temperature.

g) Transfer 4 ml mixed solution into 1-cm plastic cuvette and measure the absorbance at 760 nm in an UV-visible spectrophotometer.

h) Subtract of the absorbance of the blank from all readings and created a calibration curve form the standards.

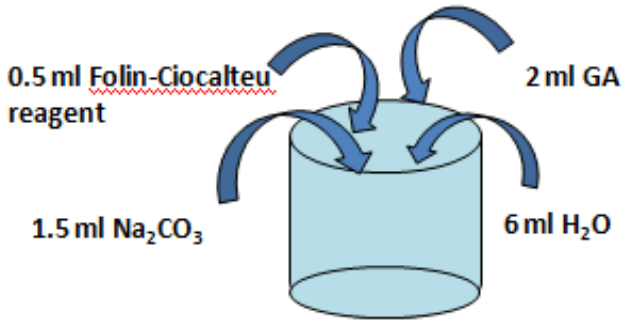

Figure 11: Determination of standard curve by Folin-Ciocalteau colorimetry

Concerning for the total phenol content, the analysis steps are similar with the standard curve determination except the change of gallic acid to polyphenol solution in step a. In addition, bulk samples were analyzed by FC assay to evaluate the molecule on the surface after functionalization.

3.2 Standard curve

A standard curve is a type of graph used as a quantitative research technique. Multiple samples with known properties are measured and graphed, which then allows the same properties to be determined for unknown samples by interpolation on the graph. The samples with known properties are the standards, and the graph is the standard curve. In this case, gallic acid is the known material and phenolic is the unknown molecule. To draw a standard curve, at least five point of absorbance of gallic acid need to be detected.

3.2.1 Calibration standard preparation

Gallic acid (97.5–102.5% titration, G7384, Sigma-Aldrich) is used as the calibration standard and six concentrations with an increasing order were prepared as described in Table 3. Since the concentration is relative low, dilution step by step is employed. Dissolve 50 mg gallic acid in 50 ml double distilled water and mix the solution with magnetic stirring. Dilute 10 ml to 100 ml to obtain 0.1 mg/ml concentration. Then dilute 1, 2, 1, 2, 3 and 4 ml to 40, 20, 10, 10, 10 and 10 ml with water, respectively, to prepare the six concentrations for standard curve. In addition, the detection of each point was tripled to analyze the standard deviation.

Table 3 Six points of concentration for standard curve

Points	1	2	3	4	5	6
Concentration (mg/ml)	0.0025	0.005	0.01	0.02	0.03	0.04

3.2.2 Sodium carbonate solution

In FC method, 20 % sodium carbonate (anhydrous, ≥99.5%, granular, Sigma-Aldrich) solution is needed for the reaction. Dissolve 10 g reagent-grade sodium carbonate in 50 ml double distilled water. Then stir with a magnetic stirring till all the powder was dissolved. At last, filter the solution and store it at room temperature.

3.3 Determination of total phenolic content

3.3.1 Solution preparation

250 mg grape skin extracts were dissolved in 50 ml double distilled water and mixed with magnetic stirred (figure 12) to obtain a solution with concentration 5 mg/ml, and then store the solution in refrigerator at 4 ℃.

Figure 12: Heating magnetic stirrer

50 mg green tea extracts were dissolved in 50 ml double distilled water and mixed with magnetic stirred to obtain a solution with concentration 1 mg/ml, and then store the solution

in refrigerator at 4 ℃.

3.3.2 Determination by Folin-Ciocalteau colorimetry

The determination of polyphenol content is similar to the determination of standard curve. In brief, place 2 ml polyphenol solution into a container followed by 6 ml double distilled water. Then add 0.5 ml Folin-Ciocalteau reagent and swirl to mix and incubate 1 to 8 minutes at room temperature. After incubated for 2 hours at room temperature, the solution was transferred to cuvette and detected the absorbance at 765 nm by UV-visible spectroscopy.

4 Surface functionalization of bioactive glasses

As described in figure 13, synthesized bioactive glass was prepared as bulk or powder samples. The first step of the functionalization process is sample washing in order to expose the hydroxyl groups (-OH) on its surface. The target molecule can be grafted on the surface exploiting the –OH groups directly or indirectly.

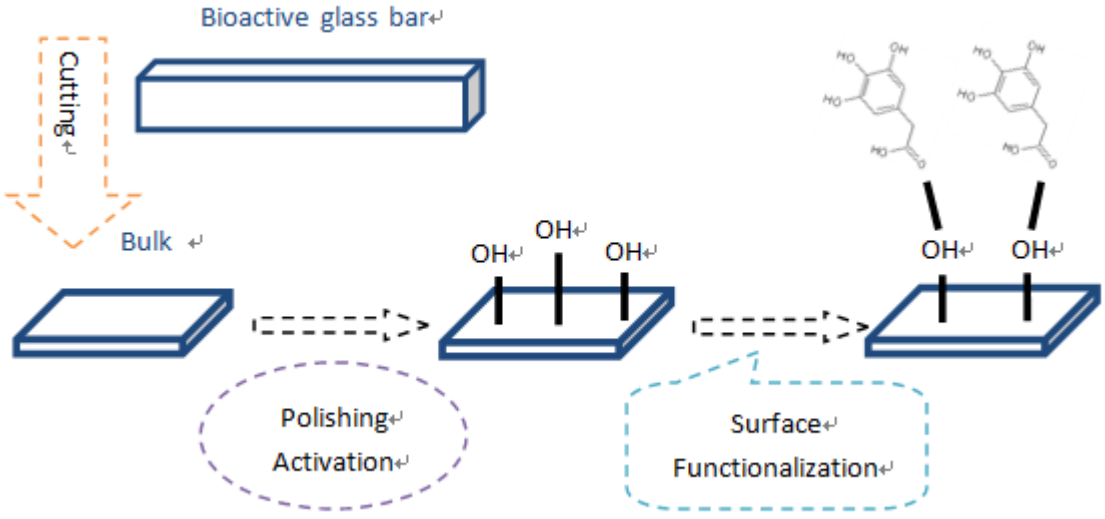

Figure 13: Surface functionalization of bioactive glasses with biological molecule

4.1 Surface activation

Surface activation is the first step in functionalization process in order to remove the contaminants on the surface as well as expose the reactive hydroxyl groups. The cleaning treatment condition has been selected according to a previous study on functionalization of bioactive glasses performed by the research group [14]. In the cited reference, different treatments were compared by contact angle measurement and XPS analysis in order to characterize surface modification (hydroxyls exposition and bioactivity reactions). The optimal treatment has been chosen as the one that allows high hydroxylation in a controlled and reproducible way, without the beginning of bioactivity reaction (such as hydroxyls condensation to form silica gel).

4.1.1 Hydroxyl exposure of SCNA and CEL2

The surface activation of SCNA and CEL2 include three passages for both bulk and powder samples:

a) Samples washing in acetone for 5 min in an ultrasonic bath to remove contaminants

b) Samples washing three times in double distilled water for 5 min in ultrasonic bath to favour -OH groups exposition

c) Samples air drying in cabinet at room temperature

This method is according to the previous work in our lab [1] and the presence of hydroxyls groups onto samples surface has been investigated by means of XPS.

4.1.2 Hydroxyl exposure of SC-45

In order to bond with bioactive molecules, the surface of glass-ceramic should be firstly activated. Since SC-45 is a silica-based glass-ceramic, the surface can be easily functionalized by activating the -OH groups after the contact with an aqueous medium. According to previous work in our lab [15], the optimization condition of surface treatment has been selected. Both the bulk and powder samples were soaked in double-distilled water for 7 days in incubator at 37 ℃ without refreshing the solution.

4.2 Gallic acid grafting

Gallic acid was directly grafted on the surface of SCNA, CEL2 and SC-45, since it presents functional groups able to link directly with -OH groups on the glass surface. Gallic acid solution with concentration of 1 mg/ml in double distilled water was prepared by dissolving GA in double-distilled water for about 2 hours under magnetic stirring. For each glass bulk or powder sample, 5 ml of 1.0 mg/ml gallic acid solution was employed. Then, samples (both bulk and powder ones) with activated surface were soaked in gallic acid solution for 24 hours at 37 ℃ in incubator. In addition, in order to prevent the light irradiation of gallic acid, which is a light-sensitive molecule, all the containers were covered with aluminum foils. After functionalization, bulks and powers were separated from the solution and washed twice in double distilled water. Finally, the glass samples were air dried in cabinet at room temperature. The solutions were stored in refrigerator for further analysis. The GA grafted samples were labeled as SCNA+GA, CEL2+GA and SC-45+GA, respectively.

4.3 SCNA and CEL2 modified with acidified gallic acid

In order to investigate the effect of pH on the glass and molecule behavior, SCNA and CEL2 were modified by citric acid addition to acidify GA solution. 0.5 M citric acid (CA, Citric Acid Monohydrate, ACS reagent 99.0-102.0%, Sigma-Aldrich) in double distilled water was added drop wise to 1.0 mg/ml GA solution till the pH was 3.0. The procedures of functionalization are the same as GA grafting. The acidified GA grafted samples were labeled as SCNA+GA+CA and CEL2+GA+CA.

4.4 SC-45 modified with buffered gallic acid

With the aim to evaluate effect of pH on both the glass-ceramic and molecule behavior, SC-45 was functionalized with buffered gallic acid solution, prepared dissolving gallic acid in citric acid-sodium citrate buffer The citric acid-sodium citrated buffer system was employed and the pH range of the buffer is from 3.0 to 6.2. In this case, pH 3.0 was selected by mixing 82 ml 0.1 M citric acid and 18 ml 0.1 M sodium citrate solution. The preparation of buffer solution and buffered gallic acid was described as follows:

a) Weight 2.1 g citric acid monohydrate ($C_6H_8O_7$•H_2O, M. wt. 210.14 g/mol, Sigma-Aldrich) and add 100 ml double distilled water under magnetic stirring mixing to obtain 0.1 M citric acid solution.

b) Dissolve 2.94 g trisodium citrate dihydrate, ($C_6H_5O_7Na_3$•$2H_2O$, M. wt. 294.12 g/mol, Sigma-Aldrich) in 100 ml double distilled water and mix the solution with magnetic stirring to get 0.1 M sodium citrate solution.

c) Transfer 82 ml 0.1 M citric acid solution and mixed with 18 ml 0.1 M sodium citrate solution to obtain the buffer solution with pH 3.0.

d) 50 mg gallic acid was dissolved in 50 ml above-mentioned buffer solution and mixed under magnetic stirring to obtain the buffered gallic acid solution.

Some samples were treated with the pure buffer solution (without gallic acid) in order to study the effect of the citric acid-sodium citrate buffer on SC-45.

Each sample of SC-45 bulk and powder was modified with 5 ml buffer solution and 5 ml buffered gallic acid solution, respectively, through the same method as gallic acid grafting. The buffer grafted and buffered GA grafted samples were named as SC-45+BUF and SC-45+GA-BUF, respectively.

4.5 Grape polyphenol and tea polyphenol grafting

The grafting of grape polyphenol (GP) and tea polyphenol (TP) is similar to the grafting of gallic acid on the surface of SCNA and CEL2. Both grape polyphenol and tea polyphenol were directly grafted with concentration of 5.0 mg/ml and 1.0 mg/ml, respectively, in double distilled water. Grape polyphenol solution was prepared by dissolving 250 mg grape skin extracts in 50 ml double-distilled water for about 2 hours under magnetic stirring. Tea polyphenol solution was obtained by dissolving 50 mg green tea extracts in 50 ml double-distilled water for about 2 hours under magnetic stirring. For each glass bulk or powder sample, 5 ml of 5.0 mg/ml GP solution as well as 1.0 mg/ml TP solution were employed. Then, samples (both bulk and powder ones) with activated surface were soaked in GP solution and TP solution for 24 hours at 37 ℃ in incubator. In addition, in order to prevent the light irradiation all the containers were covered with

aluminum foils. After functionalization, bulks and powers were separated from the solution and washed twice in double distilled water. Finally, the glass samples were air dried in laminar flow cabinet (figure 14) at room temperature. The solutions were stored in refrigerator for further analysis.

Figure 14: Laminar flow cabinet

4.6 Surface functionalization of SC-45 with folic acid

4.6.1 Silanization of SC-45

Silaniazation, which has been chosen because it is a well known technique for traditional glass functionalization, is the second step in the surface functionalization process in order to promote and stabilize the bonding between material and molecule. The background of our lab has transferred this technique to reactive glasses and glass-ceramics [14]. 3-amminopropyltriethoxysilane ($H_2N\ (CH_2)_3\ Si\ (OC_2H_5)_3$, APTES, 99% Aldrich) has been employed in order to introduce amino groups as functionalities. The main procedure can be described as follows:

a) 35 µl of 3-aminopropyltriethoxysilane has been dissolved in 150 ml of ethanol to obtain a solution

b) SC-45 bulks or powders were soaked in this solution maintained for 6 h at room temperature.

c) A thermal treatment has been processed for 1 h at 100 ℃ in oven to stabilize the silane-surface bonding

d) Samples were washed three times in ethanol for 5 minutes in ultrasonic bath in order to remove the un-bounded molecules.

e) Dry again for 1h at 100 ℃ in a furnace.

The silanization was investigated by XPS analysis (Al source, Surface Science Instruments, M-Probe), since it was able to detect the nitrogen atom and characterize amino groups on the glass surface.

4.6.2 Folic acid grafting

At first, a solution of folic acid (Folic acid ⩾ 97%, Sigma-Aldrich) in DMSO (Dymethyl sulfoxide ⩾ 99%, ACS reagent, Sigma-Aldrich) has been prepared by dissolving 4.5 mg folic acid in 5 ml DMSO and adding 4.5 mg DCC (Dicyclohexyl carbodiimide ⩾99%, Sigma-Aldrich) to obtain a 5 ml mixed solution for each SC-45 glass-ceramic sample (bulk or powder). Then, the silanized glass-ceramic samples have been soaked in this mixed solution for 2 h at 25 ℃ followed by washing sample twice in double distilled water. In the end, the functionalized glass samples were air dried under a laminar flow cabinet to avoid contaminations. After completely dried, the samples were packed in paper-PE bags with welding machine (figure 15) and stored in dark for XPS analysis, while the powder samples were stored in bottles covered by aluminum foils for further analysis.

Figure 15: Welding machine and packed samples

4.7 Antioxidant analysis of SC-45 powder before and after functionalization

Powder samples of SC-45 washed, SC-45+GA, SC-45+BUF and SC-45+BUF-GA were suspended in a buffered solution (PB, pH 7.4) of H_2O_2 in the presence of DMPO as a spin trap to test the release of HO • radicals in buffer solution. The electron paramagnetic resonance spectroscopy (EPR) spectra were recorded on aqueous suspension after 10, 30 and 60 minutes of incubation.

5 Analysis techniques for surface functionalization

5.1 UV-visible spectroscopy [16-18]

Ultraviolet–visible spectroscopy or ultraviolet-visible spectrophotometry (UV-Vis or UV/Vis) refers to absorption spectroscopy or reflectance spectroscopy in the ultraviolet-visible spectral region. This means that light in visible and adjacent range is employed. The absorption intensity in the visible ranges directly influences the color of the chemicals involved.

Many molecules absorb ultraviolet or visible light. The absorbance of a solution increases as attenuation of the beam increases. The absorbance (A) could be stated by Beer-Lambert's Law as:

$$A = \varepsilon bc = \log_{10} (I/I_0)$$

Where b is the path length of sample; c represents the concentration of compound in solution; ε is a constant of proportionality, called absorbtivity; I_0 the intensity of the incident light at a given wavelength; I is the transmitted intensity.

The principle of ultraviolet-visible absorption can be described as molecules containing π-electrons or non-bonding electrons (*n*-electrons) can absorb the energy in the form of ultraviolet or visible light to excite these electrons to higher anti-bonding molecular orbitals.

The absorption of UV or visible radiation corresponds to the excitation of outer electrons. There are three types of electronic transition which can be considered:

i. Transitions involving π, σ, and *n* electrons (figure 16)

ii. Transitions involving charge-transfer electrons

iii. Transitions involving *d* and *f* electrons

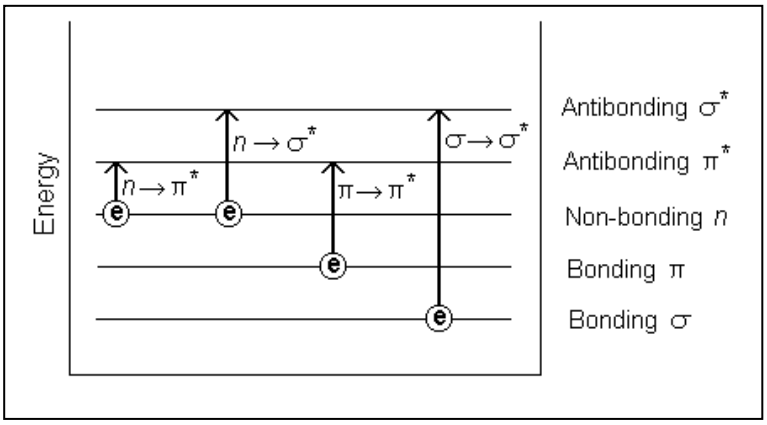

Figure 16: Possible electronic transitions of π, σ, and *n* electrons

A UV-visible spectrophotometer (figure 17) is a device used to study ultraviolet-visible spectroscopy. It measures the intensity of light passing through a sample (*I*), and compares it with the intensity of light before it passes through the sample (I_0). The ratio of *I* and I_0 is named as the transmittance, which is usually expressed as a percentage (% T). The absorbance (A) is based on the transmittance:

$$A = - \log (\% T / 100 \%)$$

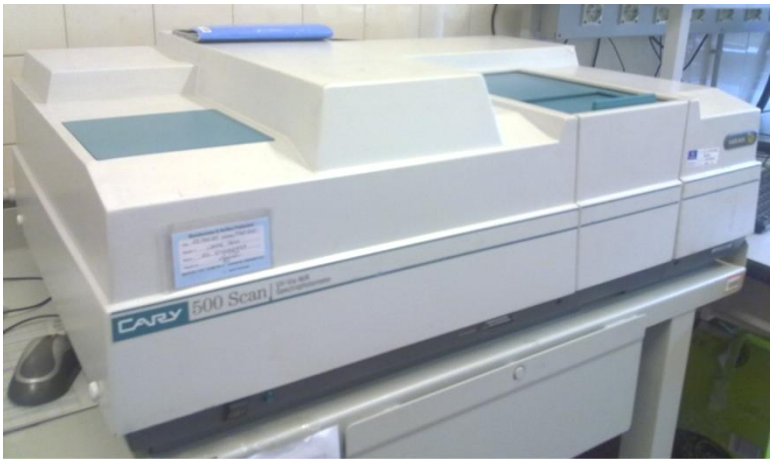

Figure 17: Cary ® 500 Scan UV-visible spectrophotometer

As showed in figure 18, the basic parts of a spectrophotometer include a light source, a holder, a diffraction grating or monochromator to prepare the different wavelengths of a light, and a detector. The radiation source is often a Tungsten filament (300-2500 nm), a deuterium arc lamp which is continuous over the ultraviolet region (190-400 nm), and more recently light emitting diodes (LED) and Xenon Arc Lamps for the visible wavelengths. The detector is typically a photomultiplier tube, a photodiode, a photodiode array or a charge-coupled device (CCD).

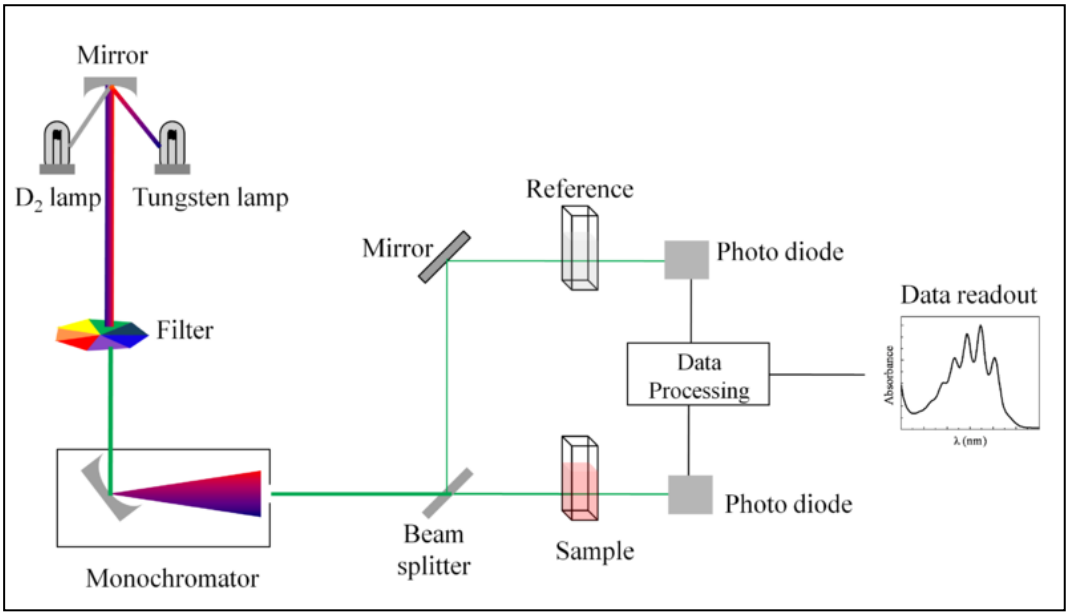

Figure 18: Schematic of UV- visible spectrophotometer

UV/Vis spectroscopy is routinely used in analytical chemistry for the quantitative determination of different analytes, such as transition metal ions, highly conjugated organic compounds, and

biological macromolecules. Moreover, UV spectroscopy plays a role as detector of other methodology such as HPLC. Samples for spectroscopic analysis are commonly solutions but solids and gases may also be studied.

In the present thesis UV-Visible spectroscopy was employed for the quantification of gallic acid and total phenols by the Folin-Ciocalteau method describe in the previous paragraphs (figure 17).

5.2 Fourier Transform Infrared Spectroscopy (FTIR)

5.2.1 Introduction of Fourier Transform Infrared Spectroscopy (FTIR) [19-22]

Fourier transform infrared spectroscopy is used to obtain an infrared spectrum of absorption, emission, photoconductivity or Raman scattering of liquid, solid or gas on the basis of interaction of infrared radiation with sample. FTIR techniques analyze molecular vibrations induced by the IR radiation (400 - 4000 cm-1). These techniques schematize atoms as masses joined by bonds with spring-like properties.

An FTIR Spectrometer (figure 19) is an instrument which acquires broadband NIR to FIR spectra. Unlike a dispersive instrument, i.e. grating monochromator or spectrograph, FTIR spectrometers collect all wavelengths simultaneously. This feature is called the Multiplex or Felgett Advantage.

Figure 19: FTIR spectrometers

The information provided by FTIR can identify unknown materials; determine the quality or consistency of a sample; determine the amount of components in a mixture. Figure 20 exhibited the optical diagram of an FTIR spectrometer.

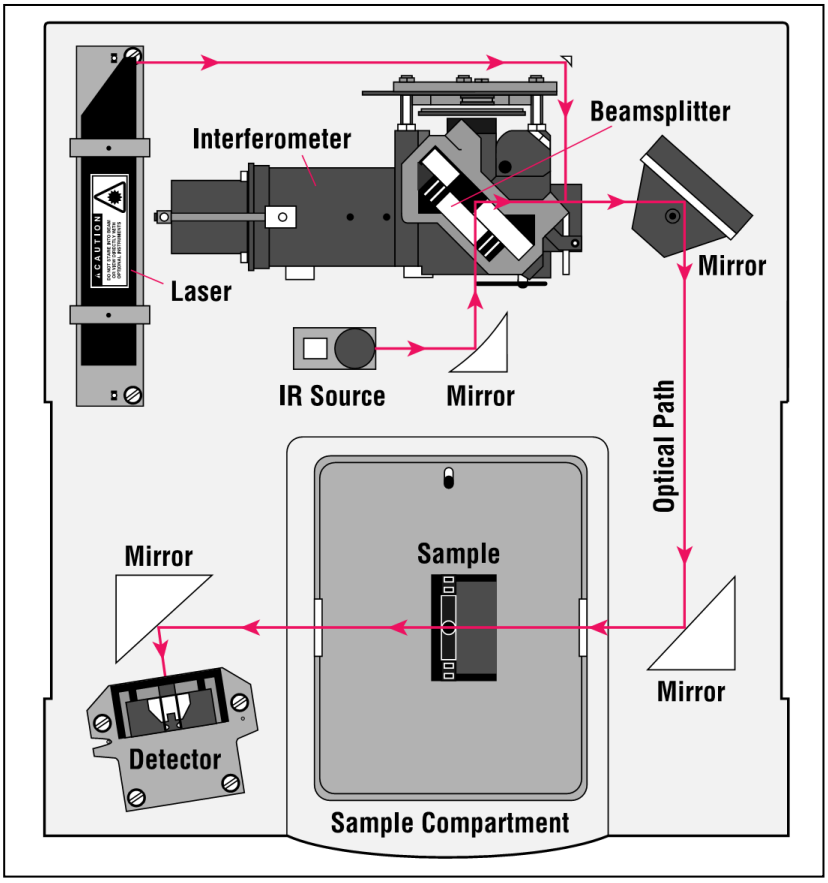

Figure 20: Optical diagram of an FTIR spectrometer

The normal instrumental analysis process is as follows (figure 21):

a) The Source: Infrared energy is emitted from a glowing black-body source. This beam passes through an aperture which controls the amount of energy presented to the sample (and, ultimately, to the detector).

b) The Interferometer: The beam enters the interferometer where the "spectral encoding" takes place. The resulting interferogram signal then exits the interferometer.

c) The Sample: The beam enters the sample compartment where it is transmitted through or reflected off of the surface of the sample, depending on the type of analysis being

accomplished. This is where specific frequencies of energy, which are uniquely characteristic of the sample, are absorbed.

d) The Detector: The beam finally passes to the detector for final measurement. The detectors used are specially designed to measure the special interferogram signal.

e) The Computer: The measured signal is digitized and sent to the computer where the Fourier transformation takes place. The final infrared spectrum is then presented to the user for interpretation and any further manipulation

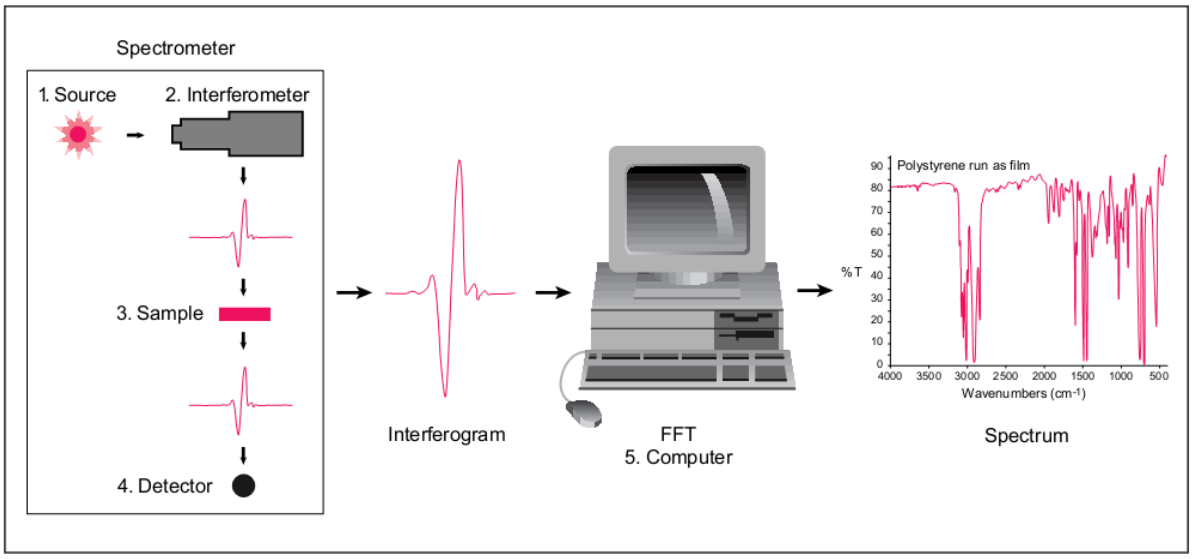

Figure 21: Normal instrumental analysis process of FTIR Spectrometer

Some of the major advantages of FTIR over the dispersive technique include high analysis speed, high sensitivity, mechanical simplicity and internally calibration etc. These advantages, along with several others, make measurements made by FT-IR extremely accurate and reproducible. Thus, it is a very reliable technique for positive identification of virtually any sample.

5.2.2 Sample preparation for FTIR

In this thesis, functionalized powder sample were dried and stored for FTIR analysis. The glass powder and KBr with a ratio of 2 mg/198 mg for each pellet were completely mixed and pressed with the mould as showed in figure 22 to obtain a pellet sample for analysis.

FTIR technique was employed for the evaluation of surface chemical composition of bare and functionalized glasses.

Figure 22: Mould for KBr pellet

5.3 Scanning Electron Microscopy (SEM) [22-24]

The scanning electron microscope (SEM) is a type of electron microscope that produces images of a sample by scanning it with a focused beam of high-energy electrons to generate a variety of signals at the surface of solid specimens. The signals that derive from electron-sample interactions reveal information about the sample including external morphology (texture), semi-quantitative chemical composition, and crystalline structure and orientation of materials making up the sample. The electron beam is generally scanned in a raster scan pattern, and the beam's position is combined with the detected signal to produce an image.

In most applications, data are collected over a selected area of the sample surface, and a 2-dimensional image is generated that displays spatial variations in surface properties. Conventional SEM techniques can scan areas ranging from approximately 1 cm to 5μm in width with a magnification from 20× to approximately 30000×. Furthermore, SEM is capable of performing analysis of selected point locations on the sample surface; the approach is especially useful in qualitatively or semi-quantitatively determining chemical compositions (combination with EDS), crystalline structure as well as crystal orientations (with EBSD).

The fundamental principle of SEM is that accelerated electrons in an SEM carry significant amounts of kinetic energy, and this energy is dissipated as a variety of signals produced by electron-sample interactions when the incident electrons are decelerated in the solid sample. These signals mainly include secondary electrons (which produce SEM images), backscattered electrons (BSE), diffracted backscattered electrons (EBSD, used for determination of crystal structures and orientations of minerals), photons (characteristic X-rays, that are used for elemental analysis and continuum X-rays), visible light (cathodoluminescence-CL), as well as heat. Secondary electrons and backscattered electrons are commonly employed to image samples. Thereinto, secondary electrons do great contributions to exhibit morphology and topography on samples, while backscattered electrons are most valuable for illustrating contrasts in composition in multiphase samples. X-ray is generated by inelastic collisions between the incident electrons and electrons in discrete orbitals (shells) of atoms in the sample. When the excited electrons go back to lower energy orbital, the X-ray is produced with a fixed wavelength which depends on the energy difference of electrons in different element. Hence, the element in a sample will be excited by the electron beam and yield a characteristic X-ray.

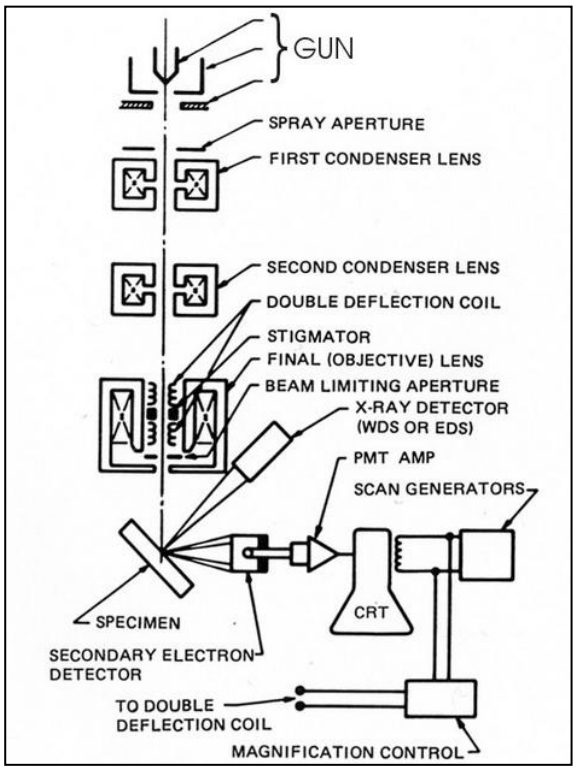

Figure 23: Schematic of SEM characteristic components

Scanning electron microscopy instrumentation is commonly consisted of several essential components including the following (figure 23):

a) Electron Source ("Gun")

b) Electron Lenses

c) Sample Stage

d) Detectors for all signals of interest

e) Display / Data output devices

f) Infrastructure Requirements

In addition, the infrastructure requirements include power supply, vacuum system, cooling system, vibration-free floor as well as room free of ambient magnetic and electric fields.

In the present thesis SEM and EDS analyses were performed in order to evaluate the reaction of bioactive glasses and glass ceramic in the functionalization media, both from a morphological and chemical point of view.

5.4 X-ray photoelectron spectroscopy (XPS) [25-28]

X-ray Photoelectron Spectroscopy (XPS), also known as Electron Spectroscopy for Chemical Analysis (ESCA) is a widely used technique to investigate the chemical composition of surfaces. XPS is a kind of surface-sensitive quantitative spectroscopic technique that measures the elemental composition at the parts per thousand range, empirical formula, chemical state and electronic state of the elements that exist within a material. XPS spectra are obtained by irradiating a material with a X-rays beam and simultaneously measuring the kinetic energy and number of electrons escaping from the top 0 to 12 nm of the material being analyzed. During XPS measurement, an ultra-high vacuum (UHV) < 10^{-9} Torr (< 10^{-7} Pa) condition is required.

As showed in figure 24, the XPS instrumentation commonly includes essential parts as follows:

a) Electron energy analyzer

b) X-ray source

c) Ar ion gun

d) Neutralizer

e) Vacuum system

f) Electronic controls

g) Computer system

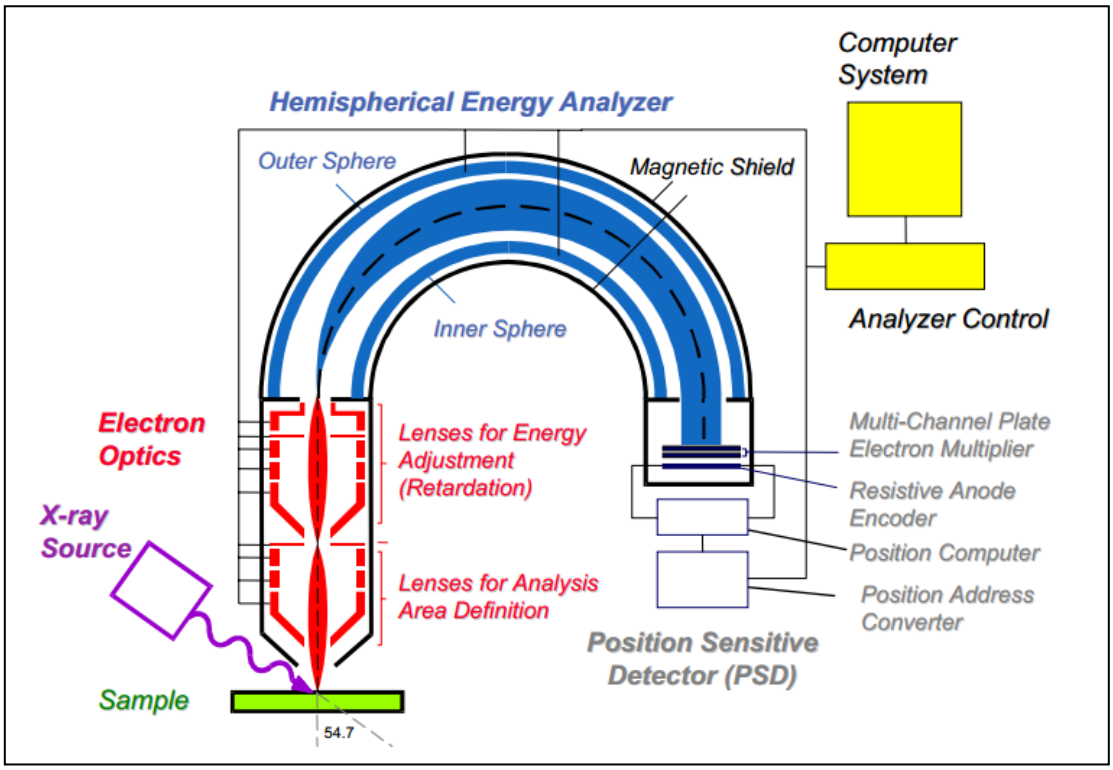

Figure 24: X-ray Photoelectron Spectrometer

XPS is based on the theory of photoelectric effect (figure 25a) outlined by Einstein in 1905 and photoemission for analysis (figure 25b) proposed by Kai Siegbahn.

The energy of a photon of all types of electromagnetic radiation is given by the Einstein relation:

$$E = h \nu$$

Where h is Planck constant (6.62×10^{-34} J s) and ν is the frequency (Hz) of the radiation.

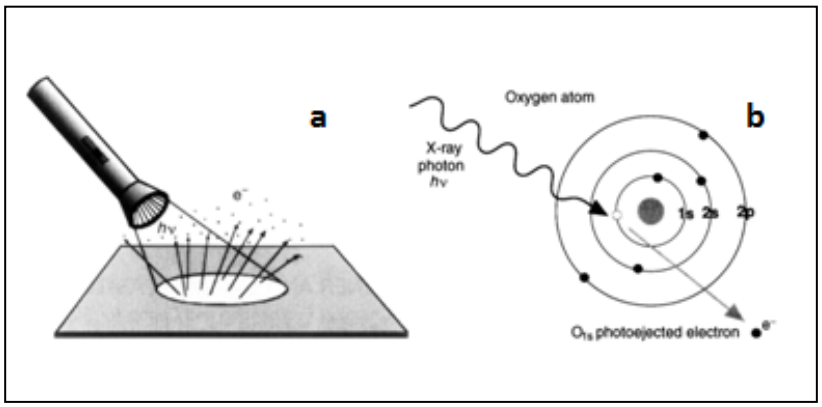

Figure 25: (a) Photoelectric effect and (b) photoemission

A photoemission process can be described by an energy balance:

$$BE = h\nu - KE - \Phi spec$$

Where BE represents electron binding energy; KE is electron kinetic energy; Φspec represents for spectrometer work function.

Through XPS analysis, some information of sample analyzed could be obtained:

a) Identification of elements near the surface and surface composition

b) Local chemical environments

c) Oxidation states of transition metals

d) Valence band electronic structure

As a result of the obtained information, XPS is commonly empolyed to measure:

a) Elemental composition of the surface

b) Empirical formula of pure materials

c) Elements that contaminate a surface

d) Chemical or electronic state of each element in the surface

e) Uniformity of elemental composition across the top surface (line profiling or mapping)

f) Uniformity of elemental composition as a function of ion beam etching (depth profiling)

Reference

[1] Verné E, M Miola, Vitale-Brovarone C, et al. Surface silver-doping of biocompatible glass to induce antibacterial properties. Part I: massive glass. J Mater Sci Mater Med 2009; 20: 733-740

[2] Chen QZ, Thompson ID, Boccaccini AR. 45S5 Bioglass® derived glass-ceramic scaffolds for bone tissue engineering. Biomaterials 2006; 27: 2424-2425

[3] Vitale Brovarone C, Verné E, Robiglio L, et al. Biocompatible glass-ceramic materials for bone substitutions. J Mater Sci:Mater Med 2008; 19: 471-478

[4] Bretcanu O, Verné E, Cöisson M, et al. Temperature effect on the magnetic properties of the coprecipitation derived ferrimagnetic glass-ceramics. J Magn Magn Mater 2006; 300: 412-417

[5] Bretcanu O, Verné E, Cöisson M, et al. Magnetic properties of the ferrimagnetic glass-ceramics for hyperthermia. J Magn Magn Mater 2006; 305: 529-533

[6] Singh J, Rai GK, Upadhyay AK, et al. Antioxidant phytochemicals in tomato (Lycopersicon esculentum). Ind J Agric Sci 2004; 74: 3-5

[7] Polewski K., Kniat, S., Slawinska, D., 2002. Gallic acid, a natural antioxidant, in aqueous and micellar environment: spectroscopic studies. Curr. To p. Biophys. 26, 217-227.

[8] Yen, G.C., Duh, P. D., Tsai, H.L., 2002. Antioxidant and pro-oxidant properties of ascorbic acid and gallic acid. Food Chem. 79, 307-313.

[9] JW Miller. Folic acid. Encyclopedia of Human Nutrition, Encyclopedia of Human Nutrition, 2005, 2: 262-269

[10] Cho YJ, Hong JY, Chun HS, et al. Ultrasonication-assisted extraction of resveratrol from grapes. J Food Eng 2006; 77: 725-730

[11] Vuong QV, Golding JB, Stathopoulos CE, et al. Optimizing conditions for the extraction of catechins from green tea using hot water. J Sep Sci 2011; 34: 3099-3106

[12] Wiseman S, Waterhouse A, Korver O. The health effects of tea and tea components: opportunities for standardizing research methods. Crit Rev Food Sci Nutr 2001; 41: 387-412

[13] Singleton VL and Rossi JA. Colorimetry of total phenolics with phosphomolybdic-phosphotungstic acid reagents. Am J Enol Vitic 1965; 16: 144-158

[14] Vernè E, Vitale-Brovarone C, Bui E, et al. Surface functionalization of bioactive glasses. J Biomed Mater Res DOI: 10.1002/jbm.a.32153.

[15] Verné E, Miola M, Ferraris S, et al. Surface activation of a ferrimagnetic glass-ceramic for antineoplastic drugs grafting. Adv Eng Mater 2010; 12: 309-319

[16] http://en.wikipedia.org/wiki/Ultraviolet%E2%80%93visible_spectroscopy

[17] http://teaching.shu.ac.uk/hwb/chemistry/tutorials/molspec/uvvisab1.htm

[18] http://teaching.shu.ac.uk/hwb/chemistry/tutorials/molspec/beers1.htm

[19] http://en.wikipedia.org/wiki/Fourier_transform_infrared_spectroscopy

[20] http://mmrc.caltech.edu/FTIR/FTIRintro.pdf

[21] http://www.newport.com/Introduction-to-FTIR-Spectroscopy/405840/1033/content.aspx

[22] http://serc.carleton.edu/research_education/geochemsheets/techniques/SEM.html

[23] http://www.purdue.edu/rem/rs/sem.htm

[24] http://www.ammrf.org.au/myscope/sem/background/

[25] http://mmrc.caltech.edu/SS_XPS/XPS_PPT/XPS_Slides.pdf

[26] http://www.phi.com/surface-analysis-techniques/xps.html

[27] http://pire-ecci.ucsb.edu/pire-ecci-old/summerschool/papers/vohs1.pdf

[28] http://en.wikipedia.org/wiki/X-ray_photoelectron_spectroscopy#Peak_identification

Chapter V

Results and discussions

1 Introduction

In this thesis, two types of bioactive glasses (SCNA and CEL2) and one kind of bioactive and ferrimagnetic glass-ceramic (SC-45) have been employed for the functionalization. Three types of molecules, gallic acid, grape polyphenol and tea polyphenol were grafted to bioactive glasses, while gallic acid has either been used for SC-45 functionalization. This chapter, which constitutes the core of this thesis, is divided in to four sections and each of them devoted to deal with one of the research theme: i) surface functionalization of SCNA and CEL2 with gallic acid; ii) surface functionalization of SCNA and CEL2 with polyphenol extracted from grape skin; iii) surface functionalization of SCNA and CEL2 with polyphenol extracted from green tea ; iv) surface functionalization of SC-45 with gallic acid and buffered gallic acid and v) surface functionalization of SC-45 with folic acid.

2 Surface functionalization of SCNA and CEL2 with gallic acid

Bioactive glasses are very attractive materials and widely investigated for many years with the applications in bone reconstruction. SCNA and CEL2 are two types of silica-based bioactive glasses with different level of reactivity (CEL2 possesses a higher reactivity). In this section, gallic acid (GA) as a model molecule of polyphenol family was grafted to the surface of bioactive glasses and, in order to study of effect of pH, acidified gallic acid with citric acid was employed for the functionalization as well.

2.1 Macroscopic observations on the samples

Figure 2-1 exhibited the SCNA and CEL2 bulk samples before and after functionalization process. As far as CEL2 is referred, after modification with gallic acid, the color of bulk sample transferred from colorless to brown. Similar changes of color were also found on the surface of CEL2 grafted by gallic acid with citric acid (CA) addition. On the other hand, no significant color variation was observed on the surface of SCNA functionalized by GA as well as GA+CA.

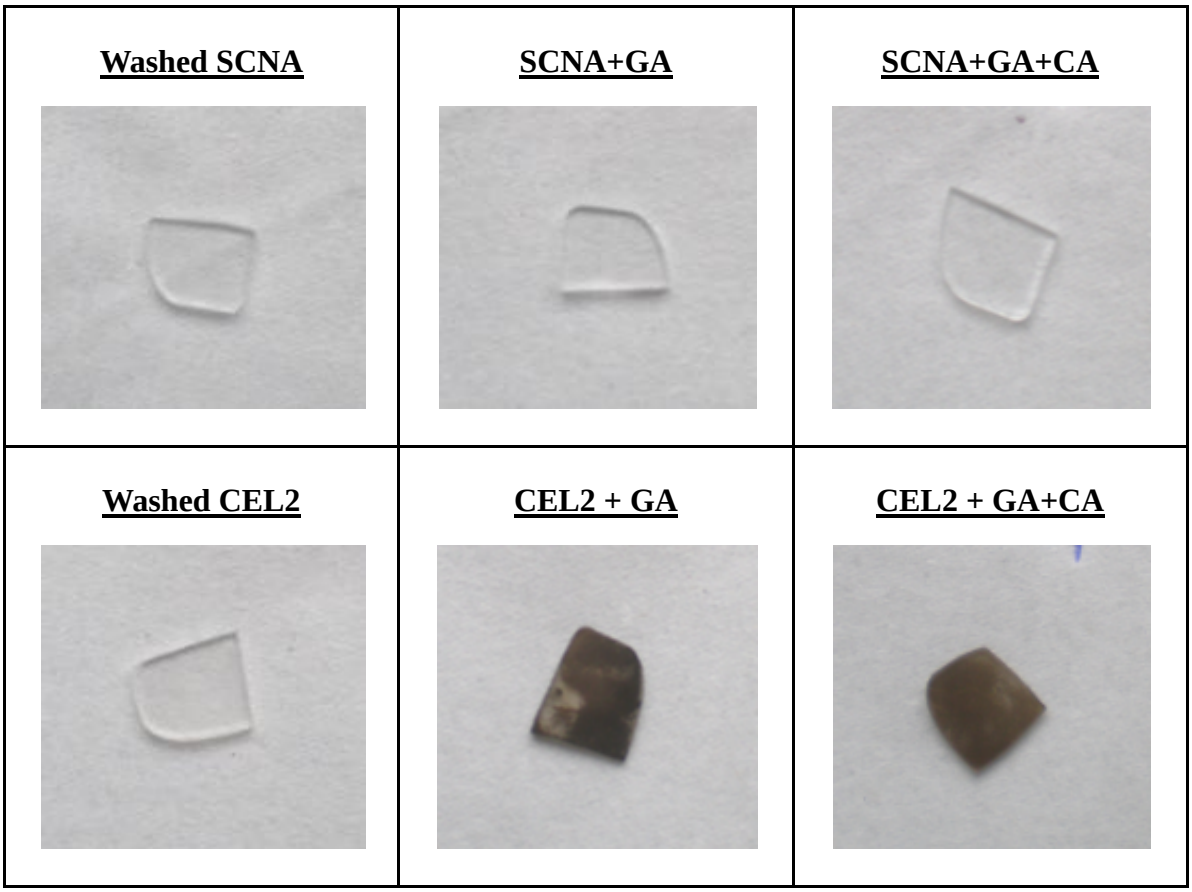

Figure 2-1: Glass bulks appearances before and after functionalization

Both SCNA and CEL2 powder samples were only functionalized by GA, and after solution was moved away, the powder appearances were observed in figure 2-2. The color of CEL2 powder transferred from white to brown, which was similar to bulk sample. However, compared with SCNA bulk, powder sample exhibited significant color changes from white to brown.

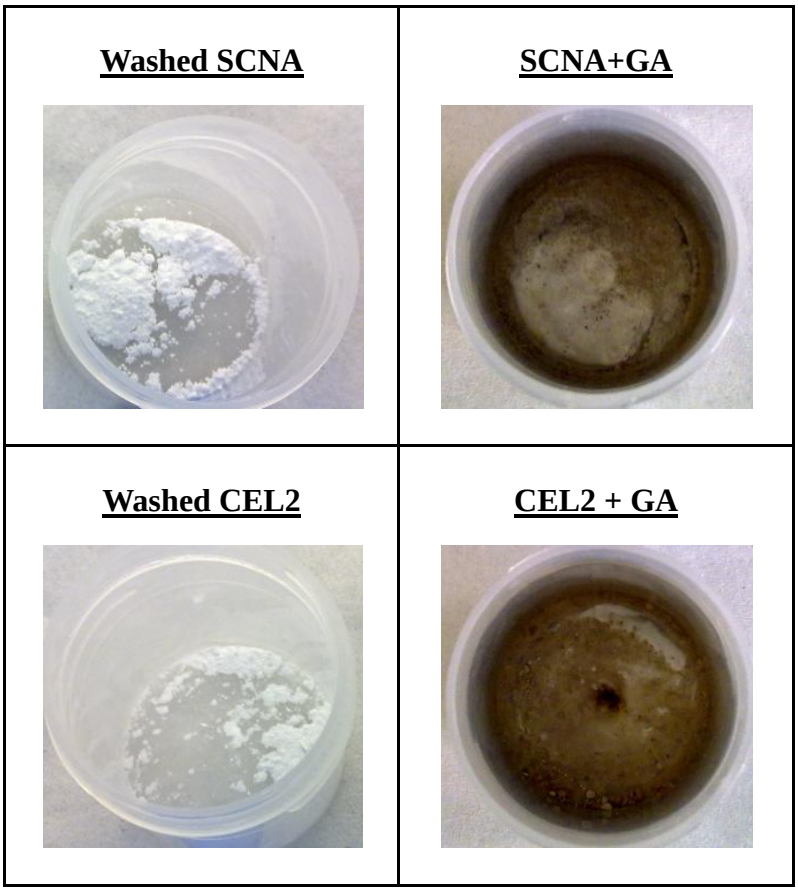

Figure 2-2: Glass powder appearances before and after functionalization

Figure 2-3 reported the color of gallic acid, gallic acid with citric acid and uptake solution after functionalization. GA solution in which the bulk samples were soaked for 24 hours exhibited a color change from colorless to dark green after CEL2 bulks were removed out. As for uptake solution of SCNA functionalization, no significant color change was observed. With the addition of citric acid, the mixed solution presented a light green after reacting with CEL2. It means that citric acid can reduce the color change in the uptake solution.

Figure 2-3: Gallic acid, gallic acid with citric acid and uptake solution after functionalization

2.2 pH measurement

In order to investigate the effect of pH and the addition of citric acid, pH value of GA solution was measured before and after soaking SCNA and CEL2 bulks for 24 hours with a pH-meter (figure 2-4) and the results were showed in figure 2-5. It should be underlined that, in the starting step, both two glasses were soaked in the GA solution, whose pH value was 3.22 ± 0.30 without the addition of CA.

Figure 2-4: Crison ® pH meter

After functionalization, notable changes of pH from acidic value to alkaline in uptake solution of both glasses could be observed, especially in the case of more reactive glass (CEL2) and the

powder samples (Table 2-1). In this case, the pH value is 3.45 for SCNA bulk and 7.99 for SCNA powder, 7.34 for CEL2 bulk and 8.68 for CEL2 powder.

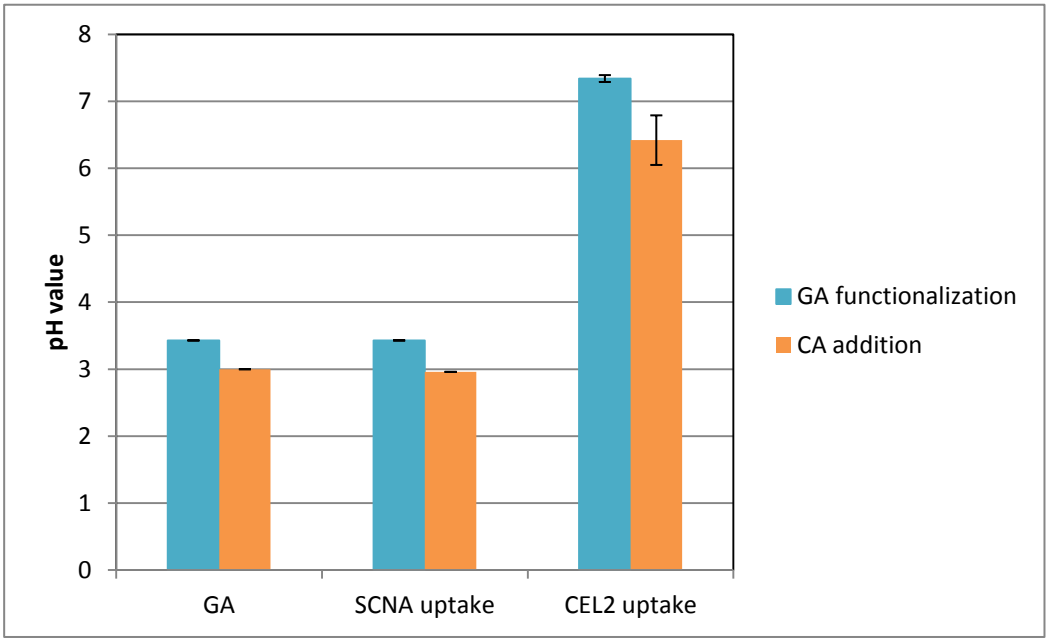

Figure 2-5: pH value of GA uptake solution before and after 24 hours soaking of different glass bulks, and the effect of CA addition in surface functionalization

Table 2-1 pH value of GA uptake solution before and after 24 h soaking of SCNA and CEL2 powders

Samples	**GA**	**SCNA+GA**	**CEL2+GA**
pH value	3.22	7.99	8.68

In general, the amorphous silica network of bioactive glasses can be attacked by water through the breaking of oxygen bridges and the forming of hydroxyl group, when glass is soaking in aqueous solution. The formation of –OH group could be promoted by the ion exchange between Na^+ from glass network and H_3O^+ from the aqueous solution. When an acid solution was employed, the –OH formation will be facilitated by the increase of ion exchange [1].

According to literature [2], the environment of an aqueous solution where bioactive glasses are soaked can transfer to an alkaline one with a static model of soaking, even if the solution was the

buffered simulated body fluids. The reason may be the decrease amount of H_3O^+ in the solution by ion exchange with Na^+.

Furthermore, an alkaline environment promotes a further hydroxylation of silica-based glasses through a direct disruptive action on the silica network catalyzed by the –OH anions in the solution. The promotion effect is much stronger on bioactive glasses characterized by high reactivity such as CEL2 than on almost inert glasses. Since the powder samples provided a larger surface area for reaction, the ion change was stronger than the bulk sample. As a result of basic environment, the catechol groups on GA structure can be oxidized and generate quinone groups [3]. This process leaded to the typical brownish color observed both on the glass surface and in uptake solution.

With addition of citric acid, the basification was weakened but not completely overcame. The pH value of uptake solution could be kept below 7.00, in fact this value is reported in literature as a favorable pH for the transition of GA structure from phenol group to quinone ones [3]. As a result, a strong color change of CEL2 uptake solution was significantly reduced compared with the one without CA addition.

2.3 UV-Vis measurements

2.3.1 Standard curve: gallic acid as the calibration standard

The standard calibration curve (figure 2-6) was obtained by the combination of Folin-Ciocalteau colorimetry (chapter IV) and UV-Vis spectroscopy after the reaction between Gallic acid solutions (different concentrations ranged from 0.0025 to 0.04 mg/ml) and Folin-Ciocalteau reagent.

In this case, GA solution, the calibration standard was prepared with six different concentrations (Table 2-2) to detect the absorbance at 760 nm by UV absorption technique. Moreover, absorbance detection was repeated at least three times to estimate the uncertainty, marked in figure 2-6 as the error bar. The correlation coefficient of this curve is 0.9997,

which represented for an extremely good linear relationship.

Table 2-2 concentrations of GA and absorbance

Number	Concentration [mg/ml]	Absorbance Mean±SD
1	0.0025	0.074204±0.001477
2	0.005	0.134941±0.002894
3	0.01	0.259997±0.005529
4	0.02	0.491553±0.00066
5	0.03	0.709862±0.012044
6	0.04	0.933102±0.007839

(n = 3 mean±SD)

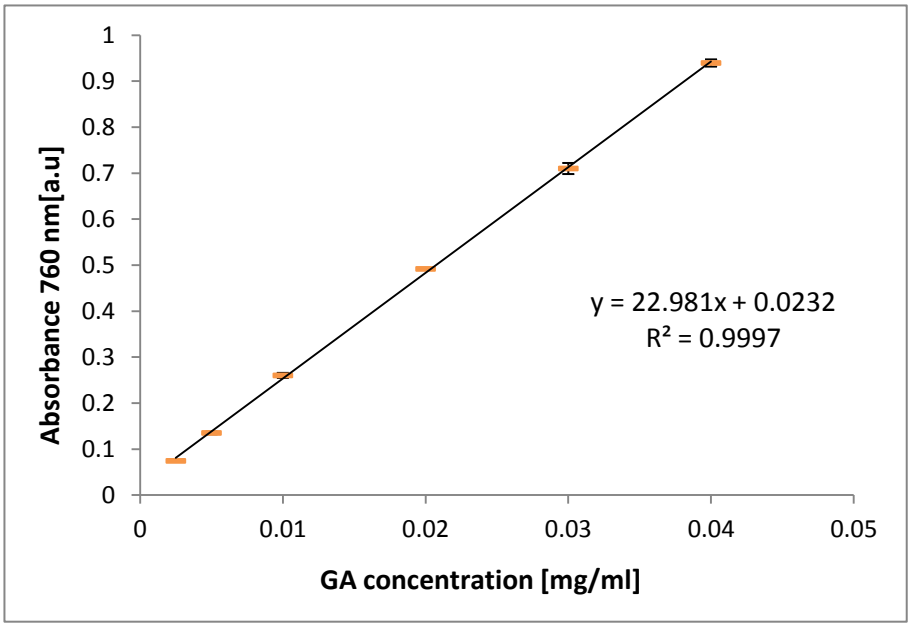

Figure 2-6: Standard calibration curve with GA as standard

2.3.2 Uptake solution analyzed by UV

In order to evaluate the consumption of gallic acid during the functionalization process, the amount of gallic acid in solution, both before and after grafting, was determined by Folin-Ciocalteau colorimetry and UV-Vis spectroscopy. On the basis of standard calibration curve, the amount of gallic acid was calculated.

The bar diagram in figure 2-7 exhibited the concentration of original gallic acid and gallic acid remaining in the uptake solution after soaking SCNA bulk and powder samples as well as CEL2 bulk and powder samples. In general, a decrease of gallic acid concentration can be observed in uptake solution of all samples, which means gallic acid was depleted during functionalization. Furthermore, it is notable that CEL2 consumed more gallic acid than SCNA, no matter bulk and powder samples (the value are 0.3293 and 0.9092 mg/ml, respectively). The reason could be that CEL2 has a higher surface reactivity with more –OH group exposure. Moreover, during functionalization process, the high reactivity of CEL2 could lead to the condensation of –OH groups and promote the formation of silica gel layer which can absorb and retain an additional amount of gallic acid.

Compared to bulk samples, powder samples of both glasses showed a higher depletion of gallic acid due to their larger specific surface area to bind more gallic acid molecules. In fact, the reduction in the amount of gallic acid in the functionalization medium is extremely high for both glass powders. On the other hand, it should be noticed that the strongly basic pH of solution recorded after modification of CEL2 (bulk and powder) and SCNA (powder) samples can affect and change the molecular structure of gallic acid and may lead to a different behavior during reaction with Folin-Ciocalteau’s reagent.

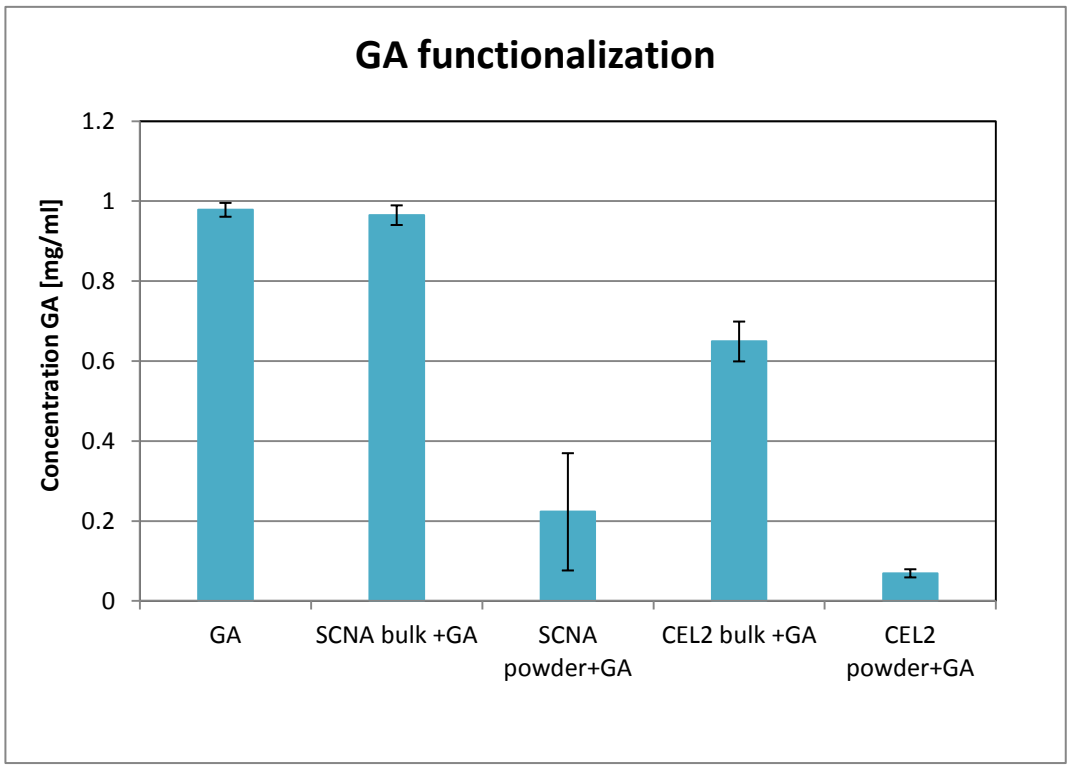

Figure 2-7: UV photometric results for GA uptake solution before and after 1 day soaking of different glass samples

The effect of citric acid addition to gallic acid solution on gallic acid depletion after functionalization is reported in figure 2-8. Compared to gallic acid without citric acid introduction, an apparent reduction of gallic acid uptake can be observed for both SCNA and CEL2 bulk samples. The reason may be that the significant reduction of the gallic acid content after functionalization without citric acid addition was partly attributed to an effective bond with glass and partly to the structure change of gallic acid when it is in a basic solution. At the same time, the observable depletion of gallic acid after citric acid introduction partly evidenced the success of grafting to some extent.

In order to evaluate the reversibility of grafting, citric acid was added in the uptake solution after soaking CEL2 bulk with and without citric acid addition to obtain a solution with pH 3.0. The consumptions of gallic acid content were 0.3064 and 0.3140 in uptake solution of CEL2+GA and CEL2+GA+CA with citric acid addition after functionalization, respectively. The results suggest that with the change of pH the grafting is stable to some extent.

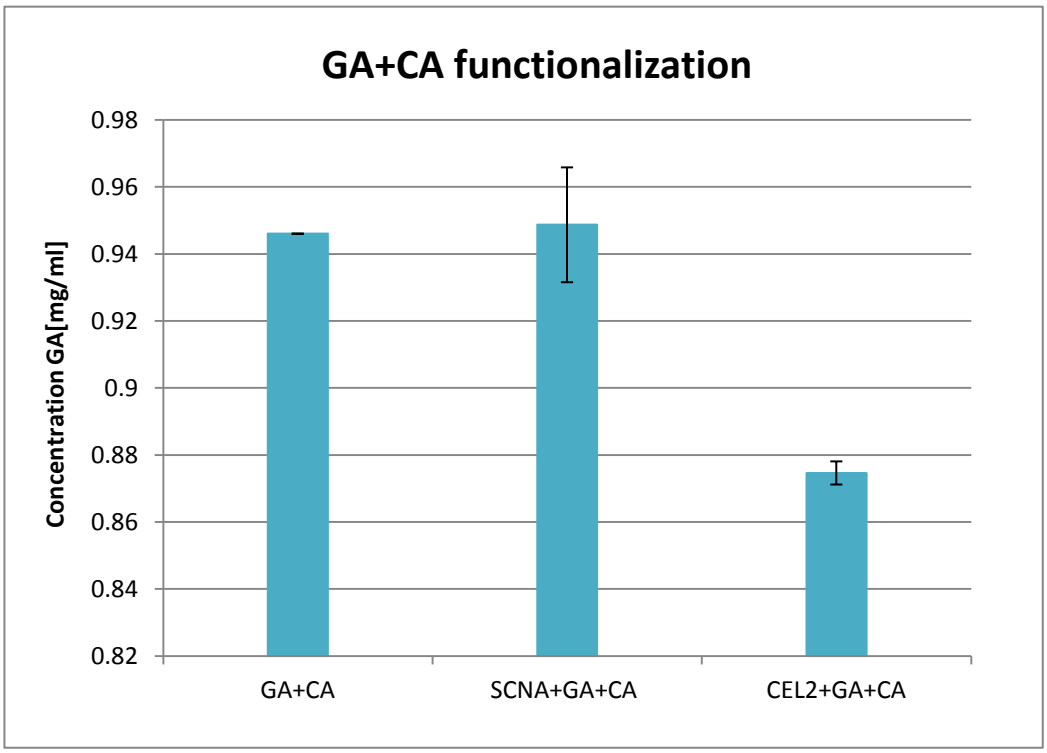

Figure 2-8: UV photometric results for GA+CA uptake solution before and after 1 day soaking of different glass samples

2.3.3 Functionalized bulk samples analyzed by UV

Bulk samples of SCNA and CEL2 were investigated after soaked in gallic acid solution for 24 hours by reacting with Folin-Ciocalteau's reagent (figure 2-9) cooperated with UV-Vis spectroscopy in order to determine the amount of gallic acid grafted on sample surface. The bar diagram in figure 2-10 exhibited the amount of gallic acid remaining on the bulk samples after functionalization. There was nearly no gallic acid detected on the surface of SCNA bulks while a relatively high amount of gallic acid remained on the surface of CEL2 bulks. The results were reasonable in comparison with the consumption amount of gallic acid due to the different reactivity level of two glasses. Another reason may be the amount of gallic acid on SCNA surface is too low to be detected by Folin-Ciocalteau colorimetry.

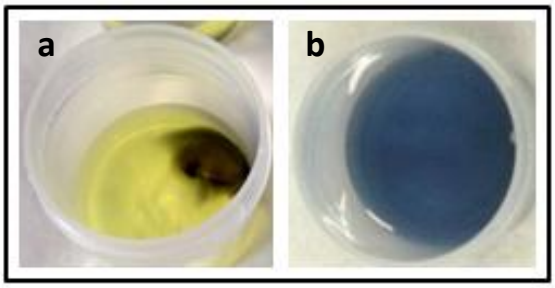

Figure 2-9: a) GA grafted bulk sample in FC reagent and b) uptake after 2h incubation

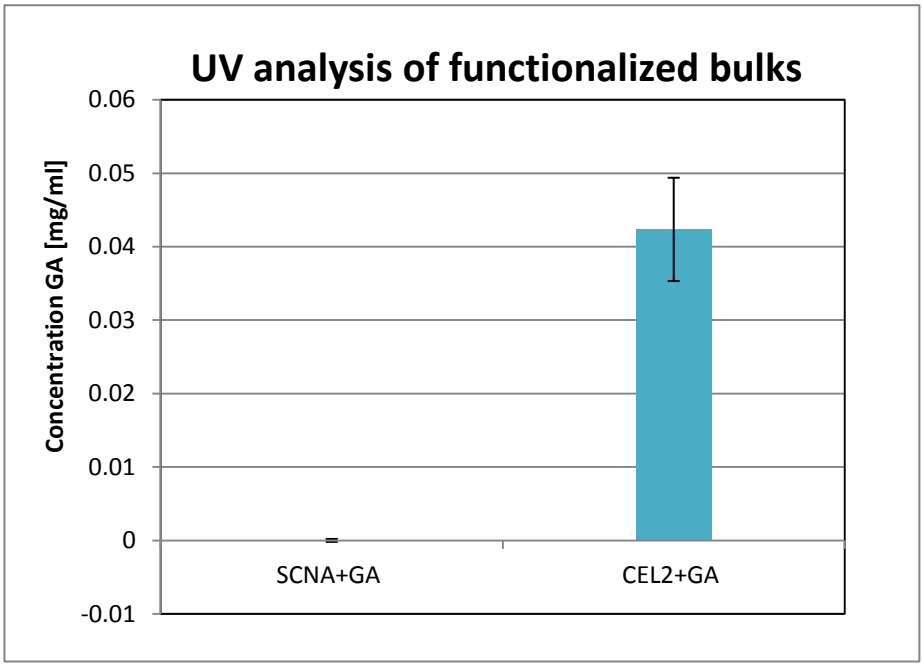

Figure 2-10: UV photometric results for SCNA and CEL2 bulk samples uptake after 1 day soaking in gallic acid solution

2.3.4 Release test in double distilled water

The release of both two types of glass powder sample after gallic acid functionalization process were investigated for one day release and one week release. The effectiveness was evaluated by gallic acid content in the release uptake solution after powder samples were incubated for 1 day and 1 week with the combination of UV and Folin-Cilcalteau colorimetry. From the bar diagram in figure 2-11, generally speaking, the release amount of gallic acid from SCNA and CEL2 powders were low with a value below 0.004 mg/ml (GA). Moreover, the release of both powder samples decreased along with the increase of time. Compared with

CEL2 powder, SCNA powder could release a higher amount of gallic acid for both 1 day release and 1 week release. The low release effectiveness may suggest the strong bond between glass surface and gallic acid molecules.

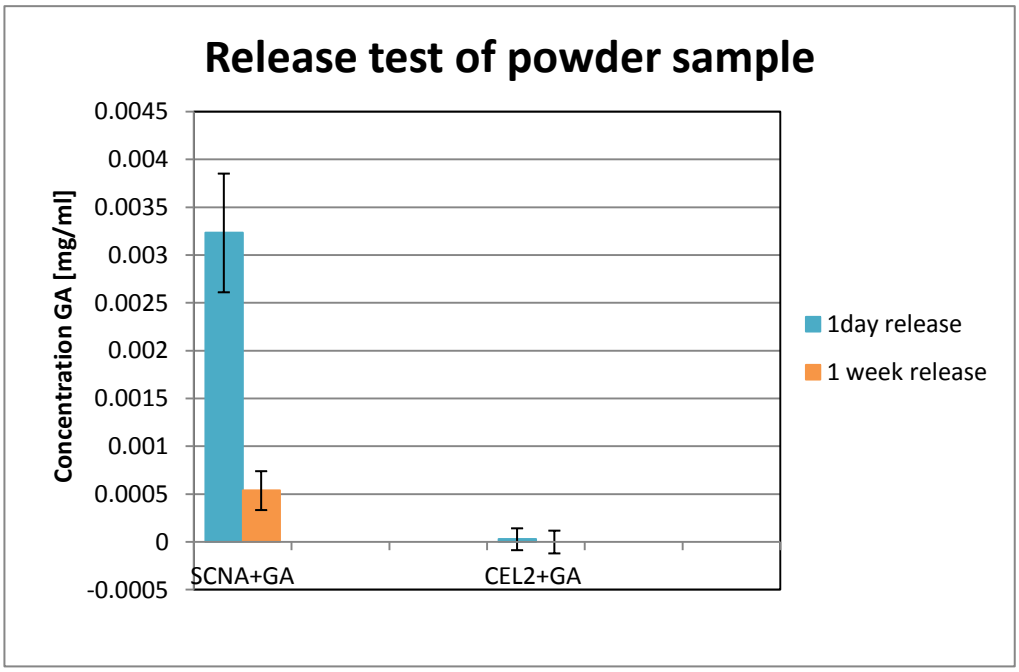

Figure 2-11: Release test of SCNA and CEL2 powder grafted by GA for 1 day and 1 week

2.4 XPS analysis

XPS was employed to characterize the chemical composition and kind of chemical bond on the outermost surface layer of the washed SCNA and CEL2 bulk samples as well as bulks grafted by gallic acid and gallic acid with addition of citric acid. Results were exhibited by the following spectra including survey spectra and detailed analyses of carbon and oxygen regions. The samples were named as follows:

i. SCNA (just washed sample)

ii. SCNA+GA

iii. SCNA+GA+CA

iv. CEL2 (just washed sample)

v. CEL2+GA

vi. CEL2+GA+CA

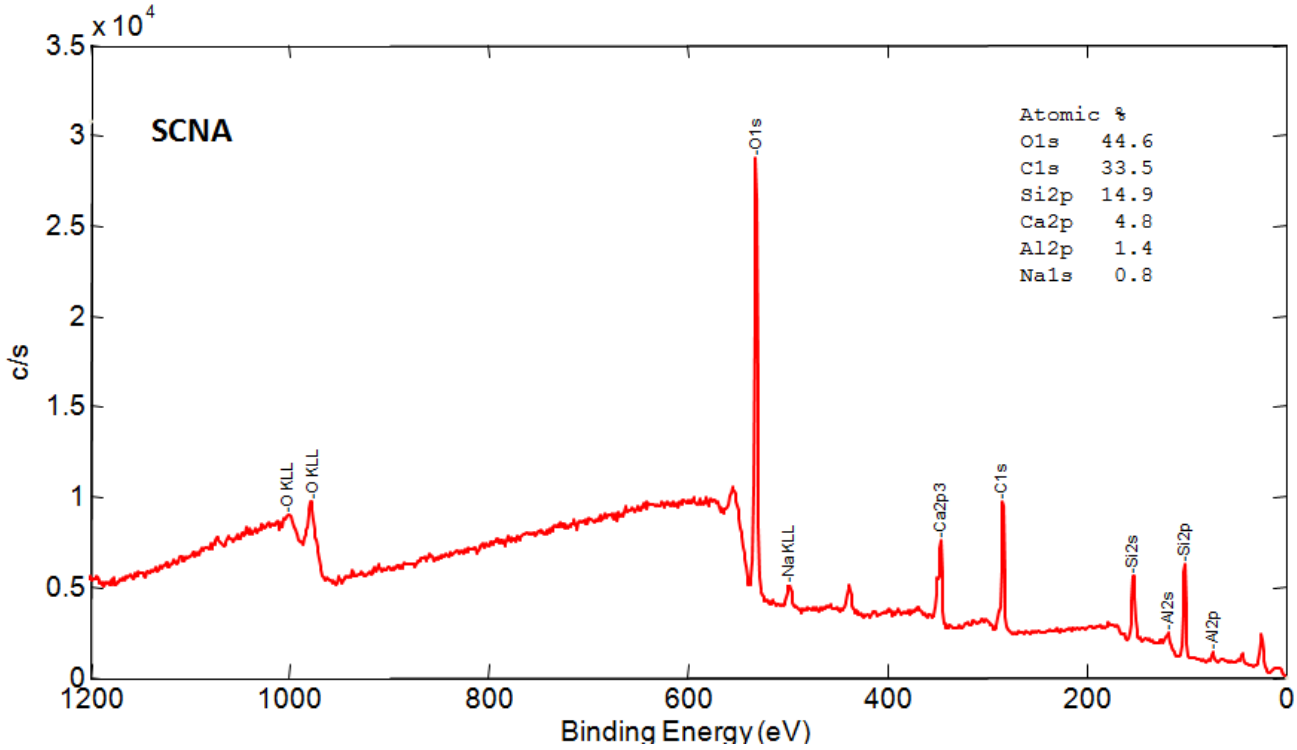

Figure 2-12: Survey spectra of SCNA

The survey spectra (figure 2-12) of washed SCNA highlighted all elements present on glass surface. Signals of elements from glass composition were observed. Carbon, which is commonly present in the first surface layers of materials, was also observed in this non-functionalized sample due to the unavoidable atmospheric contaminations. The atomic percentage of sodium was low, since the sodium atom stayed inside the glass matrix.

Figure 2-13 showed the detailed XPS analysis in carbon region of SCNA bulks. It can be observed that, a notable signal at about 284.8 eV was detected on surface of washed SCNA, which can be attributed to unavoidable hydrocarbon contaminants on reactive surface as widely mentioned in literature for XPS analysis of reactive materials [4]. A weak signal at about 289.38 eV can be assigned to carbonates [5]

The detailed analysis spectra (figure 2-14) of oxygen region underlined the presence of the characteristic signals for oxides at 531.7 eV, silica at 532.35 eV as well as hydroxyls at 533.54 eV as reported in literature related to surface activation [6].

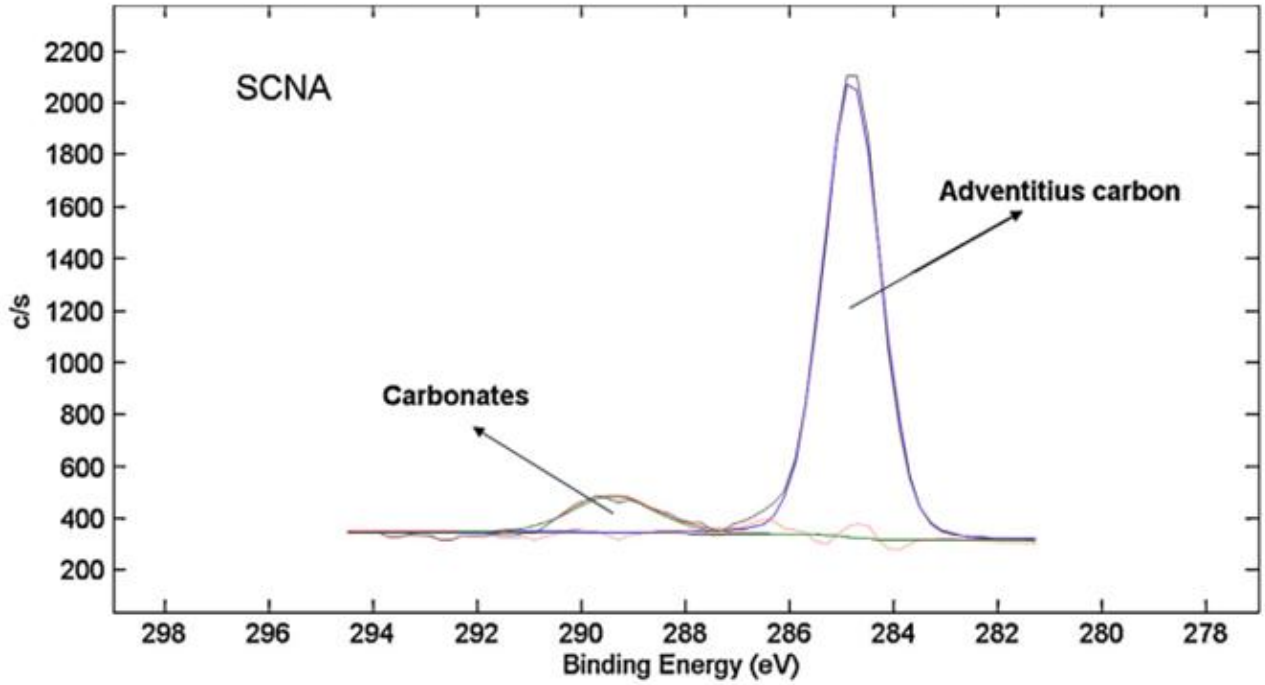

Figure 2-13: XPS detailed analysis of carbon region for SCNA washed sample

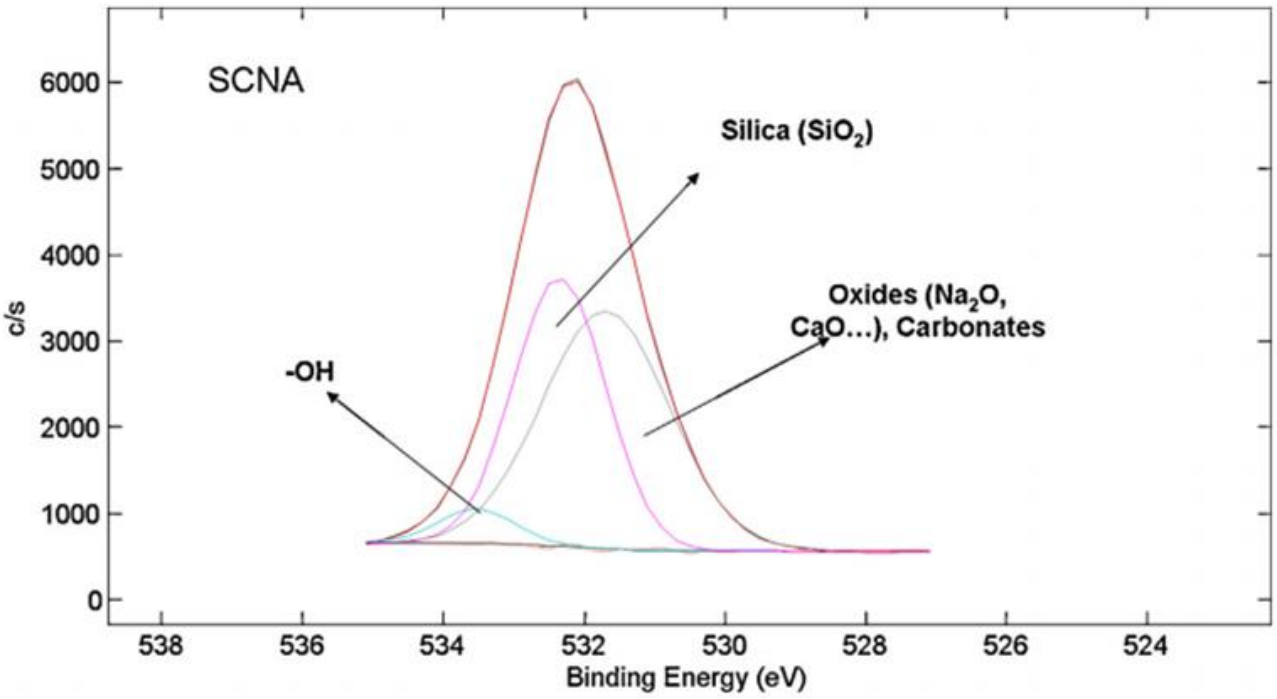

Figure 2-14: XPS detailed analysis of oxygen region for SCNA washed sample

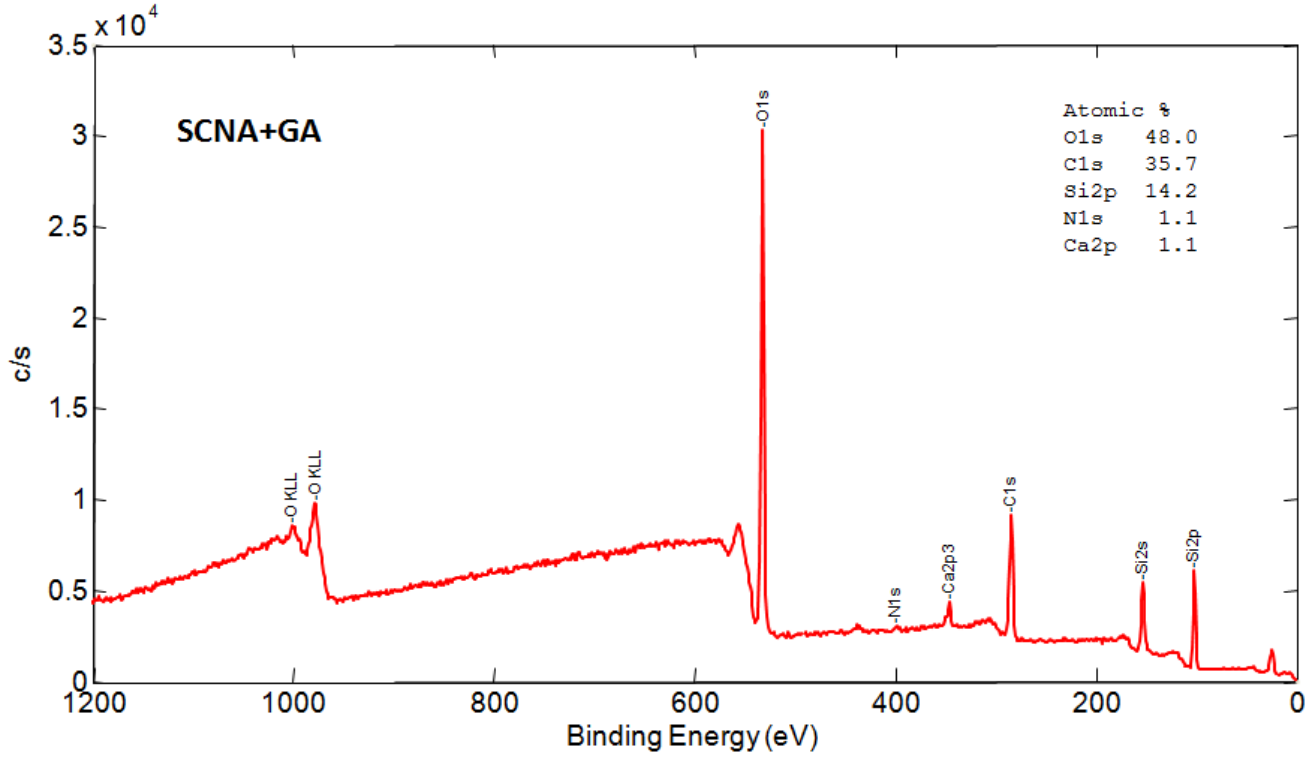

Figure 2-15: Survey spectra of SCNA+GA

The survey spectra (figure 2-15) of SCNA functionalized with gallic acid highlighted all elements present on glass surface. Signals of elements from glass composition were observed.

In detailed analysis spectra of carbon region on SCNA+GA (figure 2-16), different contributions can be detected after gallic acid functionalization. In particular, the signal of carbonate disappeared. Together with the peak of carbon contaminants at 284.83 eV, other two peaks at 286.23 eV and 288.22 eV were observed. They can be attributed to C-O and C=O bonds respectively, according to literature [7-10]. Similar results have been reported on gallic acid functionalized surfaces [9].

Figure 2-17 showed the detailed analysis spectra of oxygen region on SCNA bulk after gallic acid modification. A notable increase in the –OH signal at 533.58 eV further evidenced the presence of gallic acid. Peak at 531.71can be attributed to oxides but also to C=O bonds [11].

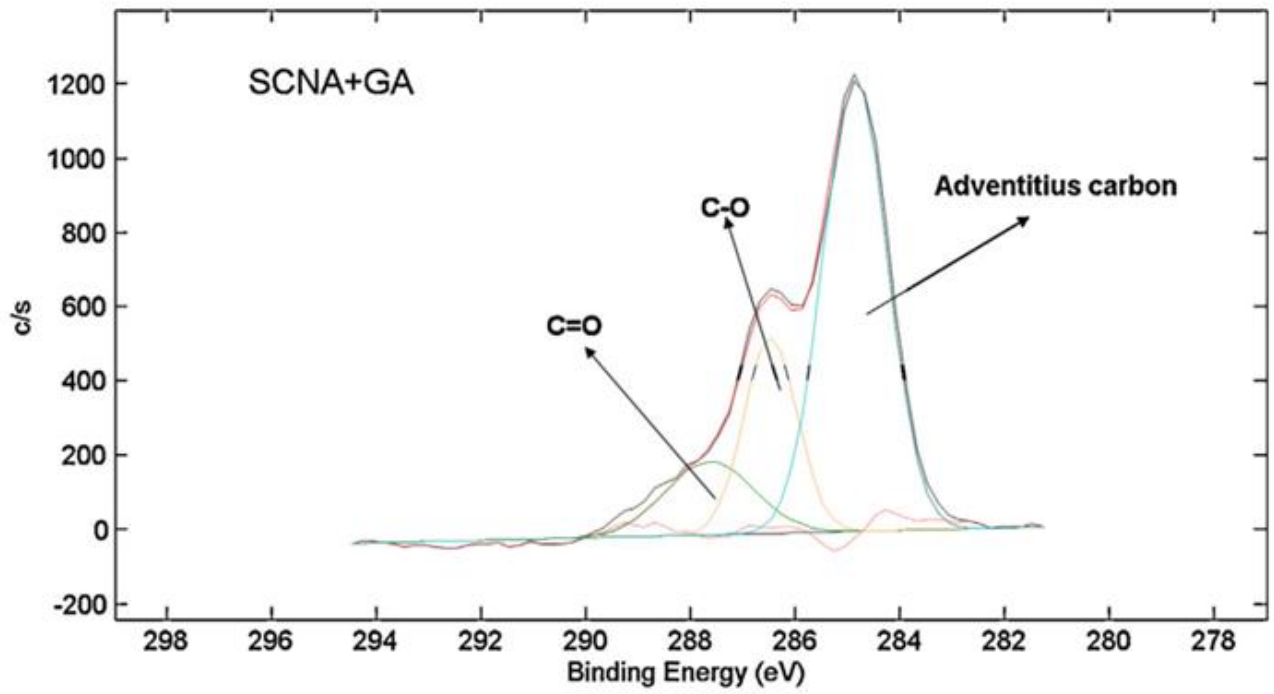

Figure 2-16: XPS detailed analysis of carbon region for SCNA+GA sample

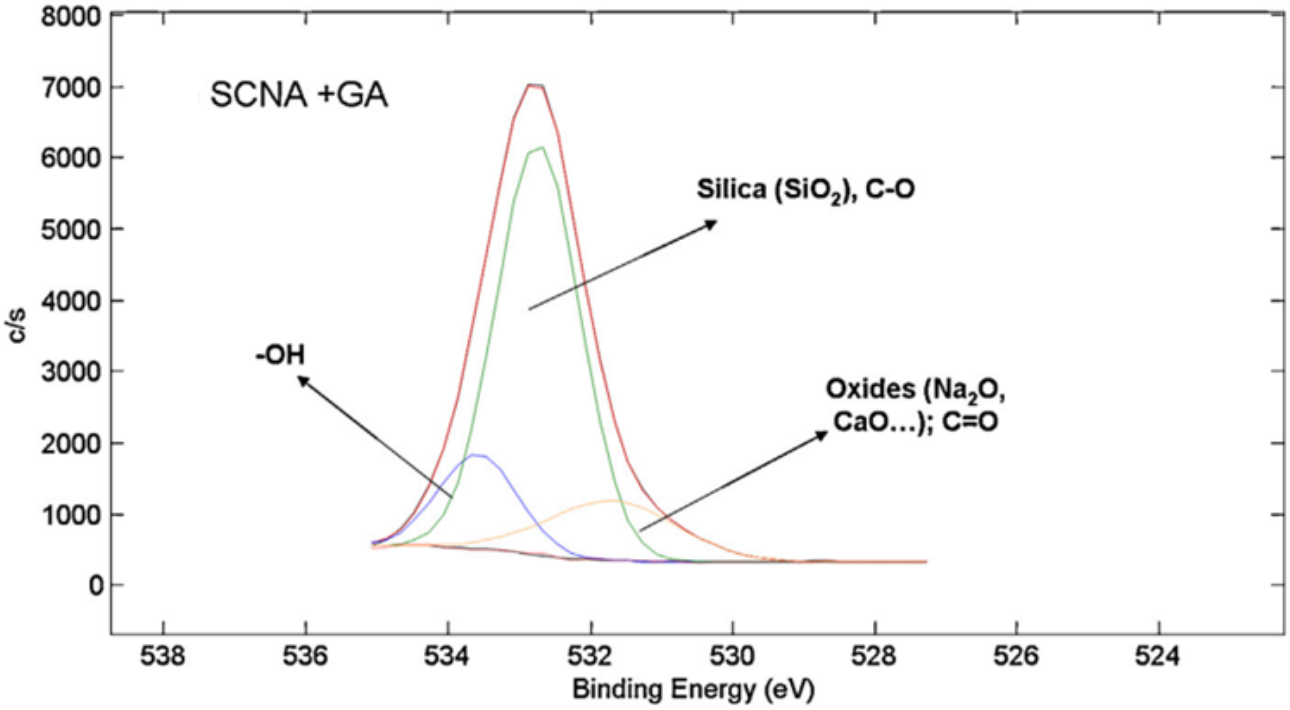

Figure 2-17: XPS detailed analysis of oxygen region for SCNA+GA sample

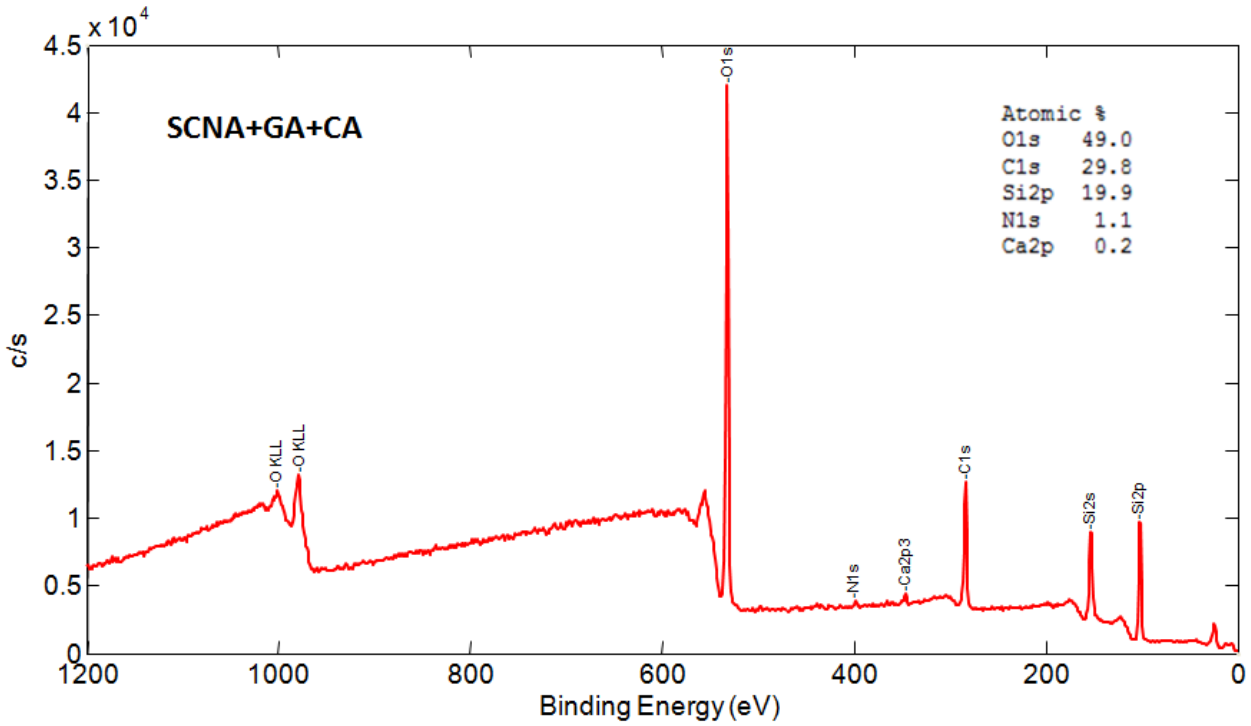

Figure 2-18: Survey spectra of SCNA+GA+CA

Figure 2-18 displayed the survey spectra of SCNA functionalized by gallic acid with addition of citric acid. It highlighted all elements present on glass surface. Signals of elements from glass composition were observed.

After functionalization with addition of citric acid, a reduction of C=O signal (at about 288 eV) can be observed compared to the one without citric acid in detailed analysis of carbon region (figure 2-19). This result confirms the possibility of citric acid to inhibit the oxidation of gallic acid to quinone.

In the detailed analysis of oxygen region (figure 2-20), a significant decrease in signals of –OH group at about 533.5 eV as well as signal of C=O at about 531.6 eV can be detected in accordance to the results obtained in carbon region.

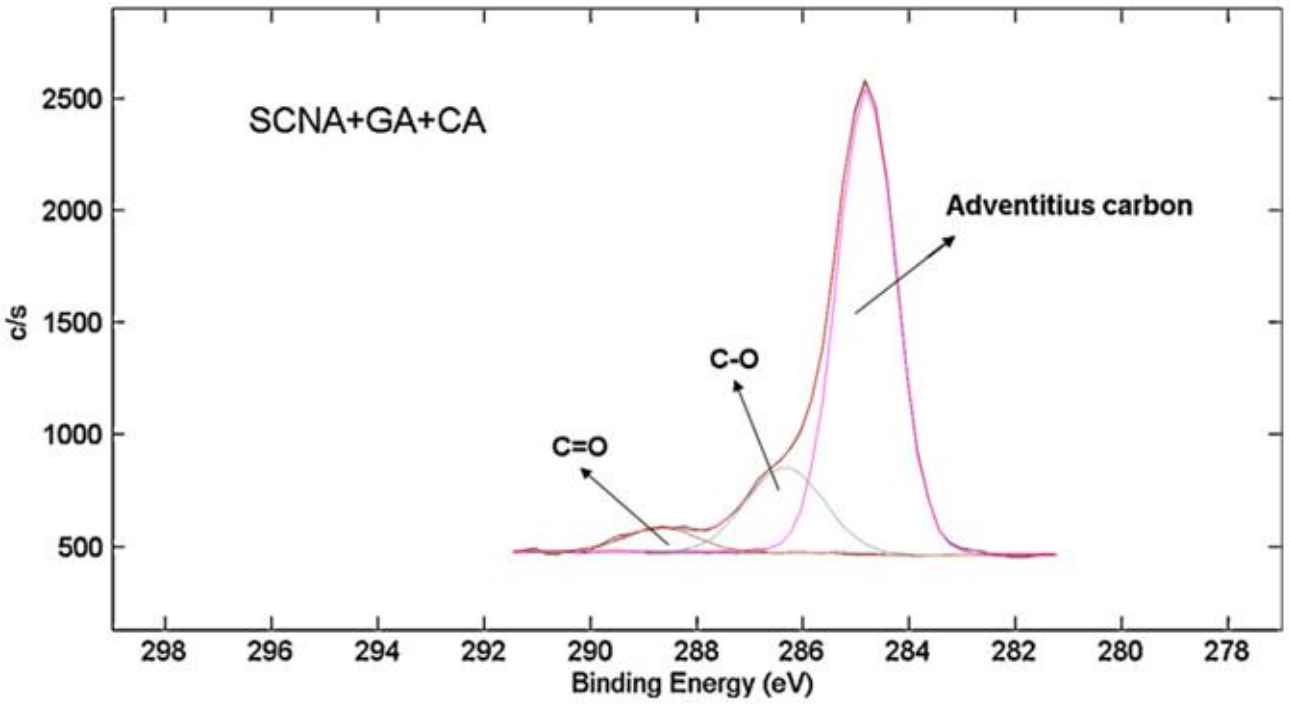

Figure 2-19: XPS detailed analysis of carbon region for SCNA+GA+CA sample

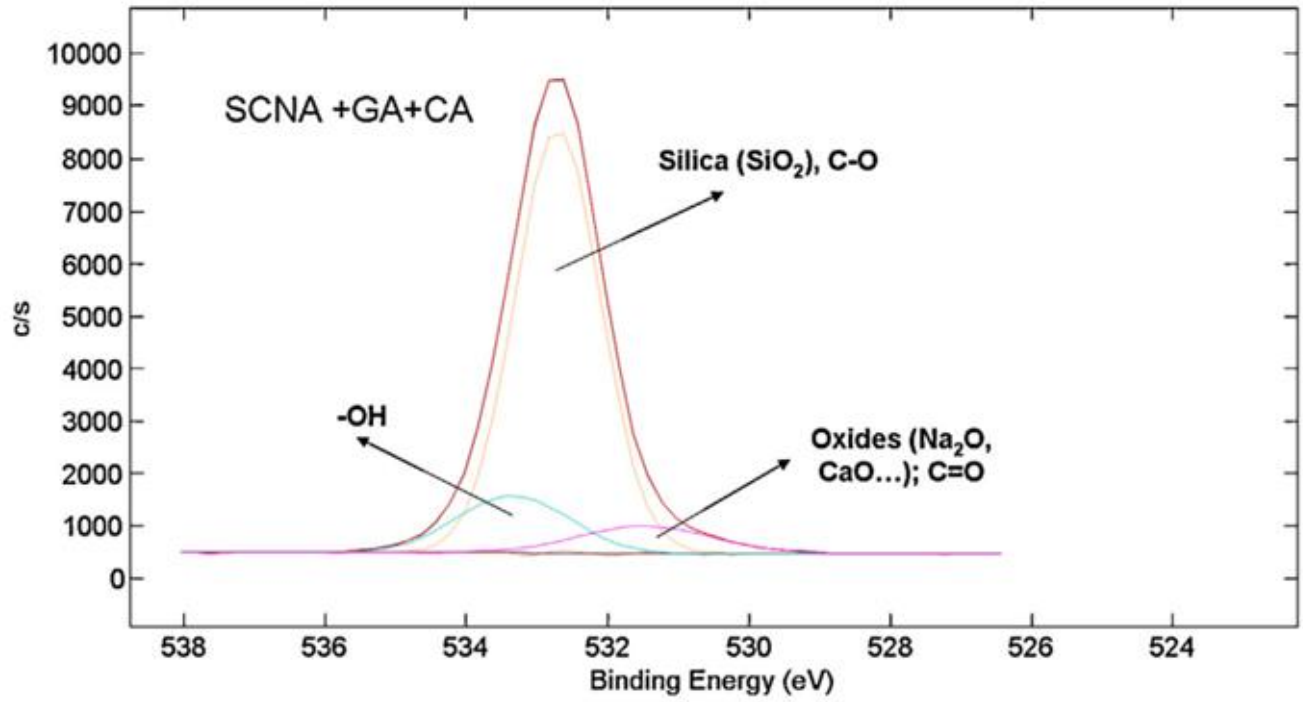

Figure 2-20 XPS: detailed analysis of oxygen region for SCNA+GA sample

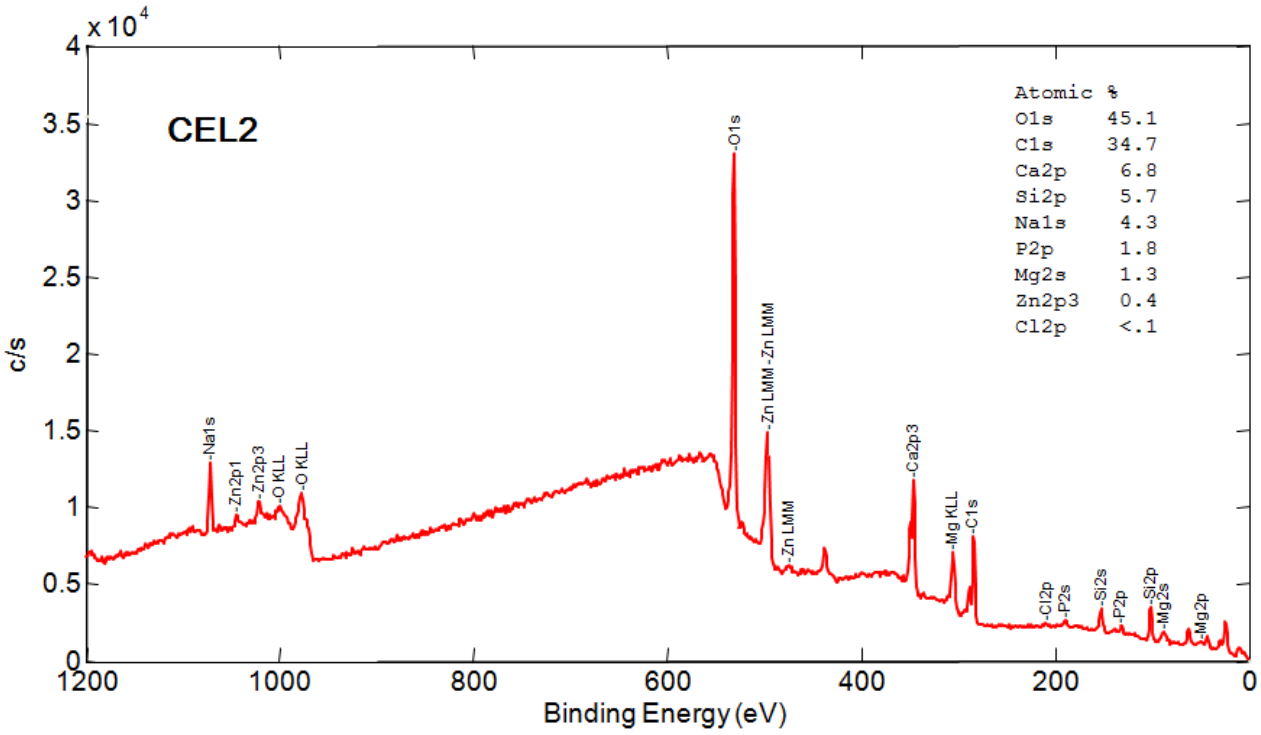

Figure 2-21: Survey spectra of CEL2 washed sample

The survey spectra (figure 2-21) of washed CEL2 highlighted all elements present on glass surface. Signals of elements from glass composition were observed, including oxygen, calcium, silicon, magnesium and sodium. Carbon, which is commonly present in the first surface layers of materials, was also observed in this non-functionalized sample due to the unavoidable atmospheric contamination.

Figure 2-22 showed the detailed XPS analysis of carbon region of CEL2 bulks. It can be observed that, a notable signal at about 284.85 eV was detected on surface of washed CEL2, which can be attributed to unavoidable hydrocarbon contaminants on reactive surface as widely mentioned in literature for XPS analysis of reactive materials [4]. Compared to SCNA, a signal at about 289.66 eV with higher intensity can be assigned to carbonates [5]

The detailed analysis spectra (figure 2-23) of oxygen region underlined the presence of the characteristic signals for oxides at 530.84 eV, silica at 531.63 eV as well as hydroxyls at 533.26 eV as reported in literature related to surface activation [6]. It should be underlined that the signal of –OH is stronger than that of SCNA due to the higher reactivity of CEL2 with more

–OH groups exposed on the surface.

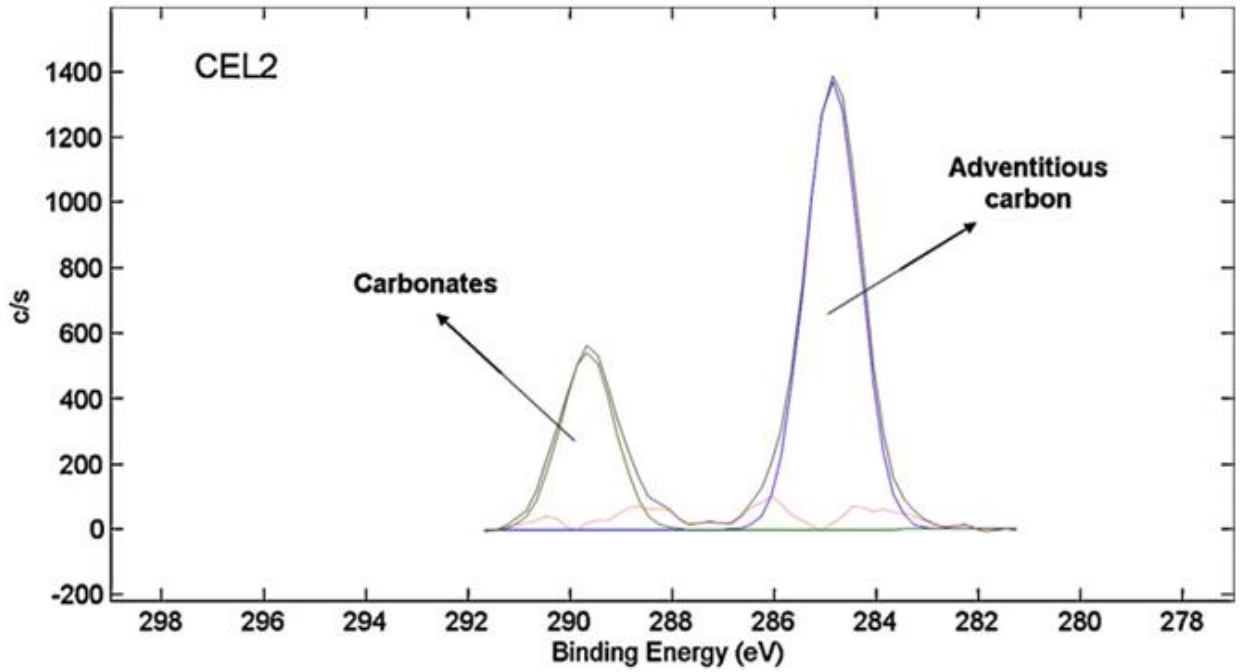

Figure 2-22: XPS detailed analysis of carbon region for CEL2 washed sample

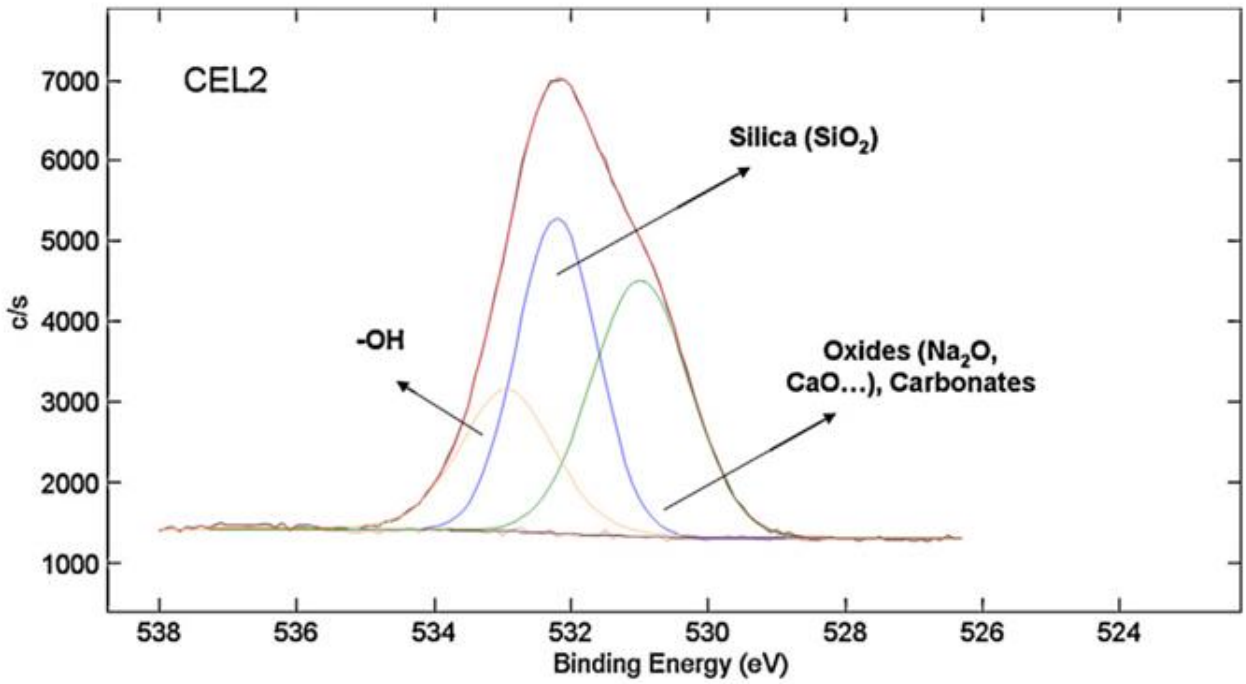

Figure 2-23: XPS detailed analysis of oxygen region for CEL2 washed sample

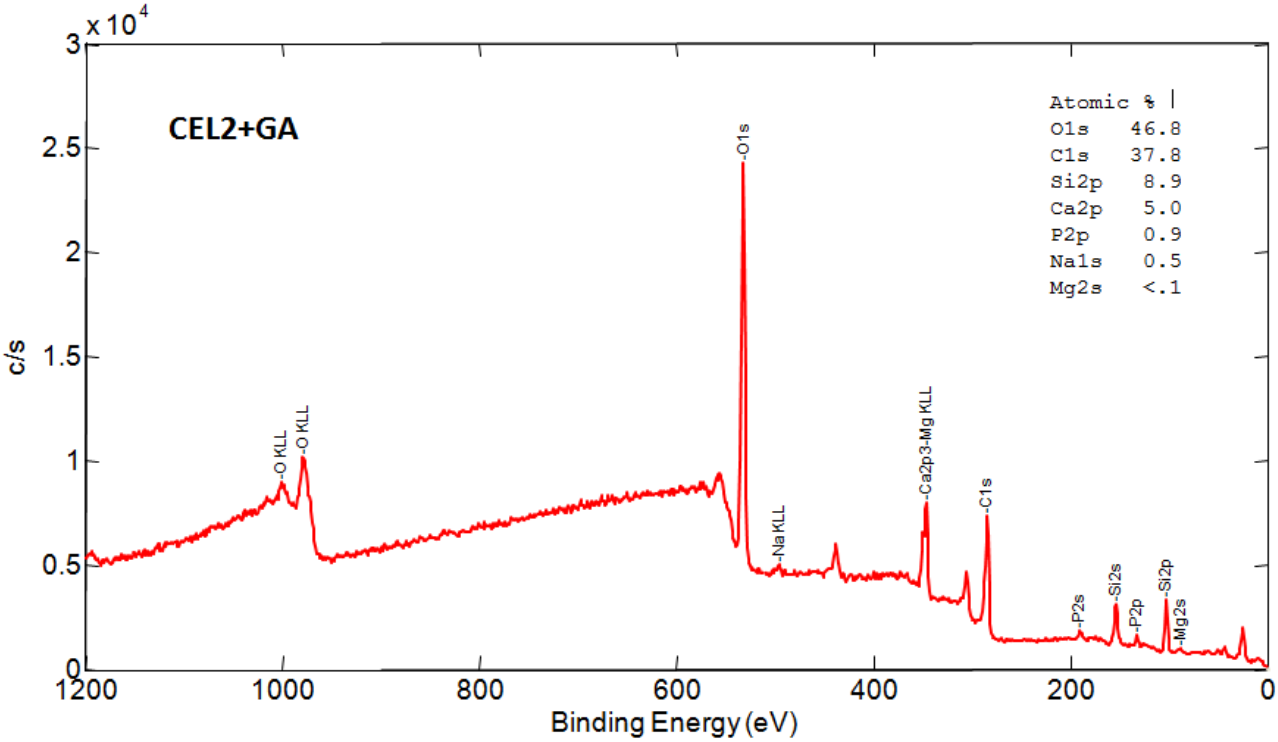

Figure 2-24: Survey spectra of CEL2+GA sample

The survey spectra (figure 2-24) of CEL2 functionalized with gallic acid highlighted all elements present on glass surface. Signals of elements from glass composition were observed, including oxygen, calcium, silicon, phosphorus, magnesium as well as carbon. Sodium content was lower probably due to the ion exchange with the aqueous solution.

In detailed analysis spectra of carbon region on CEL2+GA (figure 2-25), different contributions can be detected after gallic acid functionalization. In particular, the signal of carbonate disappeared. Together with the peak of carbon contaminants at 284.83 eV, other two peaks at 286.23 eV and 288.22 eV were observed. They can be attributed to C-O and C=O bonds according to literature [7, 8].

Figure 2-26 showed the detailed analysis spectra of oxygen region on CEL2 bulk after gallic acid modification. A significant increase in the –OH signal at 533.59 eV further evidenced the presence of gallic acid. Peak at 531.35 eV can be attributed to oxides but also to C=O bonds [11].

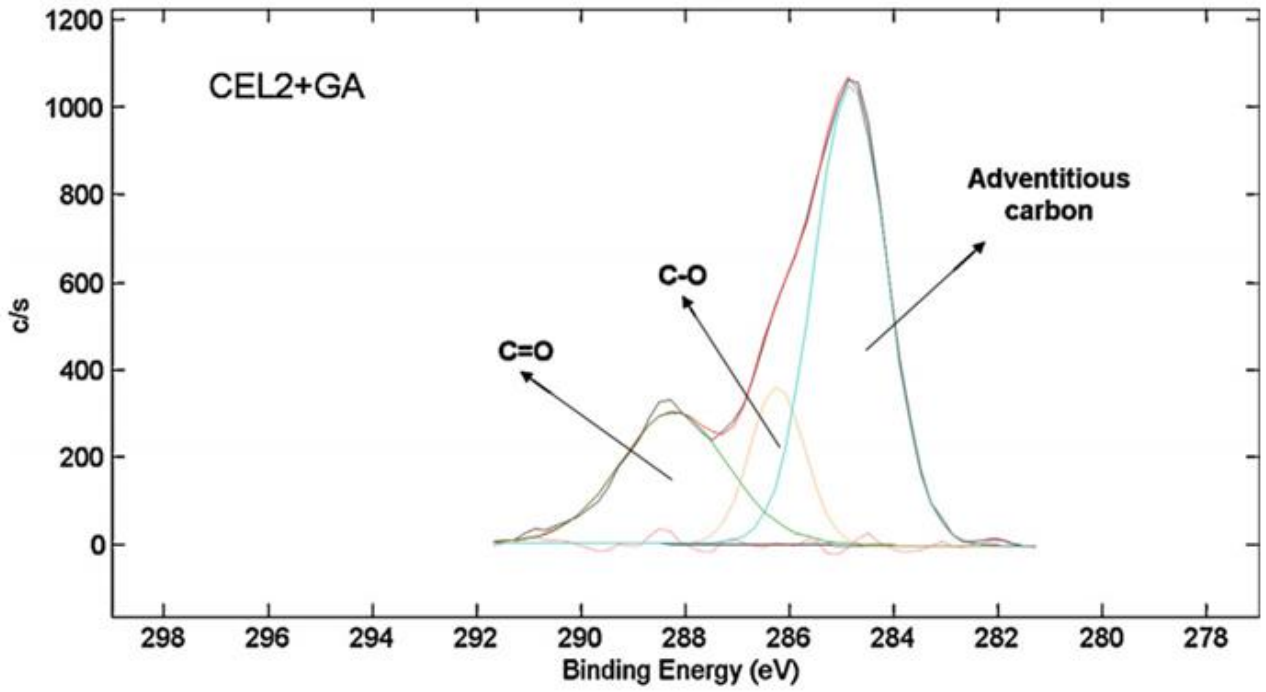

Figure 2-25: XPS detailed analysis of carbon region for CEL2+GA sample

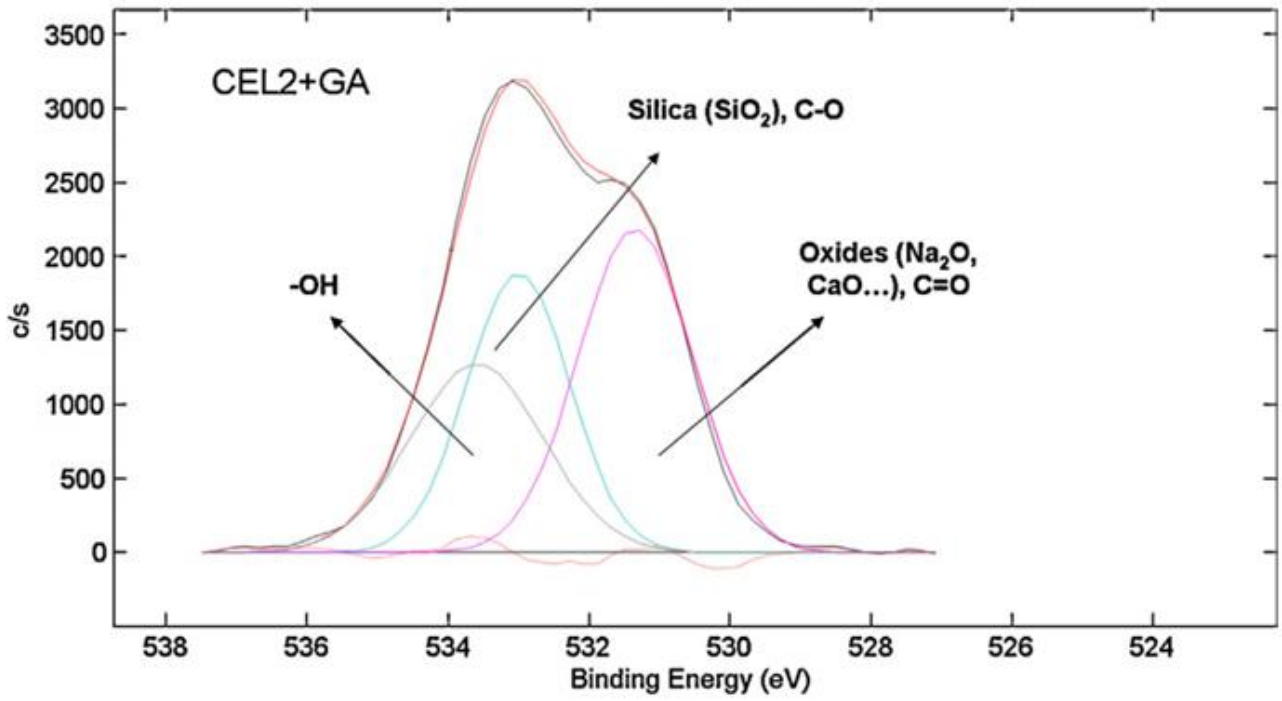

Figure 2-26: XPS detailed analysis of oxygen region for CEL2+GA sample

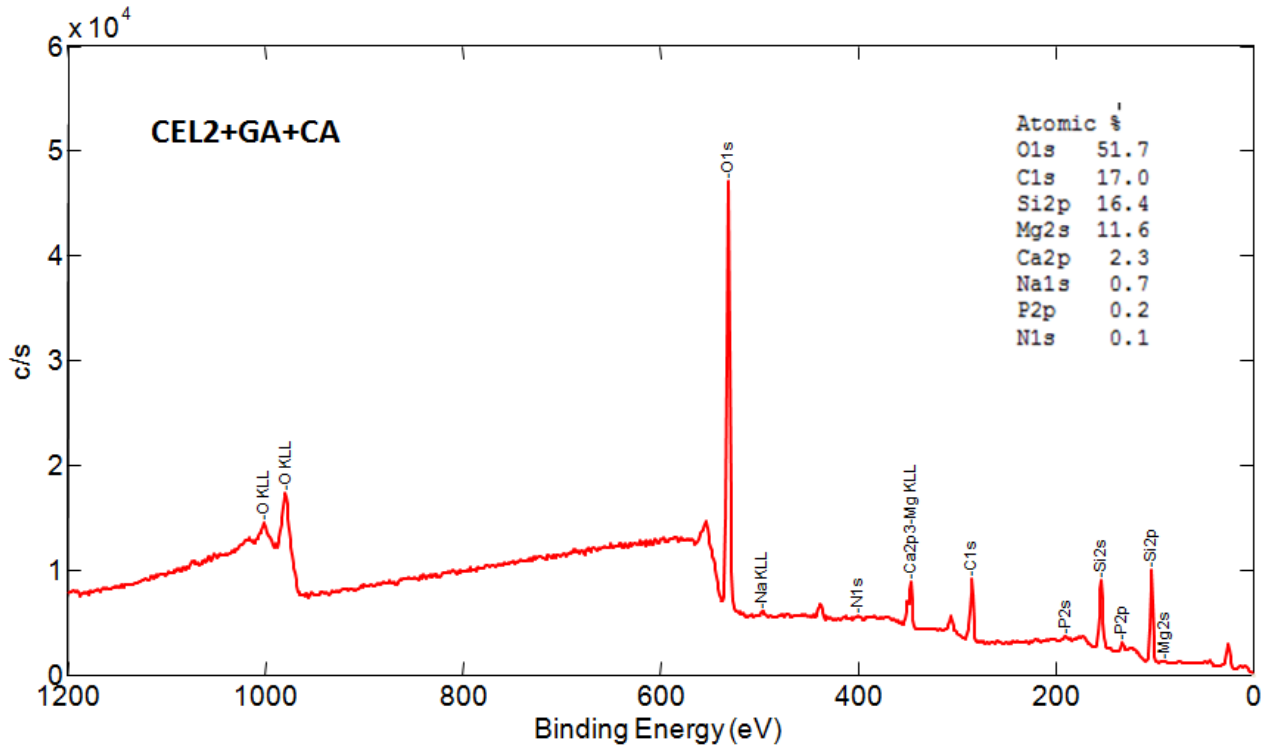

Figure 2-27: Survey spectra of CEL2+GA+CA sample

Figure 2-27 displayed the survey spectra of CEL2 functionalized by gallic acid with addition of citric acid. Signals of elements from glass composition were observed, including calcium, silicon, phosphorus, magnesium as well as carbon. Also, on this sample, sodium was present with a low atomic percentage probably due to the ion exchange with solution.

Similar to SCNA, after functionalization with addition of citric acid, a reduction of C=O signal (at about 288 eV) can be observed compared to the one without citric acid in detailed analysis of carbon region (figure 2-28). This result confirms the possibility of citric acid to inhibit the oxidation of gallic acid into quinone.

In the detailed analysis spectra of oxygen region (figure 2-29), a significant decrease in signals of –OH group at about 533.5 eV as well as signal of C=O at about 531.6 eV could be detected in accordance to the results obtained in carbon region.

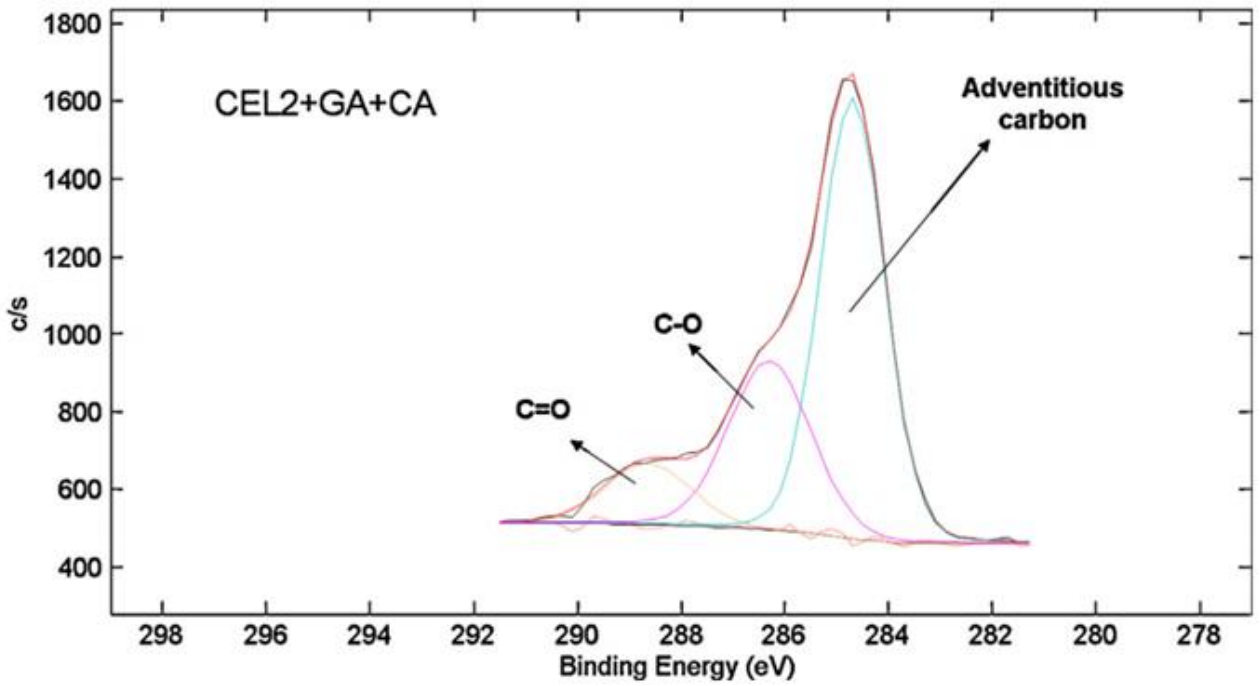

Figure 2-28: XPS detailed analysis of carbon region for CEL2+GA+CA sample

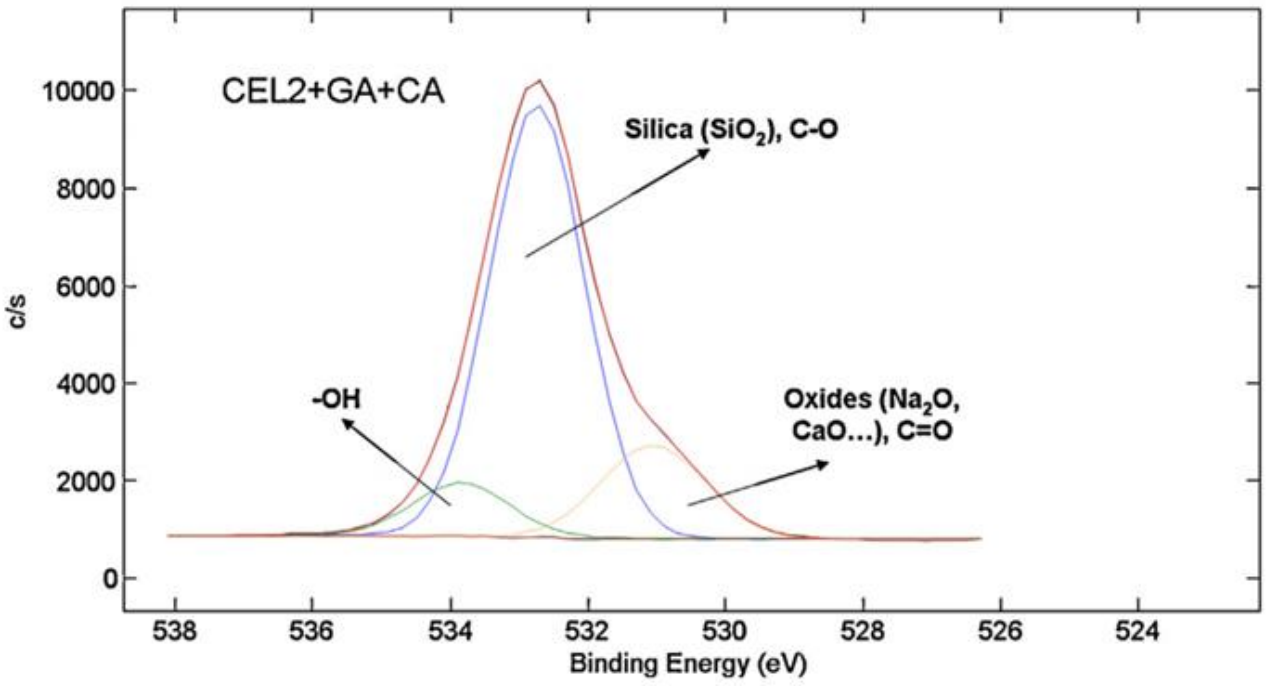

Figure 2-29: XPS detailed analysis of oxygen region for CEL2+GA+CA sample

Table 2-3 XPS atomic percentage analysis of bulk samples

Element [at%]	SCNA			CEL2		
	Washed	GA	GA+CA	Washed	GA	GA+CA
O	44.6	48.0	49.0	45.1	46.8	51.7
C	33.5	35.7	29.8	34.7	37.8	17.0
Si	14.9	14.2	19.9	5.7	8.9	16.4
Ca	4.8	1.1	0.2	6.8	5.0	2.3
Al	1.4	-	-	-	-	-
Na	0.8	-	-	4.3	0.5	0.7
P	-	-	-	1.8	0.9	0.2
Mg	-	-	-	1.3	<0.1	11.6
Other	-	1.1	1.1	<0.5	-	0.1

The atomic percentage analysis of elements detected by means of the survey analysis was listed in Table 2-3. It can be observed that on surface of both washed SCNA and CEL2 samples, a certain amount of unavoidable carbon contaminants stilled remained, even though a washing treatment has been performed as widely reported in the literature for XPS analysis of reactive materials [12-14].

After functionalization with gallic acid, a certain increase in surface carbon and oxygen content can be detected on both SCNA and CEL2 surfaces. However, with the addition of citric acid in the functionalization medium, a reduction in the surface carbon content and a more evident increase in the oxygen content were observed.

Through the analysis of surface chemical composition, a notable decrease in sodium and calcium content could be detected for both glasses due to the ion exchange process between bioactive glass surface and the grafting solution.

In addition, after GA grafting, no change of the silicon content happened to SCNA, while for gallic acid grafted CEL2, a significant increase of silicon content could be observed in comparison with washed CEL2. The increase in the surface silicon content was observed after functionalization with addition of citric acid for CLE2 and also for SCNA. These observations suggest certain dissolution of the glass matrix in the functionalization medium added with citric acid, which result in a higher SiO_2 exposition and higher removal of adventitious carbon.

2.5 SEM analysis

The SEM-EDS analyses were performed to analyze the surface morphology of the samples, as well as their chemical composition on bulks before and after gallic acid grafting to obtain clear evidence about the difference in the substrate reactivity.

SCNA washed

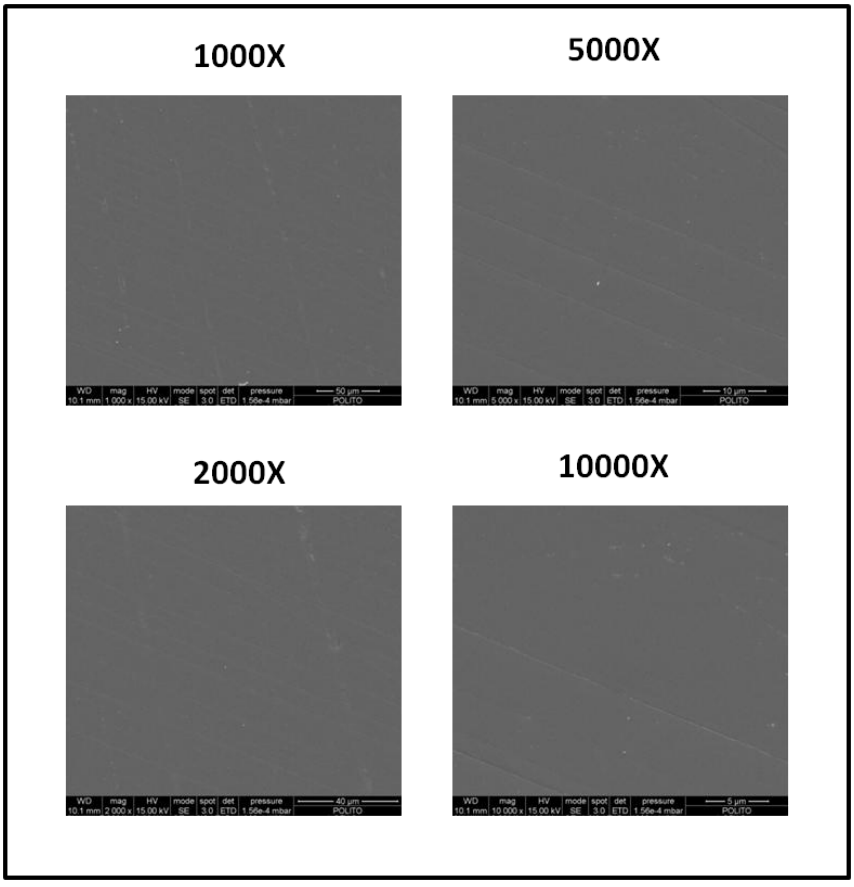

Figure 2-30: SEM images of washed SCNA samples with different magnifications

Figure 2-30 exhibited the images of washed SCNA bulk with different magnifications from 1000 × to 10000×. A uniform surface was present with slightly polishing lines.

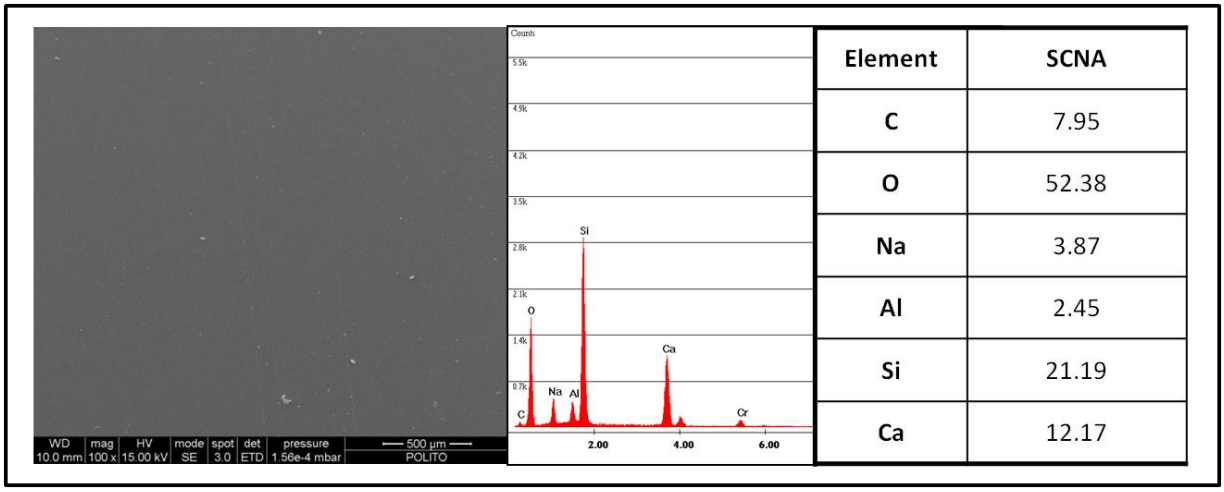

Element	SCNA
C	7.95
O	52.38
Na	3.87
Al	2.45
Si	21.19
Ca	12.17

Figure 2-31: SEM images and EDS analysis of SCNA washed

EDS analysis (figure 2-31) demonstrated the elements detected on SCNA and all elements of glass composition were observed such as oxygen, silicon, sodium, calcium as well as aluminum. Carbon was present on the surface, which is ascribed to contaminant on the surface.

SCNA+GA

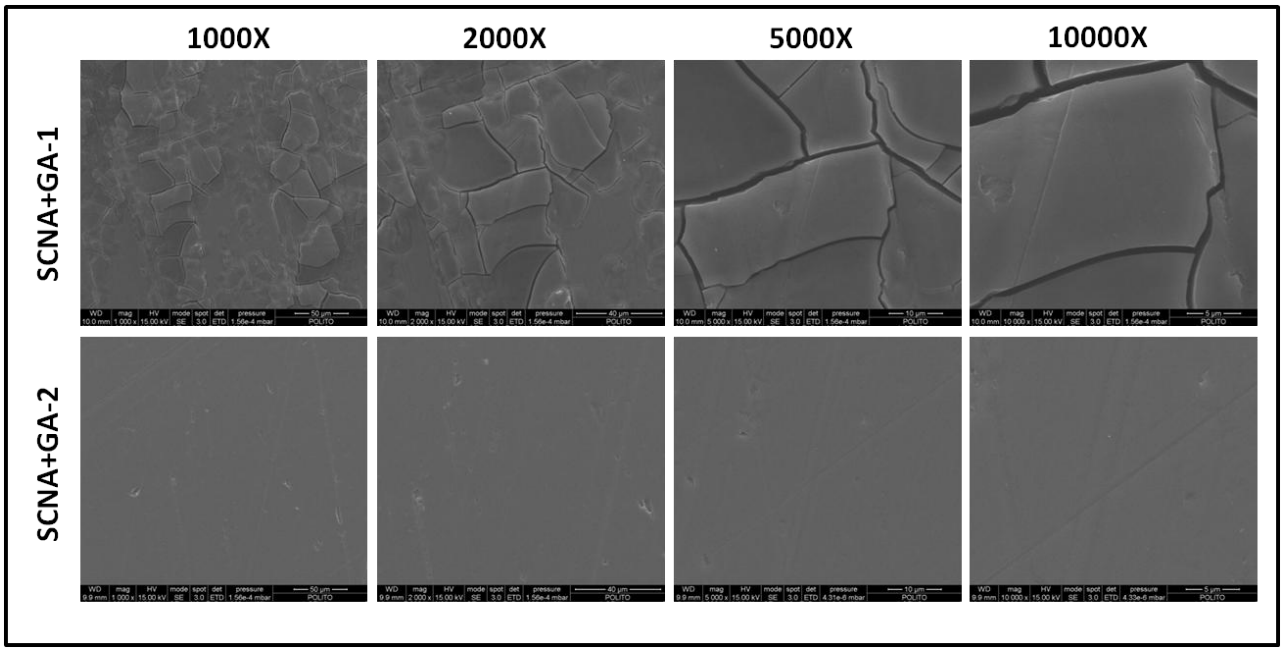

Figure 2-32: SEM images of gallic acid grafted SCNA samples with different magnifications in

two areas

In order to investigate the homogeneity of surface morphology, two different areas were selected and analyzed by SEM. Figure 2-32 displayed the images from two different areas named as SCNA+GA-1 and, respectively, with magnification of 1000×, 2000×, 5000× and 10000×.

After grafting with gallic acid, two different surface morphologies can be observed in SCNA+GA-1 and SCNA+GA-2. SCNA+GA-1 area presents a quite cracked surface with the typical morphology of the silica gel layer, while the other area showed a uniform surface which is analogous to the washed SCNA.

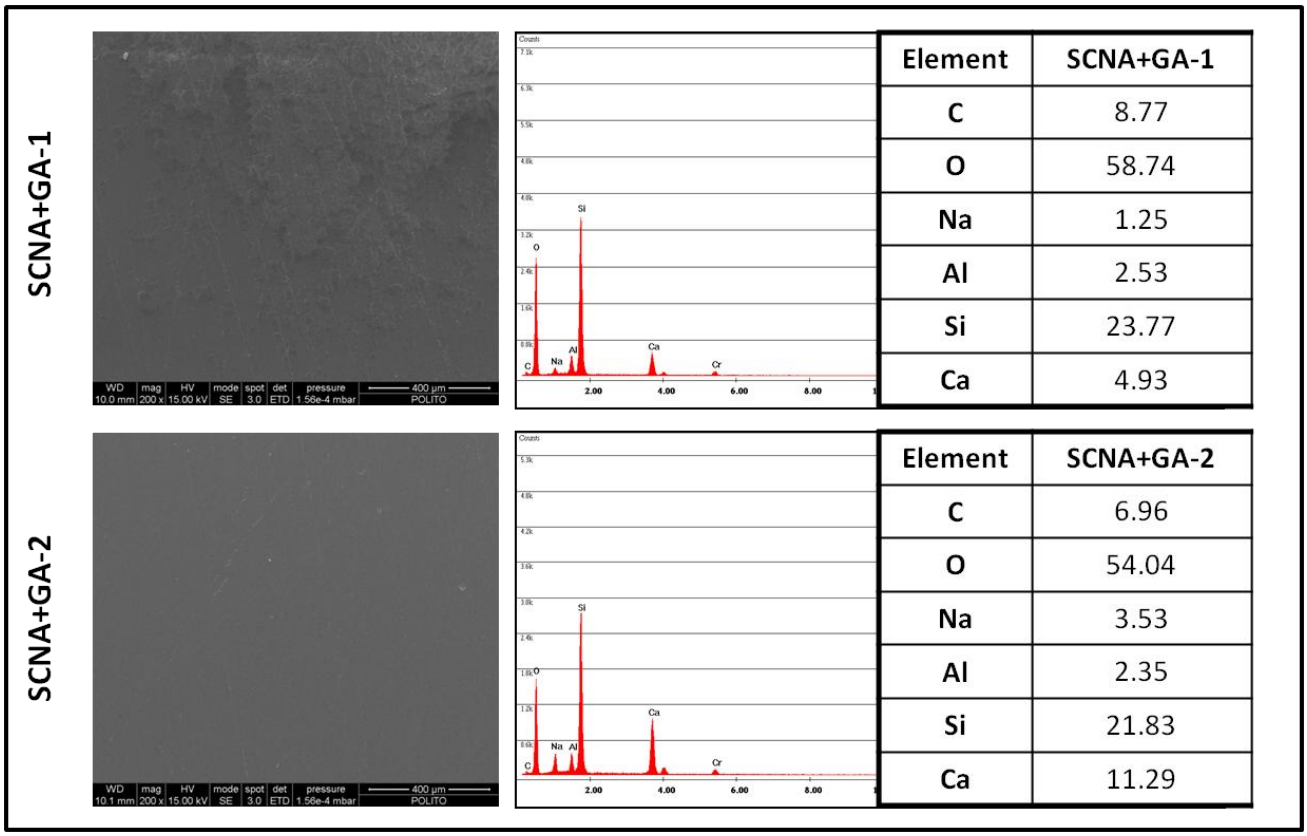

Element	SCNA+GA-1
C	8.77
O	58.74
Na	1.25
Al	2.53
Si	23.77
Ca	4.93

Element	SCNA+GA-2
C	6.96
O	54.04
Na	3.53
Al	2.35
Si	21.83
Ca	11.29

Figure 2-33: SEM images with a magnification 200×and EDS analysis on chemical composition of gallic acid grafted SCNA in two areas

EDS analysis (Tables in figure 2-33) demonstrated a higher enrichment of carbon atomic percentage as well as depletion of sodium and calcium for SCNA+GA-1 area, if compared to SCNA+GA-2 area, which is closer to the just washed sample. It means that the surface reactivity

of SCNA is not uniform; and this phenomenon may be ascribed the slower reaction kinetics of this material.

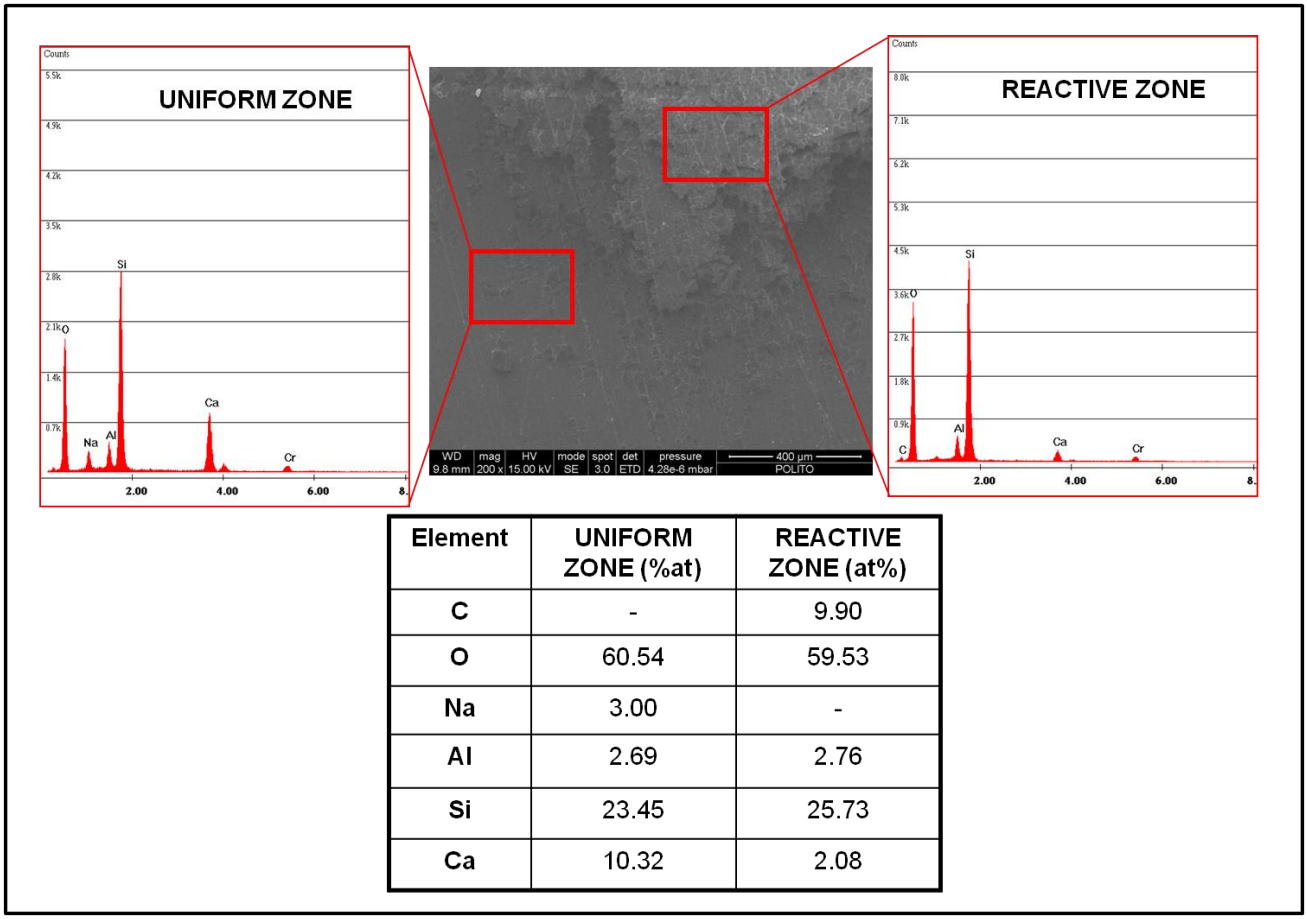

Element	UNIFORM ZONE (%at)	REACTIVE ZONE (at%)
C	-	9.90
O	60.54	59.53
Na	3.00	-
Al	2.69	2.76
Si	23.45	25.73
Ca	10.32	2.08

Figure 2-34: SEM images with a magnification 200×and EDS analysis on chemical composition of gallic acid grafted SCNA in two specific zones: the reactive zone and the uniform zone

In order to further evaluate the chemical composition of the gallic acid grafted surface, EDS analysis was performed in two zones as showed in figure 2-34: i) reactive zone and ii) uniform zone.

Compared with the chemical composition of uniform zone, a significant enrichment of carbon could be detected due to the contribution of gallic acid grafting. In addition, a notable depletion of sodium and calcium could be observed; this phenomenon could be ascribed to the relatively intense ion-exchange between the material and solution.

CEL2

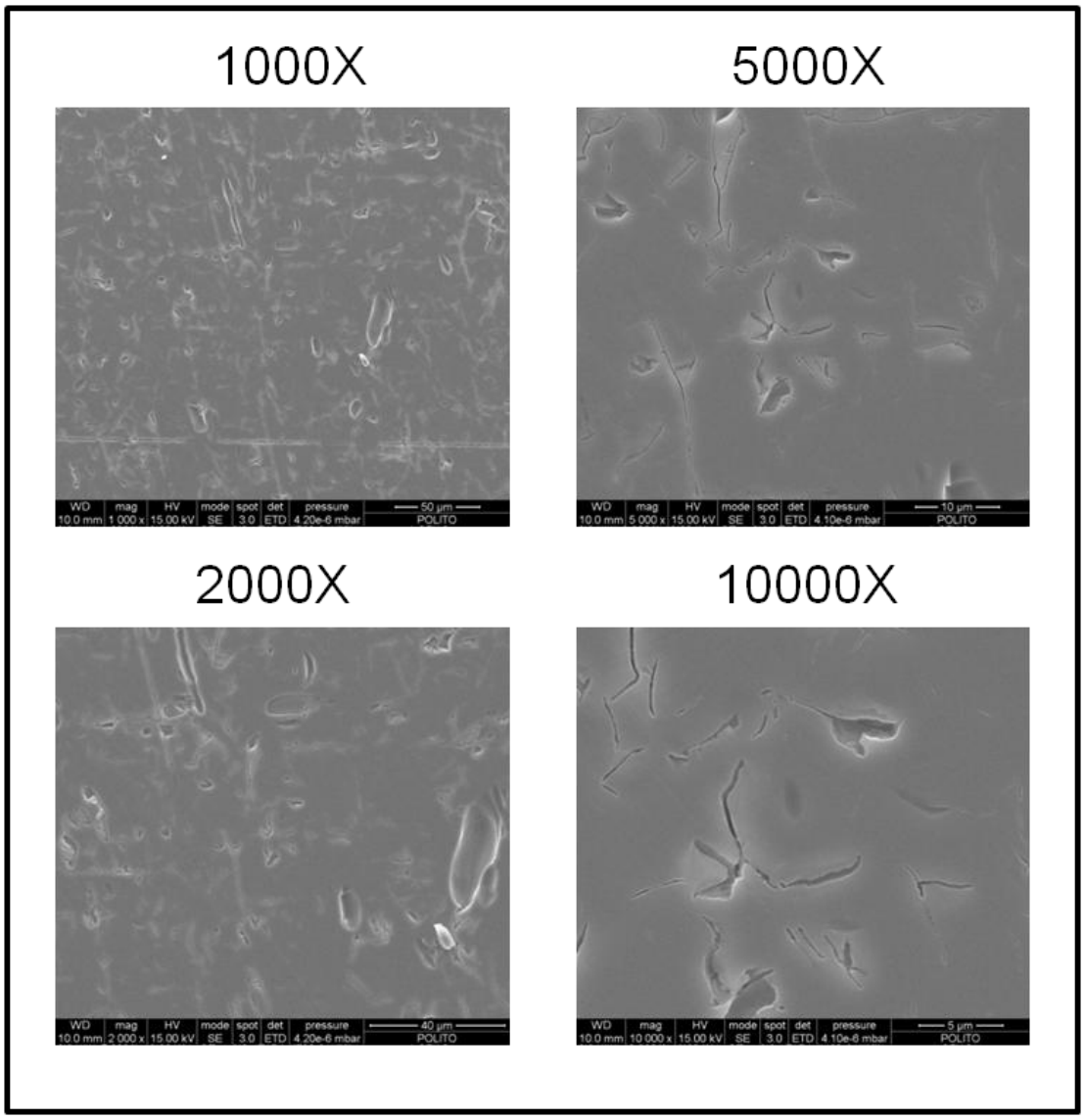

Figure 2-35: SEM images of washed CEL2 samples with different magnifications

Figure 2-35 exhibited the images of washed CEL2 bulk with different magnifications ranged from 1000× to 10000×. All the images showed a uniform surface with slightly polishing spots and cracks.

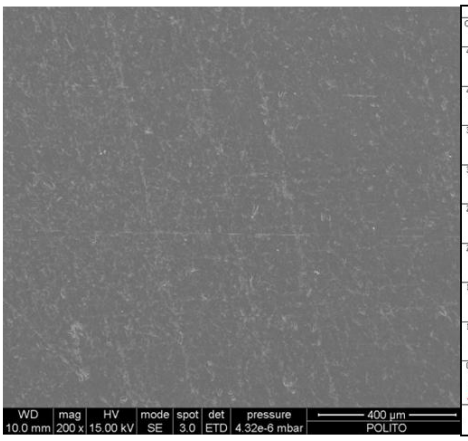

Element	CEL2
C	8.57
O	49.63
Na	8.89
Mg	3.42
Si	15.84
P	2.26
K	2.54
Ca	8.85

Figure 2-36: SEM images with 200× and chemical composition by EDS analysis of CEL2 washed bulks

EDS analysis (figure 2-36) evidenced all elements of glass composition including oxygen, silicon, sodium, calcium, phosphorus, potassium as well as magnesium. The presence of carbon is due to the unavoidable atmospheric contamination on the surface.

CEL2+GA

Since the morphology of CEL2 grafted with gallic acid was uniform on all the sample surface, only one area was selected for SEM investigation. Figure 2-37 displayed the images with magnification of 1000×, 2000×, 5000× and 10000×.

After grafting with gallic acid, CEL2 bulks were completely covered by a cracked layer with the typical morphology of silica gel. Compared with the washed CEL2, EDS analysis (Tables in figure 2-38) demonstrated a notable increase of carbon content on gallic acid grafted CEL2 surface as well as significant depletion of sodium and calcium due to the higher reactivity of glass surface.

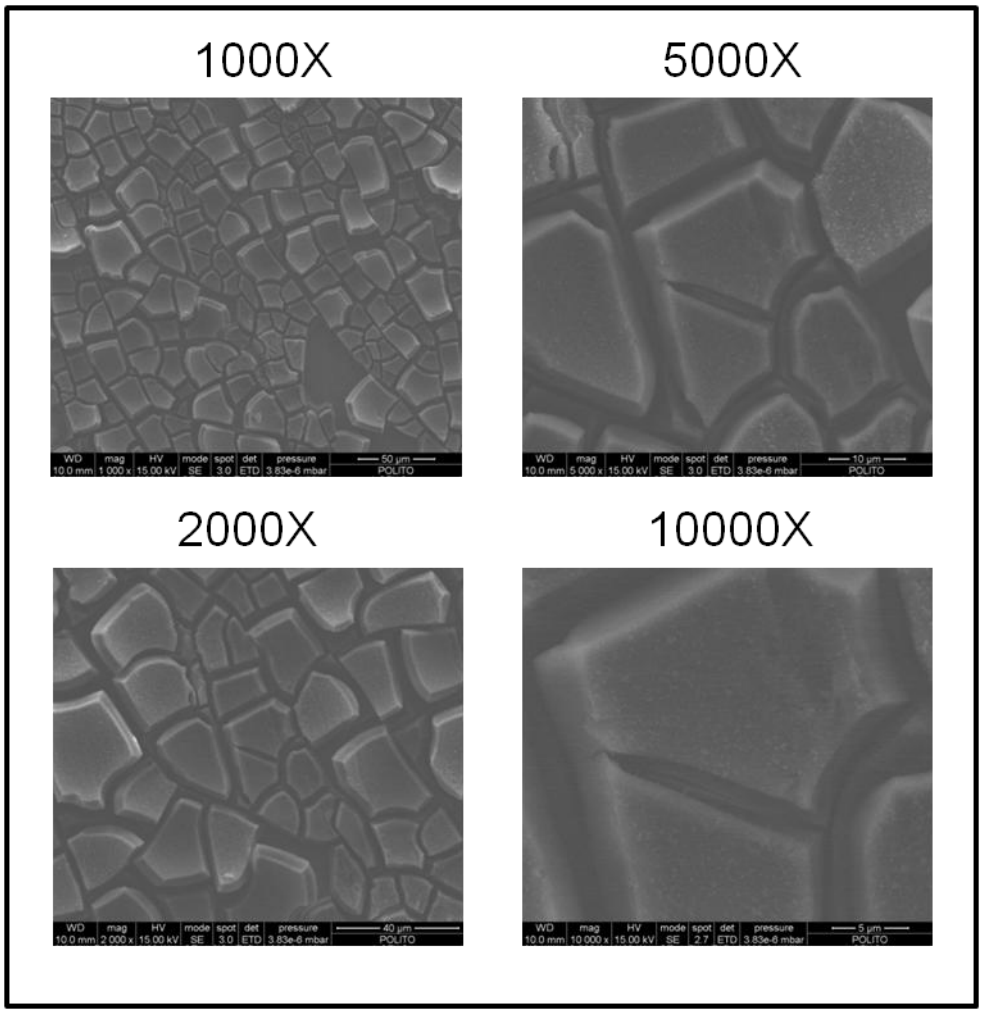

Figure 2-37: SEM images of gallic acid grafted CEL2 samples with different magnifications

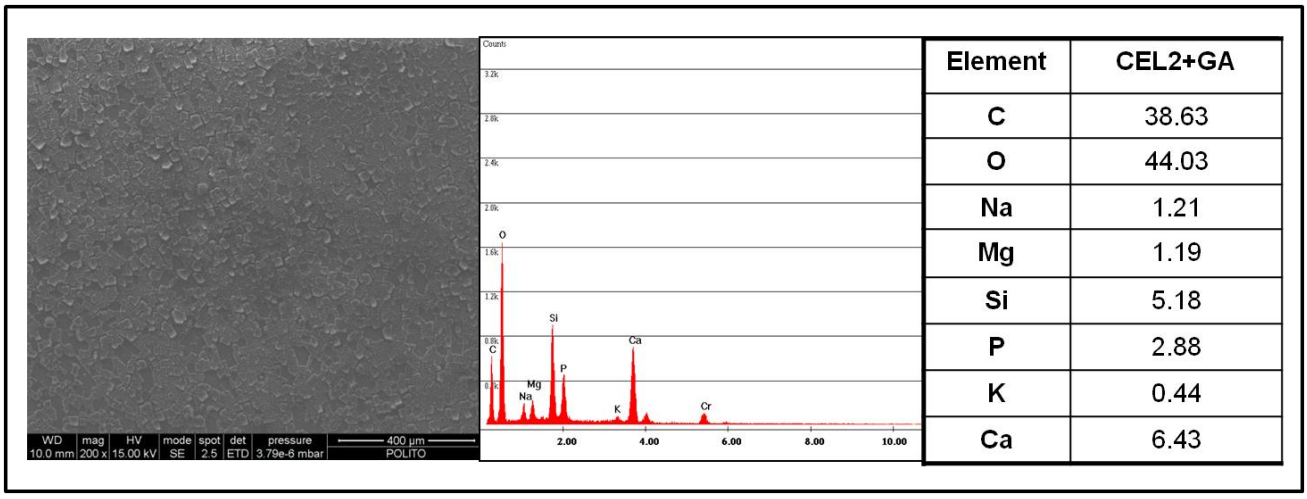

Element	CEL2+GA
C	38.63
O	44.03
Na	1.21
Mg	1.19
Si	5.18
P	2.88
K	0.44
Ca	6.43

Figure 2-38: SEM images with a magnification 200×and EDS analysis on chemical composition of gallic acid grafted CEL2

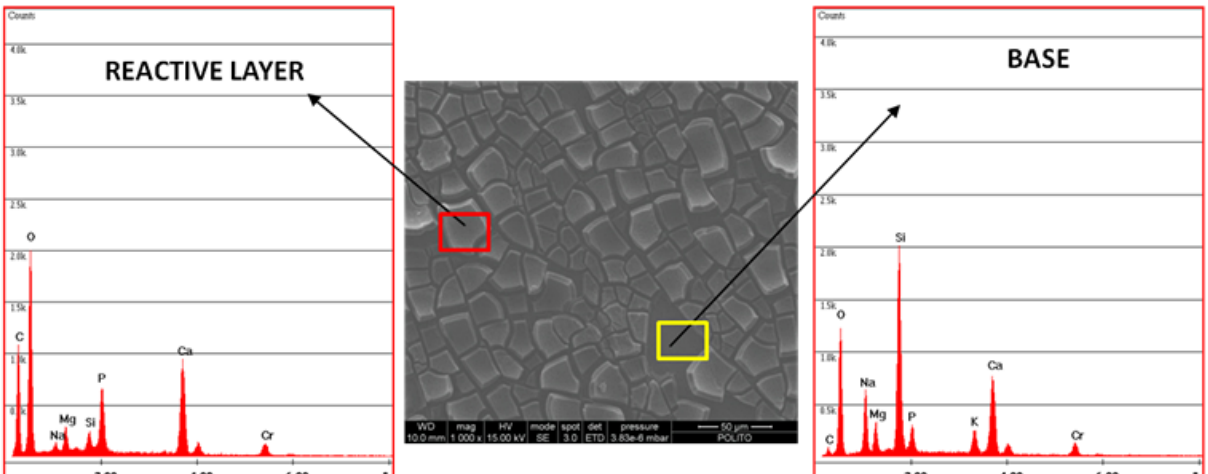

Element	REACTIVE LAYER	BASE
C	44.50	9.85
O	42.94	47.76
Na	0.52	7.09
Mg	1.26	2.84
Si	0.91	16.69
P	3.32	2.59
K	-	2.84
Ca	6.56	10.33

Figure 2-39: SEM images with a magnification 200×and EDS analysis on chemical composition of gallic acid grafted CEL2 in two specific zones: The reactive zone and the base zone

In order to further evaluate the chemical composition of the gallic acid grafted surface, EDS analysis was performed in two zones as showed in figure 2-39: i) reactive layer and ii) base zone.

Compared with the chemical composition of base zone, a significant increase of carbon could be detected on the reactive layer, due to the contribution of gallic acid grafting. In addition, a notable depletion of sodium and calcium can be observed; this phenomenon can be ascribed to the relatively intense ion-exchange between the material and solution.

2.6 FTIR analysis

FTIR was employed to analyse the functional groups of both SCNA and CEL2 glass powder before and after functionalization with gallic acid.

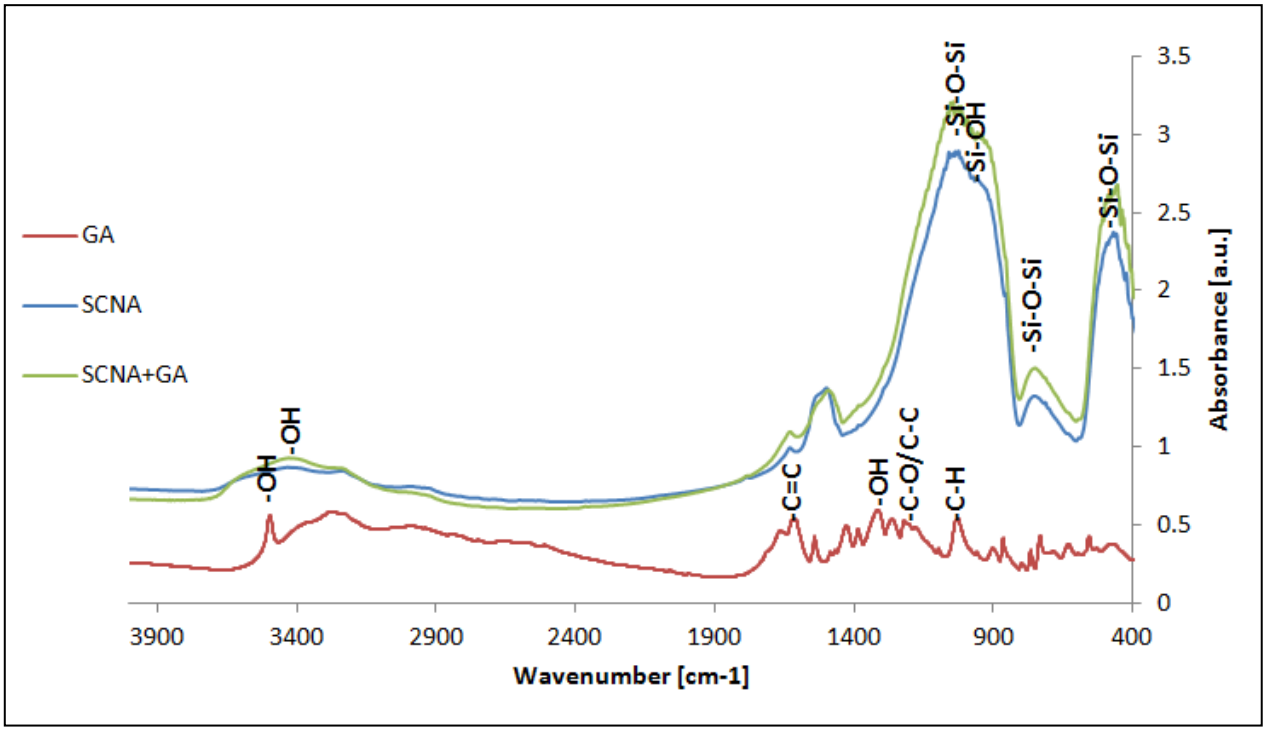

Figure 2-40: FTIR spectra of GA, washed SCNA and SCNA+GA

As for the gallic acid spectra (figure 2-40, 2-41), the typical polyphenolic characteristics were showed with the existence of a phenolic ring –OH stretching within the 3200-3550 cm^{-1}, and –OH in plane bending at about 1322 cm^{-1}, an aromatic ring C=C stretching within1450-1600 cm^{-1}, and C-O/C-C stretching vibrations within 1200-1300 cm^{-1}, deformation of C-H aromatic at about 1024cm^{-1}, as well as δcc benzene ring vibration at about 732 cm^{-1} [15, 16].

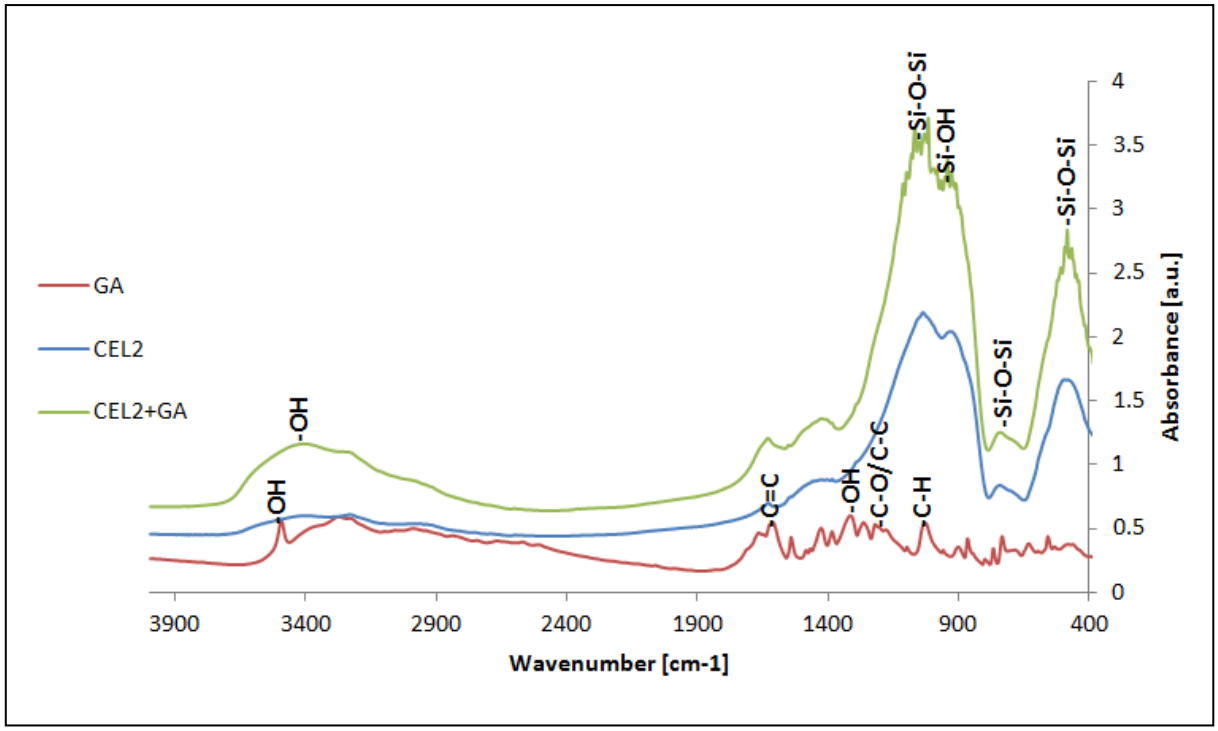

Figure 2-41: FTIR spectra of GA, washed CEL2 and CEL2+GA

The FTIR spectra of two glasses are dominated by the vibrational bands due to Si-O vibrational modes: Si-O-Si stretch, Si-O alkali stretch and S-O bend and Si-O rock as showed in figure 2-39, 2-40. Both two bioactive glasses showed very strong absorption at 1000-1200 cm-1, assigned to Si-O-Si asymmetric stretching mode. Peaks at about 760 cm^{-1} and 460 cm^{-1} are assigned to symmetric stretching and rocking vibration of Si-O-Si band, respectively. The observed peak around 960 cm^{-1} present on both glasses is assigned to non-bridging oxygen together with the surface silanols (Si-OH) groups. In addition, the surface silanol groups are confirmed by presence of a broad band in the region from 3000cm^{-1} to 3400 cm^{-1}, which represents the vibration of different hydroxyl groups [17-19].

After gallic acid grafting, the absorbance intensity of board peak in the region of 3000-3400 cm^{-1} increased and the peak became narrow compared with that of the washed glasses. This phenomenon can ascribed to the bonding of gallic acid to enhance the signal of –OH group.

3 Surface functionalization of SCNA and CEL2 with polyphenol extracted from grape skin

Natural grape polyphenols (GP) were extracted through a conventional solvent extraction methodology with 80% ethanol as the solvent. The grape polyphenols extracts were freeze dried and then grafted to the surface of two bioactive glasses (SCNA and CEL2) with different bioactivity level. Techniques such as UV together with Folin-Ciocalteau colorimetry, XPS, SEM were employed to evaluate the effectiveness of surface functionalization on the basis of the previous research on galic acid grafting. The aim of this research is the combination of bioactive propertied of bioactive glasses with the health-promoting benefits and good biocompatibility of polyphenols.

3.1 Total phenol content analysis

The total polyphenol content was evaluated by UV-Vis spectroscopy with Folin-Ciocalteau colorimetry as described in Chapter IV and calculated with function below according to the standard calibration curve:

$$\text{Absorbance} = 22.981 * \text{Concentration}_{(GA)} + 0.0232$$

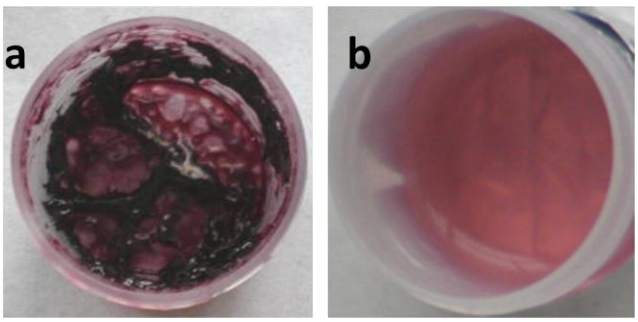

Figure 3-1: (a) Grape polyphenol extract after freeze drying and (b) polyphenol aqueous solution

Figure 3-1 showed the images of grape polyphenol extracts after freeze drying and the polyphenol aqueous solution for functionalization. Both the grape polyphenol extracts and the aqueous solution presents a purple color due to the polyphenol composition, which always

includes proanthocyanidins as mentioned in Chapter I.

Table 3-1 total phenol content of GP

Sample	Phenol content (mg/ ml GA)	Phenol mass mg/ g extract
1	0.07296 ± 0.00369	14.59201 ± 0.00074
2	0.07084 ± 0.02197	14.16867 ± 0.00439

N=3 mean ± SD

Table 3-1 listed the phenol content of grape phenol extract from two extractions. No significance difference of phenol content could be observed in these two extractions. The results revealed the repeatability and stability of extraction methodology. In addition, through calculation, there are 14.59 mg and 14.17 mg of phenols in 1 g of extract, respectively.

3.2 Macroscopic observations on the samples

Figure 3-2 exhibited the SCNA and CEL2 bulk samples before and after functionalization process. As far as CEL2 is referred, it is evidenced that after modification with grape phenol, the color of bulk sample changed from colorless to light brown. Similar changes of color were also found on the surface of CEL2 grafted by grape phenol with citric acid (CA) addition. On the other hand, the color variation was almost absent on the surface of SCNA functionalized by GP as well as GP+CA.

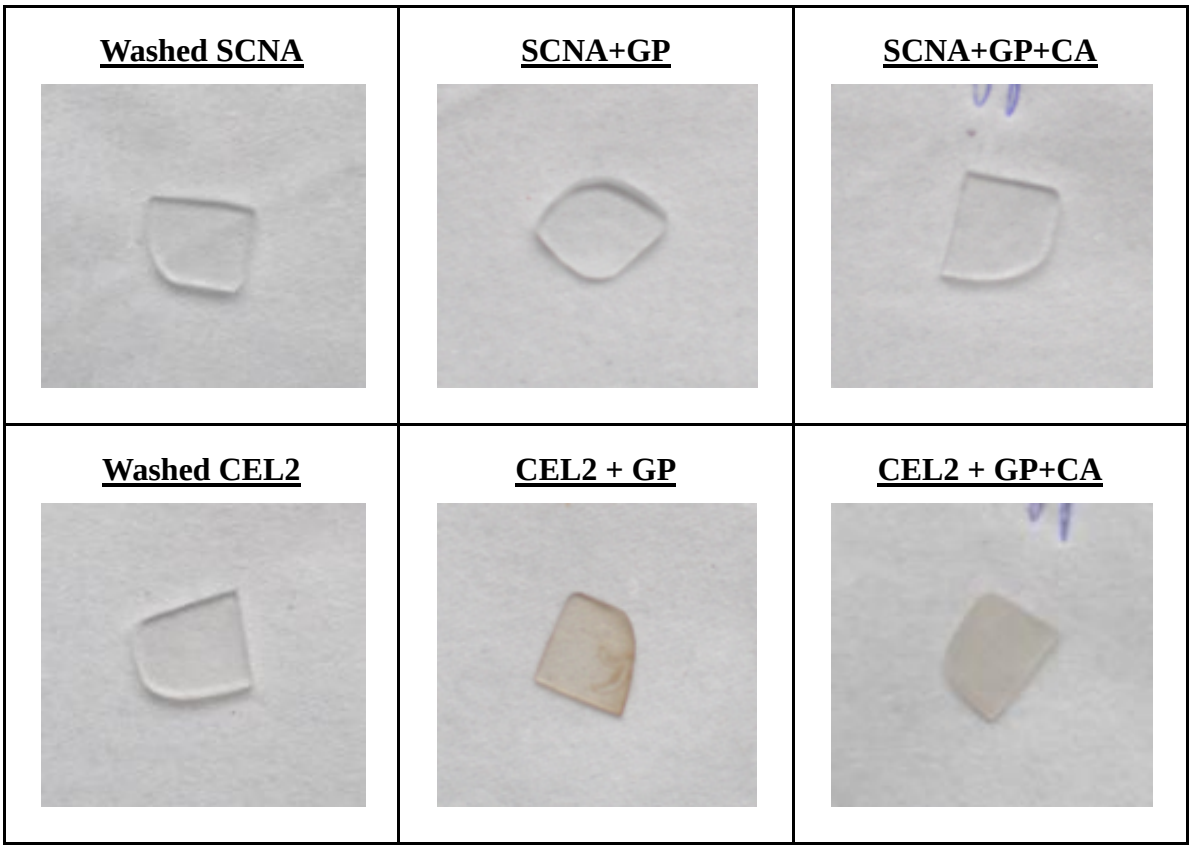

Figure 3-2: Glass bulks appearances before and after functionalization

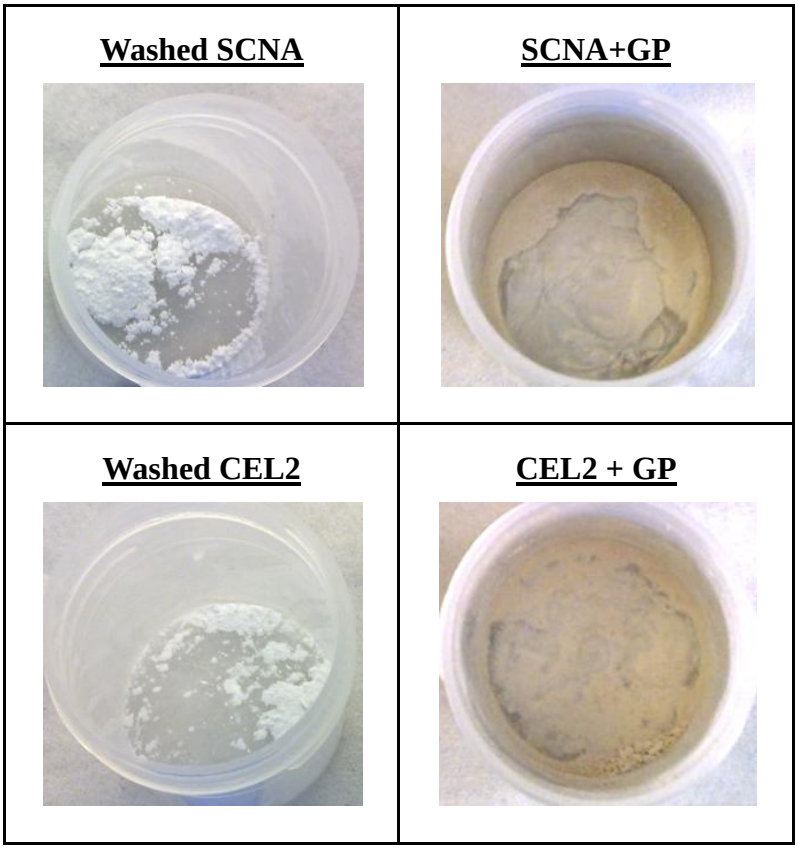

Figure 3-3: Glass powder appearances before and after functionalization

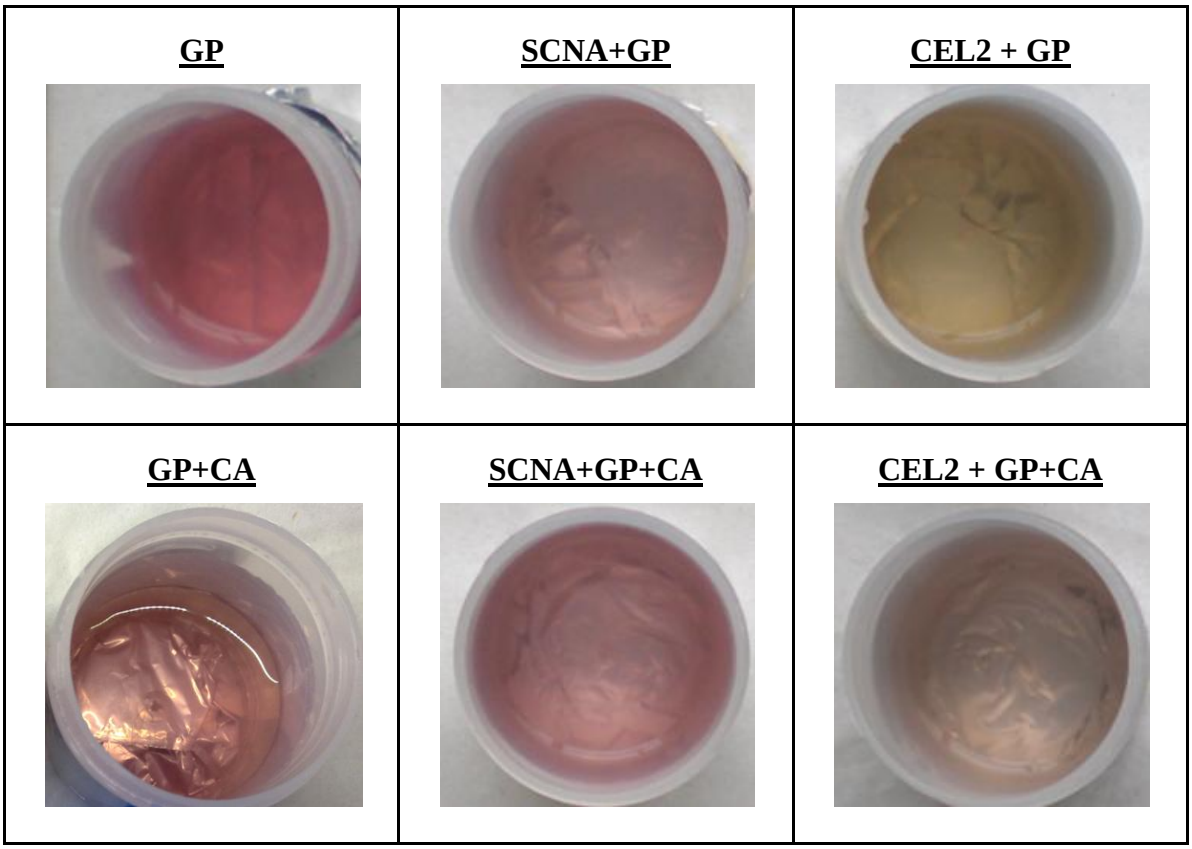

Figure 3-4: Phenol solution, phenol solution with citric acid and uptake solution after functionalization

Both SCNA and CEL2 powder samples were just functionalized by grape phenol without citric acid, and after solution was moved away, the powder appearances were observed in figure 3-3. The color of CEL2 powder transferred from white to light brown, which was similar to bulk sample. Compared with SCNA bulk, powder sample exhibited significant color changes from white to light brown. However, the color variation is not as significant as gallic acid functionalization (chapter V, section 2.1), since the phenol content of GP is lower than GA.

Grape phenol aqueous solution in which the bulk samples were soaked for 24 hours exhibited a color change from pink to yellow after CEL2 bulks were removed out. As for uptake solution of SCNA functionalization, the color became lighter. With the addition of citric acid, the mixed solution presented a light orange after reacting with CEL2, while after SCNA was removed out, the color of solution seemed similar to the one without citric acid. The color variation is the results of depletion and oxidation of pigment component in the grape phenol extracts [20].

3.3 pH measurement

The effect of pH and the addition of citric acid were investigated through measuring pH value of GP solution before and after soaking SCNA and CEL2 samples (bulk and powder) for 24 hours with pH meter. Figure 3-5 demonstrated the results.

It should be underlined, as described previously for the gallic acid functionalization, that in the present setup, both of the glasses were soaked in the grape phenol solutions, which are characterized by a fairly acid pH value (3.61 ± 0.23) without the addition of CA.

As described in the previous research on gallic acid functionalization, a significant ion release can be ascribed to bioactive glasses in aqueous media and it is enhanced by an acidic environment. The ion exchange between the glass and the solution induces a significant increase of the solution pH for static soaking models as reported in literature [1] and confirmed by experimental results (figure 3-5).

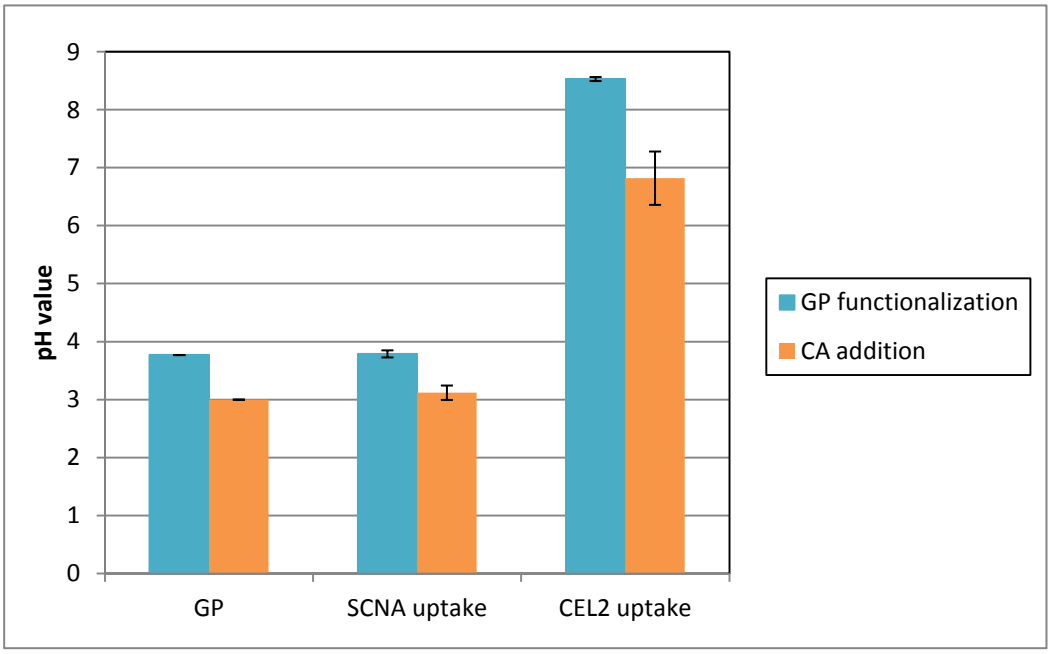

Figure 3-5: pH value of GP uptake solution before and after 24 hours soaking of different glass bulks, and the effect of CA addition in surface functionalization

After functionalization, notable changes of pH from acidic value to alkaline in uptake solution of both glasses could be observed, especially in the case of more reactive glass (CEL2) and the powder samples (Table 3-2). In this case, the pH value is 3.79 for SCNA bulk and 9.54 for SCNA powder, 8.53 for CEL2 bulk and 10.68 for CEL2 powder. These data confirmed the one previously obtained with gallic acid.

Table 3-2 pH value of GP uptake solution before and after 24 h soaking of SCNA and CEL2 powders

Samples	**GP**	**SCNA+GP**	**CEL2+GP**
pH value	3.61	9.54	10.06

According to literature, an alkaline environment promotes a further hydroxylation of silica-based glasses as well as the oxidation of catechol groups in phenols into quinone groups, resulting in the color changes on the bulk samples and in uptake solutions. Since the significant pH change of CEL2 samples, the colors varied greatly.

With addition of citric acid, the basification was weakened but not completely overcome (figure 3-5). The pH value of uptake solution could be kept below 7.00 that the literature reports a favorable pH for the transition of phenolic components from phenol group to quinone ones [3]. As a result, a strong color change of CEL2 uptake solution was significantly reduced compared with the one without CA addition.

3.4 UV-Vis analysis

3.4.1 Uptake solution analyzed by UV

In order to evaluate the depletion of grape phenols during the functionalization process, the amount of phenols in uptake solution of both before and after grafting was measured by Folin-ciocalteau colorimetry with UV-Vis spectroscopy. The amount of phenols was calculated based on the equation from standard calibration curve.

The bar diagram in figure 3-6 demonstrated the phenol content in original phenol solution as well as in the uptake solution after soaking SCNA bulk and powder samples, and CEL2 bulk and powder samples. Generally, a depletion of phenols content can be observed in all uptake solution samples. A notable decrease of phenol content was observed on CEL2 bulk (the value is 0.0548 mg/ml) compared with SCNA bulk samples (the value is 0.0732 mg/ml). Furthermore, a higher consumption of biomolecules can be underlined for powder samples when compared to bulk ones. Both of results are in accordance with the ones obtained with gallic acid functionalization on glass samples (chapter V, section 2.3.2). As far as the powders are concerned, the capability to bond larger amount of biomolecules can be ascribed to the larger surface area in comparison with bulk samples. Considering the different bioactivity levels of two bioactive glasses, the higher ability of CEL2 in binding phenols can be assigned to its higher reactivity with more –OH group exposure. The formation of a porous silica gel layer during functionalization process can lead to the absorption an additional amount of phenol molecules. In addition, the structural change of phenol molecules in alkaline environment can be another reason for the phenol content reduction, as previously studied for gallic acid functionalization (chapter V, section 2.3.2).

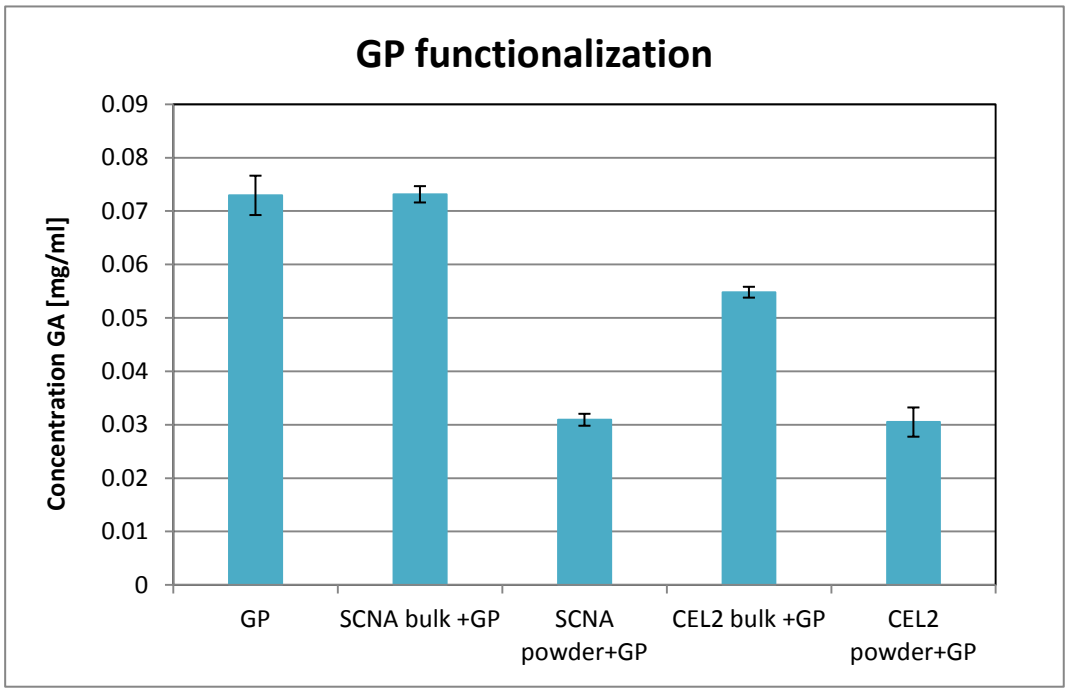

Figure 3-6: UV photometric results for GP uptake solution before and after 1 day soaking of different glass samples

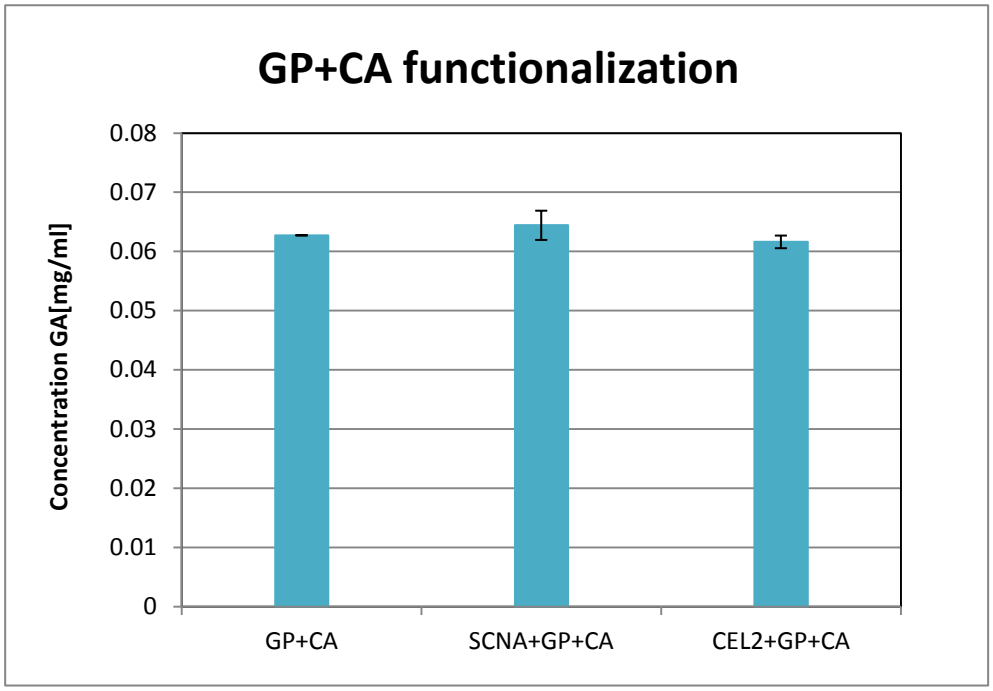

Figure 3-7: UV photometric results for GP+CA uptake solution before and after 1 day soaking of different glass bulk samples

The effect of citric acid (CA) addition in the functionalization medium of bulk samples is reported in figure 3-7. A decrease of phenol consumption can be observed in the uptake solutions, especially in CEL2 with addition of citric acid (figure 3-7) when compared with the ones without CA (figure 3-6). As described in gallic acid functionalization (chapter V, section 2.3.2), it can be supposed that the strong basification induced by bioactive glasses (and especially by CEL2) soaking can lead to the partial change in the structure of the molecules and the impossibility to detect them by the Folin&Ciocalteau method. CA addition allows the maintenance of uptake solution pH below 7.00 reducing the structural change of phenols. A moderate reduction in the phenols content of CA-added grape polyphenols (figure 3-7) solutions after glass functionalization was detected. However, the uptake of a fraction of molecules on samples surface. will be demonstrated by other analysis in the following paragraphs.

3.4.2 Functionalized bulk samples analyzed by UV

After grafting with grape phenols, bulk samples of SCNA and CEL2 were investigated by

reacting with Folin-Ciocalteau's reagent (figure 3-8) cooperated with UV-Vis spectroscopy to evaluate the amount of phenol molecule on the bulk surface after functionalization and the results were reported in bar diagram figure 3-9. The amount of phenols on the surface of SCNA was low and could not be detected by UV. However, on the surface of CEL2, a relatively higher amount of grape phenols was detected. The results are in accordance with the depletion of grape phenols in uptake solution due to the different reactivity level of two glasses.

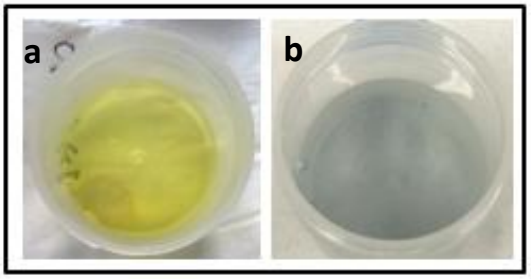

Figure 3-8: a) GP grafted bulk sample in FC reagent and b) uptake after 2h incubation

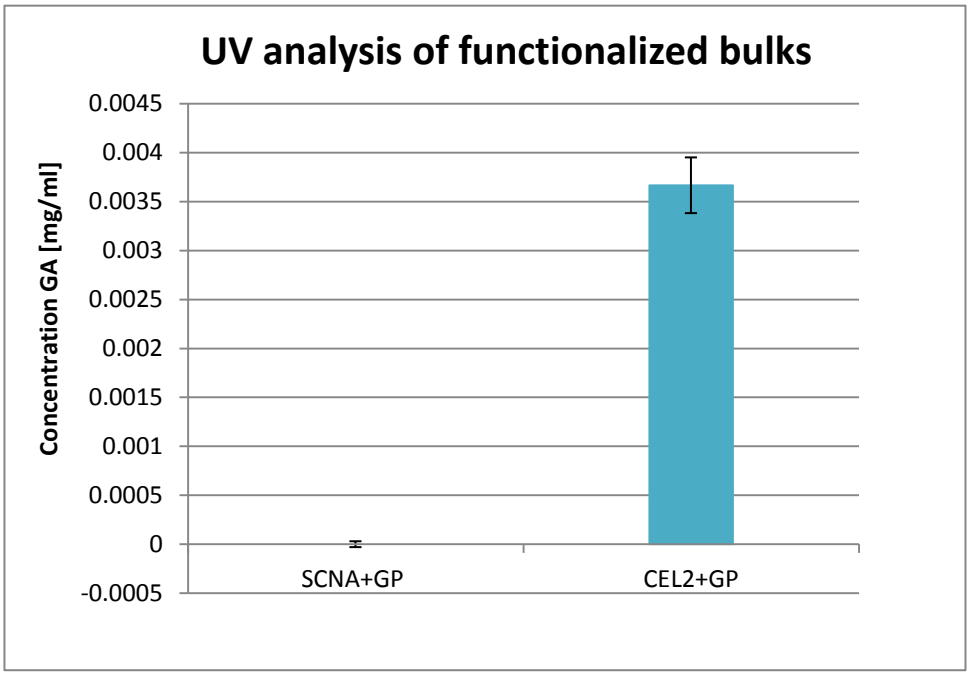

Figure 3-9: UV photometric results for phenol content on functionalized SCNA and CEL2 bulk samples

3.4.3 Release test in double distilled water

The release test was performed by soaking powder samples of two types of glasses after functionalization with grape phenol for 1 day and 1 week and analyzing through UV with Folin-Ciocalteau method. In general, the release amount of grape phenols from SCNA and CEL2 powders were extremely low and the UV was not able to evaluate the amount. The low release effectiveness may suggest the strong bond between glass surface and grape phenol molecules. These results are in accordance with the ones obtained for gallic acid functionalization of the same glasses (chapter V, section 2.3.4).

3.5 XPS analysis

XPS was employed to characterize the chemical composition and chemical groups on the surface of the just pretreated SCNA and CEL2 bulk samples as well as bulks grafted by grape phenols and grape phenols with addition of citric acid. Results were reported by the following spectra including survey spectra and detailed analyses of carbon and oxygen regions. The samples were named as follows:

i. SCNA (just washed sample)

ii. SCNA+GP

iii. SCNA+GP+CA

iv. CEL2 (just washed sample)

v. CEL2+GP

vi. CEL2+GP+CA

SCNA washed

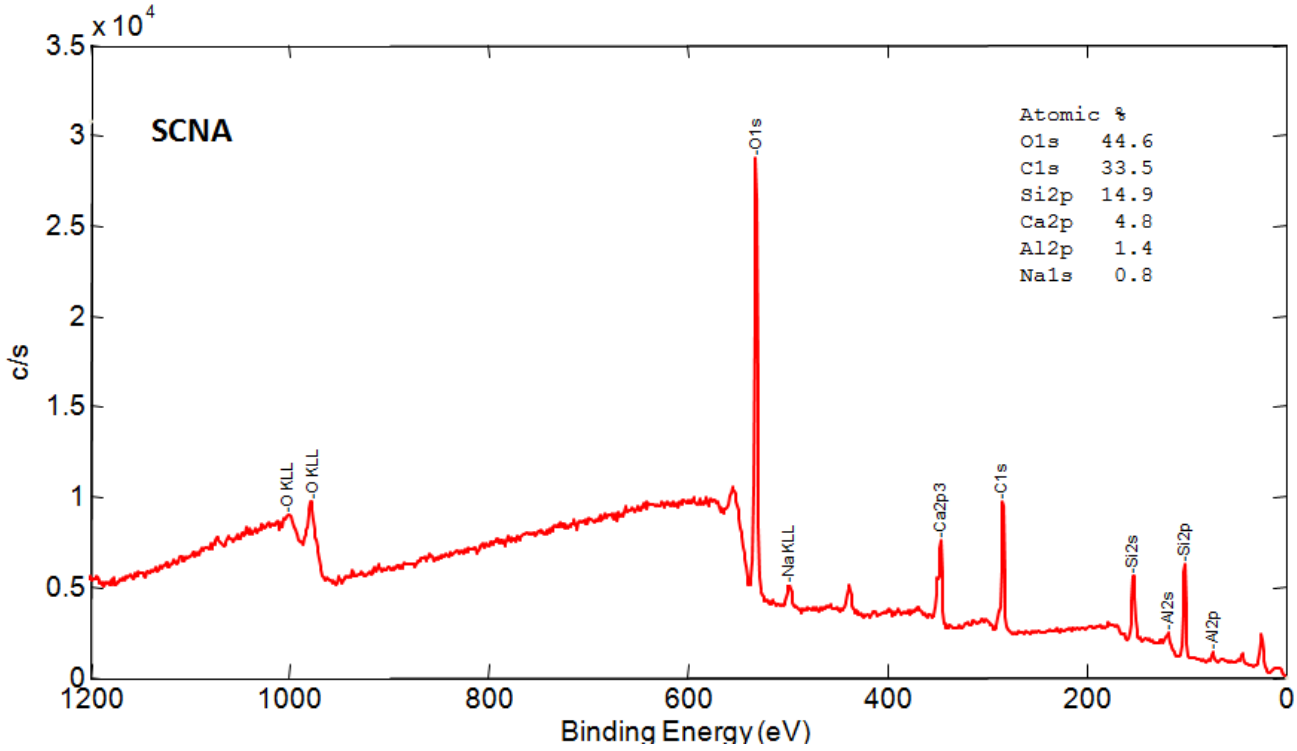

Figure 3-10: survey spectra of washed SCNA

The survey spectra (figure 3-10) of washed SCNA highlighted all elements present on glass surface. Signals of elements from glass composition were observed, including oxygen, calcium, silicon, aluminum and sodium. Carbon, which is commonly present in the first surface layers of materials, was also observed in this non-functionalized sample due to the unavoidable atmospheric contamination as reported in the literature [12, 13] and already observed for gallic acid functionalization (Chapter V, section 2.4).

Figure 3-11 reports the detailed analysis of carbon region of SCNA. Two main contributions can be observed at about 284.8 eV and 289.4 eV. The front could be attributed to unavoidable contaminations and the latter could be assigned to carbonates.

In the detailed analysis spectrum of oxygen region (figure 3-12), typical signals of oxides (at 531.7 eV) , silica (532.35 eV) and hydroxyl groups (533.54 eV) can be observed as reported in the literature related to surface activation [6].

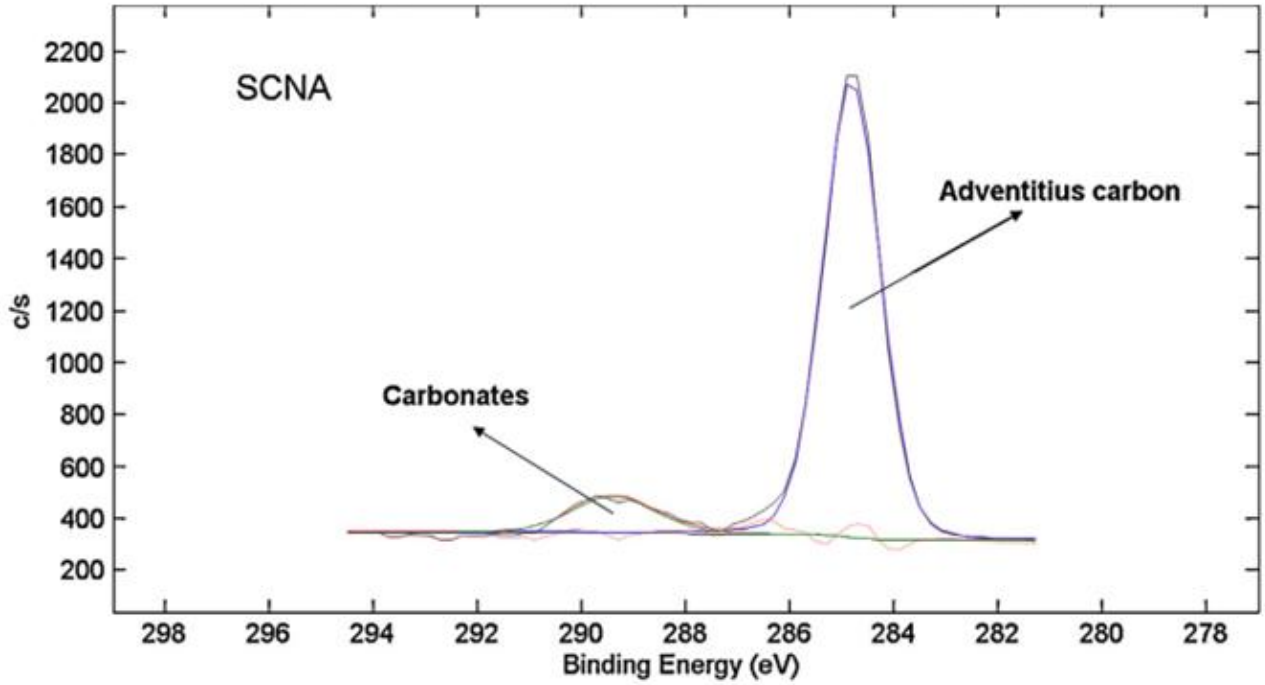

Figure 3-11: XPS detailed analysis of carbon region for SCNA washed sample

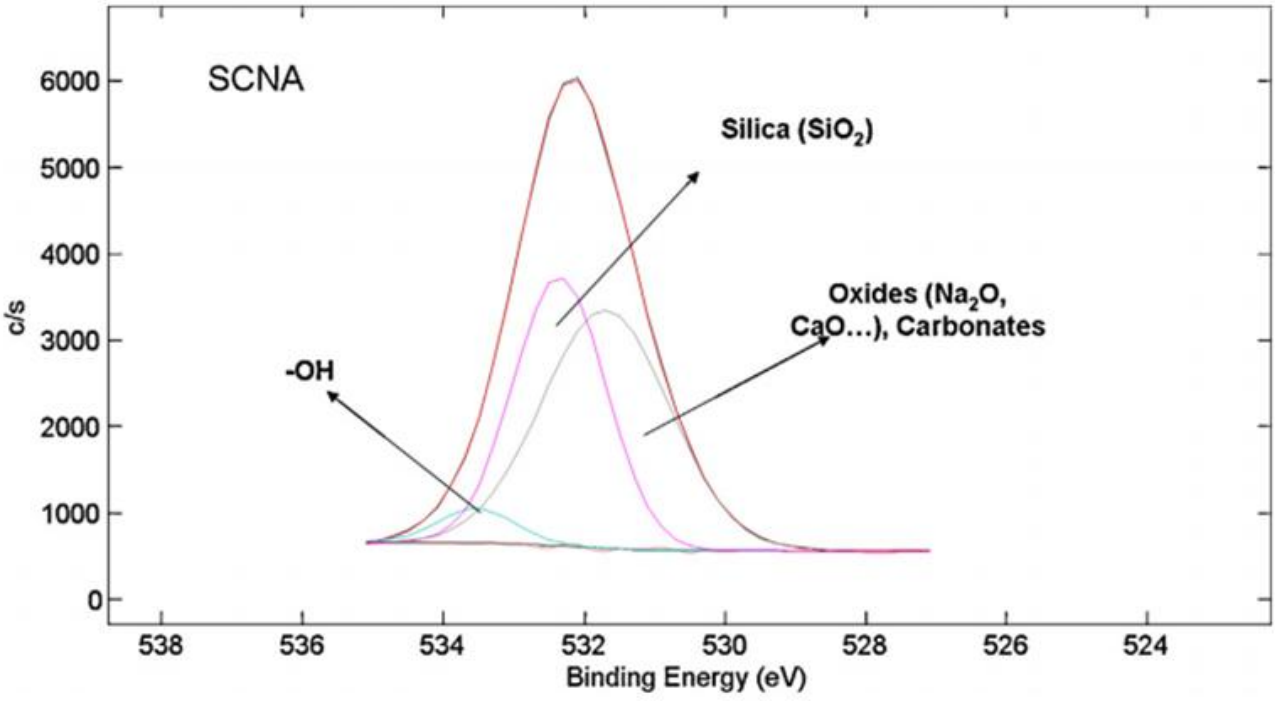

Figure 3-12 XPS detailed analysis of oxygen region for SCNA washed sample

SCNA+GP

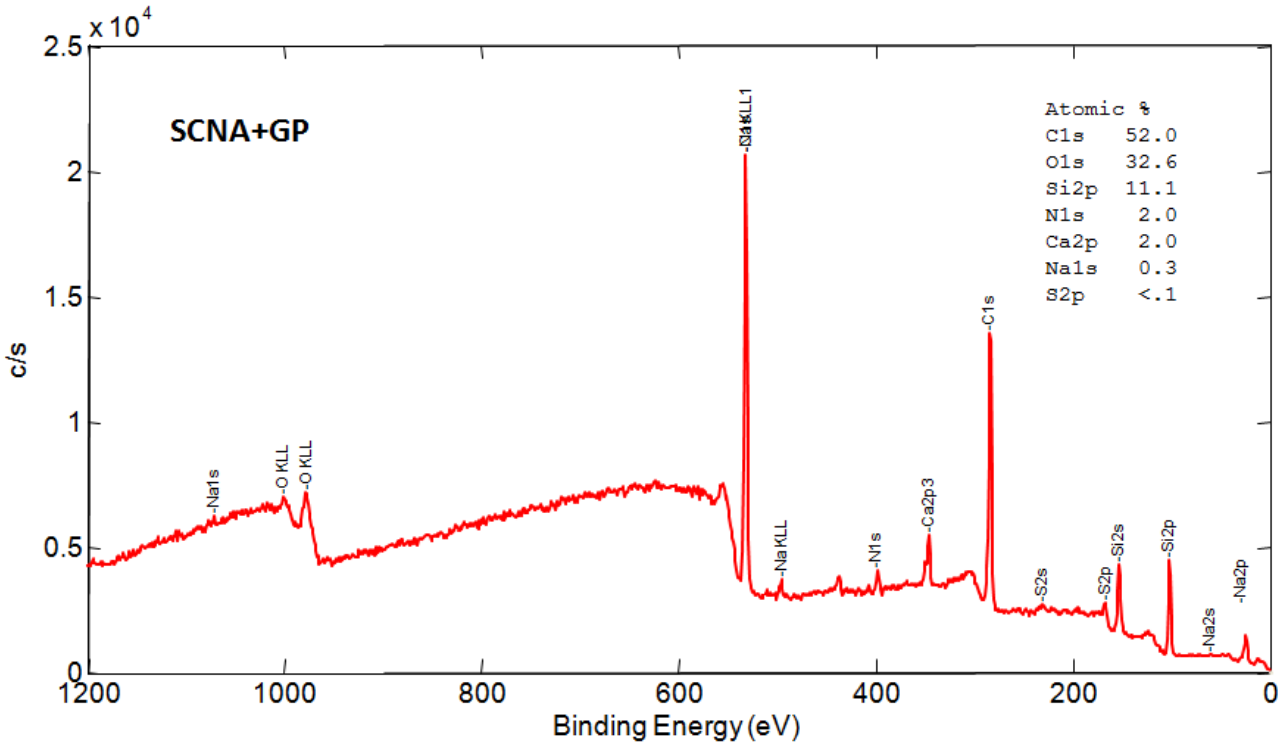

Figure 3-13: Survey spectra of SCNA+GP

Figure 3-13 reports the survey spectrum of SCNA functionalized with grape phenols highlighted all elements present on glass surface. Signals of elements from glass composition were observed, including oxygen, calcium, silicon, aluminum, sodium as well as carbon.

In detailed analysis spectra of carbon region on SCNA+GP (figure 3-14), different contributions can be detected after grape phenol functionalization. In particular, the signal of carbonates disappeared. The appearance of two new contributions at 285.93 eV and at 288.08 eV was observed. They can be attributed to C-O and C=O, respectively. Compared with gallic acid funtionalization, same signals were detected with a lower intensity (chapter V, section 2.4).

Figure 3-15 reports the detailed analysis of oxygen region, signals of silica and –OH groups are still present on SCNA bulk after phenol grafting. Hydroxyls peaks confirmed the grafting of phenol. Signals at about 531.6 eV can be attributed to both oxides and C=O groups.

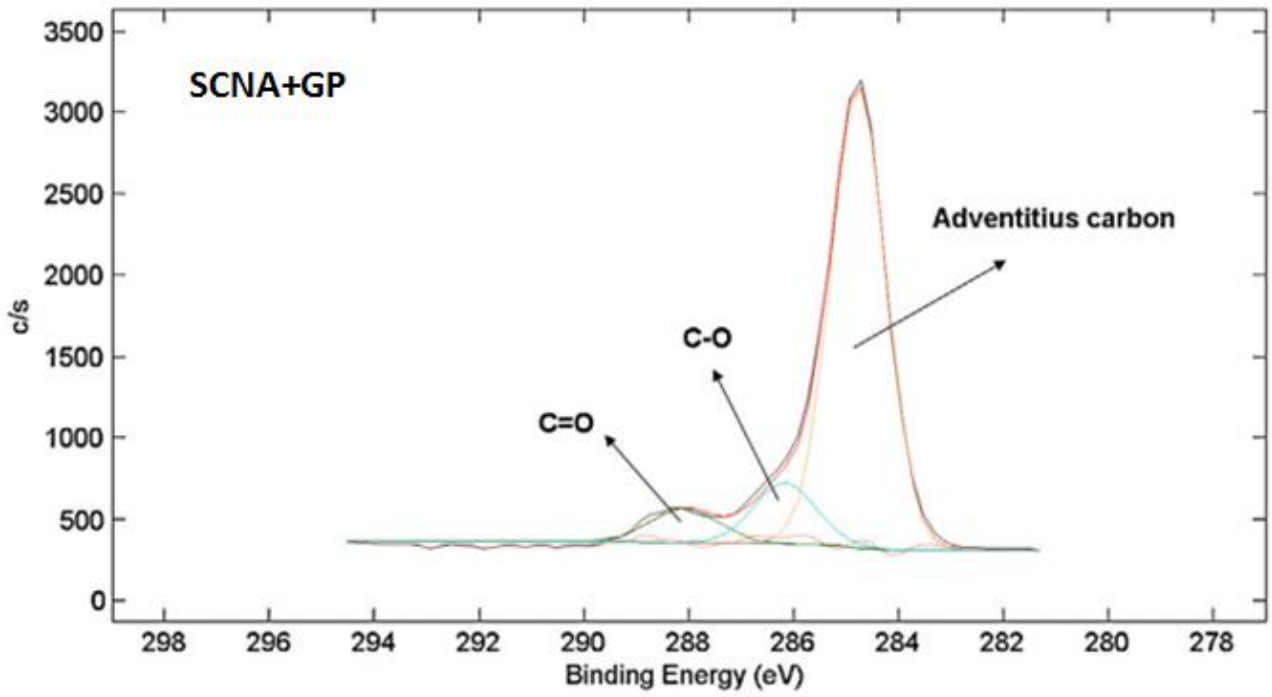

Figure 3-14: XPS detailed analysis of carbon region for SCNA+GP sample

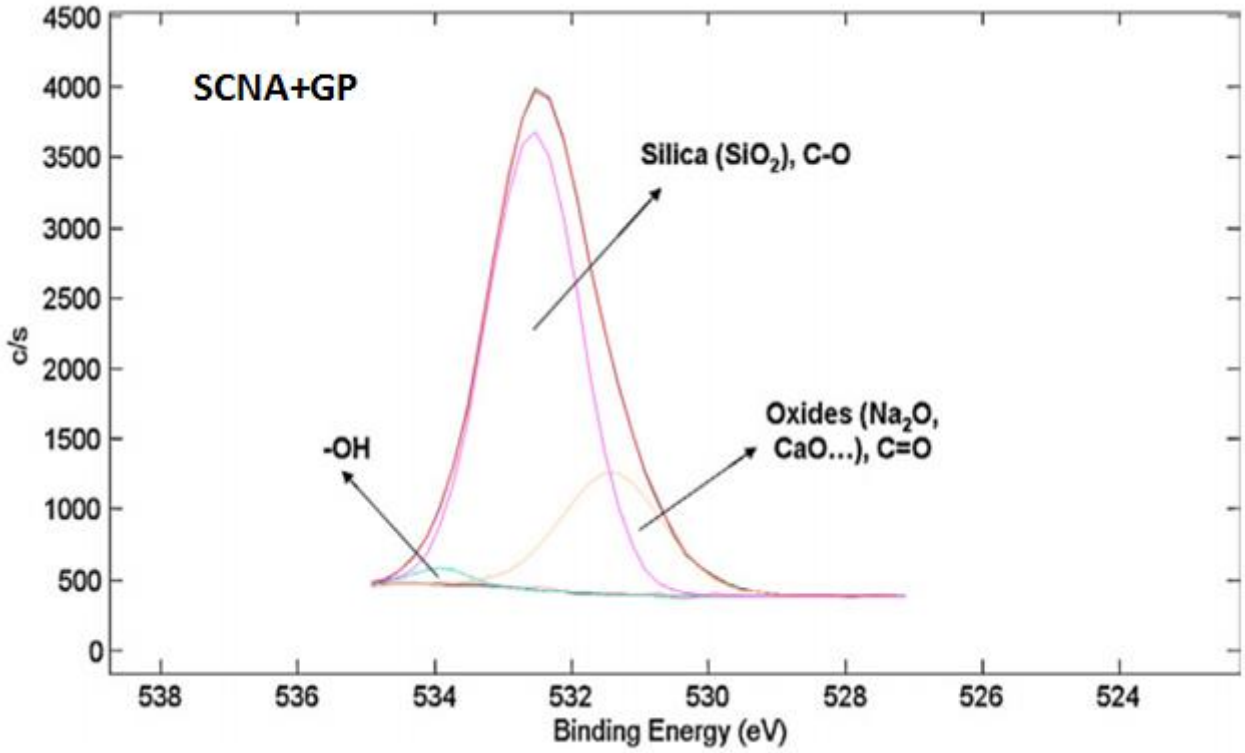

Figure 3-15: XPS detailed analysis of oxygen region for SCNA+GP sample

SCNA+GP+CA

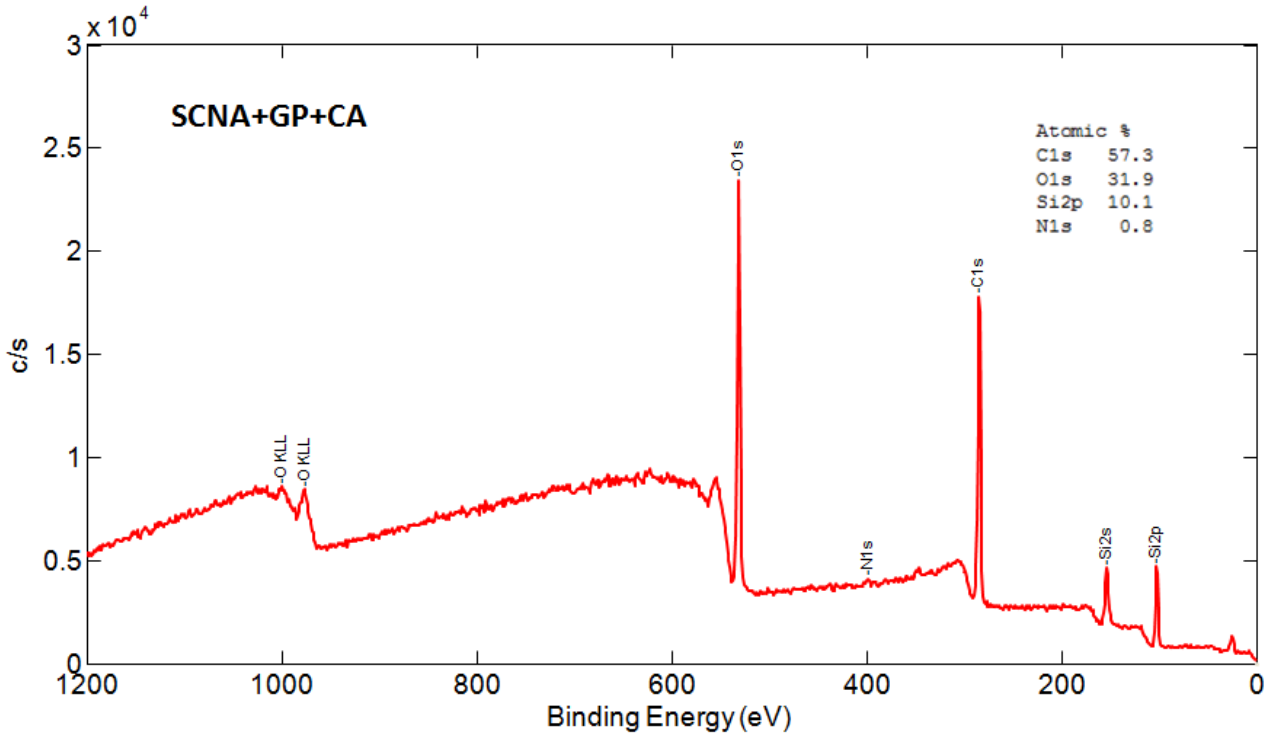

Figure 3-16: Survey spectra of SCNA+GP+CA

Figure 3-16 presents the survey spectra of SCNA functionalized by phenol with addition of citric acid. All elements present on glass surface are listed. Signals of elements from glass composition were observed.

With addition of citric acid as observed for gallic acid grafted samples, a reduction of C=O signal can be observed compared to the one without citric acid in detailed analysis of carbon region (figure 3-17). This result confirms the ability of citric acid to inhibit the oxidation of phenol molecule to quinone.

In the detailed analysis of oxygen region (figure 3-18), a reduction in signals of -OH group as well as signal of C=O could be detected in accordance with the results obtained for gallic acid grafted bioactive glasses (chapter V, section 2.4).

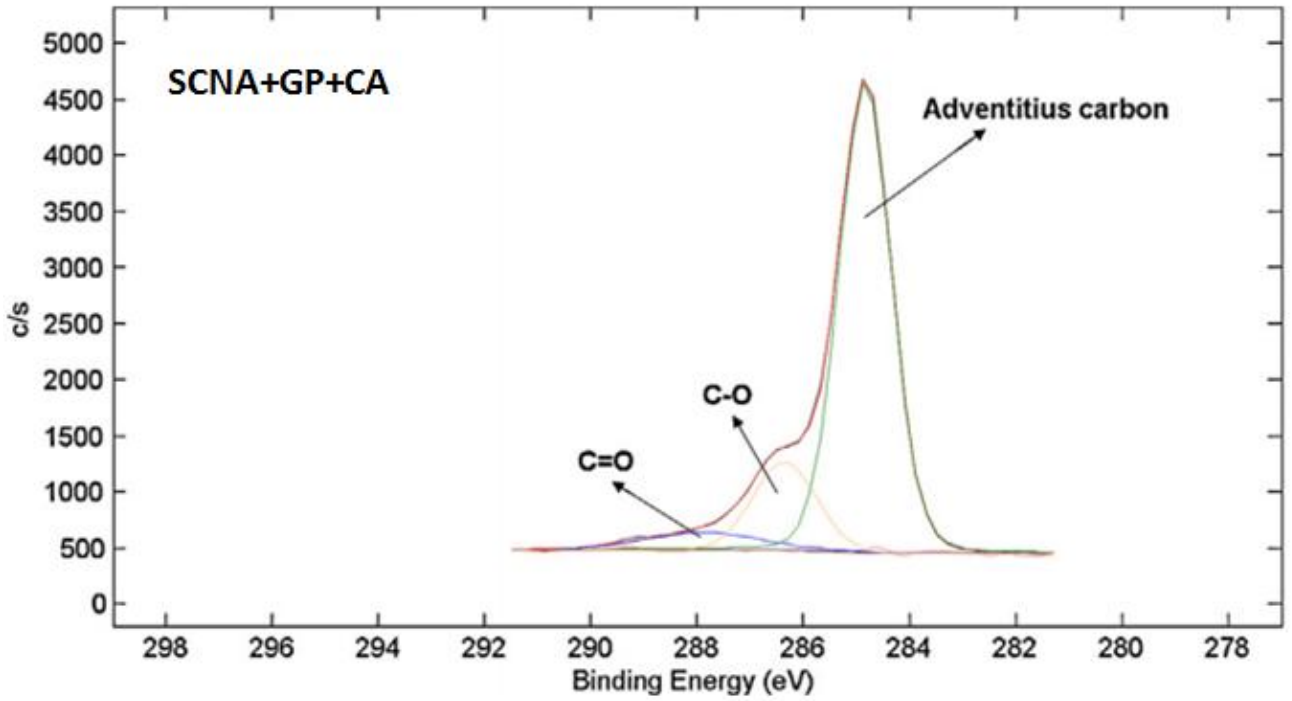

Figure 3-17: XPS detailed analysis of carbon region for SCNA+GP+CA sample

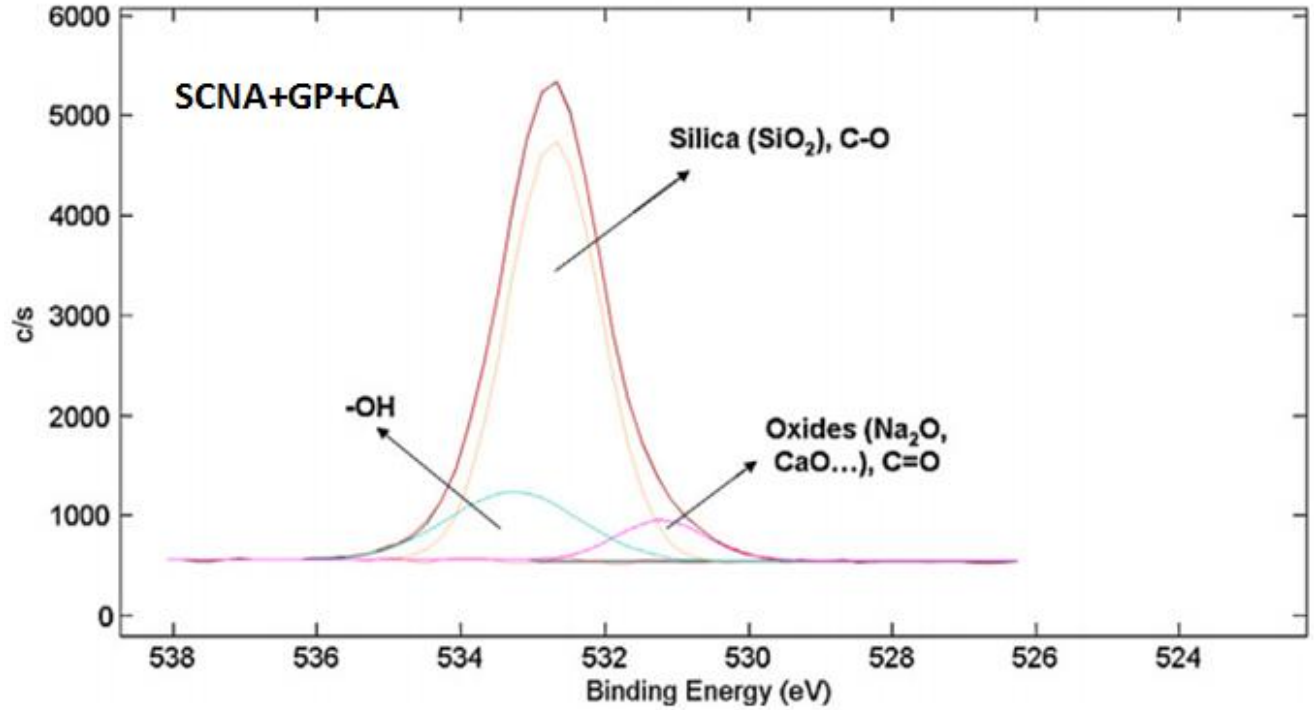

Figure 3-18: XPS detailed analysis of oxygen region for SCNA+GP+CA sample

CEL2 washed

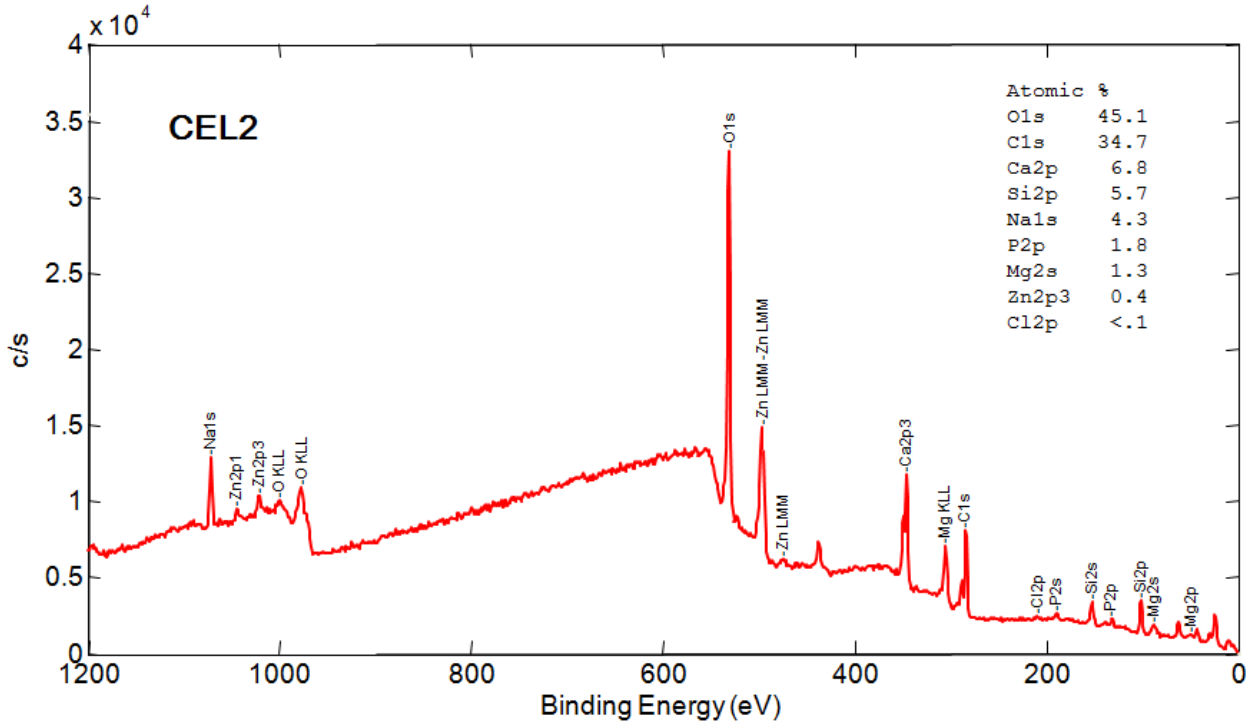

Figure 3-19: Survey spectra of CEL2 washed sample

The survey spectrum (figure 3-19) of washed CEL2 highlights all elements present on glass surface, as observed for gallic acid functionalization (chapter V, section 2.4). Signals of elements from glass composition were observed. Carbon, which is commonly present in the first surface layers of materials, was also observed in this non-functionalized sample due to the unavoidable atmospheric contaminations [13, 14].

Figure 3-20 shows the detailed analysis of carbon region of CEL2 bulk sample. A notable signal at about 284.85 eV is present on surface of washed CEL2, which can be attributed to unavoidable hydrocarbon contaminants on reactive surfaces [13, 14]. Compared to SCNA, the signal at about 289.66 eV presents a higher intensity and can be assigned to carbonates [5].

In the detailed analysis (figure 3-21) of oxygen region, the presence of the characteristic signals for oxides at 530.84 eV, silica at 531.63 eV as well as hydroxyls at 533.26 eV can be observed. It can be underlined that the signal of –OH is stronger than that of SCNA due to the higher

reactivity of CEL2 with more –OH groups exposed on the surface.

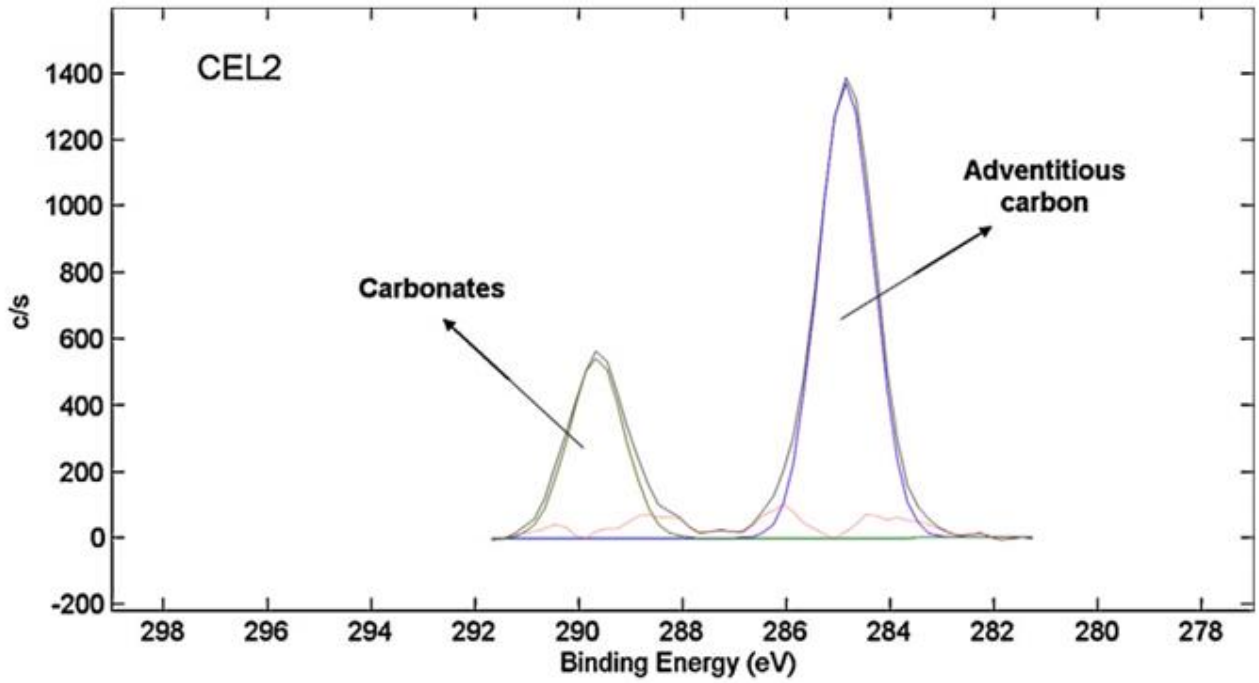

Figure 3-20: XPS detailed analysis of carbon region for CEL2 washed sample

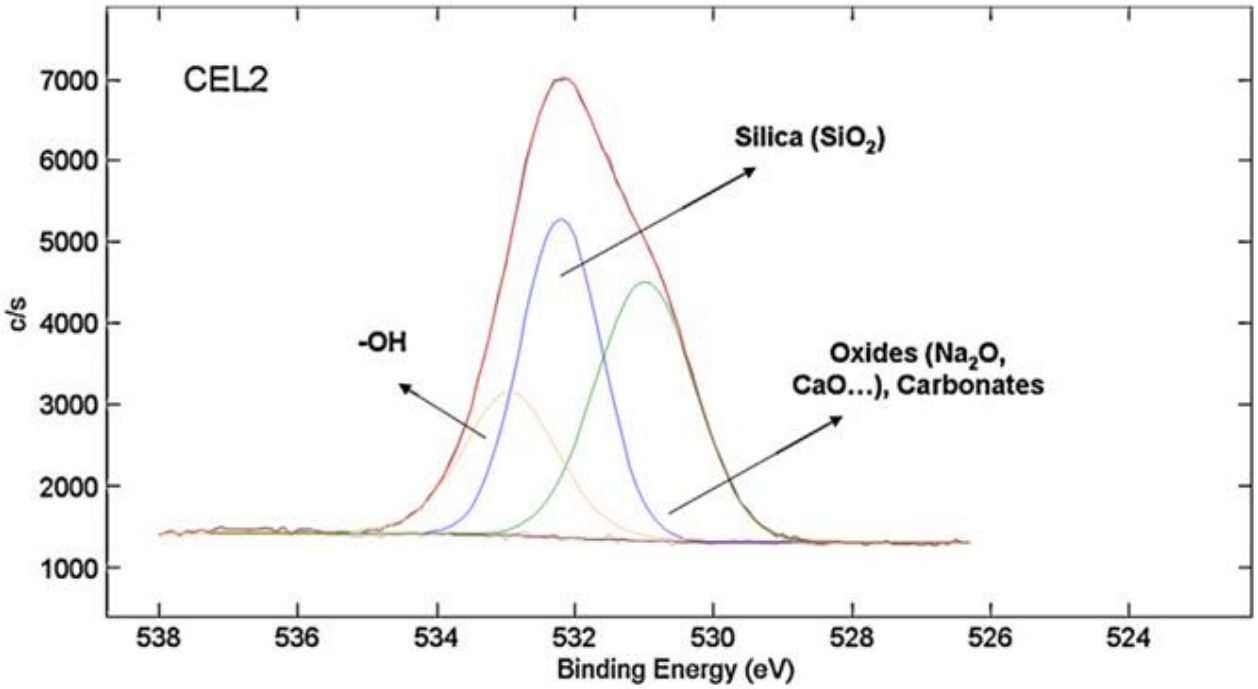

Figure 3-21: XPS detailed analysis of oxygen region for CEL2 washed sample

CEL2+GP

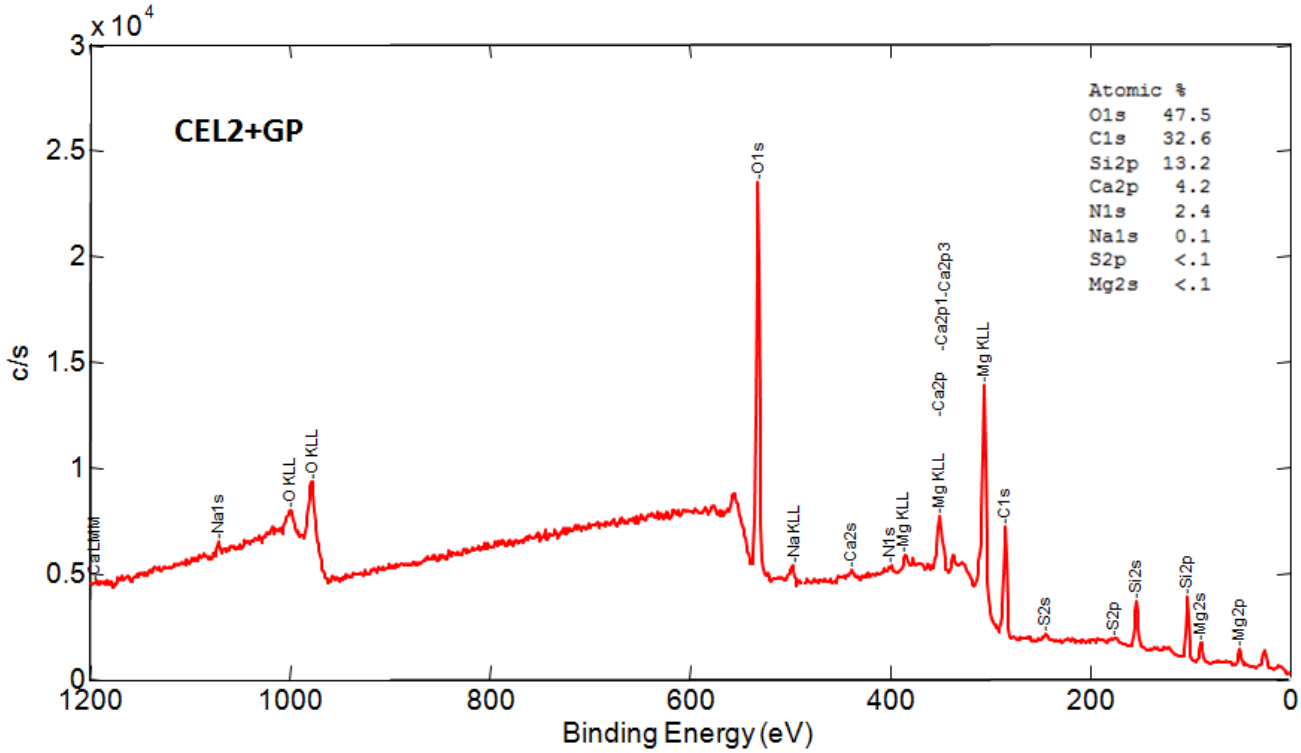

Figure 3-22: Survey spectra of CEL2+GP

The survey spectrum (figure 3-22) of CEL2 functionalized with grape phenols highlights all elements present on glass surface. Compared with the only washed sample, A certain reduction in the sodium and calcium content can be correlated with the ion release in the functionalization medium, while the increase in silicon content can be attributed to the silica gel formation.

In detailed analysis of carbon region of CEL2+GP (figure 3-23), different contributions can be detected after phenols functionalization. First, the signal of carbonate and the new peak at 286.16 eV and 288.79 eV can be observed and they can be attributed to C-O and C=O bonds respectively.

Figure 3-24 exhibits the detailed analysis of oxygen region of CEL2 bulk after grape phenols grafting. A significant increase in the –OH signal at 533.59 eV further confirms the phenols grafting. Peak at 531.6 eV can be attributed to oxides but also to C=O bonds [11].

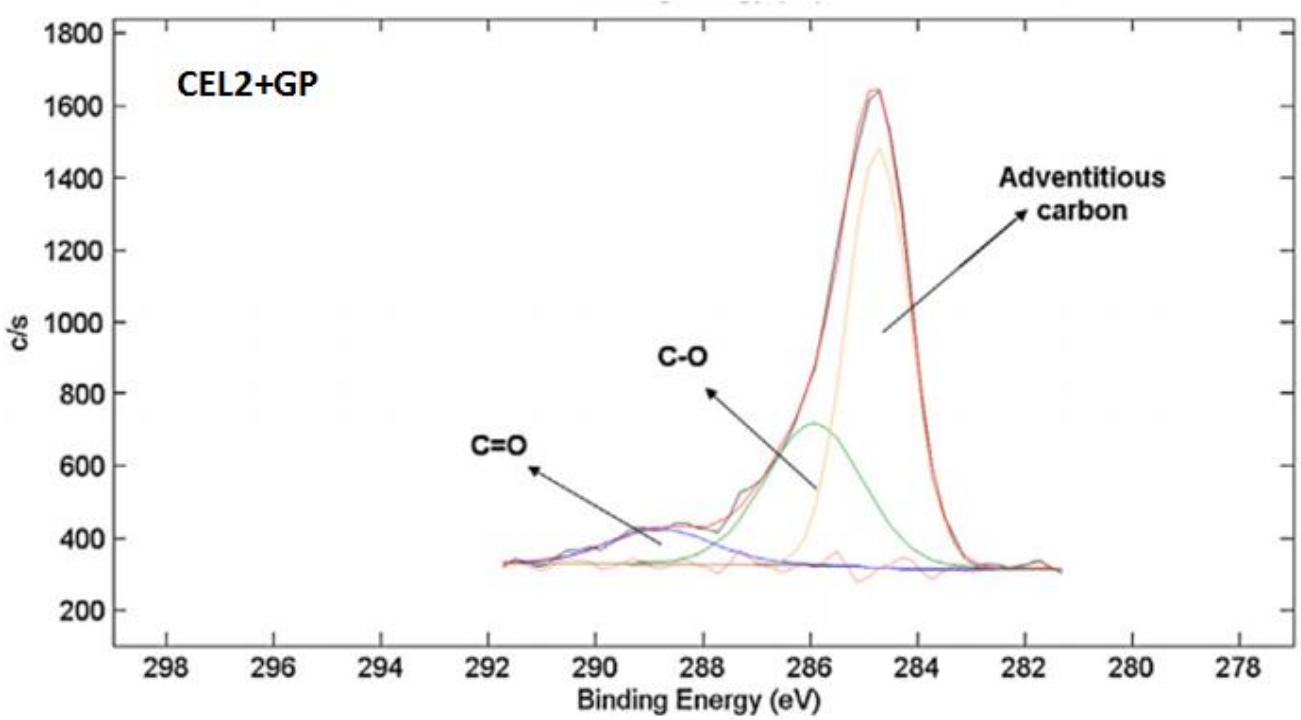

Figure 3-23: XPS detailed analysis of carbon region for CEL2+GP sample

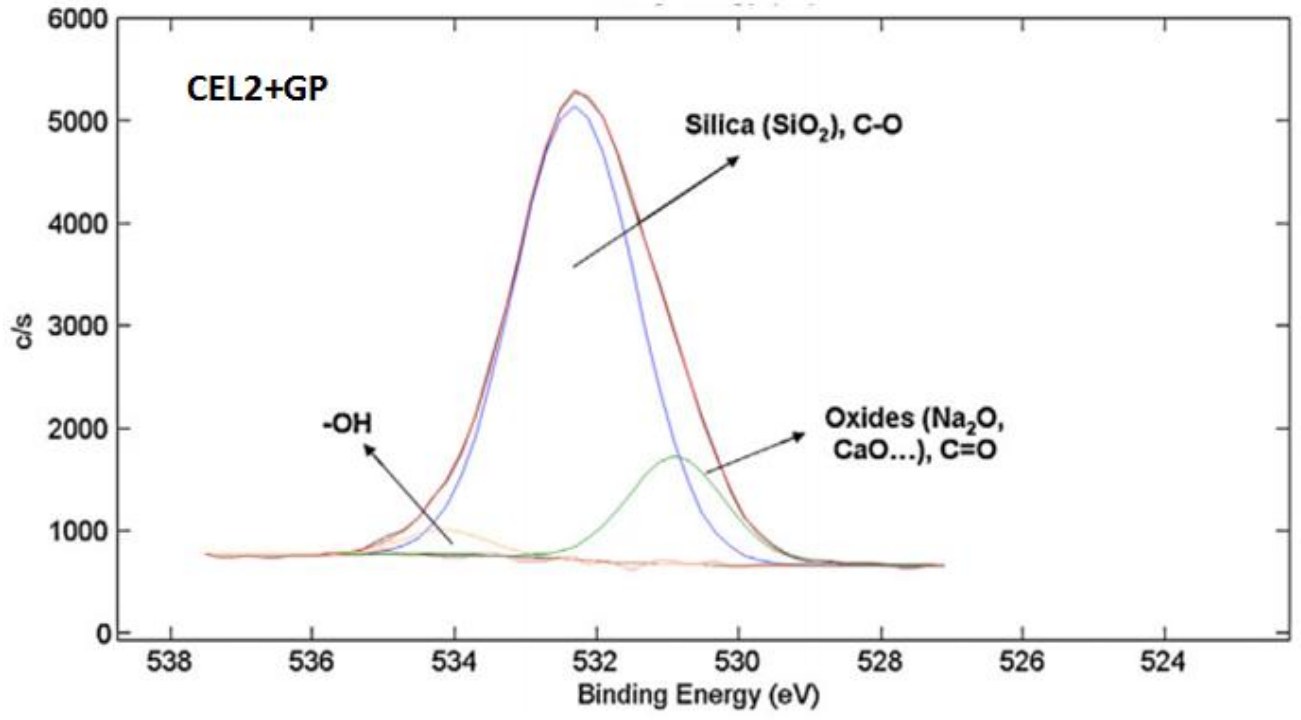

Figure 3-24: XPS detailed analysis of oxygen region for CEL2+GP sample

CEL2+GP+CA

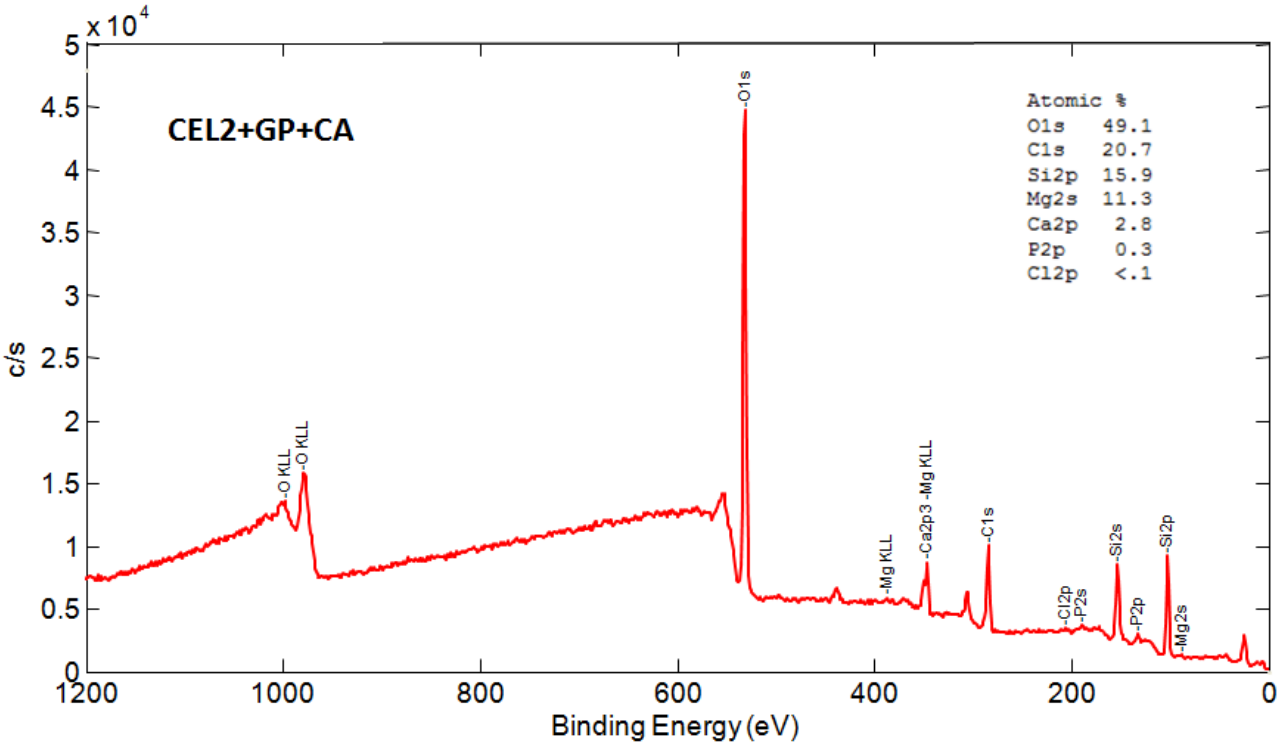

Figure 3-25: Survey spectra of CEL2+GP+CA

The survey spectrum of CEL2 functionalized by grape phenols with addition of citric acid is reported in figure 3-25. It highlights all elements present on glass surface. A certain reduction in the sodium and calcium content can be correlated with the ion release in the functionalization medium, while the increase in silicon content can be attributed to the silica gel formation

Similar to SCNA, after functionalization with addition of citric acid, a reduction of C=O signal can be observed in the detailed analysis of carbon region (figure 3-26). This result confirms the ability of citric acid to inhibit the oxidation of phenol into quinone.

In the detailed analysis of oxygen region (figure 3-27), a significant decrease in signals of –OH group as well as signal of C=O can be detected in accordance with the results obtained in gallic acid functionalization (chapter V, section 2.4).

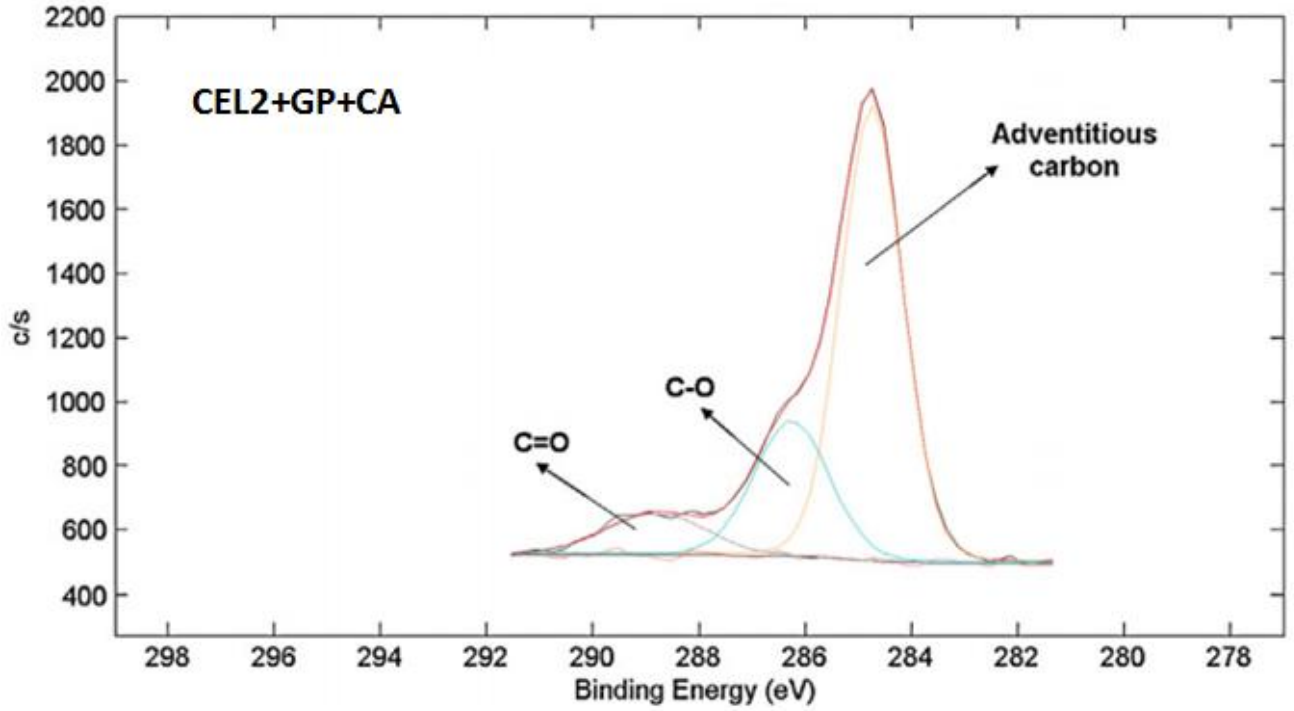

Figure 3-26: XPS detailed analysis of carbon region for CEL2+GP+CA sample

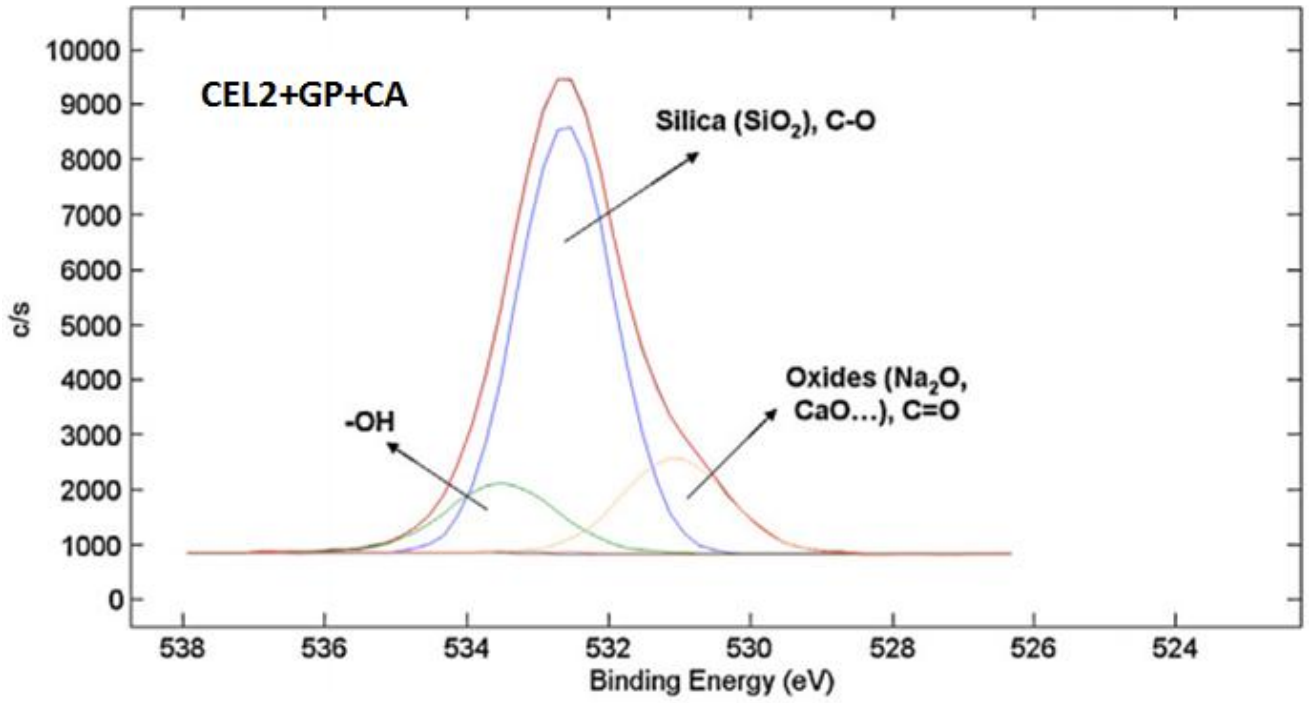

Figure 3-27: XPS detailed analysis of oxygen region for CEL2+GP+CA sample

Table 3-3 XPS atomic percentage of elements in the analyzed samples

Element [at%]	SCNA			CEL2		
	Washed	GP	GP+CA	Washed	GP	GP+CA
O	44.6	32.6	31.9	45.1	47.5	49.1
C	33.5	52.0	57.3	34.7	32.6	20.7
Si	14.9	11.1	10.1	5.7	13.2	15.9
Ca	4.8	2.0	-	6.8	4.2	2.8
Al	1.4	-	-	-	-	-
Na	0.8	0.3	-	4.3	0.1	-
P	-	-	-	1.8	-	0.3
Mg	-	-	-	1.3	<0.1	11.3
Other	-	<2.1	0.8	<0.5	<2.4	<0.1

Table 3-3 reports the comparison between atomic percentages of elements on the surface of bioactive glasses before and after phenol functionalization, with and without citric acid addition.

It can be observed that on surface of both washed SCNA and CEL2 samples, a certain amount of unavoidable carbon contaminants still remained, even though a washing treatment has been performed as widely reported in the literature for XPS analysis of reactive materials [12-14].

The reduction in calcium and sodium after phenol grafting demonstrates the ion exchange between glasses and the solution due to the material reactivity. At the same time, the increase in the silicon content on CEL2 samples confirms a more evident reaction which can lead to the formation of a silica gel layer, as discussed in the SEM paragraph.

After phenol grafting, the total carbon and oxygen contents on the surface show a not consistently trend. A certain increase in surface carbon can be detected on SCNA while a decrease on CEL2 surfaces. The detailed analyses of carbon and oxygen regions, discussed in

the previous paragraphs, allow a more precise discussion of the surface functionalization.

3.6 SEM analysis

The SEM-EDS analysis was performed to analyze the surface morphology of the samples, as well as their chemical composition on bulks before and after phenol grafting to obtain clear evidence about the difference in the substrate reactivity.

SCNA washed

Figure 3-28 exhibits the images of washed SCNA bulk with different magnifications from 1000 × to 10000×. A uniform surface is present with slightly visible polishing lines.

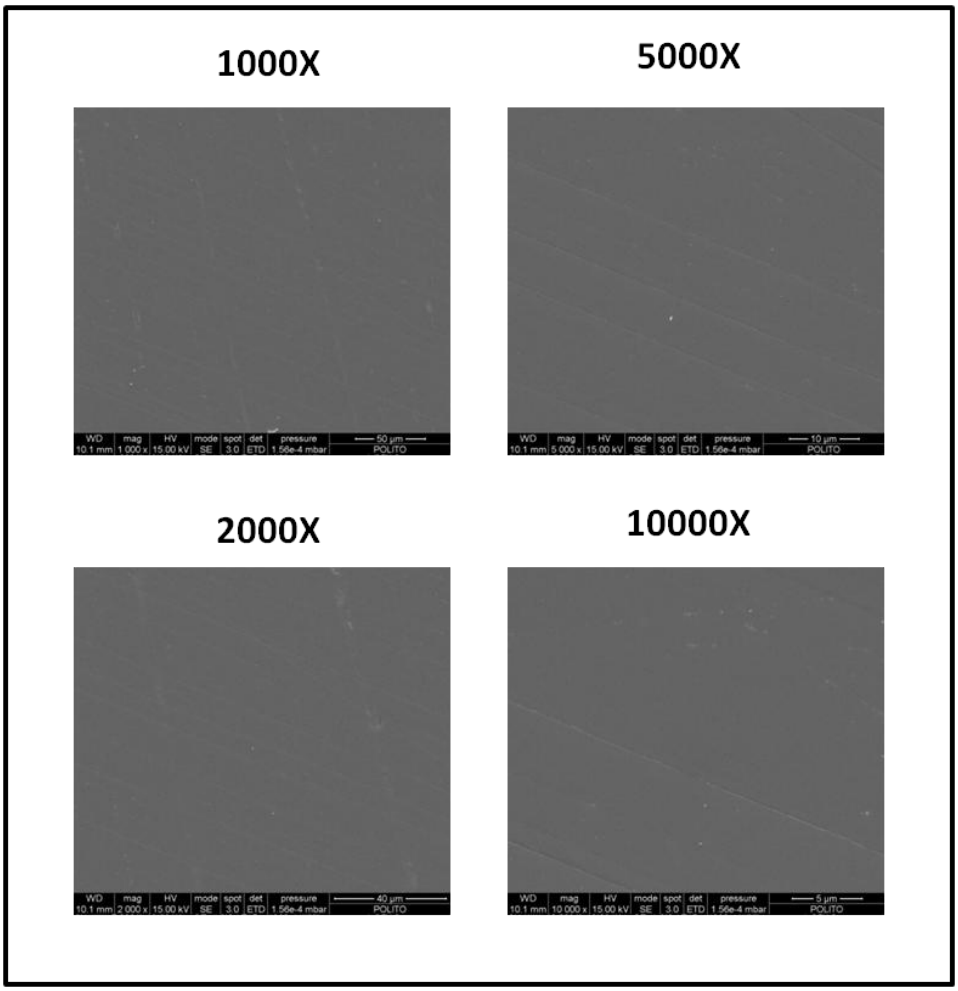

Figure 3-28: SEM images of washed SCNA samples with different magnifications

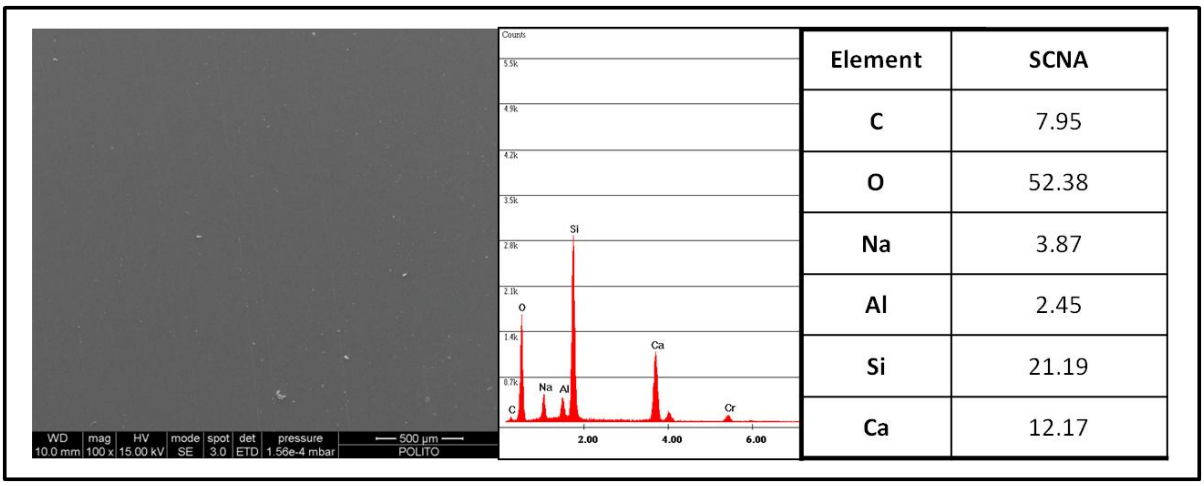

Element	SCNA
C	7.95
O	52.38
Na	3.87
Al	2.45
Si	21.19
Ca	12.17

Figure 3-29: SEM images and EDS analysis of SCNA washed

EDS analysis (figure 3-29) evidences the presence of the typical elements of glass composition (such as oxygen, silicon, sodium, calcium as well as aluminum). A small amount of carbon has also been reported and can be ascribed to surface contaminations.

SCNA+GP

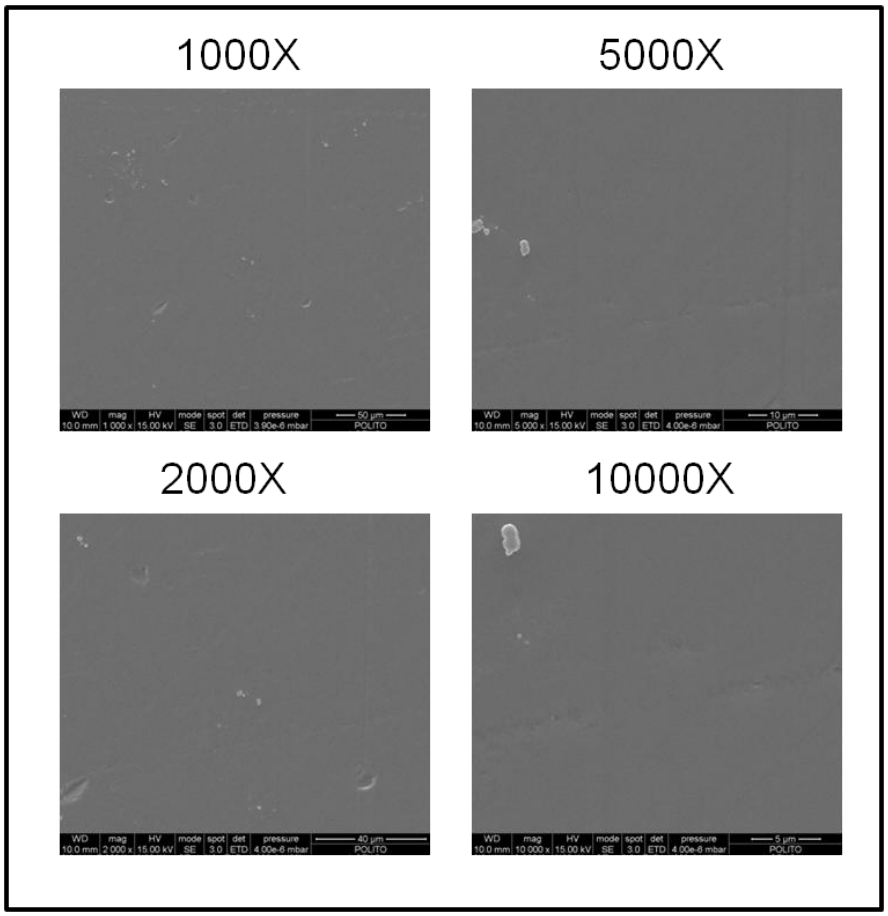

Figure 3-30: SEM images of SCNA+GP samples with different magnifications

In general, the surface of SCNA+GP showed a homogeneous morphology. Figure 3-30 shows the images with magnification of 1000×, 2000×, 5000× and 10000×. No significant changes can be observed from these images compared with the washed sample (figure 3-28). The reason may be the low reactivity of SCNA and the low amount of phenol molecules in grape phenol solution.

EDS analysis (figure 3-31) demonstrates a slight enrichment of carbon as well as depletion of sodium and calcium.

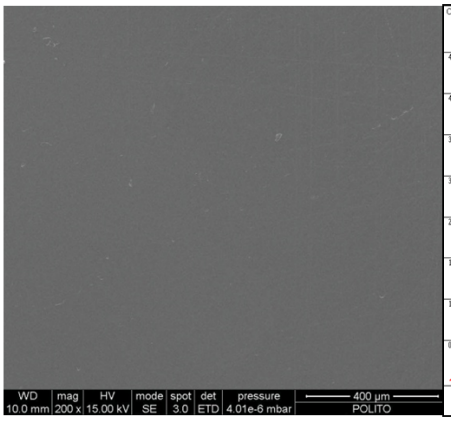

Element	SCNA+GP
C	8.04
O	51.85
Na	3.69
Al	2.58
Si	20.95
Ca	12.90

Figure 3-31: SEM images and EDS analysis of SCNA+GP

CEL2

Figure 3-32 exhibits the images of washed CEL2 bulk with different magnifications ranged from 1000× to 10000×. All the images show a uniform surface with slightly polishing spots and cracks.

EDS analysis (figure 3-33) detects all the elements of glass composition (oxygen, silicon, sodium, calcium, phosphorus, potassium as well as magnesium). The presence of a small amount of carbon is due to the unavoidable atmospheric contamination on the surface.

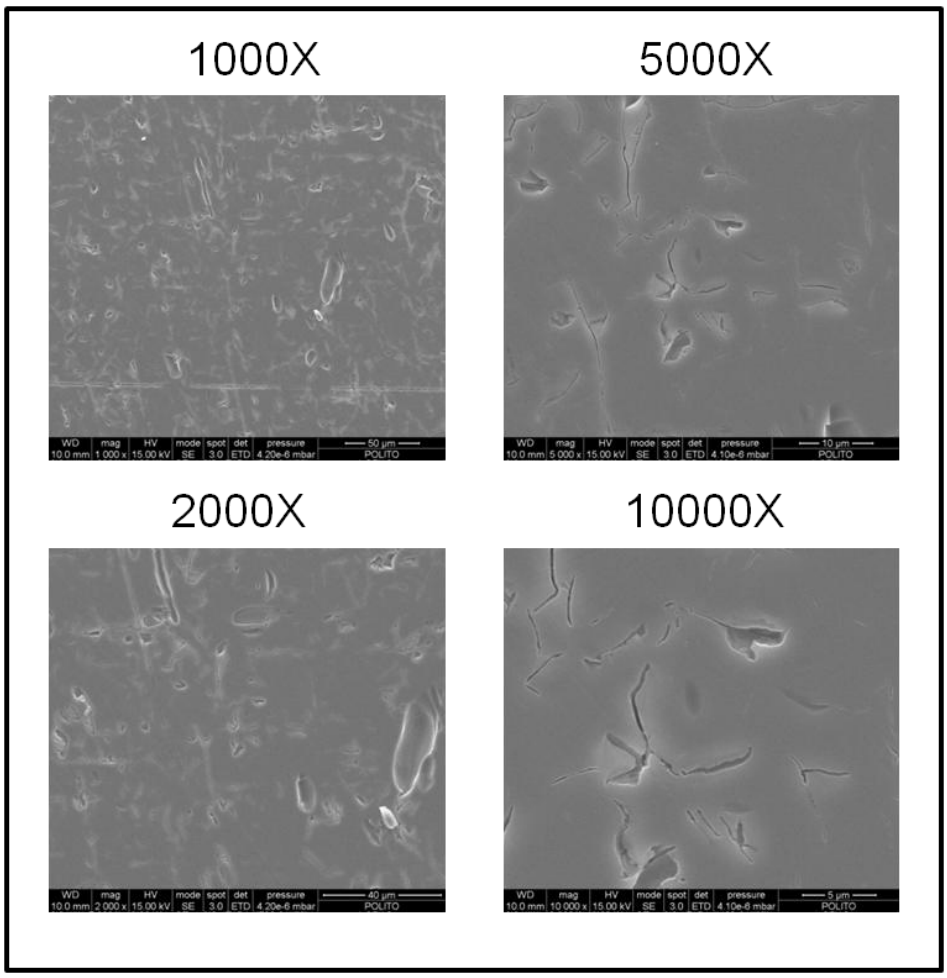

Figure 3-32: SEM images of washed CEL2 samples with different magnifications

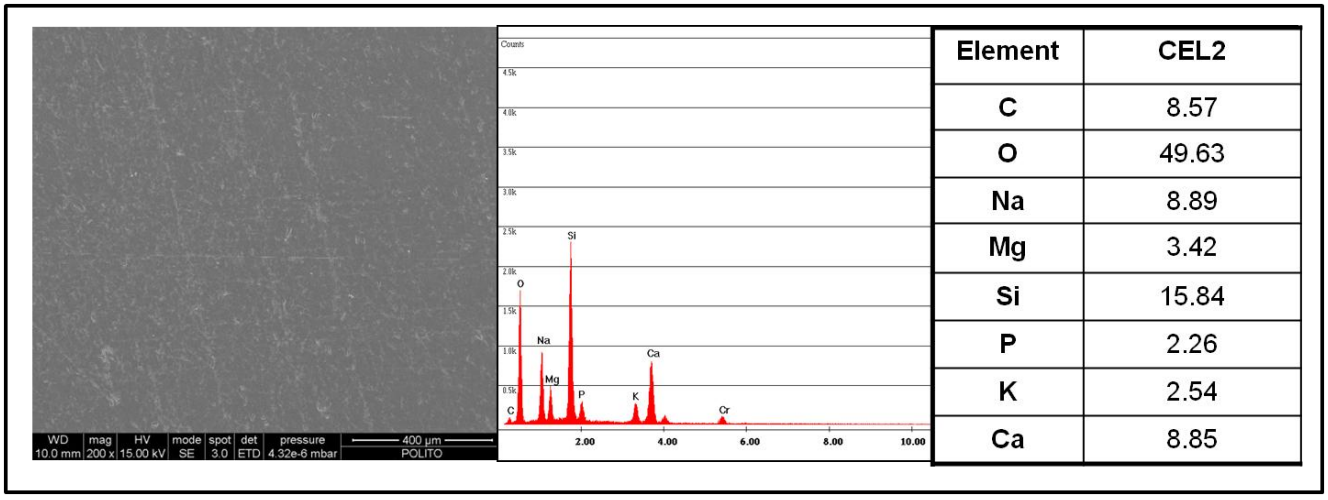

Element	CEL2
C	8.57
O	49.63
Na	8.89
Mg	3.42
Si	15.84
P	2.26
K	2.54
Ca	8.85

Figure 3-33: SEM images with 200× and chemical composition by EDS analysis of CEL2 washed bulks

CEL2+GP

The images of CEL2 grafted with grape phenols (Figure 3-34) shows a conformably cracked morphology through SEM investigation. Figure 3-33 displays the images with magnification of 1000×, 2000×, 5000× and 10000×.

After grafting with phenol, CEL2 bulks were completely covered by a cracked layer with the typical morphology of silica gel. Compared with the washed CEL2, EDS analysis (Tables in figure 3-35) demonstrates a notable increase in the carbon content on phenol grafted CEL2 surface as well as significant depletion of sodium and calcium due to the higher reactivity of glass surface.

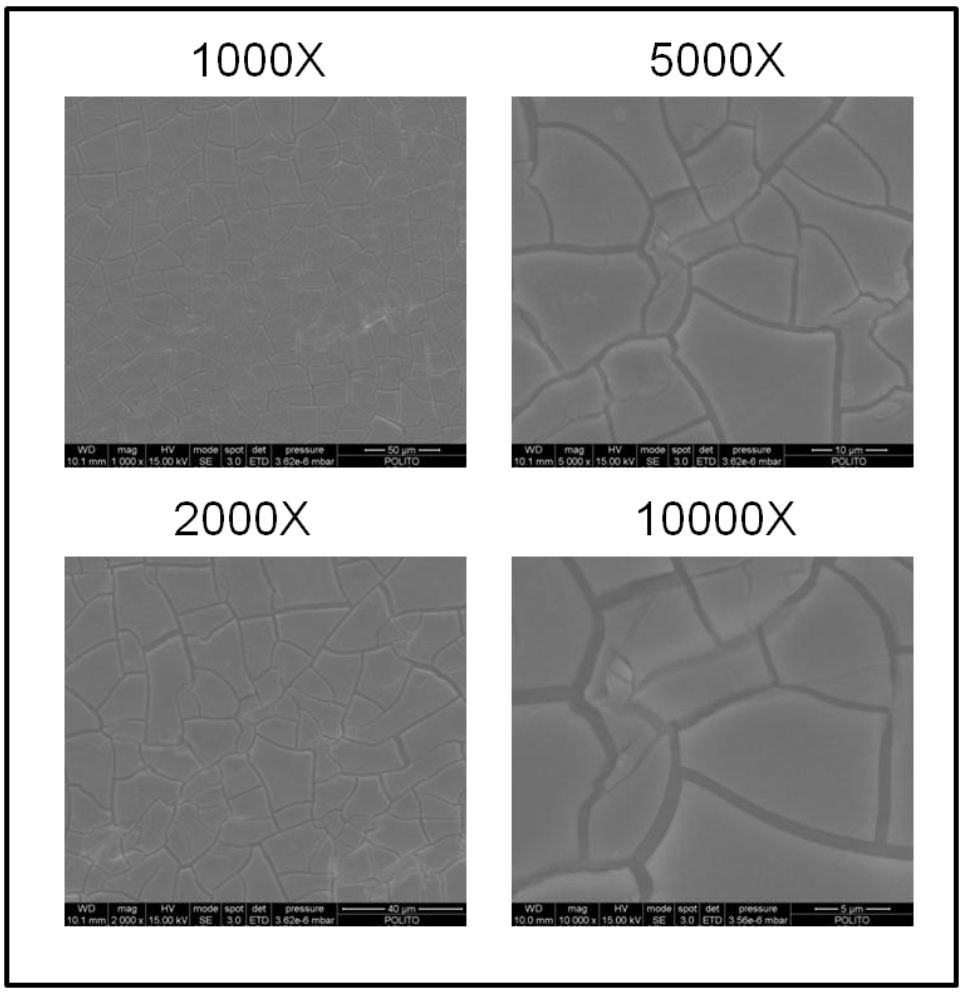

Figure 3-34: SEM images of CEL2+GP samples with different magnifications

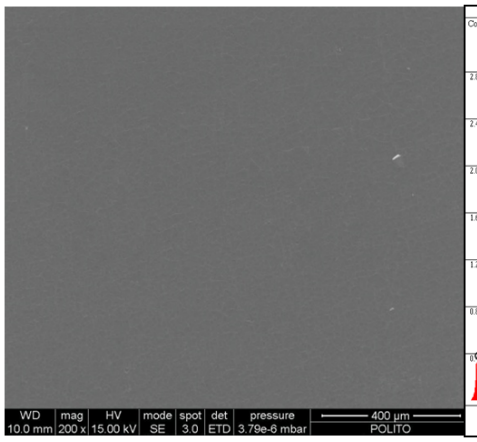

Element	CEL2+GP
C	28.63
O	47.84
Na	1.91
Mg	2.44
Si	5.09
P	5.73
K	0.65
Ca	8.07

Figure 3-35: SEM images with 200× and chemical composition by EDS analysis of CEL2 +GP bulks

3.7 FTIR analysis

FTIR was employed for the analysis of the functional groups of both SCNA and CEL2 glass powder before and after functionalization with grape phenols.

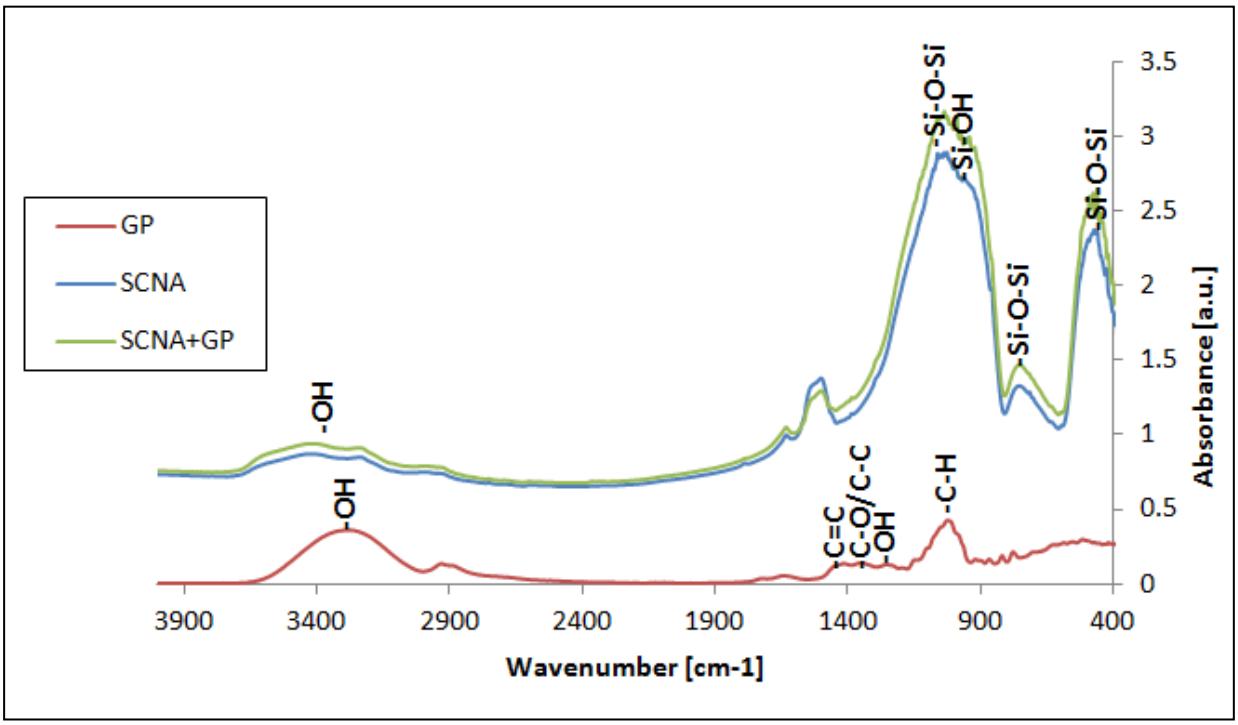

Figure 3-36: FTIR spectra of phenol, washed SCNA and SCNA+GP

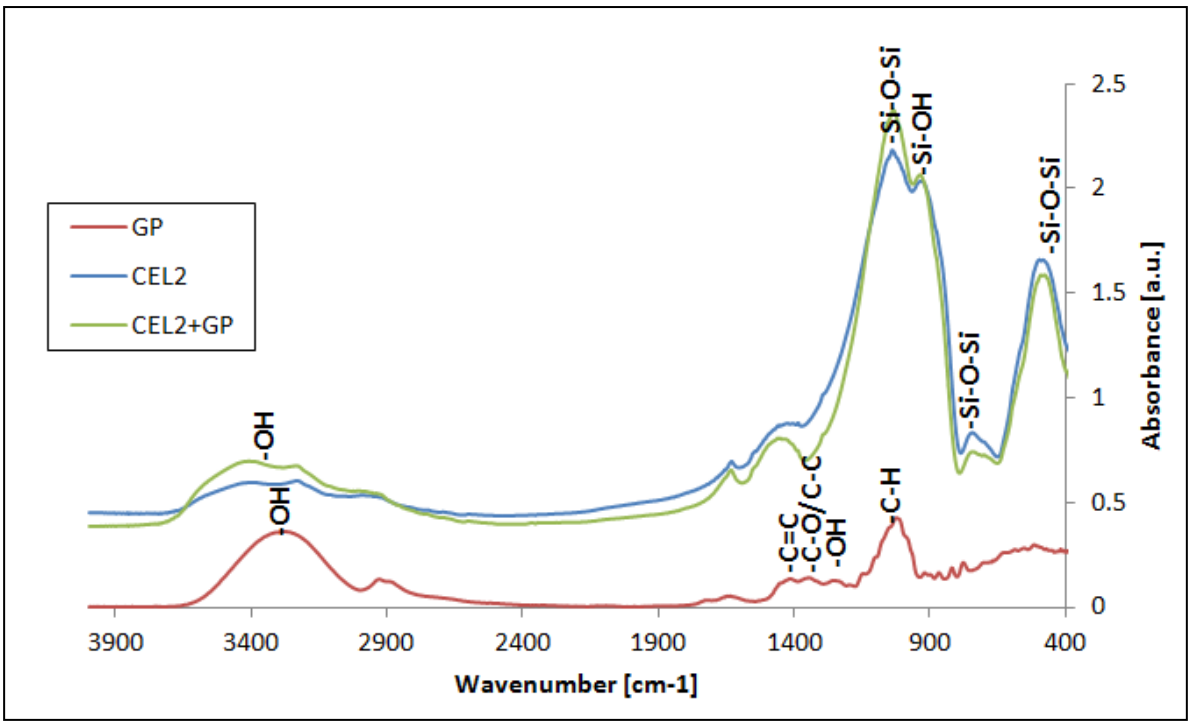

Figure 3-37: FTIR spectra of phenol, washed CEL2 and CEL2+GP

As for the grape phenol spectra (figure 3-36, 3-37), the typical polyphenolic characteristics were observed, including the existence of a phenolic ring –OH stretching within the 3200-3550 cm^{-1}, and –OH in plane bending at about 1322 cm^{-1}, an aromatic ring C=C stretching within1450-1600 cm^{-1}, and C-O/C-C stretching vibrations within 1200-1300 cm^{-1}, deformation of C-H aromatic at about 1024cm^{-1}[15, 16].

The FTIR spectra of two glasses are dominated by the vibrational bands due to Si-O vibrational modes: Si-O-Si stretch, Si-O alkali stretch and S-O bend and Si-O rock as showed in figure 3-40, 3-41 as reported in gallic acid grafting. The strong absorption at 1000-1200 cm-1 is assigned to Si-O-Si asymmetric stretching mode while peaks at about 760 cm^{-1} and 460 cm^{-1} are attributed to symmetric stretching and rocking vibration of Si-O-Si band, respectively. The peak observed around 960 cm^{-1} present on both glasses is assigned to non-bridging oxygen together with the surface silanols (Si-OH) groups. In addition, the surface silanol groups are confirmed by presence of a broad band in the region from 3000cm^{-1} to 3400 cm^{-1}, which represents the vibration of different hydroxyl groups [17-19].

After phenol grafting, the absorbance intensity of board peak in the region of 3000-3400 cm^{-1}

increased and the peak became narrow compared with that of the washed glasses. This phenomenon can ascribed to the bonding of phenol to enhance the signal of –OH group. In other parts of the spectra, similar to gallic acid functionalziation, no significant changes of the peak can be observed due to the low amount of phenols on the glass surface as well as the strong signal from glass oxides, which covers the absorbance intensity of phenol to some extent.

4 Surface functionalization of SCNA and CEL2 with polyphenol extracted from green tea

Natural tea polyphenols (TP) were extracted through a conventional solvent extraction methodology with two types of solvents: 80% ethanol and double distilled water, respectively. The extract yield and total phenol content were investigated by UV-Vis spectroscopy with Folin-Ciocalteau colorimetry. Tea polyphenols (TP, ethanol extracts) were grafted to the surface of two bioactive glasses (SCNA and CEL2) with different bioactivity level. Techniques such as UV-Vis spectroscopy together with Folin-Ciocalteau colorimetry and XPS were employed to evaluate the effectiveness of surface functionalization on the basis of the previous research on grape phenol grafting (chapter V, section 3).

4.1 Total phenol content and extract yield analysis

The total polyphenol content was evaluated by UV-Vis spectroscopy with Folin-Ciocalteau colorimetry as described in Chapter IV and calculated with the standard calibration curve:

$$\text{Absorbance} = 22.981 * \text{Concentration}_{(GA)} + 0.0232$$

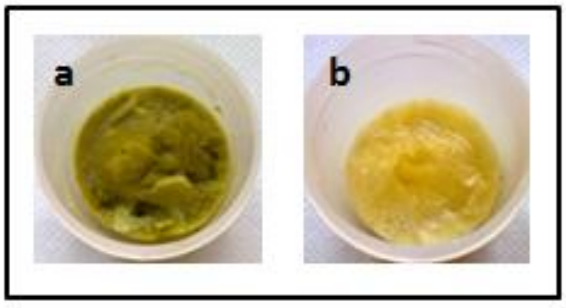

Figure 4-1: Freeze dried tea polyphenol extracts from (a) 80% ethanol extraction (b) double distilled water extraction

Figure 4-1 reports the images of polyphenol extracts with 80 % ethanol (a) and double distilled water (b) after freeze drying. The ethanol extract presents a green color while the water extracts showed a yellow color due to the compositional differences as mentioned in Chapter I.

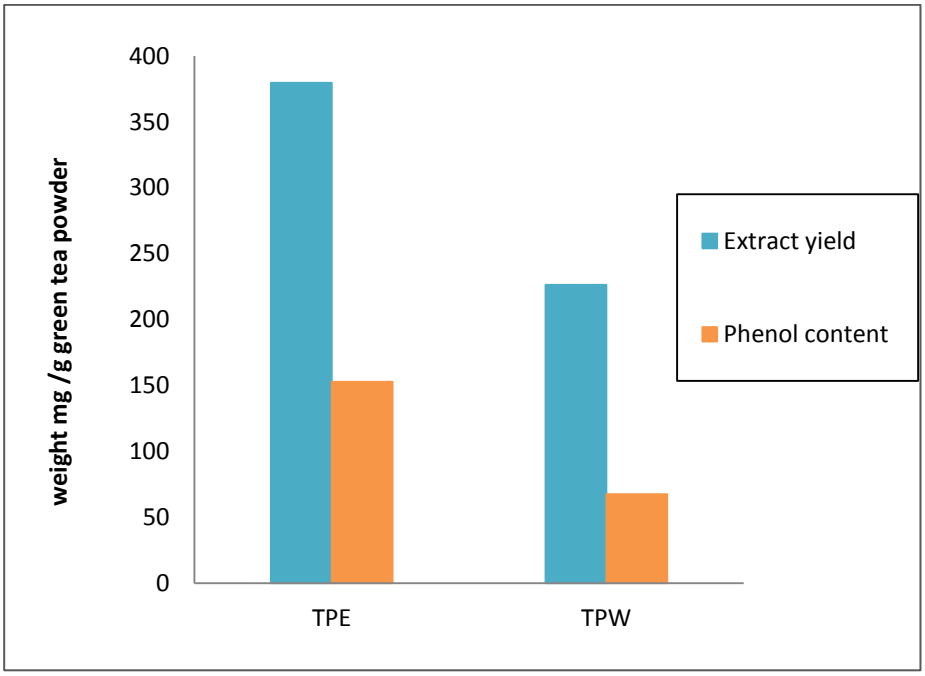

Figure 4-2: Phenol content and extract yield of two types of extract

In order to evidence the presence of polyphenols in extracts as well as evaluate effectiveness of two solvents, phenol content and extract yield were analyzed by Folic-Ciocalteau colorimetry with UV-Vis spectroscopy and results are presented in in figure 4-2. 379.7 mg crude tea polyphenol (TPE) can be isolated with 80 % ethanol, while 226.3 mg with double distilled water (TPW) from 1 g grinded green tea,. As far as the total phenol content was concerned, tea polyphenols from ethanol have a higher phenol content than the water extracts. Since the extracts from ethanol exhibited a higher extract yield and total phenol content, in the subsequent research, this extracts were employed for the functionalization and named as TP.

4.2 Macroscopic observations on the samples

SCNA and CEL2 bioactive glasses, in the form of slices and powders, were functionalized with tea polyphenols (extracted with water-ethanol solvent system) as described in (chapter IV, section2.3.4) of materials and methods section.

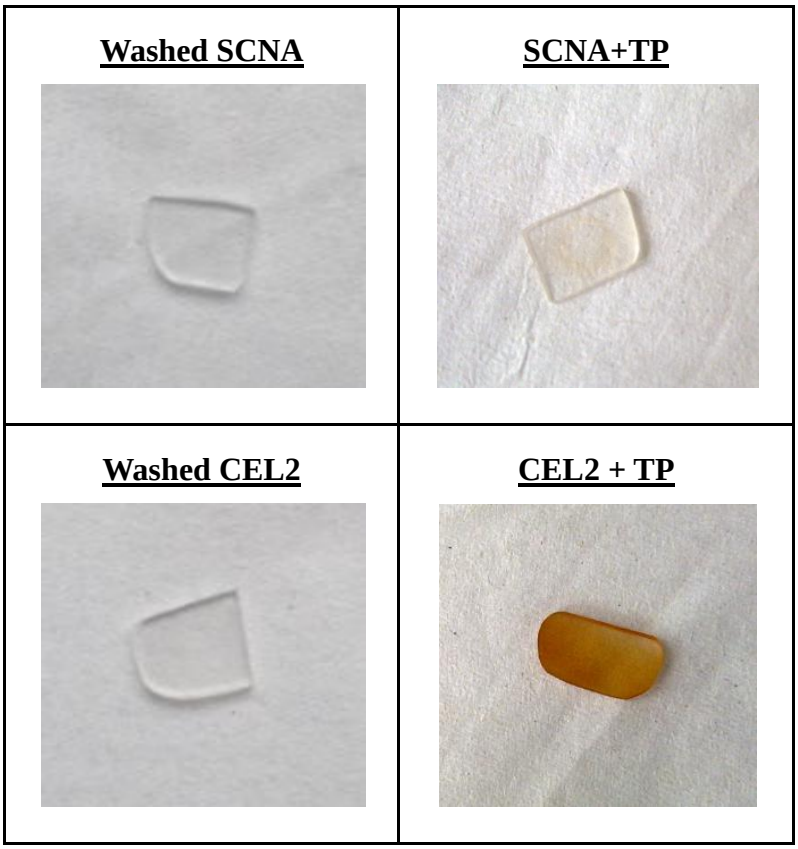

Figure 4-3: Glass bulks appearances before and after TP functionalization

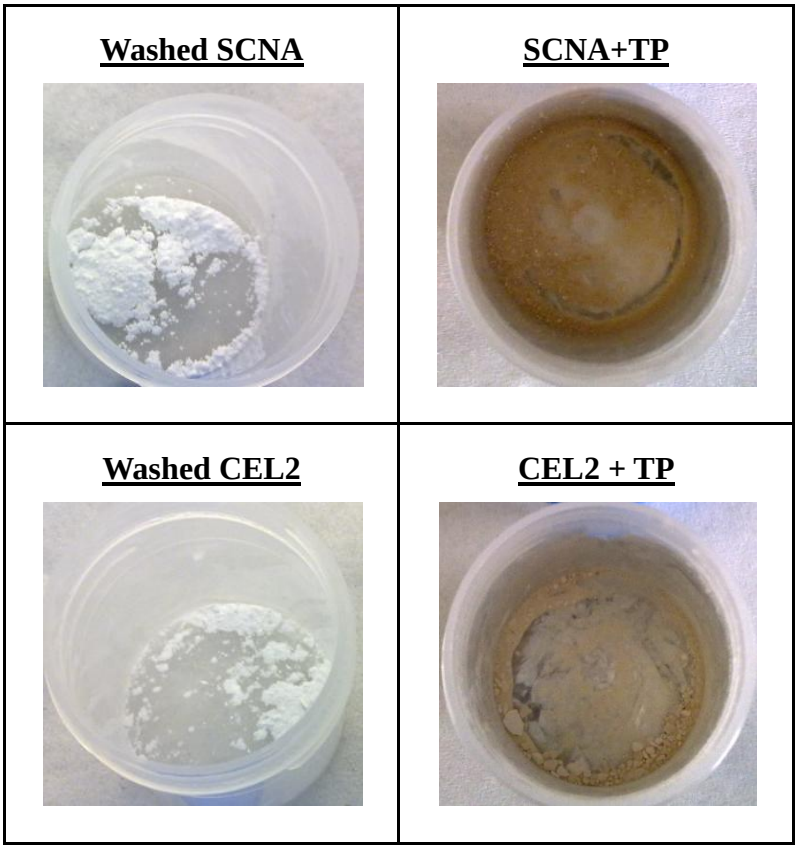

Figure 4-4: Glass powder samples appearances before and after TP functionalization

Figure 4-3 shows the SCNA and CEL2 bulk samples before and after TP functionalization process. As far as CEL2 is referred, it is evident that after modification with tea polyphenols, the color of bulk samples changes from colorless to brown. On the other hand, the color variation is almost absent on the surface of SCNA functionalized by TP.

Both SCNA and CEL2 bulk and powder samples were functionalized with tea polyphenol, and after solution was moved away, the powder appearances were observed in figure 4-4. The color of CEL2 powder changes from white to light brown, which was similar to bulk sample. Compared with SCNA bulk, powders exhibit a significant color changes from white to brown. However, the color variation is not as significant as gallic acid funtionalization but the change is greater than that of grape phenol functionalization.

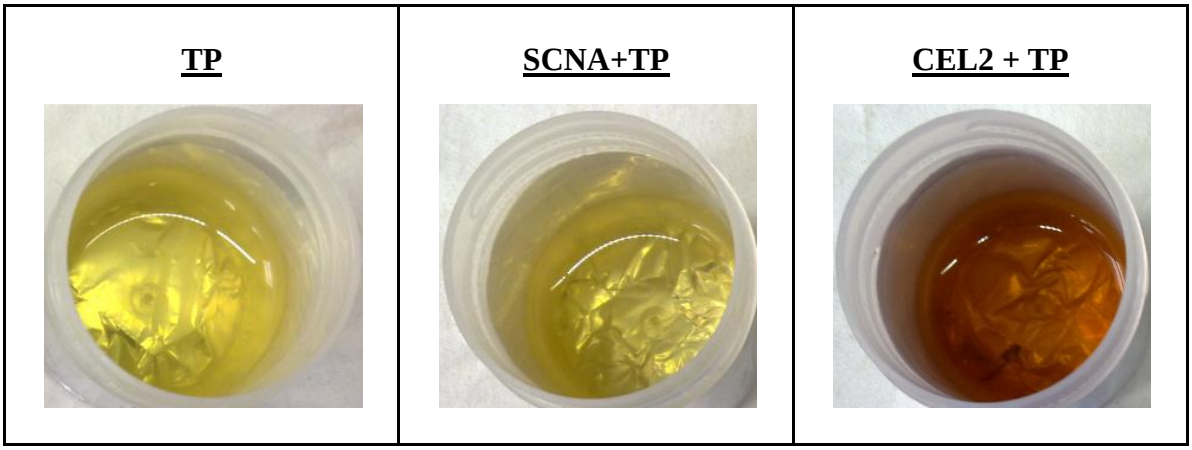

Figure 4-5: Tea polyphenol solution and uptake solution after functionalization of SCNA and CEL2 bulk samples

The original tea polyphenol solution presents a yellow color. Figure 4-5 exhibits the color change of uptake solution of tea polyphenols in which SCNA and CEL2 bulks were soaked for 24 hours. After SCNA bulks were removed out, the tea polyphenol uptake varied from yellow to light yellow while the uptake solution for CEL2 functionalization changed into brown color.

4.3 pH measurement

The effect of pH was investigated through measuring pH value of TP uptake solutions before and after soaking of SCNA and CEL2 samples (bulks and powders) for 24 hours. The results are reported in figure 4-6.

As described previously for the gallic acid and grape phenols functionalization (chapter V, section 2.2 and 3.3), the pH of the starting TP solution used for the functionalization is acidic, in this case the pH has a value of 5.11 ± 0.0.

The ion exchange between the glass and the solution induces a significant increase of the solution pH for static soaking models as described and confirmed in the previous research on gallic acid and grape phenol functionalization (chapter V, section 2.2 and 3.3). Similar variations of pH value can be observed in uptake solution of both glass bulks and powders after TP functionalization.

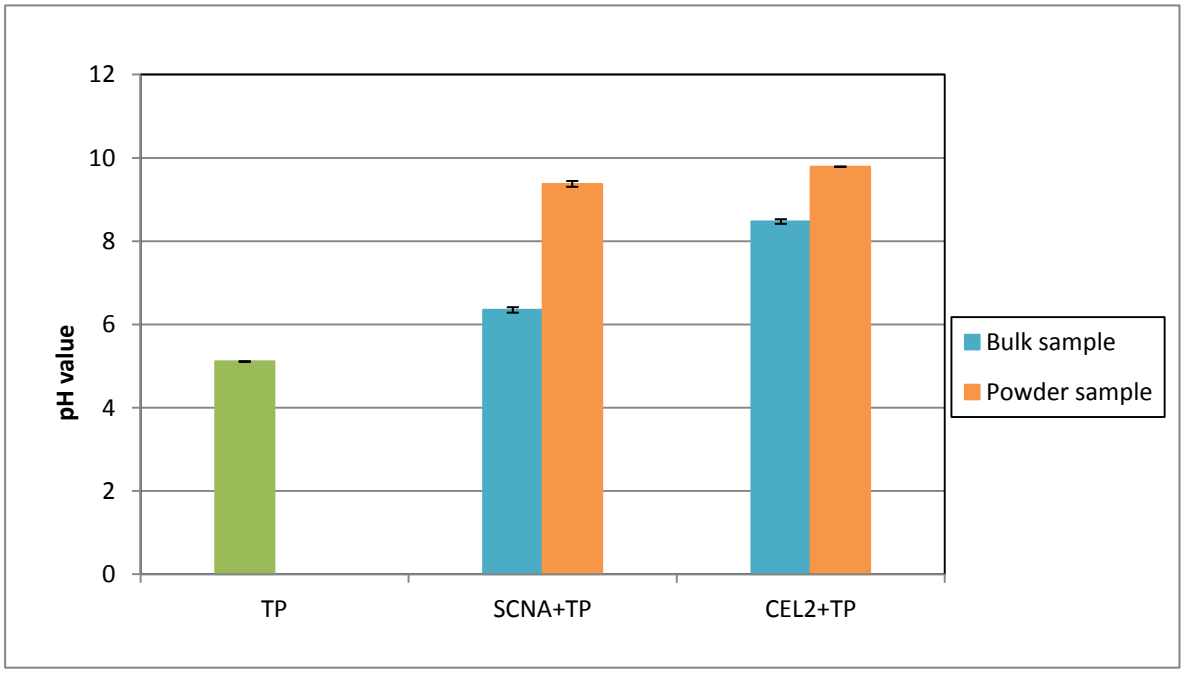

Figure 4-6: pH value of TP uptake solution before and after 24 hours soaking of different glass bulks and powders

After functionalization, notable changes of pH from acidic value to alkaline in uptake solution of

both glasses can be observed, especially in the case of more reactive glass (CEL2) and the powder samples (figure 4-6). In this case, the pH value is 6.35 ± 0.06 for SCNA bulk and 9.38 ± 0.07 for SCNA powders, 8.47 ± 0.05 for CEL2 bulk and 9.79 ± 0.0 for CEL2 powders. These data confirmed the one previously obtained with gallic acid as well as grape phenols (chapter V, section 2.2 and 3.3).

4.4 UV-Vis analysis

4.4.1 Uptake solutions analyzed by UV

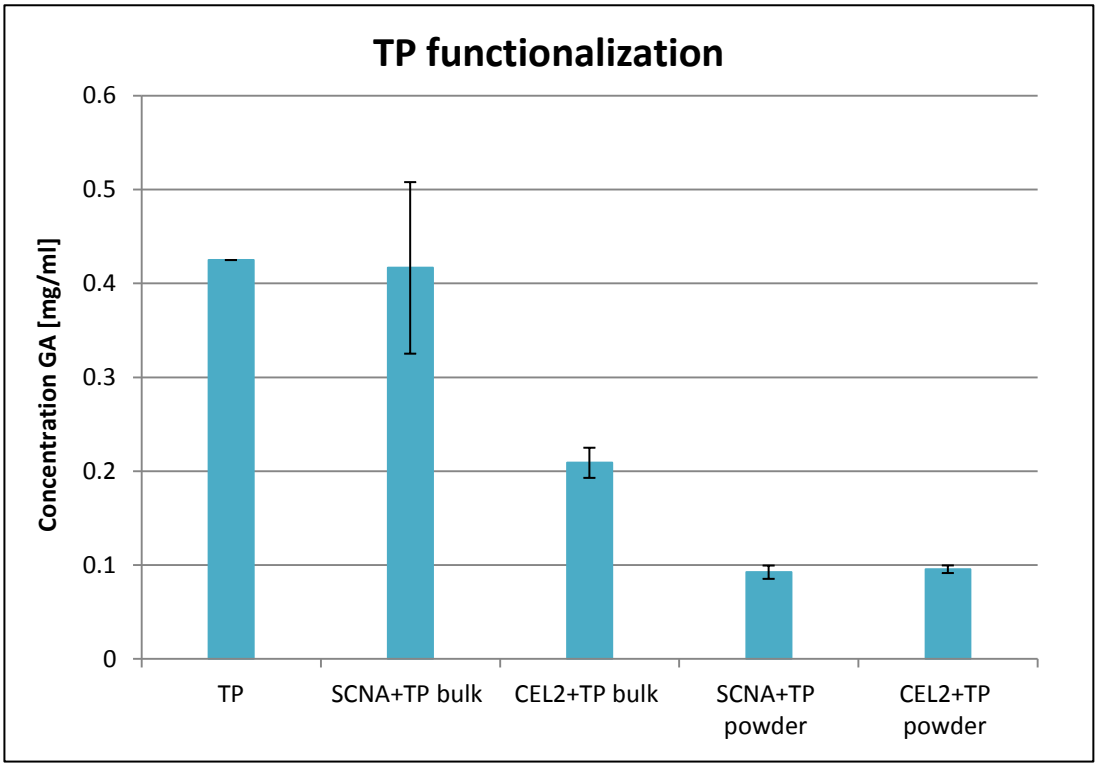

Figure 4-7: UV photometric results for TP uptake solution before and after 24 hours soaking of different glass samples

The depletion of tea polyphenols during the functionalization process was investigated by means of Folin-Ciocalteau colorimetry with UV-Vis spectroscopy on uptake solutions before and after glass soaking. The amount of tea polyphenols content was calculated on the basis of the equation from standard calibration curve (chapter V, section 2.3.1).

The bar diagram in figure 4-7 shows the phenol content in original phenol solution as well as in the uptake solution after soaking SCNA bulk and powder samples, and CEL2 bulk and powder samples. In general, the depletion of phenol content can be observed in all uptake solutions, as reported in gallic acid and grape phenol functionalization (chapter V, section 2.3.2 and 3.4.1). If compared with SCNA bulk samples, the CEL2 bulks were able to bond more biomolecule and significantly decreased the phenol content to 0.2091 mg/ml. Furthermore, a higher consumption of biomolecules can be underlined for both powder samples (the values are 0.0925 and 0.0957 mg/ml, respectively) when compared to bulk ones. The results are in accordance with the ones obtained with gallic acid and grape phenol functionalization on glass samples (chapter V, section 2.3.2 and 3.4.1).

As far as the powders are concerned, the capability to bond more biomolecules can be ascribed to the larger surface area. Considering the different bioactivity levels of two bioactive glasses, the higher ability of CEL2 in binding phenols can be assigned to its higher reactivity with more –OH group exposure and formation of a porous silica gel layer during functionalization process (chapter V, section 2.3.2 and 3.4.1). In addition, the structural change of phenol molecules in alkaline environment can be another reason for the phenol content reduction, as previous study for gallic acid and grape phenol functionalization (chapter V, section 2.3.2 and 3.4.1).

4.4.2 Functionalized bulk samples analyzed by UV

In order to evaluate the amount of phenol molecules on the bulk surface after functionalization, bulk samples of SCNA and CEL2 were analysed by reacting with Folin-Ciocalteau's reagent (figure 4-8) and observing the reaction solution with UV-Vis spectroscopy. The results are reported in bar diagram in figure 4-9.

The amount of phenols on the surface of SCNA is too low to be detected by UV. However, on the surface of CEL2, a relatively higher amount of tea polyphenol has been detected. The results are in accordance with the depletion of tea polyphenol in uptake solution due to the different reactivity level of two glasses.

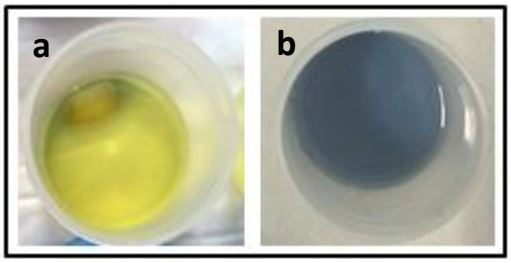

Figure 4-8: a) TP grafted bulk sample in FC reagent and b) uptake after 2h incubation

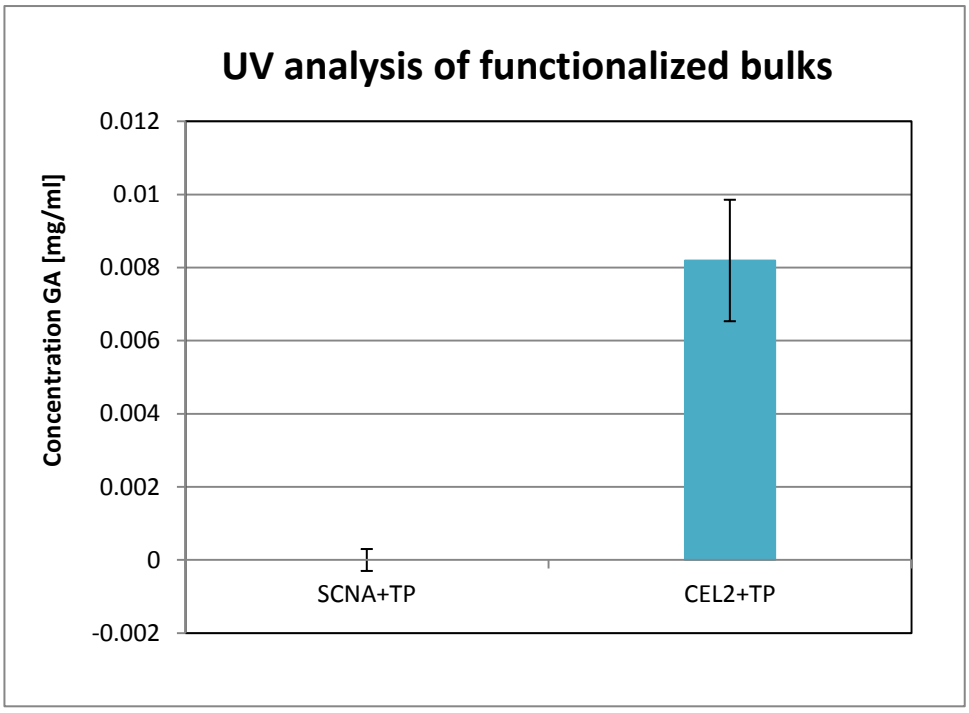

Figure 4-9: UV photometric results for phenol content on functionalized SCNA and CEL2 bulk samples

4.5 XPS analysis

With the aim to confirm the presence of tea polyphenols on material surface, XPS was employed to characterize the chemical composition and chemical groups on the surface of the just washed SCNA and CEL2 bulk samples as well as bulks grafted with tea polyphenols. Results have been reported by the following spectra including survey spectra and detailed analyses of carbon and oxygen regions. The samples were named as follows:

i. SCNA (just washed sample)

ii. SCNA+TP

iii. CEL2 (just washed sample)

iv. CEL2+TP

SCNA washed

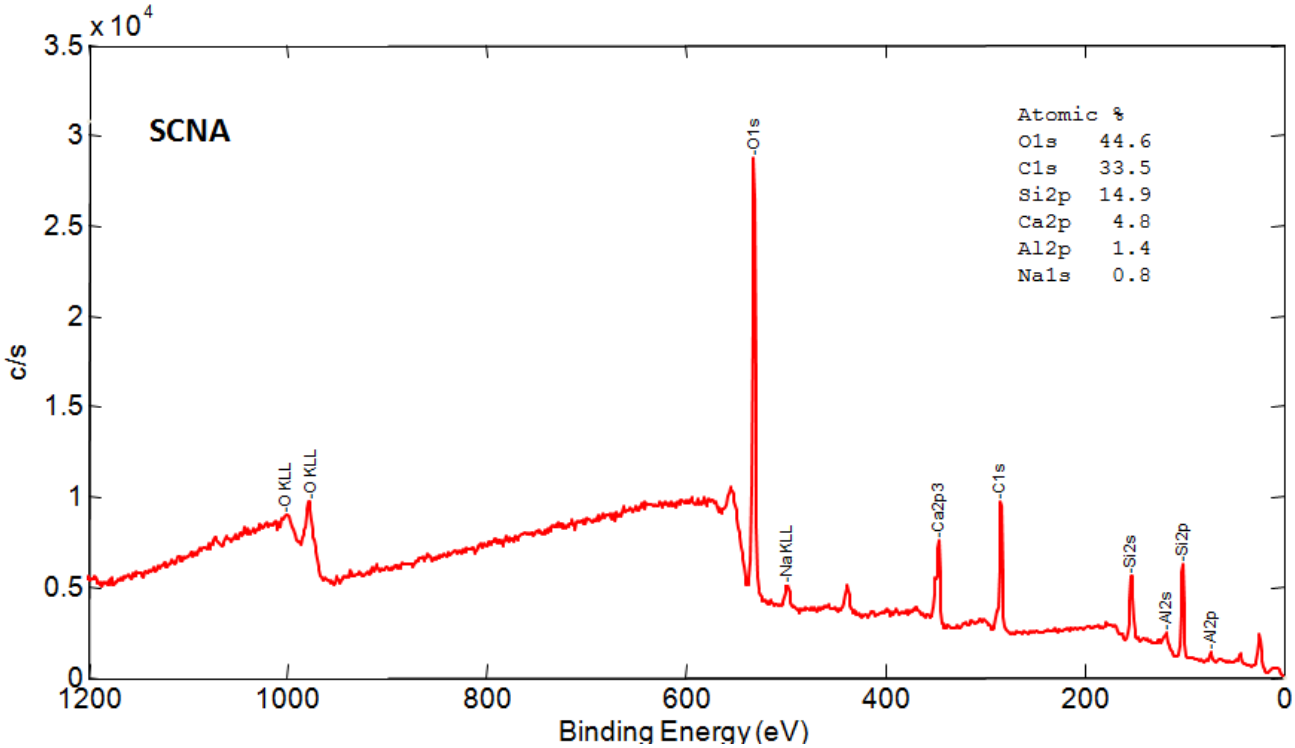

Figure 4-10: Survey spectra of washed SCNA

Signals of all elements from glass composition were highlighted in the survey spectrum (figure 4-10) of washed SCNA. Signals of elements characteristic of glass composition can be observed, including oxygen, sodium, calcium, silicon, aluminum. Carbon, which is commonly present in the first surface layers of reactive materials, has also been observed in this non-functionalized sample due to the unavoidable atmospheric contaminations, as reported in gallic acid and grape phenol functionalization (chapter V, section 2.4 and 3.5).

Figure 4-11 reports the detailed analysis of carbon region of washed SCNA. Two main contributions can be observed at about 284.8 eV and 289.4 eV, they can be attributed to unavoidable contaminations and carbonates, respectively [13, 14].

In the detailed analysis spectrum (figure 4-12) of oxygen region, typical signals of oxides (at 531.7 eV), silica (532.35 eV) and hydroxyl groups (533.54 eV) can be observed, as reported in the literature related to surface activation [6].

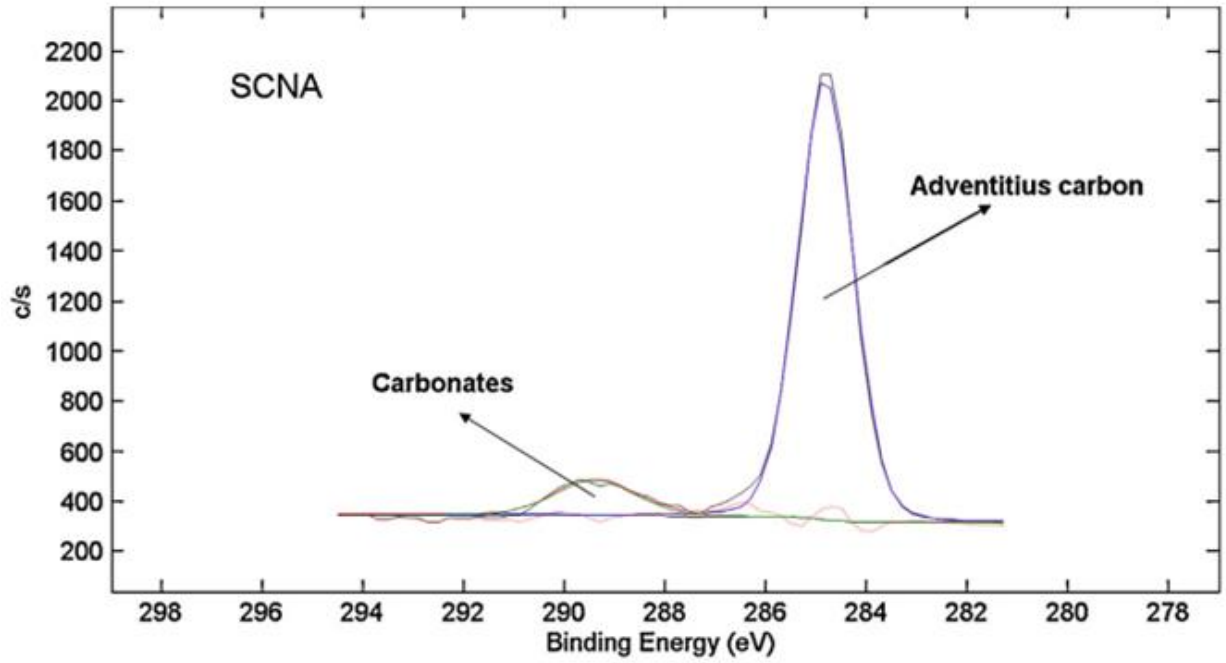

Figure 4-11: XPS detailed analysis of carbon region for SCNA washed sample

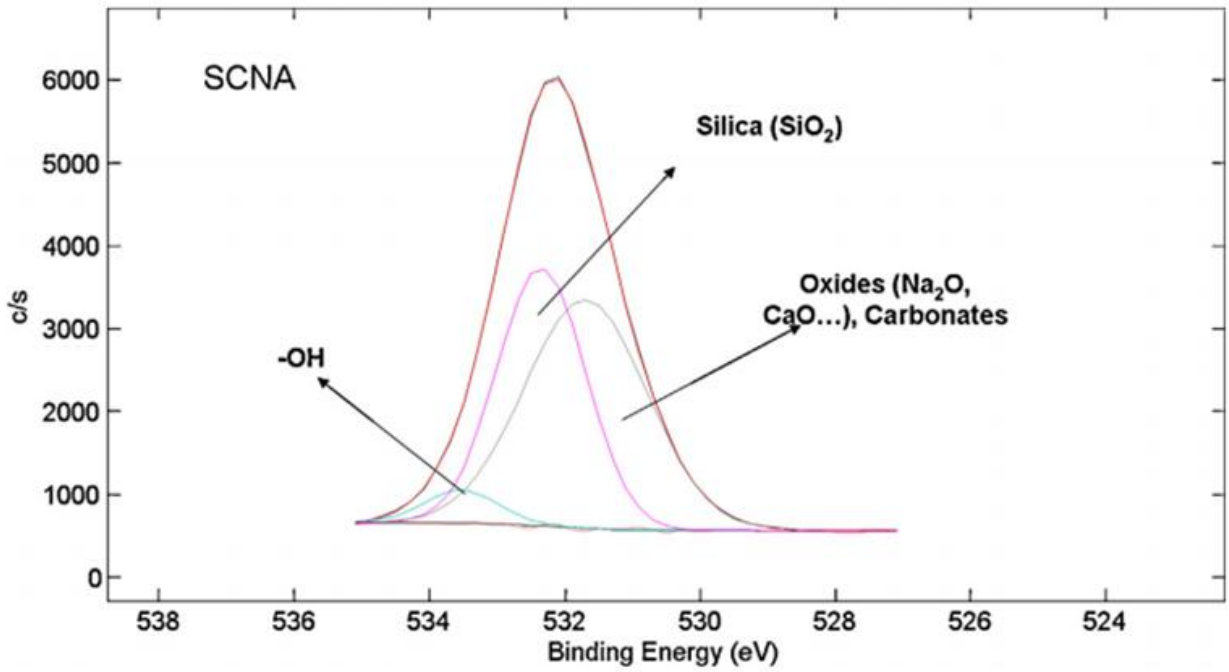

Figure 4-12: XPS detailed analysis of oxygen region for SCNA washed sample

SCNA+TP

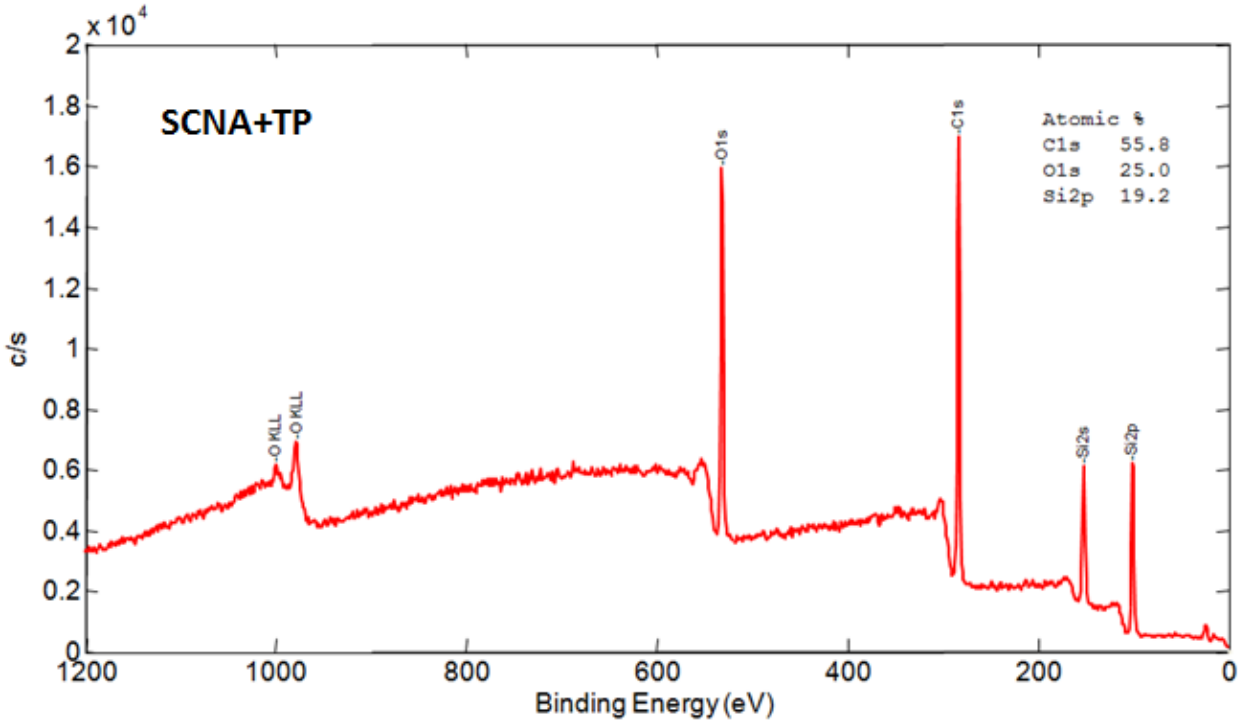

Figure 4-13: Survey spectra of SCNA+TP

The survey spectrum of SCNA functionalized with tea polyphenols (figure 4-13) highlights only silicon and oxygen as characteristic elements of the glass composition, while no signals for sodium and calcium can be detected. Ion release in the functionalization medium can be an explanation of this result. Moreover a significant increase in the carbon content can be pointed out.

Figure 4-14 presents the detailed analysis of carbon region on SCNA+TP. After tea polyphenols functionalization, carbonate signals disappears and two new contributions at 285.12 eV and at 288.96 eV appears near to the contaminants one. They can be attributed to C-O and C=O, respectively.

Figure 4-15 reports the detailed analysis of oxygen region. A small signal for OH groups is still present and can be related also to tea polyphenol grafting. A signal at about 532.36 eV can be attributed to both silica and C-O bonds, while the small one at about 530.96 eV can be attributed

to both oxides and C=O groups.

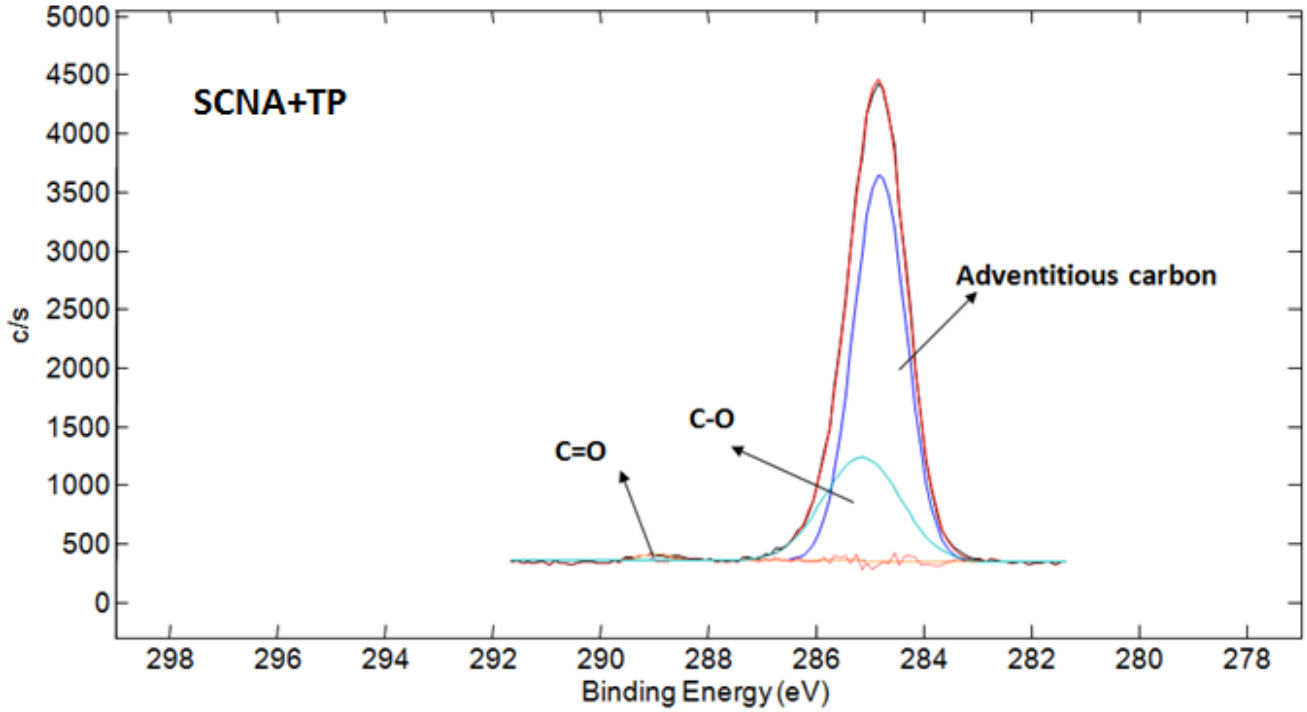

Figure 4-14: XPS detailed analysis of carbon region for SCNA +TP sample

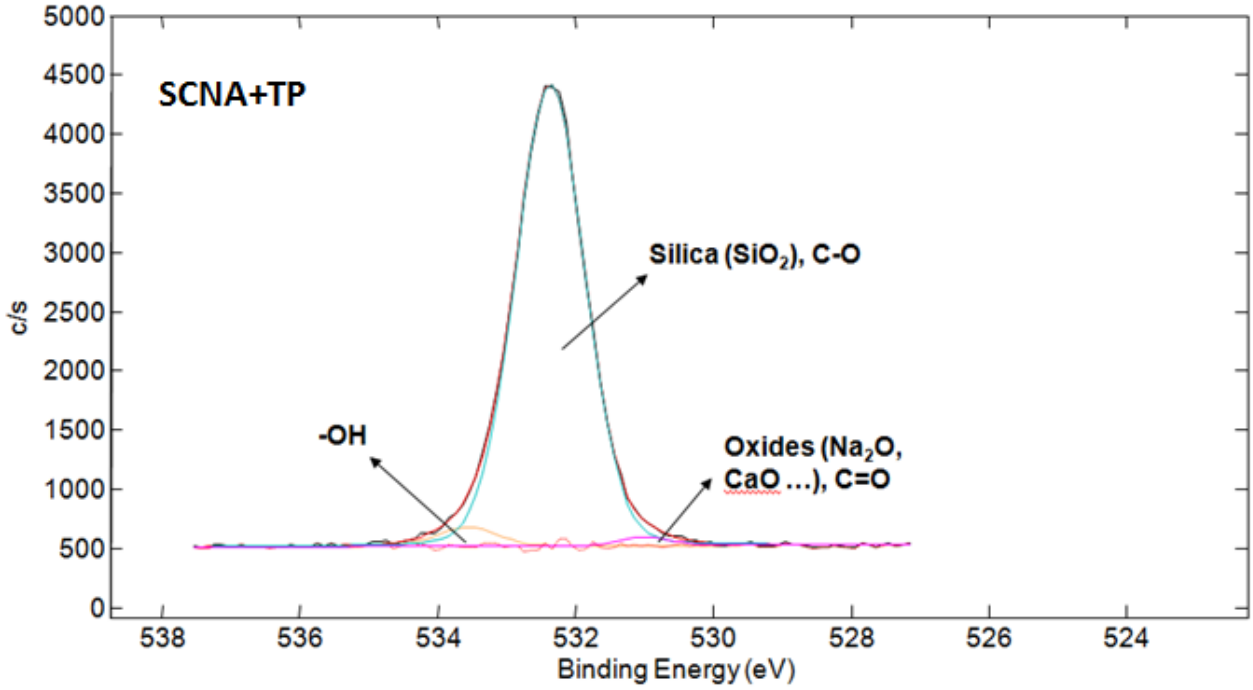

Figure 4-15: XPS detailed analysis of oxygen region for SCNA+TP sample

CEL2 washed

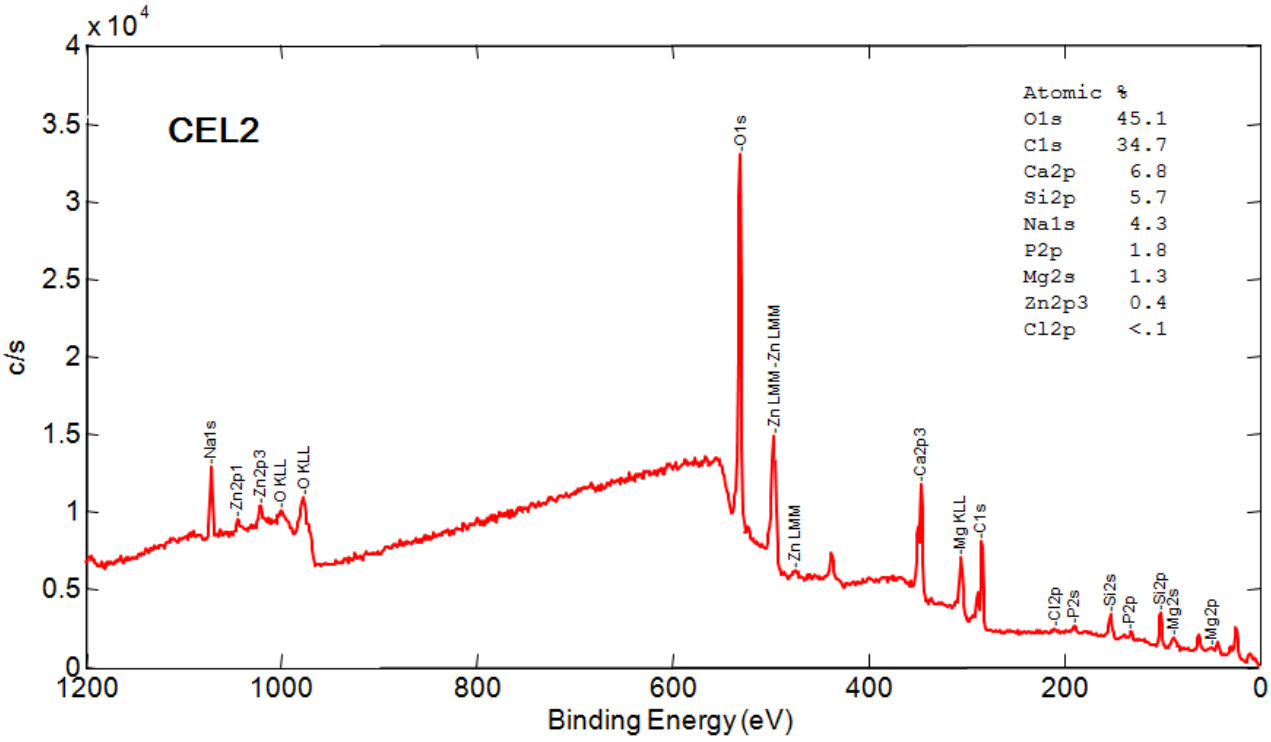

Figure 4-16: Survey spectra of CEL2 washed sample

All elements present on glass surface were highlighted in the survey spectra (figure 4-16) of washed CEL2, as reported in gallic acid and grape phenol functionalization. Signals of elements from glass composition were observed, including oxygen, calcium, silicon, magnesium and sodium. Carbon was also observed in this non-functionalized sample due to the unavoidable atmospheric contamination [13, 14]. The content of magnesium, sodium and calcium are lower that the starting composition probably due to the release of ion in aqueous solution.

In the detailed analysis of carbon region of washed CEL2 (figure 4-17), a notable signal at about 284.85 eV can be detected, and it can be attributed to unavoidable hydrocarbon contaminants on reactive surfaces [13, 14]. A signal at about 289.66 eV can also be observed, it can be attributed to carbonates [5] and it presents and higher intensity if compared to the one observed on washed SCNA (figure 4-10), because of the higher reactivity of CEL2.

In the detailed analysis (figure 4-18) of oxygen region, the presence of the characteristic signals

for oxides at 530.84 eV, silica at 531.63 eV as well as hydroxyls at 533.26 eV can be observed, as reported in gallic acid and grape phenol functionalization (chapter V, section 2.4 an 3.5).

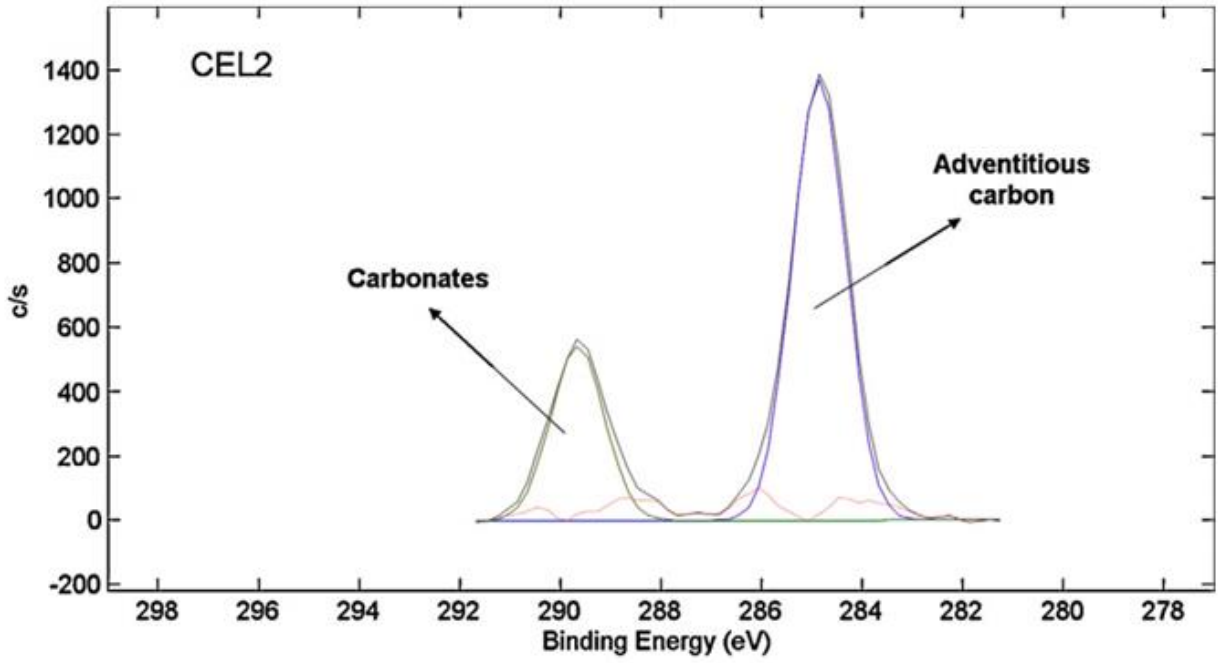

Figure 4-17: XPS detailed analysis of carbon region for CEL2 washed sample

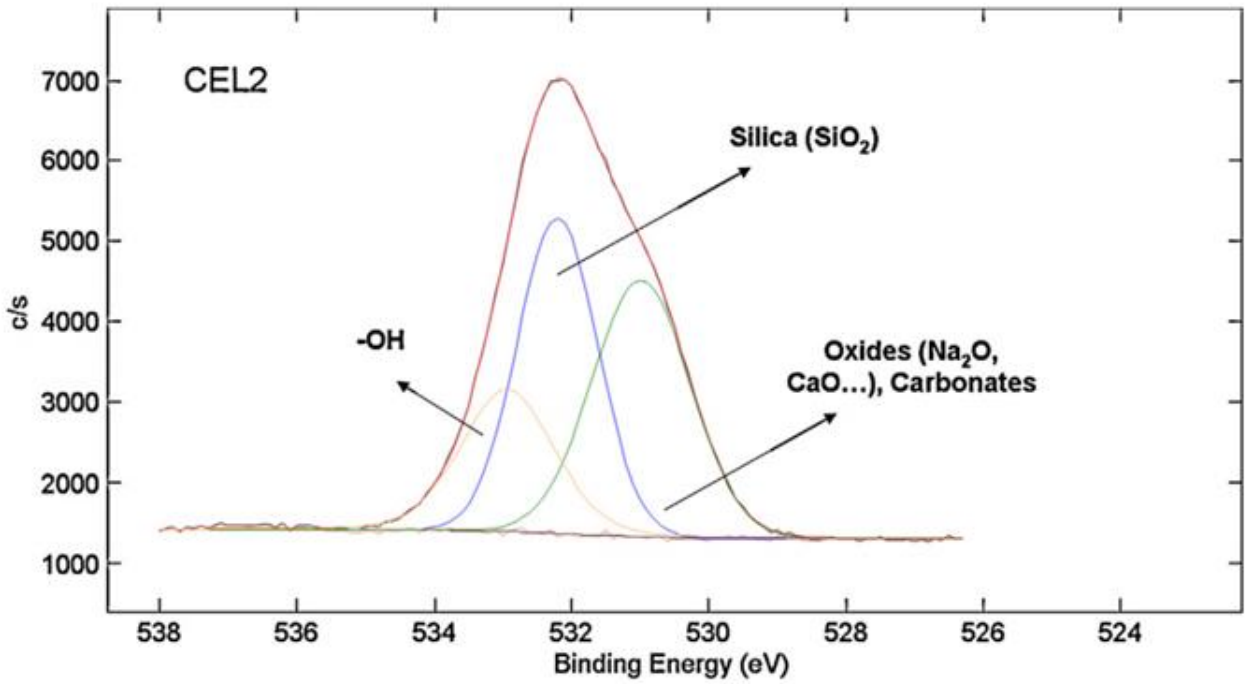

Figure 4-18: XPS detailed analysis of oxygen region for CEL2 washed sample

CEL2+TP

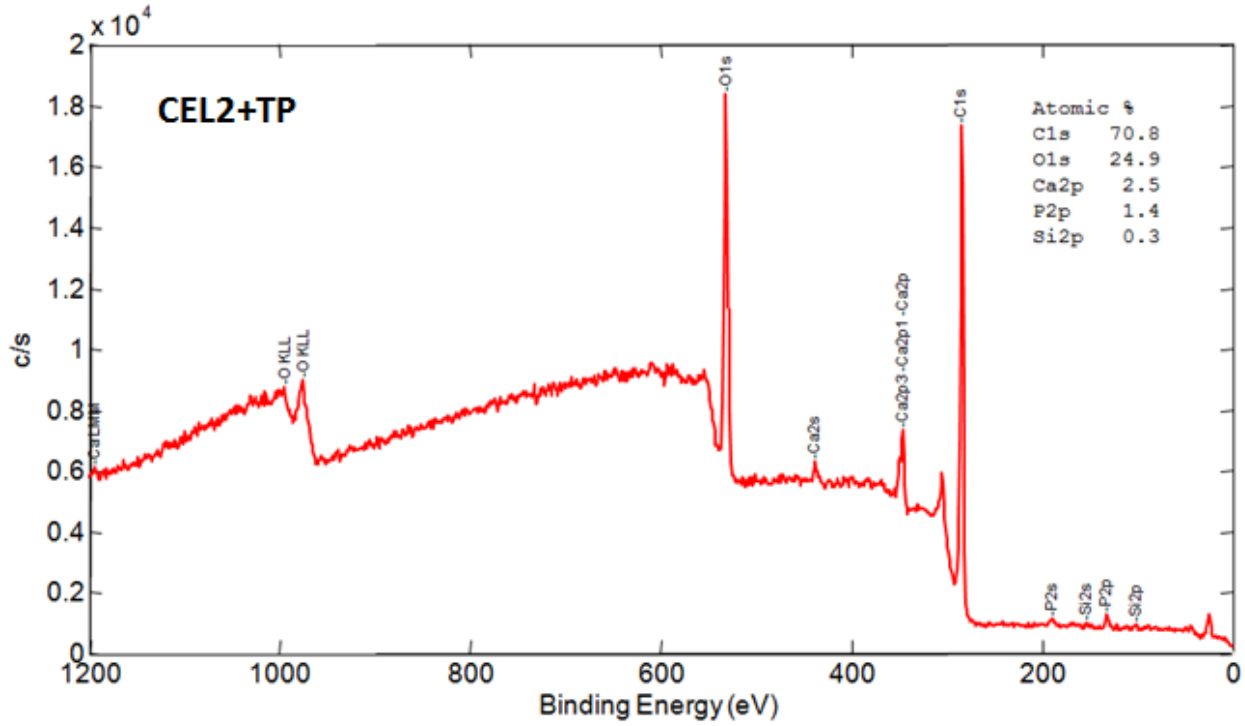

Figure 4-19: Survey spectra of CEL2+TP

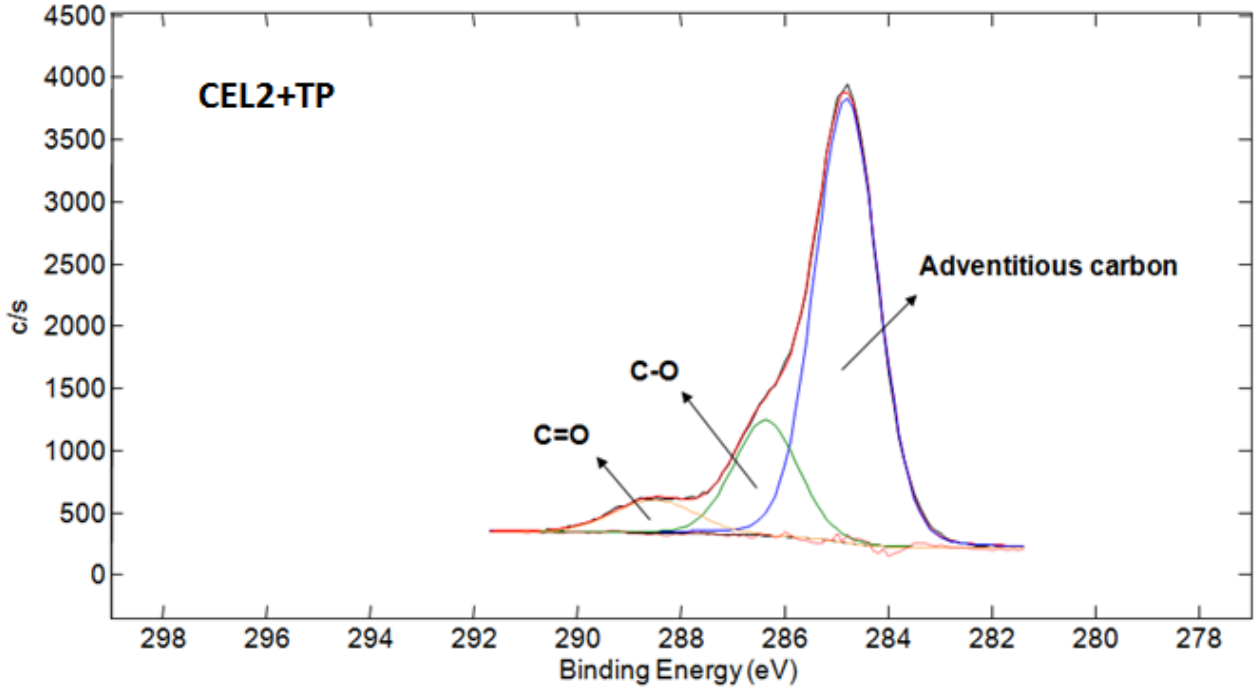

Figure 4-20: XPS detailed analysis of carbon region for CEL2+TP sample

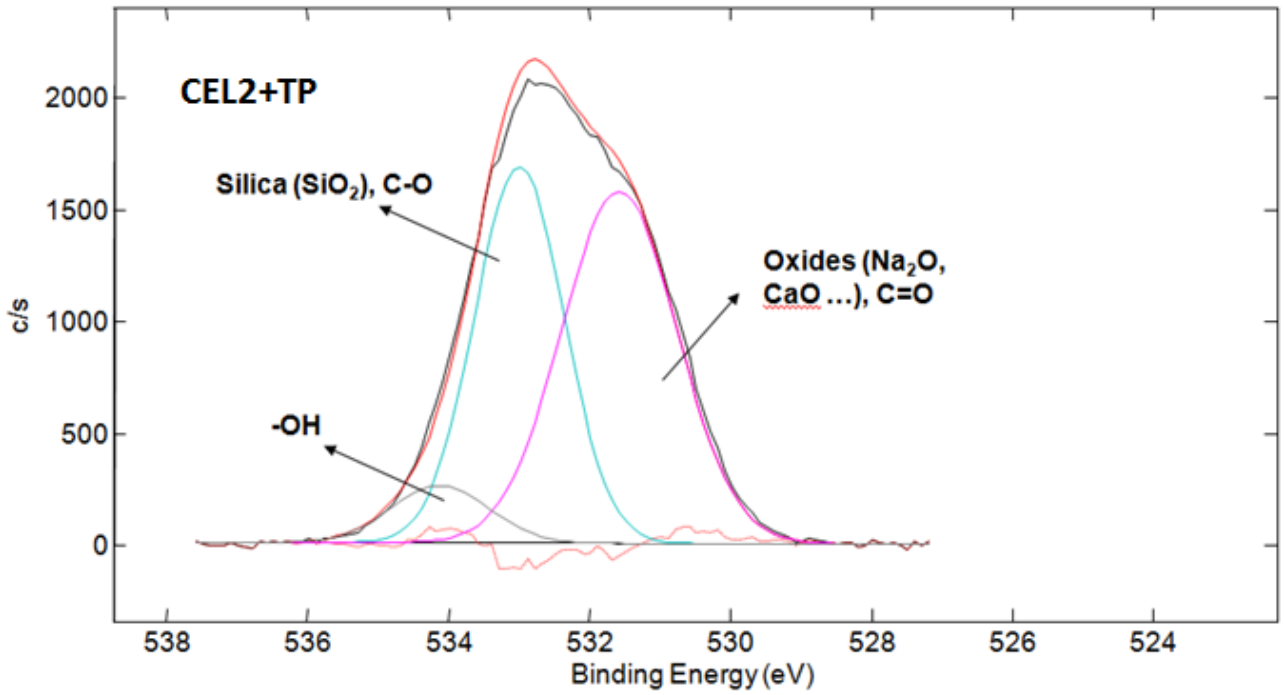

Figure 4-21: XPS detailed analysis of oxygen region for CEL2+TP sample

The survey spectrum (figure 4-19) of CEL2 functionalized with tea polyphenol highlighted all elements present on glass surface, including oxygen, calcium, silicon, phosphorus, as well as carbon. Magnesium was absent and the decrease of calcium and silicon content was observed. The reason may be that tea polyphenol grafting covers the reactive layer of glass.

In the detailed analysis of carbon region on CEL2+TP (figure 4-20), different contributions can be observed after phenol functionalization. First, the signal of carbonate and one new contributions can be observed at 286.34 eV and 288.48 eV and can be attributed to C-O and C=O bonds, respectively.

Figure 4-21 reports the detailed analysis of oxygen region on CEL2 bulk after tea polyphenol modification. The presence of –OH signal at 533.59 eV can be attributed to tea polyphenol grafting. Peak at 531.6 eV and 532.98 eV can be attributed to oxides /C=O bonds and silica/C-O bonds respectively; they are a further confirmation of phenol grafting and are in accordance with the results obtained for gallic acid and grape phenol grafting (chapter V, section 2.4 and 3.5).

Table 4-1 XPS atomic percentage of elements in the analyzed samples

Element [at%]	SCNA		CEL2	
	Washed	**TP**	**Washed**	**TP**
O	44.6	25.0	45.1	24.9
C	33.5	55.8	34.7	70.8
Si	14.9	19.2	5.7	0.3
Ca	4.8	-	6.8	2.5
Al	1.4	-	-	-
Na	0.8	-	4.3	-
P	-	-	1.8	1.4
Mg	-	-	1.3	-
Other	-	-	<0.5	-

Table 4-1 reports the atomic percentages of elements on the surface of bioactive glasses before and after tea polyphenol functionalization.

It can be observed that on surface of both washed SCNA and CEL2 samples, a certain amount of unavoidable carbon contaminants stilled remained, even though a washing treatment has been performed as widely reported in the literature for XPS analysis of reactive materials [12-14].

A significant increase of carbon content on both glasses after tea polyphenol functionalization can be observed. Compared with SCNA, the content of carbon on CEL2 surface increases up to 70.8 due to its higher reactivity that leads to notable effectiveness of tea polyphenol grafting.

The calcium and sodium were almost absent on the surfaces of both glasses after functionalization due to the ion exchange between molecule and glass surface, and the results are in accordance with the pH value variations. Concerning for CEL2, the decrease of silicon

content is the result of tea polyphenol bonding with reaction layer to cover the glass silica gel.

5 Surface functionalization of SC-45 with gallic acid and buffered gallic acid

SC-45 is a type of bioactive and ferrimagnetic glass-ceramics. This peculiar feature suggests it as a potential candidate for cancer treatment. In this section, gallic acid (GA) as a model molecule of polyphenol family was grafted to the surface of SC-45 bioactive glass-ceramic. In order to study the effect of pH, citric acid and sodium citrate buffer system was employed for the functionalization. Techniques such as UV together with Folin-Ciocalteau colorimetry, XPS, SEM were employed in order to evaluate the effectiveness of surface functionalization on the basis of the previous research on gallic acid grafting.

5.1 Macroscopic observations on the samples

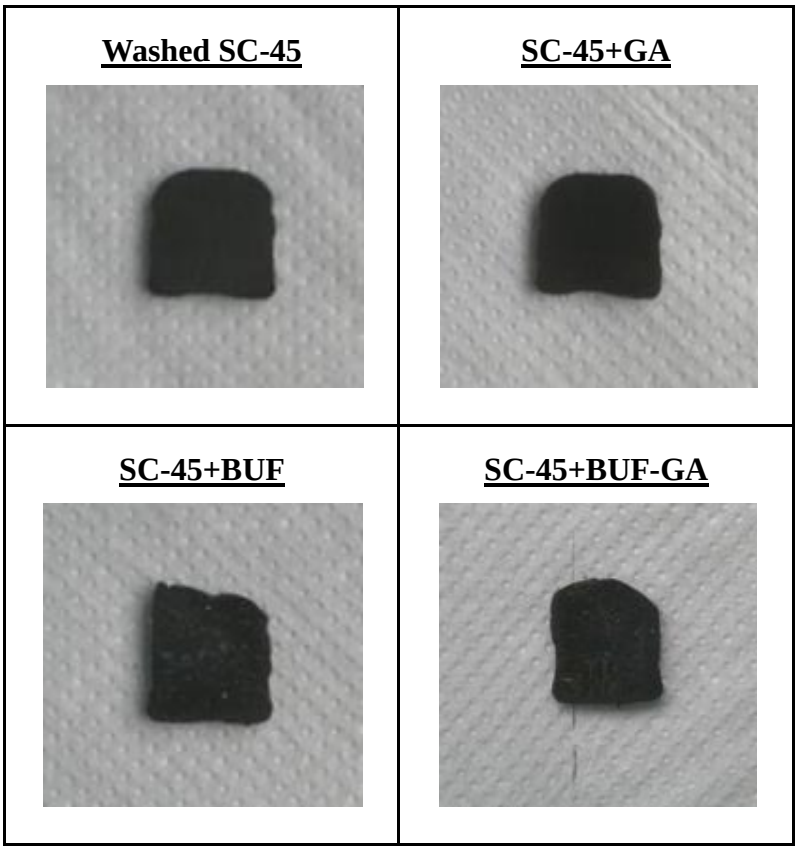

Figure 5-1: Glass bulks appearances before and after functionalization

Bulk and powders samples of SC-45 were prepared as described in Chapter IV, and were

subsequently functionalized with gallic acid (GA), through direct anchoring to the hydroxyl groups on surface with or without citric acid-sodium-citrate buffer. Some samples were treated only with the buffer (without gallic acid) in order to evaluate the effect of citric acid-sodium-citrate buffer on the glass-ceramic surface. The functionalized samples were named as SC-45+GA, SC-45+BUF and SC-45+BUF-GA, respectively.

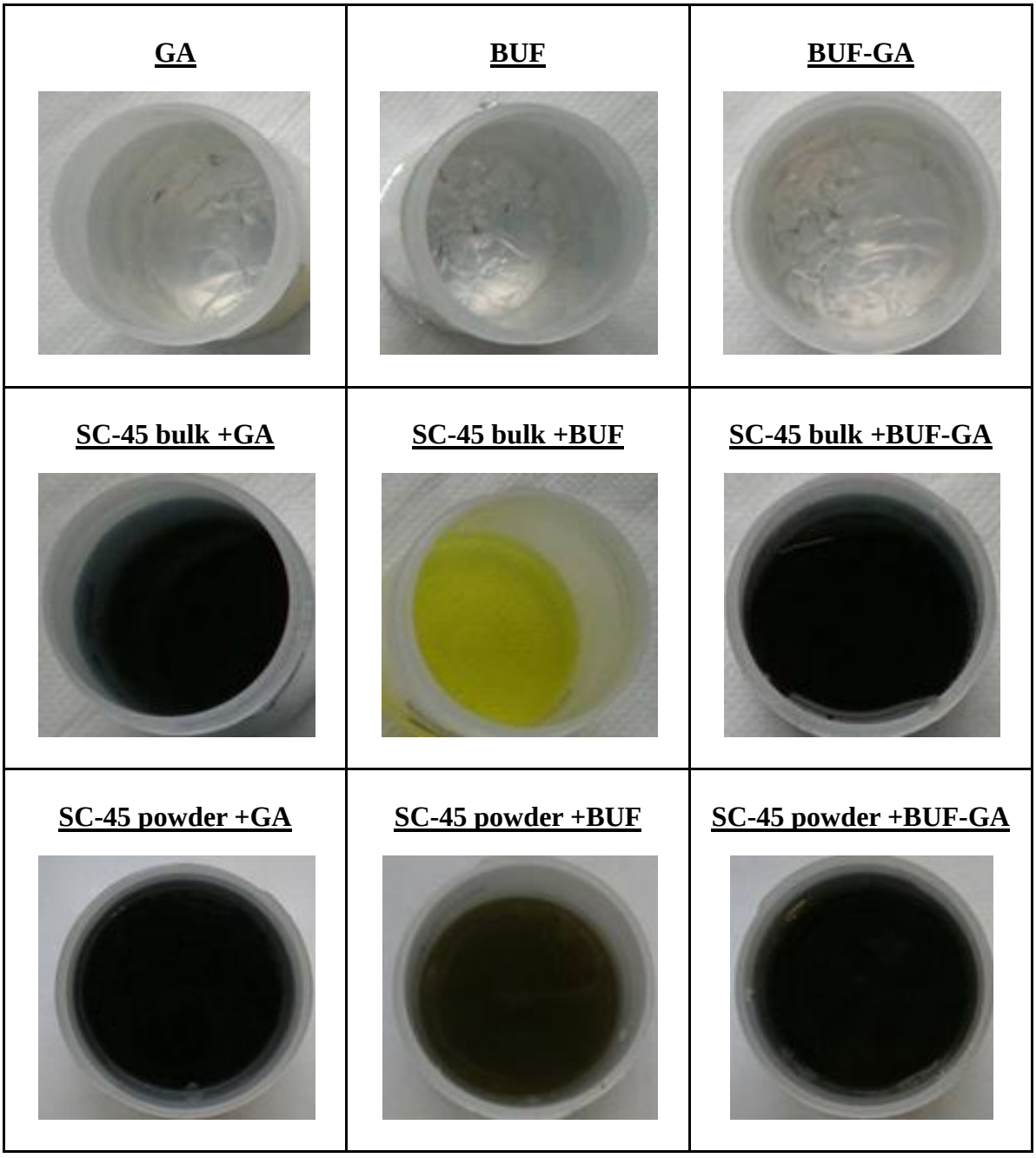

Figure 5-2: Gallic acid, buffer solution and buffered gallic acid as well as their uptake solution after functionalization

Figure 5-1 exhibits the observations from the macroscopic point of view on functionalized samples in comparison with samples not functionalized. It can be observed that the appearance of SC-45 bulk functionalized with only gallic acid is almost the same as washed SC-45, while the surface of SC-45 treated with buffer and buffered gallic acid is more soft or grainy and presents some white deposits. Compared with gallic acid grafted SC-45 bulk, the other two bulks with the presence of buffer showed a lower consistency with superficial white deposits.

Figure 5-2 presents the appearance of gallic acid solution, buffer solution as well as buffered gallic acid solution before and after soaking SC-45 bulks and powders for 24 hours at 37 ℃. A notable color change from colorless to dark can be observed in uptake solution after gallic acid and buffered gallic acid grafting. This phenomenon can be assigned to the bond between gallic acid and iron to form the iron-gallates complex, which has a typically dark color [21]. The uptake solution of buffer after functionalization varied into yellow (bulk samples) or brown (powder samples) due to the chelating capability of citric acid to bond with iron and calcium and resulting in the color variation. It must be underlined that formation of white deposits can be observed after functionalization with the presence of buffer.

5.2 pH measurement

In order to investigate the effect of pH, pH values of GA solution, buffer solution as well as buffered gallic acid solution were measured, with a pH meter, before and after soaking SC-45 bulks and powders for 24 hours and the results are reported in figure 5-3 and Table 5-1.

Three types of original solution (gallic acid, buffer, buffered gallic acid) have an acidic pH value (3.21, 2.99, and 3.02, respectively). After functionalization, the pH value increased in all kinds of uptake solutions as the glass has released ions which tend to basify the solution. This effect is more substantial in the case of powders due to their greater surface area.

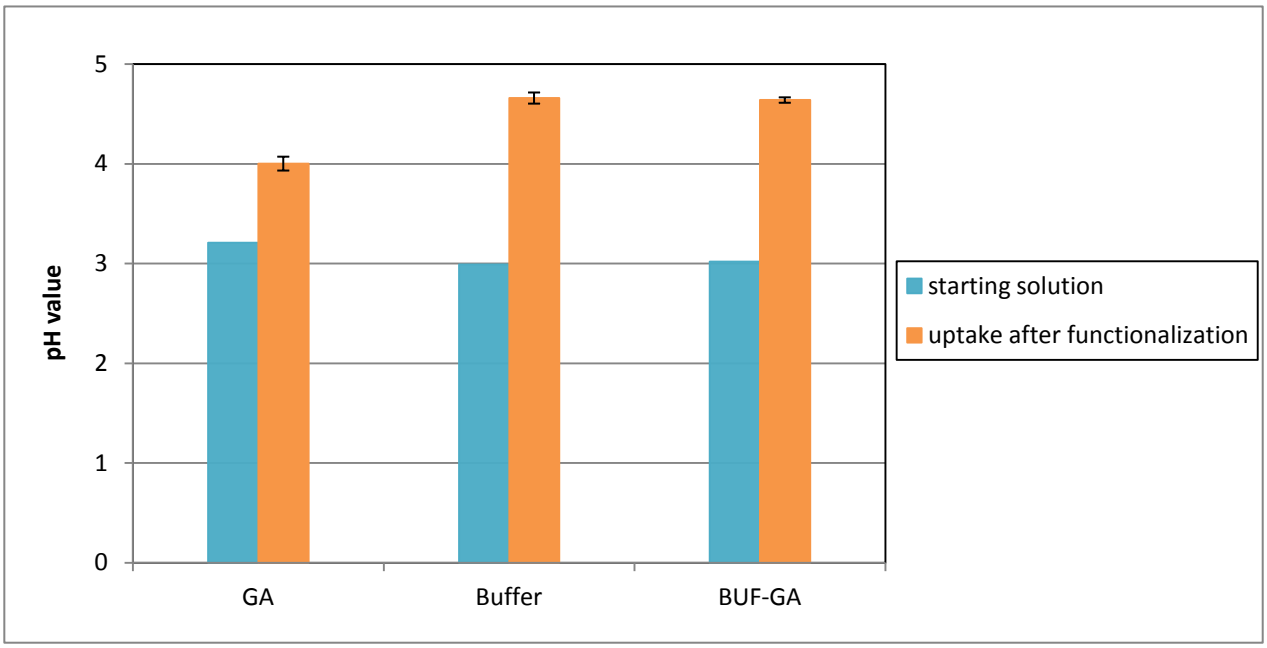

Figure 5-3: pH value of GA, buffer and BUF-GA uptake solution before and after 24 hours soaking SC-45 bulks

Table 5-1 pH value of GA, buffer and BUF-GA uptake solution before and after 24 hours soaking SC-45 powders

Samples	pH value
GA	3.21
Buffer	2.99
BUF-GA	3.02
SC-45+GA	8.07 ± 0.126
SC-45+BUF	4.72 ± 0.060
SC-45+BUF-GA	4.56 ± 0.042

In the case of functionalization with buffered gallic acid, the effect of buffer solution can be clearly observed for powder samples, as it has a pH much lower than the same material immersed in a solution of gallic acid in water. On the contrary, for the bulk samples no significant effect can be observed, namely measuring almost the same pH value in the case of functionalization with or without buffer.

5.3 UV-Vis measurements

5.3.1 Uptake solution analyzed by UV

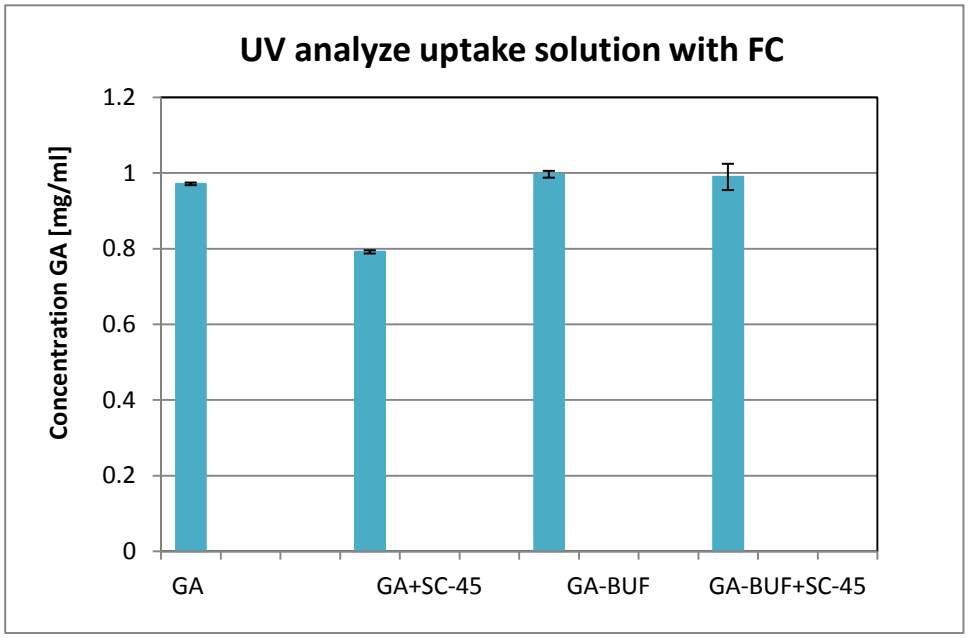

Figure 5-4: UV photometric results for GA and buffered gallic acid uptake solution before and after 1 day soaking of SC-45 bulk

In order to evaluate the depletion of gallic acid during the functionalization process as well as the effect of buffer, the amount of gallic acid in uptake solution (gallic acid and buffered gallic acid) was determined by Folin-Ciocalteau colorimetry and UV-Vis spectroscopy. The results are reported in figure 5-4.

The bar diagram in figure 5-4 exhibits the concentrations of original gallic cid and buffered gallic acid are approximately 1mg/ml which are in accordance with solutions concentration as prepared. It can be observed that the decrease of gallic acid content is greater in uptake solution for samples functionalized with only gallic acid than samples grafted with buffered gallic acid. It can be due to the different functionalization of two cases, in particular the presence of buffer solution inhibit the adhesion of gallic acid to the surface. The possible reason can be that gallic acid tends to bind to the –OH groups exposed on the surface of glassy matrix, while with the presence of buffer, since the majority of the glass surface

dissolved in the solution, the effectiveness of functionalization can be decreased.

5.3.2 Functionalized bulk samples analyzed by UV

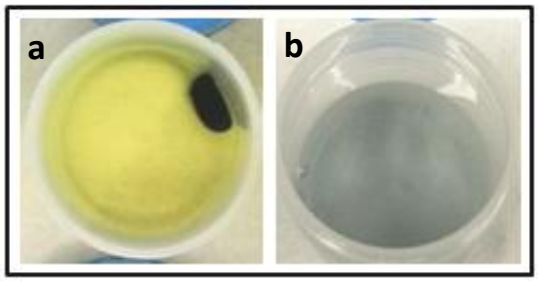

Figure 5-5: a) GA grafted SC-45 bulk in FC reagent and b) uptake after 2h incubation

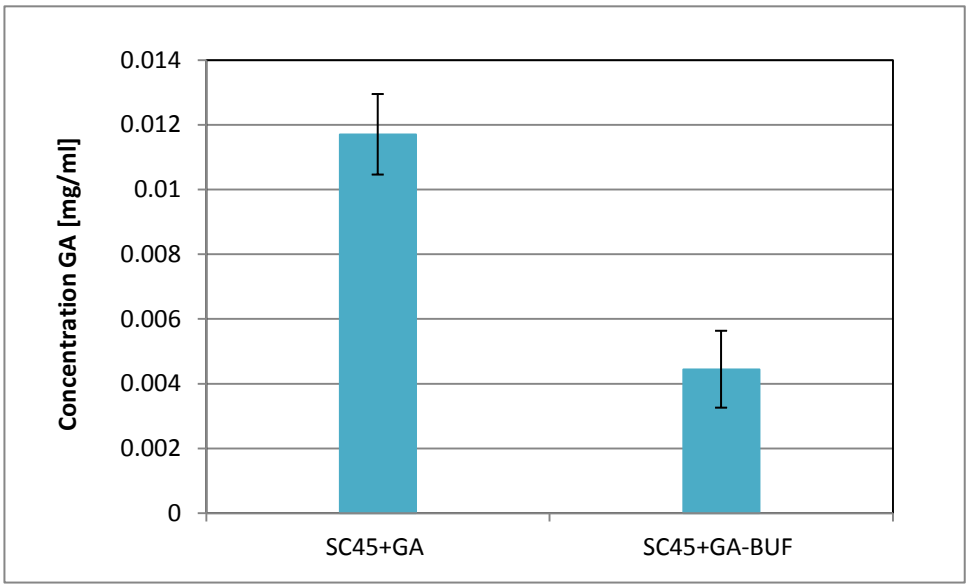

Figure 5-6: UV photometric results for gallic acid content on gallic acid and buffered gallic acid functionalized SC-45 bulk samples

Bulk samples of SC-45 were investigated after soaking in gallic acid solution and buffered gallic acid solution for 24 hours by reacting with Folin-Ciocalteau's reagent (figure 5-5) cooperated with UV-Vis spectroscopy. The bar diagram (figure 5-6) exhibits the amount of gallic acid remaining on the bulk samples after functionalization. It can be underlined that the amount of gallic acid on washed SC-45 and SC-45+BUF were almost zero after reaction with Folin-Ciocalteau's reagent. In general, after GA and BUF-GA grafting, a certain amount of gallic acid was detected on both samples, while the amount is higher on bulks functionalized

with only gallic acid than that grafted with BUF-GA. The results are reasonable, since the depletion of gallic acid in uptake solution of sample grafted with only gallic acid is higher than that of buffered gallic acid.

5.3.3 Release test in double distilled water

Table 5-2 Gallic acid amount in uptake after 3h and 24 release test

Samples	Release time [h]	Gallic acid content of release [mg/ml]
SC-45+GA	3	-0.00013 ± 0.000219
SC-45+BUF-GA	3	0.002142 ± 0.002799
SC-45+GA	24	0.000105 ± 0.000252
SC-45+BUF-GA	24	-0.00047 ± 0.000105

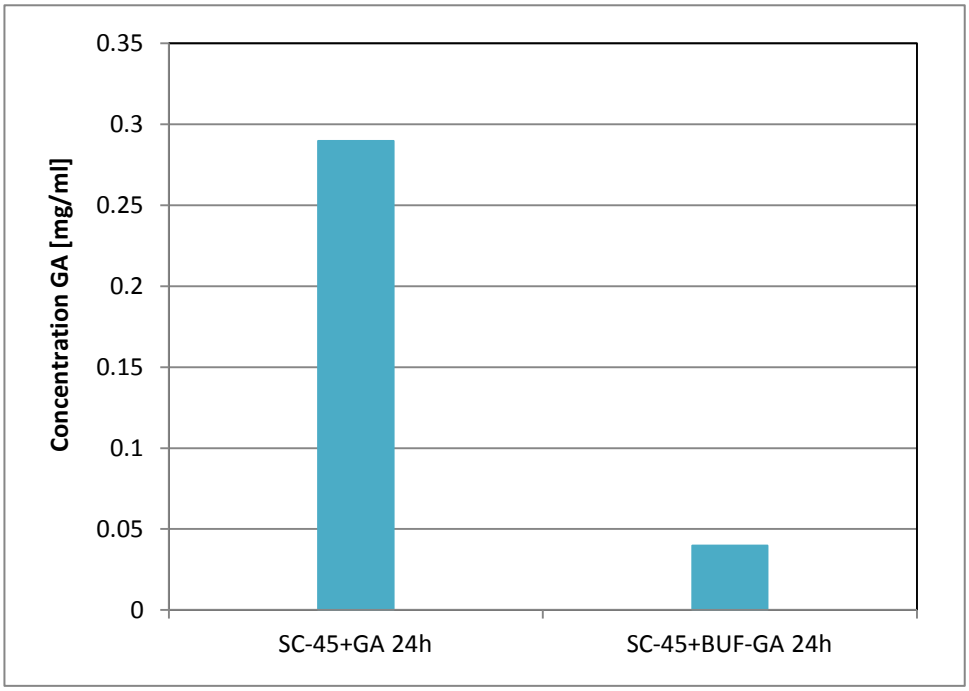

Figure 5-7: UV photometric results for gallic acid content on gallic acid and buffered gallic acid functionalized SC-45 bulk samples after 24h release

With the aim to evaluate the release of gallic acid from functionalized surfaces, the release

solutions as well as the functionalized bulks were analyzed after 3 h and 24 h release. Table 5-2 listed the results of gallic acid content in release solutions of 3 h and 24 h release, respectively. However, overall neither the bulks grafted with only gallic acid nor that grafted with buffered gallic acid present a release of gallic acid in double distilled water.

Bulks after 24 h release were investigated with Folin-Ciocalteau colorimetry in order to further study the release test and evaluate the maintenance of the molecule on glass-ceramic surface after water soaking. From bar diagram in figure 5-7, on both samples, the presence of gallic acid can be observed and moreover the bulk only grafted with gallic acid contains larger amount of gallic acid than that grafted with BUF-GA. The results are also in accordance with the analysis on bulks before release test. As a result, it can be inferred that it is nearly impossible to release gallic acid from SC-45 due to the strong bond between GA and glass-ceramics.

5.4 XPS analysis

XPS was employed to characterize the chemical composition and the kind of chemical bonds on the surface of the just washed SCNA and CEL2 bulk samples as well as bulks grafted with gallic acid and gallic acid citric acid-sodium citrate buffer. Survey spectra and detailed analyses of carbon and oxygen regions hqave been considered. The samples are named as follows:

i. Washed SC-45

ii. SC-45+GA

iii. SC-45+BUF

iv. SC-45+BUF-GA

Washed SC-45

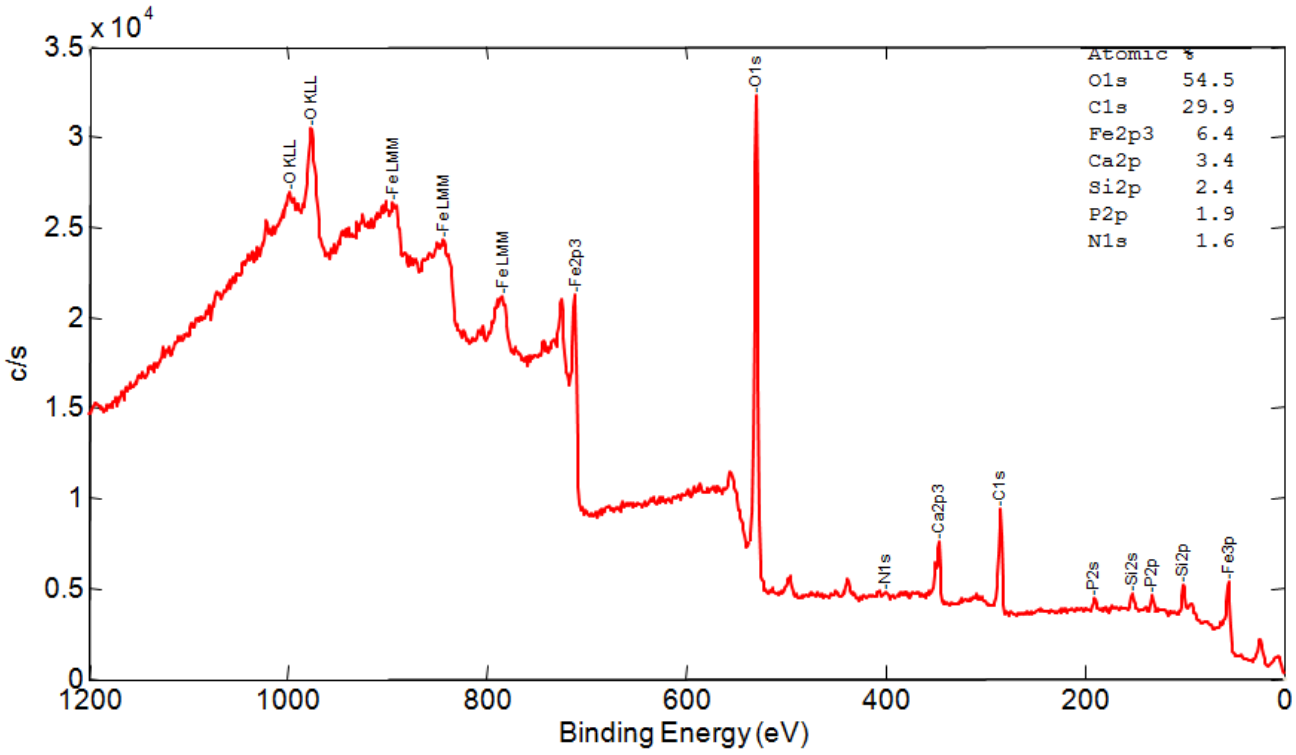

Figure 5-8: Survey spectra of washed SC-45

Figure 5-8 presents the survey spectrum of washed SC-45, in which the elements present on the surface of bulk samples are highlighted. Elements from glass-ceramic composition can be observed, including oxygen, iron, calcium, phosphorus, and silicon. The presence of carbon and nitrogen on the first surface layer of materials, even in non-functionalized samples, is due to the unavoidable atmospheric contaminants [13, 14]. It can be noted that sodium has not been detected; this phenomenon can be attributed to the ion release of the glass-ceramic in the washing media, as previously observed for SCNA and CEL2 glasses (chapter V, section 2.4).

Figures from 5-9 to 5-12 exhibit the spectra of the detailed regions of carbon, oxygen, iron and silicon.

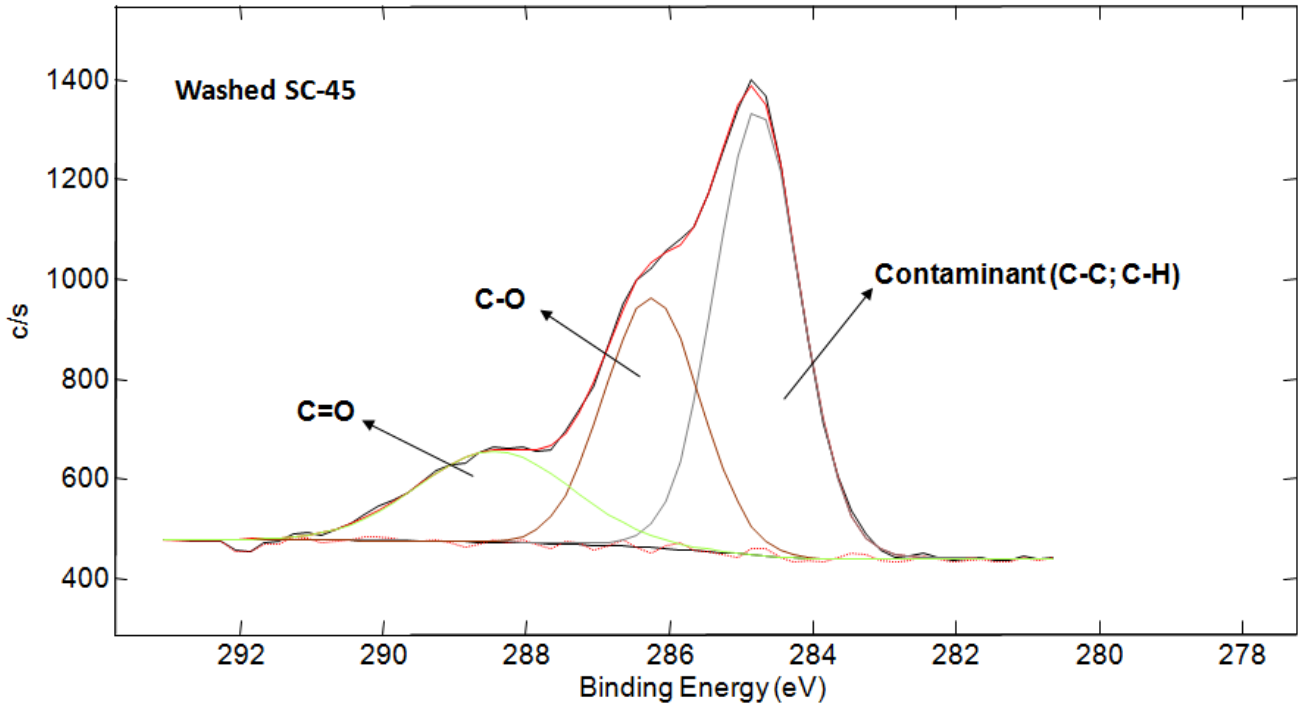

Figure 5-9: XPS detailed analysis of carbon region for washed SC-45 sample

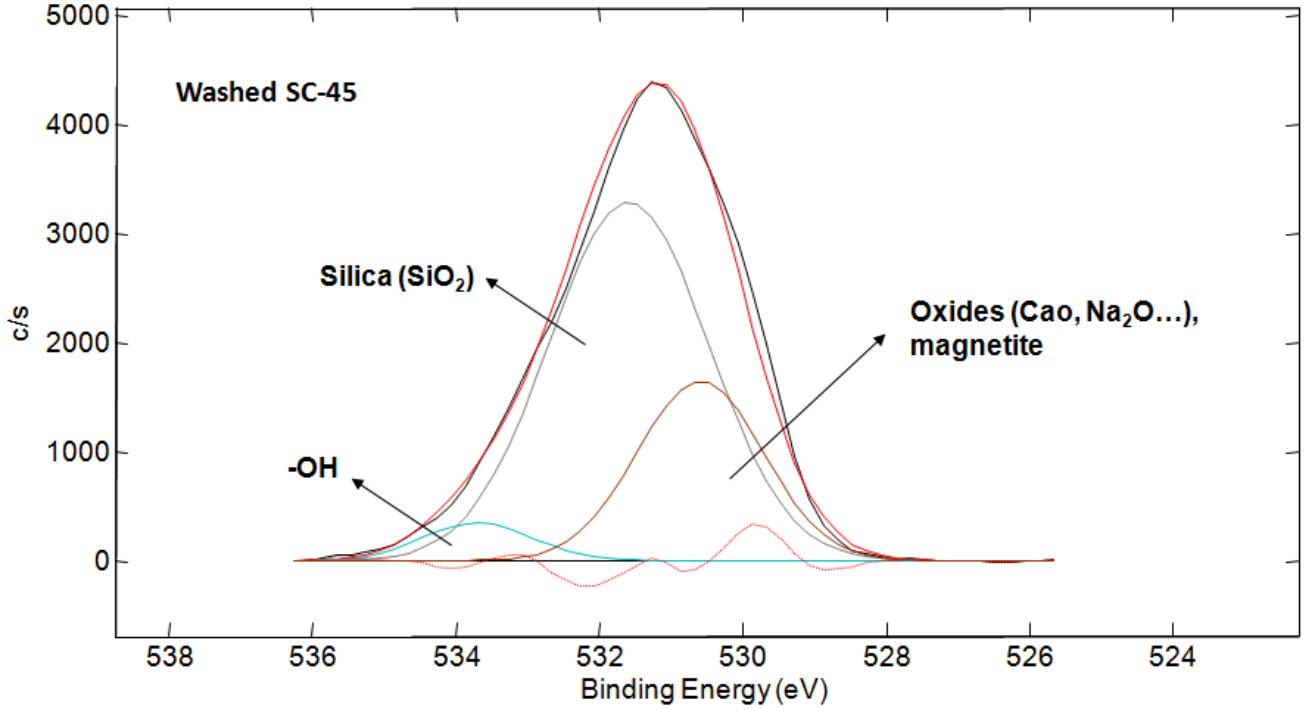

Figure 5-10: XPS detailed analysis of oxygen region for washed SC-45 sample

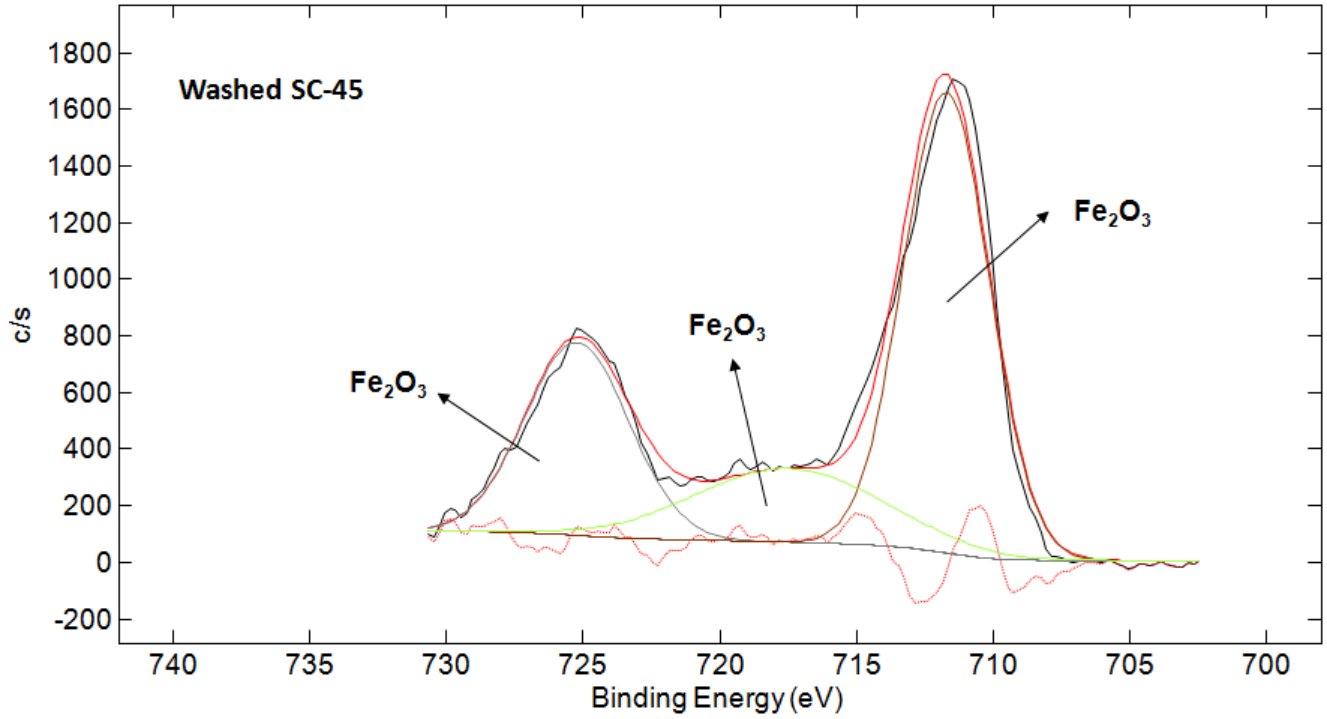

Figure 5-11: XPS detailed analysis of iron region for washed SC-45 sample

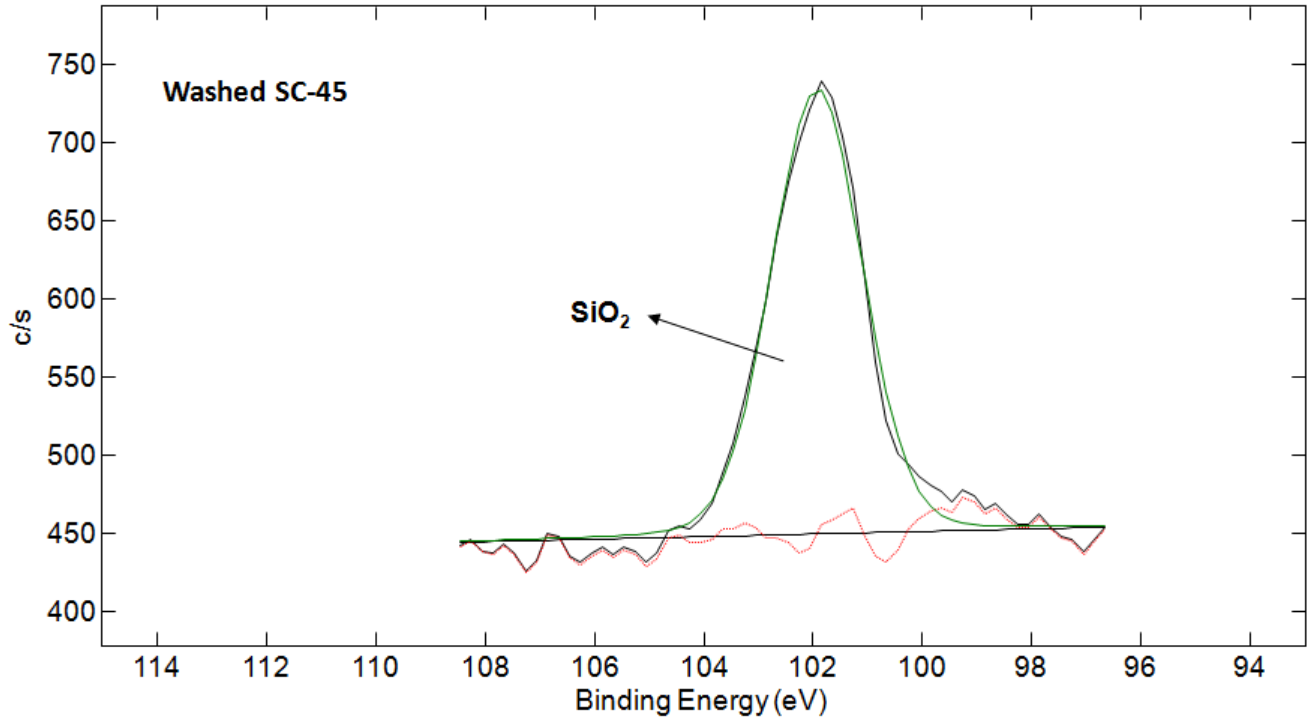

Figure 5-12: XPS detailed analysis of silicon region for washed SC-45 sample

In figure 5-9, the detailed analysis spectrum of carbon region shows a signal at about 284.77 eV which can be attributed to environmental contaminants, as the reactive surface easily absorb hydrocarbons from the atmosphere. Other signals at 286.25 eV and 288.44 eV are assigned to C-O and C=O bond respectively [22-24].

Figure 5-10 presents the spectrum of the detailed analysis of oxygen region. It can be observed that oxygen is bound to different element of glass-ceramics, in particular, the silicon with the notable signals present at 531.58 eV. The contribution at about 530.58 eV is assigned to oxides from glass matrix. Peaks at about 533.69 are attributed to surface hydroxyl groups which confirmed the exposure of –OH on material surface. It can be noted that through XPS it is possible to observe the surface hydroxyls while in FTIR spectra (chapter V, section 5.6) this signal is absent. This result can be explained considering the different penetration depths of the two techniques, few microns for FTIR and few nanometers for XPS. The OH-rich layer interests just for nanometers of the glass-ceramic surface and consequently only XPS can clearly detect it. In the detailed analysis spectrum of iron region (figure 5-11), three contributions have been detected and all of them can be attributed to Fe_2O_3. It is possible that the analysis was carried out on the lamella of hematite, or that those signals corresponded to magnetite, as it is given by $Fe_2O_3 + FeO$.

In detailed analysis spectrum of silicon region (figure 5-12), only one peak at 101.92 eV has been detected and attributed to silica (SiO_2), confirming that the washing step effectively induce hydroxyls exposition without their condensation to silica gel [25].

SC-45+BUF

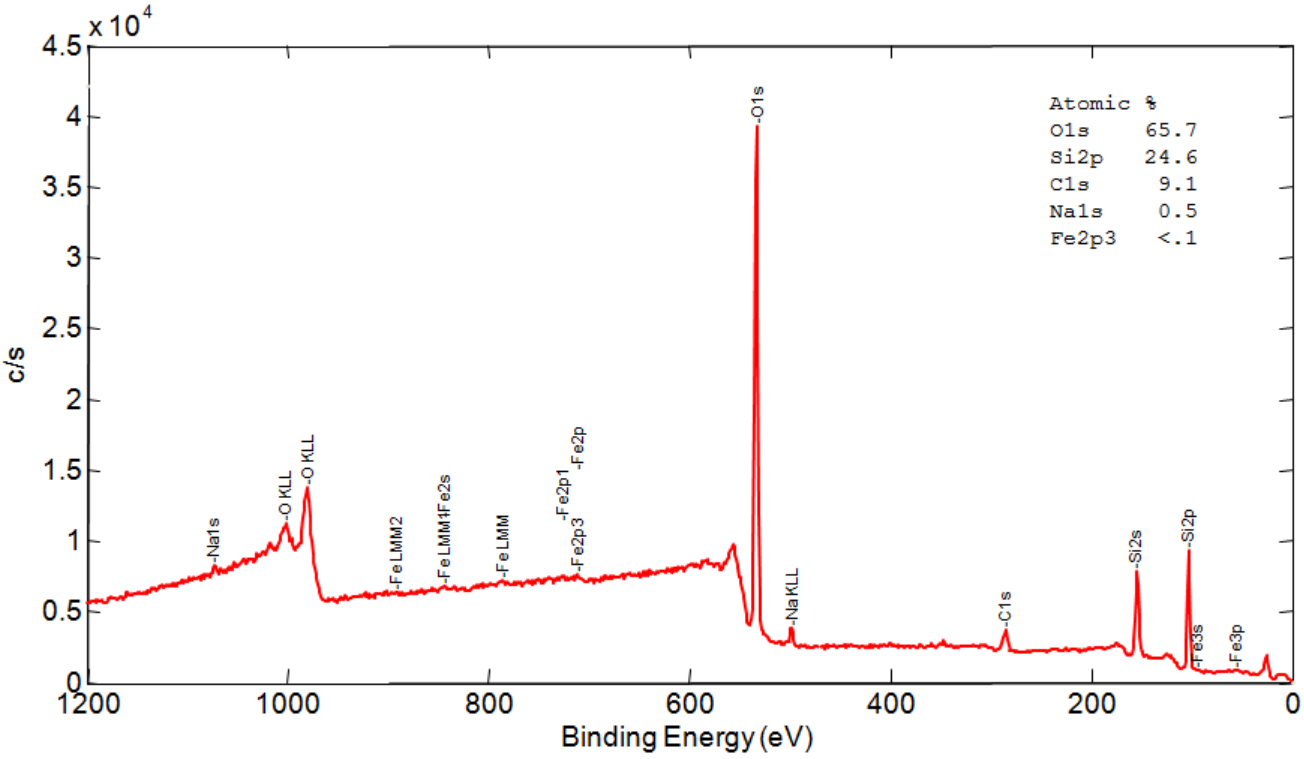

Figure 5-13: Survey spectra of SC-45+BUF

Figure 5-13 shows the survey spectrum of SC-45+BUF, in which all elements present on the surface of bulk samples are highlighted. Elements from glass-ceramic composition can be observed, including oxygen, calcium and silicon. Sodium and calcium are almost absent due to the ion exchange between washing solutions and buffer and SC-45 and also to the bond with citric acid which is a strong chelator for calcium ions. It can be observed that the signal of iron is almost absent, while strong signals of silicon and oxigen are present. It can be supposed that after the etching occurred by the action of the buffer, only a thin silica-rich film was detected as the result of ionic dissolution from the glass matrix.

Figure 5-14 reports the detailed spectrum of carbon region for SC-45+BUF; it can be observed that the intensity of peak of the contamination decreased if compared with the pretreated SC-45. The signal at 286.03 eV corresponds to alcohols, and then it can be attributed to the C-OH bond of citric acid. The third peak at 288.64 eV, corresponded to the C=O of non-reactive COOH

group [26], and of COO^- groups from calcium citrate, as discussed in (chapter V, section 5.5.1 and 5.6).

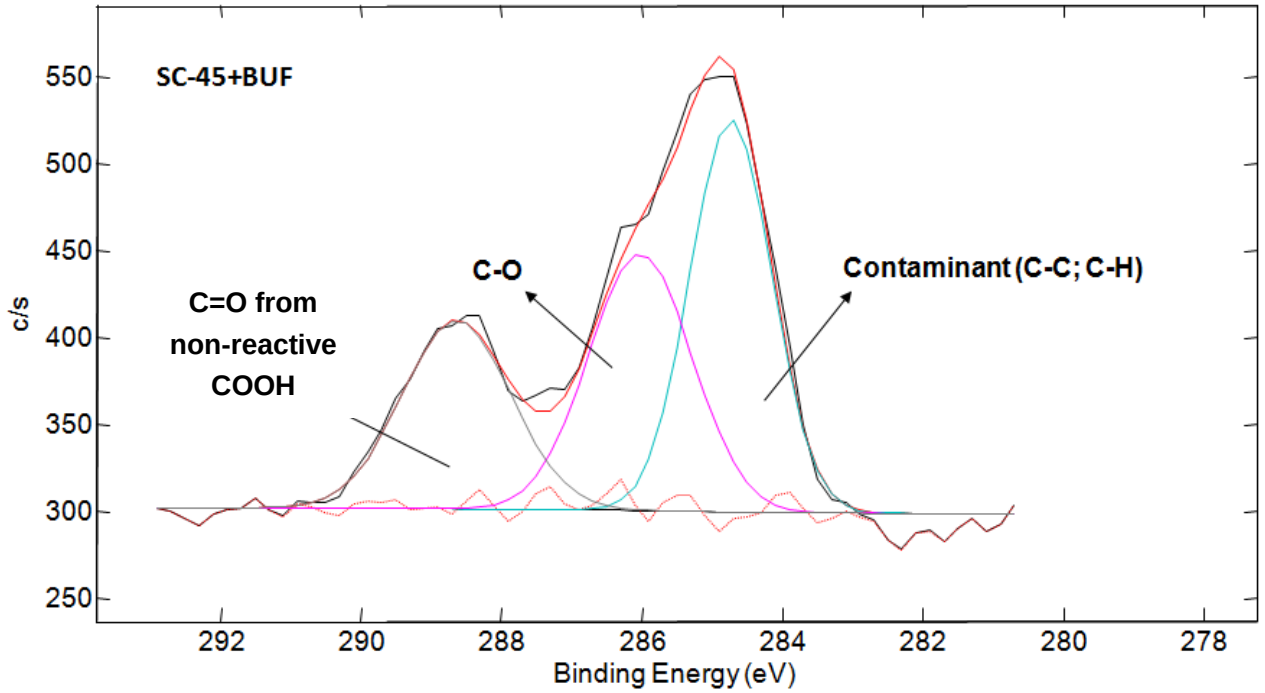

Figure 5-14: XPS detailed analysis of carbon region for SC-45+BUF sample

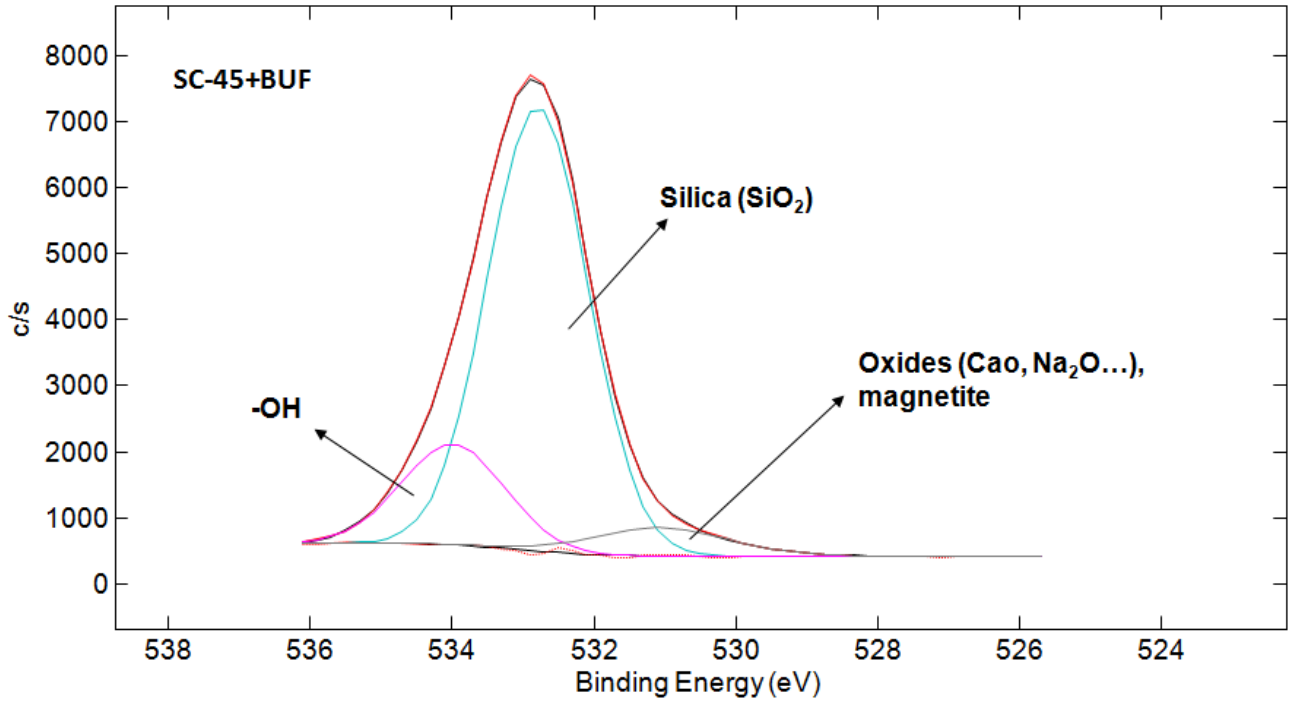

Figure 5-15: XPS detailed analysis of oxygen region for SC-45+BUF sample

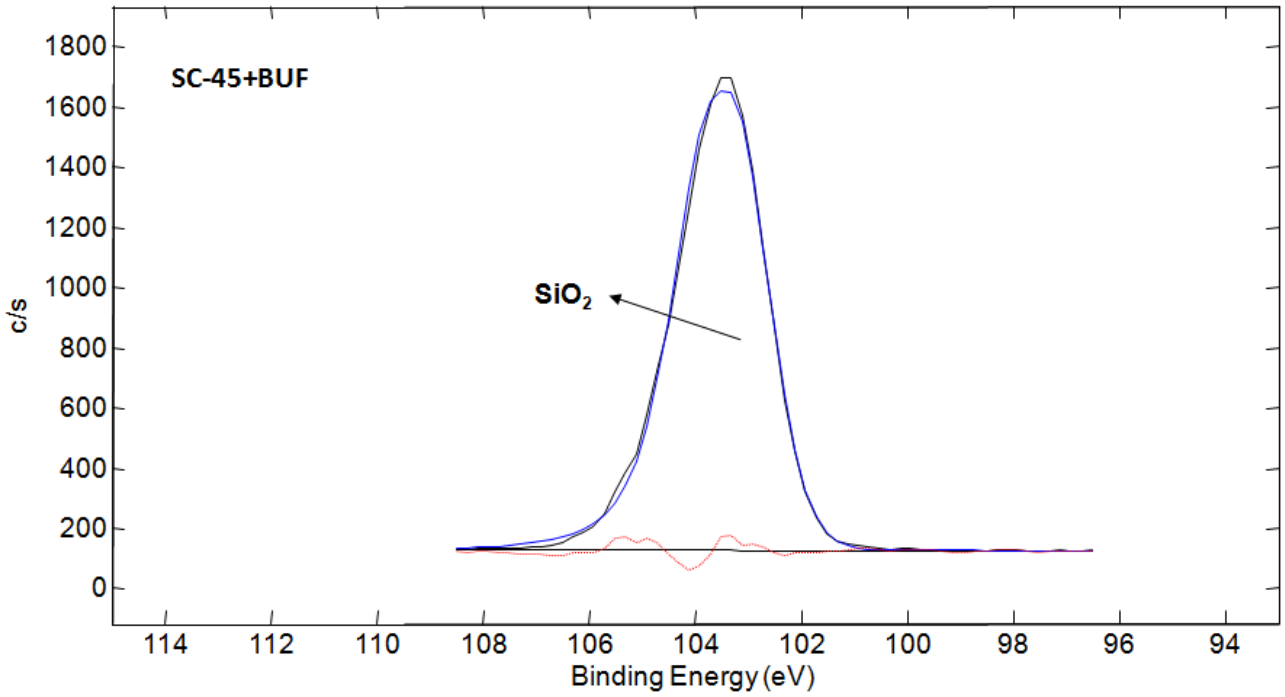

Figure 5-16: XPS detailed analysis of silicon region for SC-45+BUF sample

Figure 5-15 shows the detailed analysis spectrum of oxygen region for SC-45+BUF. It can be observed that the signals of oxides from glass structure are greatly reduced compared to the pretreated SC-45 (figure 5-9) due to the dissolution of glass matrix in buffer solution, which was observed in subsequent analysis of SEM images (chapter V, section 5.5.1).

In the detailed spectrum of silicon region (figure 5-16), a single peak at 103.37 eV can be observed. This signal is located at band energy where typically signal of silica gel can be detected; however, in the presence of silica gel, two peaks of silica at lower energy are usually detected. In this case, instead only one peak was observed and therefore it is not appropriated to assign the signal to silica gel. Hence, it is assumed that the signal is from silica despite it has higher binding energy. Another reason may be that the signal at 101.92 eV detected in the pretreated sample is attributed to the silicate glass matrix, while buffer tends to dissolve the glass matrix and leads to the formation of a more disrupted network of silica, which confirms the macroscopic appearance of SC-45+BUF with soft or grainy surfaces.

SC-45+GA

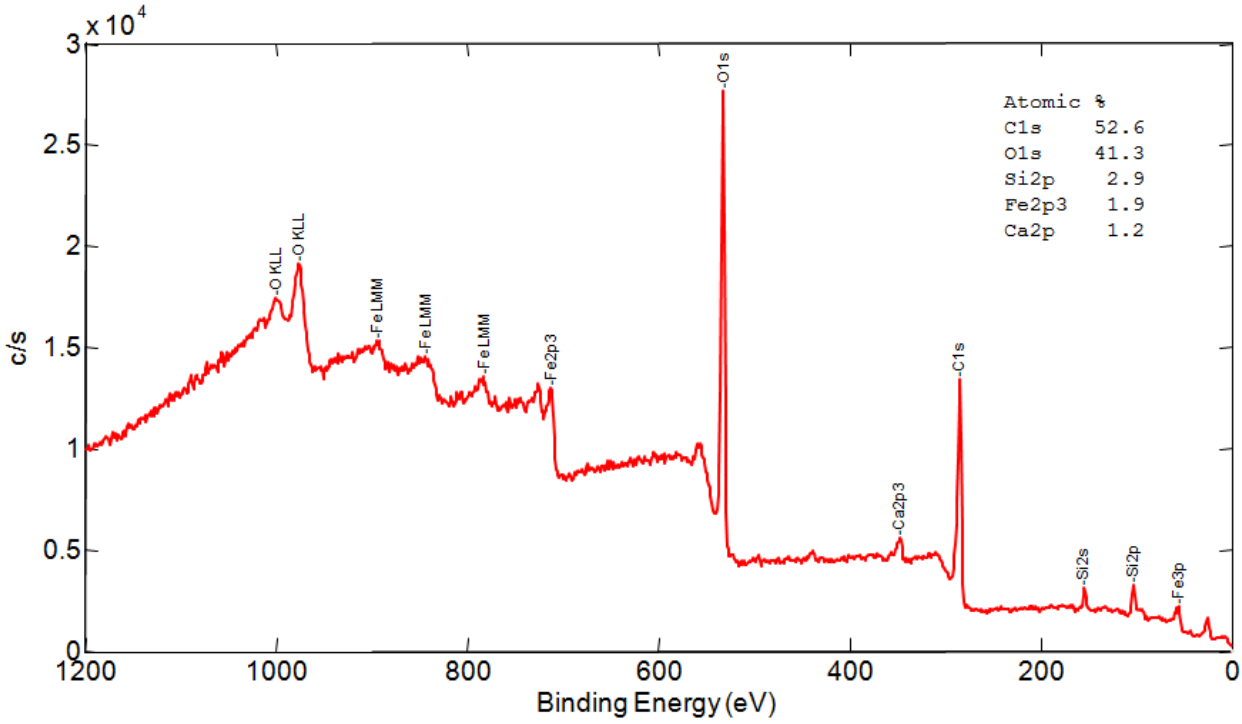

Figure 5-17: Survey spectra of SC-45+GA

Figure 5-17 presents the survey spectrum of SC-45+GA, in which all elements present on the surface of bulk samples are highlighted. Elements including oxygen, iron, calcium, silicon from glass-ceramic composition can be observed. On this bulk sample, sodium has not been detected as well, as reported in washed SC-45 and SC-45+BUF. The signal of carbon is significantly higher if compared to ones detected on washed (figure 5-7) and buffer treated (figure 5-12) samples, it can be attributed to the sum of atmospheric contaminants and grafted gallic acid.

In figure 5-18 (detailed spectrum of carbon region), the contribution at lower energies is shifted, if compared to the peak of contaminants on the washed SC-45, toward higher energies and partially cover the possible contribution at 286.03 eV of C-O. The peak at 288.29 eV,attributed to C=O groups, is still present. So, for this sample the carbon region is not of univoque interpretation and does not allow an attribution to gallic acid groups.

In the detailed spectrum of oxygen region in figure 5-19, two main contributions can be

observed. Compared to washed SC-45 (figure 5-9) and SC-45+BUF (figure 5-14), the signals of oxides from glass matrix disappeared. The intensity of signal at 532.36 eV attributed to –OH group presents a significant increase and this phenomenon can be assigned to the grafting of gallic acid. Moreover the other peak at 531.04 eV could be attributed to silica or oxides from glass structure.

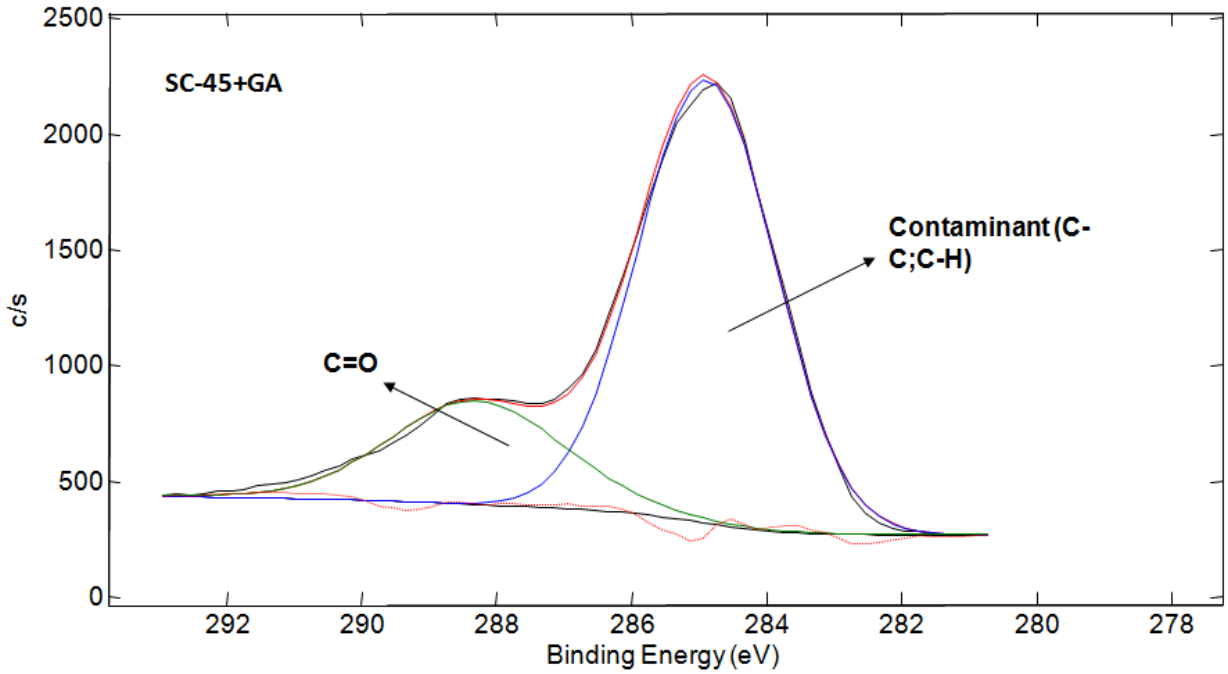

Figure 5-18: XPS detailed analysis of carbon region for SC-45+GA sample

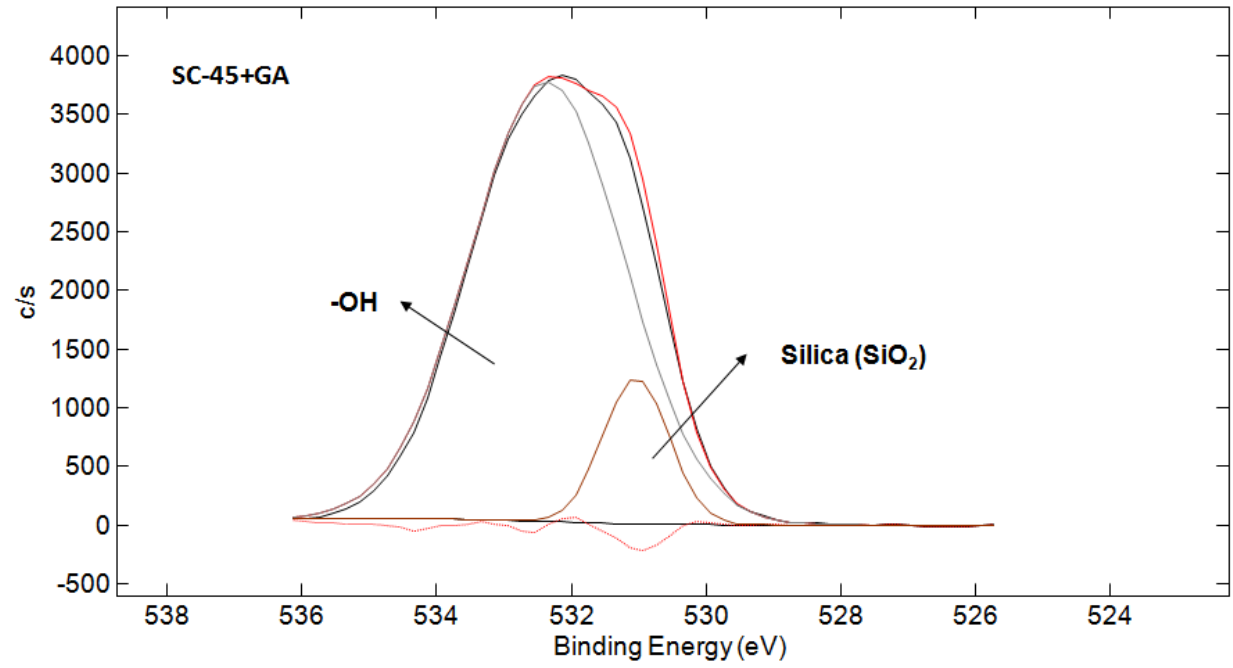

Figure 5-19: XPS detailed analysis of oxygen region for SC-45+GA sample

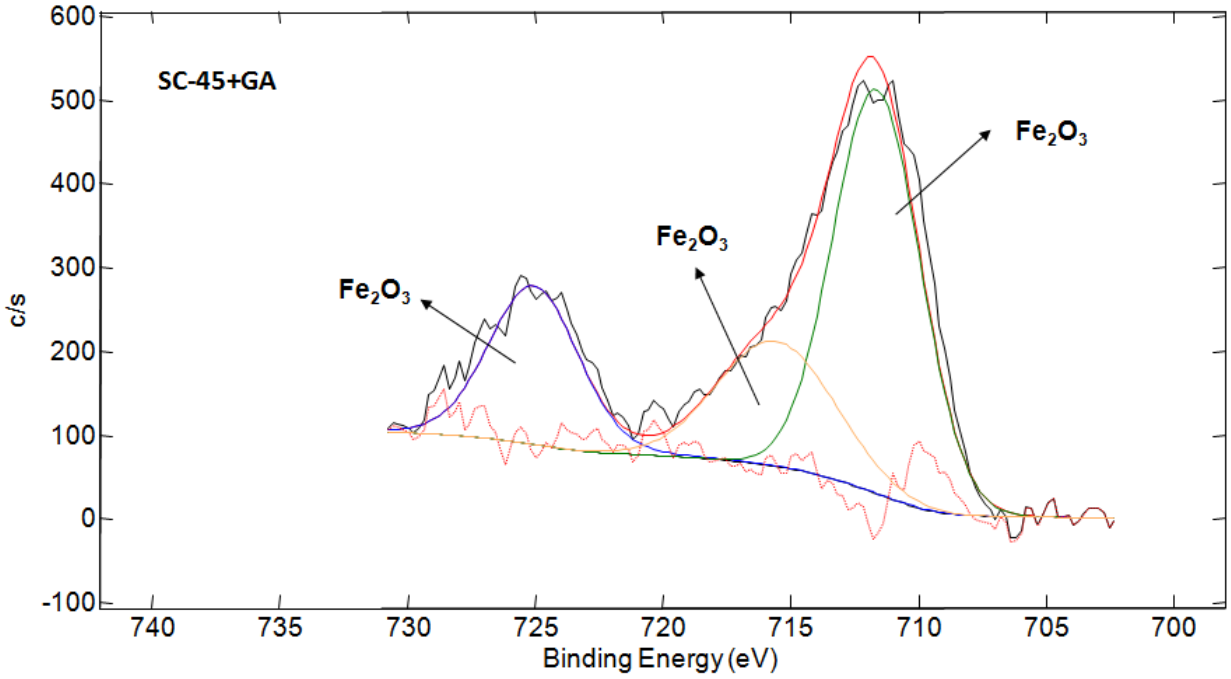

Figure 5-20: XPS detailed analysis of iron region for SC-45+GA sample

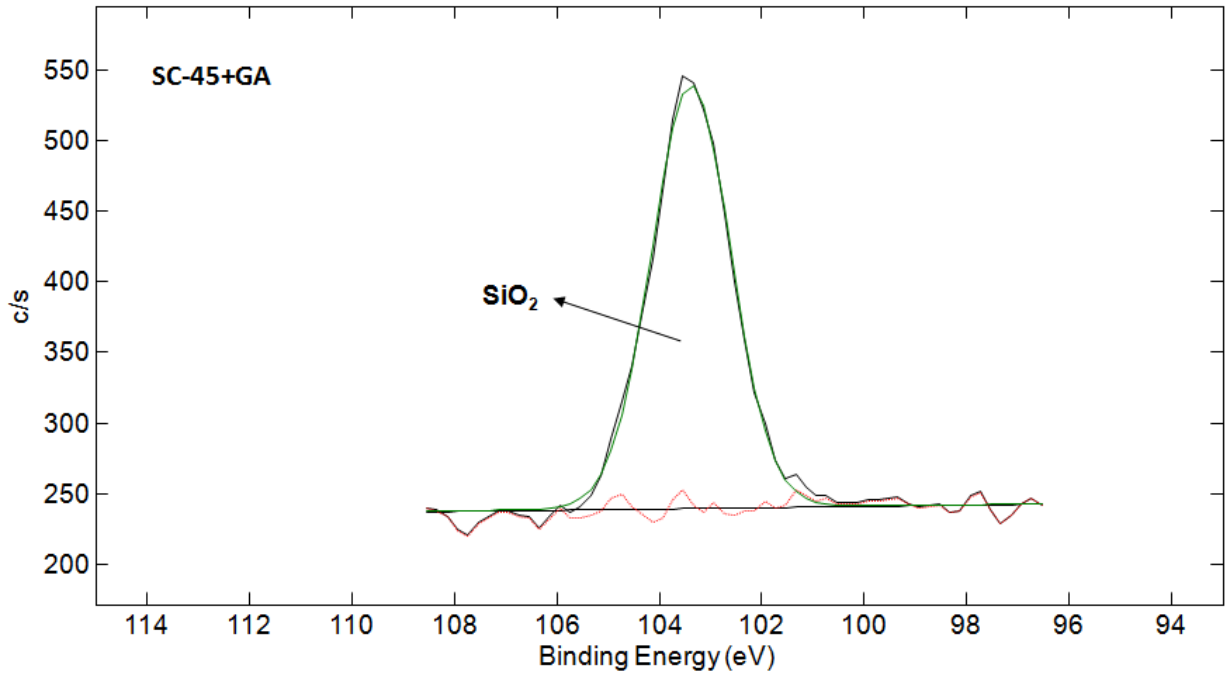

Figure 5-21: XPS detailed analysis of silicon region for SC-45+GA sample

From the detailed spectrum of iron region (figure 5-20), similar peaks to washed SC-45 were observed and attributed to Fe_2O_3 hematite or magnetite.

As for the silicon region analysis (figure 5-21), a single peak at 103.38 eV was detected and attributed to silica as reported for SC-45+BUF.

SC-45+BUF-GA

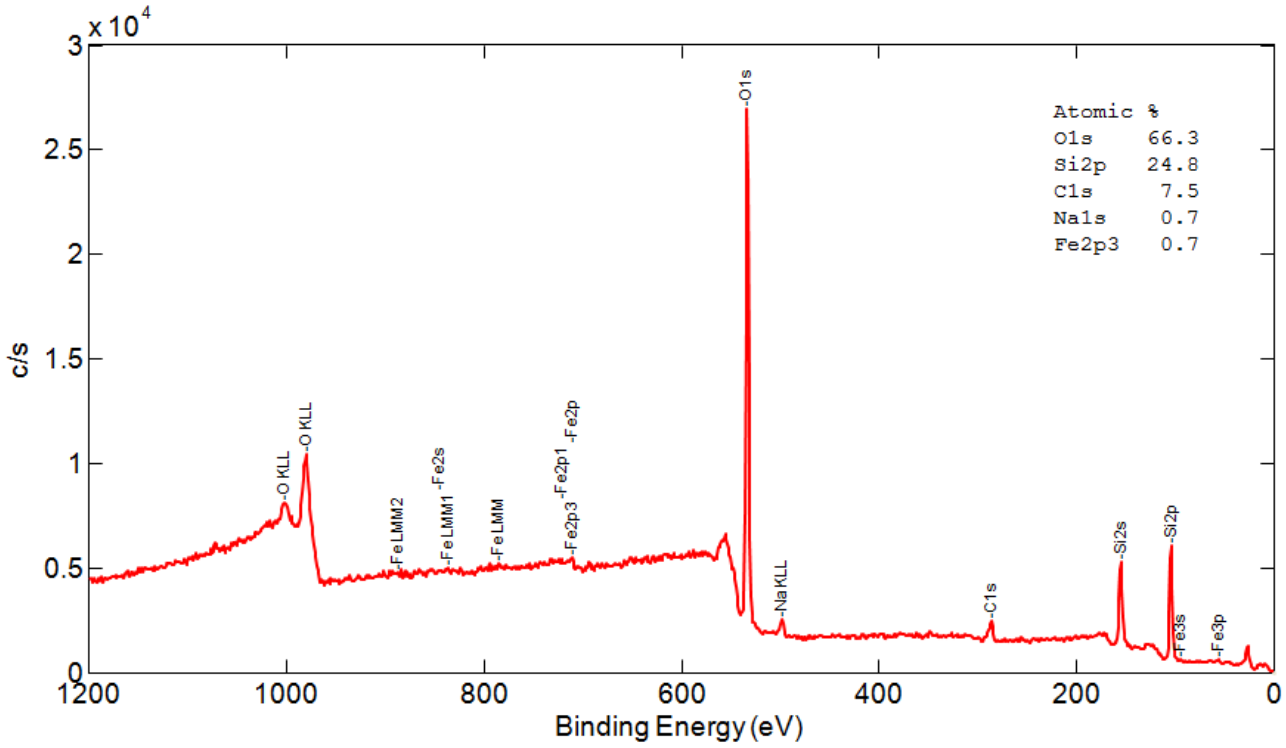

Figure 5-22: Survey spectra of SC-45+BUF-GA

Figure 5-22 presents the survey spectrum of SC-45+BUF-GA, in which all elements present on the surface of bulk samples are highlighted. Elements including oxygen, iron, sodium and silicon from glass-ceramic composition have been observed. On this bulk sample, calcium was absent due to the binding with citric acid of the buffer. Moreover, the signal of iron is very low as reported in SC-45+BUF sample, while strong signals of silicon and oxigen are present. It can be supposed that after the etching occurred by the action of the buffer, only a thin silica-rich film was detected as the result of ionic dissolution from the glass matrix. The presence of carbon is very low, despite the presence of gallic acid.

The detailed analysis of carbon region (figure 5-23) underlines that the peak related to contaminants or gallic acid in SC-45+BUF-GA increased if compared with SC-45+BUF. Similar results can be found in SC-45+GA if compared with the washed SC-45. While the signal at 286.17 eV become weaker than SC-45+BUF and it can be attributed to C-O in citric acid or

gallic acid. The peak at 288.81 eV, assigned to C=O, presents a slightly higher intensity than the sample SC-45+BUF, as a result of the binding of citrate and calcium or gallic acid.

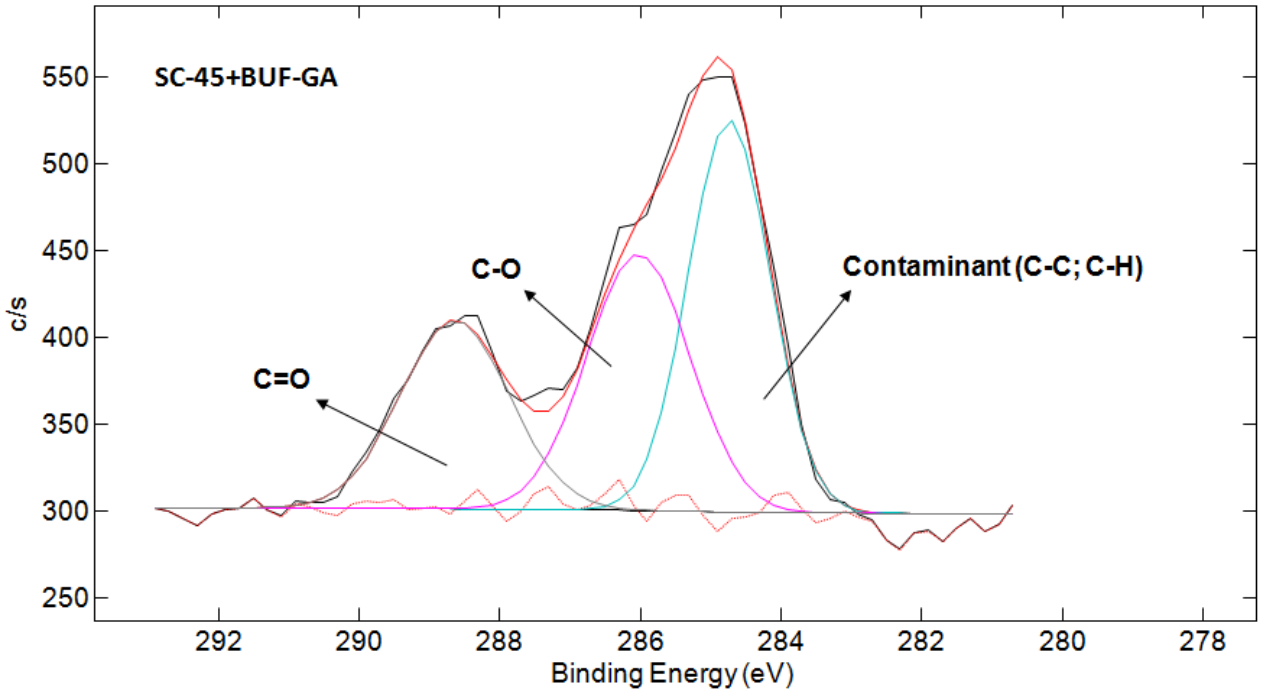

Figure 5-23: XPS detailed analysis of carbon region for SC-45+BUF-GA sample

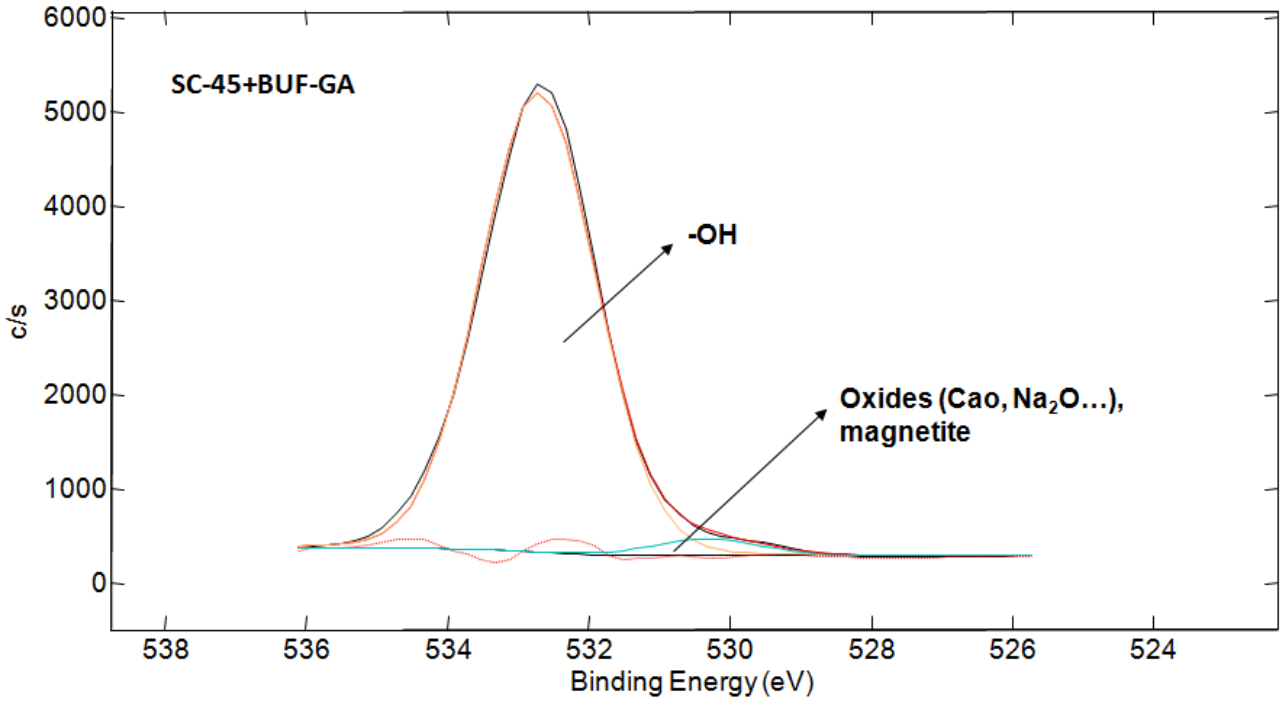

Figure 5-24: XPS detailed analysis of oxygen region for SC-45+BUF-GA sample

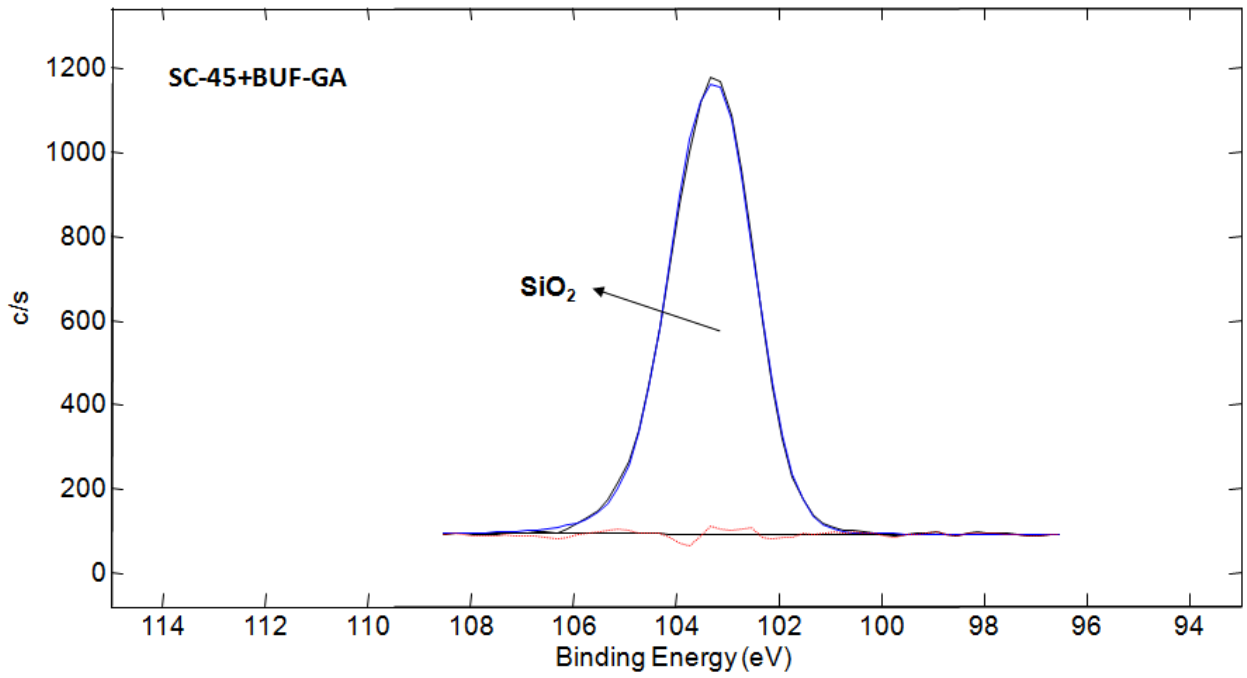

Figure 5-25: XPS detailed analysis of silicon region for SC-45+BUF-GA sample

Two peaks have been detected in the detailed analysis spectrum of oxygen region (figure 5-24). A weak signal at 530.31 eV and an extremely strong signal at 532.71 eV are attributed to oxides of glass or oxygen in Fe_2O_3, and –OH group respectively. The intensity of –OH signals presents an increase tendency, due to the grafting of gallic acid.

As for silicon region analysis (figure 5-25), as in the previous two spectra, a single peak at 103.22 eV is detected and can be attributed to silica.

Table 5-3 listed XPS the atomic percentage of washed SC-45, SC-45+BUF, SC-45+GA SC-45+BUF-GA bulk samples.

A significant increase of carbon content can be observed on SC-45+GA bulk sample due to the contribution of gallic acid.

It can be noted that compared with the washed sample, sodium, calcium as well as phosphorus are almost absent on functionalized bulks due to the bond between gallic acid and citric acid as

well as the dissolution of glass surface. Moreover, the iron content decreased after functionalization.

The silicon content is higher in samples with buffer than that without buffer. Since samples immersed in the buffer was dissolved to obtain a surface owning almost magnetite crystals with a thin silica layer on them. The one without buffer bonded large quantity of gallic acid which may cover the silica layer. This will confirmed by results obtained from SEM / EDS and UV with the Folin-Ciocalteau colorymetry.

Table 5-3 XPS atomic percentage analysis of bulk samples

Element	Washed SC-45	SC-45+BUF	SC-45+GA	SC-45+BUF-GA
O	54.5	65.7	41.3	66.3
C	29.9	9.1	52.6	7.5
Fe	6.4	<0.1	1.9	0.7
Ca	3.4	-	1.2	-
Si	2.4	24.6	2.9	24.8
P	1.9	-	-	-
N	1.6	-	-	-
Na	-	0.5	-	0.7

5.5 SEM analyses

The SEM-EDS analyses have been performed in order to analyze the surface morphology of the samples, as well as their chemical composition before and after gallic acid grafting to obtain clear evidence about the difference in the substrate reactivity.

5.5.1 SC-45 bulk sample

Washed SC-45

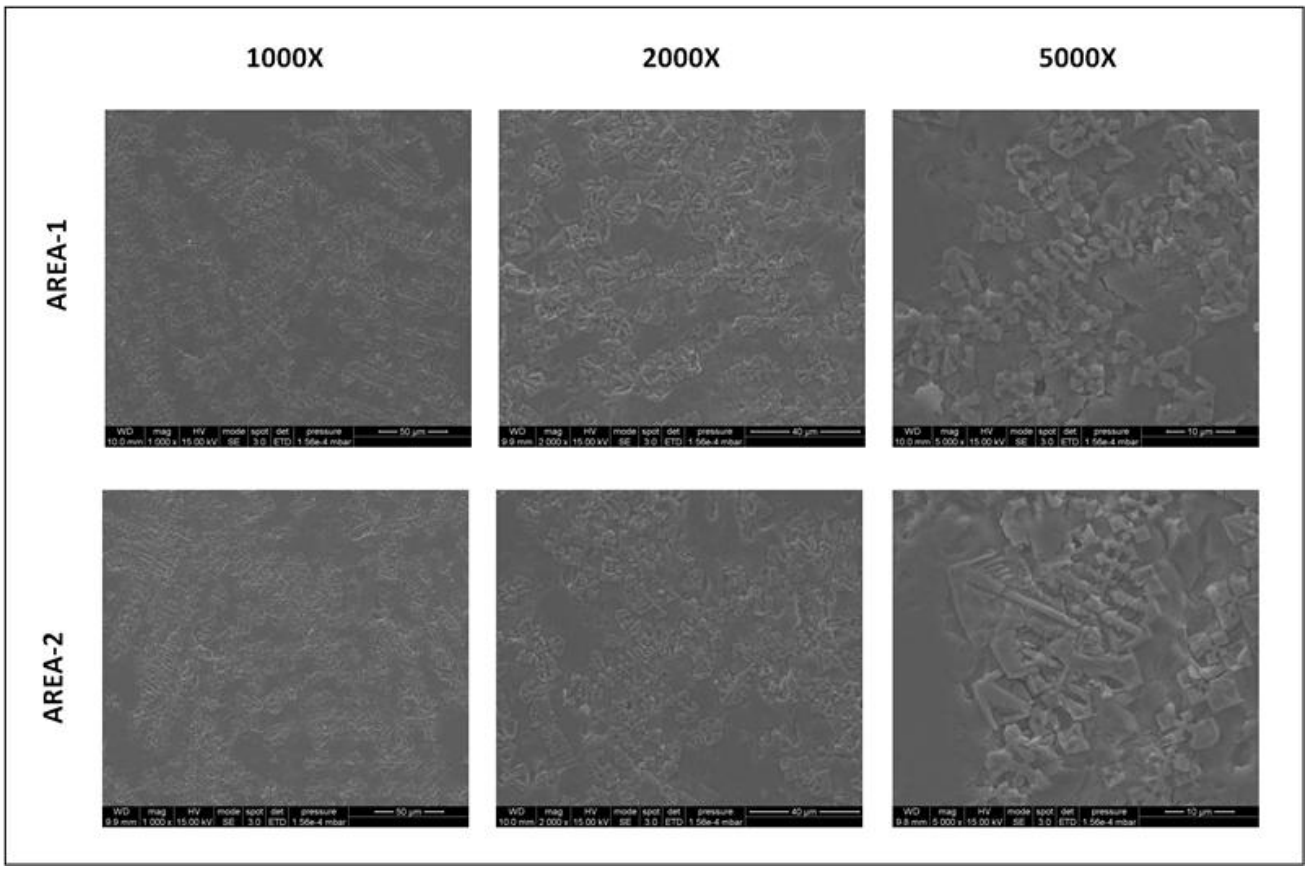

Figure 5-26: SEM images of washed SC-45 samples with different magnifications in two different areas

Figure 5-26 reports the SEM images of washed SC-45 with magnifications of 1000×, 2000× and 5000× in two different areas in order to analyze the morphology and homogeny of the glass-ceramic surface. It can be noted that the glass-ceramic surface is homogeneous, since different areas have similar morphological structures. In both areas magnetite crystals, embedded in the glass matrix, can easily be observed.

Figure 5-27 shows an SEM image with the corresponding EDS analysis of washed SC-45. It can be observed that all elements of glass-ceramic composition are present in the surface, including oxygen, iron, silicon, sodium, calcium and phosphorus. A small amount of carbon attributed to environmental contamination can be detected as well, as widely reported in literature, and already observed in XPS analyses. Cr signal is due to sample metallization for SEM observation.

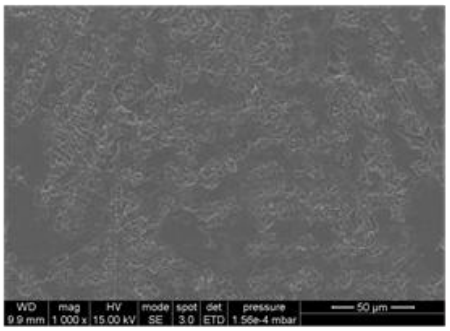

Element	SC-45 wash
C	10.8
O	53.79
Na	3.56
Si	8.17
P	0.99
Ca	4.76
Fe	17.92

Figure 5-27: SEM images and EDS analysis of washed SC-45

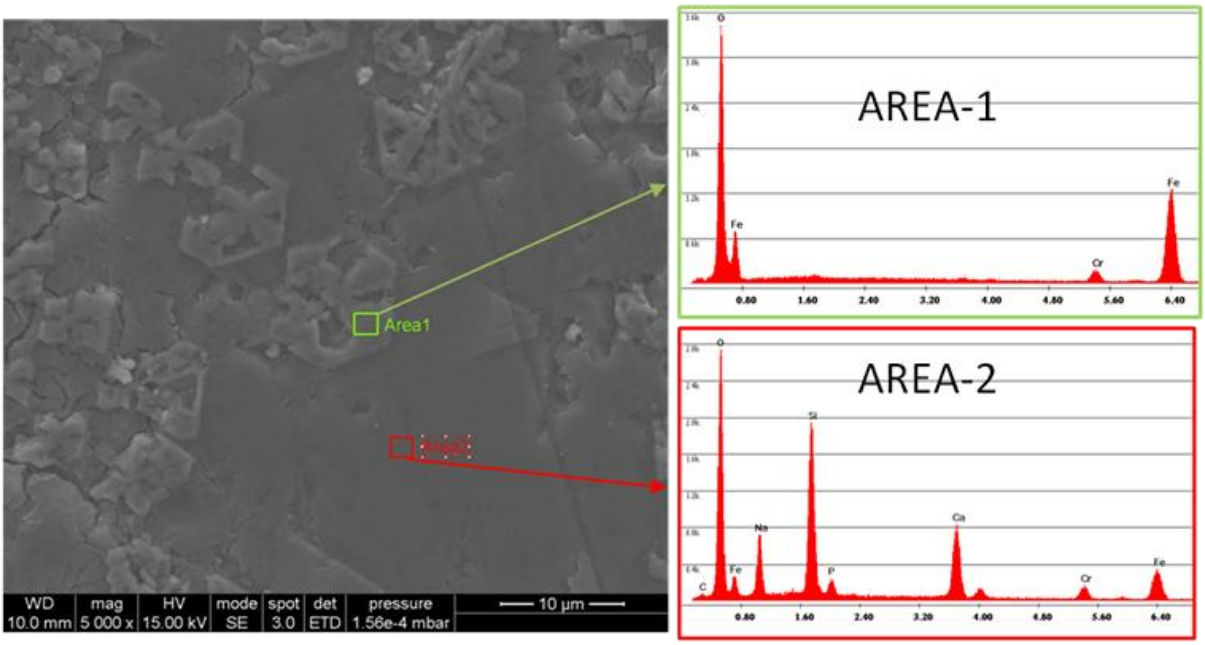

Element	AREA 1 [%at]	AREA 2 [%at]
C	-	5.62
O	55.44	55.43
Na	-	7.87
Si	-	13.33
P	-	1.2
Ca	-	7.89
Fe	44.56	8.66

Figure 5-28: SEM images with a magnification 5000×and EDS analysis on chemical composition of washed SC-45 in two specific areas

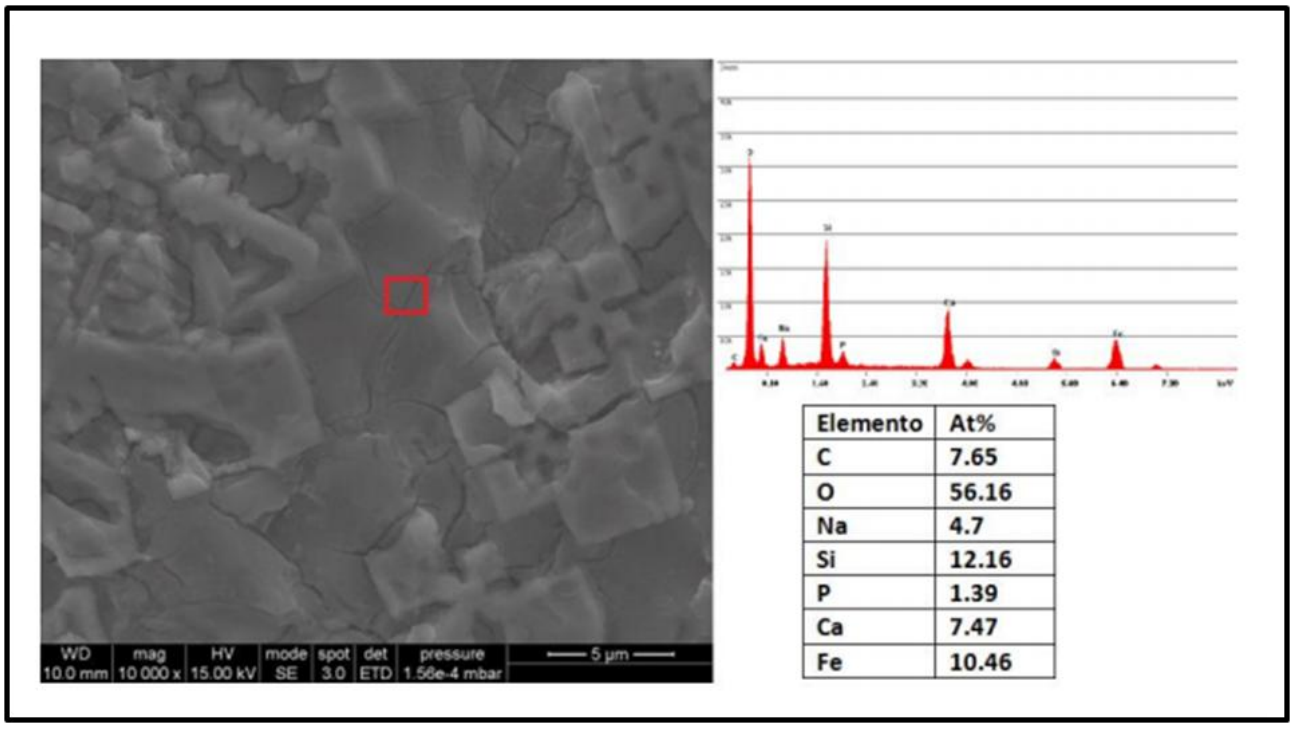

Elemento	At%
C	7.65
O	56.16
Na	4.7
Si	12.16
P	1.39
Ca	7.47
Fe	10.46

Figure 5-29: SEM images with a magnification 10000× specific on the cracks with EDS analysis in the surface region

Figure 5-28 reports the SEM images with a magnification 5000×and EDS analyses of washed SC-45 in two specific areas. It can be found that in area 1 only oxygen and iron can be detected and together with the morphology of this area, the presence of magnetite crystals can be confirmed. While in area 2, all elements from glass-ceramic composition have been detected with an increase of silicon content compared with the washed sample, probably due to the formation of silica gel layer.

Figure 5-29 shows an SEM image (magnification 10000×) with the corresponding EDS analysis on the cracked surface layer in order to investigate more in depth the nature of the reaction layer. . The composition is similar to the characteristic elements of glass. The higher amount of oxygen and silicon can be related to the formation of a thin reaction layer made of silica gel, in this point.

SC-45+GA

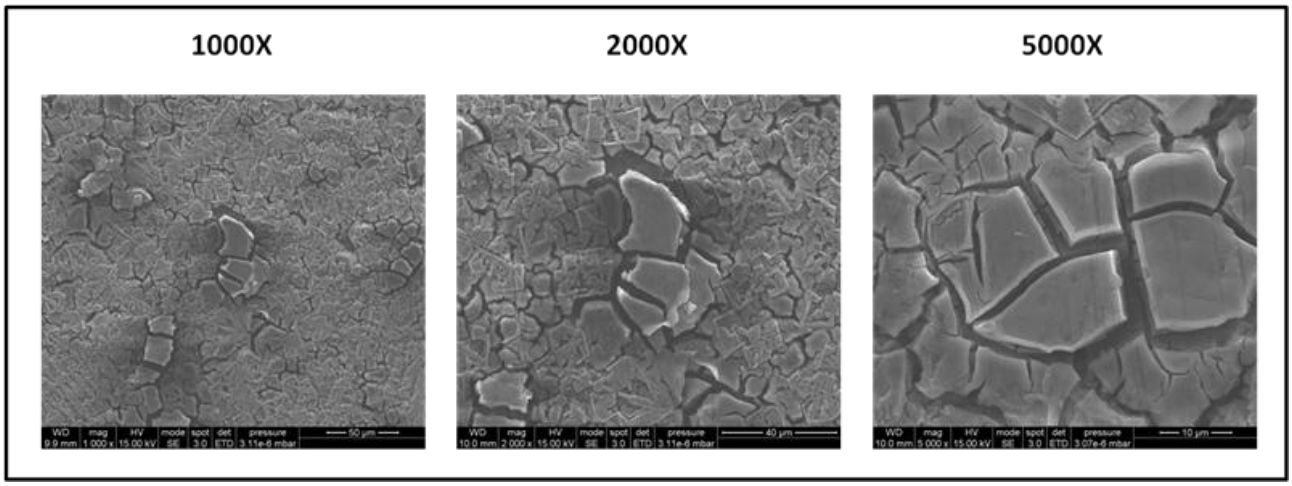

Figure 5-30: SEM images of SC-45+GA samples with different magnifications

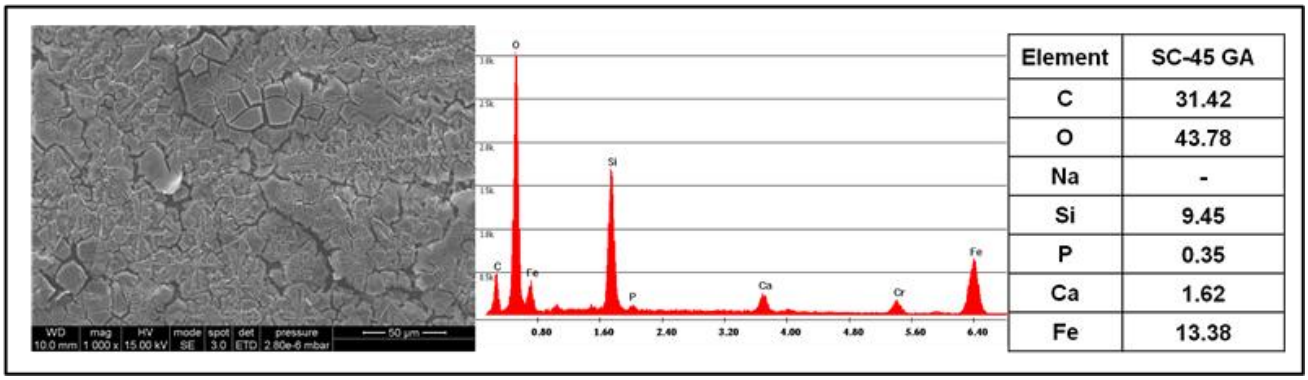

Element	SC-45 GA
C	31.42
O	43.78
Na	-
Si	9.45
P	0.35
Ca	1.62
Fe	13.38

Figure 5-31: SEM images and EDS analysis of SC-45+GA

Figure 5-30 reports SEM images of SC-45+GA samples with magnifications of 1000×, 2000× and 5000×. In comparison with the only washed sample, the process of functionalization with gallic acid induces a greater reactivity in the glass. In fact, a surface reaction layer can clearly be observed and it results in a surface full of cracks. It is also noted that the edges of the crystals are less tidy, and this can be due to a reaction layer above the crystals themselves.

Figure 5-31 shows the SEM images and EDS analysis of SC-45+GA. A significant increase of carbon content can be observed compared to the washed sample and assigned to the contribution of gallic acid considering equal environmental contamination on the samples. In addition, all elements of glass constituents have been detected by EDS. Sodium has not been detected

probably because of its release in the solution as well as a surface coverage of silica gel layer with gallic acid.

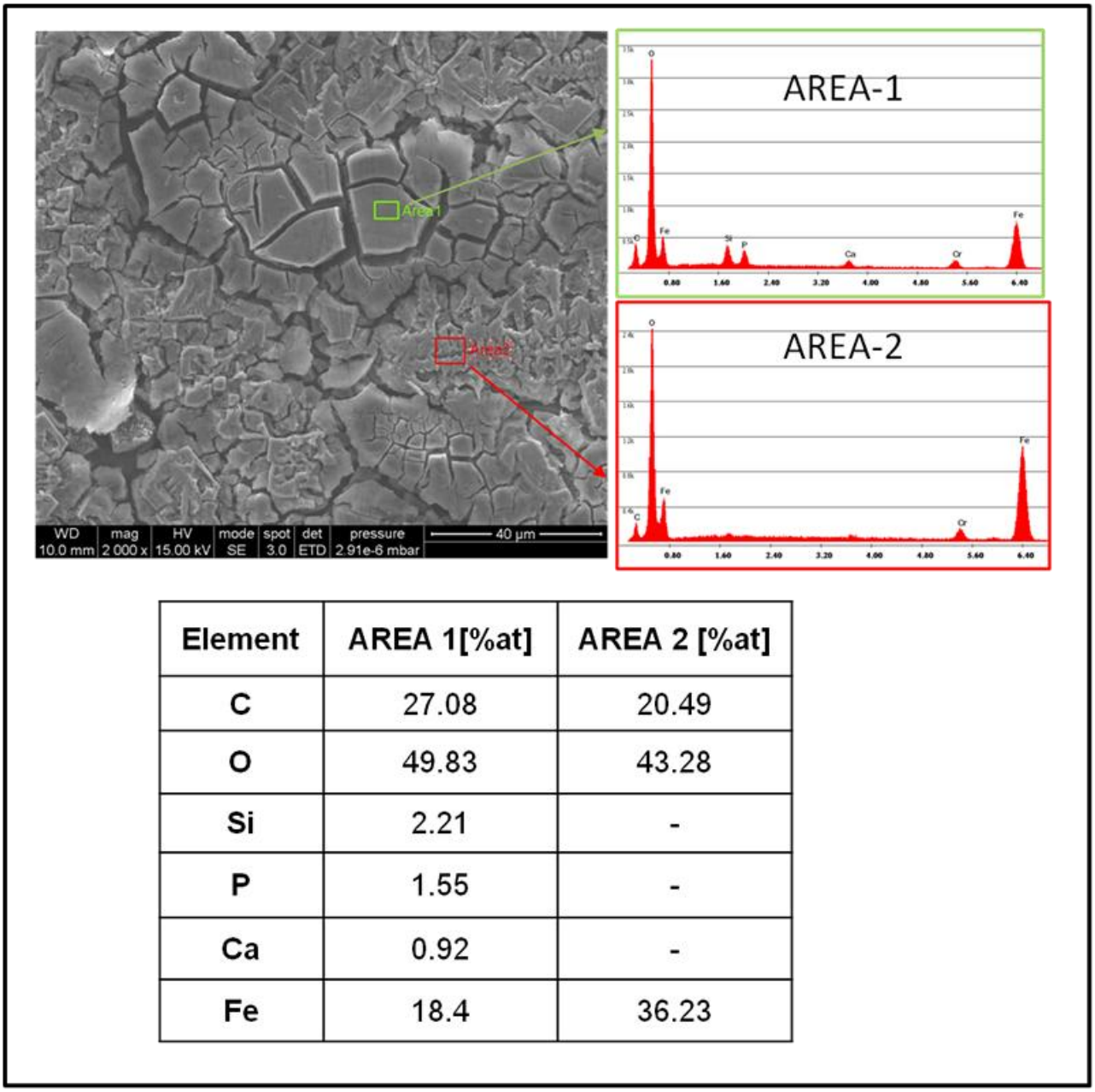

Element	AREA 1[%at]	AREA 2 [%at]
C	27.08	20.49
O	49.83	43.28
Si	2.21	-
P	1.55	-
Ca	0.92	-
Fe	18.4	36.23

Figure 5-32: SEM images with a magnification 2000×and EDS analysis on chemical composition of SC-45+GA in two specific areas

Figure 5-32 listed SEM images with a magnification 2000×and EDS analysis on chemical composition of SC-45+GA in two specific areas which were selected to analyze the crack and reactive layer. From morphological observations, Area 1 seems as silica gel layer grafted with gallic acid while area 2 can be recognized as magnetite crystals. The EDS analyses underline a notable increase in the carbon content in area 1, which can be a confirmation the grafting of

gallic acid. In area 2, a higher amount of iron and oxygen can be detected, confirming the presence of magnetite crystals.

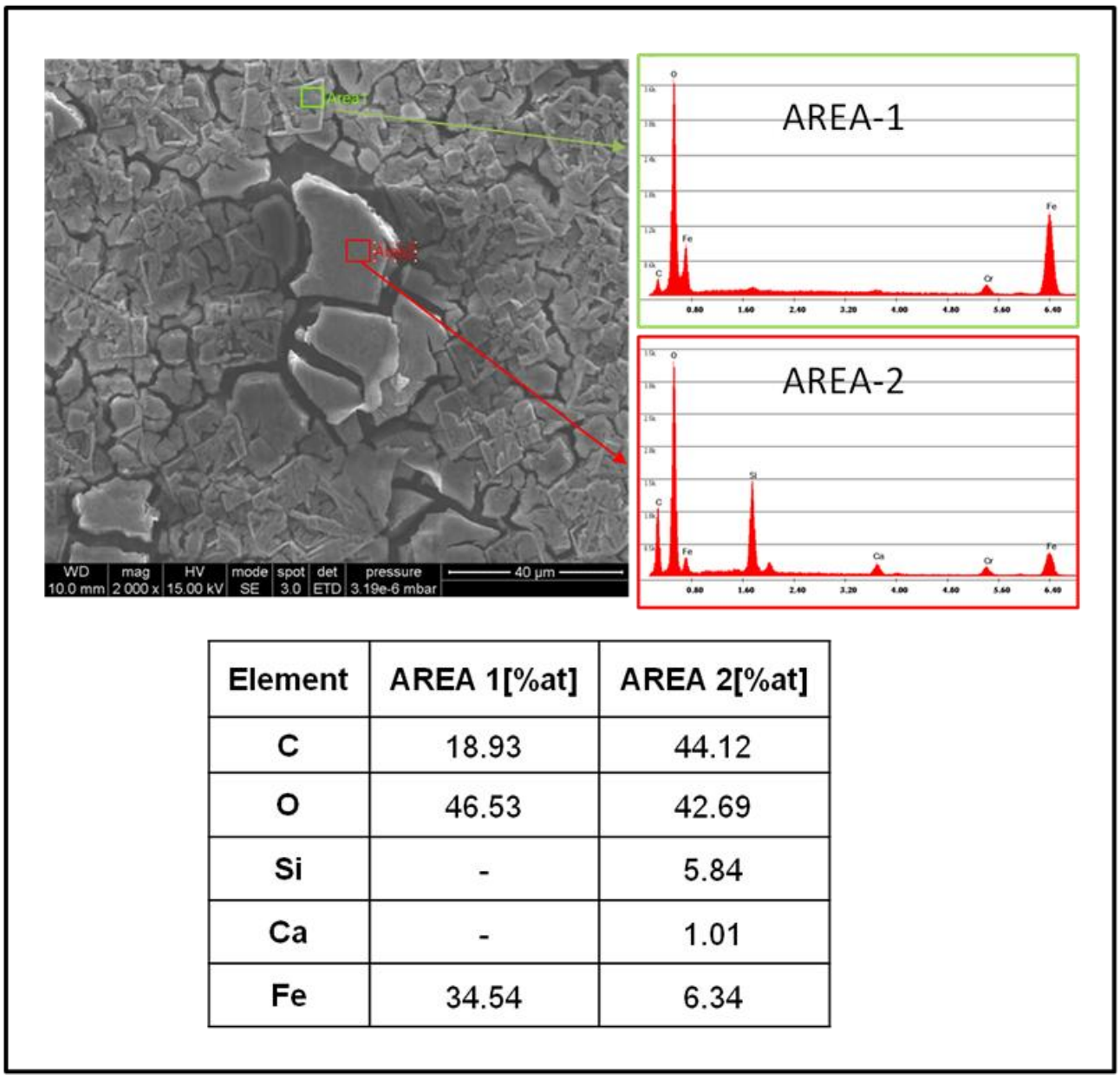

Element	AREA 1[%at]	AREA 2[%at]
C	18.93	44.12
O	46.53	42.69
Si	-	5.84
Ca	-	1.01
Fe	34.54	6.34

Figure 5-33: SEM images with a magnification 2000×and EDS analysis on chemical composition of SC-45+GA in two specific areas

Figure 5-33 showed the SEM images with a magnification 2000×and EDS analysis on chemical composition of SC-45+GA in two specific areas (different areas from figure 5-29 with similar morphology). Similar results have been obtained from the morphology observation as well as the EDS analysis. This result further proved the grafting of gallic acid and the presence of magnetite crystals in this sample.

SC-45+BUF

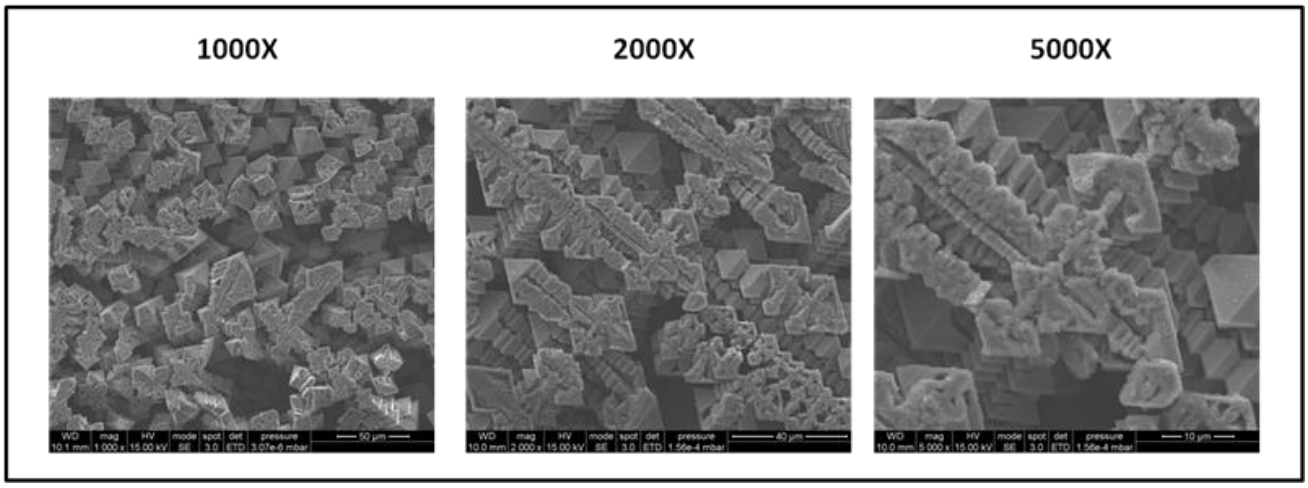

Figure5-34: SEM images of SC-45+BUF samples with different magnifications

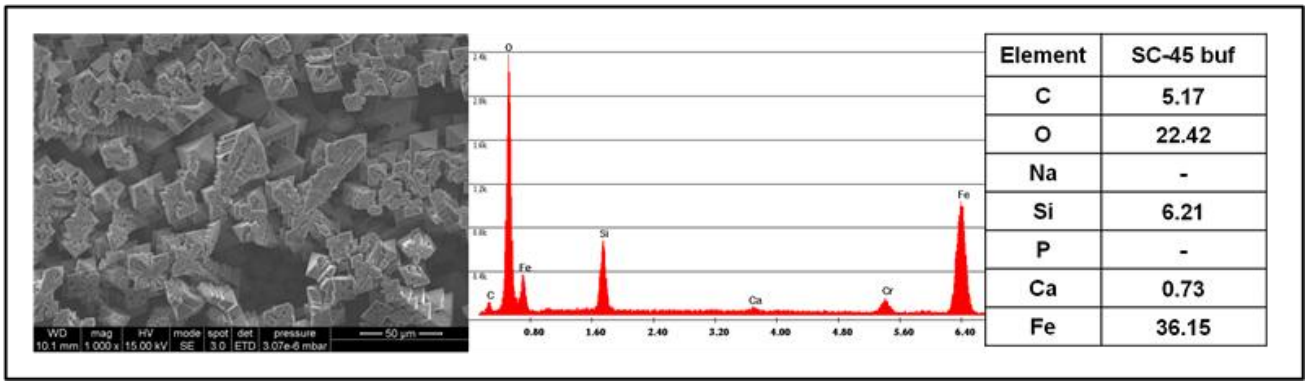

Element	SC-45 buf
C	5.17
O	22.42
Na	-
Si	6.21
P	-
Ca	0.73
Fe	36.15

Figure5-35: SEM images and EDS analysis of SC-45+ BUF

Figure 5-34 exhibits SEM images of SC-45+BUF samples with magnifications of 1000×, 2000 × and 5000×. In comparison with the only washed sample (figure 5-23), the amorphous glassy matrix appears significantly reduced while magnetite crystals are clearly visible. In addition some slats are clearly observable and they can be traced to hematite crystals.

Figure 5-35 reports the SEM images and EDS analysis of SC-45+BUF. It can be noted that the content of carbon decreased while iron content increased compared with the washed sample due to the dissolution of glass matrix in buffer. The results are in accordance with the morphology observation in figure 5-31.

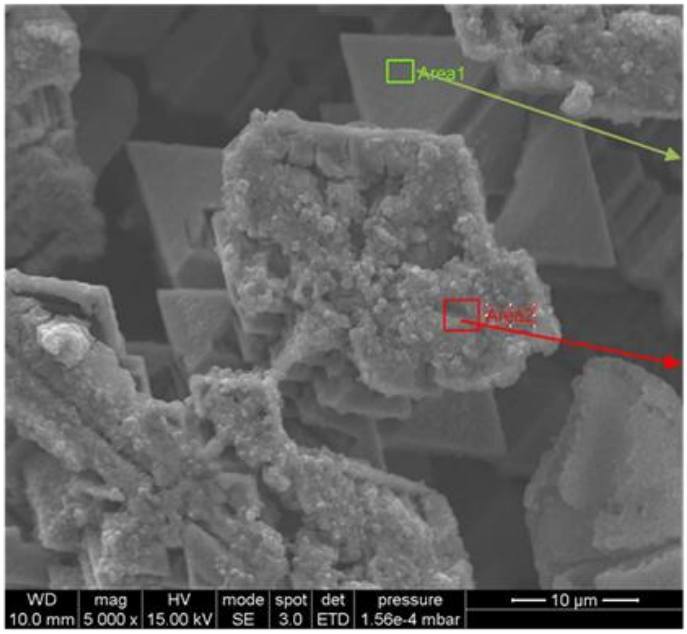

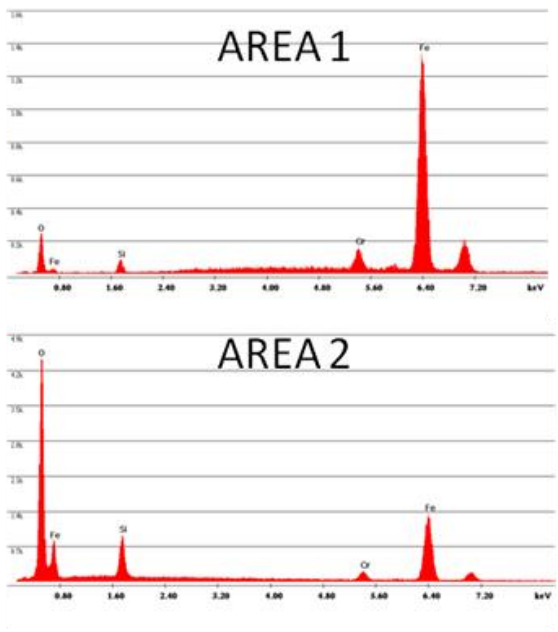

Element	AREA 1 [at %]	AREA 2 [at %]
O	8.53	56.89
Si	1.86	7.07
Fe	89.61	36.05

Figure 5-36: SEM images with a magnification 5000×and EDS analysis on chemical composition of SC-45+BUF in two specific areas

Two specific areas have been selected to analyze the chemical composition and the SEM images with a magnification 5000× and EDS analysis results are reported in figure 5-36. In both areas only iron, oxygen and silicon have been detected. Area 1 with extremely high iron is mainly magnetite crystals but with less amount of residual glass matrix, while area 2 can be assigned to magnetite crystals with a part of residual glassy matrix as observed from the image.

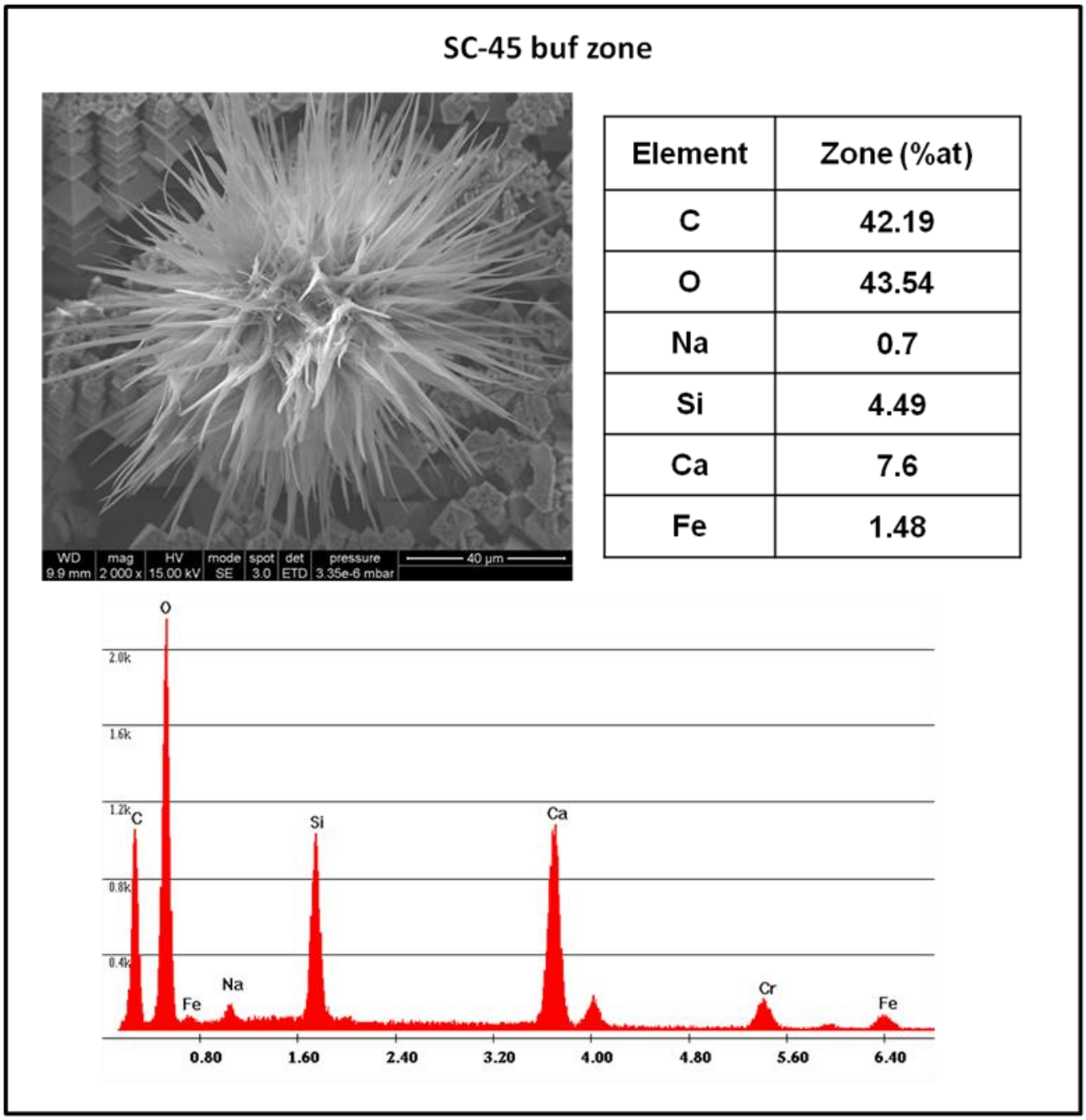

Figure 5-37: SEM images with a magnification 2000× and EDS analysis of white deposits on SC-45+BUF surface

Figure 5-37 shows the image and EDS analysis of white deposits on bulk surface. It can be underlined that the carbon and calcium content are very high on these deposits. It is assumed as salts of calcium, probably calcium citrate. The further confirmation will be subsequently carried out with FTIR (chapter V, section 5.6).

SC-45+BUF-GA

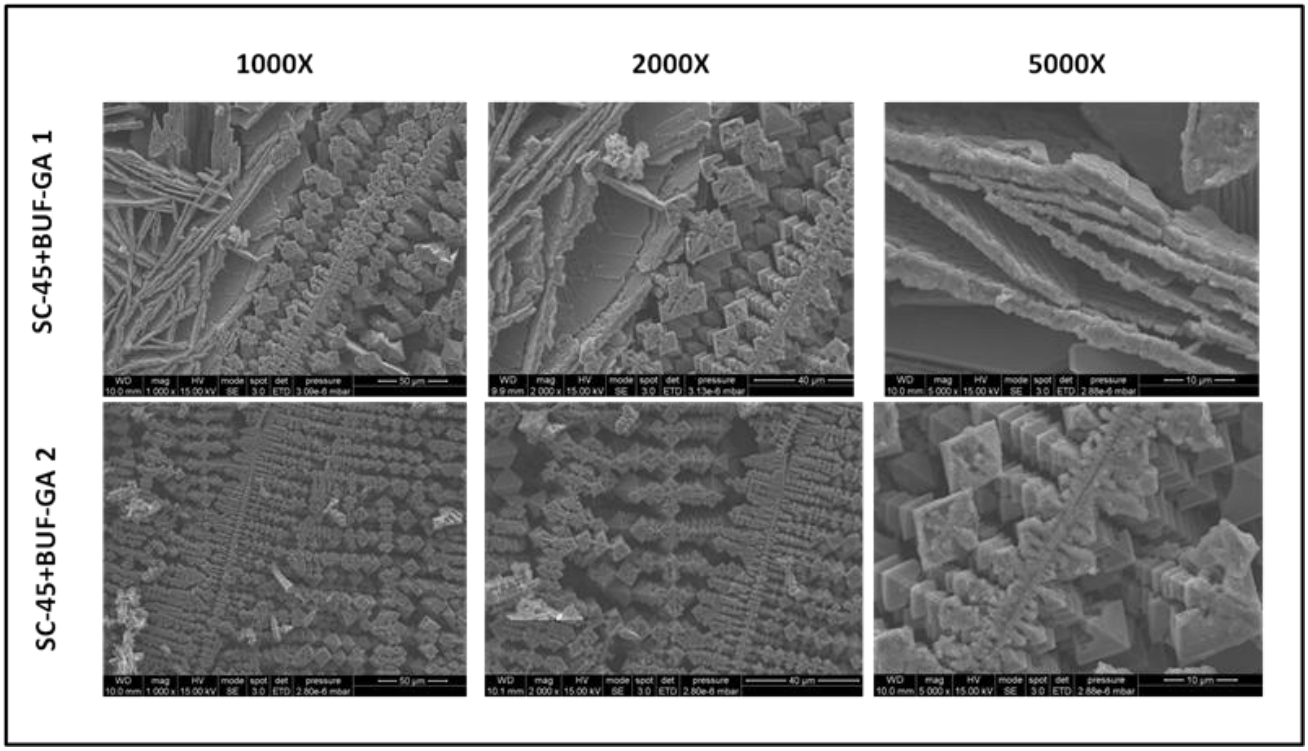

Figure 5-38: SEM images of SC-45+BUF-GA samples with different magnifications

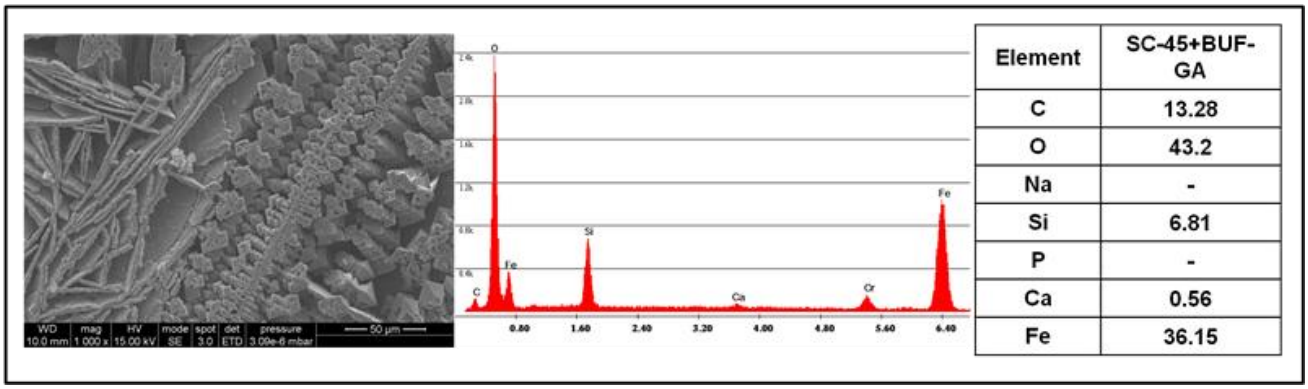

Element	SC-45+BUF-GA
C	13.28
O	43.2
Na	-
Si	6.81
P	-
Ca	0.56
Fe	36.15

Figure 5-39: SEM images and EDS analysis of SC-45+ BUF-GA

Figure 5-38 exhibits SEM images of SC-45+BUF-GA samples with magnifications of 1000×, 2000× and 5000× in two different areas. It can be observed that in the presence of buffer, the majority of the glassy matrix surface has gone into solution leaving magnetite crystals and hematite, as has already observed for the bulk sample immersed in buffer. In addition, the wrinkled layers can be seen, which also present in other samples and likely assigned to residual amorphous phase on the crystals. This suggests that the dissolution of the amorphous phase

happens in presence of the buffer. The phenomenon is explicable by considering the acidic pH of this solution and the strong chelating effect of citrate for iron and calcium.

Figure 5-39 shows the SEM images and EDS analysis of SC-45+BUF-GA. On the surface of this sample, iron and oxygen are particularly present, confirming the SEM observation that suggestedthe presence of magnetite crystals and hematite lamellae. The carbon content is much lower if compared to the one on the sample only grafted with gallic acid. The reason may be that the dissolution of the amorphous phase reduces the possibility of bonding between the molecule and the surface of the material.

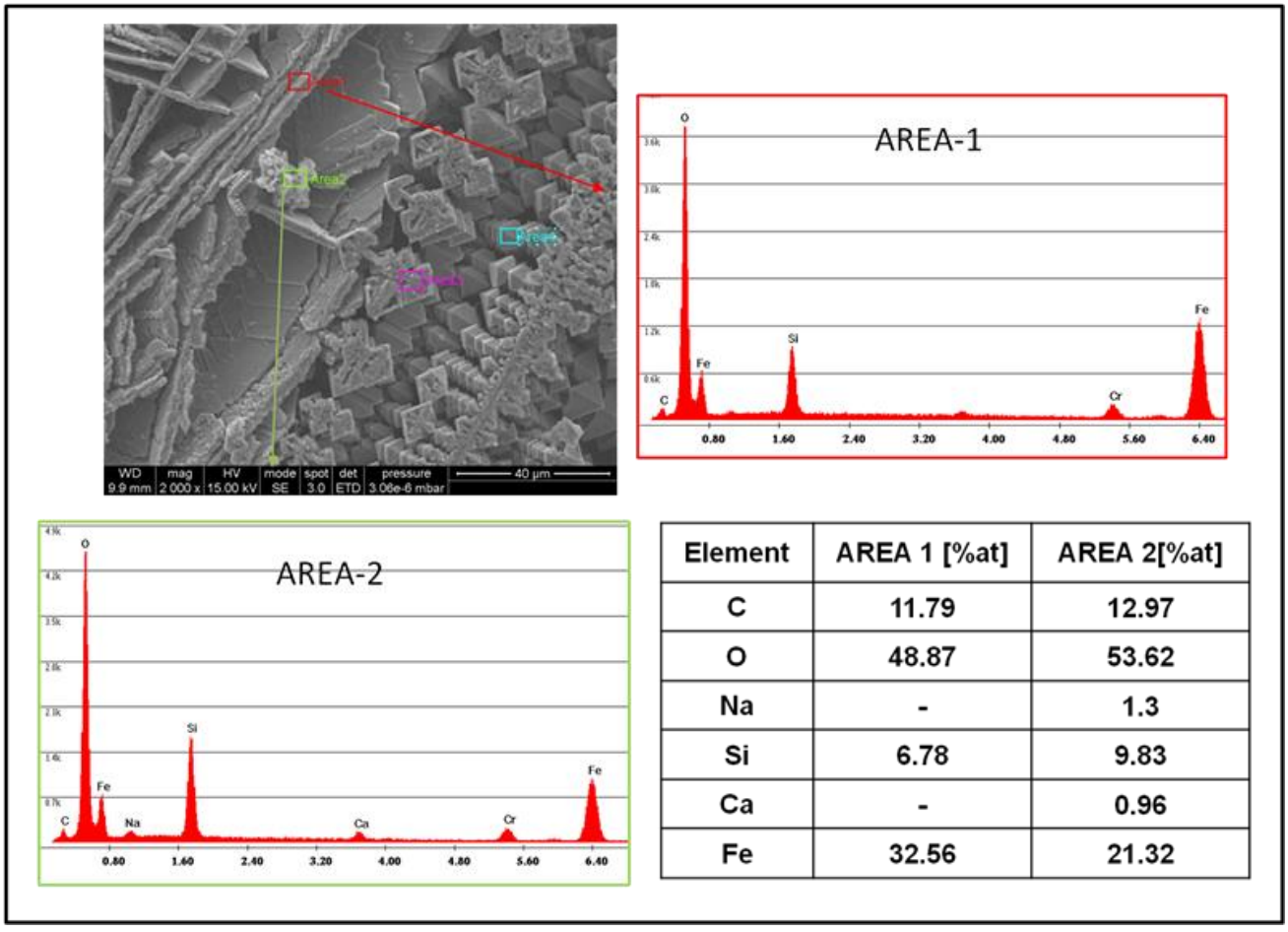

Element	AREA 1 [%at]	AREA 2[%at]
C	11.79	12.97
O	48.87	53.62
Na	-	1.3
Si	6.78	9.83
Ca	-	0.96
Fe	32.56	21.32

Figure 5-40: SEM images with a magnification of 2000×and EDS analysis on chemical composition of SC-45+BUF-GA in area 1 and area 2

Figure 5-40 and 5-41 report the SEM images with a magnification of 2000× and EDS analysis in four different areas on SC-45+BUF-GA bulk surface. The areas are: 1) thick blades (hematite), 2) possible residual amorphous phase surface, 3) magnetite crystals and 4) deepest portion.

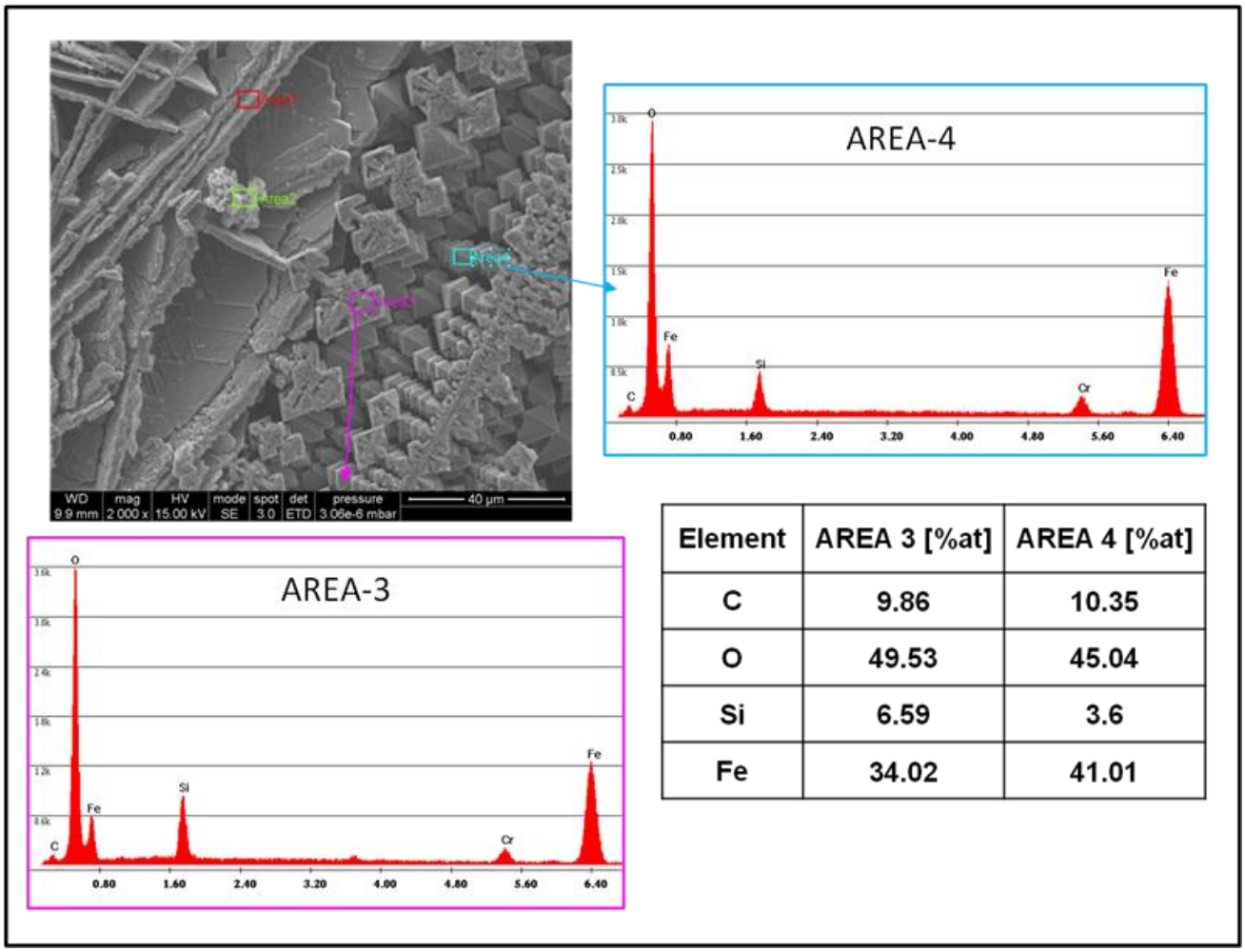

Element	AREA 3 [%at]	AREA 4 [%at]
C	9.86	10.35
O	49.53	45.04
Si	6.59	3.6
Fe	34.02	41.01

Figure 5-41: SEM images with a magnification 2000×and EDS analysis on chemical composition of SC-45+BUF-GA in area 3 and area 4

From the EDS analysis, iron, oxygen, silicon and carbon can be observed in area 1. Together with the morphology, it can be deduced that this area is made up of magnetite crystals coated with thin layer of glass matrix, as evidenced by the presence of small amount of silicon. Almost all components of the glass can be detected in area 2 with particular high iron content. It suggests that this area refers to a residual glassy matrix positioned over magnetite crystals. Elements of area 3 are similar to that of area 1, except more iron and less carbon. The EDS analysis of area 4 demonstrated a high amount of iron, and together with the morphological observation, it can be assumed that the area 4 is reported to a magnetite crystal.

SC-45+BUF-GA zone

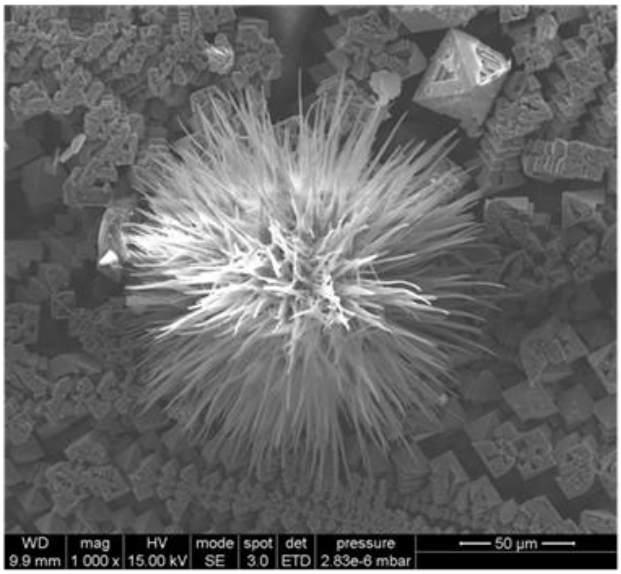

Element	Zone (%at)
C	39.06
O	42.3
Na	1.34
Si	5.14
Ca	9.91
Fe	2.24

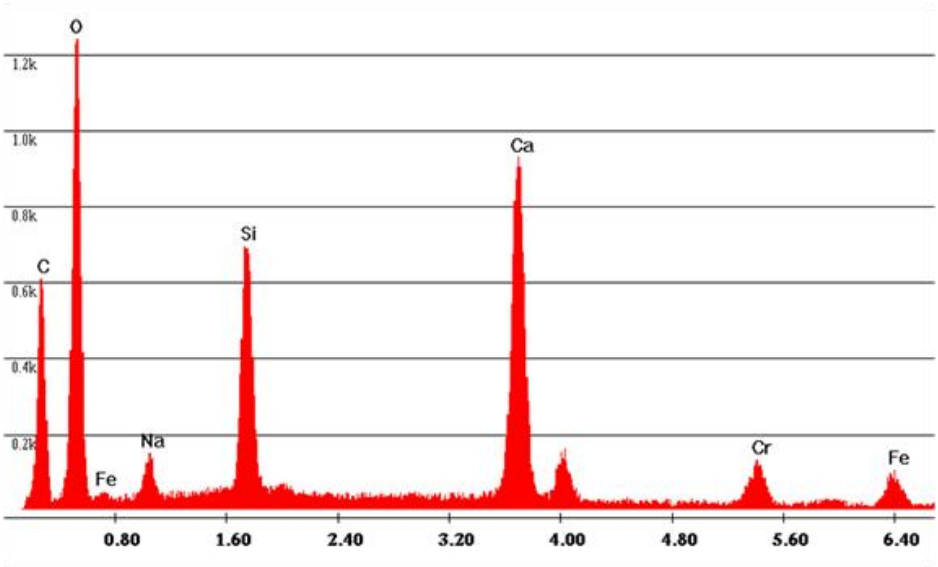

Figure 5-42: SEM images with a magnification 1000× and EDS analysis of white deposits on SC-45+BUF-GA surface

Figure 5-42 showed the image and EDS analysis of white deposits on bulk surface of SC-45+BUF-GA. The morphology and the chemical composition are similar to that of SC-45+BUF (figure 5-37). It is assumed as salts of calcium, probably calcium citrate. The further confirmation will be carried out with FTIR (chapter V, section 5.6).

Table 5-4 atomic percentages of elements from EDS analyses of bulk samples

Element	washed SC-45	SC-45 + GA	SC-45 + BUF	SC-45+ BUF-GA
C	10.8	31.42	11.78	13.28
O	53.79	43.78	41.54	43.20
Na	3.56	-	-	-
Si	8.17	9.45	6.33	6.81
P	0.99	0.35	-	-
Ca	4.76	1.62	-	0.56
Fe	17.92	13.38	40.36	36.15

Table 5-4 reports the atomic percentages of elements from EDS analyses of bulk samples. It can be underlined that carbon content significantly increases after functionalization with gallic acid compared to the washed sample. This change is not notable between the sample soaked in the buffer and buffered gallic acid, as described previously, probably due to the strong dissolution of the glassy matrix by buffer, which inhibits the bond between gallic acid and the surface. The presence of the buffer indicates another obvious difference: the higher iron content in these samples. However, opposite results of iron content has been obtained by XPS analysis. This phenomenon is reasonable, considering the different penetration depths of two techniques, few microns for SEM and few nanometers for XPS. Hence, the magnetic crystals and hematite in valley are not able to be detected by XPS. In addition, a slight difference of calcium content can be observed due to the strong chelating between buffer and calcium, and resulting in generation of stable compounds.

5.5.2 SC-45 powder samples

Washed SC-45

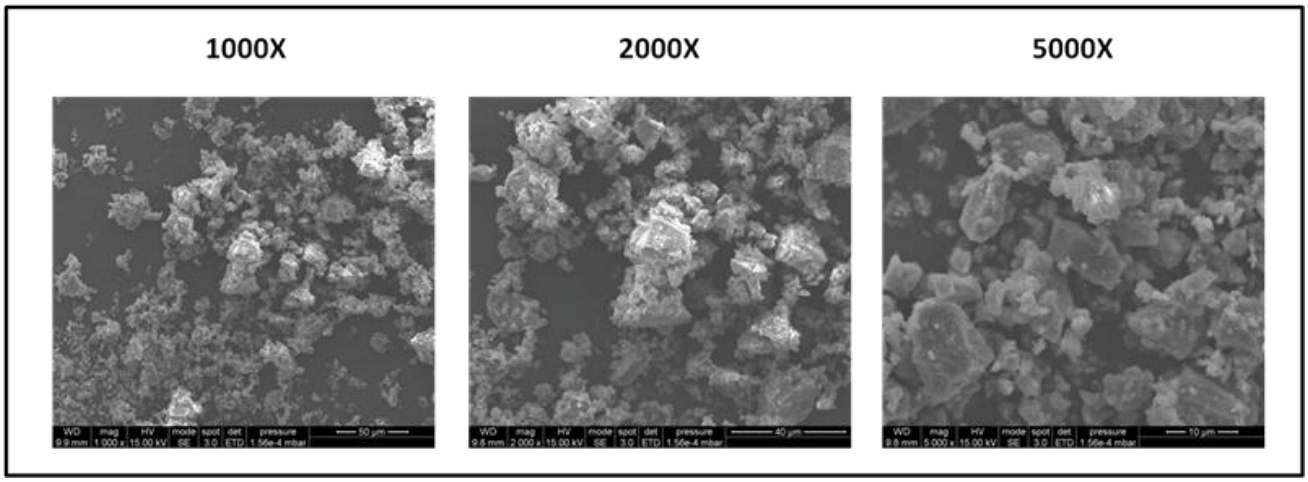

Figure 5-43: SEM images of washed SC-45 powders with different magnifications

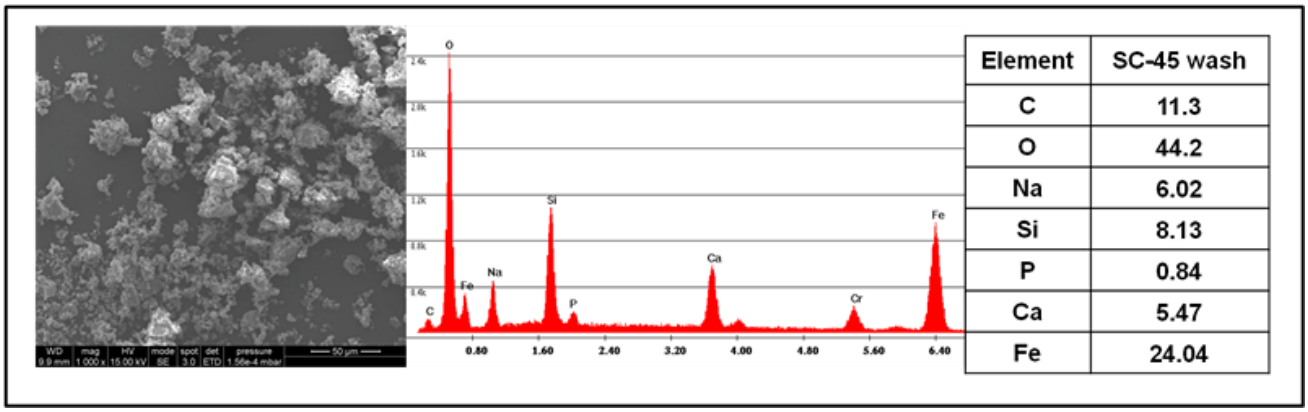

Element	SC-45 wash
C	11.3
O	44.2
Na	6.02
Si	8.13
P	0.84
Ca	5.47
Fe	24.04

Figure 5-44: SEM images and EDS analysis of washed SC-45 powder

Figure 5-43 and 5-44 reports the SEM images and EDS analysis of washed SC-45 powder. From the SEM images, we can verify that the average size of the powder is less than 20 μm as prepared by sieving through a sieve with mesh-size of 20μm. Some aggregates of powder can be observed while magnetite crystals are not clearly visible since they are inside the glass matrix.

From EDS analysis, in general, similar composition of glass can be detected as obtained from bulk sample. However, powder presents higher carbon content than bulk sample. This result can be assigned to the small size of powder which deposited on an adhesive based on carbon.

SC-45+GA

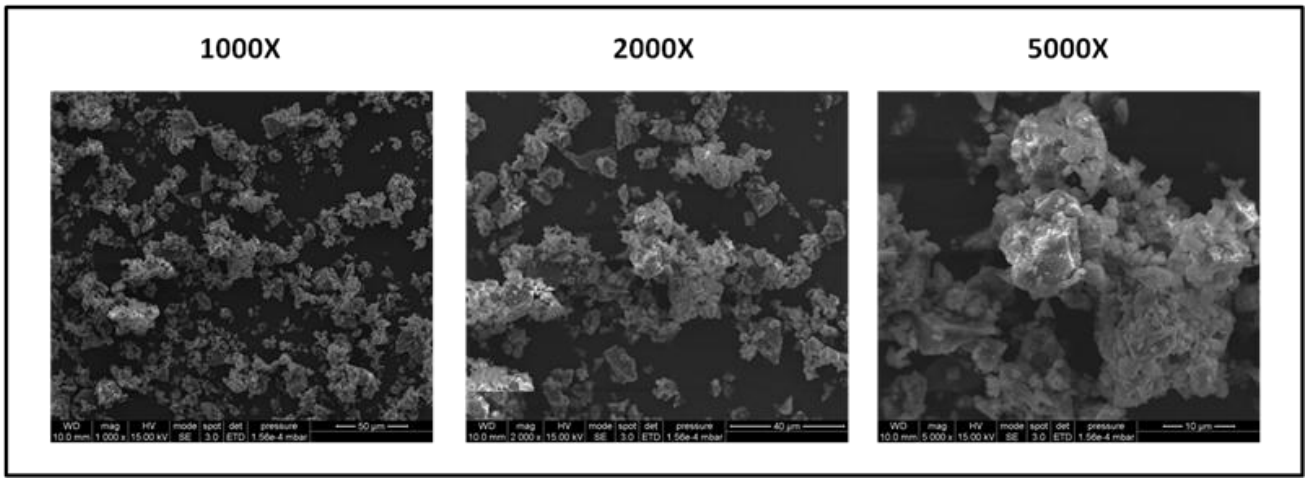

Figure 5-45: SEM images of SC-45+GA powders with different magnifications

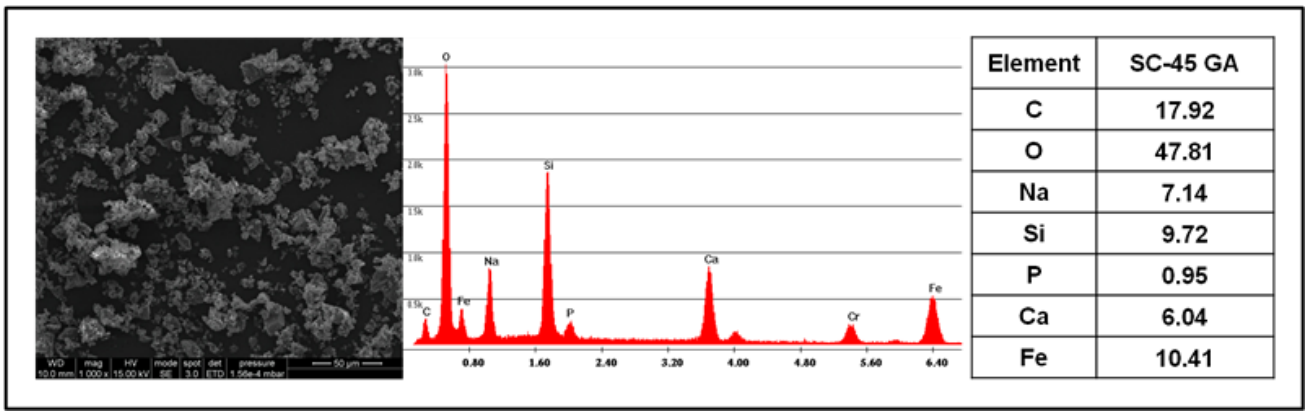

Element	SC-45 GA
C	17.92
O	47.81
Na	7.14
Si	9.72
P	0.95
Ca	6.04
Fe	10.41

Figure 5-46: SEM images and EDS analysis of SC-45+GA powder

Figure 5-45 and 5-46 reports the SEM images and EDS analysis of SC-45+GA powder. The appearance of the powders is similar to that of washed ones. As for the morphology of the powders, also in this case magnetite crystals can't be observed and it is assumed that they are immersed in the glass matrix.

From EDS analysis, the atomic percentages of the different elements is similar to that obtained from washed powders except a slight difference of iron and carbon. In this case, the iron content decreased while the carbon content increased probably due to the presence of gallic acid on the surface. However it must be underlined that semi-quantitative analyses on powders are not precise due to the significant contribution of carbon adhesive tape.

SC-45+BUF

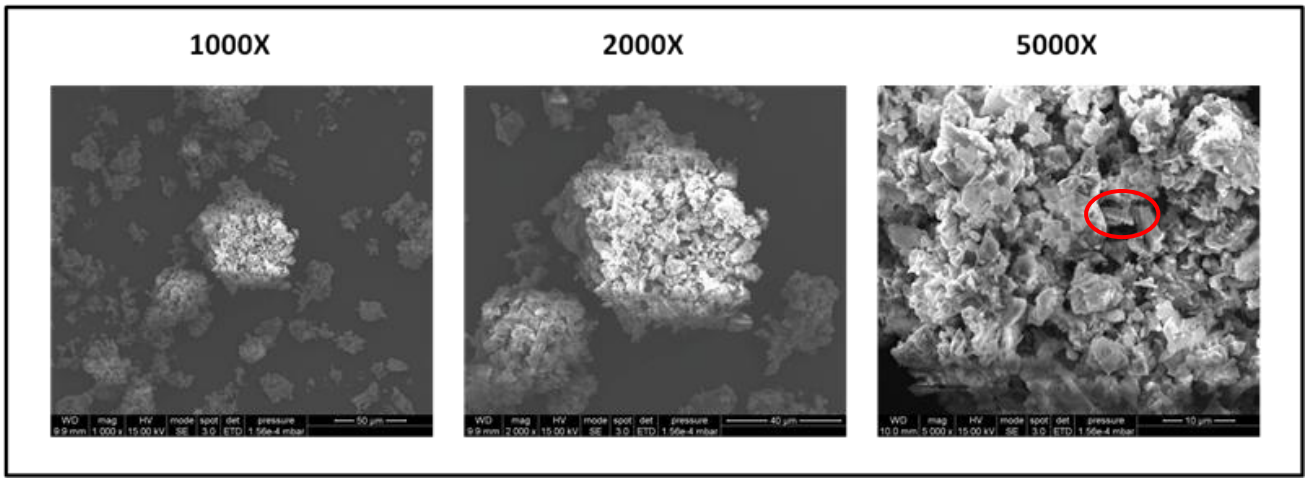

Figure 5-47: SEM images of SC-45+BUF powders with different magnifications

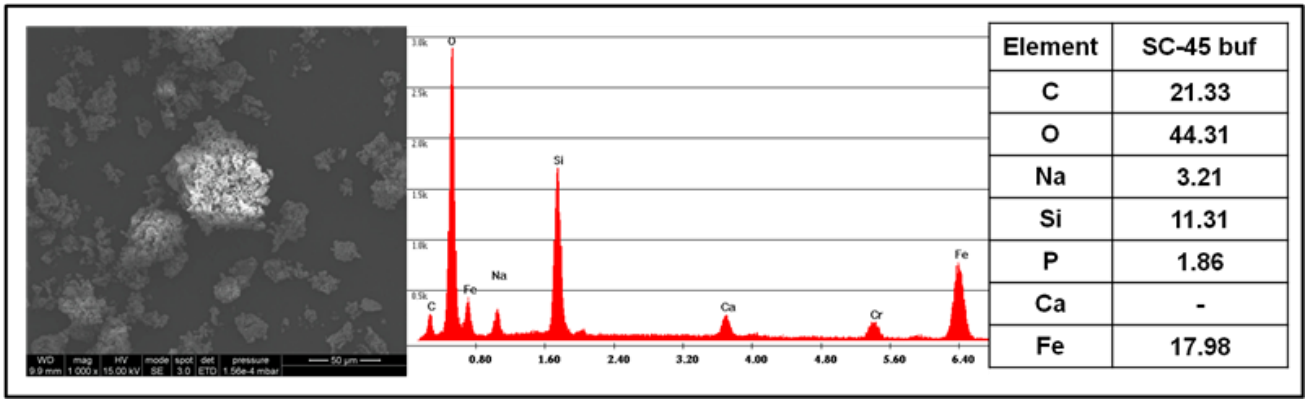

Element	SC-45 buf
C	21.33
O	44.31
Na	3.21
Si	11.31
P	1.86
Ca	-
Fe	17.98

Figure 5-48: SEM images and EDS analysis of SC-45+BUF powder

Figure 5-47 and 5-48 reports the SEM images and EDS analysis of SC-45+BUF powder,. The appearance of SC-45+BUF powder is slightly different from the washed powder in dimensions of powder size. In this case, the powder size is smaller, with minimum size of less than 5 μm. It also seems that these powders tend to aggregate compared with the washed sample. Moreover some magnetite crystals can be observed.

From EDS analysis, nearly no difference was found in composition of this powders compared with powders studied previously. In addition, higher carbon content was observed even compared to SC-45+GA due to the deposition of calcium salts, probably calcium citrate as observed in bulk samples.

SC-45+BUF-GA

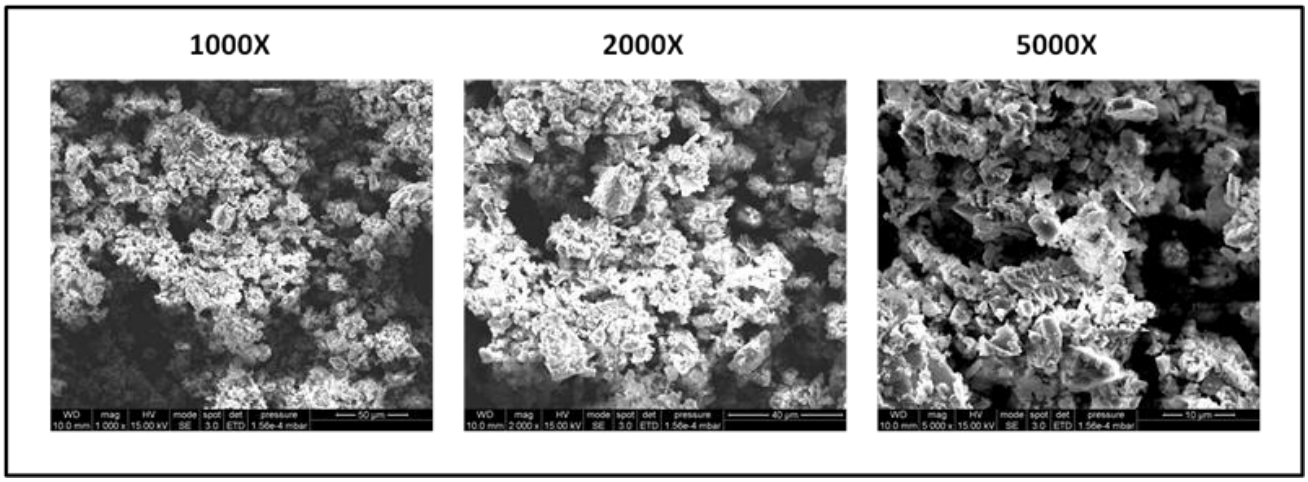

Figure 5-49: SEM images of SC-45+BUF-GA powders with different magnifications

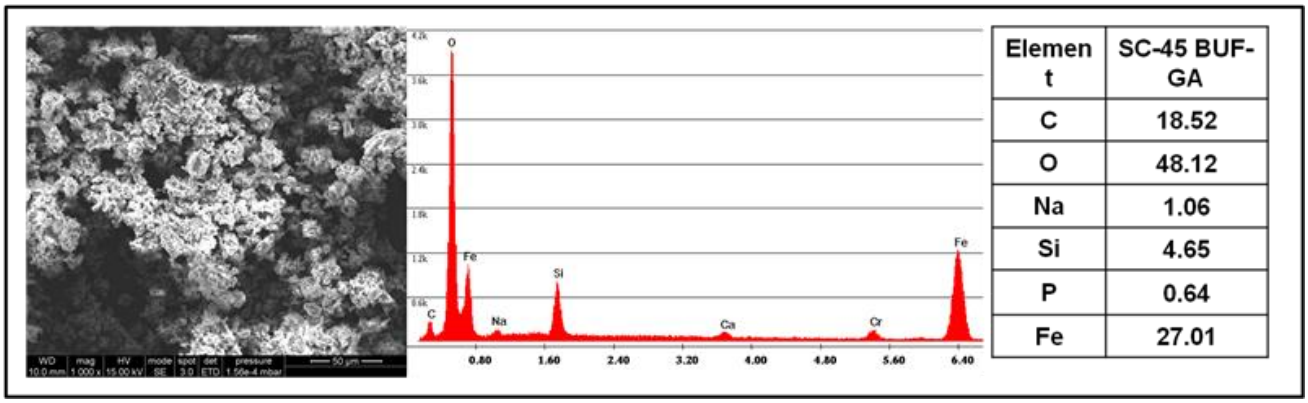

Element	SC-45 BUF-GA
C	18.52
O	48.12
Na	1.06
Si	4.65
P	0.64
Fe	27.01

Figure 5-50: SEM images and EDS analysis of SC-45+BUF-GA powder

Figure 5-49 and 5-50 shows the SEM images and EDS analysis of SC-45+BUF-GA powder. The appearance of the powders is similar to that treated only with the buffer in both morphology and dimensions. In comparison to the sample grafted with only GA, there is a greater aggregation of the powders, as observed in powder soaked in buffer. Moreover, in some regions the presence magnetite crystals can be observed, as seen in the bulk and in just buffer treated powders. As for EDS analysis, it can be underlined that functionalization with the presence of buffer leads to higher iron content due to the dissolution of glass matrix as observed in the bulk samples. These powders, compared with those soaked in the buffer only, seem to have an atomic percentage of less carbon, in contrast to what would be expected for the presence of gallic acid bonded to the

surface. This result can support a less effective functionalization of the glass-ceramic in the presence of buffer as already observed for bulk samples. However it must be underlined that quantitative analyses on powders are not precise due to the significant contribution of carbon adhesive tape.

5.6 FTIR analyses

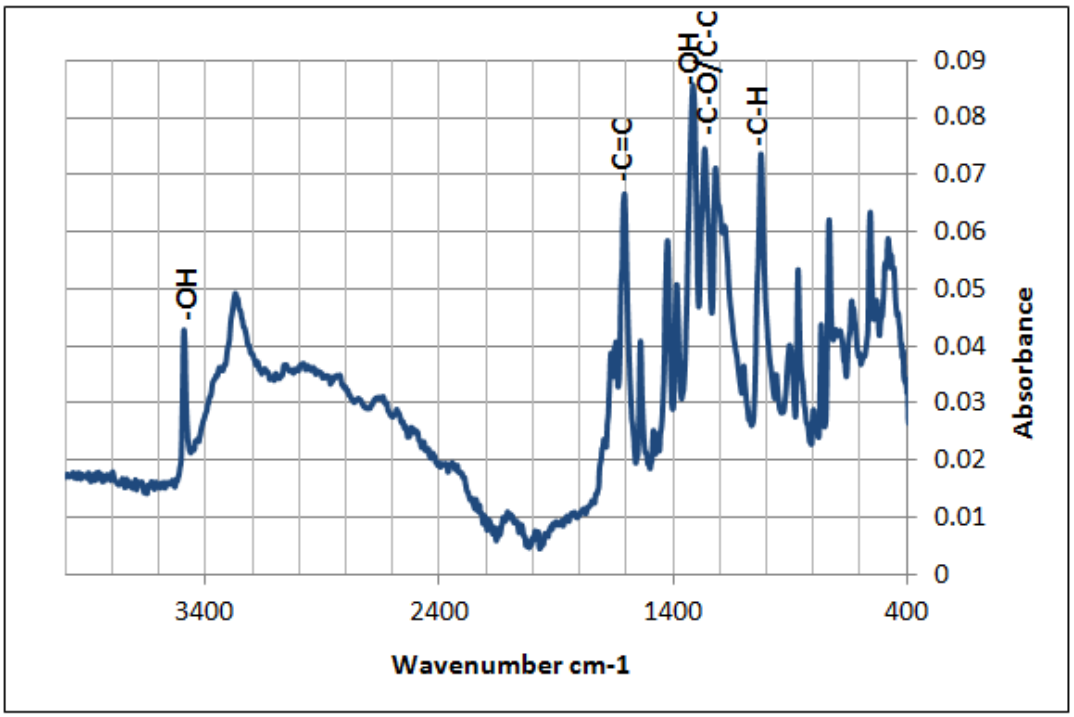

Figure 5-51: FTIR spectra of gallic acid (with KBr)

From FTIR spectra of gallic acid (figure 5-51), the typical polyphenolic characteristics were showed with the existence of a phenolic ring –OH stretching within the 3200-3550 cm^{-1}, and –OH in plane bending at about 1322 cm^{-1}, an aromatic ring C=C stretching within1450-1600 cm^{-1}, and C-O/C-C stretching vibrations within 1200-1300 cm^{-1}, deformation of C-H aromatic at about 1024cm^{-1}, as well as δ-benzene ring vibration at about 732 cm^{-1} [15, 16].

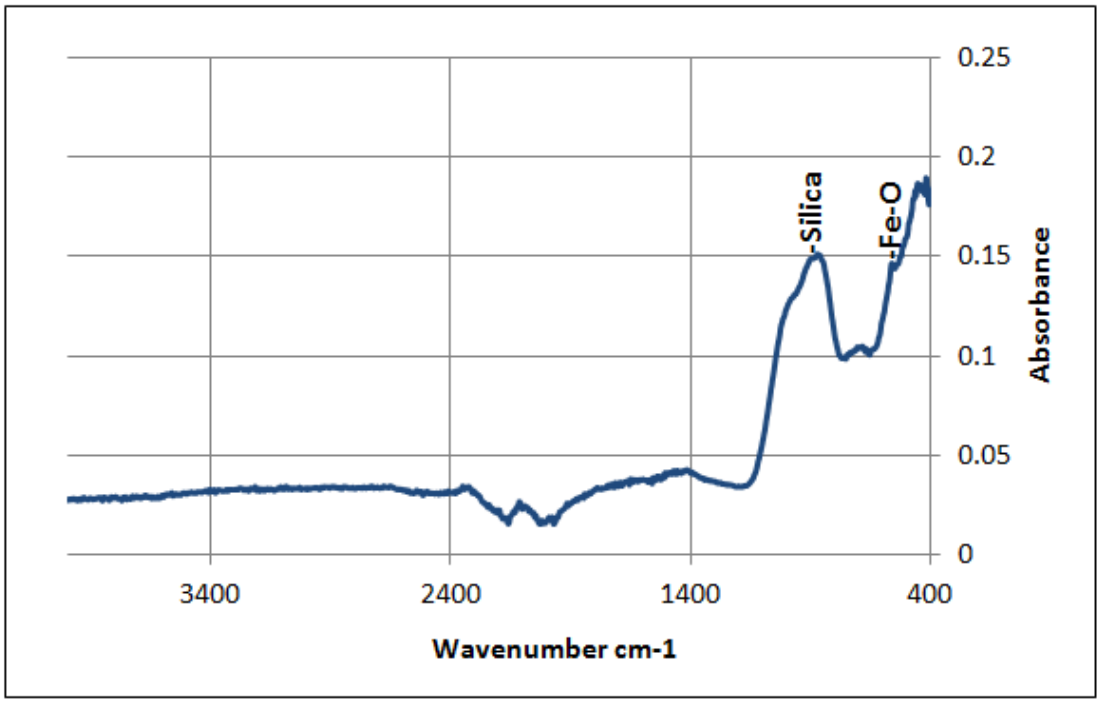

Figure 5-52: FTIR spectra of washed SC-45

From FTIR spectra (figure 5-52) of washed SC-45, the peaks at 889.8 cm^{-1} show the existence of silica and peaks at 558.2 cm^{-1} are related to iron oxide (Fe-O stretching) [24].

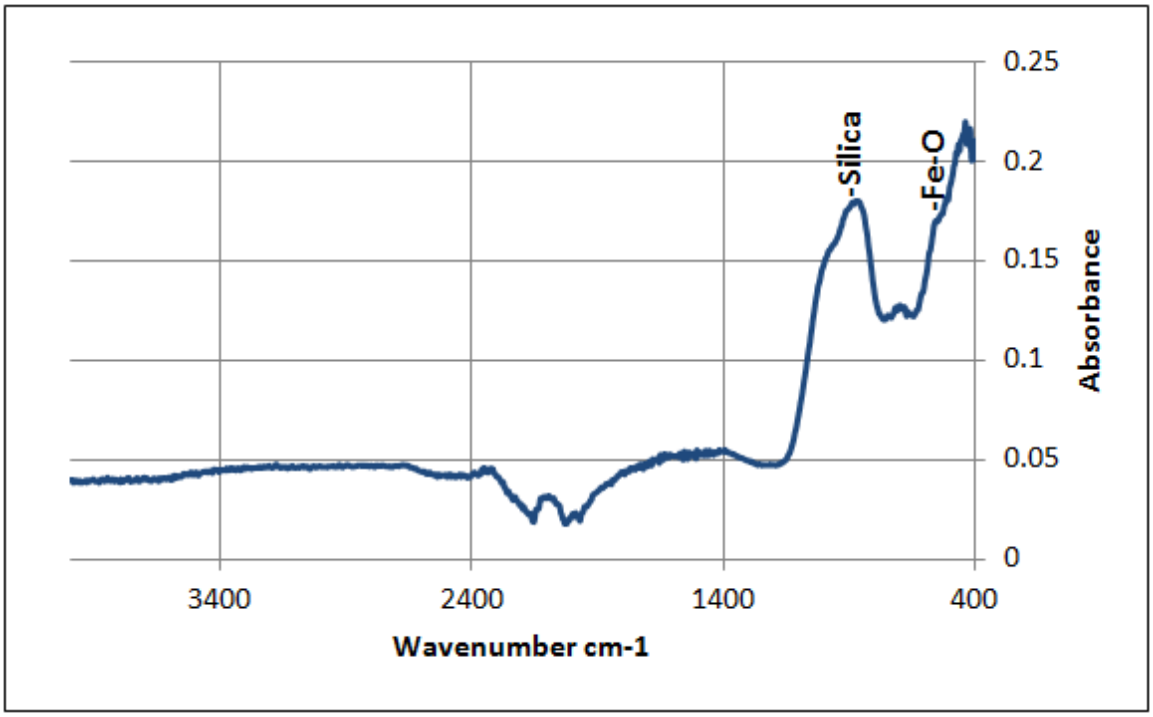

Figure 5-53: FTIR spectra of SC-45+GA

From FTIR spectra of SC-45+GA in figure 5-53, the signal of silica and magnetite or hematite at 871.4 cm^{-1} and 539.8 cm^{-1} can be detected respectively [27, 28]. No signal for gallic acid has been recorded. Probably the molecular layer is too this to be detected by this technique considering the high signal of the substrate.

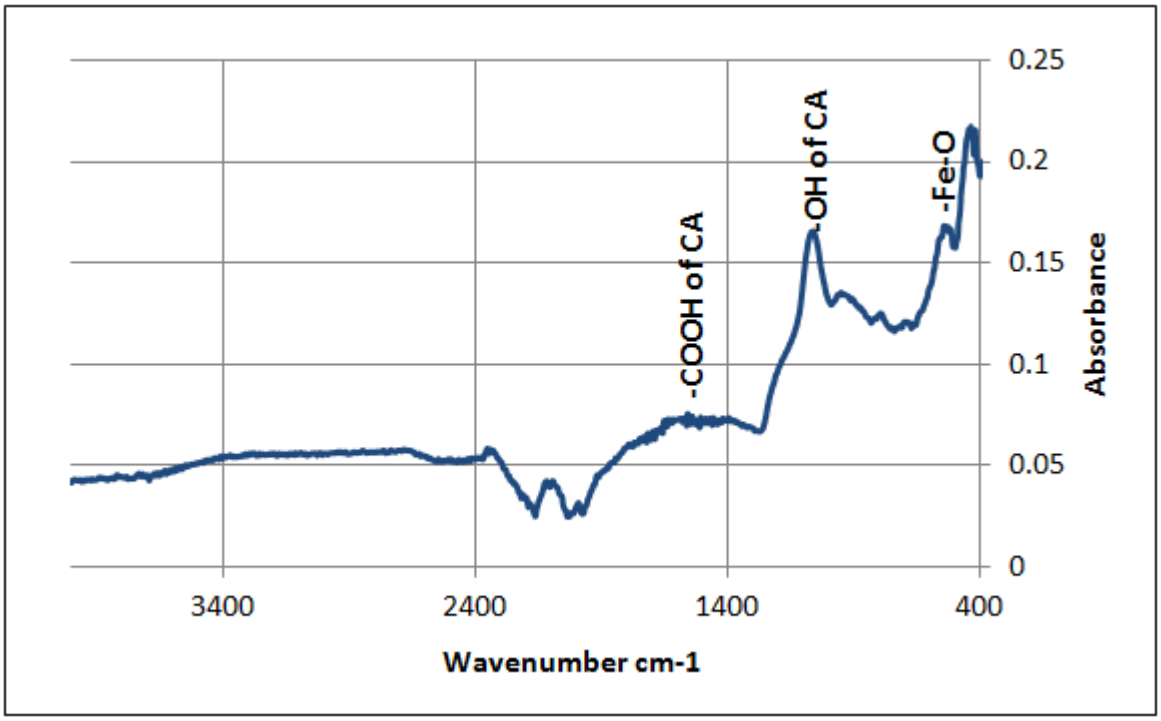

Figure 5-54: FTIR spectra of SC-45+BUF

From FTIR spectra of SC-45+BUF in figure 5-54, typical peaks of Fe-O stretching at 539.9 cm^{-1} were observed, which may correspond to the or magnetite or hematite [27, 28]. The absence of peaks of silica is in accordance with the observation in the SEM images due to the dissolution of amorphous glassy matrix. Signals at 1565 cm^{-1} and 1055 cm^{-1} may be attributed to asymmetrical stretching of the COOH group of citric acid and the symmetrical stretching of the -OH group of citric acid.

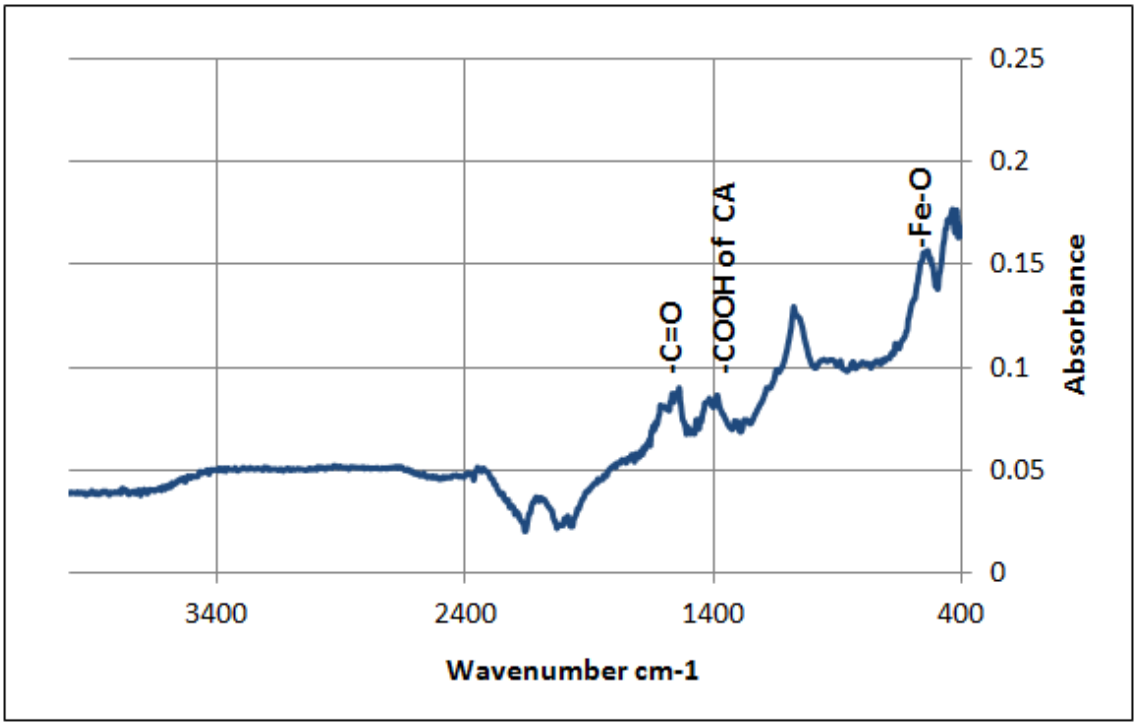

Figure 5-55: FTIR spectra of SC-45+BUF-GA

From FTIR spectra of SC-45+BUF-GA in figure 5-55, a peak corresponding to the stretching Fe-O can be observed with position at 554.0 cm^{-1} between that for hematite (540 cm^{-1}) and magnetite (570 cm^{-1}). Peaks at 1574 cm^{-1} and 1372 cm^{-1} can be attributed to asymmetrical stretching of the C=O of -COOH group, symmetric stretching of the –COO group from citric acid or calcium citrate, whose signals are at 1400 cm^{-1} (figure 5-55). Peaks at 1058 cm^{-1} are attributed to the symmetric stretching of the OH group of citric acid.

Figure 5-56 reported the FTIR spectra of commercial calcium citrate, deposit in SC-45+BUF and deposit in SC-45+BUF-GA. It can be observed that the graphs obtained are identical, therefore it can be concluded that the white deposits present on the samples that have been in contact with the citrate buffer are actually citrates of calcium.

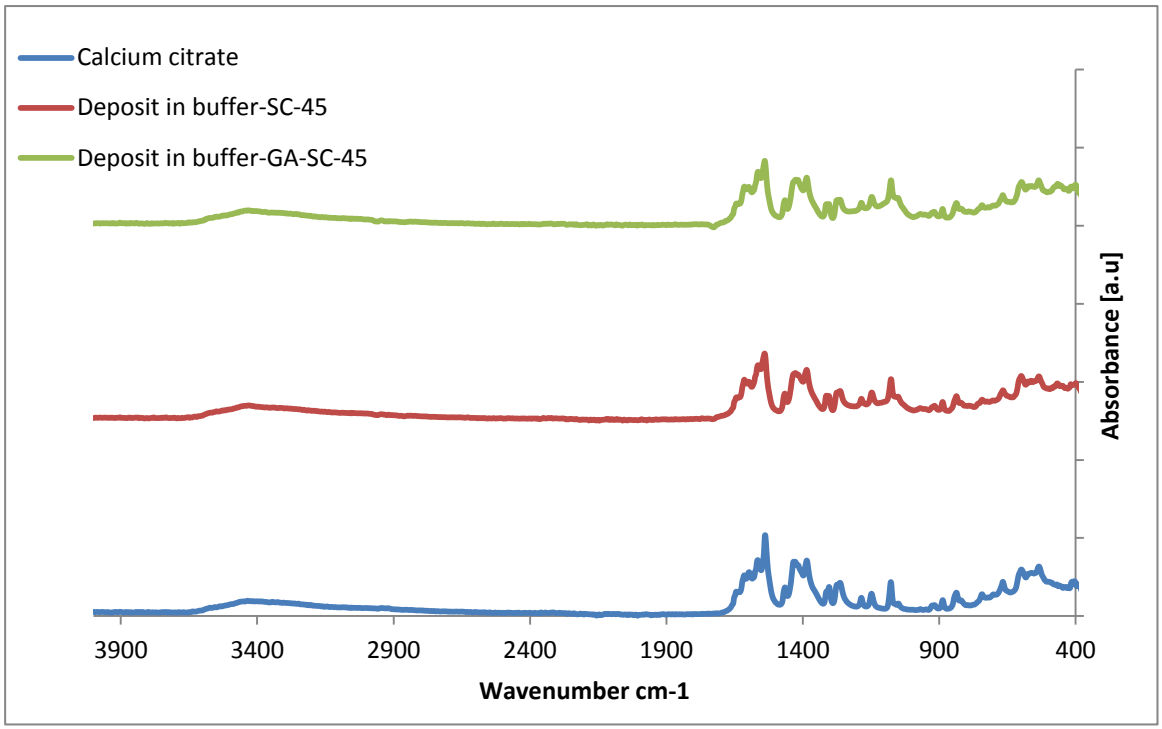

Figure 5-56 FTIR spectra of calcium citrate, deposit in SC-45+BUF and deposit in SC-45+BUF-GA

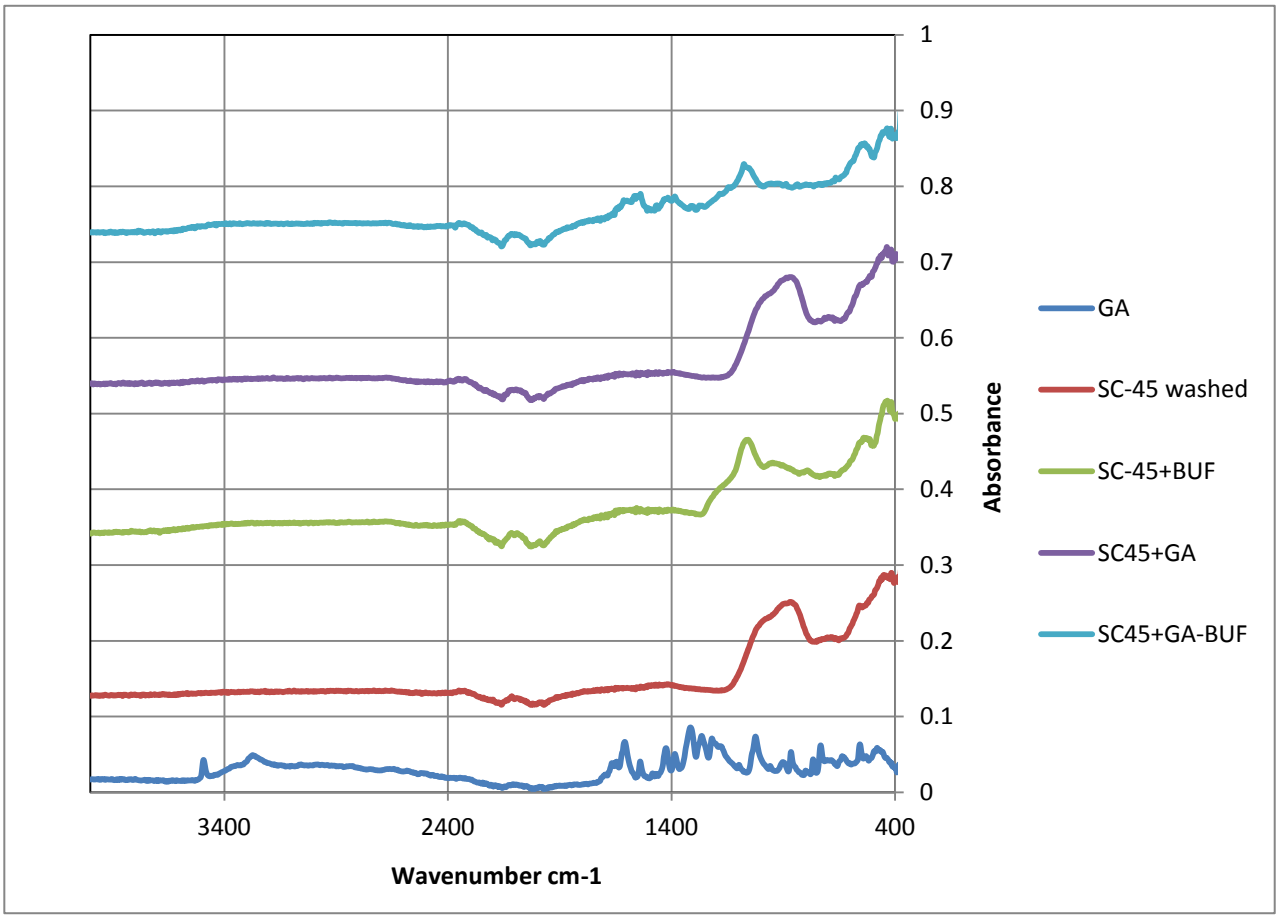

Figure 5-57: FTIR spectra of all the samples analyzed

Figure 5-57 reports the FTIR spectra of all the samples analyzed.No significant differences have been observed in spectra of the four samples of SC-45 (washed, GA, BUF, GA+BUF) for wave numbers from 2000 cm^{-1} to 4000 cm^{-1}. In particular, the peaks of hydroxyls were not clearly observed.

A board peak in the range of 1400-1500 cm^{-1} is present on powders of washed SC-45, SC-45+GA and SC-45+BUF, while for the powders of SC-45+ BUF-GA, two distinct peaks at 1574.2cm^{-1} and 1371.6 cm^{-1} have been observed and can be attributed to the link between magnetite and citric acid or, the C=C stretching of the aromatic ring and the vibration of the phenolic -OH group of the gallic acid or calcium citrate, respectively.

A peak at about 1055 cm^{-1} can be observed on the two samples treated with the buffer, they can be attributed to a link between citric acid and magnetite (symmetric stretching of the OH group citric acid). A peak at about 880 cm^{-1} can be observed for washed SC-45 and SC-45+GA samples but not for the ones treated with the buffer. This signal can be attributed to silica, and its behavior confirms the dissolution of the silica-based glassy matrix for buffer treated surfaces.

According to literature [24, 25], the peak at 575 cm^{-1} is related to stretching Fe-O of magnetite (Fe_3O_4); and peak at 539.85 cm^{-1} is attributed to hematite. SC-45+BUF-GA present a signal at 554.02 cm^{-1} that can be attributed to the Fe-O stretching vibration of magnetite or hematite, since peak located within the range of characteristic wavelength of these two iron oxides.

5.7 Antioxidant properties

Powder samples of SC-45 washed, SC-45+GA, SC-45+BUF and SC-45+BUF-GA were suspended in a buffered solution (PB, pH 7.4) of H_2O_2 in the presence of DMPO as a spin trap to test the release of HO • radicals in buffer solution. The electron paramagnetic resonance spectroscopy (EPR) spectra were recorded on aqueous suspension after 10, 30 and 60 minutes of incubation.

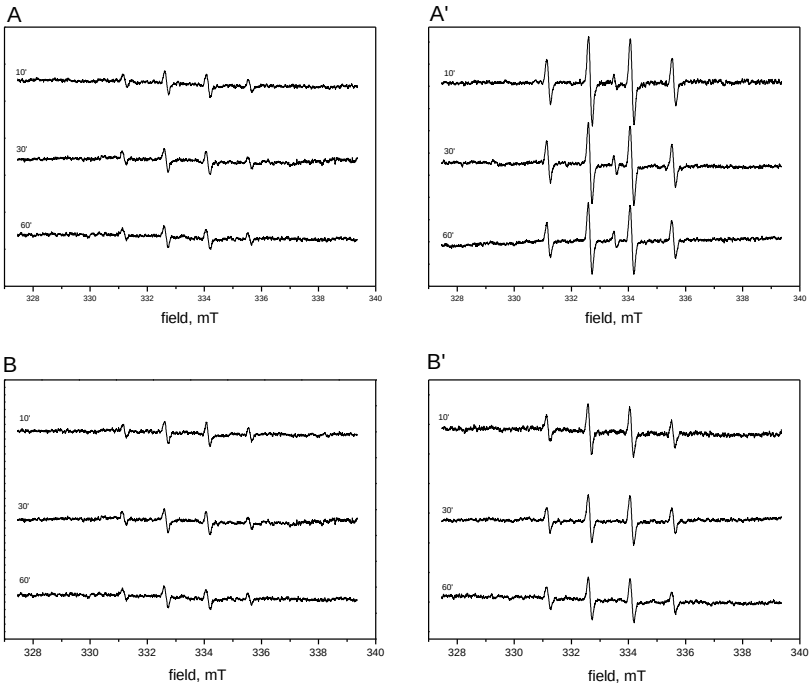

Figure 5-58 HO• radicals release by suspensions in buffer solution of A) washed SC-45, A') SC-45+GA, B) SC-45+BUF and B') SC-45+BUF-GA in the presence of H_2O_2 using DMPO as a spin trap.

In general (figure 5-58), all samples are able to generate HO• radicals suggesting a reactivity of Fenton. Moreover, for all samples, that a radical production which remains constant over time is observed. Washed SC-45 and SC-45+BUF produced similar amount of radicals, while samples after modification with gallic acid, an increase of reactivity can be detected for both samples, which suggests the pro-oxidant activity of gallic acid [29].The reason can be that when phenolic are under the condition which favor their autoxidation, such as high pH with high concentration of iron or with the presence of oxygen, they tend to behave like prooxidant [30] as described in chapter 1, section 4.2.1.3. However, a number of recent researches investigated the pro-oxidant effects of phenol and have also been suggested as potential mechanisms for cancer prevention [31-33] by induction of apoptosis and inhibition of cell proliferation [34, 35] as well as effect on cell signaling [36, 37].

In the spectra recorded in the presence of SC-45+GA, the signal of HO• appears superimposed, while that of SC-45+BUF-GA is not yet identified. This phenomenon can be assigned to an inhibitory effect of the citrate buffer on the generation of this radical.

6 Surface functionalization of SC-45 with folic acid

In addition to gallic acid grafting, SC-45 bulk and powder samples have been silanized and functionalized with folic acid (FA). The combination of folic acid and SC-45 may provide a new method for tumor detection and hyperthermia treatment. Techniques such as XPS and FTIR were employed in order to evaluate the effectiveness of surface functionalization. The names of samples and techniques for characterization are listed in Table 6-1.

Table 6-1 Names and analysis techniques employed

Sample name	Treatment	Analysis
Washed SC45	Hydroxylation	XPS
SC45+SIL	Hydroxylation and silanization	XPS
SC45+SIL+DCC+FA	Hydroxylation, silanization and FA grafting	XPS, FTIR

6.1 XPS analysis

The atomic percentages of the elements are listed in Table 6-2 after detected on sample surfaces (washed SC-45, SC-45+SIL, SC-45+SIL+DCC) at different steps of functionalization process by XPS. Although a good clean degree can be obtained by washing, a certain amount of unavoidable carbon contaminants still remain on the surfaces as described in literature [13, 14]. After silanization, on SC45 surface an increase in surface carbon content can be noticed compared with the washed one, while a further increase of carbon can be observed on the folic acid grafted samples. This phenomenon suggests the contribution of APTES and FA. In addition, that nitrogen nearly absent on washed SC45 surface appeared on silanized and FA grafted samples can be a first index of presence of APTES and FA on the surface.

Table 6-2 XPS atomic percentages of elements in the analyzed samples

Element [at %]	Washed SC45	SC45+SIL	SC45+SIL+DCC+FA
O	54.5	43.8	36.3
C	29.9	40.0	46.5
N	1.6	5.0	9.2
Fe	6.4	4.0	4.0
P	1.9	1.0	0.8
Si	2.4	4.8	2.3
Ca	3.4	0.7	0.7
Na	-	0.7	0.1

Washed SC-45

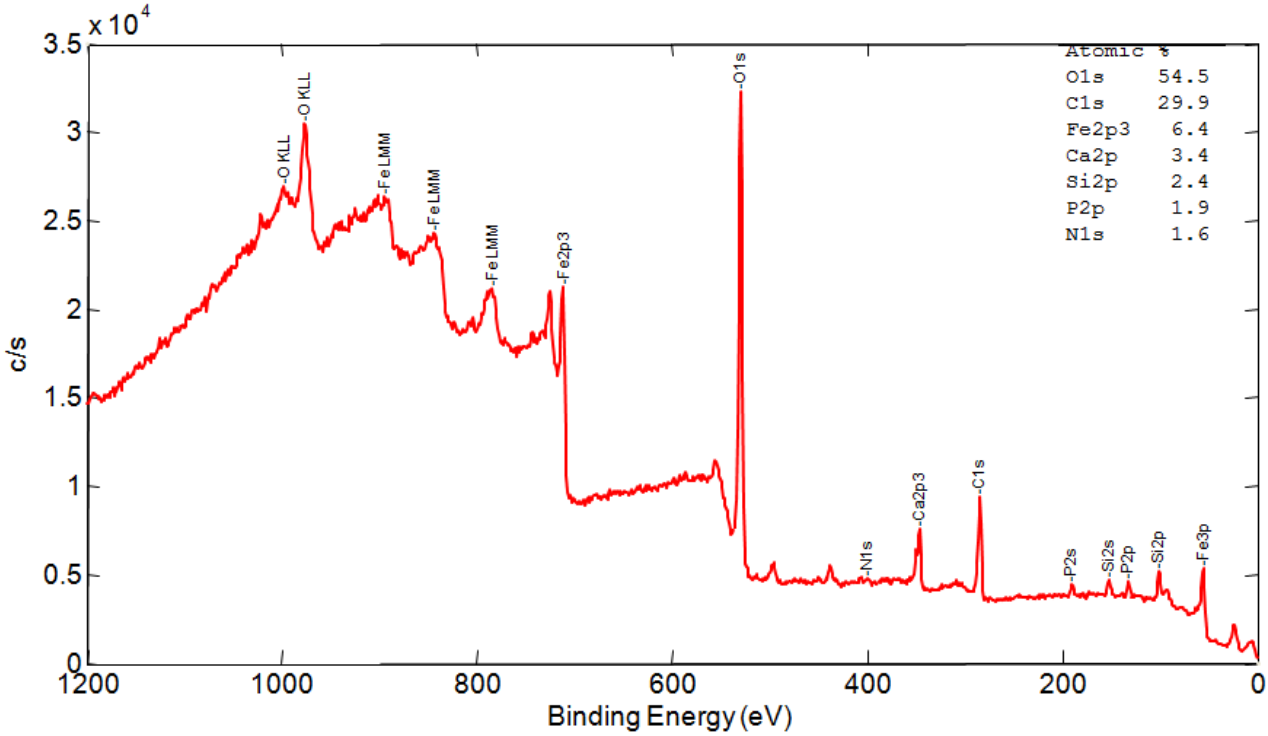

Figure 6-1: Survey spectra of washed SC-45

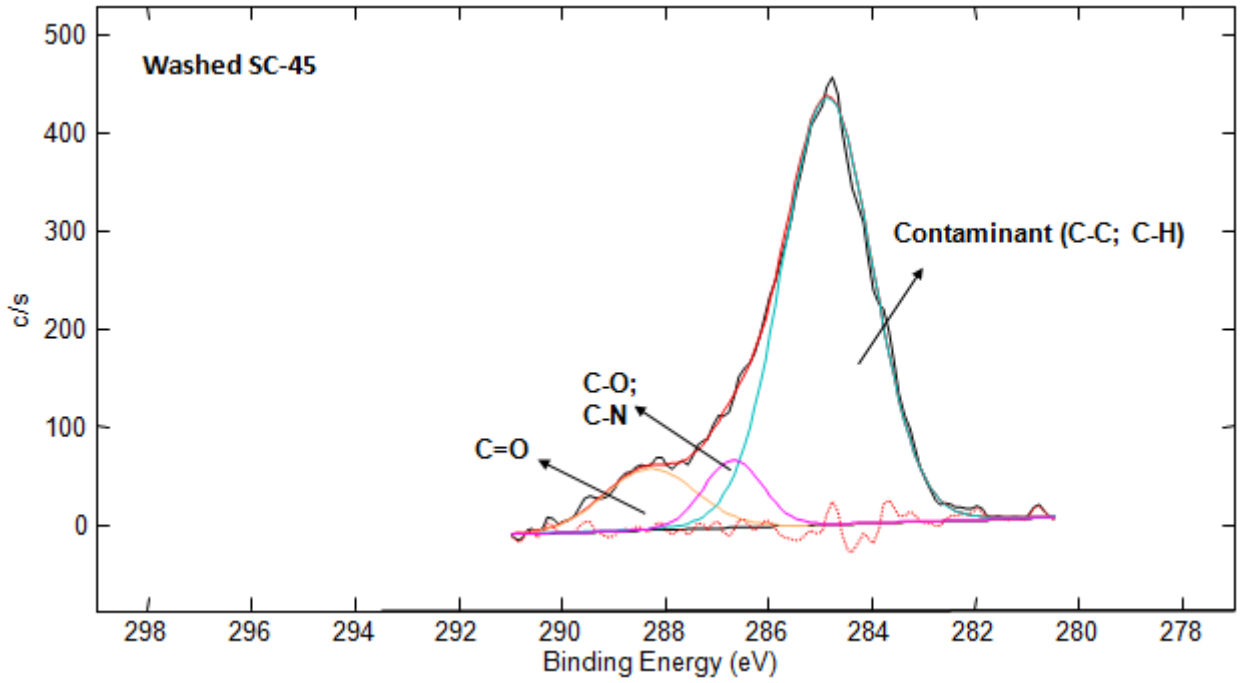

Figure 6-2: XPS detailed analysis of carbon region for washed SC-45 samples

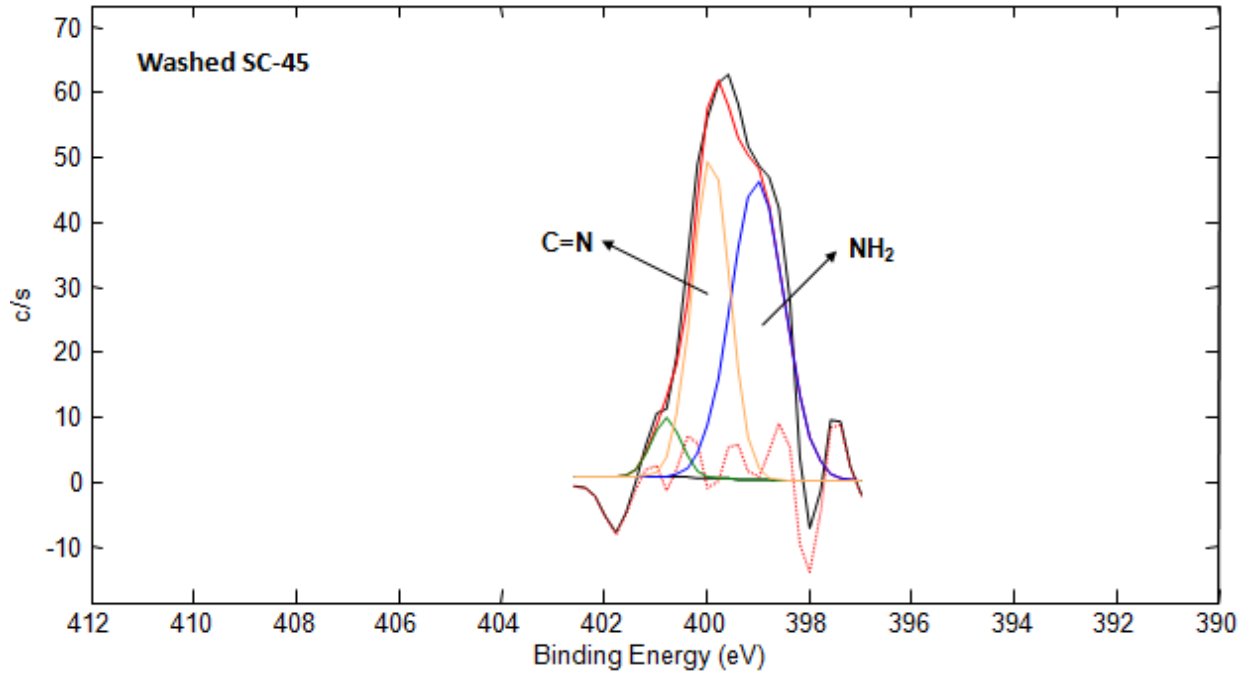

Figure 6-3: XPS detailed analysis of nitrogen region for washed SC-45 samples

Figure 6-1 presents the survey spectrum of washed SC-45, in which the elements present on the surface of bulk samples are highlighted. Elements from glass-ceramic composition can be

observed, including oxygen, iron, calcium, phosphorus, and silicon. The presence of carbon and nitrogen on the first surface layer of materials, even in non-functionalized samples, is due to the unavoidable atmospheric contaminants [13, 14]. It can be noted that sodium has not been detected; this phenomenon can be attributed to the ion release of the glass-ceramic in the washing media, as previously observed for SCNA and CEL2 glasses (chapter V, section 2.4).

In figure 6-2, the detailed analysis spectrum of carbon region shows a signal at about 284.88 eV which can be attributed to environmental contaminants, as the reactive surface easily absorb hydrocarbons from the atmosphere. Other signals at 286.25 eV and 288.44 eV are assigned to C-O /C-N and C=O bond respectively [6, 22-24]; they are very small on this sample and can be attributed to contamination too.

Figure 6-3 presents the spectrum of the detailed analysis of nitrogen region. Signals at 399.01 eV and 399.92 eV can be assigned to $–NH_2$ and C=N in the contaminants, respectively according to literature [38, 39].

SC-45+SIL

Figure 6-4 shows the survey spectrum of SC-45+SIL, in which all elements present on the surface of bulk samples are highlighted. Elements from glass-ceramic composition can be observed, including oxygen, calcium and silicon. It can be observed that the content of nitrogen as well as carbon content increased notably, due to the contributions of APTES.

In figure 6-5, the detailed analysis spectrum of carbon region shows a signal at about 284.92 eV which can be attributed to environmental contaminants and in this case, it can also assigned to the characteristic carbon bond (C-C) present in APTES as described in [14]. Other signals at 286.71 eV and 288.17 eV are assigned to C-O /C-N and C=O bond respectively [22-24].

In the detailed spectrum of nitrogen region in figure 6-6, the main contributions at about 400.26 eV can be observed and attributed to NH_2 from APTES molecule. The other peak with lower intensity can be assigned to C=N and CONH in contaminants [13].

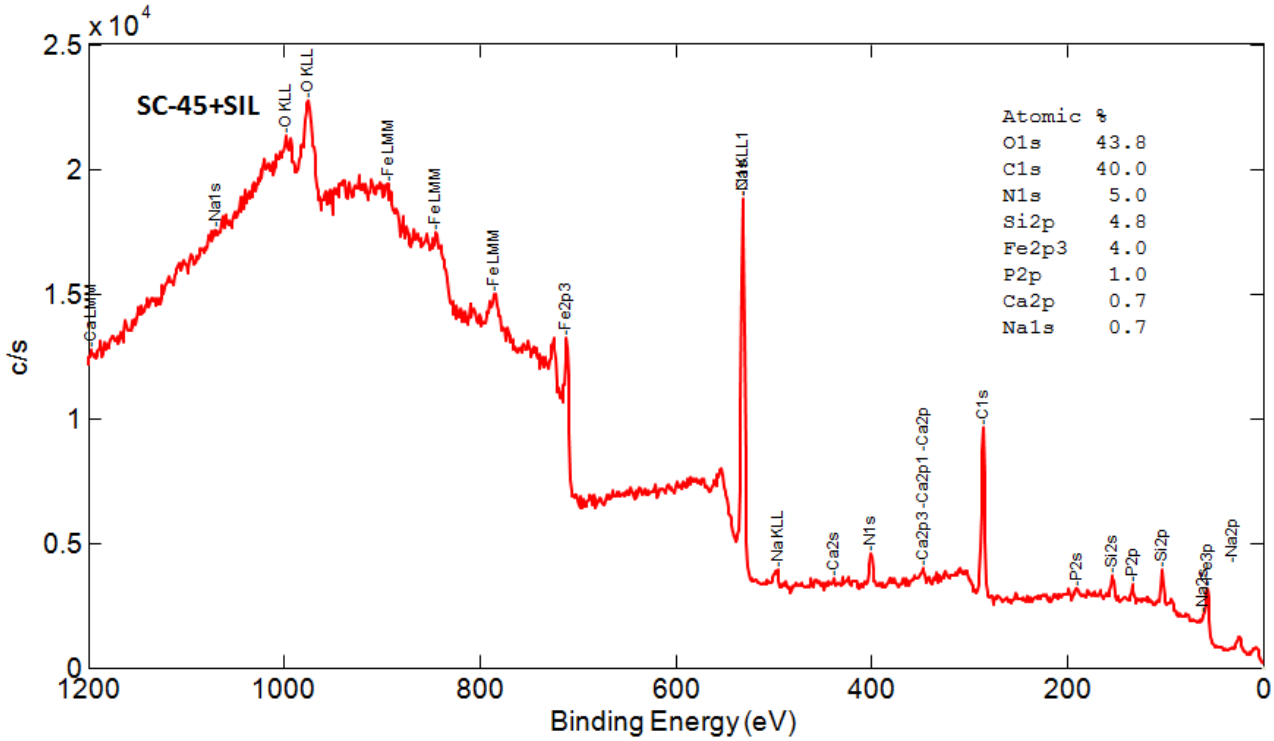

Figure 6-4: Survey spectra of SC-45+SIL

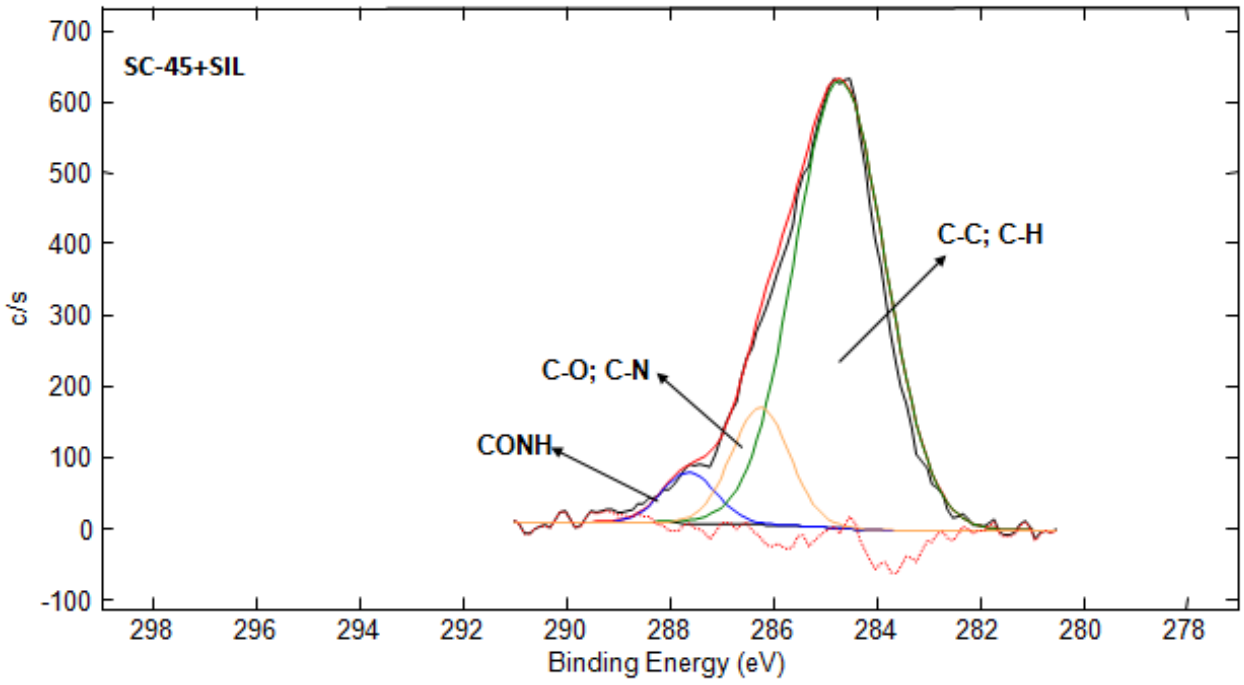

Figure 6-5: XPS detailed analysis of carbon region for SC-45+SIL samples

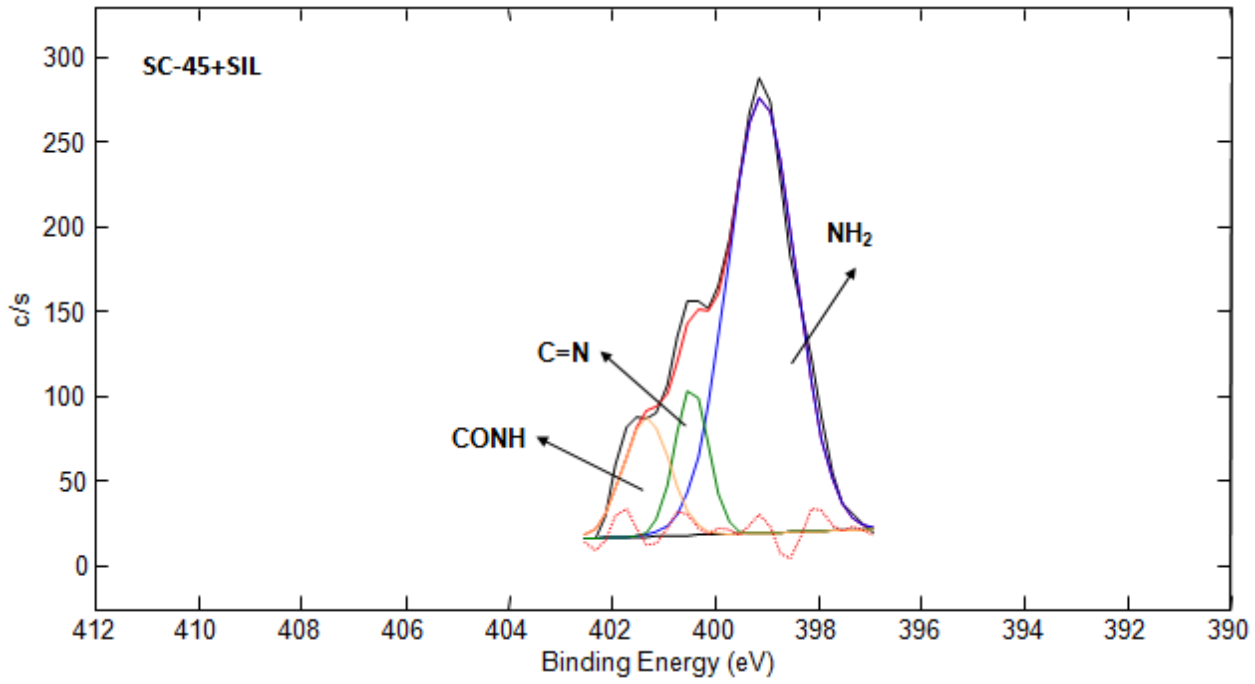

Figure 6-6: XPS detailed analysis of nitrogen region for SC-45+SIL samples

SC-45+SIL+DCC+FA

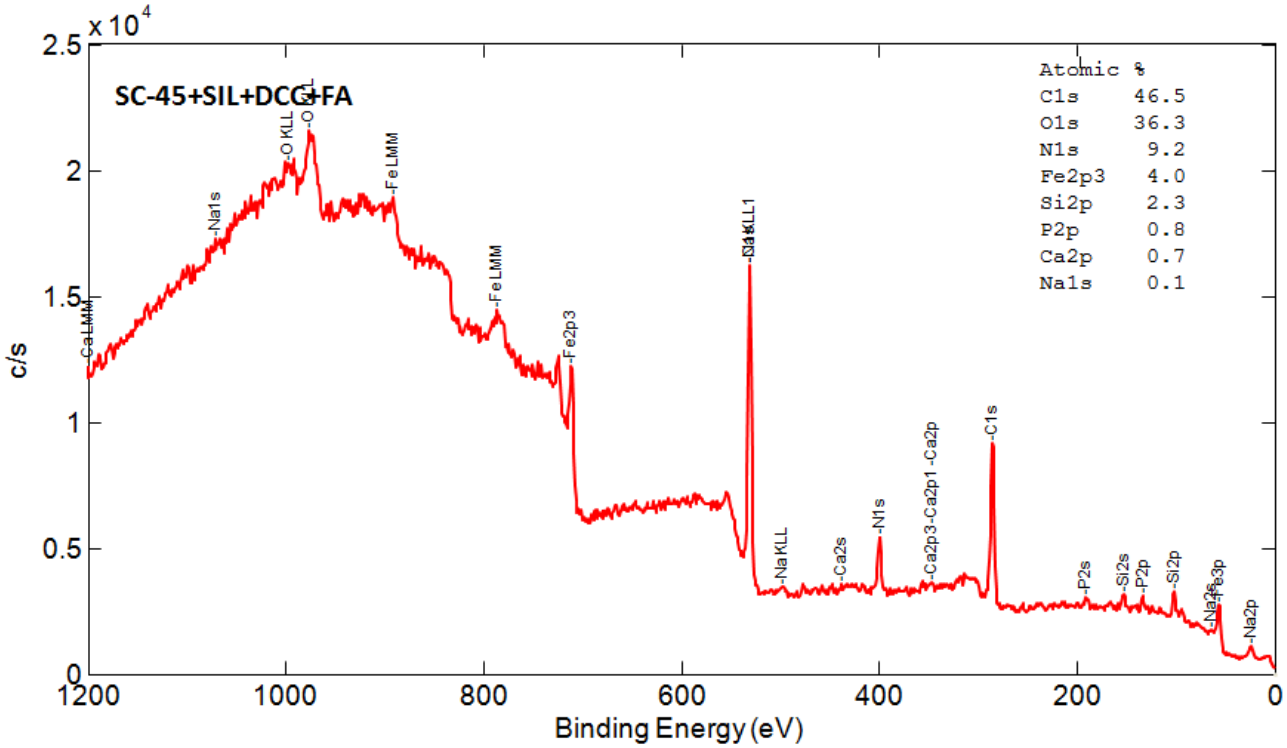

Figure 6-7: Survey spectra of SC-45+SIL+DCC+FA

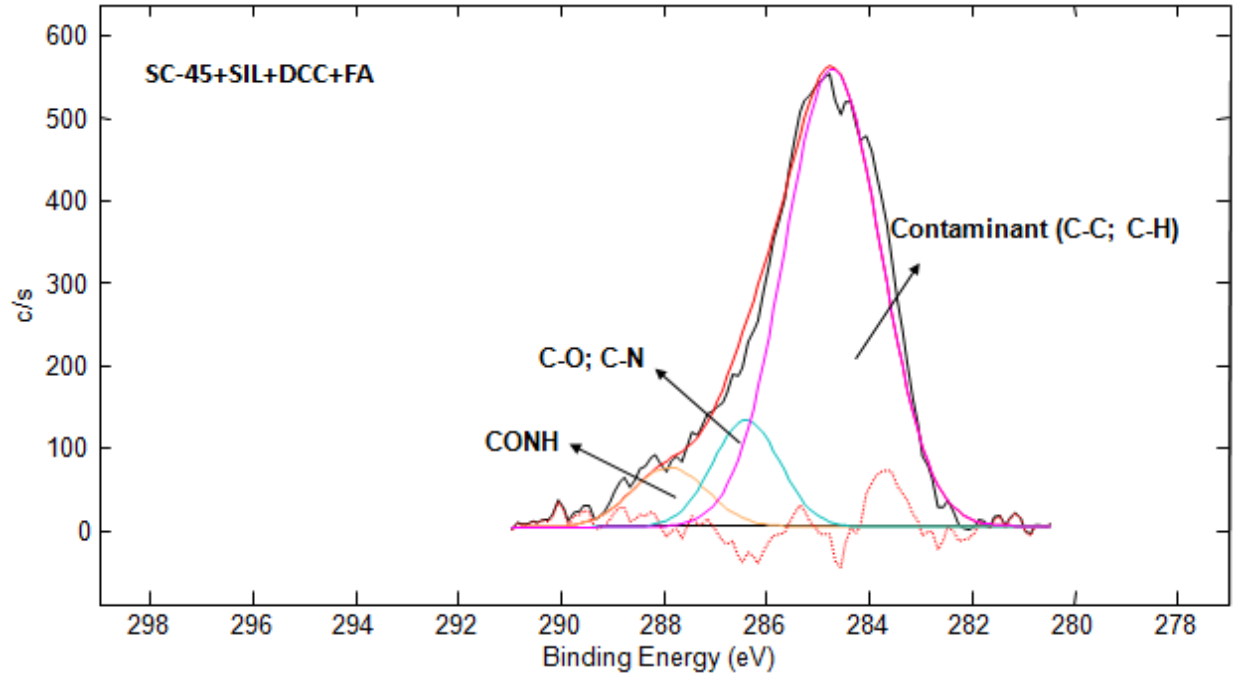

Figure 6-8: XPS detailed analysis of carbon region for SC-45+SIL+DCC+FA samples

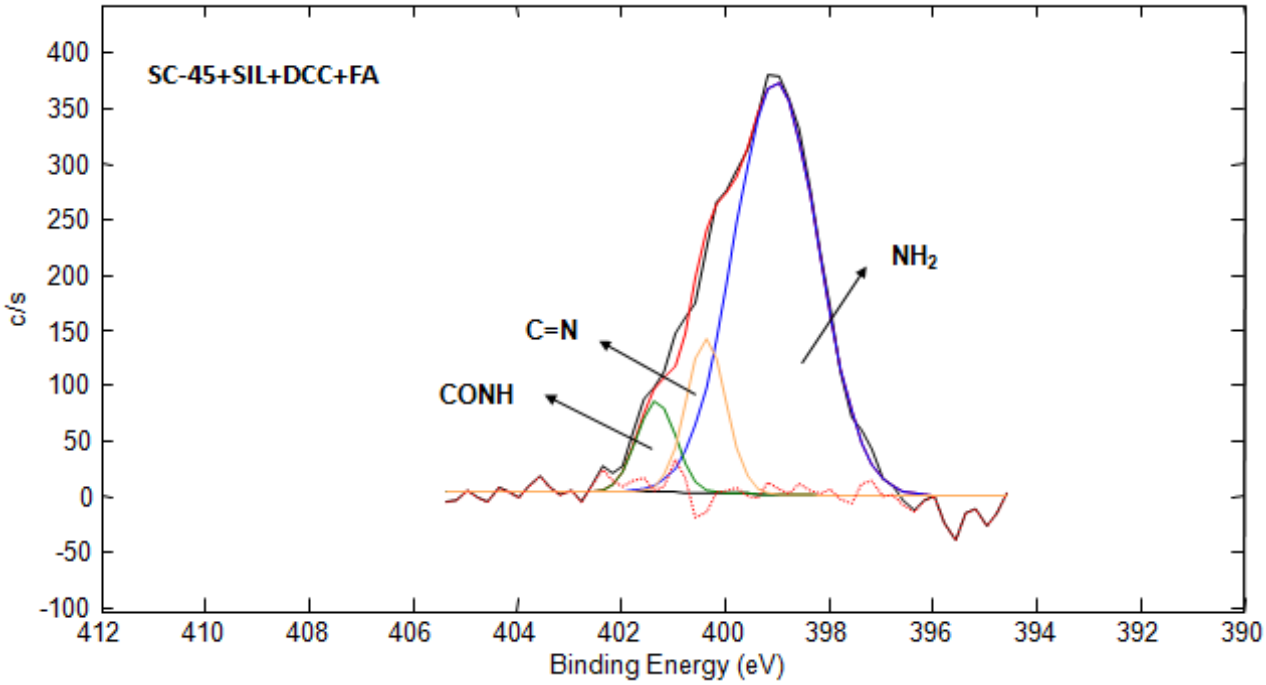

Figure 6-9: XPS detailed analysis of nitrogen region for SC-45+SIL+DCC+FA samples

Figure 6-7 presents the survey spectrum of SC-45+SIL+DCC+FA, in which all elements present on the surface of bulk samples are highlighted. Elements including oxygen, iron, calcium, silicon from glass-ceramic composition can be observed. It should be underlined that a significantly

increase of carbon and nitrogen can be observed, if compared with SC-45+SIL. It can be assumed that the contribution of folic acid molecule leads to the increase.

In figure 6-8 (detailed spectrum of carbon region), the main contribution at about 284.71 can be attributed to C-C bond in APTES molecule as well as the contaminants from atmosphere. It should be noticed that signal of C=O on washed SC-45 and SC-45+SIL at about 288.3 eV disappeared and instead a new contribution at 287.89 eV was detected. According to literature, it can be assigned to CONH group in folic acid structure [14].

In spectrum of nitrogen region (figure 6-9), signals at 399.1 eV can be assigned to NH_2 group in APTES as well as that in folic acid structure. Another peak at 400.35 eV can be corresponded to C=N bond in folic acid. In addition, the signal with higher energy at about 401.31 eV can be correlated to NHCO bonds of folic acid [14].

6.2 FTIR analysis

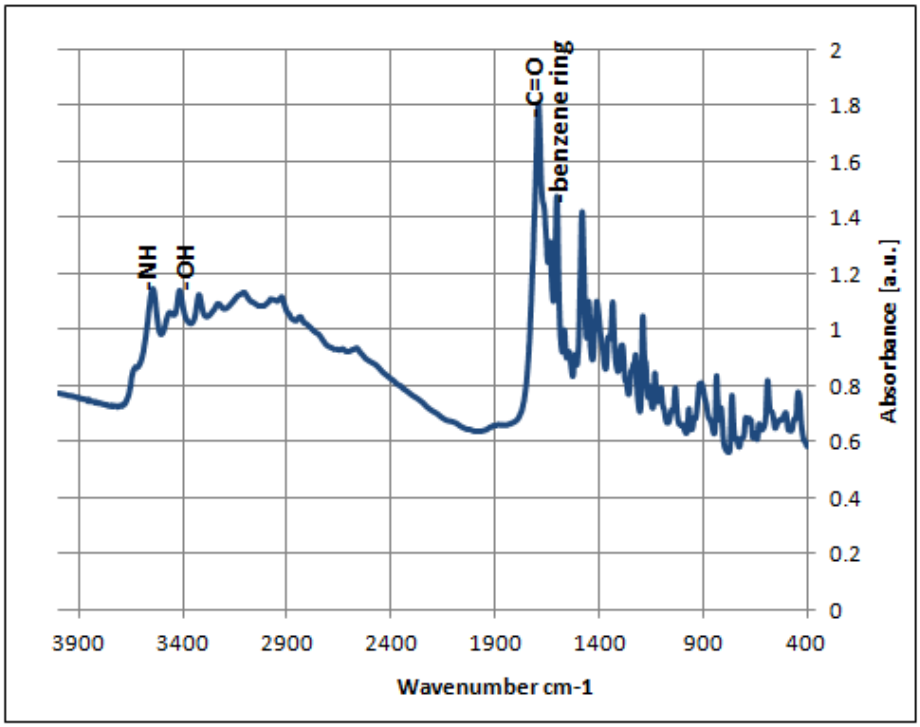

Figure 6-10: FTIR spectra of folic acid

Folic acid spectrum (figure 6-10) evidences the characteristic peaks of the molecule: the bands between 3600 and 3400 cm^{-1} are due to the hydroxyl (–OH) stretching bands of glutamic acid moiety and –NH group of PT ring. Peak at 1690 cm^{-1} is due to the vibration of C=O, while the peak at 1605 cm^{-1} relates to benzene ring as described in literature [38].

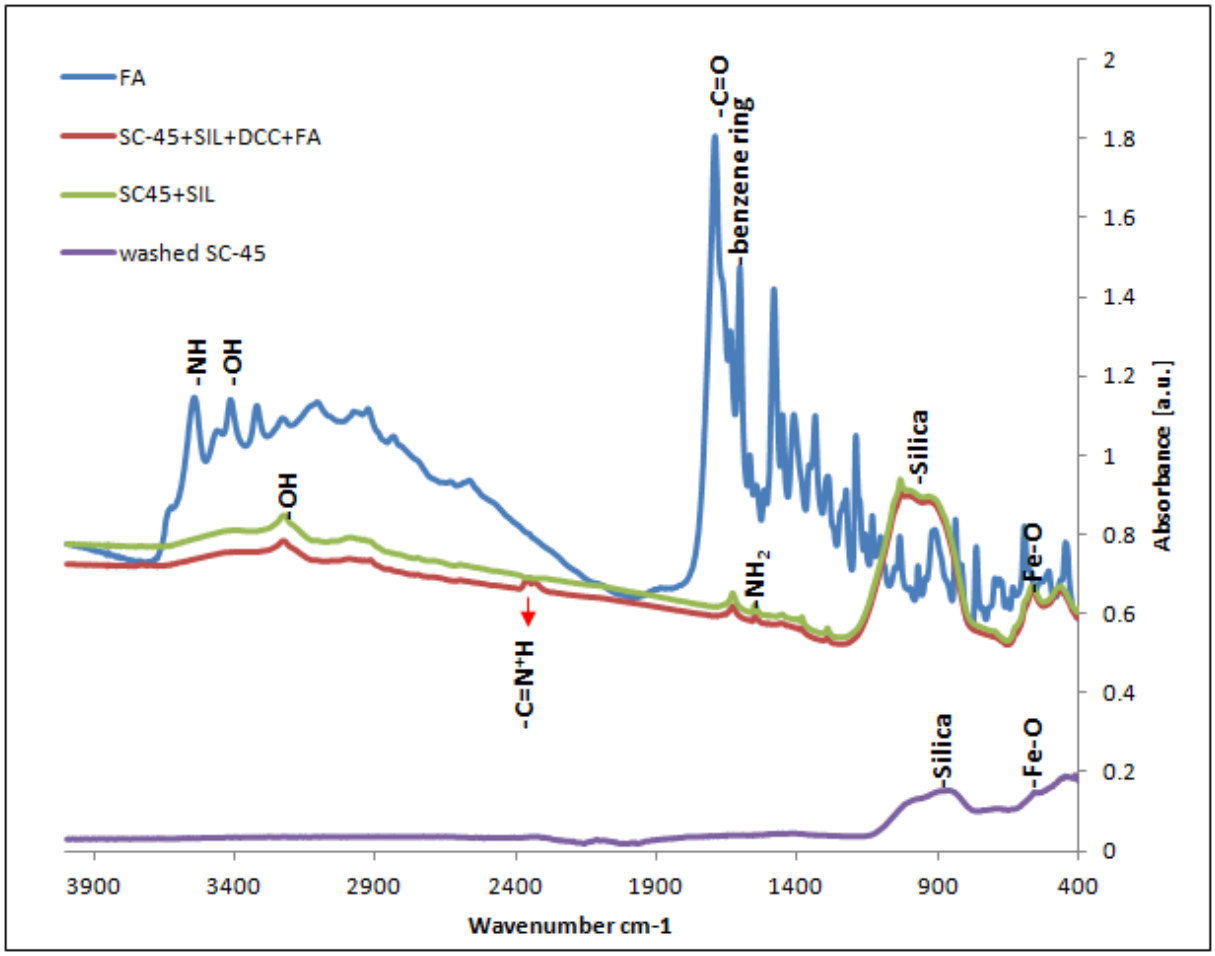

Figure 6-11: FTIR spectra of folic acid, washed SC-45, SC-45+SIL and SC-45+SIL+DCC+FA

Figure 6-11 reports the comparison among FTIR spectra of folic acid, washed SC-45, SC-45+SIL and SC-45+SIL+DCC+FA. The washed SC-45 powders present the typical signal for silica at 928 cm^{-1} and iron oxides at about 558 cm^{-1}. After silanization, in addition to the signals of silica and iron oxide, signals of -OH groups can be observed at 3230 cm^{-1}, while the appearance of peaks at about 1553 cm^{-1} can be assigned to amino group of APES molecule [38, 39], if compared with washed SC-45. With DCC activation and folic acid grafting, the presence of peak at about 2384 cm^{-1} can be ascribed to N^{+}-H stretching vibration band of $C=N^{+}H$- on PT

ring from folic acid structure as described in the literature [38].

References

[1] Vernè E, Vitale-Brovarone C, Bui E, et al. Surface functionalization of bioactive glasses. J Biomed Mater Res 2009; 90A: 981-992

[2] Vernè E, Bretcanu O, Balagna C, et al. Early stage reactivity and in vitro behaviour of silica-based bioactive glasses and glass–ceramics. J Mater Sci: Mater Med 2009; 20: 75-87

[3] Yang Z, Wu J, Wang X, et al. Inspired chemistry for a simple but highly effective immobilization of vascular endothelial growth factor on gallic aicd functionalized plasma polymerized film. Plasma Processes Polym 2012; 9: 718-725

[4] Textor M, Sittig C, Frauchiger V, Tet al. Properties and biological significance of natural oxide films on titanium and its alloys. In: Titanium in Medicine (Eds.: Tengvall P, Textor M, Thomsen P), Springer-Verlag: Berlin, Heidelberg, New York, 2001; pp: 171-230

[5] X-Ray Photoelectron Spectroscopy Reference pages, 2013, C1s Carbonates: http://www.xpsfitting.com/2011/03/c-1s-carbonates.html, Copyright M. C. Biesinger (http://www.xpsfitting.com/),

[6] Vernè E, Ferraris S, Vitale-Brovarone C, et al. Alkaline phosphatase grafting on bioactive glasses and glass-ceramics. Acta Biomater 2010; 6: 229-240

[7] Mowlder JF, Stickle WF, Sobol PE, et al. Handbook of X-Ray Photo-electron Spectroscopy: A Reference Book of Standard Spectra for Identification and Interpretation of XPS Data, Physical Electronic, USA, 1995.

[8] Naumkin AV , Kraut-Vass A, Gaarenstroom SW, Powell CJ, NIST X-ray Photo-electron Spectroscopy Database, NIST Standard Reference Database 20, Version 4.1, 2013, http://srdata.nist.gov/xps/selEnergyType.aspx, 2012 copyright by the U.S. Secretary of Commerce on behalf of the United States of America.

[9] Yang Z, Wu J, Wang X, et al. Inspired chemistry for a simple but highly effective immobilization of vascular endothelial growth factor on GA functionalized plasma polymerized film. Plasma Processes Polym 2012; 9: 718-725

[10] Qiao G, Su J, He M. Effect of (-)-epigallocatechin gallate on electrochemical behavior and surface film composition of Co–Cr alloy used in dental restorations. Dent Mater J 2012; 31: 564-574

[11] He L, Wu H, Gao S, et al. Silver nanoparticles stabilized by tannin grafted collagen fiber: Synthesis, characterization and antifungal activity. Ann Microbiol 2012; 62: 319-327

[12] Morra M, Cassinelli C, Buzzone G, et al. Surface chemistry effects of topographic modification of titanium dental implant surfaces, 1 surface analysis. Int J Oral Maxillofac Implants 2003; 18: 40-45

[13] Ferraz MP, Monteiro FJ, Santos JD. $CaO–P_2O_5$ glass hydroxyapatite double layer plasma spray coating: in vitro bioactivity evaluation. J Biomed Mater Res 1999; 45: 376-383

[14] Ferraris S, Perero S, Vernè E, et al. Surface functionalization of Ag–nanoclusters–silica composite films for biosensing. Mater Chem Phys 2011; 130: 1307-1316

[15] Mohammad YG, Mohd ZH. Controlled release study of an anti-carcinogenic agent, gallate from the surface of magnetite nanoparticles. J Phys Chem Solids 2012; 73: 936-942

[16] Kong XG, Jin L, Wei M, et al. Antioxidant drugs intercalated into layered double hydroxide: Structure and in vitro release. Appl Clay Sci 2010; 49: 324-329

[17] Vaid C, Murugavel S. Alkali oxide containing mesoporous bioactive glasses: Synthesis, characterization and in vitro bioactivity. Mater Sci Eng C 2013; 33: 959-968

[18] Pirayesh H, Nychka JA. Sol-Gel Synthesis of Bioactive Glass-Ceramic 45S5 and its in vitro Dissolution and Mineralization Behavior. J Am Ceram Soc 2013; 96: 1643-1650

[19] Wang H, Chen X, Wang Y, et al. Preparation and characterization of the system SiO_2-CaO-P_2O_5 bioactive glasses by microemulsion approach. J Wuhan University Technology-Mater Sci Ed 2013; 1053-1057

[20] Xia EQ, Deng GF, Guo YJ, et al. Biological activities of polyphenols from grapes. Int J Mol Sci 2012; 11: 622-646

[21] Rouchon-Quillet V, Remazeilles C, Bernard J, et al. The impact of gallic acid on iron gall ink corrosion. Applied physics A, 2004; 79 (2), 389-392

[22] Miller DJ, Biesinger MC, McIntyre NS. Interactions of CO_2 and CO at fractional atmosphere pressures with iron and iron oxide surfaces: one possible mechanism for surface contamination? Surf Interface Anal 2002; 33: 299-305

[23] http://www.xpsfitting.com/2008/10/using-adventitious-carbon-for-charge.html

[24] http://xpssimplified.com/elements/carbon.php

[25] Vern è E, Miola M, Ferraris S, et al. Surface activation of a ferrimagnetic glass-ceramic for antineoplastic drugs grafting. Adv En Mater 2010; 12: 309-319

[26] Yoshida Y, Van Meerbeek B, Nakayama Y, et al. Adhesion to and Decalcification of Hydroxyapatite by Carboxylic Acids. Journal of Dental Research, 2001; 80 (6): 1565-1569

[27] Nigam S, Barick KC, Bahadur D. Development of citrate-stabilized Fe_3O_4 nanoparticles: Conjugationand release of doxorubicin for therapeutic applications. J Magn Magn Mate 2011; 323: 237-243

[28] Bruce IJ, Taylor J, Todd M, et al. Synthesis, characterisation and application of silica-magnetite nanocomposites. J Magn Magn Mate 2004; 284: 145-160

[29] Yen GC, Duh PD, Tsai HL. Antioxidant and pro-oxidant properties of ascorbic acid and gallic acid. Food Chem 2002; 79: 307-313

[30] Lambert JD, Elias RJ. The antioxidant and pro-oxidant activities of green tea polyphenols: A role in cancer prevention. Arch Biochem Biophys 2010; 501: 65-72

[31] Hou Z, Sang S, You H, et al. Mechanism of action of (−)-epigallocatechin-3-gallate: aAuto-oxidation-dependent inactivation of epidermal growth factor receptor and direct effects on growth inhibition in human esophageal cancer KYSE 150. CellsCancer res 2005; 65: 8049-8056

[32] G Shen, Xu C, Hu R, et al. Comparison of (−)-epigallocatechin-3-gallate elicited liver and small intestine gene expression profiles between C57BL/6J mice and C57BL/6J/Nrf2 (−/−) mice. Pharm

Res 2005; 22: 1805-1820

[33] Butt MS, Sultan MT. Green tea: nature's defense against malignancies Crit Rev Food Sci Nutr 2009; 49: 46347

[34] Yang GY, Liao J, Li C, et al. Effect of black and green tea polyphenols on c-jun phosphorylation and H2O2 production in transformed and non-transformed human bronchial cell lines: possible mechanisms of cell growth inhibition and apoptosis induction. Carcinogenesis 2000; 21: 2035-2039

[35] Nakagawa H, Hasumi K, Woo JT, et al. Generation of hydrogen peroxide primarily contributes to the induction of Fe(II)-dependent apoptosis in Jurkat cells by (−)-epigallocatechin gallate. Carcinogenesis 2004; 25: 1567-1574

[36] Liang YC, Lin-shiau SY, Chen CF, et al. Suppression of extracellular signals and cell proliferation through EGF receptor binding by (2)-epigallocatechin gallate in human A431 epidermoid carcinoma cells. J Cell Biochem 1997; 67: 55-65

[37] M Muzolf-Panek, Gliszczynska-Swiglo A, de Haan L, et al. Role of catechin quinones in the induction of EpRE-mediated gene expression. Chem ResToxicol 2008; 21: 2352-2360

[38] He YY, Wang XC, Jin PK, et al. Complexation of anthracene with folic acid studied by FTIR and UV spectroscopies. Spectrochim Acta A 2009; 72: 876-879

[39] Figaroa S, Louisy-Louis S, Lambert J, et al. Adsorption studies of recalcitrant compounds of molasses spent wash on activated carbons. Water res 2006; 40: 3456-3466

Conclusions

Two types of sources were employed for the natural polyphenol extraction. One is red grape (Barbera) from Italy, while the other is green tea (Longjing) from China. Both the grape polyphenol (GP) and tea polyphenol (TP) were extracted by conventional solvent extraction. The solvent system used for GP extraction was water-ethanol (20:80, v/v) solution, while two solvent systems, which were water and water-ethanol (20:80, v/v), respectively, were adopted in TP extraction. Through Folin-Ciocalteau colorimetry and calibration curve (linear correlation coefficient R^2=0.9997), the presence and total phenol content of both polyphenol in the freeze dried extracts was determined. The total phenol content of grape polyphenol is 14.6 mg/g (freeze dried extracts). Considering the total phenol content of tea polyphenol, the phenol masses from 1 g green tea leaves were 152.8 mg (extracted from water-ethanol system) and 67.4 mg (extracted from double distilled water system). Compared with the tea polyphenol extracted from water system, tea polyphenol from water-ethanol exhibited a higher yield and total phenol content.

In this thesis, two silica-based bioactive glasses (SCNA and CEL2) with different surface reactivity were prepared as bulk and powder samples for functionalization with one model molecule (gallic acid, GA) and two natural biomolecules (grape polyphenols and tea polyphenols). After surface activation, hydroxyl groups were exposed on the material surface followed by gallic acid, grape polyphenol as well as tea polyphenol grafting.

Through Folin-Ciocalteau colorimetry combined with UV-vis spectroscopy, the depletion of GA, GP and TP in uptake solution and the content of these molecules on functionalized bulk samples were evaluated. The results suggest not only the uptake of molecule on glass surface during functionalization but also the grafting of the three types of molecules on bioactive glass samples. All three types of molecules displayed a similar tendency that the depletion of GA, GP and TP in uptake solutions and the amount of these molecules on functionalized bulks increased along with the glass reactivity from SCNA to CEL2 as well as the surface area from bulk samples to powder samples.

XPS analysis of samples after GA, GP and TP anchoring evidenced characteristic peaks for GA and polyphenol on functionalizaed samples.

Concerning for the gallic acid and grape polyphenol functionalization, citric acid addition in the fictionalization medium made it possible to preserve the structure of gallic acid and phenol molecule during grafting. Moreover, SEM observation of the surfaces confirmed the different reactivity of two types of glasses. In fact, a significant reaction layer with a uniformly cracked morphology was observed on CEL2 surfaces for both gallic acid and grape polyphenol, while only several reactive zones can be seen on gallic acid grafted SCNA samples.

In aspect of the depletion in uptake solution as well as three molecules amount on functionalized surface, gallic acid grafting exhibited the most significant results probably due to its higher phenol content and purity, followed by tea polyphenol and the last one is grape phenol. Furthermore, through the macroscopic observation, the greatest color changes on bulk sample and in uptake solution before and after functionalization were, in order gallic acid, tea polyphenol and grape polyphenol. In addition, pH changes showed similar tendency as well.

SC-45, a bioactive and ferrimagnetic glass-ceramic belonging to the system $CaO\text{-}SiO_2\text{-}P_2O_5\text{-}Na_2O\text{-}Fe_2O_3\text{-}FeO$ was also investigated as bulk and powder samples functionalized with gallic acid and buffered gallic acid (citric acid-sodium citrate buffer system) in this thesis. The glass-ceramic samples have been functionalized using the strategy of directly anchoring gallic acid to the hydroxyl groups on material surface exposed by soaking in water for 7 days. Considering the sensitivity of gallic acid in pH changes, the functionalization was performed not only using a solution of GA in water, but also with a solution of GA in citrate buffer (pH 3.0).

Analysis through Folin-Ciocalteau colorimetry and UV-vis spectroscopy demonstrated gallic acid depletion in uptake solution after grafting and the presence of gallic acid on functionalized bulks, especially for samples functionalized without citrate buffer. XPS analysis confirmed the appearance of characteristic signals of the molecule anchored on the samples functionalized with gallic acid as well as a significant increase of carbon content, but not observed for buffered gallic acid grafting. Surface morphology of the samples subjected to the different treatments has been observed by SEM / EDS: i) pretreated glass-ceramics presented magnetite crystals immersed in a glassy matrix; ii) gallic acid functionalized sample induced the formation of a significant reaction layer on surface; iii) buffer

treated samples (both with and without GA) showed a strong dissolution of amorphous surface with the exposure of magnetite crystals and hematite with small residual amorphous phase. On the buffer treated samples (both with and without GA), the precipitation of calcium citrates has been observed. The semi-quantitative analysis of the surface chemical composition (EDS) has revealed a greater concentration of carbon in the samples functionalized with GA (without buffer) compared to the pretreated ones; this phenomenon is not observed in the samples treated with the buffer. In addition, none of the samples showed the capacity to release gallic acid in water for immersion up to 24h. It is therefore possible that the gallic acid tends to bind to the hydroxyl exposed from the glass matrix and the link seems quite strong as there is no evidence of release water. As a result, the functionalization effectiveness of SC-45 with gallic acid (without buffer) is greater than that with the presence of buffer since the glass-ceramics after treated with buffer tend to dissolved and thus the possibility of bond with molecule is decreased. If compared with bioactive glasses also employed in this thesis, the reactivity of SC-45 is higher than SCNA and the results can be evidenced by the depletion of gallic acid in uptake solution, the amount of molecule on functionalized bulk surface as well as the formation of a uniformly cracked reaction layer. However, since SC-45 is a kind of glass-ceramic, its morphology is different from that of bioactive glasses and magnetic crystals have been observed by SEM.

To summarize, this thesis demonstrates that both model molecule and natural biomolecules can be coupled with synthetic inorganic materials. The results are quite new and creative in the surface functionalization field, since it proves the possibility to prepare smart biomaterials able to combine typical inorganic activity of biomaterials with specific biological properties of natural molecules. In vitro cellular tests are planned in order to verify the biological behavior of the modified materials. Moreover, analysis will be performed to determine the composition of polyphenol extracts as well as the biological activities of functionalized glass and glass-ceramic samples.

Publications

In journals:

1. **Xin Zhang**, Sara Ferraris, Enrico Prenesti, Enrica Vernè. Surface functionalization of bioactive glasses with natural molecules of biological significance, Part I: Gallic acid as model molecule. Applied Surface Science, 287 (2013) 329–340

2. **Xin Zhang**, Sara Ferraris, Enrico Prenesti, Enrica Vernè. Surface functionalization of bioactive glasses with natural molecules of biological significance, Part II: Grafting of polyphenols extracted from grape skin. Applied Surface Science, 287 (2013) 341–348

3. **Xin Zhang**, Sara Ferraris, Enrico Prenesti, Enrica Vernè. Surfacce functionalization of bioactive galsses with natural molecules of biological significance: grafting of polyphenol extracted from green tea. (to be submitted)

4. **Xin Zhang**, Sara Ferraris, Enrico Prenesti, Enrica Vernè. Surfacce functionalization of bioactive and ferrimagnetic galss-ceramics (SC45) with gallic acid and buffered gallic acid (to be submitted)

Proceedings:

1. Baino F., Balagna C., Bruno M., Ferraris M., Ferraris S., Gallo M., Miola M., Novajra G., Pan G., Perero S., Spriano S., Tallia F., Vernè E., Vitale-Brovarone C., **Zhang X**. Smart biomaterials with tailored properties. In: Terzo Congresso Gruppo Nazionale di Bioingegneria, Roma (Italy), 26-28 Giugno 2012.

2. **Xin Zhang**, Sara Ferraris, Enrica Vernè, Alberto Venturello, Enrico Prenesti. Surface functionalization of bioactive and ferrimagnetic glass-ceramics (SC-45) with gallic acid and folic acid. In: the 10th IASTED International Conference on Biomedical Engineering, Innsbruck (Austria), 13-15 February 2013.

3. Ferraris S., **Zhang X**., Prenesti E., Vernè E. Polyphenols grafting to bioactive glasses and glass-ceramics. In: Congresso Società Italiana Biomateriali, Baveno (VB), 3-5 giugno 2013.

4. **Xin Zhang**, Sara Ferraris, Enrica Vernè. Surface Functionalization of Bioactive Glasses with Natural Polyphenols. In 25th European Conference on Biomaterials, Madrid (Spain), 8-12 September, 2013.

Acknowledgements

At first, I wish to thank my supervisor, Dr. Enrica Vern é and Dr. Enrico Prenesti (Universi à di Torino) for their kind guidance, great help and useful advice during my research activities. Moreover, I should give my great appreciation to Dr. Sara Ferraris who was my valuable experiment partner and did contributions to result discussion.

Secondly, I would like to thank all my Lab mates and colleagues, especially Dr. Giorgia Novajra, Dr. Auristela de Miranda, Dr. Matteo Bruno, Dr. Qiuling Chen and Dr. Xinrui Song with whom I shared many happy moments during research.

Finally, acknowledgement must also be given to my dear families especially my mother for their support and concerns during the past years.

Torino, December 2013